



# Sampling Surface and Subsurface Particle-Size Distributions in Wadable Gravel- and Cobble-Bed Streams for Analyses in Sediment Transport, Hydraulics, and Streambed Monitoring

Kristin Bunte  
Steven R. Abt



## Abstract

---

Bunte, Kristin; Abt, Steven R. 2001. Sampling surface and subsurface particle-size distributions in wadable gravel- and cobble-bed streams for analyses in sediment transport, hydraulics, and streambed monitoring. Gen. Tech. Rep. RMRS-GTR-74. Fort Collins, CO: U.S. Department of Agriculture, Forest Service, Rocky Mountain Research Station. 428 p.

This document provides guidance for sampling surface and subsurface sediment from wadable gravel- and cobble-bed streams. After a short introduction to streams types and classifications in gravel-bed rivers, the document explains the field and laboratory measurement of particle sizes and the statistical analysis of particle-size distributions. Analysis of particle parameters, including shape, density, and bulk density are also discussed. The document describes the spatial variability of bed-material particle sizes as well as the horizontal and vertical structure of particle deposits. The discussion of sampling procedures and equipment helps the user to make appropriate selections that support the sampling objective. Sample-size estimates may be obtained from empirical data or computed from statistical relationships between sample size and accuracy. The document explains a variety of methods, their usage and prerequisites. A detailed discussion of sampling schemes guides the user to select appropriate spatial sampling patterns necessary to produce representative samples.

---

**Keywords:** Particle-size analysis, spatial variability of bed-material size, sampling procedures, sampling equipment, sample size, spatial sampling schemes.

## Authors

---

**Kristin Bunte** is a Fluvial Geomorphologist and Research Associate at the Engineering Research Center, Department of Civil Engineering, Colorado State University. She received M.S. and Ph.D. degrees in geography from the Freie Universität Berlin in Germany.

**Steven R. Abt** is Professor and Associate Dean for Research and Graduate Studies, College of Engineering, Colorado State University, and a Professional Engineer. He received M.S. and Ph.D. degrees in civil engineering from Colorado State University.

You may order additional copies of this publication by sending your mailing information in label form through one of the following media. Please specify the publication title and number.

<b>Telephone</b>	(970) 498-1392
<b>FAX</b>	(970) 498-1396
<b>E-mail</b>	rschneider@fs.fed.us
<b>Web site</b>	<a href="http://www.fs.fed.us/rm">http://www.fs.fed.us/rm</a>
<b>Mailing Address</b>	Publications Distribution Rocky Mountain Research Station 240 West Prospect Road Fort Collins, CO 80526

---

*The use of trade or firm names in this publication is for reader information and does not imply endorsement by the U.S. Department of Agriculture of any product or service*

---

# **Sampling Surface and Subsurface Particle- Size Distributions in Wadable Gravel- and Cobble-Bed Streams for Analyses in Sediment Transport, Hydraulics, and Streambed Monitoring**

**Kristin Bunte  
Steven R. Abt**



Prepared in support of the National Stream Systems Technology Center mission to enable land managers to “secure favorable conditions of water flows” from our National Forests.



## **Preface**

---

The Stream Systems Technology Center of the Rocky Mountain Research Station, U.S. Forest Service, initiated the generation of this compendium of methods because National Forest System streams are dominated by gravel caliber material and sound guidelines for characterizing the bed material of gravel- and cobble-bed streams are needed by hydrologists, fisheries and aquatic biologists, and geomorphologists. This project was initiated to meet Forest Service needs and at the same time provide an encyclopedia of approaches as a basis for the Federal Interagency Sedimentation Project Task Committee to adopt selected methods as standard approaches in the future. Work on this reference was initiated by an ad hoc team convened by Larry Schmidt of the Stream Systems Technology Center. The team included Ron Copeland, U.S. Army Corps of Engineers, Phil Zrymiak, Environment Canada, Randy Parker, U.S. Geological Survey, and Jim Fogg, Bureau of Land Management.

Streambed analysis and sampling in gravel-bed rivers have received increasing attention, especially over the last few years. Publishing activity reflects this trend. During the late 1970s and the 1980s, one or two papers were published per year on gravel-bed sampling procedures, sample size estimates, or sampling schemes. This number has risen to about five to seven papers per year during the 1990s. Despite the interest in the topic, a comprehensive compilation of these approaches is lacking and users need a reference to guide them through the multi-layered aspects of bed-material sampling.

The work presented is intended to fill this gap. Obviously attempting to comprehensively synthesize a rapidly evolving technology is impossible. This effort represents our knowledge at this point in time. Consequently, the user must exercise judgment in applying the approaches provided herein to specific sampling projects. To make the best choice of methods, the user should have knowledge about gravel-bed rivers and the processes forming them. The selection of a sampling program (where, how, and how much to sample) significantly influences the outcome.

## **Acknowledgments**

---

This publication was made possible through a partnership between the Rocky Mountain Research Station, National Stream Systems Technology Center and the Colorado State University, Engineering Research Center. The authors appreciate the helpful contributions and assistance of John Gray, Tom Lisle, Sue Hilton, Dave Dawdy, Paul Bakke, Mike McNamara, Mark Weinhold, Mohammed Samad, and Pete Klingeman. A special thanks to John Buffington, John Potyondy, and John Ritter for their significant effort in carefully reviewing this document and to Kurt Swingle and Louise Kingsbury who helped edit the final manuscript.



# Contents

---

Preface .....	i
Acknowledgments .....	i
Copyrighted Materials .....	x
List of Notations and Units .....	xiv
<b>1. Introduction .....</b>	<b>1</b>
<b>1.1 Gravel- and cobble-bed streams: Distinctions from other streams .....</b>	<b>1</b>
<b>1.2 Bed-material sampling and guidelines .....</b>	<b>2</b>
1.2.1 Aspects of bed-material sampling in gravel- and cobble-bed streams .....	2
1.2.2 Interdependency between sampling methods and study objectives .....	4
1.2.3 Deficiencies in existing guidelines .....	4
1.2.4 What these guidelines are intended to do .....	5
1.2.5 Guidelines are no substitute for experience .....	5
<b>1.3 Classification of gravel- and cobble-bed streams .....</b>	<b>6</b>
1.3.1 The Montgomery-Buffington stream classification .....	6
1.3.2 The Rosgen stream classification .....	7
1.3.3 Differences between the Rosgen and the Montgomery- Buffington classifications .....	9
1.3.4 Sediment source: self-formed versus relict/non-fluvial streams .....	12
1.3.5 Wadable and non-wadable streams .....	13
<b>2. Particle analysis .....</b>	<b>14</b>
<b>2.1 Size analysis .....</b>	<b>14</b>
2.1.1 Particle axes .....	14
2.1.2 Particle sizes and size classes .....	16
2.1.2.1 <i>The Wentworth scale of particle sizes</i> .....	17
2.1.2.2 <i>Particle size in <math>\phi</math>-units</i> .....	17
2.1.2.3 <i>Particle size in <math>\psi</math>-units</i> .....	19
2.1.3 Sieving and manual measurements of particle size .....	20
2.1.3.1 <i>Square-hole sieves</i> .....	20
2.1.3.2 <i>Relation between b-axis size and square-hole sieve sizes</i> .....	21
2.1.3.3 <i>Round-hole sieves</i> .....	23
2.1.3.4 <i>Center of class and mean particle b-axes length per size class</i> .....	23
2.1.3.5 <i>Comparison of sieve results using round-hole and square-hole sieves</i> ....	24
2.1.3.6 <i>Templates</i> .....	25
2.1.3.7 <i>Rulers and calipers</i> .....	27
2.1.3.8 <i>Pebble-box</i> .....	28
2.1.3.9 <i>Lab sieving</i> .....	30
2.1.3.10 <i>Field sieving, weighing, volume determination, and counting</i> .....	32
2.1.4 Computation of the particle-size distribution .....	38
2.1.4.1 <i>Particle-size frequency and cumulative frequency distribution</i> .....	38
2.1.4.2 <i>Percentiles and their computation</i> .....	40
2.1.4.3 <i>Testing for various distribution types</i> .....	42

2.1.5	Computation of particle distribution parameters .....	56
2.1.5.1	<i>Graphic, or percentile methods (geometric and arithmetic)</i> .....	57
2.1.5.2	<i>Moment, or frequency distribution method</i> .....	60
2.1.5.3	<i>Central tendency (mode, median, and mean)</i> .....	62
2.1.5.4	<i>Standard deviation and sorting</i> .....	65
2.1.5.5	<i>Skewness</i> .....	73
2.1.5.6	<i>Kurtosis</i> .....	78
2.1.5.7	<i>Comparison between methods</i> .....	80
2.1.5.8	<i>Percent fines</i> .....	82
2.1.5.9	<i>Bimodality</i> .....	83
<b>2.2</b>	<b>Shape analysis</b> .....	<b>85</b>
2.2.1	Compact, platy, bladed, and elongated particle shapes .....	86
2.2.2	Sphericity .....	88
2.2.2.1	<i>Indication of fluvial transport distance</i> .....	88
2.2.2.2	<i>Indication of particle transportability</i> .....	89
2.2.3	Roundness or angularity: analytical and visual approaches .....	90
2.2.4	Shape/roundness matrix: visual field classification .....	91
2.2.5	Pivot angles and their computation .....	93
2.2.6	Sample size for shape analysis .....	97
<b>2.3</b>	<b>Particle density, specific weight, specific gravity, and submerged specific weight ..</b>	<b>98</b>
<b>2.4</b>	<b>Bulk density, porosity, and void ratio</b> .....	<b>100</b>
<b>3.</b>	<b>Spatial variability of bed-material size</b> .....	<b>107</b>
<b>3.1</b>	<b>Downstream fining</b> .....	<b>107</b>
<b>3.2</b>	<b>Surface bed-material sizes within a reach</b> .....	<b>108</b>
3.2.1	Morphology of the bar-unit with pools, riffles, and bars .....	108
3.2.2	Bed-material particle-sizes on pools, riffles, and bars .....	113
3.2.2.1	<i>Helical flow and bed-material size in a bar unit</i> .....	113
3.2.2.2	<i>Riffle-related features: rapids, runs, glides, and pool-exit slopes</i> .....	116
3.2.2.3	<i>Coarsest parts of the reach: pools, riffles, and bar heads</i> .....	117
3.2.3	Stream morphology and particle-sizes in B-type and A-type streams .....	122
3.2.4	Effect of large woody debris and other stream blockages on stream morphology and particle sizes .....	123
3.2.5	Bed-material particle sizes around boulders .....	127
<b>3.3</b>	<b>Vertical variability in bed-material size</b> .....	<b>128</b>
3.3.1	Sedimentary processes causing vertical stratification .....	128
3.3.1.1	<i>The coarse surface layer: armoring and pavement</i> .....	130
3.3.1.2	<i>Mechanisms of fine sediment intrusion into open framework gravel</i> .....	131
3.3.2	Implications of vertical stratification for bed-material sampling .....	132
<b>3.4</b>	<b>Bed-surface structures</b> .....	<b>133</b>
3.4.1	Transverse and longitudinal bedforms .....	133
3.4.2	Imbrication .....	136
3.4.3	Clustering .....	137
3.4.4	Horseshoe vortex scour .....	138

3.4.5	Cobble embeddedness and protrusion .....	139
3.4.6	Gravel sheltered in pockets .....	141
3.4.7	Implications of bed-surface structures for bed-material sampling .....	141
<b>4.</b>	<b>Sampling procedures and equipment .....</b>	<b>143</b>
<b>4.1</b>	<b>Surface sampling .....</b>	<b>144</b>
4.1.1	Pebble counts along transects .....	146
4.1.1.1	<i>Heel-to-toe walks and sampling along a measuring tape .....</i>	<i>146</i>
4.1.1.2	<i>Sources of errors in pebble counts .....</i>	<i>148</i>
4.1.1.3	<i>Operator bias against small particles .....</i>	<i>149</i>
4.1.1.4	<i>Operator bias against and towards cobbles and boulders .....</i>	<i>154</i>
4.1.1.5	<i>Statistical detectability of operator bias .....</i>	<i>156</i>
4.1.1.6	<i>Sampling frame for bias reduction in particle identification .....</i>	<i>158</i>
4.1.1.7	<i>Measuring, recording and analyzing pebble count data .....</i>	<i>164</i>
4.1.2	Grid sampling .....	166
4.1.2.1	<i>Grid sizes and spatial scale .....</i>	<i>166</i>
4.1.2.2	<i>Photographic grid counts .....</i>	<i>166</i>
4.1.3	Areal sampling .....	170
4.1.3.1	<i>Manual sampling .....</i>	<i>171</i>
4.1.3.2	<i>Adhesive sampling .....</i>	<i>172</i>
4.1.3.3	<i>Photographic areal sampling .....</i>	<i>178</i>
4.1.3.4	<i>Photographic (areal) analyses in other scales .....</i>	<i>182</i>
4.1.3.5	<i>Visual particle-size estimates .....</i>	<i>184</i>
<b>4.2</b>	<b>Volumetric sampling .....</b>	<b>188</b>
4.2.1	Armor layer .....	188
4.2.1.1	<i>Definition and description .....</i>	<i>188</i>
4.2.1.2	<i>Thickness and sampling depth of the armor layer .....</i>	<i>188</i>
4.2.2	Subsurface, subarmor, and unstratified bed material .....	191
4.2.2.1	<i>Definition and description .....</i>	<i>191</i>
4.2.2.2	<i>Sampling depth to avoid bias against large particles .....</i>	<i>192</i>
4.2.3	Procedures and sampling dimensions for dry beds .....	195
4.2.3.1	<i>Tools for shoveled samples .....</i>	<i>195</i>
4.2.3.2	<i>Sample dimensions for shoveled samples in unstratified bed material ...</i>	<i>195</i>
4.2.3.3	<i>Surface pebble count on subsurface sediment .....</i>	<i>197</i>
4.2.4	Procedures and equipment for submerged conditions .....	198
4.2.4.1	<i>Shovels .....</i>	<i>199</i>
4.2.4.2	<i>Mesh-bag scoop .....</i>	<i>200</i>
4.2.4.3	<i>Grab samples (US RBMH-80) .....</i>	<i>201</i>
4.2.4.4	<i>Backhoe .....</i>	<i>203</i>
4.2.4.5	<i>Pipe samplers and the McNeil sampler .....</i>	<i>203</i>
4.2.4.6	<i>Barrel samplers .....</i>	<i>206</i>
4.2.4.7	<i>Three-sided plywood shield .....</i>	<i>209</i>
4.2.4.8	<i>Freeze-cores .....</i>	<i>210</i>
4.2.4.9	<i>Resin cores .....</i>	<i>213</i>
4.2.4.10	<i>Hybrid samplers: combined pipe and freeze-core sampler, or excavated freeze-cores .....</i>	<i>213</i>

4.2.5	Volumetric sampling in deep water .....	215
<b>4.3</b>	<b>Conversion of sample distributions: grid - areal - volume, and number - weight ...</b>	<b>216</b>
4.3.1	Voidless cube model .....	218
4.3.2	Modified cube model .....	224
4.3.3	Conversion based on computed penetration depth .....	226
4.3.4	Split plane surface model .....	227
<b>4.4</b>	<b>Combination of two particle-size distributions .....</b>	<b>230</b>
4.4.1	Rigid combination .....	230
4.4.2	Flexible combination .....	233
4.4.3	Adjusting frequency distributions .....	237
<b>4.5</b>	<b>Recording field results .....</b>	<b>240</b>
<b>5.</b>	<b>Sample size .....</b>	<b>241</b>
<b>5.1</b>	<b>Factors affecting sample size .....</b>	<b>242</b>
<b>5.2</b>	<b>Pebble counts: number-based sample-size recommendations .....</b>	<b>245</b>
5.2.1	General form of number-based sample-size equations .....	245
5.2.2	Prespecified error around the mean .....	249
5.2.2.1	<i>Absolute error around the mean in <math>\phi</math>-units .....</i>	<i>249</i>
5.2.2.2	<i>Percent error around the mean in mm .....</i>	<i>250</i>
5.2.2.3	<i>Percent error around the mean in <math>\phi</math>-units .....</i>	<i>252</i>
5.2.2.4	<i>Percent error in <math>\phi</math> and mm for approximate lognormal distributions .....</i>	<i>253</i>
5.2.2.5	<i>Limited number of particles available for sampling (<math>N \neq \infty</math>) .....</i>	<i>254</i>
5.2.2.6	<i>Comparison between sample-size equations for errors around the mean .....</i>	<i>256</i>
5.2.2.7	<i>Effect of bed-material sorting and error on sample size .....</i>	<i>258</i>
5.2.2.8	<i>Influence of multiple operators on sampling accuracy .....</i>	<i>259</i>
5.2.2.9	<i>Computation of sample size and error in the field .....</i>	<i>260</i>
5.2.3	Specified error for all percentiles .....	261
5.2.3.1	<i>Two-stage sampling approach (ISO 1992) .....</i>	<i>261</i>
5.2.3.2	<i>Binomial distribution approach (Fripp and Diplas 1993) .....</i>	<i>264</i>
5.2.3.3	<i>Multinomial distribution approach (Petrie and Diplas 2000) .....</i>	<i>265</i>
5.2.3.4	<i>Bootstrap approach: no assumed distribution type (Rice and Church 1996b) .....</i>	<i>268</i>
5.2.3.5	<i>Summary: the relation between sample size and error .....</i>	<i>275</i>
5.2.4	Detectability of change in percent fines (Bevenger and King 1995) .....	277
5.2.4.1	<i>Sample-size determination from diagrams .....</i>	<i>278</i>
5.2.4.2	<i>Sample-size computation .....</i>	<i>281</i>
5.2.4.3	<i>Operator error in the percent fines adds to the statistical error .....</i>	<i>283</i>
<b>5.3</b>	<b>Areal sampling: area-based sample-size recommendations .....</b>	<b>283</b>
5.3.1	$D_{max}$ and geometrical considerations .....	284
5.3.2	Two-stage sampling: specified error around the median .....	285
5.3.3	Multinomial approach .....	287
<b>5.4</b>	<b>Volumetric sampling: mass-based sample-size recommendations .....</b>	<b>288</b>
5.4.1	Sample mass as a function of largest particle size .....	289
5.4.1.1	<i>Sample mass as cubic functions of <math>D_{max}</math> .....</i>	<i>290</i>

5.4.1.2	<i>National standards: non-cubic functions of <math>D_{max}</math> particle size</i> .....	295
5.4.1.3	<i>Error of the entire particle-size distribution due to the presence or absence of particles from the largest size class</i> .....	298
5.4.1.4	<i>Sample-mass reduction: truncation and readjustment at the coarse end</i> .....	299
5.4.2	Sample mass as a function of acceptable percentile errors .....	301
5.4.2.1	<i>Two-stage sampling approach (ISO 1992)</i> .....	301
5.4.2.2	<i>Computerized two-stage sampling (Hogan et al. 1993)</i> .....	304
5.4.3	Analytical computation of sample mass (Ferguson and Paola 1997) .....	308
5.4.3.1	<i>Sample mass for bias avoidance</i> .....	311
5.4.3.2	<i>Sample mass for specified acceptable error</i> .....	315
5.4.4	Comparison of error curves for low, central, and higher percentiles .....	320
5.4.4.1	<i>Symmetrical parent distributions</i> .....	320
5.4.4.2	<i>Asymmetrical parent distributions skewed towards a fine tail</i> .....	322
<b>6.</b>	<b>Spatial sampling schemes</b> .....	<b>323</b>
<b>6.1</b>	<b>Terminology and sampling principles</b> .....	<b>325</b>
6.1.1	Stream types and stream morphology .....	325
6.1.2	Length of the sampling reach .....	325
6.1.3	Homogeneous versus heterogeneous gravel deposits .....	326
6.1.4	Pilot studies .....	326
6.1.5	Spatial aspects of pebble counts .....	327
6.1.5.1	<i>Minimum sampling point spacing</i> .....	327
6.1.5.2	<i>Number of sampling points</i> .....	327
6.1.5.3	<i>Minimum sampling area</i> .....	328
6.1.5.4	<i>Measurement of particle sizes in pebble counts</i> .....	328
6.1.5.5	<i>Recording pebble count data</i> .....	329
6.1.6	Spatial aspects of volumetric sampling .....	329
6.1.6.1	<i>Layers to be sampled</i> .....	329
6.1.6.2	<i>Relation between surface and subsurface sediment size</i> .....	330
6.1.6.3	<i>Feasibility and the statistical relationship between mass of subsamples, total sample mass, and number of sampling locations</i> .....	331
<b>6.2</b>	<b>Spatially integrated or unstratified pebble counts (reach-averaged sampling)</b> .....	<b>332</b>
6.2.1	Near-homogeneous reaches: paced transects, transects along measuring tapes, and an unplanned zigzag course .....	333
6.2.2	Long and relatively homogeneous stream sections: planned zigzag course .....	334
6.2.3	Heterogeneous reaches and complex streambeds .....	336
6.2.3.1	<i>Grid sampling and lay-out of the grid</i> .....	336
6.2.3.2	<i>Grid spacing and areal extent of the sampling grid</i> .....	338
<b>6.3</b>	<b>Spatially segregated pebble counts (sampling each unit individually)</b> .....	<b>340</b>
6.3.1	Geomorphologically stratified sampling .....	340
6.3.1.1	<i>Characterization and delineation of geomorphological units</i> .....	341
6.3.1.2	<i>Grid sampling on individual geomorphological units</i> .....	341
6.3.1.3	<i>Sampling on riffles only</i> .....	342
6.3.1.4	<i>Proportional sampling on long reaches</i> .....	343

6.3.2	Sedimentary stratified sampling .....	345
6.3.2.1	<i>Visual delineation of sedimentary units (facies or patches) based on estimates of percentile particle sizes</i> .....	345
6.3.2.2	<i>Visual delineation based on a two-level characterization of particle sizes</i> .....	347
6.3.2.3	<i>Statistical delineation from systematic grid data</i> .....	348
6.3.2.4	<i>Strategies for sampling within delineated facies units</i> .....	351
6.3.2.5	<i>Area-weighted reach-averaged particle-size distribution from stratified sampling</i> .....	357
<b>6.4</b>	<b>Spatially integrated volumetric sampling (reach-averaged)</b> .....	<b>358</b>
6.4.1	Sampling a truly homogeneous reach .....	360
6.4.2	Sampling schemes for spatially integrated sampling of heterogeneous reaches ....	360
6.4.2.1	<i>Random sampling locations</i> .....	360
6.4.2.2	<i>Sampling the reach at systematic grid points</i> .....	361
6.4.2.3	<i>Random placement of sampling locations within grid cells</i> .....	362
6.4.2.4	<i>Two-stage sampling using overlaying grid systems or a small grid pattern</i> .....	363
6.4.3	Number of sampling points for systematic samples of heterogeneous reaches .....	363
6.4.3.1	<i>Large streams, no space limitation</i> .....	364
6.4.3.2	<i>Small streams, space limitation for sampling</i> .....	365
6.4.4	Subsample mass at each grid location and total sample mass within the reach .....	365
6.4.4.1	<i>Full sample at each grid location in well sorted, fine to medium gravel beds</i> .....	365
6.4.4.2	<i>Reduction of sample mass at each grid location in poorly sorted gravel- and cobble beds</i> .....	365
6.4.4.3	<i>Individually biased grab samples, empirical approach</i> .....	366
6.4.4.4	<i>Determining sampling precision from two-stage sampling with overlaying grid systems</i> .....	368
6.4.4.5	<i>Individually unbiased subsamples for assumed normal distributions</i> .....	368
6.4.4.6	<i>Comparison of subsample masses and total sample mass computed with two different approaches</i> .....	369
6.4.4.7	<i>Retroactive computation of the number of sampling points</i> .....	370
6.4.4.8	<i>Problems with collecting large samples in coarse gravel and cobble-bed streams</i> .....	370
6.4.4.9	<i>Computation of the reach-averaged particle-size distribution</i> .....	370
<b>6.5</b>	<b>Spatially segregated volumetric sampling (sampling each unit individually)</b> .....	<b>371</b>
6.5.1	Geomorphologically stratified sampling .....	371
6.5.1.1	<i>Sampling on riffles only</i> .....	371
6.5.1.2	<i>Sampling patterns and sample mass for riffle samples</i> .....	372
6.5.2	Sedimentary stratified sampling .....	373
6.5.2.1	<i>Reach-averaged information on subsurface, armor, or bulk sediment size</i> .....	373
6.5.2.2	<i>Sampling location for reach-averaged subsurface <math>D_{50}</math> size</i> .....	377
<b>6.6</b>	<b>Spatially focused sampling</b> .....	<b>379</b>
6.6.1	Sampling large particles on bar heads for stream competence analysis .....	380
6.6.2	Sampling fines in pools for analysis of fine sediment supply .....	380

<b>7. Steps of a sampling project .....</b>	<b>384</b>
<b>8. Appendix .....</b>	<b>391</b>
<b>9. References .....</b>	<b>393</b>
<b>10. Index .....</b>	<b>409</b>

## Copyrighted Materials

---

We would like to thank the following publishers, individuals, and organizations for granting permission to reproduce, quote, or modify the following figures as needed. We have made every effort to contact those we believe to be the original sources to obtain these permissions. If there have been any accidental errors, omissions, or misattributions we apologize to those concerned.

- Geological Society of America, for **Fig. 1.1**; taken from Figs. 2 and 3 on p. 600 and 601 in: Montgomery, D.R. and J.M. Buffington, 1997. Channel-reach morphology in mountain drainage basins. *Geological Society of America Bulletin* 109 (5): 596-611.
- Elsevier Science, for **Fig. 1.2**; taken from Fig. 1 on p. 174 in: Rosgen, D.L., 1994. A classification of natural rivers. *Catena* 22: 169-199.
- John Wiley and Sons, for **Fig. 2.3** and **Fig. 2.4**; taken from Fig. 3.3 on p. 51 in: Church, M., D.G. McLean and J.F. Walcott, 1987. River bed gravels: sampling and analysis. In: *Sediment Transport in Gravel-Bed Rivers*. C.R. Thorne, J.C. Bathurst and R.D. Hey (eds.).
- American Society of Civil Engineers, for **Fig. 2.5**; taken from Fig. 1 on p. 844 in: Hey, R.D. and C.R. Thorne, 1983. Accuracy of surface samples from gravel bed material. *Journal of Hydraulic Engineering*, 109 (6): 842-851.
- Society for Sedimentary Geology, for **Fig. 2.10**; taken from Fig. 1 on p. 940 in: Ibbeken, H., 1974. A simple sieving and splitting device for field analysis of coarse grained sediments. *Journal of Sedimentary Petrology* 44(3): 939-946.
- Society for Sedimentary Geology, for **Fig. 2.15**; taken from Fig. 3 on p. 1218 in: Ibbeken, H., 1983. Jointed source rock and fluvial gravels controlled by Rosin's law: a grain size study in Calabria, South Italy. *Journal of Sedimentary Petrology* 53(4): 1213-1231.
- Springer Verlag, for **Fig. 2.18**; taken from Fig. A-1 on p. 585 in: Pettijohn, J.F., P.E. Potter, and R. Siever, 1972. *Sand and Sandstone*. Springer Verlag, New York, Heidelberg, Berlin, 619 pp.
- American Geophysical Union, for **Fig. 2.21**; taken from Fig. 6 on p. 1183 in: Sambrook Smith, G.H., A.P. Nicholas and R.I. Ferguson, 1997. Measuring and defining bimodal sediments: Problems and implications. *Water Resources Research* 33 (5): 1179-1185.
- Society for Sedimentary Geology, for **Fig. 2.22**; taken from Figs. 3 and 4 on p. 66 and 67 in: Krumbein, W.C., 1941. Measurement and geological significance of shape and roundness of sedimentary particles. *Journal of Sedimentary Petrology* 11 (2): 64-72.
- University of Chicago Press, for **Fig. 2.23**; taken from Figs. 2 and 6 on p. 119 and 123 in: Sneed, E.D. and R.L. Folk, 1958. Pebbles in the lower Colorado River, Texas: a study in particle morphogenesis. *Journal of Geology* 66: 114-150.
- Society for Sedimentary Geology, for **Fig. 2.24**; taken from Plate 1 in: Krumbein, W.C., 1941. Measurement and geological significance of shape and roundness of sedimentary particles. *Journal of Sedimentary Petrology* 11 (2): 64-72.
- Society for Sedimentary Geology, for **Fig. 2.25**; taken from Figs. 1 and 2 on p. 932 in: Crofts, R.S., 1974. A visual measure of single particle form for use in the field. *Journal of Sedimentary Petrology* 44 (3): 931-934.
- Press Syndicate of the University of Cambridge, for **Fig. 2.27**; taken from Fig. 7.1 (top) on p. 112 in: Julien, P., 1995. *Erosion and Sedimentation*. Cambridge University Press, Cambridge.
- Press Syndicate of the University of Cambridge, **Fig. 2.28**; taken from Fig. 7.1 (bottom) on p. 112 in: Julien, P., 1995. *Erosion and Sedimentation*. Cambridge University Press, Cambridge

- John Wiley and Sons, for **Fig. 3.1**; taken from Fig. 11.6 (top) on p. 302 in: Church, M. and D. Jones, 1982. Channel bars in gravel-bed rivers. In: *Gravel-bed Rivers. Fluvial Processes, Engineering and Management*. R.D. Hey; J.C. Bathurst and C.R. Thorne (eds.).
- Newbury Hydraulics Ltd., for **Fig. 3.3**; taken from Fig. 3.9 on p. 76 in: Newbury, R.W. and M.N. Garboury, 1993. *Stream Analysis and Fish Habitat Design. A Field Manual*.
- John Wiley and Sons, for **Fig. 3.4**; taken from Figs. 11.1 and 11.4 on p. 295 and 299 in: Church, M. and D. Jones, 1982. Channel bars in gravel-bed rivers. In: *Gravel-bed Rivers. Fluvial Processes, Engineering and Management*. R.D. Hey; J.C. Bathurst and C.R. Thorne (eds.).
- John Wiley and Sons, for **Fig. 3.5**; taken from Figs. 2 and 4 on p. 634 and 636 in: Thompson, A., 1986. Secondary flows and the pool-riffle unit: a case study of the processes of meander development. *Earth Surface Processes and Landforms* 11: 631-641.
- American Geophysical Union, for **Fig. 3.6**; taken from Fig. 26 on p. 1379 in: Dietrich, W.E. and J.D. Smith, 1984. Bedload transport in a river meander. *Water Resources Research* 20 (10): 1355-1380.
- John Wiley and Sons, for **Fig. 3.7**; taken from Fig. 6.9 on p. 215 in: Whiting, P., 1996. Sediment sorting over bed topography. In: *Advances in Fluvial Dynamics and Stratigraphy*, P.A. Carling and M.R. Dawson (eds.).
- Blackwell Science, for **Fig. 3.8**; taken from Fig. 6.6 on p. 134 in: Church, M., 1992. Channel morphology and typology. In: *The Rivers Handbook*, Vol. 1. P. Calow and G.E. Petts, eds.
- John Wiley and Sons, for **Fig. 3.9**; taken from Fig. 8 on p. 258 in: Sear, D.A., 1996. Sediment transport processes in pool-riffle sequences. *Earth Surface Processes and Landforms* 21: 241-262.
- John Wiley and Sons, for **Fig. 3.10**; taken from Fig. 13.3 on p. 285 in: Lisle, T.E. and M.A. Madej, 1992. Spatial variation in armouring in a channel with high sediment supply. In: *Dynamics of Gravel Bed Rivers*. P. Billi, R.D. Hey, C.R. Thorne and P. Tacconi (eds.).
- Blackwell Science for **Fig. 3.11**; taken from Fig. 6.4 a on p. 130 in: Church, M., 1992. Channel morphology and typology. In: *The Rivers Handbook*, Vol. 1. P. Calow and G.E. Petts, eds.
- American Geophysical Union, for **Fig. 3.13**; taken from Fig. 1 b on p. 1904 in: Buffington, J.M. and D.R. Montgomery, 1999a. A procedure for classifying textural facies in gravel-bed rivers. *Water Resources Research* 35 (6):1903-1914.
- John Wiley and Sons, Inc., for **Fig. 3.14**; taken from Fig. 3.1 on p. 47 in: Church, M., D.G. McLean and J.F. Walcott, 1987. River bed gravels: sampling and analysis. In: *Sediment Transport in Gravel-Bed Rivers*, C.R. Thorne, J.C. Bathurst and R.D. Hey (eds.).
- Geological Society of America, for **Fig. 3.16**; taken from Fig. 1 on p. 105 in: Whiting, P.J., W.E. Dietrich, L.B. Leopold, T.G. Drake, and R.L. Shreve, 1988. Bedload sheets in heterogeneous sediment. *Geology* 16: 105-108.
- John Wiley and Sons, for **Fig. 3.18**; taken from Fig. 9.2 in: Todd, S.P., 1996. Process deduction from fluvial sedimentary structures. In: *Advances in Fluvial Dynamics and Stratigraphy*. P.A. Carling and M.R. Dawson (eds.),
- Canadian Society of Petroleum Geologists, for **Fig. 3.19**; taken from Fig. 2 on p. 79 in: Brayshaw, 1984. Characteristics and origin of cluster bedforms in coarse-grained alluvial channels. In: *Sedimentology of Gravels and Conglomerates*. E.H. Koster and R.J. Steel, (eds.), Canadian Society of Petroleum Geologists, Memoir 10: 77-85.
- John Wiley and Sons, for **Fig. 3.20**; taken from Fig. 9 a on p. 129 in: Bunte, K. and J. Poesen, 1994. Effects of rock fragment size and cover on overland flow hydraulics, local turbulence and sediment yield on an erodible soil surface. *Earth Surface Processes and Landforms* 19: 115-135.
- John Wiley and Sons, for **Fig. 4.12**; taken from Fig. 2 on p. 62 in: Ibbeken, H. and R. Schleyer, 1986. Photo sieving: a method for grainsize analysis of coarse-grained, unconsolidated bedding surfaces. *Earth Surface Processes and Landforms* 11: 59-77.

- John Wiley and Sons, for **Fig. 4.13**; taken from Fig. 3 on p. 62 in: Ibbeken, H. and R. Schleyer, 1986. Photo sieving: a method for grain size analysis of coarse-grained, unconsolidated bedding surfaces. *Earth Surface Processes and Landforms* 11: 59-77.
- American Geophysical Union, for **Fig. 4.15**; taken from Figs. 3 and 4 on p. 1906 and 1907 in: Buffington, J.M. and D.R. Montgomery, 1999a. A procedure for classifying and mapping textural facies in gravel-bed rivers. *Water Resources Research* 35 (6): 1903-1914.
- American Society of Civil Engineers, for **Fig. 4.19**; taken from Fig. 9 on p. 964 in Diplas, P. and J.B. Fripp, 1992. Properties of various sediment sampling procedures. *Journal of Hydraulic Engineering* 118 (7): 955-970.
- National Council of the Paper Industry for Air and Steam Improvement, for **Fig. 4.28**; taken from Fig. 15.3 on p. A-16 in: National Council of the Paper Industry for Air and Stream Improvement (NCASI) 1986. A comparison of four procedures for determining streambed substrate composition. Technical Bulletin 481. Source: Walkotten, W.J., 1976. An improved technique for freeze sampling streambed sediments. U.S.D.A. Forest Service Research Note PNW-281, 11 pp.
- American Fisheries Society, for **Fig. 4.30**; taken from Fig. 1 on p. 854 in: Rood, K. and M. Church, 1994. Modified freeze-core technique for sampling the permanently wetted streambed. *North American Journal of Fisheries Management* 14: 852-861.
- Chapman & Hall, for **Fig. 4.31**; taken from Fig. 4-5 on p. 54 in: Lewis, D.W. and D. McConchie, 1994. *Analytical Sedimentology*.
- American Society of Civil Engineers, for **Fig. 4.32**; taken from Fig. 5 on p. 1170 in: Kellerhals, R. and D.I. Bray, 1971. Sampling procedures for coarse fluvial sediments. *Journal of the Hydraulics Division, ASCE*, 97 (HY8): 1165-1180.
- American Society of Civil Engineers, for **Fig. 4.36**; taken from Fig. 2 on p. 541 in: Fraccarollo, L. and A. Marion, 1995. Statistical approach to bed-material surface sampling. *Journal of Hydraulic Engineering* 121 (7): 640-645.
- John Wiley and Sons, for **Fig. 5.1**; taken from Fig. 2.4 on p. 11 in: Gilbert, R.O., 1987. *Statistical Methods for Environmental Pollution Monitoring*. Van Nostrand Reinhold, New York, 320 pp.
- American Geophysical Union, for **Fig. 5.4**; taken from Fig. 4 on p. 2630 in: Marcus, W.A., S. Ladd and J. Stoughton, 1995. Pebble counts and the role of user-dependent bias in documenting sediment size distributions. *Water Resources Research* 31 (10): 2625-2631.
- Society for Sedimentary Geology, for **Fig. 5.8**; taken from Fig. 5 on p. 658 in: Rice, S. and M. Church, 1996b. Sampling surficial fluvial gravels: the precision of size distribution percentile estimates. *Journal of Sedimentary Research* 66 (3): 654-665.
- Society for Sedimentary Geology, for **Fig. 5.10**; taken from Fig. 7 on p. 660 in: Rice, S. and M. Church, 1996b. Sampling surficial fluvial gravels: the precision of size distribution percentile estimates. *Journal of Sedimentary Research* 66 (3): 654-665.
- Society for Sedimentary Geology for **Fig. 5.11**; taken from Fig. 8 on p. 661 in: Rice, S. and M. Church, 1996b. Sampling surficial fluvial gravels: the precision of size distribution percentile estimates. *Journal of Sedimentary Research* 66 (3): 654-665.
- John Wiley and Sons, for **Fig. 5.19 a-c**; taken from Fig. 2 on p. 1066 in: Ferguson, R.I. and C. Paola, 1997. Bias and precision of percentiles of bulk grain size distributions. *Earth Surface Processes and Landforms* 22 (11): 1061-1078.
- John Wiley and Sons, for **Fig. 5.20** taken from Fig. 7 on p. 1073 in: Ferguson, R.I. and C. Paola, 1997. Bias and precision of percentiles of bulk grain size distributions. *Earth Surface Processes and Landforms* 22 (11): 1061-1078.

- John Wiley and Sons, for **Fig. 5.21 a-c**; taken from Fig. 5 on p. 1070 in: Ferguson, R.I. and C. Paola, 1997. Bias and precision of percentiles of bulk grain size distributions. *Earth Surface Processes and Landforms* 22 (11): 1061-1078.
- John Wiley and Sons, for **Fig. 5.22 a-c**; taken from Fig. 7 on p. 1073 in: Ferguson, R.I. and C. Paola, 1997. Bias and precision of percentiles of bulk grain size distributions. *Earth Surface Processes and Landforms* 22 (11): 1061-1078.
- Wildland Hydrology, for **Fig. 6.7**; taken from Fig. 5-18 on p. 5-27 in: Rosgen, D.L., 1996. *Applied River Morphology*.
- American Society of Civil Engineers, for **Fig. 6.9**; taken from Fig. 8 and 9 on p. 1114 in: Crowder, D. W. and P. Diplas, 1997. Sampling heterogeneous deposits in gravel-bed streams. *Journal of Hydraulic Engineering* 123 (12): 1106-1117.
- American Society of Civil Engineers, for **Fig. 6.10**; taken from Fig. 7 on p. 1113 in: Crowder, D. W. and P. Diplas, 1997. Sampling heterogeneous deposits in gravel-bed streams. *Journal of Hydraulic Engineering* 123 (12): 1106-1117.

*Kristin Bunte and Steven Abt  
Fort Collins, May, 2001*

## List of Notations and Units

---

$a$	Particle $a$ -axis, the longest axis	mm
$a$	Coefficient	—
$a, \beta$	Confidence levels	—
$b$	Particle $b$ -axis, the intermediate axis	mm
$b$	Coefficient	—
$A$	Area	$m^2, mm^2$
$A_p$	Area covered by one particle	$m^2, mm^2$
$A_s$	Sampling area	$m^2, mm^2$
$B$	Bimodality index (Wilcock 1993)	—
$B^*$	Bimodality index (Sambrook Smith et al. 1997)	—
$c$	Particle $c$ -axis, the shortest axis	mm
$C$	Corey shape factor, similar to particle sphericity $\psi$	—
$b_m$	Mean particle $b$ -axis size	mm
$b_{m(sq)}$	Mean $b$ -axis size of particles retained on a square-hole sieve	mm
$b_{m(rd)}$	Mean $b$ -axis size of particles retained on a round-hole sieve	mm
$d$	Diameter (e.g., of a freeze core)	m
$d_p$	Penetration depth of adhesive in areal sampling	mm
$d_{Smin}$	Minimum sampling depth	cm
$D$	Particle size or particle sieve size	mm
$D_{cm}$	Particle size of the coarse mode of a distribution	mm
$D_{ci}$	Particle size of the center of the $i$ th size class	mm
$D_{dom}$	Dominant large particle diameter within an area of concern (reach)	mm
$D_e$	Vertical extent of particle embedded or buried below the bed	mm
$D_f$	Height with which a particle protrudes above the bed	mm
$D_{fm}$	Particle size of the fine mode of a distribution	mm
$D_{gm}$	Geometric mean particle size of a distribution	mm
$D_i$	Particle size of the $i$ th size class	mm
$D_{ic}$	Center of class particle size computed from the geometric mean of the upper and lower border of the size fraction (equal to logarithmic mean, or arithmetic mean of particle sizes in $\phi$ -units)	$\phi$
$D_{i(sq)}$	Particle size of the $i$ th size class on a square-hole sieve	mm
$D_{i(rd)}$	Particle size of the $i$ th size class on a round-hole sieve	mm
$D_m$	Mean particle size of a distribution	mm
$D_{max}$	Largest particle	mm
$D_{mc}$	Particle size of the weight midpoint of a sieve class; i.e., particle size that halves the particle mass per size class	mm
$D_{min}$	Smallest particle	mm
$D_{mode}$	Mode of particle size distribution	mm
$D_n$	Nominal particle diameter, $(a \cdot b \cdot c)^{1/3}$	mm
$D_p$	$p^{\text{th}}$ percentile of a particle-size distribution	mm
$D_{pass}$	Smallest sieve size through which a particle passed	mm
$D_{pass(i)}$	Smallest sieve size passed by all particles of the $i$ th size class	mm
$D_{pm}$	Mean of $p^{\text{th}}$ percentile obtained from several subsamples	mm
$D_{ret}$	Largest sieve size that retained a particle	mm
$D_{ret(i)}$	Largest sieve size retaining all particles of the $i$ th size class	mm
$D_s$	Size of sieve opening	mm
$D_t$	Total vertical extent of a particle	mm
$D_{50}$	Median particle size of a distribution	mm
$D_{84}$	84 <sup>th</sup> percentile of a particle-size distribution (subscript number refers to percentile)	mm
$D_{84m}$	Mean particle size of the $D_{84}$ in subsamples	mm
$e$	Void ratio, ratio of volume of voids to total volume	—
$e\%D_m$	Percentage error around the mean particle size in mm ( $D_m$ )	mm
$e_{\pm\phi m}$	Absolute error around the mean particle size in $\phi$ -units ( $\phi_m$ )	$\phi$

$e_{\% \phi_m}$	Percentage error around the mean particle size in $\phi$ -units ( $\phi_m$ )	$\phi$
$e_{\pm D_p}$	Absolute error around the mean particle size for the $p^{\text{th}}$ percentile in mm.	mm
$e_{\pm \phi_p}$	Absolute error around the mean particle size for the $p^{\text{th}}$ percentile in $\phi$ -units	$\phi$
$E$	Embeddedness	—
$E\%$	Percent cobble embeddedness	%
$F$	Particle form factor distinguishing between platy, bladed and elongated particle shapes	—
$f$	Frequency by weight or number of a particle-size class	—
$f_{\%}$	Percent frequency by weight or number of a particle-size class	%
$G_{\phi_i}$	Frequency of an equivalent Gaussian distribution of $\phi_i$	—
$G_{\%i}$	Percent frequency of an equivalent Gaussian distribution of $\phi_i$	%
$g$	Acceleration due to gravity = 9.81	m/s <sup>2</sup>
$i$	$i^{\text{th}}$ size class	—
$k$	Total number of size classes	—
$K$	Particle size of the bottom particle	mm
$ku$	Arithmetic kurtosis of a distribution	—
$ku_g$	Geometric kurtosis of a distribution (hypothetical)	—
$l$	Length (e.g., of a freeze core)	m
$L_{D_i}$	Frequency of an equivalent lognormal distribution of $D_i$	—
$L_{\%i}$	Percent frequency of an equivalent lognormal distribution of $D_i$	%
$m$	Mass	g, kg
$m_{D_{max}}$	Mass of the $D_{max}$ particle size	g, kg
$m_{mi}$	Mean weight of particles retained on the $i^{\text{th}}$ size class	g, kg
$m_i$	Mass of particles retained on the $i^{\text{th}}$ size class	g, kg
$m_s$	Mass of all particles contained in a sample	g, kg
$m_{ss}$	Mass of all particles contained in a subsample	g, kg
$m_{tot}$	Mass of all particles contained in the total sample	g, kg
$m_{\%i}$	Percent frequency of particle mass for the $i^{\text{th}}$ size class	%
$m_{\%cmi}$	Percent frequency of particle mass for the $i^{\text{th}}$ size class that is part of the coarse mode of the distribution	%
$m_{\%fmi}$	Percent frequency of particle mass for the $i^{\text{th}}$ size class that is part of the fine mode of the distribution	%
$n_{emb}$	Number of embedded particles	—
$n_{exp}$	Number of particles exposed on the bed surface	—
$n_i$	Number of particles retained for $i^{\text{th}}$ size class	—
$n$	Total number of particles per sample	—
$n_{\% exp}$	Percent of particles exposed on the bed surface	%
$n_i$	Number of particles retained in the $i^{\text{th}}$ size class	—
$n_{ph}$	Number of particles contained within a photographed area	—
$n_r$	Number of particles at the reference site	—
$n_s$	Number of particles at the study site	—
$n_{tot}$	Total number of samples	—
$n_2$	Second sample	—
$n_{\%i}$	Percent frequency of particle numbers for the $i^{\text{th}}$ size class	%
$\Sigma n_{\%i}$	Cumulative percent frequency of particle numbers for the $i^{\text{th}}$ size class = $p_i$	%
$p$	Porosity, ratio of volume of voids to total volume	—
$p_{i,a-w}$	Weight fraction ( $m_i/m_{tot}$ ) of the $i^{\text{th}}$ size class of an area-by-weight particle-size distribution	—
$p_{i,0}$	Weight fraction ( $m_i/m_{tot}$ ) of the $i^{\text{th}}$ size class of a volume-by-weight size-distribution converted from an area-by-weight distribution	—
$p_{i,v-w}$	Weight fraction ( $m_i/m_{tot}$ ) of the $i^{\text{th}}$ size class of a volume-by-weight particle-size distribution	—
$p_s$	Proportion of fines in bed material at a study site	—

$P_r$	Proportion of fines in bed material at a reference site	—
$P_{v,0}$	Porosity, ratio of volume of voids to total sediment volume (bulk)	—
$p$	Probability associated with $z_p$ values	—
$p$	Percentile (in decimals)	—
$P_i$	Percentile of a cumulative distribution for $i^{\text{th}}$ size class (in decimals)	—
$P_{Ai}$	Percentile for $i^{\text{th}}$ size class of an areal sample	—
$P_{Gi}$	Percentile for $i^{\text{th}}$ size class of a grid sample	—
$P_{ri}$	Percentile for $i^{\text{th}}$ size class of a sample using a rigid combination method	—
$P_{fi}$	Percentile for $i^{\text{th}}$ size class of a sample using a flexible combination method	—
$P$	Particle roundness index	—
$P_m$	Mean particle roundness index for a deposit	—
$P_{cm}$	Proportion of sediment contained in the coarse distribution mode	mm
$P_{fm}$	Proportion of sediment contained in the fine distribution mode	mm
$P_{1m}$	Proportion of sediment contained in the primary distribution mode	mm
$P_{2m}$	Proportion of sediment contained in the secondary distribution mode	mm
$q$	Number of subsamples	—
$r$	Number of replicate samples for a given sample or subsample size	—
$r$	Largest radius of a circle that can be inscribed into a corner of a particle	mm
$R$	Largest radius of a circle that can be inscribed into the entire particle	mm
$R_{Di}$	Frequency of an equivalent Rosin distribution of $D_i$	—
$R_{\%i}$	Percent frequency of an equivalent Rosin distribution of $D_i$	%
$s$	Sample standard deviation, or sorting coefficient of an approximately normal distribution	mm or $\phi$
$s_{Dm}$	Standard deviation of the mean particle size in subsamples	mm or $\phi$
$s_{50}$	Standard deviation of the median particle size $D_{50}$ in subsamples	mm or $\phi$
$s_g$	Geometric standard deviation or sorting coefficient of a sample distribution	—
$sk$	Arithmetic skewness of a distribution	—
$sk_g$	Geometric skewness of a distribution	mm, mm <sup>2</sup>
$s_p$	Standard error around percentile $p$	mm or $\phi$
$s_R$	Sorting coefficient for a Rosin distribution	mm or $\phi$
$s_I$	Sorting coefficient as computed by Inman (1952)	$\phi$
$S$	Particle compactness	—
$V$	Volume (e.g., of a freeze core)	m <sup>2</sup>
$V_s$	Volume of sediment without pores	m <sup>3</sup> , liter
$V_t$	Total volume of sediment	m <sup>3</sup> , liter
$V_v$	Volume of voids or pores in sediment	m <sup>3</sup> , liter
$z_p$	Values of the x-axis of a true, bell-shaped normal distribution	—
$\Phi$	Pivot angle, angle of repose, intergranular friction angle	°
$\phi$	Particle size unit = $-\log_2(D)$	$\phi$
$\phi_m$	Arithmetic mean particle size of a distribution	$\phi$
$\phi_i$	Particle size in $\phi$ -units of the $i^{\text{th}}$ size class	$\phi$
$\phi_{ci}$	Particle size in $\phi$ -units of the center of the $i^{\text{th}}$ size class	$\phi$
$\phi_{m1}$	Particle size of the primary distribution mode	$\phi$
$\phi_{m2}$	Particle size of the secondary distribution mode	$\phi$
$\phi_{50}$	Median particle size of a distribution	$\phi$
$\phi_{84}$	84 <sup>th</sup> percentile of a particle-size distribution (subscript number refers to percentile)	$\phi$
$\phi_p$	$p^{\text{th}}$ percentile of a particle-size distribution	$\phi$
$\gamma$	Specific weight $\rho \cdot g$	g/cm <sup>2</sup> ·s <sup>2</sup> , kg/m <sup>2</sup> ·s <sup>2</sup>
$\mu$	Distribution mode	mm or $\phi$
$\pi$	Dimensionless constant, 3.141	—

$\rho$	Density	$\text{g/cm}^3, \text{kg/m}^3$
$\rho_f$	Fluid density	$\text{g/cm}^3, \text{kg/m}^3$
$\rho_s$	Density of a sediment particle	$\text{g/cm}^3, \text{kg/m}^3$
$\rho'_s$	Submerged particle density	$\text{g/cm}^3, \text{kg/m}^3$
$\rho_b$	Sediment bulk density	$\text{g/cm}^3, \text{kg/m}^3$
$\rho_{sub}$	Subsurface sediment bulk density	$\text{g/cm}^3, \text{kg/m}^3$
$\sigma$	Standard deviation of the population distribution	any unit
$\Sigma$	Sum	any unit
$\psi$	Particle size unit, = $\log_2(D) = -\phi$	$\psi$
$\psi$	Particle sphericity	—
$\psi_r$	Effective particle settling sphericity	—

# 1. Introduction

---

## 1.1 Gravel- and cobble-bed streams: distinctions from other streams

Gravel- and cobble-bed streams are principally distinguished from sand- and boulder-bed streams by their particle-size distributions. Gravel-bed streams have a mean particle size in the range of 2 - 64 mm, and cobble-bed streams in the range of 64 - 256 mm (Table 1.1). By contrast, sand-bedded streams contain bed-material that is mostly less than 2 mm, and boulder-bed streams are comprised of mostly boulders and have a mean particle size larger than 256 mm.

Table 1.1: Stream classification based on the median bed-material particle size.

Stream type	Range of median bed-material particle size (mm)
Sand-bed stream	0.063 - 2
Gravel-bed stream	2 - 64
Cobble-bed stream	64 - 256
Boulder-bed stream	256 - 4096

Gravel- and cobble beds usually contain some sand, typically less than 10% in mountainous areas, and maximally up to about 50%. In mountain areas, gravel- and cobble bed streams may also contain large boulders. Thus, the entire range of bed-material particle size can span five orders of magnitude (i.e., from fine sand of 0.06 mm to boulders of 4000 mm). This wide range causes complex interactions between particles of different sizes during erosion, transport, deposition, and causes spatially heterogeneous beds that complicate bed-material sampling.

Gravel- and cobble-bed streams differ from sand- and boulder-bed streams not only by particle size, but also with respect to the appearance of the stream (morphology) and the environment in which the stream occurs (topographic setting). Sand-bed streams often have low gradients and occur in valleys or on broad plains, whereas most boulder-bed streams have steep gradients and are found in mountain environments, although exceptions exist for both. Gravel- and cobble-bed streams are commonly found in moderately steep mountain valleys and where streams enter plains near mountains. The distinction between sand-, gravel-, cobble-, and boulder-bed streams is included in the stream classification by Rosgen (1994) that is discussed in Section 1.3.2.

## **1.2 Bed-material sampling and guidelines**

### **1.2.1 Purpose of bed-material sampling**

The majority of bed-material sampling work is undertaken in order to obtain information on the particle-size distribution of the riverbed. Information on bed-material particle size is needed for a variety of purposes that can be grouped into three major areas:

- 1) Streambed monitoring for detecting watershed impacts, analyzing stream habitat, and evaluating the success of mitigation efforts,
- 2) Computations of flow hydraulics, bedload transport rates transport capacity and flow competence to analyze and predict stream behavior, and
- 3) Advancement in the understanding of stream processes.

Information on particle shape is also needed for predicting bed stability and the onset of scour by balancing entraining versus resisting forces, as well as for analyzing the source and travel distance of sediment.

### **1.2.1 Aspects of bed-material sampling in gravel- and cobble-bed streams**

Stream studies quantify bed-material particle size by analyzing the frequency distribution of particle sizes contained within a bed-material sample. However, sampling bed-material in gravel- and cobble-bed streams is different from sampling in sand- and boulder-bed streams. Sand-bedded streams may be sampled by taking about a cup-full of sediment from several locations distributed more or less systematically over the streambed. Differentiation between surface and subsurface sediment is usually not necessary, and a shovel is often sufficient as a sampling device. Thus sampling bed-material in sand-bedded streams is a relatively straight-forward task. Ashmore et al. (1988) provide detailed guidelines for bed-material sampling in sand-bedded streams.

Sampling bed-material in gravel- and cobble-bed streams is a more complicated enterprise and forces the user to make a number of informed decisions on the study methods that depend on the study objective and the stream condition. Prior to sampling, the user needs to decide where in the stream samples are to be taken. Sampling may need to cover a large area of the streambed about 5-7 channel widths long, or concentrates on a downstream sequence of riffles or pools.

Gravel- and cobble-bed streams usually have surface sediment that is coarser than the sediment below the surface. The degree of difference between surface and subsurface sediment is tied to the flow regime and upstream sediment supply. The user needs to identify the appropriate bed-material strata (i.e., layer) to be sampled for a given study objective. Some objectives require sampling particles exposed to the surface, other studies sample the armor layer that extends from the surface down to a depth of 1 or 2 large particles. Still other studies sample the subsurface sediment below the surface, or compare sediment from different layers (strata) within the bed.

Particles on the surface, in the subsurface, and in the armor layer are sampled by different techniques. For example, particles may be picked off the stream surface (pebble count), or the subsurface sediment may be dug up after surface particles or the armor layer has been removed. There are a number of sub-procedures for sampling each strata; surface particles may be collected along a grid, or all particles within a small area may be collected (areal sample, or the streambed surface may be analyzed from photographs. Equipment and techniques that may be used for sampling subsurface sediment depend on the sampling objective, the size of the bed material in the stream, and on whether the streambed is dry or inundated.

Gravel- and cobble-bed streams may have a relatively uniform particle-size distribution over distances several stream widths long (homogeneous bed). Alternatively, the streambed may be composed of many areas with different particle-size distributions, or of areas in which particle-size distributions change from coarse to fine (heterogeneous bed). It may be difficult to find areas that are both spatially homogeneous and large enough for collecting a surface sample. In any case, the user needs to select a spatial sampling strategy (sampling scheme) that matches study objectives and stream conditions. This requires deciding on the areal extent of the streambed to sample, and the spatial pattern with which particles are selected. Sampling may extend in some systematic patterns over the entire area (spatially integrated), or the user may choose to sample in locations representative for a particular streambed area or sample spatially focused on streambed areas of concern. Alternatively, the stream reach may be segregated into sub-areas that are then sampled individually (spatially segregated).

Bed-material sampling should also provide information on the statistical precision of the sampling result. Ideally, a desired level of precision is selected before the study begins. Different relations between sample size and precision may be consulted to determine how large the sample needs to be in terms of particle numbers, of sediment weight, or how many parallel samples need to be taken. Investigators are frequently surprised by the large sample sizes necessary. Several hundred particles may have to be collected for one pebble count, while the mass of volumetric samples needed may be several hundred kg or more.

The physical act of collecting representative samples in gravel-and cobble-bed streams may be challenging. Individual fine particles located between large clasts on the bed may be difficult to pick up, while cobbles and boulders may be too heavy or too wedged in the bed surface to dislodge. Cold water makes it difficult to work bare-handed in mountain streams, and the flow may be fast or deep. The sample mass needed for statistical accuracy is usually large, and sampling sites may not have vehicle access.

After all the samples are taken, the final part of bed-material sampling is performing a particle-size analysis. This involves sieving the sample as well as selecting particle-size parameters and statistical analyses suitable for demonstrating sampling results.

### **1.2.2 Interdependency between sampling methods and study objectives**

Bed-material strata, the sampling procedures and equipment, the sampling scheme, the sampling precision and ensuing sample size, and the particle-size analysis used in the study must be thoughtfully selected to provide useful information. For the most part, their selection depends on study objectives and on the streambed conditions encountered.

There is a dependency between study methods and study aim. A study performed in a given streambed may yield different results if different methodological approaches are used. Consequently, studies with similar objectives that use different methods generally fail to produce comparable results. Since results from bed-material sampling projects are method specific, the user needs to describe the methods used clearly, so that a comparable study can be done at a different location or time. Similarly, a clear description of sampling and analysis methods is essential for readers to assess the meaning and reliability of published results.

### **1.2.3 Deficiencies in existing guidelines**

There is an abundance of literature that demonstrates sampling equipment, compares and suggests sampling procedures, recommends sample sizes, proposes sampling schemes, presents alternative particle-size parameters or computational methods, and describes findings of specific bed-material studies. This methodological diversity, and the ongoing debates on the general appropriateness of methods or their applicability in specific situations, leave the field person with an abundance of techniques from which to choose. However, there is little guidance for deciding if a particular method is suitable for a given study and a given stream.

Faced with this diversity, stream studies tend to resort to so-called “standard methods”. For example, the 100-particle Wolman (1954) pebble-count is often considered a standard method for surface particles, or the McNeil and Ahnell (1964) sampler is commonly used for volumetric bed-material samples in submerged conditions. These methods have attained “standard” status, and are described and applied on numerous occasions, primarily because they are relatively quick and easy to perform. However, presumed standard methods, although desirable, are not generally applicable.

Current guidelines on stream studies include the description of a few widely-used methods but are not a comprehensive source of information on bed-material sampling in general. Some guidelines focus on specific fluvial environments, such as large alluvial gravel-bed rivers (Yuzyk and Winkler 1991), or on specific sampling aims, such as the evaluation of aquatic habitat (Platts et al. 1883; Hamilton and Bergersen 1984). The paper by Church et al. (1987) and the guidelines by Ramos (1996) provide perhaps the widest coverage of bed-material sampling to date.

None of the current guidelines for bed-material sampling and analysis (Platts et al. 1883; Williams et al. 1988; Edwards and Glysson 1998; ISO 1992; Yuzyk and Winkler 1991;

Hamilton and Bergersen 1984; Church et al. 1987; Ramos 1996), and few published papers provide specific information on bed-material sampling in small mountain streams with coarse beds. Sampling these environments is particularly difficult because bed-material particle sizes extend over a wide range - from sand to boulders. Streambeds are often perennially inundated, and scour and deposition around large woody debris leads to a spatially diversified streambed.

#### **1.2.4 What these guidelines are intended to do**

These guidelines explain the various aspects of bed-material sampling in gravel- and cobble-bed streams and discuss the proper application, scope, and limitations of sampling methods. This includes the explanation of bed-material strata, the procedures and equipment used for sampling, a discussion of the spatial scheme to be employed, the relation between sample size and precision, and methods of particle-size analysis. These guidelines are meant to provide the user with a wide range information from which to select methods and approaches suitable for a given study in a given fluvial setting. Information used to compile these guidelines was mostly found in published papers, government documents, monographs, and the authors' field studies.

#### **1.2.5 Guidelines are no substitute for experience**

The physical processes acting in mountain streams are quite complex. Stream morphology and spatial variability of bed-material size are not only affected by fluvial processes, but also by near-stream and off-stream sedimentary processes. Such complex, multi-process environments require professional experience for meaningful field work. Unfortunately, government agencies and consulting companies frequently desire simple guidelines that advocate methods requiring little field time and that can be followed by inexperienced field personnel.

For quality results, field work needs to be performed or closely guided by experienced personnel. An inexperienced crew cannot determine sampling locations and sample size if these decisions depend on recognizing geomorphic, hydraulic, and sedimentary processes of various scales and magnitude. Such assessments require knowledge and familiarity with fluvial processes.

Operator training is extremely important. When selecting particles from a predefined streambed location, or even when measuring particle sizes in a preselected sample of rocks, there is less variability between the results of experienced operators than between those obtained by novices. Field personnel need to be trained to perform procedures accurately, to avoid bias, and to use equipment that reduces operator induced error. No guidelines, these included, can substitute for operator experience and training.

### 1.3 Classification of gravel- and cobble-bed streams

Gravel- and cobble-bed rivers have different appearances because stream gradients, bed-material particle-size distributions, large woody debris content, the cross-sectional channel shape, and stream morphology<sup>1</sup> may be different between streams. The diversity of resulting stream forms makes it useful to classify streams.

Stream classifications are educational in and of themselves. They make the user aware of different cross-sectional shapes of the stream and the flood plain, of the different morphological parts of a stream, the specifics of the interactions between flow and sedimentation, and the resulting stream types. This knowledge leads to an understanding that stream morphometry<sup>2</sup>, stream morphology, flow hydraulics and sedimentation processes respond to controlling agents such as flow regime, quantity and size of sediment supplied, and channel gradient. Besides an understanding of stream behavior, a familiarity with the terminology used in stream classifications helps clarify communication.

From the variety of stream classifications available, two recent stream classification systems, Montgomery and Buffington (1993, 1997, 1998), and Rosgen (1994, 1996) are explained below. These two classification systems are currently used most often in the U.S. Readers are encouraged to become acquainted with them, not only because their terminology will be used in this document, but also to acquire an understanding for the variety of stream types and processes common in gravel- and cobble-bed streams.

#### 1.3.1 The Montgomery-Buffington stream classification

Montgomery and Buffington (1993, 1997) developed a stream classification to describe streams found in the Pacific Northwest. The steep mountain ranges and the short distance to the Pacific coast result in a sequence of predominant landforms: steep valleys and hillslopes in the upper watersheds, gentler valleys in the middle watersheds, and low gradient valleys at the end of the watershed. In accordance with those landforms, the classification system differentiates between five stream types: *cascades*, *step-pool*, *plane-bed*, *pool-riffle*, and *dune-ripple* streams, listed in the order of decreasing stream gradient (Table 1.2). Those streams have a distinctly different morphology because the interaction between flow hydraulics and sedimentary processes, particularly the amount of energy dissipated by the turbulence of flow, differs in each of the stream types. Although bed-material size generally decreases from cascades to dune-ripple streams, it is not a discriminating feature of the classification. Longitudinal and planform illustrations of the five stream types are shown in Fig. 1.1.

---

<sup>1</sup> Morphology characterizes a (fluvial) object through a descriptive term, e.g., a riffle and a pool.

<sup>2</sup> Morphometry describes the physical dimensions of a (fluvial) object through measurements, e.g., the width and depth of a streambed.

Table 1.2: Stream classification by Montgomery and Buffington (after Montgomery and Buffington 1997, 1998)

Stream gradient, range and mode (m/m)	Stream type	Typical bed material	Dominant sediment source	Dominant sediment storage	Typical pool spacing*
0.03 - 0.20 (0.08 - 0.20)	Cascades	Cobble-boulder	Fluvial, hillslopes, debris flows	Around flow obstructions	< 1
0.02 - 0.09 (0.04 - 0.08)	Step-pool	Cobble-boulder	Fluvial, hillslopes, debris flows	Bedforms	1 - 4
<0.02 - 0.05 (0.02 - 0.04)	Plane-bed, forced pools	Gravel-cobble	Fluvial, bank failure, debris flows	Overbank	None
<0.001- 0.03 (0.01)	Pool-riffle	Gravel	Fluvial, bank failure	Overbank, bedforms	5 - 7
< 0.001	Dune-ripple	Sand	Fluvial, bank failure bedforms	Overbank,	5 - 7

*Values in parentheses are the modes of the observed stream gradient distribution; \* in terms of channel widths*

### 1.3.2 The Rosgen stream classification

The Rosgen classification (1994, 1996) uses an alphanumeric code to classify streams based on five morphometric parameters of the stream channel and its flood plain:

- entrenchment ratio, i.e., ratio of the width of the flood-prone area inundated by flows having twice the maximum depth of bankfull flow to the width of the bankfull channel (i.e., a measure of flood plain width),
- width-depth ratio at bankfull flow,
- sinuosity, i.e., stream length to valley length,
- stream gradient, and
- median bed-surface particle size.

The five parameters are used to distinguish seven main stream types identified by capital letters A to G. Each main stream type has a number assigned that reflects the bed-material particle size. Streams with boulder-, cobble- and gravel beds have the numbers 2, 3, and 4, respectively and are the only stream types referred to in the context of these guidelines. Uncapitalized letters a, b and c are used to specify stream gradients outside the typical range for a main stream type. For example, a stream classified as Bc3 is a B-type stream (B), with a cobble bed (3) but a gradient within the range of 0.001 - 0.02 more typical of C-type streams (c). Morphological characteristics of the mayor stream types in the Rosgen classification are presented in Table 1.3. Fig. 1.2 shows the stream types in longitudinal, cross-sectional and plan views and provides bed-material sizes and morphometric criteria for the 41 delineated stream types.

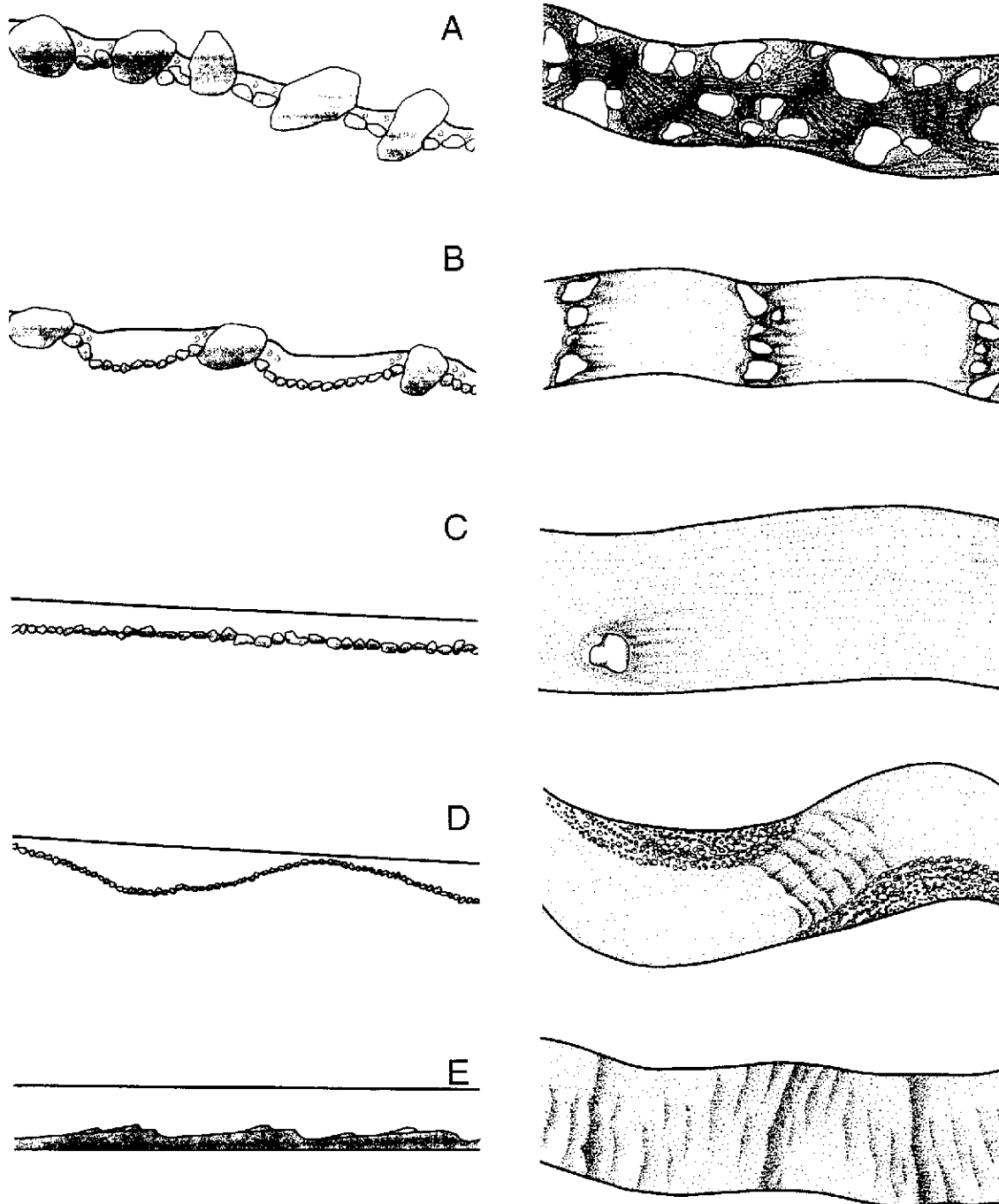


Fig. 1.1: Schematic longitudinal (left) and planform (right) illustration of the five stream types at low flow: (A) **Cascade** with nearly continuous highly turbulent flow around large particles; (B) **Step-pool** channel with sequential highly turbulent flow over steps and more tranquil flows through intervening pools; (C) **Plane-bed** channel with an isolated boulder protruding through otherwise uniform flow; (D) **Pool-riffle** channel with exposed bars, highly turbulent flow over riffles, and more tranquil flow through pools; and (E) **Dune-ripple** channel with dune-ripple bedforms. (Slightly altered and reprinted from Montgomery and Buffington (1997), by permission of the Geological Society of America).

Table 1.3: Morphological characteristics of the major Rosgen stream types

Stream Type	Morphological characteristics
A	<b>Step-pool, or cascading:</b> plunge and scour pools, high energy, low sediment storage, stable;
B	<b>Riffles and rapids:</b> some scour pools, bars rare, stable;
C	<b>Pool-riffle sequences:</b> meandering, point bars, well developed floodplain, banks stable or unstable;
D	<b>Braided:</b> multiple channels, shifting bars, scour, deposition, high sediment supply, eroding banks;
DA	<b>Anastomosing:</b> multiple channels, pool-riffle, vegetated floodplain, adjct. wetlands, stable banks;
E	<b>Meadow meanders:</b> well-developed floodplain, riffle-pool, relative high sediment conveyance;
F	<b>Valley meanders:</b> incised into valleys, poor floodplain, pool-riffle, banks stable or unstable;
G	<b>Gullies:</b> incised into hillslopes and meadows, high sediment supply, unstable banks, step-pool.

### 1.3.3 Differences between the Rosgen and the Montgomery-Buffington classifications

The Rosgen and the Montgomery–Buffington stream classifications differ in several points which include:

#### *Basis for classification*

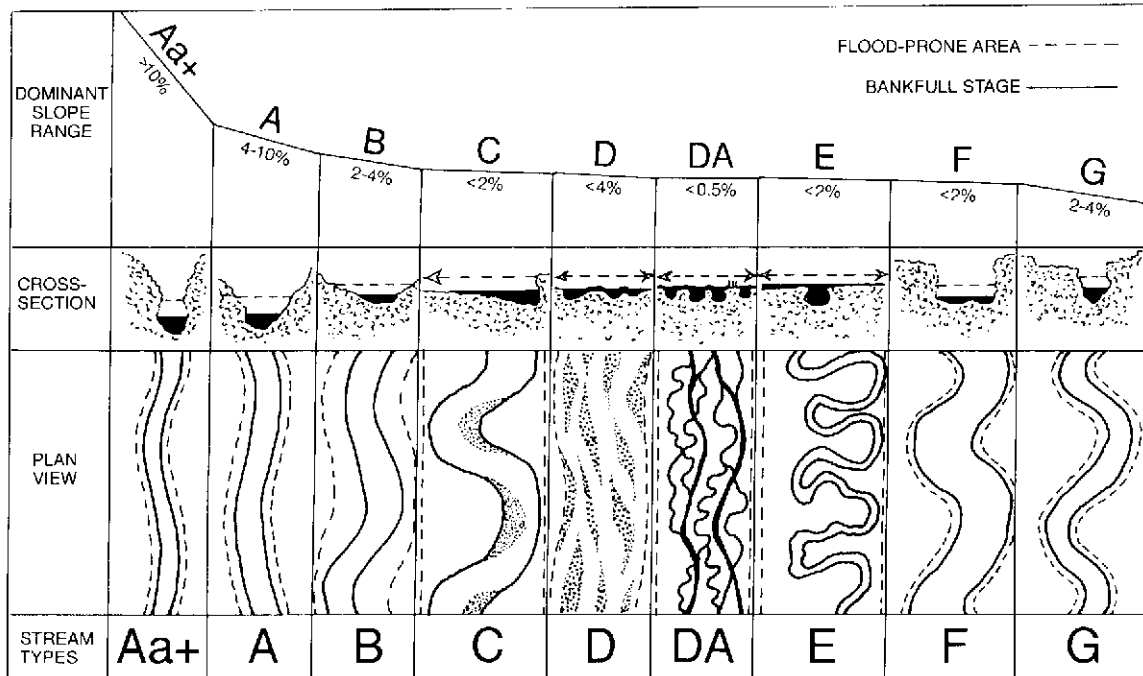
The Rosgen classification is based on morphometric parameters and precisely differentiates between streams of different slope gradients, width-depth ratios, sinuosity, and entrenchment. The Montgomery–Buffington classification is based on stream types commonly found in the Pacific Northwest where streams traverse the relatively short distance between steep headwaters and sea level in a succession of different stream types. From steep terrain to low gradient, these stream types have an increasing potential to show a morphological response to changes in water and sediment yield.

#### *Appearance of the classification system*

The Rosgen classification presents a non-intuitive alphanumeric code. The large number of stream types thus classified can be discouraging for the novice user. The Montgomery–Buffington classification presents five stream types using commonly known fluvial terminology.

#### *Applicability*

Based on morphometric parameters, the Rosgen classification system is applicable to any streambed, thus exceeding the range of streams addressed in this manual. The Montgomery–Buffington classification is best suited to describe gravel-, cobble-, and boulder-bed streams in mountainous terrain, from steep headwaters to low gradient valleys and plains, and thus describes the stream types addressed in these guidelines.



Dominant Bed Material	A	B	C	D	DA	E	F	G
1 BEDROCK								
2 BOULDER								
3 COBBLE								
4 GRAVEL								
5 SAND								
6 SILT/CLAY								
ENTRH.	<1.4	1.4-2.2	>2.2	N/A	>2.2	>2.2	<1.4	<1.4
SIN.	<1.2	>1.2	>1.4	<1.1	1.1-1.6	>1.5	>1.4	>1.2
W/D	<12	>12	>12	>40	<40	<12	<12	<12
SLOPE	.04-.099	.02-.039	<.02	<.04	<.005	<.02	<.02	.02-.039

Fig. 1.2: Rosgen's stream classification. Longitudinal, cross-sectional and plan views of mayor stream types (top); Cross-sectional shape, bed-material size, and morphometric delineative criteria of the 41 mayor stream types (bottom). (Redrawn from Rosgen (1994), by permission of Elsevier Science B.V).

### *Correspondence between the two classification systems*

The three stream types step-pool, plane-bed, and pool-riffle, distinguished by the Montgomery-Buffington classification generally correspond to the stream types A, B, and C in the Rosgen classification. The mode of slope gradients observed for these three stream types in the Montgomery-Buffington classification corresponds fairly well to the slope gradients assigned to A, B, and C streams by Rosgen (Fig. 1.3). The Montgomery-Buffington classification provides a wide range of observed slopes, which may overlap between stream types, thus uniting streams with morphometric differences into one stream type if the hydraulic and sedimentary processes are similar. The Rosgen classification creates numerous subgroups, thus differentiating between stream types with slight morphometric differences.

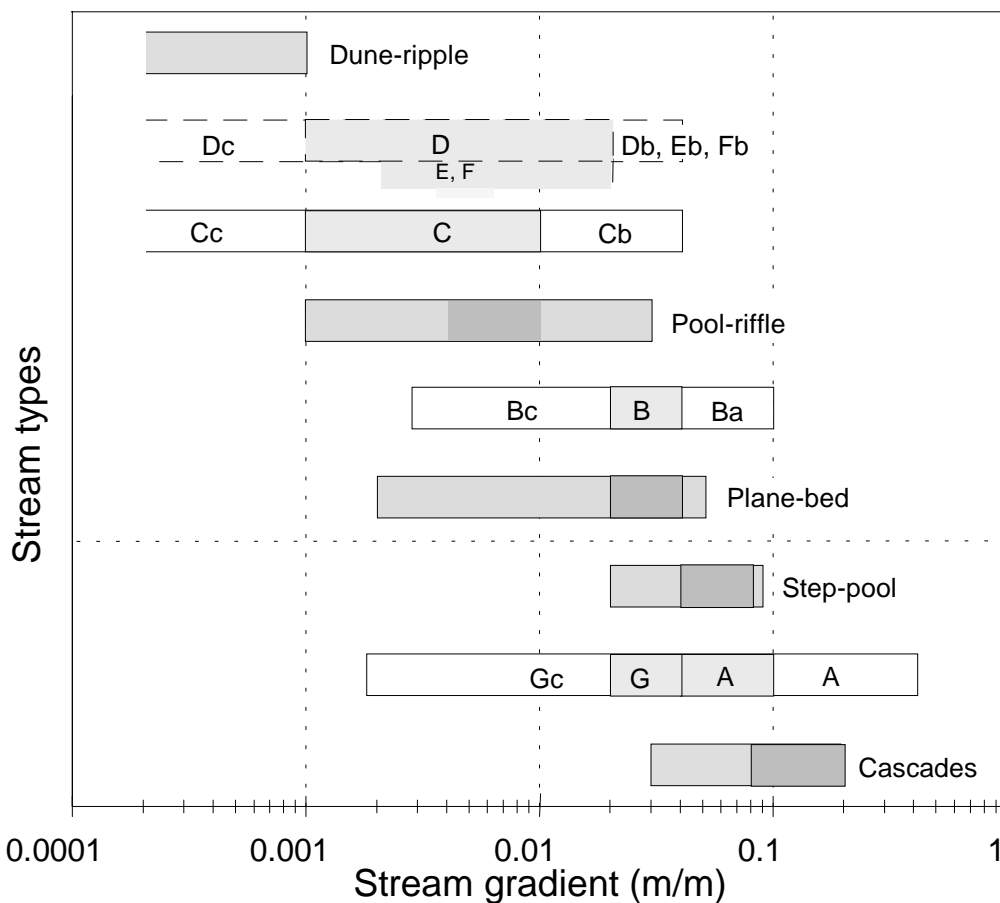


Fig. 1.3: Comparison of stream gradients in the Montgomery-Buffington (1997,1998), and the Rosgen (1994, 1996) classification. The Montgomery-Buffington stream types are pool-riffle, plane-bed, step-pool, and cascades. The light shading indicates the range of observed stream gradients, the dark shading indicates the mode. The letters refer to the Rosgen classification. Light shading indicates the main stream type, whereas subtypes with steeper or gentler stream gradients have no shading. Open-ended boxes indicate stream gradients given in terms of "larger than", or "smaller than".

### 1.3.4 Sediment source: self-formed versus relict/non-fluvial streams

The distinction between self-formed and relict/non-fluvial gravel-bed rivers is not explicitly part of current classification systems, but this distinction is important because it affects all aspects of bed-material sampling in gravel-bed rivers.

#### *Self-formed streams*

Self-formed streams receive their sediment supply almost entirely from upstream (fluvial) sources, the local bed, and erosion of banks composed of sediment transported under the current transport regime. Stream morphology and sediment sizes are exclusively controlled by the interaction between flow and sediment. Consequently, the streambed contains no particles larger than those that can be moved during the highest floods. Because sediment in self-formed streams is not coupled to hillslopes and other non-fluvial sources, such stream systems are also referred to as *uncoupled* streams.

#### *Relict/non-fluvial streams*

Relict/non-fluvial streams can receive much of their sediment from non-fluvial sources such as:

- mass movements (debris flows, landslides, avalanches, etc.),
- rock-fall from canyon walls,
- intensive slope wasting, bank undercutting and slumping,
- downcutting into glacial deposits from which the stream unearths large boulders that may be of commonly untransportable size, and
- erosion of bank material deposited under a different regime of flow or sediment supply.

Streams receiving sediment supply from relict-fluvial and non-fluvial sources are often referred to as *coupled*. Coupled streams are common in mountain areas, where nearby hillslopes and glacial deposits contribute to the off-stream sediment supply. The presence of large cobbles and boulders may cause unsystematic spatial variability of bed-material size. Obstacles in the stream flow create local hydraulics that control sedimentation patterns and inhibit the development of a stream morphology expected for a stream with a given gradient, stream flow, and supply of transportable sediment.

Self-formed and relict-non-fluvial streams can be difficult to distinguish in the field, if off-stream sediment supply is low or occurs only sporadically. Whiting and Bradley (1993) defined the likelihood of debris flows reaching the stream for regions prone to debris flows based on the ratio of valley width to stream width. For example, debris flows *seldom* reach a small stream 5 m wide if the valley is more than 250 m wide, but *occasionally* in a valley 50-250 m wide. *Most* debris flows would enter the stream if the valley was 25-50 m wide, and *all* debris flows enter the stream if stream width is equal to valley width. An aspect not considered in this definition is that streams often take a winding course through the valley, being close to the valley wall and even undercutting the hillslopes at some locations. Here, streams can easily receive off-stream sediment, even in wide valleys.

### **1.3.5 Wadable and non-wadable streams**

These guidelines applies to gravel- and cobble-bed streams that are generally wadable. Nevertheless, most of the techniques discussed in this document could also be applied to deeper streams if a team of experienced divers were available. Some sampling techniques and equipment may have to be adjusted to fit underwater conditions.

Wadable streams are easier to sample when less water is in the channel. In some streams, the annual low flow exposes only a small proportion of the bed, so that wading and sampling techniques that work in submerged conditions are required year-round. In other streams, much of the bed is exposed during low flows, which makes those times preferable for many sampling studies.

Within the range of wadable flows, fast flowing water often causes more sampling difficulties than deep water. Not only is there a safety hazard when venturing into fast flow with velocities exceeding 1.5 m/s (Abt et al. 1989), but sampling results are likely to become inaccurate and biased in fast water. Fine particles can easily be washed from an operator's hand, and fast flow, often combined with turbid water, does not allow the operator to visually distinguish individual particles on the channel bottom. This requires that much of the work be performed by feel. Fast flow adds to the difficulty of extracting large or wedged particles from the bed.

Sampling in locally deep flow has its challenges as well because it makes some stream locations inaccessible to wading or an operator may not be able to touch the stream bottom by hand without getting his face wet. However, problems posed by deep water can often be mitigated, for example by visually estimating the size class of a particle to be included in the sample, or by sampling with long-handled scoops while using a flotation device. Relatively warm water may encourage getting wet in swimming clothes, but submersion or diving in cold water requires dry suit equipment.

## 2. Particle analysis

---

Particle analysis in gravel-bed rivers includes the analysis of particle size, particle shape, particle density and bulk density. These four topics are presented and discussed below.

### 2.1 Size analysis

Particle-size analysis comprises the measurement and analysis of the three particle axes that define the three-dimensional shape of a particle. For many applications, it is much more convenient to characterize particle size by only one variable, such as the length of the intermediate particle axes or the size of the sieve on which a particle was retained. Once the sizes of particles are determined, they are statistically analyzed, so that particle-size distributions and statistical parameters characterizing them can be compared between streams or over time. The mean particle size on a streambed, a particular particle-size percentile, a characteristic large particle size, as well as the entire spectrum of particle sizes all affect the hydraulics of flow as well as bedload transport rates. Studies concerned with the mechanics of particle entrainment, particle transport and deposition need to include the description and comparison of particle shapes.

#### 2.1.1 Particle axes

The analyses of particle sizes and particle shape parameters are based on the length of three mutually perpendicular particle axes: the *longest* (*a*-axis), the *intermediate* (*b*-axis), and the *shortest* (*c*-axis) axis. The demand for the *a*, *b*, and *c*-axes being truly the longest, the intermediate, and the shortest axes agrees with the demand for perpendicularity of the three particle axes only if the particle shape is ellipsoidal (e.g., like a lightly-worn bar of soap). Particles with a rhombic shape cannot fulfill both demands, and this might leave the user confused on whether to base particle identification on the absolute lengths of particle axes or on perpendicularity. The identification of the *a*- and the *b*-axes is affected most by this discrepancy, whereas the position and length of the *c*-axis is usually clear.

The crucial point is whether the analysis starts with the definition of the *a*-axis as the longest axis, with the *b*-axis following as the longest intermediate axis perpendicular to the *a*-axis as done in the Canadian guidelines (Yuzyk and Winkler 1991) (Fig. 2.1), or whether the analysis starts with identifying the *b*-axis as the “shortest axis of the maximum projection plane (the plane with the largest area) perpendicular to the *c*-axis” (Gordon et al. 1992. 198-199). If the *a*-axis is subsequently defined as perpendicular to the *b*-axis, then the *a*-axis is not necessarily the longest distance between two points on a given particle. The *b*- and *a*-axes are along the heavy black arrows ***a*** and ***b*** in Fig. 2.1 according to the definition by Gordon et al. (1992).

Differences in the definition of the  $a$ - and  $b$ -axis are most pronounced in particles of rhombic shape (Fig. 2.2, left).  $a$ - and  $b$ -axes follow the gray stippled lines  $a$  and  $b$  when defined according to Yuzyk and Winkler (1991), and along the black solid lines  $a$  and  $b$  according to the definition by Gordon et al. (1992). Both lines  $a$  and  $b$  are longer than  $a$  and  $b$ .

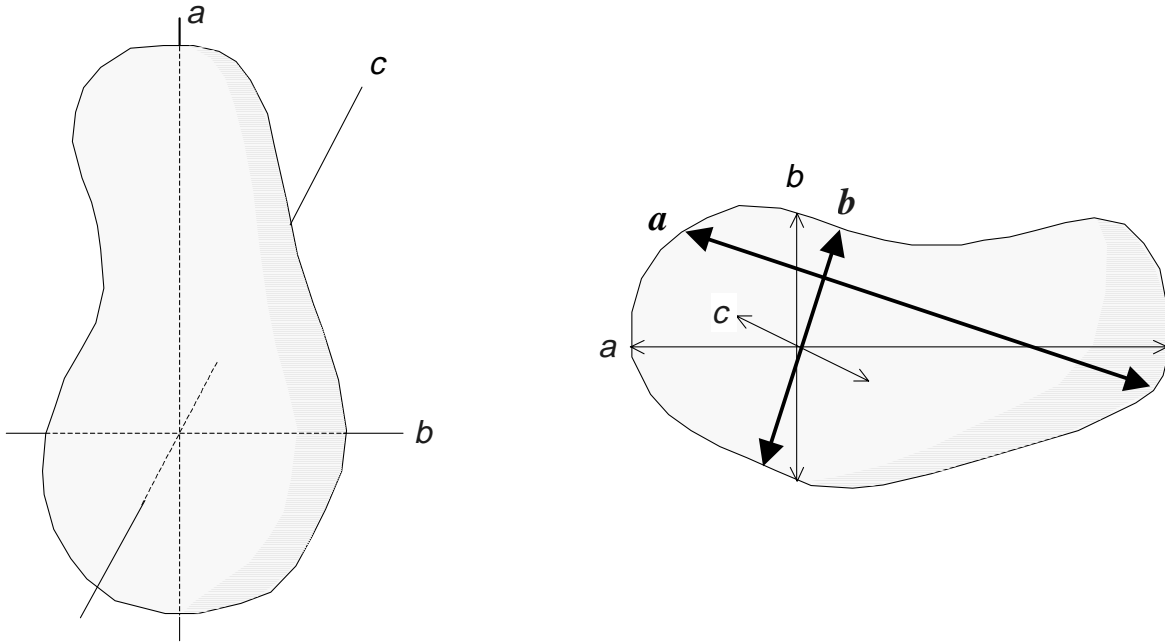


Fig. 2.1: Definition of particle axes (Redrawn after Yuzyk 1986, and Yuzyk and Winkler 1991).

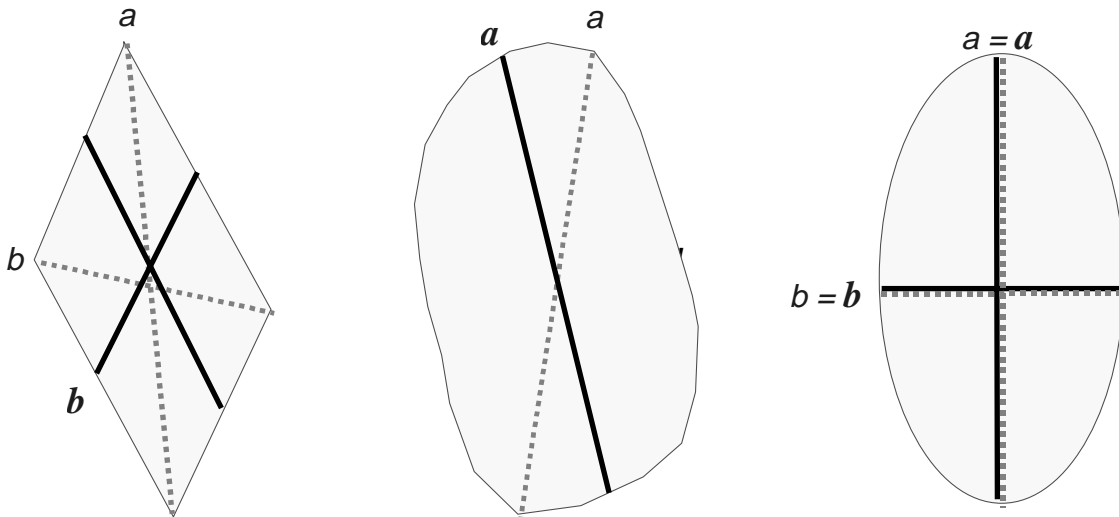


Fig. 2.2: Discrepancy in  $b$ - and  $a$ -axes definitions for rhombic, irregular ellipsoidal, and ellipsoidal particle shapes.

The differences in the two axis definitions become irrelevant for smooth ellipsoidal shapes (Fig. 2.2). Consequently, the definition of particle *b*-axes should be unproblematic for well rounded and ellipsoidal particles in alluvial streams in which all particles experienced a long fluvial transport. However, particle-axes measurements can be difficult in mountain streams with a non-fluvial sediment supply, or in headwaters where fluvial transport is short and the particles can be angular and rhomboidal.

Ultimately, the study aim needs to decide how particle axes are measured. If hand-measured *b*-axis lengths are to be compared with sieve sizes, *b*-axis measurement should simulate the way a particle drops through a sieve opening. Measurements of *a*- and *c*-axis then follow the rules of perpendicularity. Measurements of *b*-axis lengths automatically follow this procedure if templates are used. The *b*-axis measurements performed with rulers, calipers, and the pebble box on rhomboid particles (Section 2.1.3) are prone to orient the *b*-axis perpendicular to the longest (*a*-axis), which is least problematic to identify. Such *b*-axis measurements tend to produce longer *b*-axis lengths than template measurements.

### 2.1.2 Particle sizes and size classes

The size of a particle can be determined in three different categories: the actual *b*-axis length, the nominal diameter, and the particle-sieve diameter. The three approaches are used for different purposes.

#### *Actual b-axis length*

Measuring the actual lengths of particle *b*-axes in units of mm or cm may be important for studies that are concerned with a small range of particle sizes, a range smaller than distinguished by two consecutive sieves in a standard sieve set. An example for such a study is the determination of the dominant particle size. This is computed as the arithmetic mean of particle *b*-axes measured on about 30 large, but not the very largest, particles found within a deposit.

#### *Nominal diameter*

If the mass or volume of a particle is of more importance for a study than the particle *b*-axis length or the sieve diameter, the nominal diameter is used. The nominal diameter is a three-dimensional approach and describes particle size by its smallest characteristic diameter. The *nominal diameter* denotes the diameter a particle would assume if its volume was expressed as a sphere and is computed from:

$$D_n = (a \cdot b \cdot c)^{1/3} \tag{2.1}$$

$D_n$  is directly related to particle volume  $V_D = \frac{\pi}{6} (a \cdot b \cdot c)^3$ .

### ***Particle sieve-diameter***

Particles contained in a sediment deposit are commonly analyzed by grouping particles of various sizes into particle size-classes that correspond to the size of sieve openings. The particle sieve-size can be defined as the smallest sieve size through which a particle can pass ( $D_{pass}$ ) or as the largest sieve size through which the particle did not pass, the retaining sieve size ( $D_{ret}$ ). For a given particle, passing or retaining sieve size differs by one size class, thus, it is important to indicate whether reference is made to the passing or retaining sieve size. Particle sieve-diameter also depends on whether sieves with square or round-holes were used; whereas for particles of equal weight, sieve diameter varies with particle shape (Sections 2.1.3.1, 2.1.3.4, and 2.1.3.5).

Sieve diameter and nominal diameter are identical for spheres and ellipsoidal particles with certain axes ratios such as  $a = 3/2 b$ , and  $c = 2/3 b$ , but deviate for other particle shapes. Compared to a sphere with an identical  $b$ -axis, a disc has a smaller  $D_n$  due to its small  $c$ -axis, whereas the  $D_n$  of a rod-shaped particle exceeds that of a sphere because of its long  $a$ -axis. Acknowledgment of this discrepancy can become important because sedimentation, i.e., erosion, transport, and deposition of particles, is tied to particle weight and shape (particularly the area projected towards the direction of flow). The analysis of particle shape is discussed in Section 2.2.

#### **2.1.2.1 The Wentworth scale of particle sizes**

If particle size-classes progress in a linear scale, e.g., 10, 20, 30 mm, the frequency of particles per size class in fluvial gravel tends to be approximately logarithmically distributed. Logarithmic distributions are statistically more difficult to work with than normal distributions. In order to obtain an approximately normal distribution of particle sizes, particle-size classes were made to increase by a factor of 2 (Wentworth scale). Thus, particle sizes in units of mm double in consecutively larger size classes (2 - 4 mm, 4 - 8 mm, 8 - 16 mm, 16 - 32 mm, etc.). These size classes are grouped into six major particle-size categories - boulders, cobbles, gravel, sand, silt and clay (Table 2.1). Silt and clay content are rarely analyzed in studies of gravel-bed rivers, thus, these size categories are included only in an abbreviated form in Table 2.1.

The mass of a spherical particle increases by a factor of 8, when the particle diameter doubles. This 8-fold range of particle mass per size class is quite large, and many studies therefore carry out particle-size analyses in size classes half as large as the Wentworth classes (see sieve sizes in Section 2.1.3).

#### **2.1.2.2 Particle size in $\phi$ -units**

The frequency distribution of the weight or number of particles per size class tends to follow approximately a lognormal distribution (Section 2.1.4.3) when particle sizes are expressed metrically in mm. Consequently, the arithmetic mean particle size and the arithmetic median particle size are not the same (mean is usually larger than median). If a

Table 2.1: Size gradation for sediment in the range of sand to boulders (Wentworth scale)

Description of particle size		$\phi = -\log_2$	mm	$\psi = \log_2$
<b>Boulder</b>	very large	- 12.0	4096	12.0
		- 11.5	2896	11.5
	large	- 11.0	2048	11.0
		- 10.5	1448	10.5
	Medium	- 10.0	1024	10.0
		- 9.5	724	9.5
	small	- 9.0	512	9.0
<hr/>		<b>- 8.0</b>	<b>256</b>	<b>8.0</b>
<b>Cobble</b>	large	- 7.5	181	7.5
		- 7.0	128	7.0
	Small	- 6.5	90.5	6.5
<hr/>		<b>- 6.0</b>	<b>64</b>	<b>6.0</b>
<b>Gravel</b>	very coarse	- 5.5	45.3	5.5
		- 5.0	32	5.0
	coarse	- 4.5	22.6	4.5
		- 4.0	16	4.0
	medium	- 3.5	11.3	3.5
		- 3.0	8	3.0
	fine	- 2.5	5.66	2.5
		- 2.0	4	2.0
very fine	- 1.5	2.83	1.5	
<hr/>		<b>- 1.0</b>	<b>2</b>	<b>1.0</b>
<b>Sand</b>	very coarse	- 0.5	1.41	0.5
		0	1	0
	coarse	+ 0.5	0.707	- 0.5
		+ 1.0	0.500	- 1.0
	medium	+ 1.5	0.354	- 1.5
		+ 2.0	0.250	- 2.0
	fine	+ 2.5	0.177	- 1.5
		+ 3.0	0.125	- 3.0
very fine	+ 3.5	0.088	- 3.5	
<hr/>		<b>+ 4.0</b>	<b>0.063</b>	<b>- 4.0</b>
<b>Silt</b>		<hr/>		
<hr/>		<b>+ 8.0</b>	<b>0.0039</b>	<b>- 8.0</b>
<b>Clay</b>		<hr/>		
<hr/>		<b>+ 12.0</b>	<b>0.00024</b>	<b>- 12.0</b>

particle-size distribution was truly logarithmic, log transformation of particle-size units would produce a normal distribution. It is desirable to work with normal distributions, because standard statistical procedures can be used to analyze them.

Any kind of logarithmic transformation, e.g., the simple log of the particle size  $D$ , i.e.,  $\log(D)$ , applied to the original data will produce a normal distribution. However, in order to obtain convenient, integer values after a log transformation, sedimentologists and geomorphologists (Krumbein 1934) expressed particle size  $D$  as the negative logarithm to

the base of 2 and called the result the  $\phi$ -scale.  $\phi$ , spelled out as phi, is the Greek letter for  $f$ . Particle sizes in  $\phi$ -units are computed from particle sizes  $D$  in units of mm by

$$\phi_i = -\log_2(D_i) \quad (2.2)$$

Since the negative logarithm to the base of 2 is not routinely programmed in scientific calculators it needs to be computed from

$$\phi = -\frac{\log(D_i)}{\log(2)} \quad (2.3)$$

Since  $\log(2) = 0.3010$ , this expression can be simplified to

$$\phi_i = \frac{-\log(D_i)}{0.301} = -3.3219 \log(D_i) \quad (2.4)$$

For example,  $-3.3219 \log(64) = -3.3219 \cdot 1.8062 = 6.0$ . Conversely, particle sizes  $D$  in units of mm are obtained from particle sizes in  $\phi$ -units by

$$D_i = 2^{-\phi_i} \quad (2.5)$$

This expression can easily be solved by scientific calculators or spreadsheet programs. An alternative expression dating from the time of logarithmic and exponential tables is

$$D_i = e^{-\phi_i \ln(2)} = 10^{-\phi_i \log(2)} = 10^{-0.301 \phi_i} \quad (2.6)$$

Table 2.1 presents particle sizes in units of mm and  $\phi$ .

### 2.1.2.3 Particle size in $\psi$ -units

The  $\phi$ -transformation produces positive values for particle sizes smaller than 1 mm and negative values for particle sizes larger than 1 mm. This feature is convenient for studies that focus on sand and smaller sediment. However, this feature is inconvenient for studies in gravel-bed rivers, because having smaller, negative numbers for larger particle sizes is

counterintuitive. Consequently, the  $\psi$ -scale was developed (Greek letter  $\psi$  spelled out as *psi*) which produces increasingly larger values as particle sizes increase from sand to boulders.  $\psi$ -units are the negative values obtained in  $\phi$ -units ( $\psi = -\phi$ , or  $\phi = -\psi$ ).  $\psi$ -units are computed from particle size  $D$  in units of mm by

$$\psi_i = \log_2(D_i) \quad (2.7)$$

By analogy to Eq. 2.2, this expression is solved by

$$\psi_i = \frac{\log(D_i)}{\log(2)} \quad (2.8)$$

which can be simplified to  $\psi_i = 3.3219 \log(D_i)$ . For example,  $3.3219 \log(64) = 3.3219 \cdot 1.8062 = 6.0$ . Particle sizes in  $\psi$ -units are provided in Table 2.1. Particle size  $D$  in mm-units is obtained from particle sizes in  $\psi$ -units by

$$D_i = 2^\psi = e^{\psi \ln(2)} = 10^{\psi \log(2)} \quad (2.9)$$

### 2.1.3 Sieving and manual measurements of particle size

The size of gravel particles can be measured manually or by sieving. The different equipment used in both approaches can affect the results. This makes it necessary to compare different methods of particle-size measurements and to determine conversion factors.

Sieving usually employs square-hole sieves, although some labs still have round-hole sieves. Square- and round-hole sieves produce different size gradation curves, especially for flat particles. Manual particle-size measurements traditionally use rulers and calipers. These devices are prone to operator error that can be avoided by using templates (Section 2.1.3.6). Notwithstanding operator error, ruler and template measurements differ to the same degree as do size gradations based on round-hole and square-hole sieves. Pebble boxes are a handy device if all three particle axes are to be measured (Section 2.1.3.8) because they help to reduce operator error and speed up the measurements.

#### 2.1.3.1 Square-hole sieves

Square-hole mesh wire sieves are the standard laboratory sieves for sand and gravel. They have size gradations between 0.063 and 64 mm. Sieve sizes, i.e., the side length of the mesh width  $D_s$ , typically advance as a logarithmic series based on 2, i.e.,

$$D_s = 2^x \quad (2.10)$$

where  $x$  usually assumes values in increments of 0.5, so that  $D_s$  advances in 0.5 units of  $\phi$  or  $\psi$  (Table 2.1). For sediment from gravel-bed rivers, a stack of sieves in 0.5  $\phi$  units usually has 64 mm as the coarsest sieve, and consecutive smaller sieves have mesh widths of 45.3, 32, 22.6, 16, 11.3, 8, 5.66, 4, 2.83, and 2 mm. If the sand fraction is of concern, sieve sizes continue with 1.4, 1.0, 0.71, 0.5, 0.35, 0.25, 0.18, 0.125, 0.088, and 0.063 mm. Sieves typically used in the United States produced by the American Society for Testing and Materials (ASTM E-11) follow the 0.5  $\phi$  or  $\psi$ -gradation only approximately for particle sizes in the gravel range. This deviation stems from expressing particle-size classes as fractions of an inch. Sieves that retain particles larger than 22.6 and 11.3 mm are commonly labeled 22.4 and 11.2 mm, suggesting an arithmetic mean between  $-4.5 \phi$  ( $=22.6$  mm) and  $7/8$  inch ( $= 22.2$  mm). Likewise, the 11.2 mm sieve size is the mean between  $-3.5 \phi$  ( $=11.3$  mm) and  $7/16$  inch  $= 11.1$  mm. Sometimes, ASTM E-11 sieves indicate three different mm sizes for the same sieve size. The “45 mm” ( $1\frac{3}{4}$  inch) sieve, for example, sometimes indicates 44.45 mm, the mm equivalent of  $1\frac{3}{4}$  inch, sometimes 45.3 mm, the exact mm equivalent of  $-5.5 \phi$ , and sometimes 45 mm, which is an intermediate value between the two. This discrepancy is problematic if size classes are first expressed in mm, and then mathematically converted to  $\phi$  or  $\psi$ -units for further particle-size analysis.

Sieving in 0.5  $\phi$ -units is recommended for many sampling projects in gravel-bed rivers. However, some study objectives may require sieving in 0.25  $\phi$ -increments, while for others units of 1.0  $\phi$  may be sufficient.

### 2.1.3.2 Relation between $b$ -axis size and square-hole sieve sizes

Particles found within one 0.5  $\phi$  sieve class can have  $b$ -axes lengths that range over a factor of almost 2. The smallest  $b$ -axis length of a particle retained on a  $-4.5 \phi = 22.6$  mm sieve is 22.7 mm, the largest  $b$ -axis length is 45.2 mm. For a given particle shape, the range of  $b$ -axes lengths is  $\sqrt{2} \cong 1.41$ . Perfect spheres have the smallest  $b$ -axes. The smallest sphere retained on the 22.6-mm sieve has a  $b$ -axis of 22.7 mm, whereas the largest sphere to fit through the  $-5 \phi = 32$ -mm sieve has a  $b$ -axis of 31.9 mm. Extremely flat particles have the largest  $b$ -axes, ranging from 31.9 to 45.2. Thus, the flatter the particle, the larger the  $b$ -axis that fits through a square sieve opening (Fig. 2.3). Particle flatness can be expressed by the ratio of shortest to intermediate axis  $c/b$ . The relation between the ratio of a square-hole sieve opening  $D_s$  to  $b$ -axis size and particle flatness (i.e., the ratio of  $c/b$ ) is given by Eq. 2.11 and shown in Fig. 2.4. Fig. 2.4 can likewise be used to illustrate the ratio

$$\frac{D_s}{b} = \sqrt{\frac{1}{\sqrt{2}} \cdot 1 + \left(\frac{c}{b}\right)^2} \quad (2.11)$$

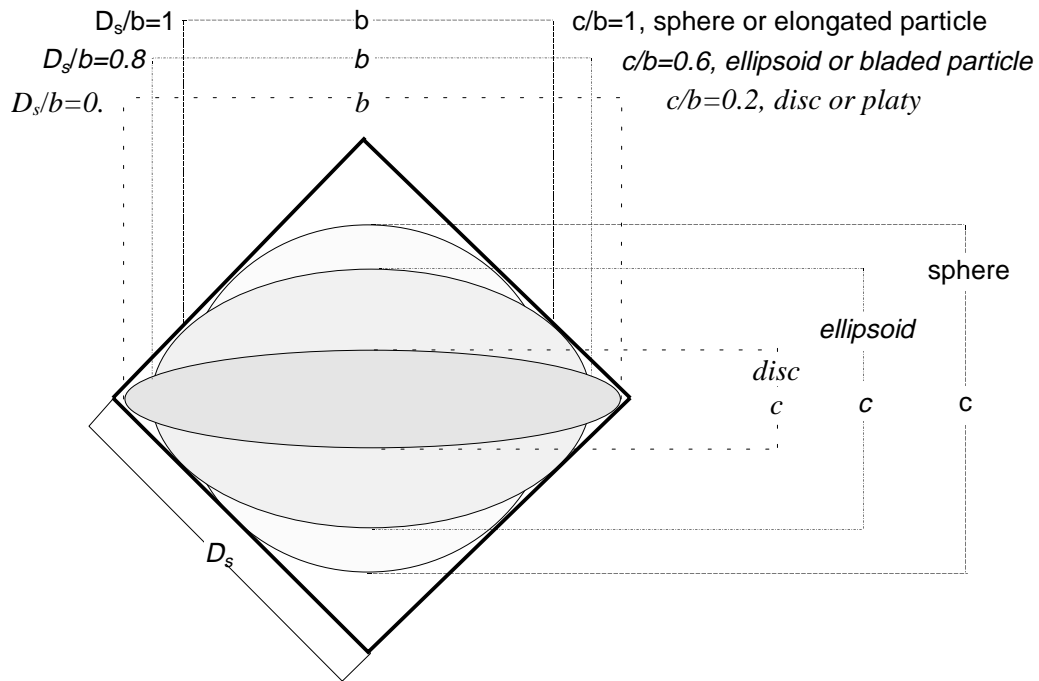


Fig. 2.3: Illustration of effect of particle shape on largest  $b$ -axis size to fit through a square-hole sieve (Redrawn from Church et al. 1987; by permission of John Wiley and Sons, Ltd.).

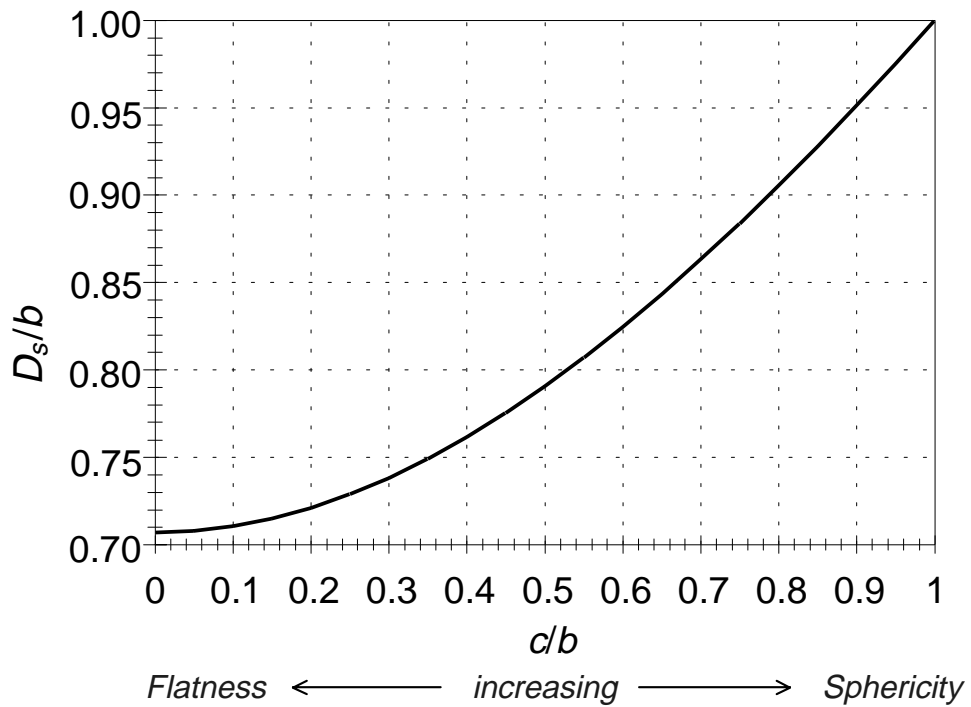


Fig. 2.4: Ratio of square-hole sieve opening  $D_s$  to measured  $b$ -axis size as a function of particle flatness, i.e., the ratio of  $c/b$  (Redrawn from Church et al. 1987; by permission of John Wiley and Sons, Ltd.).

of square-hole sieve size to round-hole sieve size for various degrees of particle flatness (Section 2.1.3.5).

### 2.1.3.3 Round-hole sieves

Some sieves consist of metal plates with round borings of the diameter  $D_s$ . Since square-hole sieves and round-hole sieves have openings of different shapes, both sieves produce different sieve results, except for particles with perfect spherical shapes. A sphere with a diameter of 3.99 mm fits through both a round-hole and a square-hole sieve of 4 mm, and a ball 46 mm in diameter is likewise retained on both the square and the round-hole sieve of 45 mm. However, sieving ellipsoidal or flat particles with both sieve types produces different gradation curves (i.e., cumulative frequencies). Differences in mean particle  $b$ -axes length and conversion factors between round and square-hole sieve results are discussed in Sections 2.1.3.4 and 2.1.3.5.

### 2.1.3.4 Center of class and mean particle $b$ -axes length per size class

Sometimes, computations require that an entire particle-size class is represented by a single particle-size value. Commonly, this value is taken as the “center of class”,  $D_c$ , which is the hypothetical *sieve* size between the retaining and the passing sieve size.  $D_c$  is therefore determined from the logarithmic mean between the retaining sieve size  $D_{ret}$  and the next larger, passing sieve size  $D_{pass}$  which is equal to the diagonal of the retaining sieve size.

$$D_c = 10^{\left(\frac{\log(D_{ret}) + \log(D_{pass})}{2}\right)} \quad (2.12)$$

For example, center of class for the 16 mm sieve is  $D_c = 10^{(\log 16 + \log 22.6)/2} = 19.02$  mm. In terms of  $\phi$ -units, the center of class is the arithmetic mean between the retaining and the passing sieve size. Thus,  $\phi_c$  for the -4 to -4.5  $\phi$  size class is  $(-4 + -4.5)/2 = 4.25 \phi = 19.03$  mm. Eq. 2.12 can likewise be expressed by the best-fit regression between  $D_c$  and  $D_{ret}$ , which yields the linear function

$$D_c = -0.00284 + 0.841 D_{ret} \quad (2.13)$$

The center of class  $D_c$  (the central sieve size between the retaining and the passing sieve) is only equal to the particle size of the weight midpoint  $D_{mc}$  of the sediment between the retaining and the passing sieves if a sufficiently fine gradation of sieve sizes is chosen (Folk 1966). In order to avoid an imbalance between  $D_c$  and  $D_{mc}$ , fluvial gravel ranging from sand to cobbles should rather be sieved in increments of 0.5  $\phi$  than in increments of 1.0  $\phi$ .

### ***Mean particle b-axes length per size class***

The center of class  $D_c$  is not generally equal to the (geometric) mean particle  $b$ -axis length  $b_m$  within that size class and thus can usually not be used as a substitute for  $b_m$ .  $D_c$  and  $b_m$  are only identical for perfect spheres.  $D_c$  for the size class 16 to 22.6 mm is 19.02 mm. The range of spheres retained on the 16-mm sieve extends from 16.1 to 22.5 mm with a geometric mean of 19.03 mm.

The  $b$ -axes sizes of very flat particles retained on a given sieve are a factor of up to  $\sqrt{2} \cong 1.4$  larger than the  $b$ -axes of spheres, extending from 31.9 to 22.5 mm, with a geometric mean of 26.8 mm. Thus, for a sediment mixture of spheres and very flat particles, the geometric mean  $b$ -axis length of particles retained on the 16-mm sieve would be somewhere within the range of 19 and 26 mm.

### ***Uneven distribution of particle sizes per sieve class***

Fluvial gravel particles are usually not of equal particle shape, particularly not in mountainous areas where bed material comprises a variety of particle shapes due to highly variable transport distances of particles within a reach. This variety of shapes produces an uneven, and approximately normal, distribution of particle  $b$ -axes lengths within one sieve class. Small particles are scarce on a sieve because small particles are only retained if they are spherical, while flat particles of the same  $b$ -axis length are not retained. Large particles are scarce on a sieve because only those large particles that are flat are passed through the next larger sieve, while round particles of the same  $b$ -axis size are retained on that larger sieve. The mid-size range of particles per sieve class comprises all particle shapes, thus mid-sized particles make up the majority of particles per sieve class. Using round-hole sieves, the passing sieve retains all particles with a  $b$ -axis larger than the passing sieve size (instead of letting the flat ones through). Thus, the majority of particles retained on a round-hole sieve are close to the passing sieve size when sieving sediment of mixed particle shapes.

#### **2.1.3.5 Comparison of sieve results using round-hole and square-hole sieves**

Sieving a given particle mixture with a set of square-hole sieves produces a finer size distribution than would be obtained from sieving the same particle mixture with round-hole sieves. This is because a round-hole sieve may retain particles that are not retained on a square-hole sieve of the same size. For example, an ellipsoidal particle with a  $b$ -axis of 50 mm and a  $c$ -axis of 30 mm will not pass through a 45-mm round-hole sieve, but will pass through a 45-mm square-hole sieve. Thus, this 50-mm particle will be tallied as larger than 45 mm when using round-hole sieves, and as smaller than 45 mm when using square-hole sieves.

If all particles of the sample are of the same and known shape, results from round-hole and square-hole sieving are convertible. Conversion factors between round-hole and square-hole sieves range from 0.71 for extremely flat particles to 1.0 for spheres (Church et al. 1987) and Fig. 2.4 can be used for conversion between round and square-hole sieve

results. Fluvially transported particles in wadable gravel-bed streams are most likely to be approximately ellipsoidal in shape and therefore are likely to have a conversion factor between 0.8 and 0.9. Note that particle shapes may vary between different size classes or different lithologies. Thus, different conversion factors may have to be applied within one sample to account for this fact.

### 2.1.3.6 Templates

During field studies, gravel particle sizes are best determined with templates because template measurements provide higher accuracy than measurements with rulers and using templates reduces variability between different operators. A template, also called a gravelometer, is a thin aluminum or plastic plate with several sieve-sized square-holes. The holes usually correspond to the sizes of standard 0.5  $\phi$ -increment sieve sets, starting at 2 mm, and reaching to 128 or 180 mm, depending on the size of the template. Templates can also be designed with holes in 1, or 0.25  $\phi$ -increments (Fig. 2.5). A gravelometer made of plastic, about 25 by 30 cm in size, and 0.5 cm thick, can be purchased from Hydro Scientific in Great Britain (Fig. 2.6). U.S. Government agencies can purchase templates from the Federal Interagency Sedimentation Project (FISP) in Vicksburg, Mississippi<sup>1</sup>. The FISP gravelometer US SAH-97 is made of aluminum, is 0.32 cm thick, and has 14 square-holes in 0.5  $\phi$ -units ranging from -1 to -7.5  $\phi$  (2 to 180 mm). The overall dimensions are 28 by 34 cm (Fig. 2.7).

Templates are especially useful for pebble counts (Section 4.1.1. and 4.1.2). The operator picks up a particle and pushes the particle through various holes. The aim is to determine a particle's sieve diameter either in terms of "*not passing or larger than*" the hole of a given size, or in terms of "*passing or smaller than*" the hole of a given size. The "larger than" approach records the largest hole size (i.e., sieve size  $D_s$ ) that is smaller than the particle diameter (equivalent to the sieve size on which the particle was retained). Particle size is tallied as "larger than  $D_s$ " where  $D_s$  is the next smaller hole size. The "smaller than" approach records the smallest hole size through which the particle could be passed (equivalent to sieve size through which the particle could pass), and tallies the particle as "smaller than  $D_s$ ", where  $D_s$  is the next larger hole size. For example, a rock with a 60 mm  $b$ -axis would be tallied in the larger than 45 mm class using the "larger than" approach, or as smaller than 64 mm in the "smaller than" approach. It does not matter which approach is followed, as long as one approach is followed consistently. The "larger than" approach seems to be more intuitively connected to note taking when sieving, equivalent to recording the weight of particles "retained on the sieve" with the sieve size  $D_s$ . The "smaller than" approach, equivalent to recording the weight of particles "passing a sieve" eliminates one step in the computation of cumulative frequency distribution, which is customarily computed as "percent of particles finer than" or "percent passing", but seems to be less intuitive.

---

<sup>1</sup> For further information contact FISP at (601) 634-2721.

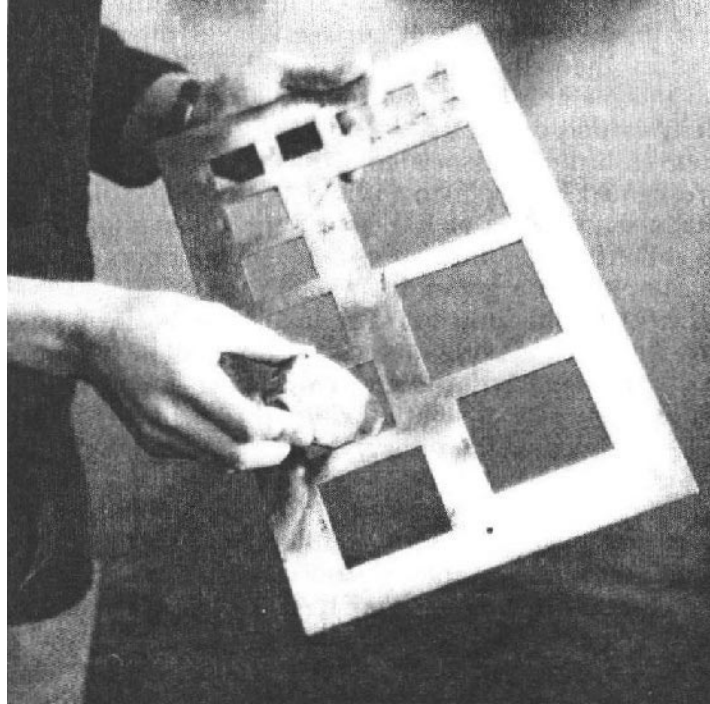


Fig. 2.5: Template in  $0.25 \phi$ -units used by Hey and Thorne (1983); Reproduced by permission of the American Society of Civil Engineers.

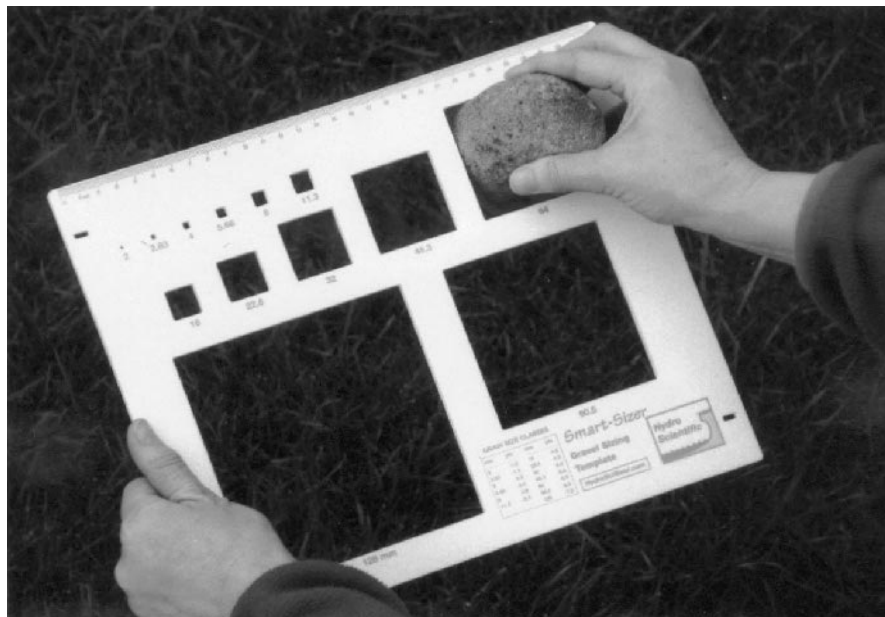


Fig. 2.6: Template available from Hydro Scientific Limited, Stratford-on-Avon, Warwickshire CV37 8EN, UK, Fax/phone:+44-1789-750965, email: HydroSci@aol.com; website: <http://members.aol.com/HydroSci>. Photo courtesy of Hydro Scientific.

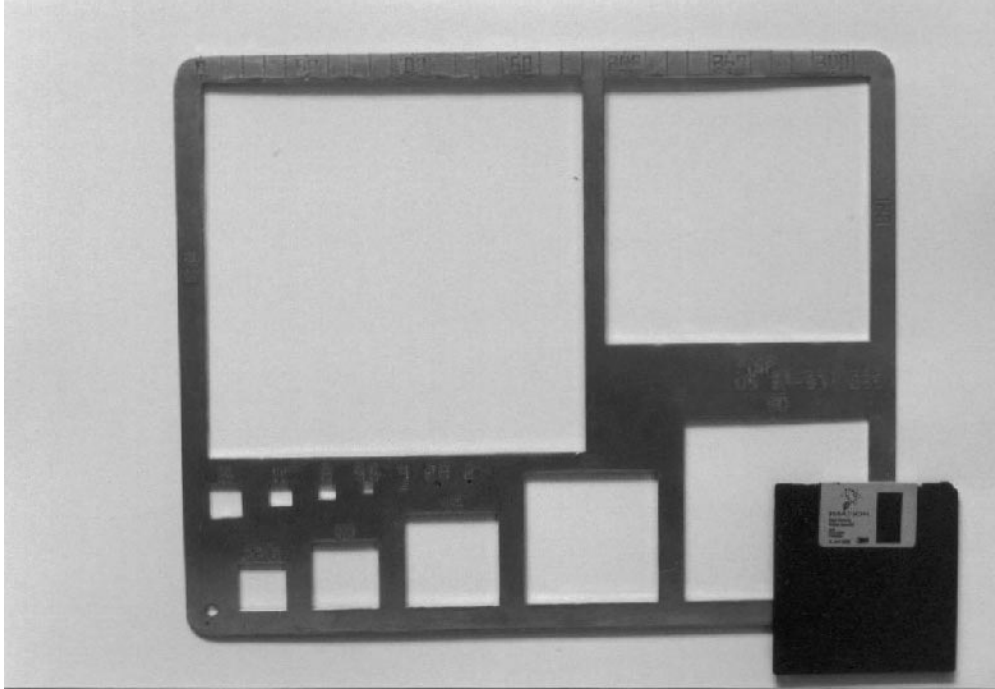


Fig. 2.7: Template US SAH-97, produced by the Federal Interagency Sedimentation Project, website: <http://fisp.wes.army.mil/>.

Measuring particle sizes with templates is expedient because the appropriate “larger than” or “smaller than” hole size can usually be determined on the first or second try. Templates are also useful for field sieving individual bulk samples. Template measurements are preferable to ruler and caliper measurements for particle-size analyses because potential errors arising from improperly defining the *b*-axis (Section 2.1.1), or from misreading the ruler can be avoided (Hey and Thorne 1983; Stream Notes, April 1996). The magnitude of errors avoided by template measurements becomes apparent if replicate *b*-axes measurements with rulers are performed on re-measured rocks. The same operator can usually reproduce particle *b*-axis measurements correctly. However, when multiple operators re-measure pre-measured particles using a ruler, individual operators produce different results (Wohl et al. 1996). Differences between operators’ results are more pronounced when angular particles shapes, and particle structures due to layering or metamorphic processes make the correct identification of the *b*-axis difficult (Marcus et al. 1995). The use of templates largely eliminates these measurement errors.

#### 2.1.3.7 Rulers and calipers

Some field studies measure the particle *b*-axis size with a ruler. This procedure is only recommended if the study focuses on measuring particle sizes within a fairly narrow range. An example is the determination of the dominant large particle size from among perhaps 30 large, but not the largest, particles within a given sampling area.

Measuring the particle  $b$ -axes size with a ruler or caliper is not recommended in studies that tally  $b$ -axes measurements in  $\phi$  units. First, ruler measurements are prone to error because the operator has to accurately determine the orientation of the  $b$ -axis (Marcus et al. 1995). Secondly, ruler measurements do not correspond to measurements made with templates, or square-hole sieves. Ruler measurements correspond to measurements with round-hole sieves. Thus, when comparing or merging ruler with template measurements, the same procedures as discussed in Section 2.1.3.5 apply, and particle sizes need to be converted, using for example Fig. 2.4. Finally, no additional information on particle size is gained from measuring  $b$ -axes to the nearest mm with a ruler or calipers, if these measurements are then tallied in  $0.5\text{-}\phi$  size classes.

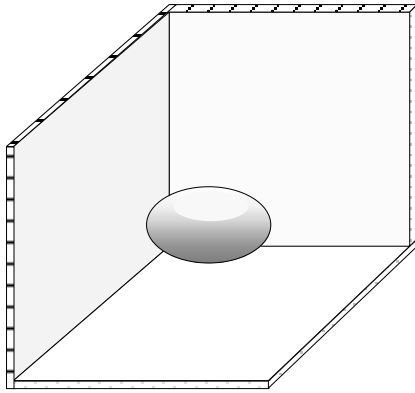
Tallying particle sizes in  $\phi$  units assumes that particle sizes are normally distributed in terms of  $\phi$  units. This assumption does often not hold in a strict statistical sense for particle-size distributions from gravel beds. Nevertheless, a normal distribution is often assumed for convenience, so that standard statistical procedures can be used (Section 2.1.4.3). However, if the assumption of a normal distribution cannot be accepted, measuring particle  $b$ -axes lengths to the nearest mm or cm allows for more options in the statistical analysis.

Rulers, or better, calipers, are appropriate for analyses of particle shape in the lab when particle axes are measured by a person aware of the difficulties involved in proper identification of the three particle axes. If large quantities of pebbles need to be measured, a pebble-box (Section 2.1.3.8) may be needed.

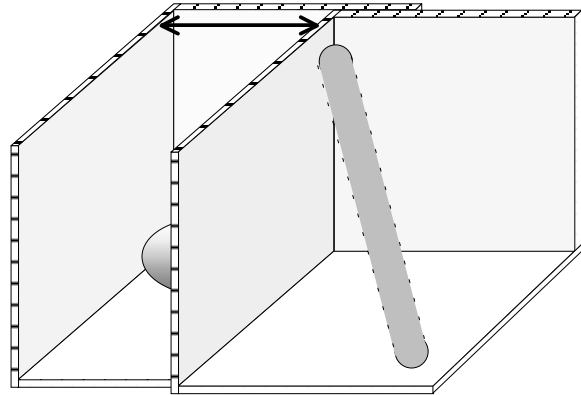
#### 2.1.3.8 Pebble-box

The pebble-box was developed by Ibbeken and Denzer (1988) who conducted several large studies of gravel particle shapes. The pebble-box is a convenient device for easy measurements of the three particle axes because it does not require repositioning the particles between measurements, as ruler measurements do, and ensures all three measured particle axes are at right angles. A pebble-box can be constructed of two 3-sided corner pieces each formed by joining the edges of 3 square pieces of plywood. The dimension of the box depends of the particle sizes to be measured. A box 15 - 20 cm along the sides, made of plywood 0.5 - 1 cm thick is suitable for pebbles and small cobbles. A diagonal handle made from a broomstick or a dowel stick is attached to one of the corner pieces (Fig. 2.8). Thin clear plastic rulers in cm and mm gradations are glued to the two top edges and the front edge of the corner piece with no handle. The “zero” marks of all rulers need to be in the corner, so that the distance from the corner can be read.

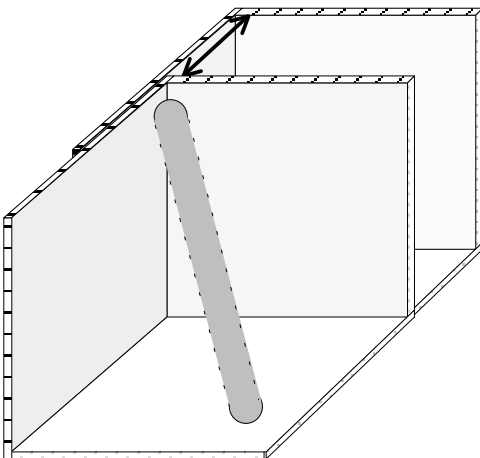
To measure the three axes a pebble is pushed into the corner of the first pebble-box. The second pebble-box (the one with the handle) is alternately placed along the top, side, and front of the pebble in the box. The length of each particle axis can then be read on the tape measures. The pebble-box is particularly useful when measuring the three axes of a



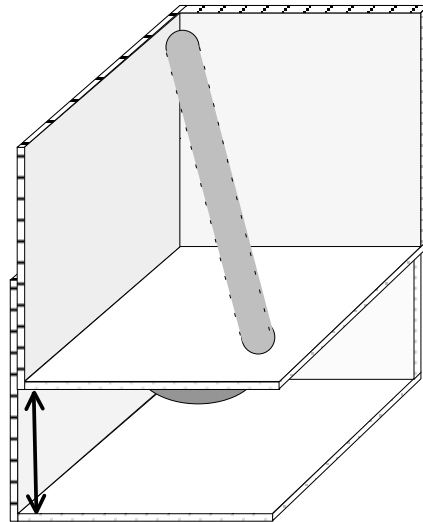
(1) A particle in the stationary corner piece



(2) Measuring the longest axis



(3) Measuring the intermediate axis



(4) Measuring the shortest axis

Fig. 2.8: Measuring the three particle axes with the pebble-box.

large number of particles. It takes about 20 minutes to measure 100 particles if a second operator records the measurements.

Particle *b*-axes measurements with the pebble-box are similar to measurements with a ruler, or caliper. Thus, particle sizes need to be converted if they are to be compared to particle sizes determined with square-hole sieves (Fig. 2.3 and Section 2.1.3.5). Compared to sieve or template measurements, pebble-box measurements may slightly overpredict the *b*-axes of rhombic or diamond-shaped particles. Particles of this shape

tend to align in the box in such a way that *b*-axes are measured across the largest width, rather than parallel to the sides of the particle (i.e., along the stippled line *b* instead of the solid line *b* in Fig. 2.2).

### 2.1.3.9 Lab sieving

Sediment from gravel-bed rivers is usually dried before sieving<sup>2</sup>. Wet sediment can be dried on metal pans (e.g., disposable 10-inch pie plates). Two or three days of exposure to air at room temperature is usually sufficient to dry gravel, but the drying process can be accelerated by placing the sediment in an oven at 90°C (194°F) overnight. Particles should be allowed to cool to room temperature before sieving and weighing, not only to avoid burning oneself, but also to avoid measuring an increase in particle weight as the particle absorbs air moisture during the cooling phase.

For sieving, the gravel from one or more pie plates is poured into the sieve stack that has a sieve pan at the bottom. The amount of sediment that can be sieved at a time depends on the number of sieves used and on the particle sizes. It is important not to overfill the sieves. As a rule of thumb, particles should not cover the sieves in a layer more than one or two particles thick. Filled in this way, the sieving process takes about 10 minutes when sieves are mounted on a shaker (ROTAP), a sieving apparatus that automatically shakes and taps the sieve stack. If an automatic shaker is not available, the shaking and tapping motion can be imitated by placing the sieve stack onto the floor. The operator sits on a stool in front of the stack, rotating, and tilting the stack forward and backward. A piece of wood placed under the sieve stack protects the floor and the sieves from damaging each other, and provides a hard enough surface when sieving in the field. Gravel particles larger than 8 mm may not require a full 10 minutes of shaking, but particles might still be sieved out of fine gravel and sand after 10 minutes. Some particles will get stuck in the sieves and should be removed and added to the sample before sieving the next subsample. Scrubbing the backside of the sieve and tapping the mesh and the sides of the sieve with a long handled fine wire brush helps clean the fine gravel sieves. Gentle prying with a screw-driver removes particles stuck in larger and more sturdy sieves. Care must be taken not to damage the sieve.

The weighing process depends on the weight range of the scale available in the lab. Sieved size fractions are weighed individually for each sieved subsample for small range scales, but individual size fractions from all subsamples should be combined for large range scales.

It is recommended to prepare data sheets with one column for retaining (or passing) sieve sizes, and one or several other columns for the weight retained on each sieve, depending on the number of subsamples into which the entire sample had to be divided for the sieving process. The example data sheet shown in Fig. 2.9 is for gravel and further differentiation of the sand into size fractions was not needed for that study. Particle weight is usually

---

<sup>2</sup> *Wetsieving as a measure of particle dispersion is not necessary for gravel and sand.*

recorded in grams or in kg. If the scale has only English units, those should be recorded on the data sheets. Unit conversions and all subsequent computations such as adding subsample mass, calculating frequencies and cumulative frequencies should be performed at a later stage after all data have been entered into a spreadsheet program.

Stream:		Date/Time:			
Person sieving:					
Standard sieve set: yes / no    ROTAP: yes / no					
Sieving duration:            (min)					
Notes:					
Particle size (mm or $\phi$ )	Mass (g) of subsample				
	1	2	3		n
Total					
64					
45.3					
32					
22.6					
16					
11.3					
8					
5.6					
4					
2.8					
2					
<2					

Fig. 2.9: Example data sheet for sieve analysis.

The range of the scale permitting, each subsample should be weighed as a total before sieving. Close correspondence between the total weight and the summed weight of all size fractions makes sure that all recordings are accurate. If this control is not available, it is important to double-check the proper recording of each value. All samples should be retained and put back into their sample bags until after the particle-size analysis, so that samples can be re-measured if results suggest errors.

### ***Sample splitting***

The fine part of a large sediment sample from a gravel bed consists of fine gravel and sand, and might weigh 10 – 20 kg. This is considerably more sediment than is needed for a representative particle-size analysis of this size range (see, e.g., Fig. 5.14 for required sample mass for a given  $D_{max}$  particle size). It might therefore be useful to split the sample before sieving. A sample is best split using a sample splitter. A riffle splitter consists of a hopper under which a series of up to about 10 equally sized compartments is located. The

bottom outlets of the compartments are alternately directed to the left or the right side of the splitter (see riffle splitter in Fig. 2.10).

Sediment is poured evenly along the entire length of the hopper, making several passes from side to side. The compartments funnel the sediment alternately to the left or the right side of the splitter where the sediment is caught in containers. This process splits the sample in half. Usually, the compartmentalization does not induce sediment sorting, so that an approximately equal amount of sediment of near-equal size distribution is contained in each of the two containers. However, the sediment to be split in a splitter must be dry. Otherwise, fine particles may cling to the compartment walls and produce subsamples with less fines than the original sample.

One passage through the sample splitter divides the sample in half. If one only needs  $1/8^{\text{th}}$  of the total sample mass, the sample is run through the splitter 3 times, one portion is discarded each time, the remaining portion is split again. If the splitting aim is to obtain a subsample with about  $1/5^{\text{th}}$  of the total sample mass, the sample is first split into 8 subsamples, two of which are discarded. Three of the  $1/8^{\text{th}}$  splits are combined and split again to yield a subsample that has  $3/16^{\text{th}}$  of the total sample volume.

Only one of the subsamples is sieved, unless the operator chooses to sieve several subsamples in order to compute the accuracy of the sieving result (see two-stage sampling, Section 5.4.2.1).

#### 2.1.3.10 Field sieving, weighing, volume determination, and counting

##### *Field sieving, templates and sieve sets*

The sample mass required for a good statistical analysis of particle sizes is often approximated by 20 - 100 times the mass of the  $D_{max}$  particle size. This amounts to 160 - 800 kg in a gravel bed with a  $D_{max}$  of 180 mm (Section 5.4.1.1). Unless vehicle access of the field site and to the lab is excellent, such large samples can best be accommodated by sieving the coarse portion of the sample down to 16 or 11.3 mm in the field.

Field sieving requires a relatively large open and dry work space, and dry weather so that particles can air dry. The surfaces of pebbles air-dry within a day even under overcast skies, provided particles are well spread out on tarps. The weight difference between air-dried and oven-dried particles is usually negligible for pebbles and cobbles, but can make a difference for sand, or for highly porous particles that retain a measurable amount of water. The drying process in the field can be accelerated by using black plastic perforated landscaping cloth instead of tarps, because the fine perforation prevents water puddles on the cloth, and the black color heats up quickly in the sun. Landscaping cloth is light-weight, especially when precut into long strips, but not very durable, and some of the fine sand may pass through the perforation.

After particles are air-dried, any dry sand sticking to larger rocks is brushed off before sieving. Cobbles and boulders larger than the largest sieve size or template hole are

measured with calipers or a ruler. All three axes are measured, and the corresponding sieve diameter of those particles is estimated from the particle *b*- and *c*-axis dimensions.

The equipment used to sieve cobbles and pebbles in the field depends on the scale of the sampling event. A few tarps, one or two templates, a few sturdy plastic shopping bags, and a hanging scale are sufficient for small sample volumes of only a few buckets. Such a field sieving kit is also recommended when working at a remote, hike-in, field site. Starting with the largest particles on the tarp, each particle is picked up and its size class is measured with a template. This task is actually less daunting than it might appear at first. For example, a sample of 135 kg from a gravel-bed stream might only contain 26 particles larger than 64 mm, but these account for 35% of the total weight of the sample (Table 2.2). Continuing with field sieving down to the 22.6 or 16 mm size class, which requires handling roughly 600-1000 particles, analyzes 2/3 to 3/4 of the total sample weight already. Particles of a given size class are collected in plastic bags, or in piles on an extra tarp. The particles of each size class are then weighed using the hanging scale. Alternatively, the number of particles per size class may be counted, and that number can be converted into mass per size class at a later stage.

If the site has vehicle access or is a short distance away from the vehicle, it is advisable to take a lab sieve set to the field when sieving larger volumes of gravel. Less bulky than a stack of lab sieves is a (home-made) sieve box consisting of a frame (approximately 0.2 by 0.3 m, 0.1 m high, into which screens of different mesh width can be inserted (Tom Lisle, pers. comm, 1998)<sup>3</sup>. Particles sieved into different size classes are collected on tarps, pails, plastic tubs, or in strong ziploc bags, depending on the extent of the sampling project. After sieving, particles of a size class can either be weighed, or counted.

There is no rule regarding the lowest sieve size for field sieving, although fine gravel and sand can probably be sieved more conveniently in the lab. If the unsieved portion of the sample is large, it can be split in the field so that sufficient sediment for the remaining largest particle-size class is taken to the laboratory for a standard sieve analysis. A subsample mass of 6 kg is quite sufficient if particles larger than 16 mm have been removed in the field (Eq. 5.40 and Fig. 5.14 provides a relation between required sample mass for a given  $D_{max}$  particle size). One method of splitting a sample in the field is to distribute scoops of sediment from the sample alternately into a series of empty buckets. The number of buckets used depends on the desired sediment mass for the subsample. The first scoop goes into bucket 1, the second into bucket 2, etc, until all sediment from the sample is evenly distributed. The volume and the mass in each bucket should be equal. A sturdy ladle works well for scooping sandy and fine gravelly sediment. The number of all subsamples is recorded, but only one of the subsamples is then taken to the lab. Well thought out field sieving equipment is essential when undertaking an extensive field-sampling program. The minimum field equipment consists of a large rockable sieve-box (ca. 0.5 by 0.5 m, and 0.15 m high) with exchangeable pieces of meshwire corresponding sieving and splitting apparatus to the field site. The device (Fig. 2.10) consists of a frame,

---

<sup>3</sup> Research Hydrologist, Pacific Southwest Forest and Range Experiment Station, Arcata, CA.

to sieve sizes. When sieving tons<sup>4</sup> of sediment, Ibbeken (1974) recommends bringing a approximately 0.5 by 0.5 m, and 0.7 m high, into which a sieve and a sample splitter can be inserted. The bottom of the frame is connected to a springy and rockable stand (old lab stool). Two operators can sieve 0.5 - 1 tons of gravelly sediment per day with this apparatus. The large masses of sediment to be handled require a large number of tarps and tubs, and a robust field scale for weighing.

### ***Particle weighing***

Particles collected per sieve class can be weighed in the field using an accurate hanging scale that is best hung from a strong tree branch, or from a tripod. The particles to be weighted are placed into a plastic shopping bag. Such bags have negligible weight, but do not withstand much use, so a supply is necessary.

Two scales with different ranges are useful if the sample contains large cobbles and small boulders. Particle weight per size class in a unimodal sample of about 150 kg from a gravel-bed ranges between 1 and 20 kg (Table 2.2). Thus, a scale with a 0.1 - 10 kg is suitable. Within the 100 g gradation, readings can be visually interpolated to the nearest 10 or 20 g. If the weight per sieve class exceeds 10 kg, particles are weighed in two batches. Large cobbles and small boulders are weighed individually. If their individual weight exceeds 10 kg, a scale with a larger range is needed, or the particle weight is computed by measuring particle volume and multiplying by an assumed particle density.

### ***Determination of particle volume***

It may be useful to determine particle volume in the field. If all particles are of known density, weight can be computed from particle volume. If particles are of distinctly different densities, such as volcanic rocks that range from massive basalt to vesicular pumice that floats on water, it is useful to determine both particle volume and weight to compute particle density. A tall, straight-walled, bucket with a known diameter and a holding capacity of about 3 to 5 gallons can be used for measuring particle volume. The bucket is filled with water to about half its capacity and the water level is read before and after the cobble is completely submerged. The bucket should stand on a level surface when reading the water level. If a level surface is not available, the bucket can be shimmed until level, using a builder's level to verify that the bucket is horizontal. If that is not possible, the water level needs to be read at several locations and averaged.

---

<sup>4</sup> Ton (English units) = 907.185 kg = 2000 lb; Metric ton = 1,000 kg = 2,204.63 lb.

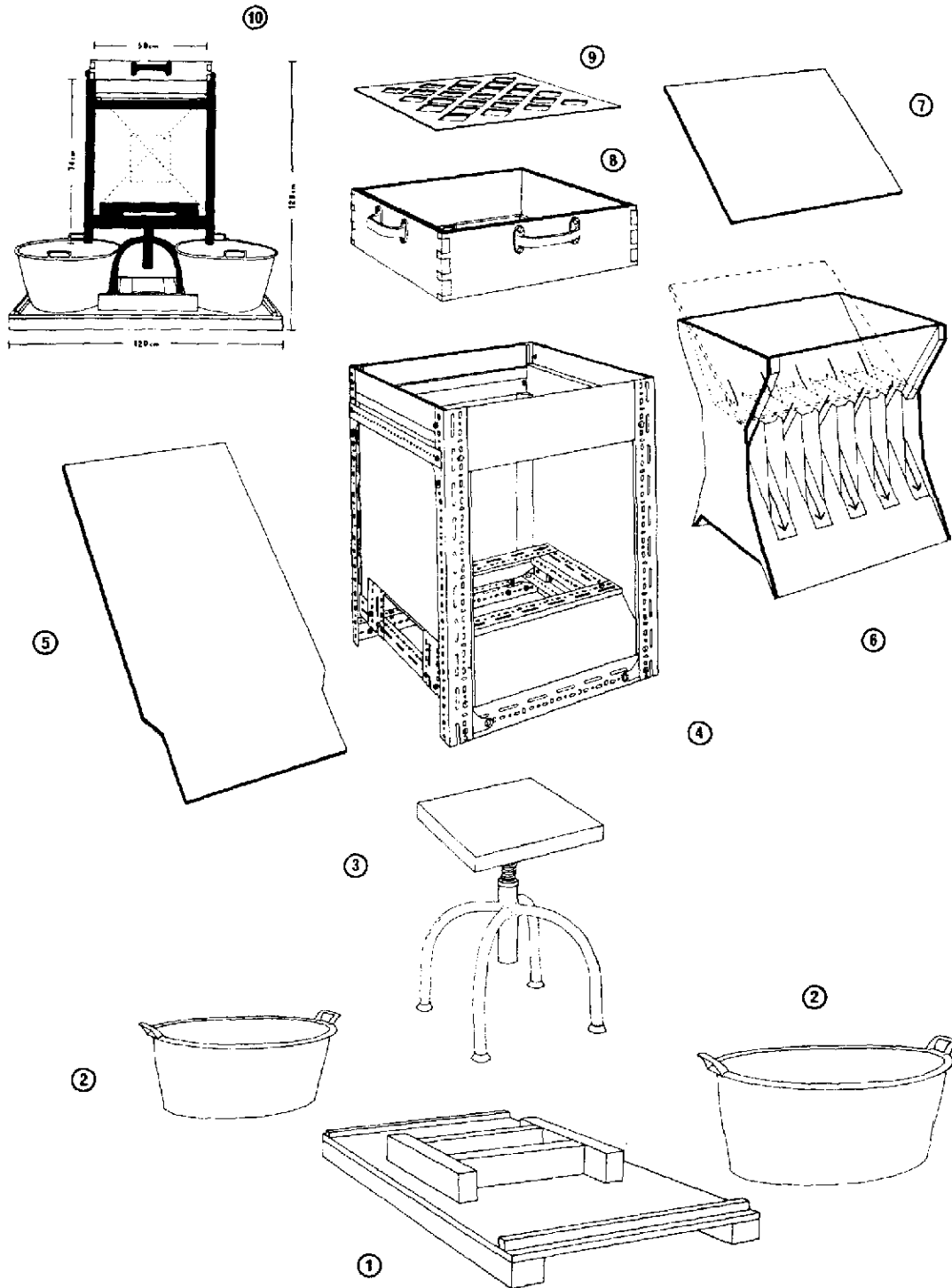


Fig. 2.10: A sieving and splitting device: (1) basal plate, (2) catch bins, (3) rockable, springy stand, (4) central frame, (5) deflecting board, (6) riffle splitter, (7) splitter board, (8) screen frame, (9) screen, (10) assembled device with general measurements (Reprinted from Ibbeken (1974), by permission of the Society of Sedimentary Geology).

Table 2.2: Example of the number of particles and weight per size class in a volumetric bed-material sample. Particles finer than 8 mm were not counted.

Size Class (mm)	No. of Particles	Weight (kg)	% Finer by Weight
256	0	0	100
180	1	16	88
128	1	6	84
90	5	10	76
64	19	14	65
45	66	18	52
32	169	16	40
22.6	326	11	32
16	716	9	25
11.3	1519	7	20
8		6	16
5.6		5	13
4		4	10
2.8		4	7
2		2	5
<2		7	4
		$\Sigma = 135$	

Water levels can be read more easily if a clear plastic tube is mounted along the outside of the bucket. The tube is connected to the inside of the bucket through a hole at the top and the bottom of the bucket. Thus, the water level in the bucket is equal to the water level in the tube outside of the bucket. A ruler mounted next to clear plastic tubing and a drop of dye in the tubing makes the reading even easier. Again, it is essential that the bucket is level.

### ***Particle counting***

Counting the number of particles per sieve class is an option if conditions are unfavorable for field weighing. Since the laboratory sieve analysis of sand and pebble particle sizes is mass based, the number of particles counted per sieve class needs to be converted to mass as well. A generalizable relationship can be obtained from the following study.

A relation between mean weight of particles  $m_{mi}$  (g) and the retaining sieve size  $D_{ret(sq)i}$  (in mm) was established for six bedload- and bed-material samples from mountain gravel-bed rivers with mainly granitic or andesite petrology. Particle shapes within a sample varied, ranging from compact to elongated. A power function in the form of  $m_{mi} = a D_{ret(sq)i}^b$  was fitted through the data and yielded a coefficient of determination  $r^2 = 0.999$  (Fig. 2.11). Particle density and shape, as well as measurement errors cause slight variability between samples, but for six sediment samples from various gravel-bed streams examined in a study

by the authors, coefficients ranged between 0.0024 and 0.0036, while exponents ranged between 2.92 and 3.04. The mid point of all coefficients and exponents obtained for mean particle weight per square-hole sieve size yielded the equation

$$m_{mi} = 0.00307 (D_{ret(sq)i})^{2.98} \quad (2.14)$$

where  $m_{mi}$  is the mean weight of particles (g) and  $D_{ret(sq)i}$  is the retaining sieve size (in mm) Eq. 2.14 is applicable to mountain gravel-bed streams where bed material comprises a variety of different particle shapes and where a particle density of approximately  $2.65 \text{ g/cm}^3$  can be assumed.

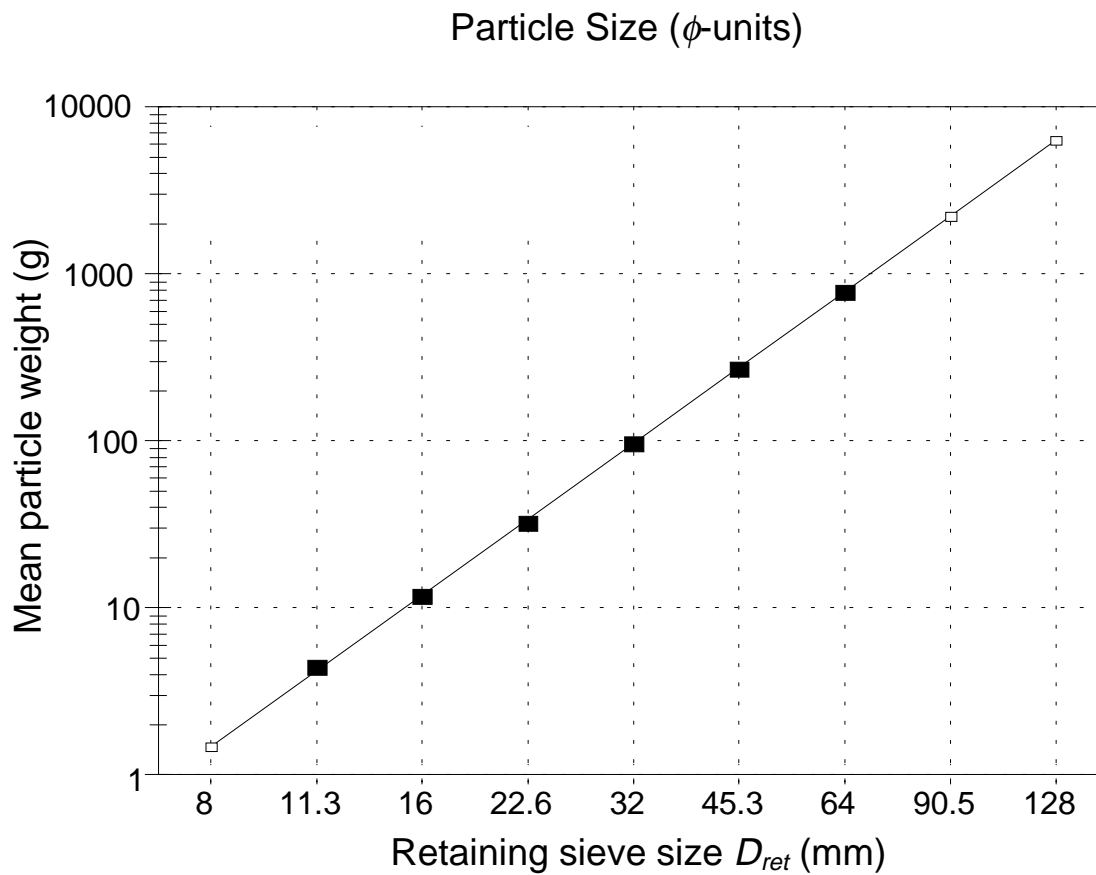


Fig. 2.11: Measured mean particle weight for sieve sizes in  $0.5 \phi$ -increments for square-hole sieves (■) and the regression function (□). Sediment from Squaw Creek, MT.

## 2.1.4 Computation of the particle-size distribution

The statistical analysis of a bed-material sample starts with computing a particle-size frequency and percentage frequency-distribution from which a cumulative frequency distribution is computed in the third step. Percentiles are determined from the cumulative distribution curve, and used by themselves, for example when comparing  $D_{50}$  sizes, or to derive particle-distribution parameters such as mean, sorting (i.e., standard deviation) and skewness that characterize the distribution as a whole. Particle-distribution parameters can also be computed directly from a frequency distribution (moment methods).

### 2.1.4.1 Particle-size frequency and cumulative frequency distribution

The result of a laboratory or field particle size-analysis is a record of particle weight (or particle numbers) retained on each sieve size (see data sheet in Section 2.1.3.9). The weight per size class is then entered into a spreadsheet table (see column 1 and 2 in Table 2.3) for all subsequent computations. The first step of analysis is to compute the percentage weight or number frequency for each size class. The weight or number of particles in each size class is divided by the total sample weight or particle number and multiplied by 100 (column 3). The result can be plotted as a percentage frequency distribution (histogram) using a bar graph (Fig. 2.12). Next, the percentage of particle weight or numbers retained on each sieve is converted into the percentage of particle weight or number passing the next larger sieve size (column 4).

For example, a record showing 9.1% of particle weight retained on sieve size 32 mm becomes 9.1% of particle weight passing the sieve size of 45 mm. The percentage particle weight or particle number per size class is then summed starting with the finest size class. This leads to a cumulative weight distribution (column 5) in terms of percent *finer than* or *percent finer* the indicated size class. The cumulative distribution curve could theoretically also be computed in terms of percent coarser or percent retained, but the percent finer or percent passing approach is the commonly used approach for particle-size distributions.

The cumulative particle size-distribution curve (Table 2.3), also called the *sieve curve*, or the *gradation curve*, is plotted with the particle-size classes from column 1 or 2 as the abscissa (x-axis, horizontal), and the percent finer by weight (column 5) on the ordinate (y-axis, vertical) (Fig. 2.12). If the analysis is based on frequency-by-number, such as in a pebble-count, the percent finer by number is plotted on the ordinate. If particle sizes are expressed in  $\phi$ -units, the x-axis is kept linear. If particle sizes are expressed in mm, the x-axis should be expressed in a logarithmic scale. Alternatively, the mm-sizes of particle size-classes can be plotted in equally spaced increments along the x-axis (as in bar or line graphs). Segments of the cumulative distribution curve are connected by straight lines.

Data plotting is often the first step of analysis, especially when dealing with a sample from a new stream site. Visualization of the frequency histogram and the cumulative frequency

Table 2.3: Example of a particle-size analysis for a 103 kg sample of subsurface sediment taken at mid-stream in a mountain gravel-bed stream (Squaw Creek, MT).

(1a)	(1b)	(2)	(3)	(4)	(5)	(6) Percentiles				(7)
x-axis: Size of sieve (mm)	( $\phi$ )	<u>Weight retained on sieve</u> (kg)	y <sub>1</sub> -axis: <u>Weight retained</u> (%)	Weight passing sieve (% finer)	y <sub>2</sub> -axis: Cumulative weight (cum. % finer)	( $\phi_p$ )	( $\phi$ )	( $D_p$ )	(mm)	
<2	<-1	6.7	6.5	-	-					
2	-1.0	2.3	2.3	6.5	6.5	$\phi_5$	-0.89	$D_5$	1.8	
2.8	-1.5	2.5	2.4	2.3	8.8					
4	-2	2.6	2.5	2.4	11.2					
5.6	-2.5	3.7	3.6	2.5	13.7					
8	-3.0	5.3	5.1	3.6	17.3	$\phi_{16}$	-2.82	$D_{16}$	7.1	
11.3	-3.5	7.8	7.6	5.1	22.4					
16	-4.0	9.6	9.4	7.6	30.0	$\phi_{25}$	-3.67	$D_{25}$	12.7	
22.6	-4.5	10.9	10.6	9.4	39.4					
32	-5.0	9.3	9.1	10.6	50.0	$\phi_{50}$	-5.00	$D_{50}$	32.0	
45	-5.5	11.4	11.1	9.1	59.1					
64	-6.0	12.2	10.9	11.1	70.1					
90.5	-6.5	7.4	7.2	10.9	81.1	$\phi_{75}$	-6.22	$D_{75}$	74.7	
128	-7.0	5.4	5.3	7.2	88.2	$\phi_{84}$	-6.70	$D_{84}$	104.3	
181	-7.5	6.6	6.5	5.3	93.5					
256	-8.0	<u>0.0</u>	<u>0.0</u>	6.5	100.0	$\phi_{95}$	-7.61	$D_{95}$	195.8	
total:		102.7	100.0							

distribution provides a first impression of the data and is helpful for interpretation. If the graph is used mainly for demonstrative or visualization purposes, the y-axis is usually plotted in a linear scale. If percentile values are to be read off the graph, plotting the y-axis on probability paper increases the accuracy with which the particle size of small and large percentiles can be read.

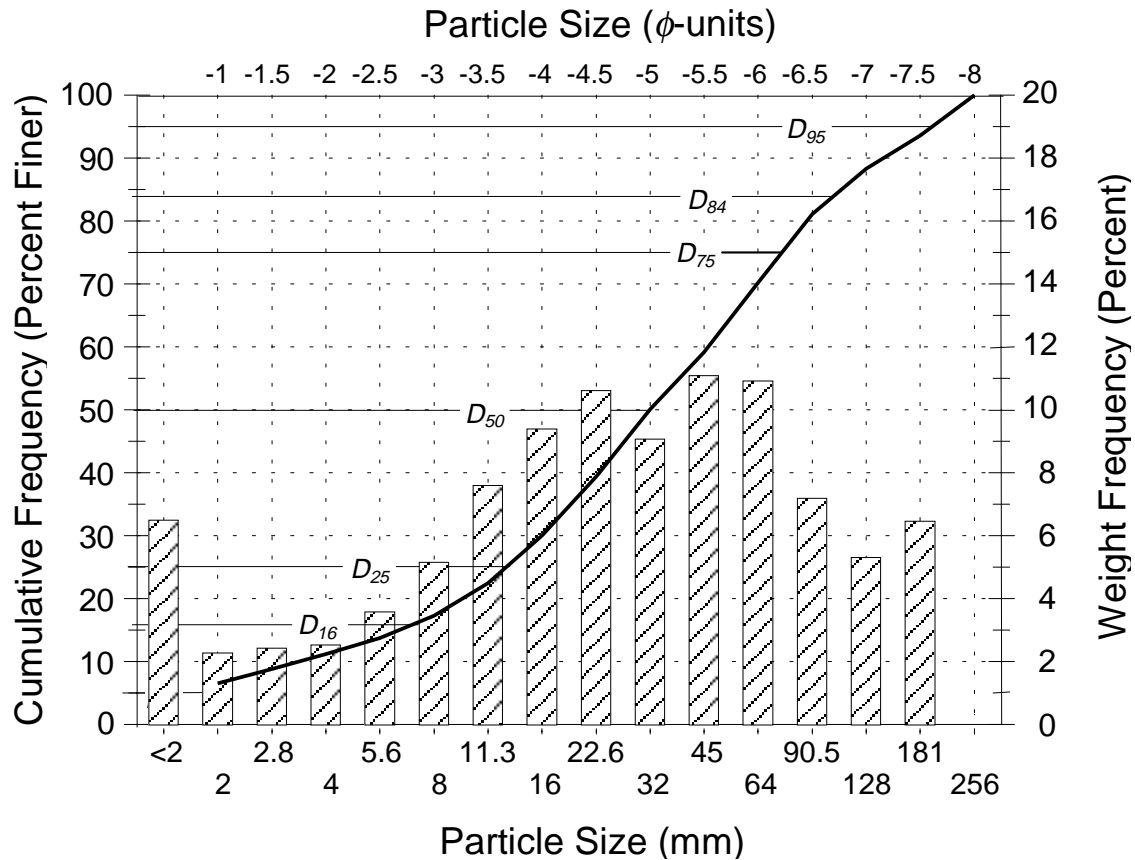


Fig. 2.12: Frequency distribution (histogram with hatched bars) and cumulative frequency distribution curve (thick line) with indicated percentile values for data listed in Table 2.3.

#### 2.1.4.2 Percentiles and their computation

Two sediment mixtures of different particle sizes are usually distinguished by comparing several of the percentile values of the two distributions or the parameters derived from the percentiles. A percentile is a sediment size indicated by the cumulative distribution curve for a particular “percent finer” value. For example, the sediment size for which 80% of the sediment sample is finer is the “80th percentile”. The notation is  $D_{80}$ , where  $D$  represents particle size (in mm) and the subscript “80” denotes 80%. The  $D_{50}$  is the median point of the distribution that divides the distribution in two equal parts. The particle size for which 25% of the distribution is finer is the 25th percentile, or the  $D_{25}$ . The  $D_{25}$  and  $D_{75}$  are also called quartiles. Theoretically, any percentile value can be used for comparison, but customarily, the particle sizes of the  $D_{50}$ , (i.e., the median), the  $D_{25}$  and  $D_{75}$  (quartiles), the  $D_{16}$  and  $D_{84}$ , and the  $D_5$  and  $D_{95}$  are used. In a normal distribution, one standard deviation from the median encompasses all data between the  $D_{16}$  and the  $D_{84}$  and are the points on a distribution curve at which the change of curvature occurs). The  $D_5$  and  $D_{95}$  characterize the distribution tails. Data between the  $D_5$  and the  $D_{95}$  comprise almost two standard deviations on either side of the  $D_{50}$  or median. Those 7 percentiles

may be compared as individual values, or be used to compute distribution parameters such as mean, sorting (i.e., standard deviation), and skewness (Section 2.1.5).

***Reading percentiles off a graph plotted on probability paper***

Before spreadsheet programs became commonly available, percentiles were often graphically determined from the cumulative particle-size distribution curve plotted on normal probability paper. The y-axis of this graph paper extends from a small value > 0 at the lower end to a value just below 100 at the high end. Probability partitioning spreads the y-axis range at the low and the high end, while compressing the central range around 50. The x-axis is linear for particle sizes in  $\phi$ -units, and lognormal for particle sizes in mm-units. Probability graph paper in linear and logarithmic partitioning is provided in the appendix. The graph of a cumulative particle frequency-distribution approaches a straight line as particle size-distributions approach normality, or lognormality, respectively. A probability plot enables the user to read percentile values in  $\phi$ -units off the graph, but plotting by hand becomes tedious when dealing with large data sets.

***Mathematical linear interpolation***

An alternative to plotting on probability paper is to compute percentiles mathematically by linear interpolation between two known data pairs of sieve size in  $\phi$ -units and their percentile values in a cumulative distribution. Particle size-classes in mm require a logarithmic interpolation, which means that the mm size classes need to be log-transformed before the interpolation ( $\log D$ ). A particle size  $\phi_x$  of a desired percentile  $x$  in  $\phi$ -units can be computed from:

$$\phi_x = (x_2 - x_1) \cdot \left( \frac{y_x - y_1}{y_2 - y_1} \right) + x_1 \tag{2.15}$$

$y_2$  and  $y_1$  are the two values of the cumulative percent frequency just below and above the desired cumulative frequency  $y_x$  (see shaded values in Table 2.3, column 5), and  $x_2$  and  $x_1$  are the particle sizes in  $\phi$ -units associated with the cumulative frequencies  $y_2$  and  $y_1$  (see shaded values in column 1b in Table 2.3). The example below illustrates how the particle size of the percentile  $\phi_{16}$  is computed for the particle-size distribution in Table 2.3 using Eq. 2.15.

$$\phi_{16} = (-3 - -2.5) \cdot \left( \frac{16 - 13.7}{17.3 - 13.7} \right) + -2.5 = -2.82\phi \quad (= 7.1 \text{ mm}) \tag{2.15a}$$

Likewise, the  $D_{16}$  is computed from:

$$D_{16} = 10^{\left( (\log(8) - \log(5.67)) \cdot \left( \frac{16 - 13.7}{17.3 - 13.7} \right) + \log(5.67) \right)} = 7.1 \text{ mm} \quad (2.15b)$$

Note that the error incurred if the computation is performed with particle sizes in mm without log transformation is relatively small and can maximally reach 1.7 % compared to the result that would have been obtained if log transformed data were used.

#### 2.1.4.3 Testing for various distribution types

Gravel deposits are typically not made up of one particle size only, but comprise a variety of particle sizes that may take up various portions of the sediment volume. One possibility is that particle sizes of each size class (in terms of  $\phi$ -units) may comprise approximately even portions of the total sediment volume (uniform distribution). More typically, medium particle sizes comprise most of the sediment volume with little sediment in the finest and coarsest size classes (normal or log-normal distributions).

Fluvially transported sediment from gravel-bed rivers often tends to roughly approximate lognormal distributions if particle sizes are expressed in mm, or approximate normal (Gaussian) distributions if particles sizes are expressed in  $\phi$ -units which are a logarithmic transformation of particle sizes in mm. Assuming an underlying normal distribution for approximately normal particle-size distributions is convenient because normality is the prerequisite for several statistical applications. Normality is required for (1) binning particle sizes in  $\phi$ -units, for (2) confidence in the results of standard descriptive statistical procedures, as well as for (3) confidence in the results of common sample-size equations.

In a strict statistical sense, particle-size distributions in  $\phi$ -units are often not normally distributed (Church and Kellerhals 1978; Church et al. 1987; Rice and Church 1996b). The tolerable degree of departure from normality varies depending on the planned statistical analysis. Small departures from normality usually do not pose problems when applying statistics that assume normality, but large departures do. If normality is wrongly assumed, results of standard descriptive statistical parameters (e.g., the sample mean, sorting, skewness and kurtosis) may not be accurate and may not serve well to discriminate between samples.

Small departures from normality, however, can greatly affect the sample size required for sampling specified percentiles with a preset precision. For example, in distributions that have a tail of fine sediment, a lower sample size than computed from standard sample-size equations may suffice to predict the  $D_{95}$  of the distribution with a preset precision. Contrarily, sample size has to be considerable higher than computed to precisely predict the  $D_5$  (Section 5.2.3.4). Church et al. (1987) and Rice and Church (1996b) therefore recommend that no particular distribution should be assumed for sediment from gravel-bed rivers, not even for large samples for which normality is more intuitively assumed than for small samples. Equations have been developed for estimating sample size when no

particular underlying distribution type is assumed (Section 5.4.1.1). Sample mass predicted from these equations is similar to the sample size predicted by equations based on normal distributions for accurate sampling of high percentiles (Section 5.4.3). But equations based on normal distributions predict that a much lower sample mass would suffice to accurately predict central percentiles.

If a user wants to acknowledge that a particle-size distribution is not strictly normal (in terms of  $\phi$ -units), non-parametric statistics could be applied. Non-parametric statistics are necessary if the data severely deviate from normality. However, non-parametric tests are only beginning to enter mainstream statistical analyses in geomorphology, and results from a relatively unknown test might not be very convincing to a reader. The reader is referred to the statistical literature for non-parametric statistics, none of which are described in this document.

A particle-size distribution can be tested for normality and lognormality in several ways:

- visual evaluation of the plotted graph,
- regression analysis between the cumulative frequency and the respective particle-size classes,
- comparison of frequency distribution with ideal Gaussian or Rosin distributions,
- probability plot of residuals with regression analysis, and
- standard tests for normality and lognormality.

#### ***Visual evaluation of the plotted graph***

The likelihood of whether a given distribution is normal or lognormal can be estimated by plotting the cumulative size distribution of particle sizes in  $\phi$  units on normal probability paper<sup>5</sup>. Lognormal probability paper is used for plotting if particle sizes are in  $\text{mm}^5$ . The straightness of the graph is assessed visually. Ideal normal, or lognormal distributions, respectively, plot as straight lines.

Some computer based statistical packages and some newer spreadsheet programs provide plots on a probability-scaled y-axis for a visual assessment of the degree of normality or lognormality. If such a program is not available, a spreadsheet program can be used to approximate a probability scale. The first step is to compute a cumulative particle-size distribution in which the frequency is expressed in decimals, i.e., as 0.4 instead of 40%. The unsieved remaining particles, i.e., the contents of the “pan” should be excluded from this analysis.

The cumulative frequency distribution can be interpreted as the probability with which to expect a particular particle-size class. A standard normal distribution (or standard normal density function) has a given probability  $p_i$  (y-axis) for each value  $z_{pi}$  (x-axis of a bell-shaped normal distribution). The values for  $p$  and  $z_p$  are listed in tables of any general purpose statistics book. For example, probabilities of 0.5, 0.75, 0.975, and 0.99 are

---

<sup>5</sup> Provided in the appendix of this document.

obtained by  $z_p$  values of 0, 0.675, 1.96, and 2.33. Since the normal distribution is symmetrical, probabilities of  $1 - 0.99 = 0.01$ , and  $1 - 0.975 = 0.025$  are obtained by  $z_p$  values of -2.33, and -1.96, respectively. The relationship between  $z_p$  and  $p$  can also be approximated from various equations. One of the possibilities provided by Stedinger et al. (1993) is the equation

$$z_p = \frac{p^{0.135} - (1 - p)^{0.135}}{0.1975} \quad (2.16)$$

Using this equation, the  $z_p$  value associated with each probability, i.e., each decimal fraction of the cumulative particle size-distribution can be computed in a spreadsheet. In a plot of  $z_p$  values versus particle size, the resulting graph is a straight line for normally distributed samples (Fig. 2.13). Deviation from a straight line can be visually assessed by comparison with a best-fit handfitted straight line. For particle-size distributions, a deviation from a straight line is usually most pronounced in the distribution tails, a

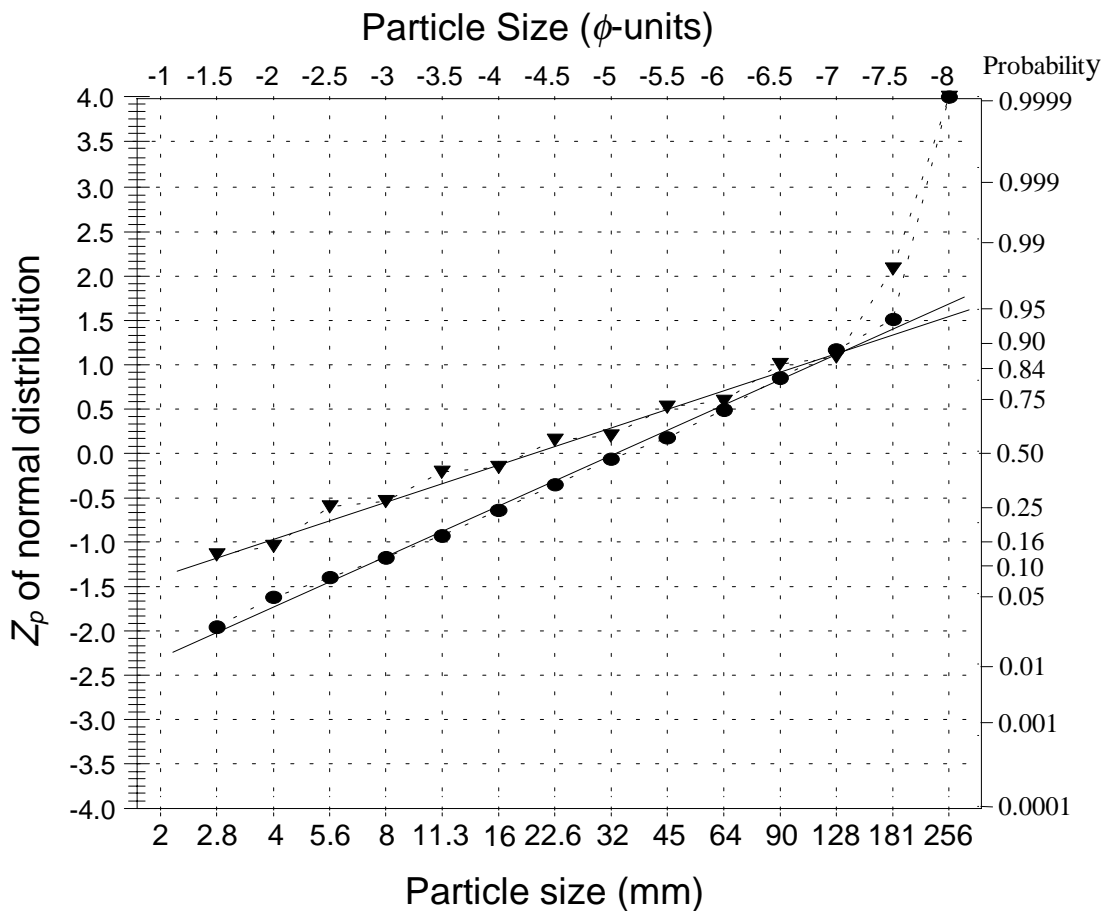


Fig. 2.13:  $Z_p$ -values versus particle size for an approximate normal distribution (●) (particle-size distribution shown on Table 2.3 and in Fig. 2.12) and a non-normal block distribution (▼).

phenomenon easily checked by the visual assessment. If the deviation of the distribution tails is pronounced, truncating the data set to the range of  $\phi_{16}$  to  $\phi_{84}$ , for example, might straighten the graph.

Caution should be used when interpreting the results of this method. The graph with the black circles in Fig. 2.13 is the particle size-distribution shown in Table 2.3 and Fig. 2.12. The plotted data points seem to resemble a normal distribution well enough to justify the assumption of a normal distribution, and hence to compute distribution parameters or the sampling accuracy for a given sample size. However, non-normal distributions do not necessarily show excessive deviation from a straight line in such plots. Even a definitely non-normally distributed data set that comprises alternate frequencies of 12, 2, 12, 2, etc. for consecutive particle-size classes yields an seemingly reasonable fit to a straight line (graph marked by black triangles in Fig. 2.13). This lack of a standard regarding the tolerable degree of deviation from a straight line is a disadvantage of the visual method.

### ***Evaluation and comparison of regression coefficients***

A regression analysis can be performed that regresses  $\ln(y)$ , with  $y$  = cumulative frequency, versus  $x$ , the particle size in  $\phi$ -units. The coefficient of determination  $r^2$  is computed for the best fit exponential regression  $y = a \cdot e^{b \cdot x}$ . The closer  $r^2$  approaches the value of 1, the closer the fit with a normal distribution. This approach is useful when comparing the goodness-of-fit to a normal distribution between two samples with a similar range of particle sizes. However, there are no standard values that  $r^2$  needs to obtain in order for the distribution to qualify as normal. This is because the value for  $r^2$  is highly dependent on the particle-size range of the sample.

### ***Comparison with best fit normal and lognormal distributions***

Another test for normality of particle-size distributions in  $\phi$ -units is to compute the normal distribution that most closely resembles the measured particle-size distribution and compare the observed and computed distribution. The difference between samples is expressed as a percentage value that then is used to compare the goodness-of-fit between samples. The standard normal distribution in its notation for grouped (i.e., “binned”) data is

$$G_{\phi_i} = \frac{1}{\sigma \cdot \sqrt{2\pi}} \cdot \exp - \left( \frac{(\phi_i - \mu)^2}{2\sigma^2} \right) \quad (2.17)$$

where  $G_{\phi_i}$  is the frequency of an equivalent Gaussian distribution for the  $i$ th size class in  $\phi$ -units,  $\phi_i$  is the particle size of the  $i$ th class in  $\phi$ -units (Schleyer 1987).  $\mu$  usually denotes the distribution mean, but Schleyer (1987) suggests that the distribution mode (i.e., the size class with the largest frequency) is a more appropriate parameter when analyzing coarse sediment samples in which the finest and the coarsest fractions may not be

representative of the population. Unrepresentative distribution tails affect the distribution mean, but not the mode. If particle frequency-distributions are too irregular in their central parts to benefit from using the distribution mode, the distribution median should be used instead. Various ways of computing a graphic arithmetic mean for particle sizes in  $\phi$ -units are explained in Section 2.1.5.3 (Eqs. 2.31 - 2.34).  $\sigma$  is the distribution standard deviation. In order to minimize the effects of possible truncation on  $\sigma$ , Schleyer (1987) suggests substituting  $\sigma$  by a sorting coefficient  $s_s$  which is computed from

$$s_s = 0.75 (\phi_{75} - \phi_{25}) \quad (2.18)$$

and focuses on the more central parts of the distribution<sup>6</sup>. The constant in Eq. 2.19 could be set to 0.5 if normality of the data was not assumed. However, using the constant of 0.75 renders the numerical values of  $s_s$  similar to the Inman sorting coefficient  $s_I$  (Eq. 2.46, Section 2.1.5.4)

If particle-size data are in mm units, correspondence with a standard lognormal distribution should be tested instead of a normal distribution. The standard lognormal distribution is given by (Gilbert 1987)

$$L_{Di} = \frac{1}{\sigma \cdot \sqrt{2\pi}} \cdot \exp - \left( \frac{(\ln D_i - D_m)^2}{2\sigma^2} \right) \quad (2.19)$$

where  $L_{Di}$  is the frequency of an equivalent lognormal distribution of the  $i$ th size class in mm.  $D_m$  is the arithmetic mean of the log-transformed data and could be computed as

$$D_m = \frac{1}{m_{tot}} \sum_{i=1}^n (D_{ci} \cdot m_i) \quad (2.20)$$

where  $D_{ci}$  is the center of class in  $\phi$ -units of  $i$ th size class,  $m_i$  is the weight of particles retained for the  $i$ th size class, and  $m_{tot}$  is the total weight of particles per sample. Eq. 2.19 can also be applied to number frequencies. In this case,  $m_i$  in Eq. 2.20 becomes  $n_i$ , the number of particles per size class, and  $m_{tot}$  becomes  $n$ , the total number of particles per sample.

Other possibilities to compute a distribution mean are shown in Section 2.1.5.3.  $\sigma$  is the distribution standard deviation and computed from

---

<sup>6</sup>  $\sigma$  denotes the standard deviation of a population,  $s$  denotes the sample standard deviation. Sorting coefficients denoted by  $s$  are an abbreviated computation of standard deviation based on a few percentiles of the distribution.

$$\sigma = \sqrt{\frac{1}{n-1} \sum_{i=1}^k (\ln D_{ci} - D_m)^2} \quad (2.21)$$

In symmetrical distributions,  $\sigma$  could be approximated by

$$\sigma = 100^{\wedge} \left( \frac{\log D_{84} - \log D_{16}}{2} \right) \quad (2.21a)$$

which is analogous to the Inman (1952) sorting coefficient  $s_I$  (Eq. 2.46). The goodness-of-fit to a Gaussian distribution is computed from the absolute differences between the cumulative percent frequency of the  $i$ th size class ( $\Sigma m_{\%i}$ ) of a bed-material sample and the cumulative percent frequency of the ideal Gaussian distribution ( $\Sigma G_{\%i}$ ). These differences are summed over all size classes  $k$  and divided by  $k-1$  (Schleyer 1987).

$$\% \text{ Gauss fit} = 100\% - \frac{1}{k-1} \cdot \sum_{i=1}^k |(\Sigma m_{\%i} - \Sigma G_{\%i})| \quad (2.22)$$

Similarly, the goodness-of-fit to lognormal distributions can be computed from:

$$\% \text{ lognormal fit} = 100\% - \frac{1}{k-1} \cdot \sum_{i=1}^k |(\Sigma m_{\%i} - \Sigma L_{\%i})| \quad (2.23)$$

The percent goodness-of-fit is affected by whether the percent frequency is allotted to the retaining sieve size  $D_{ret}$  or the center of class particle size  $D_c$ , and by how the data are summed. If the percent frequency is allotted to  $D_c$  and summed such that a 100% cumulative frequency is reached at the  $D_c$  of the largest size class, the resulting cumulative frequency is in terms of “as large as or finer than” ( $\leq$ ) the center of class of the largest size class. If the percent frequency is allotted to the retaining sieve size  $D_{ret}$ , and summed so that 100% cumulative frequency is reached at the size class above the one with the largest particle, the cumulative frequency is in terms of “smaller than” ( $<$ ), or percent finer than the indicated sieve size. Both procedures were applied to the same particle-size distribution (Table 2.3 and Fig. 2.12) to show the resulting difference (Table 2.4 and Fig. 2.14). A goodness-of-fit of 94.3% was obtained when using the center of class  $D_c$ , whereas a goodness-of-fit of 97.2% was obtained when using  $D_{ret}$ . Thus, computational consistency is important when comparing the goodness-of-fit between samples. The

Table 2.4: Computation of goodness-of-fit for particle-size distribution in Table 2.3 and Fig. 2.12.  $\phi_{25} = 3.99$ ;  $\phi_{75} = 6.3$ ;  $s_s = 1.73$  (Eq. 2.18);  $\mu = 5.75 \phi$ . Resulting goodness-of-fit (Eq. 2.22) = 97.2%.

No. of size class	Size class		Original distribution			Equivalent Gaussian distribution			Absolute difference
	$\phi_i$	$D_i$	Mass	Freq.	Cum. freq.	Eq. 2.17	Freq.	Cum. freq.	
(1)	(2)	(3)	(4)	(5)	(6)	(6)	(7)	(8)	(9)
1	1.0	2	2.3	2.4	0.0	0.005	0.3	0.3	0.3
2	1.5	2.8	2.5	2.6	2.4	0.011	0.6	0.9	1.5
3	2.0	4	2.6	2.7	5.0	0.022	1.2	2.1	2.9
4	2.5	5.6	3.7	3.8	7.7	0.039	2.1	4.2	3.5
5	3.0	8	5.3	5.5	11.5	0.065	3.5	7.7	3.8
6	3.5	11.3	7.8	8.1	17.0	0.099	5.4	13.1	3.9
7	4.0	16	9.6	10.0	25.1	0.138	7.5	20.6	4.6
8	4.5	22.6	10.9	11.4	35.2	0.178	9.6	30.2	5.0
9	5.0	32	9.3	9.7	46.5	0.210	11.4	41.5	5.0
10	5.5	45.3	11.4	11.8	56.2	0.228	12.4	53.9	2.4
11	6.0	64	11.2	11.7	68.1	0.228	12.4	66.2	1.9
12	6.5	90.5	7.4	7.7	79.8	0.210	11.4	77.6	2.2
13	7.0	128	5.4	5.7	87.4	0.178	9.6	87.2	0.3
14	7.5	181	6.6	6.9	93.1	0.138	7.5	94.7	1.6
15	8.0	256	0.0	0.0	100.0	0.099	5.4	100.0	0.0
totals:			96.0	100.0		1.85	100.0		38.9

computational difference becomes smaller as the number of particle-size classes increases, which could be achieved if the sample size is large enough to facilitate sieving in size classes of less than  $0.5 \phi$ .

### ***Comparison with best-fit Rosin distribution***

The Rosin exponential distribution was developed for coal milling purposes (Rosin and Rammler 1933, cited after Ibbeken 1983) and applies well to crushed rock. Bed-material frequency distributions that follow Rosin's distribution are skewed towards fine particles and the mode corresponds to the 36.78th percentile (Fig. 2.15) which is approximately the  $D_{63}$  if the cumulative frequency is computed as the percent finer or percent passing. The Rosin distribution is typical of jointed rock and unweathered slope sediment, and hence to sediment supplied to the stream from hillslopes (Ibbeken 1983). Thus, testing for a Rosin distribution might be worthwhile, if the bed material has a tail of fine sediment (skewed towards fines) and sediment was supplied from unstable hillslopes.

For particle-size distribution where the center of class is a distinct value representing the total class, the ideal Rosin distribution corresponding to the measured distribution is computed from (Schleyer 1987)

$$R_{Di} = \exp - \left( \frac{D_{pass(i)}}{D_{mode}} \right)^{S_R} - \exp - \left( \frac{D_{ret(i)}}{D_{mode}} \right)^{S_R} \quad (2.24)$$

where  $R_{Di}$  is the frequency of an equivalent Rosin distribution for the  $i$ th size class,  $D_{pass(i)}$  is the passing sieve size for the  $i$ th size class in mm, and  $D_{ret(i)}$  is the retaining sieve size for

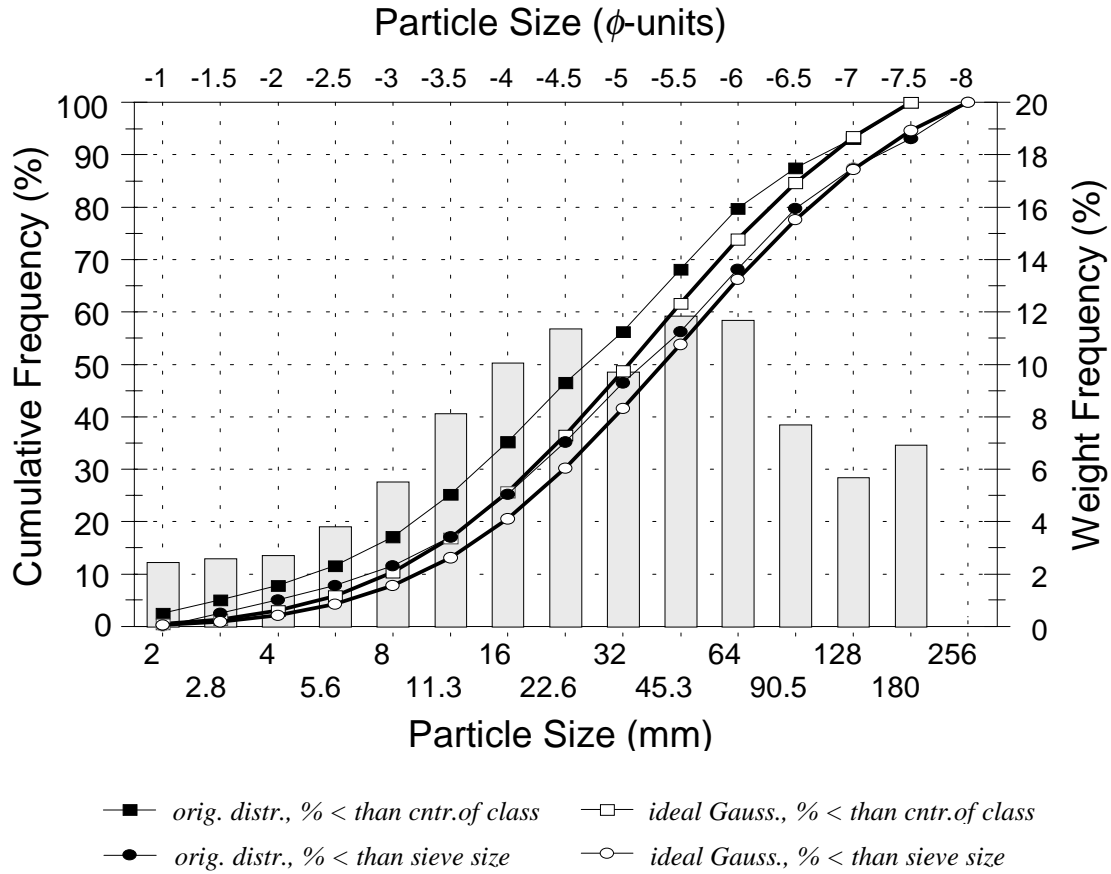


Fig. 2.14: Goodness-of-fit computations based on cumulative frequency in terms of  $\leq D_c$ , and in terms of  $< D_{ret}$  (% finer or % passing).

the  $i$ th size class in mm.  $D_{mode}$  is the mode of the distribution, and  $s_R$  is the sorting coefficient which for a Rosin distribution is computed from

$$s_R = \frac{2.15}{\phi_{68.4} - \phi_{18.4}} \quad (2.25)$$

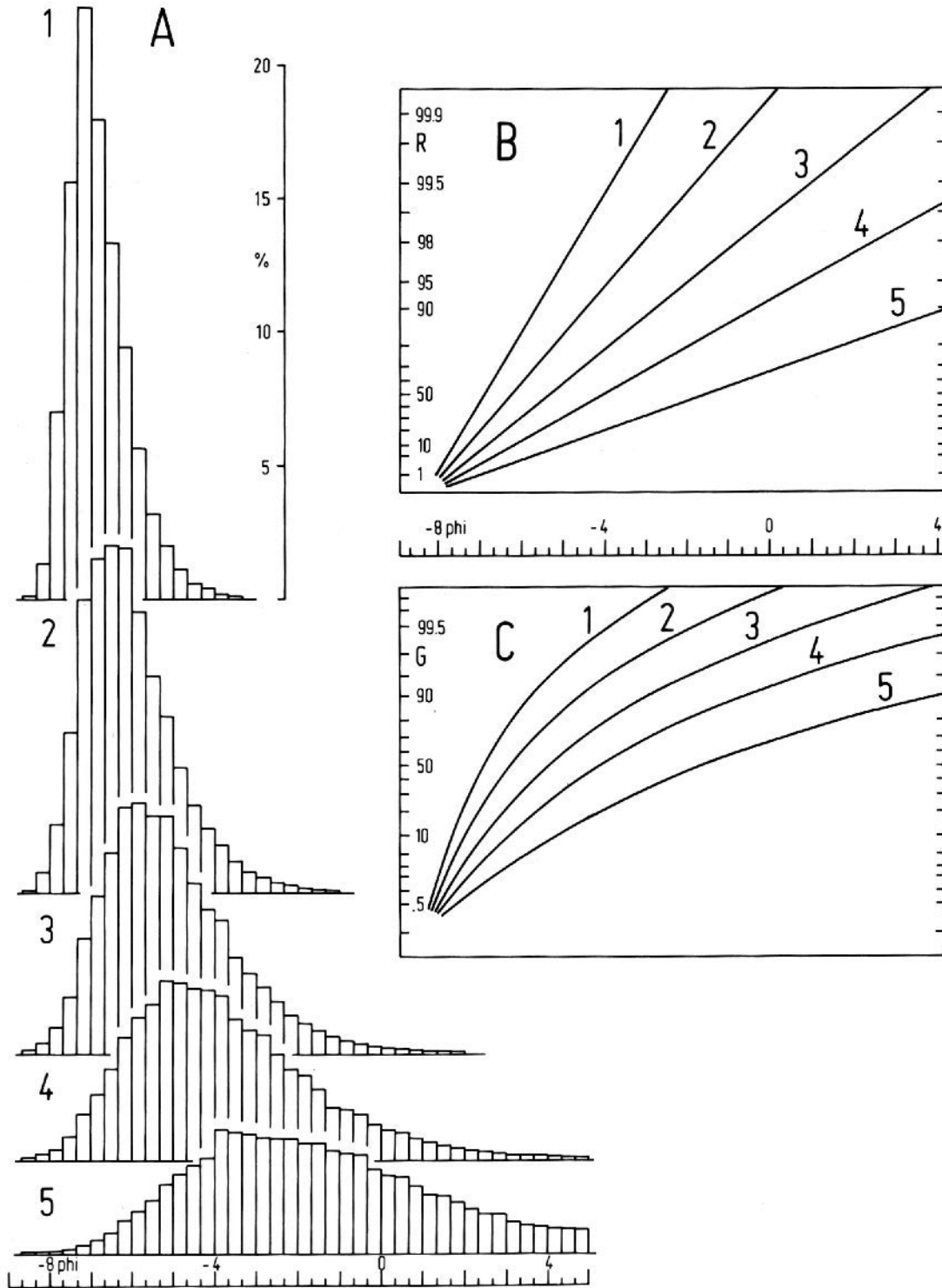


Fig. 2.15: (A) Histograms of ideal Rosin distributions, increasingly poorly sorted from 1 to 5. Cumulative frequency curves of these distributions are plotted on Rosin-coordinate probability paper (B), and on lognormal probability paper (C) (Reprinted from Ibbeken (1983), by permission of the Society of Sedimentary Geologists).

The goodness-of-fit to a Rosin distribution can be computed from (Schleyer 1987):

$$\% \text{ Rosin fit} = 100\% - \frac{1}{k-1} \cdot \sum_{i=1}^{k-1} |(\Sigma m_{\%i} - \Sigma R_{\%i})| \quad (2.26)$$

where  $\Sigma m_{\%i}$  is the cumulative percentage weight frequency of  $i$ th sieve class, and  $\Sigma R_{\%i}$  is the cumulative percentage frequency of the computed Rosin distribution for the  $i$ th sieve class, and  $k$  is the number of sieve classes.

Computed this way, the goodness-of-fit to Gaussian and Rosin distributions is *independent* of the range of the particle sizes included in the analysis and the degree of truncation of the size distribution. Hence, bed-material sediment can be partitioned into a gravel and a sand fraction, and goodness-of-fit can be computed for each part individually, a procedure useful for the analysis of bimodal sediment. Goodness-of-fit to Gaussian, or Rosin distributions is also *independent* of the degree of skewness (Section 2.1.5.5) of the bed-material distribution in question. A Gaussian size-distribution that is skewed towards fine particles does not automatically receive a good fit to a Rosin distribution, nor are good Rosin fits reserved for distributions skewed towards fines.

An analysis of the goodness-of-fit to a Gaussian or Rosin distribution can be useful in two ways: First, summary statistics used to describe particle-size distributions may not be meaningful or appropriate, if the fit to a Gaussian distribution is poor. Second, the goodness-of-fit to a Gaussian or a Rosin particle-size distribution can in and of itself serve as a means to analyze fluvial transport distance (Krumbein and Tisdell 1940; Kittleman 1964, both cited in Ibbeken 1983, and Schleyer 1987). A good fit to a normal distribution indicates that the particle-size distribution was derived due to transport controlled factors, whereas a good fit to a Rosin distribution indicates that the particle-size distribution is controlled by supply from the rock source.

#### ***Probability plot of residuals and regression analysis***

Another procedure to quantitatively evaluate normality is suggested by Neter et al. (1990). The procedure prepares a normal probability plot of residuals and conducts a regression analysis. A residual  $e_i$  in a set of  $x$ - and  $y$ -data is the difference between an observed value  $y_i$  and the value  $Y_i$  predicted from a regression analysis. For the analysis of normality, the ranked residuals  $e_i$  are plotted against the values  $E_i$  which the residuals are expected to have under normality. Near linearity of this function indicates that the distribution is near-normal. The degree of linearity, and thus the degree of normality, can be evaluated by the coefficient of correlation  $r$ . This value can be compared with table values of  $r$  for specified sample sizes and confidence levels to determine whether near-normality can be assumed.

The first step in assessing normality for particle-size frequency distributions is to compute the residuals  $e_i$  which are the positive or negative difference between the observed

cumulative percent frequency for a particle size-class  $D_i$  and the cumulative percent frequency of an equivalent Gaussian distribution (Eq. 2.17). The next step is to rank the residuals in ascending order from  $e_{i=1}$  to  $e_{i=k}$ , where  $k$  is the number of size classes. The expected value  $E_i$  of the ranked residuals under normality is computed from

$$E_i = \sqrt{\frac{\sum_{i=1}^k e_i^2}{k-2}} \cdot \left[ z \left( \frac{i-0.375}{k+0.25} \right) \right] \quad (2.27)$$

$z(A)$  is the percentile of a standard normal distribution. The table value for  $z(A)$  of e.g., 0.841 is 1.00. If  $A$  is smaller than 0.5,  $z$  is looked up under  $A-1$  and yields a negative value. For example, if  $A = 0.159$ ,  $z(0.159 - 1) = z(-0.841) = -1.00$ .

Table 2.5 shows the computation of expected values for the residuals  $E_i$  using the example particle size-distribution listed in Table 2.3 and shown in Fig. 2.13. The residuals  $e_i$  of the observed cumulative percent frequency (column 1 in Table 2.5 and column 6 in Table 2.4) and the cumulative percent frequency of the equivalent Gaussian distribution (column 2 in Table 2.5 and column 9 in Table 2.4) are computed in column 3 of Table 2.5. The residuals  $e_i$  are then ranked in ascending order (column 5 of Table 2.5). The summed term in Eq. 2.27 equals 141.02 (sum of column 6) for the example particle size-distribution, and the square-root term is  $(141.02/(15-2))^{0.5} = (10.85)^{0.5} = 3.294$ .

For the smallest residual  $e_i$  with  $i = 1$ ,  $E_i$  is computed as:

$$\sqrt{10.85} \cdot z \left( \frac{1-0.375}{15+0.25} \right) = 3.294 \cdot z(0.041) = 3.294 \cdot z(0.959) = 3.294 \cdot -1.739 = -5.728$$

For the second smallest residual  $e_i$  with  $i = 2$ ,  $E_i$  is computed as:

$$\sqrt{10.85} \cdot z \left( \frac{2-0.375}{15+0.25} \right) = 3.294 \cdot z(0.107) = 3.294 \cdot z(0.893) = 3.294 \cdot -1.243 = -4.094$$

The expected values  $E_i$  are symmetrical, so that largest and the second largest values of  $E_i$  are 5.728 and 4.094, respectively. Table 2.5 lists all values of  $E_i$  in column 10.

For a visual assessment of normality, the ranked residuals  $e_i$  are plotted against their expected values  $E_i$  (Fig. 2.16). The closer the data points fit to a straight line, the closer is the degree of normality. In addition to a visual assessment, the closeness to a straight line, and thus the degree of normality, can be mathematically quantified. To do so, the ranked residuals  $e_i$  are compared to the values expected under normality  $E_i$  by computing a linear regression function  $E_i = a \cdot e_i + b$ . The values  $E_i$  predicted from the regression function are listed in column 11 of Table 2.5 and plotted in Fig. 2.16. The coefficient of correlation  $r$  is used to indicate the departure from normality. At  $r = 1$ , the distribution is normal.

Table 2.5: Computation of normality for residuals

Orig. distr.	Gauss. distr.	residual $e_i$		ranked		$(i-0.375)$		expect.	pred.	
$\Sigma\%$	$\Sigma\%$	(1) - (2)	rank	$e_i$	$e_i^2$	$(k+0.25)$	(9) - 1	$z$	$E_i$	$E_i$
(1)	(2)	(3)	(4)	(5)	(6)	(7)	(8)	(9)	(10)	(11)
0.0	0.3	-0.29	1	-1.56	2.42	0.041	-0.959	-1.739	-5.73	-1.31
2.4	0.9	1.54	2	-0.29	0.08	0.107	-0.893	-1.243	-4.09	-0.27
5.0	2.1	2.94	3	0.00	0.00	0.172	-0.828	-0.948	-3.12	0.35
7.7	4.2	3.50	4	0.25	0.06	0.238	-0.762	-0.713	-2.35	0.85
11.5	7.7	3.80	5	1.54	2.38	0.303	-0.697	-0.516	-1.70	1.26
17.0	13.1	3.95	6	1.87	3.48	0.369	-0.631	-0.335	-1.10	1.64
25.1	20.6	4.58	7	2.18	4.77	0.434	-0.566	-0.168	-0.55	1.99
35.2	30.2	5.02	8	2.37	5.63	0.500		0	0	2.34
46.5	41.5	5.01	9	2.94	8.64	0.566		0.168	0.55	2.70
56.2	53.9	2.37	10	3.50	12.28	0.631		0.335	1.10	3.05
68.1	66.2	1.87	11	3.80	14.41	0.697		0.516	1.70	3.43
79.8	77.6	2.18	12	3.95	15.57	0.762		0.713	2.35	3.84
87.4	87.2	0.25	13	4.58	21.01	0.828		0.948	3.12	4.34
93.1	94.7	-1.56	14	5.01	25.12	0.893		1.243	4.09	4.96
100.0	100.0	<u>0.00</u>	15	5.02	<u>25.17</u>	0.959		1.739	5.73	6.00
		35.17			<u>141.02</u>					

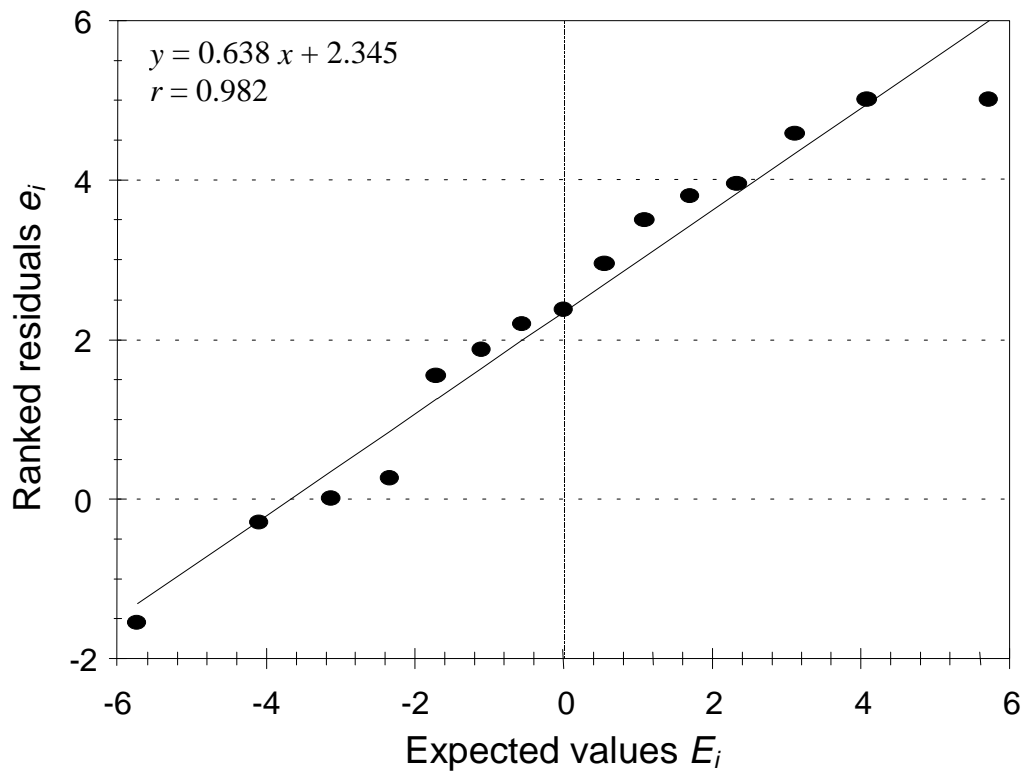


Fig. 2.16: Normal probability plot of ranked residuals versus their expected values under normality. The example particle size-distribution listed in Table 2.3 and shown in Fig. 2.12 is used for the computation.

As  $r$  becomes  $<$  than 1, the distribution departs from normality. Looney and Gullledge (1985) provide table values of  $r$  that need to be exceeded to assume near-normality for different levels of significance (Table 2.6) and number of data points used for the regression (i.e., the number of size classes  $k$ ). An  $r$ -value larger than 0.989 for  $k = 15$  indicates that the null hypothesis of normality is not rejected in 90 out of 100 cases, and not rejected in 10 out of 100 cases if  $r$  is larger than 0.951. Neter et al. (1990) suggest that departure from normality is not substantial if  $r$  exceeds the critical values for  $\alpha = 0.05$ . For  $k = 15$  this means that even if normality were true, an  $r$  as small as 0.939 would only occur in 5% of all cases. The example particle size-distribution from Table 2.3 and Fig. 2.12 obtained an  $r = 0.982$  in the probability plot (Fig. 2.16). This means that in about 70 out of 100 cases, the null hypothesis of normality is not rejected and near-normality may be correctly assumed for that particle size-distribution.

Table 2.6: Critical values for a coefficient of correlation between ordered residuals  $e_i$  and expected residual values under normality  $E_i$  when the distribution of error terms is normal (excerpt of table from: Looney and Gullledge 1985).

Number of size classes						Number of size classes					
$k$	Level of significance $\alpha$					$k$	Level of significance $\alpha$				
	0.90	0.75	0.50	0.10	0.05		0.90	0.75	0.50	0.10	0.05
5	0.988	0.977	0.960	0.903	0.880	16	0.989	0.985	0.978	0.953	0.941
6	0.986	0.977	0.962	0.910	0.888	17	0.990	0.986	0.979	0.954	0.944
7	0.986	0.978	0.964	0.918	0.898	18	0.990	0.986	0.979	0.957	0.946
8	0.986	0.978	0.966	0.924	0.906	19	0.990	0.987	0.980	0.958	0.949
9	0.986	0.980	0.968	0.930	0.912	20	0.991	0.987	0.981	0.960	0.951
10	0.987	0.980	0.970	0.934	0.918	25	0.992	0.989	0.984	0.966	0.959
11	0.987	0.981	0.972	0.938	0.923	30	0.993	0.990	0.986	0.971	0.964
12	0.988	0.982	0.973	0.942	0.928	40	0.994	0.992	0.989	0.977	0.972
13	0.988	0.983	0.974	0.945	0.932	50	0.995	0.993	0.990	0.981	0.977
14	0.989	0.984	0.976	0.948	0.935	75	0.996	0.995	0.993	0.987	0.984
15	0.989	0.984	0.977	0.951	0.939	100	0.997	0.996	0.993	0.989	0.987

### ***D'Agostino test for normality and lognormality***

One of the standard tests for normality and lognormality that is applicable to sample sizes between 50 and 1,000 is the D'Agostino test. The D'Agostino test compares the value of the test statistic  $Y$  with a table value to accept or reject the null hypothesis that a distribution is normal. If data used in this test are log-transformed, the  $Y$  statistic can likewise be used to test for lognormality. Gilbert (1987) prefers this test over the Kolmogorov-Smirnov test because the latter is invalid if the parameters of the hypothesized distribution are estimated from the data set itself.

The D'Agostino test ranks the data from smallest to largest. Hence, the test can be used for pebble-count data. In the ranked list, the smallest particle size is listed as many times as the number of particles found in that size class, then the next larger size class is listed

as many times as the number of particles found in that size class, and so on. The  $D$  statistic is computed from

$$D = \frac{\sum_{i=1}^n (i - 0.5(n + 1)) \phi_i}{n^2 \cdot s} \quad (2.28)$$

and should be determined to the 5<sup>th</sup> decimal.  $s$  is the standard deviation and is computed from:

$$s = \sqrt{\frac{1}{n-1} \sum_{i=1}^n (\phi_i - \phi_m)^2} \quad (2.29)$$

where  $\phi_m$  is the distribution mean, and  $i$  is the ranked order of the data, starting with 1 for the smallest datum, and reaching  $n$  for the largest datum. The test statistic  $Y$  is computed from:

$$Y = \frac{D - 0.28209479}{0.02998598 \sqrt{n}} \quad (2.30)$$

The null hypothesis of a normal distribution is rejected at the significance level of  $\alpha = 0.05$  if the test statistic  $Y$  is less than  $Y_{\alpha/2}$ , or greater than  $Y_{1-\alpha/2}$ . The quantiles for  $\alpha/2 = 0.025$ , and  $1-\alpha/2 = 0.975$  are listed for various sample sizes in Table 2.7. The easiest way to obtain quantiles for sample sizes not listed is by interpolation between listed sample sizes. If higher accuracy is required, the quantiles for unlisted  $n$  can be predicted from a regression analysis of the quantiles for  $\alpha/2$  and  $1-\alpha/2$  versus  $n$ .

Table 2.7: Quantiles of D'Agostino's test for normality for  $\alpha/2 = 0.025$ , and  $1-\alpha/2 = 0.975$  for  $100 < n < 500$  (abbreviated from Table A8 in Gilbert 1987, p. 262).

$n$	100	150	200	250	300	350	400	450	500
$\alpha/2$	-2.552	-2.452	-2.391	-2.348	-2.316	-2.291	-2.270	-2.253	-2.239
$1-\alpha/2$	1.303	1.423	1.496	1.545	1.528	1.610	1.633	1.652	1.668

### 2.1.5 Computation of particle distribution parameters

Particle-size distributions are commonly characterized by four distribution parameters:

- *mean*, which characterizes the central part of the distribution;
- *sorting* (i.e. *standard deviation*), or width of the distribution, which is the range of particle sizes within which a preset percentage of all data are contained;
- *skewness*, which is a measure of deviation from symmetry of a distribution; and
- *kurtosis*, which is the flatness or peakedness of the distribution.

Particle distribution-parameters were designed during the 1930's to 1950's. Apart from serving as a means for general sediment classification, ratios of various particle distribution-parameters (e.g., mean versus sorting, or sorting versus skewness) can be used to distinguish between sediments of different origins, transport modes, and the duration or distance of transport.

The literature offers a variety of possibilities for computing distribution parameters. Distribution parameters can be computed using percentiles (graphic approaches), or the percentage frequency of a distribution (frequency approaches), and both methods can be applied to particle sizes in mm (geometric approaches), or to particle sizes in  $\phi$ -units (arithmetic approaches) (Fig. 2.17). The particulars of the data sets (especially the accuracy of the distribution tails), the number of data sets to be analyzed, and the study objective play a role in the decision of which method should be used.

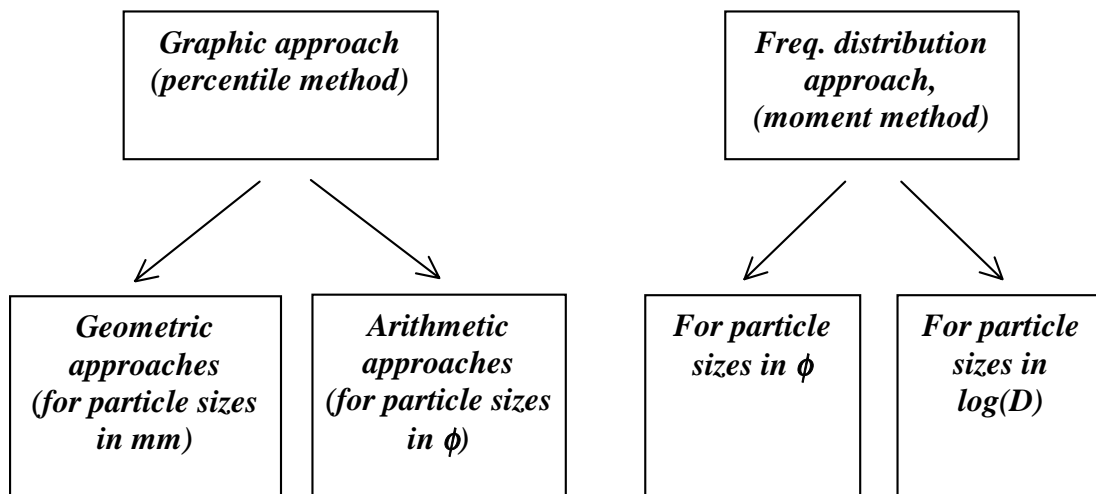


Fig. 2.17: Methods for computing particle-size distribution parameters and their applicability to particle size classes  $D$  in mm or  $\phi$ -units

Some of the methods provide identical or very similar results when applied to the same data set, whereas results from other methods may be somewhat different or not even comparable. Thus, some methods can be used interchangeably, but others cannot.

An overview of the most common approaches to compute the four distribution parameters *mean*, *sorting*, *skewness*, and *kurtosis* is provided in Table 2.8. General differences between approaches are explained in the first part of this section. Possible methods used to compute distribution parameters are discussed in the remainder of this section. Finally, all distribution parameters are computed for the example particle-size distribution shown in Table 2.3 and Fig. 2.12, and results of these computations are compared in Table 2.14.

#### 2.1.5.1 Graphic, or percentile methods (geometric and arithmetic)

Graphic methods compute distribution parameters from a few percentile values that are obtained from a cumulative particle-size frequency distribution. Traditionally, graphic methods required a plotted cumulative frequency distribution, preferably on probability paper, so that the percentiles used for the analysis could be easily read from the graph. This is still a viable, though tedious, procedure. For a computerized analysis, percentile values can be obtained from linear interpolation between the percentile values recorded for adjacent  $\phi$ -size classes on the cumulative frequency distribution, or from linear interpolation between log-transformed mm sizes (Section 2.1.4.2). This interpolation requires some time-consuming cell-by-cell computation in spreadsheet programs, so that obtaining the percentile values continues to remain the most laborious part of computing distribution parameters by graphic methods. Once the necessary percentile values are interpolated, distribution parameters can be easily computed from a variety of equations. Equations for the same distribution parameter can employ a different range and number of percentiles, and use percentiles either in  $\phi$ -units or in mm.

#### ***Percentiles in $\phi$ -units for arithmetic approaches and mm-units for geometric approaches***

The four distribution parameters: mean, sorting, skewness, and kurtosis, have the most informative value when applied to distributions that are near-normal, or almost Gaussian distributed (see Section 2.1.4.3 for analysis of distribution types). Particle-size distributions in gravel-bed rivers tend to resemble normal distributions when computed in  $\phi$ -units. The degree of normality reached is usually sufficient to compute distribution parameters, although normality may not be obtained in a strict statistical sense. Thus, arithmetic computations of particle-size distribution parameters (Folk and Ward 1957; Inman 1952) are always performed in  $\phi$ -units. A geometric approach is required if computations are preferred in mm-units, because geometric approaches compensate for the absent log transformation of particle sizes. Thus, the first step in a particle-distribution analysis is to evaluate whether the sample distribution approaches a normal, or a lognormal distribution. If the distribution is normal in  $\phi$ -units (or lognormal in mm), a graphic arithmetic approach in  $\phi$ -units, the moment method in  $\phi$ -units, or a geometric approach in mm should be used. If the distribution is normal in mm, which is less likely, mm should be used in a graphic arithmetic approach or the moment method (Fig. 2.17).

Table 2.8: Various methods for computing the distribution parameters mean, sorting, skewness, and kurtosis.

Distribution parameter	Graphic methods		Moment Method
	Geometric approaches	Mixed approach	
$n^{\text{th}}$ root computation	Particle sizes in mm	Particle sizes in $\phi$ -units	Folk & Ward (1957)
	Log computation	Trask (1932)	
Mean (central value)	Root of percentile product	Arithmetic mean of 2 or more percentiles	1st. Moment
	$\sqrt{D_{16} \cdot D_{84}}$	$\frac{D_{25} + D_{75}}{2}$	
Sorting (standard deviation)	Log of percentile ratio	Standard deviation	2nd. Moment
	$\sqrt{\frac{D_{84}}{D_{16}}}$	$\frac{\phi_{84} - \phi_{16}}{2} = \sigma_{\phi}$	
Skewness (symmetry)	Root of percentile ratio	Root of percentile ratio	Weighted percentile difference
	$\sqrt{\frac{D_{84}}{D_{75} \cdot D_{25}}}$	$\sqrt{\frac{D_{25}}{D_{75}}}$	
Skewness (symmetry)	Mean/Sorting (Friedle Index)	Mean/Mean	Mean-Median/Sorting + Mean-Median/Sorting
	$\sqrt{\frac{D_{16} \cdot D_{84}}{D_{75} \cdot D_{25}}}$	$\frac{D_{25} \cdot D_{75}}{D_{50}^2}$	
Kurtosis (peakedness)	theoret.: Sorting/Sorting	Mean-Sorting/Sorting	4th. Moment
	$\sqrt{\frac{D_{16}/D_{84}}{D_{75}/D_{25}}}$	$\frac{0.5 (\phi_{95} - \phi_5) - \sigma_{\phi}}{\sigma_{\phi}}$	
	theoret.: Sorting/Sorting	Sorting/Sorting	$\frac{\sum m_i (\phi_{ci} - \phi_m)^4}{n \cdot \sigma^4}$
			$\frac{\sum m_i (\phi_{ci} - \phi_m)^3}{n \cdot \sigma^3}$
			$\frac{\sum m_i (\phi_{ci} - \phi_m)^2}{n - 1}$
			$\frac{\phi_{16} + \phi_{50} + \phi_{84}}{3}$
			$\frac{\phi_{84} + \phi_{50} + \phi_{84}}{3}$
			$\frac{\phi_{16} + \phi_{84}}{2} = \phi_m$
			$\frac{\phi_{84} - \phi_{16}}{4} + \frac{\phi_{95} - \phi_5}{6.6}$
			$\frac{\phi_{84} - \phi_{16}}{2} = \sigma_{\phi}$
			$\frac{\phi_{16} + \phi_{84} - 2\phi_{50}}{2(\phi_{84} - \phi_{16})} + \frac{\phi_5 - 2\phi_{50}}{2(\phi_{95} - \phi_5)}$
			$\frac{\phi_{95} - \phi_5}{2.44 (\phi_{75} - \phi_{25})}$
			$\frac{D_{25} - D_{25}}{2(D_{90} - D_{10})}$
			$\frac{D_{16}/D_{84}}{D_{75}/D_{25}}$
			$\frac{\log(D_{16}/D_{84})}{\log(D_{75}/D_{25})}$
			$\frac{\log(D_{16} \cdot D_{84})}{\log(D_{75}/D_{25})}$
			$\frac{D_{25} \cdot D_{75}}{D_{50}^2}$
			$\frac{\phi_m - \phi_{50}}{\sigma_{\phi}}$
			$\frac{\phi_{16} + \phi_{84} - 2\phi_{50}}{2(\phi_{84} - \phi_{16})} + \frac{\phi_5 + \phi_{95} - 2\phi_{50}}{2(\phi_{95} - \phi_5)}$
			$\frac{\phi_{95} - \phi_5}{2.44 (\phi_{75} - \phi_{25})}$

The difference between arithmetic and geometric approaches can best be explained for the parameter “mean”. An arithmetic progression is a series of numbers in which the difference between each number and its predecessor is identical: for example, the series 2, 4, 6, 8, or the series 9, 7.5, 6, 4.5. The arithmetic mean is the sum of  $n$  terms divided by  $n$ . In a geometric progression, each term differs from its predecessor by the same factor (or multiplier) (Table 2.9), for example 2, 4, 8, 16 or -8, -2, -0.5, -0.125. The geometric mean is defined as the central term of an odd number of consecutive terms in a geometric progression. If the number of terms is even, or when the geometric progression is not known, the geometric mean is computed from the  $n$ th root of the product of  $n$  numbers (Table 2.9). An alternative to the  $n$ th root approach is the logarithmic approach, which

Table 2.9: Examples of geometric progressions with a central term, and computation of the geometric mean using the  $n$ th root, and the logarithmic approach.

Geometric progression	Ratio $t_3 : t_2 = t_2 : t_1 = \text{const.}$	Geometric mean		
		Central term	$n$ th root approach	Logarithmic approach
4, 6, 9	1.5	6	$\sqrt[3]{4 \cdot 6 \cdot 9} = 6$	$\frac{\log(4 \cdot 6 \cdot 9)}{3} = 0.78 = \log 6$
$2, 1, \frac{1}{2}, \frac{1}{4}, \frac{1}{8}$	-0.5	$\frac{1}{2}$	$\sqrt[5]{2 \cdot 1 \cdot \frac{1}{2} \cdot \frac{1}{4} \cdot \frac{1}{8}} = 0.5$	$\frac{\log(2 \cdot 1 \cdot \frac{1}{2} \cdot \frac{1}{4} \cdot \frac{1}{8})}{5} = -0.30 = \log 0.5$
$3, 3^2, 3^3$	3	$3^2$	$\sqrt[3]{3 \cdot 3^2 \cdot 3^3} = 9$	$\frac{\log(3 \cdot 3^2 \cdot 3^3)}{3} = 0.95 = \log 9$

does not require computing the  $n$ th root. This is an advantage when a calculator does not feature the  $y^x$  command. The numerical result of the geometric mean from the logarithmic approach is identical to the log of the geometric mean computed by the  $n$ th root approach.

Graphic approaches to particle distribution-parameters compute the mean from two or three percentiles. If the arithmetic mean from percentiles in  $\phi$ -units is transformed into mm-units, the result is identical to the geometric mean from the  $n$ th-root approach computed from the same percentiles in mm, and to the antilog of the mean from the geometric log approach.

### ***Number and range of percentiles used***

To compute the four distribution parameters, Inman (1952), and Folk and Ward (1957) used five different percentiles in  $\phi$ -units:  $\phi_{50}$  (the median),  $\phi_{16}$  and  $\phi_{84}$  (the percentiles at the points of curvature of a Gaussian distribution, approximately the data range of  $\pm$  one standard deviation around the mean), and  $\phi_5$  and  $\phi_{95}$  (two percentiles that characterize the tails of the distribution, the data range of approximately  $\pm$  two standard deviations around

the median). In Gaussian distributions, the particle sizes of those five percentiles are almost evenly-spaced over the particle-size range. Geometric approaches are commonly based on four percentiles:  $D_{16}$  and  $D_{84}$  (the percentiles at the point of curvature), and  $D_{25}$  and  $D_{75}$  (the two quartiles). Trask's (1932) mixed approach uses only the three quartiles  $D_{25}$ ,  $D_{50}$ , and  $D_{75}$ .

Statistical analyses are more powerful and informative when data from the entire particle-size range are included, but this holds true only if the accuracy of data is sufficiently high over the entire data range. Distribution tails are prone to sampling errors in samples from gravel-bed rivers. Small sample sizes in which the presence of a large particle accounts for 5 - 10% or more of the total sample weight cause errors at the coarse end. Operator bias against fines in pebble counts, or disregard for the spatial variability of fines within the sampling area, cause uncertainty at the fine end. If there is considerable doubt regarding the accuracy of the distribution tails, peripheral percentiles from the distribution tails should be excluded from the analysis. If the study focuses on the central tendency, the analysis should be limited to the central part of the distribution.

The accuracy of distribution parameters is increased when many percentiles are used for analysis. Up to 7 or 10 percentiles might be used, but eventually there is a trade off between the effort required for interpolating percentiles and the information gained by using a large number of percentiles. A set of 3 to 5 percentile values usually suffices when computing distribution parameters with the goal of describing and identifying a particle size-distribution. When the study objective is to detect minuscule differences between samples, more than 5 percentiles might have to be used. However, the most important factor for the ability of detecting small differences between samples is the necessity of obtaining a sufficiently large sample size (Section 5).

#### 2.1.5.2 Moment, or frequency distribution method

The frequency distribution method, also called the moment method, uses the absolute or percentage frequency of each particle size-class to compute the four moments that are related to the four distribution parameters. Computations are usually performed in  $\phi$ -units, because particle size-distributions tend to resemble a Gaussian distribution when computed in  $\phi$ , but using log-transformed particle-size classes in mm for the analysis (i.e.,  $\log D$ ) would work as well.

The moment method requires that the percentage or absolute frequency for all particle-size classes is known, including the fine and the coarse tail, and that size classes are equidistant (e.g., 0.5  $\phi$  size classes). An unsieved remainder, such as the contents of the pan, or the particle-size category "smaller than 2 mm" cannot be included in the analysis unless this sediment is further differentiated into discrete sieve classes. This measure truncates a sample at the fine end. Similarly, a sample may have to be truncated at the upper end if the percent frequency contributed by one or two particles in the largest size class is unduly high. Truncation, however, alters the shape of the distribution and thus its percentiles

and all summary statistics computed from it. Truncated samples can only be compared among each other if all samples have been truncated at the same upper and lower size classes.

The advantage of the moment method is that the computations of the distribution parameters can be completely computerized once the data are entered. This is a convenient attribute when dealing with a large number of data sets.

### ***Graphic approaches versus moment method***

Graphic approaches are mathematically easy to compute once the percentiles have been determined. However, determining the percentiles for a larger number of samples is a rather tedious and time consuming effort when applying graphic methods to a large number of samples. Graphic methods have the advantage of being both standardized and flexible. The Folk and Ward (1957) approach in  $\phi$ -units offers a rating scheme that can be used to classify samples, for example as “poorly” or “well” sorted, or “moderately” or “extremely skewed”. Flexibility, by contrast, results from the user’s choice of either focusing on central percentiles or extending the analysis to peripheral ones, depending on the accuracy of the distribution tails or the study objective. Graphic approaches can further be modified with respect to the number of percentiles used, and even by altering the computation itself. However, modifications might provide numerical values that differ from the ones obtained by “standard” approaches. If this is the case, classifications of the degree of sorting or skewness, such as those introduced by Folk and Ward (1957), may not be applicable.

The moment method is most suitable for complete and reliable particle-size frequency distributions because, apart from truncation, the user can determine only the width of particle size-classes (e.g., 0.25, 0.5, or 1  $\phi$ -units). Folk (1966) showed that the moment method overpredicts values of standard deviation if the sediment is only sieved in a few large sieve classes, and the weight midpoint is not equal to the center of class sieve size  $D_c$ . To avoid this problem, moment methods should only be applied to sediment sieved in sufficiently small increments. Particle-size classes of 0.5  $\phi$  should be appropriate for gravel-bed streams with particles ranging between sand and cobbles.

The selection of sieve classes usually needs to be made before sampling, because sieving in smaller size classes requires a larger sample size. Disadvantages of the moment method are the lack of standardized numerical values that distinguish between “poorly” and “moderately” sorted particle size-distributions, or between the degrees of skewness. The moment method is mathematically less straightforward than graphic methods, particularly for the two higher moments representing the parameters skewness and kurtosis. The power expressions of the moment equations need to be solved before they can be applied to grouped data, and the solutions become lengthy for the third and the fourth moment. However, once the solved equations are entered into spreadsheets, computations can be applied to an unlimited number of data sets. The computational rigidity, and the suitability for complete computer processing make the moment method most suitable for analyzing large numbers of samples, that have accurate tails or that can all be truncated at the same upper and lower size classes.

### 2.1.5.3 Central tendency (mode, median, and mean)

The central tendency of a particle-size distribution can be characterized by its mode, its median, and its mean.

#### ***Mode***

The mode is the center of the size class that contains most of the sediment, either in terms of weight frequency or number frequency. The mode can be computed in terms of mm sizes or in  $\phi$ -units. The particle-size distribution shown in Table 2.3 and Fig. 2.12 has its mode in the center of the size class 45.3 to 64 mm, or -5.5 to -6.0  $\phi$ . An analysis of modality determines the number of modes in a distribution. Distributions can be unimodal (one mode), bimodal (two modes), or polymodal (several modes). An irregularity of a frequency distribution in which two non-contiguous size classes have higher weight frequencies than their two neighbors, such as the size classes 45.3 and 22.6 mm in Table 2.3 and Fig. 2.12, does not qualify for bimodality. Bimodality and its computation is explained in Section 2.1.5.9.

#### ***Median***

The median is the center of the cumulative frequency distribution. The median can be computed in terms of mm sizes as  $D_{50}$  or in terms of  $\phi$ -units as  $\phi_{50}$  and is probably the most frequently used parameter in the description of gravel-bed rivers. The distribution in Table 2.3 has a  $D_{50}$  of 32 mm, and a  $\phi_{50}$  of -5.0.

#### ***Mean***

The mean can be considered as the mathematical center of a data set. Means can be computed by a variety of approaches.

Mode, median and mean are equal in symmetrical (unskewed), normally distributed data sets, but not in skewed distributions which, however, are typical of fluvial gravel sediment.

#### ***Graphic arithmetic means***

The arithmetic mean is the  $n$ th fraction of a sum of  $n$  numbers. The graphic arithmetic mean is usually computed from two or three percentiles in  $\phi$ -units that have equal distances from the median. It is assumed that particle sizes approximate a normal or Gaussian distribution when expressed in  $\phi$ -units (Section 2.1.2.2). Computations in  $\phi$ -units are usually carried out to two decimals.

Inman (1952) computes the mean from the 16<sup>th</sup> and the 84<sup>th</sup> percentile in  $\phi$ -units, both of which are equidistant to the median in a normal distribution.

$$\phi_{m,I} = \frac{\phi_{16} + \phi_{84}}{2} \quad (2.31)$$

Trask (1932) used the two quartile values.

$$\phi_{m,T} = \frac{\phi_{25} + \phi_{75}}{2} \quad (2.32)$$

Cumulative distribution curves from unrepresentatively small samples are often jagged and only little accuracy can be placed upon a particular percentile. It is anticipated that these errors tend to cancel each other out if the graphic mean is computed from several percentiles. Thus, Folk and Ward (1957) added the  $\phi_{50}$  as a third datum to the computation.

$$\phi_{m,F\&W} = \frac{\phi_{16} + \phi_{50} + \phi_{84}}{3} \quad (2.33)$$

Briggs (1977, cited after Gordon et al. 1992) extended the computation evenly over the entire data range and used nine percentile values (see also Folk 1966).

$$\phi_{m,B} = \frac{\phi_{10} + \phi_{20} + \phi_{30} + \dots + \phi_{90}}{9} \quad (2.34)$$

At some point, there is a trade-off between increased accuracy due to a large number of percentiles used for the computations and the computational effort of determining percentiles. The moment method is usually more practical if the entire data range is to be included in the analysis.

Computations of  $\phi_{m,I}$ ,  $\phi_{m,F\&W}$ , and  $\phi_{m,B}$  are identical for distributions that are symmetrical and truly normal in terms of  $\phi$ -units. In particle-size distributions skewed towards a tail of fine particles, typical of gravel-bed rivers, the particle size of  $\phi_{m,B}$  is larger than the particle size of  $\phi_{m,F\&W}$  which is larger than the particle size of  $\phi_{m,I}$ .

### ***Graphic geometric mean, square root approach***

The geometric mean is the  $n$ th root of the product of  $n$  numbers. For particle-size distributions, the geometric mean is commonly computed from the square root of two percentiles in mm (Kondolf and Wolman 1993; Yang 1996).

$$D_{gm,sq} = \sqrt{D_{84} \cdot D_{16}} \quad (2.35)$$

***Graphic geometric mean, cube root approach***

Alternatively, the cube root of three percentiles can be taken (Kondolf and Wolman 1993)

$$D_{gm,cu} = (D_{84} \cdot D_{50} \cdot D_{16})^{1/3} \quad (2.36)$$

More percentiles could be used if necessary for the study objective. When applied to the same data set, the graphic geometric mean computed in mm from the square or cube root approach is equivalent to the arithmetic mean computed in  $\phi$ -units, transformed into mm (Eq. 2.5).

***Graphic geometric mean, log approach***

The graphic geometric mean can also be computed from the mathematically more simple log approach. This is an advantage should a calculator not feature the  $y^x$  command.

$$D_{gm,log} = 10^{\left(\frac{\log(D_{16} \cdot D_{84})}{2}\right)} \quad (2.37)$$

This geometric mean is equivalent to the geometric mean computed with the square root approach in Eq. 2.35.

***Geometric mean from a frequency distribution (power approach)***

A geometric mean can also be computed from a particle-size frequency-distribution instead of percentiles. This approach ensures that the mean represents the entire particle-size distribution and does not rely only on a few percentiles. Another advantage is that this computation can be fully computerized and does not require the time consuming task of determining percentiles. Platts et al. (1983) suggest the following equation:

$$D_{gm,pw} = (D_{c1}^{m\%_1} \cdot D_{c2}^{m\%_2} \cdot \dots \cdot D_{ck}^{m\%_k})^{1/100} \quad (2.38)$$

where  $D_{c1}$  to  $D_{ck}$  are the centers of the particle-size classes 1 to  $k$ ,  $k$  is the number of size classes, and  $m\%_i$  is the percentage particle weight for the  $i$ th size class. The computations can likewise be performed for number frequencies, in which case  $m\%_i$  is substituted by  $n\%_i$ .  $D_{gm,pw}$  yields the same result as the mm-transformed mean obtained from the 1st moment method based on  $\phi$ -units.

***The first moment (arithmetic mean from a frequency distribution)***

Moment methods use all particle size-classes present and compute the arithmetic mean  $\phi_{m,frq}$  of a frequency distributions from

$$\phi_{m,frq} = \frac{1}{m_{tot}} \sum_{i=1}^n (\phi_{ci} \cdot m_i) \quad (2.39)$$

where  $\phi_{ci}$  is the center of the  $i$ th size class in  $\phi$ -units (Section 2.1.5.2),  $m_i$  is the weight of particles retained on the  $i$ th size class sieve, and  $m_{tot}$  is the total weight of particles per sample. For computation using number frequencies,  $m_i$  is substituted by  $n_i$ , the number of particles per size class, and  $m_{tot}$  by  $n$ , the total number of particles per sample. For percentage frequency distributions, the equation becomes

$$\phi_{m,frq} = \frac{1}{100} \sum_{i=1}^k (\phi_{ci} \cdot m_{\%i}) \quad (2.40)$$

where  $m_{\%i}$  is the percentage frequency by weight for particles retained on the  $i$ th size class, and  $k$  is the number of particle size-classes in the sample. For computations based on frequency by number,  $m_{\%i}$  is substituted by  $n_{\%i}$ .

***Mean in mm from a log frequency distribution (log frequency approach)***

In analogy to the arithmetic mean computed from the first moment, the mean particle size in mm  $D_m$  can also be computed from the antilog of log-transformed particle size classes in mm ( $\log D$ ) (Gordon et al. 1992)

$$D_{m,logfrq} = 10 \left( \frac{1}{100} \sum_{i=1}^k \{ \log(D_{ci}) \cdot m_{\%i} \} \right) \quad (2.41)$$

where  $D_{ci}$  is the center of class of the size classes 1 to  $k$ , and  $m_{\%i}$  is the percentage by weight for the  $i$ th size class. Alternatively,  $n_{\%i}$ , the percent frequency by number can be used instead of  $m_{\%i}$ . Results of this computation are equal to the power approach in Eq. 2.38 and equal to the arithmetic mean computed by the 1st moment in equation 2.40.

**2.1.5.4 Standard deviation and sorting**

The standard deviation ( $\sigma$ ) expresses the spread or dispersion within normally distributed data sets. Plus and minus one standard deviation ( $\sigma = \pm 1$ ) comprises the central part of

the cumulative frequency distribution that contains 68.26% of all data. Thus, one standard deviation encompasses all data within the interval of the 16<sup>th</sup> percentile ( $p_{16}$ ) and the 50<sup>th</sup> percentile ( $p_{50}$ ) because

$$p_{16\%} = 50\% - \frac{68.26\%}{2} = 50\% - 34.13\% = 15.86\% \approx 16\% \quad (2.42)$$

plus all the data between the 50<sup>th</sup> and the 84<sup>th</sup> percentile ( $p_{84}$ ) because

$$p_{84\%} = 50\% + \frac{68.26\%}{2} = 50\% + 34.13\% = 84.13\% \approx 84\% \quad (2.43)$$

Thus, the interval between the 84<sup>th</sup> and 16<sup>th</sup> percentile ( $p_{84}$  and  $p_{16}$ ) indicates the range of the mode  $\mu \pm 1$  standard deviation ( $(\mu - 1\sigma) + (\mu + 1\sigma)$ ). A distribution has a standard deviation of  $\sigma = \pm 1$  if

$$\sigma = p_{50} - p_{15.86} = 1 \quad \text{and} \quad \sigma = p_{84.13} - p_{50} = 1 \quad (2.44)$$

In symmetrical distributions, Eq. 2.44 is equal to

$$\sigma = \frac{p_{84.13} - p_{15.86}}{2} = 1 \quad (2.44a)$$

Plus and minus two standard deviations ( $\pm 2\sigma$ ) encompass 95.44% of all data, i.e., the data between the 97.72<sup>th</sup> and 2.28<sup>th</sup> percentile. A distribution has a standard deviation of  $\sigma = \pm 2$  if

$$2\sigma = \frac{p_{97.72\%} - p_{2.28\%}}{2} = 2 \quad (2.45)$$

The computation of standard deviation can become somewhat complicated for grouped data (see computation of the second moment, Eqs. 2.56 to 2.58). Therefore, sedimentologists analyze the spread or dispersion of a distribution from a sorting coefficient that is computed from a few percentiles of the distribution. The terms sorting coefficient and standard deviation are synonymous for normal distributions, and

their numerical value is identical if the distribution is truly normal. The numerical values of sorting coefficients computed for particle-size distributions in  $\phi$  units have been standardized to compare the spread or dispersion between distributions.

The sorting of a particle-size distribution can be computed in several ways. Some approaches yield identical values, some obtain identity after a transformation, while others are non-comparable. This makes it necessary to analyze the relation between different sorting coefficients.

### ***Graphic arithmetic sorting coefficients***

Particle-size distributions of fluvial sediment tend to roughly approximate normal distributions when particle sizes are expressed in  $\phi$ -sizes. In accordance to Eq. 2.44a, Inman's (1952) sorting coefficient  $s_I$  uses almost the same percentile difference, but  $s_I$  is always positive since it is the *absolute* difference, whereas the standard deviation is defined as the interval of  $\pm s$  around the mean.

$$s_I = \left| \frac{\phi_{84} - \phi_{16}}{2} \right| \quad (2.46)$$

As Inman's sorting coefficient uses two percentiles only, particle-size distributions that are quite different can have the same sorting coefficient if only those two percentiles are identical. Folk and Ward (1957) therefore include a broader range of the cumulative size-distribution curve into the sorting analysis and compute sorting as

$$s_{F\&W} = \frac{\phi_{84} - \phi_{16}}{4} + \frac{\phi_{95} - \phi_5}{6.6} \quad (2.47)$$

Folk and Ward (1957) classify the degree of sorting of fluvial sediment into 7 categories (Table 2.10). A chart for visual estimation of sorting is provided in Fig. 2.18.

The two sorting coefficients  $s_I$  and  $s_{F\&W}$  have identical results when applied to symmetrical normal distributions, although equality may not be present if the distribution is not strictly normal or somewhat skewed. However, fluvial gravel deposits that approach normal distributions in  $\phi$ -units and are only slightly asymmetrical, and which are "poorly" sorted in terms of Folk and Ward (1957), have an Inman (1952) sorting coefficient around 1.5 as well.

Table 2.10: Classification of the degree of sorting (from Folk and Ward 1957)

Sorting Coefficient	Characterization
> 4	extremely poor
2 - 4	very poor
1 - 2	poor
0.71 - 1	moderate
0.50 - 0.71	moderately well
0.35 - 0.5	well
< 0.35	very well

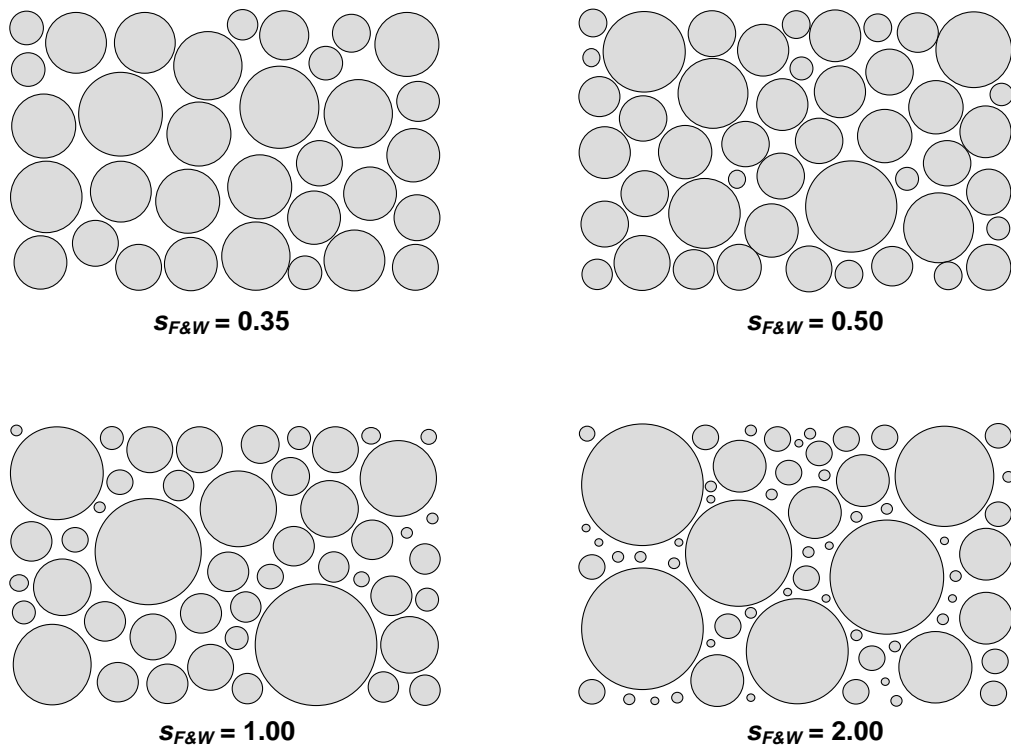


Fig. 2.18: A chart for visual estimation of sediment sorting for the same  $D_{50}$  (Redrawn from Pettijohn et al. (1972), by permission of Springer Verlag).

$\phi$ -based sorting coefficients for fluvial gravel typically range between about 0.5 and 2. Fig. 2.19 shows three example particle-size distributions with a common  $D_{50}$  of 32 mm, but with three different sorting coefficients of  $s = 0.5, 1.0,$  and  $1.5$ . Particle sizes in uncoupled gravel-bed streams might obtain a sorting coefficient of about 0.5 after a long

fluvial transport. Mountain gravel-bed streams with grain sizes ranging from sand to boulders more typically have sorting coefficients in the range of 1.5 to 2.

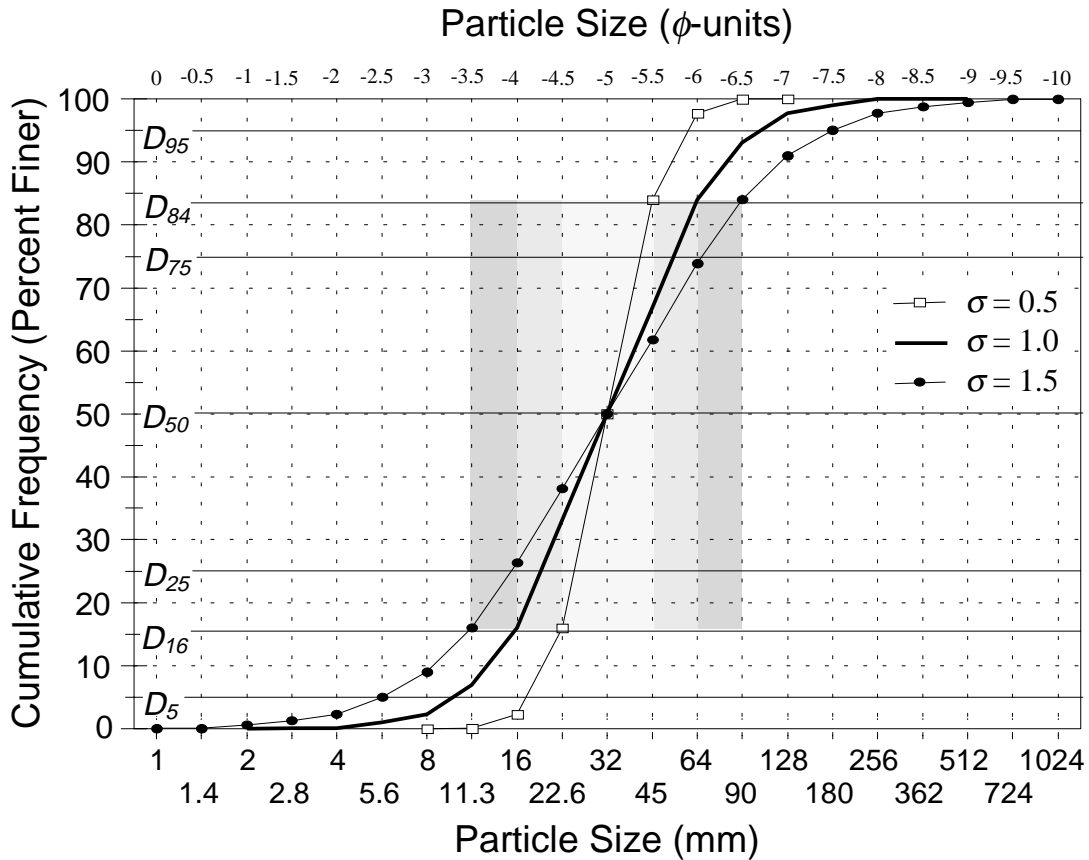


Fig. 2.19: Three particle-size distributions with a common  $D_{50}$  of 32 mm, but standard deviations of  $\sigma = 0.5$ , 1.0, and 1.5. For the curve with  $\sigma = 0.5$ , the range of one standard deviation between  $D_{16}$  and  $D_{84}$  is indicated by the lightest gray shade, for the curves with  $\sigma = 1$ , and  $\sigma = 1.5$ , the ranges of one standard deviation are indicated by the medium, and the darkest gray shade, respectively.

### ***Graphic geometric sorting coefficients, log approach***

Analogous to the standard deviation of particle sizes in  $\phi$ -units in a normal distribution where  $2s = \phi_{84} - \phi_{16}$ , and  $s = (\phi_{84} - \phi_{16})/2$ , the standard deviation of a lognormal distribution for particle sizes in mm can be expressed as (Simons and Sentürk 1992)

$$\log s = \frac{\log D_{84} - \log D_{16}}{2} = \frac{\log \left( \frac{D_{84}}{D_{16}} \right)}{2} \quad (2.48)$$

The geometric sorting coefficient  $s_{g,log}$  can be computed for percentiles in mm by taking the antilog of Eq. 2.48 which yields the same numerical results as the square root expression in Eq. 2.53.

$$s_{g,log1} = 10^{\left(\frac{\log(D_{84}) - \log(D_{16})}{2}\right)} = 10^{\left(\frac{\log\left(\frac{D_{84}}{D_{16}}\right)}{2}\right)} \quad (2.49)$$

Since the term in parenthesis in the first equation is the log of the arithmetic Inman sorting coefficient  $s_I = (\phi_{84} - \phi_{16})/2$ , results computed by  $s_{g,log1}$  and  $s_I$  are convertible. By analogy to Eqs. 2.4 and 2.3,

$$s_{g,log1} = 2^{s_I} \quad (2.50)$$

and

$$s_I = \frac{\log(s_{g,log1})}{\log(2)} \quad (2.51)$$

The log approach for a geometric sorting coefficient can include the  $D_{50}$  value, so that Eq. 2.49 can be rewritten as:

$$s_{g,log2} = 10^{\left(\log\left(\frac{\left(\frac{D_{84}}{D_{50}} + \frac{D_{50}}{D_{16}}\right)}{2}\right)\right)} \quad (2.52)$$

Eq. 2.49 and Eq. 2.52 yield identical results if distributions are symmetrical. When applied to the distribution in Table 2.3, Eq. 2.49 provides a numerical value of 3.84 which is similar but not identical to the numerical value of 3.88 provided by Eq. 2.52 for the same data set. Eq. 2.52 can be simplified by eliminating the log and the antilog. This measure yields the gradation coefficient.

### ***Gradation coefficient***

The gradation coefficient is a term used in engineering. It computes the spread of a distribution from percentiles in mm (Simons and Sentürk 1992; Julien 1995; Yang 1996)

$$s_{grad} = \frac{\left( \frac{D_{84}}{D_{50}} + \frac{D_{50}}{D_{16}} \right)}{2} \quad (2.53)$$

Eq. 2.53 may be seen as a simplified notation of the log approach in Eq. 2.52, yielding the same result. Note the conceptual difference between the terms “sorting” and “gradation” – sedimentologists refer to a sediment that spreads over a wide size range as poorly sorted, while engineers refer to a poorly sorted sediment as well graded, i.e., it has a wide range of particle sizes that is sufficient for a given application.

***Graphic geometric sorting coefficients, square root approach***

Instead of an antilog, the logarithmic expression  $\log s = (\log D_{84} - \log D_{16})/2$  in Eq. 2.48 can also be solved by a square root equation (Simons and Sentürk 1992; Julien 1995; and Yang 1996)

$$s_{g,sq} = \sqrt{\frac{D_{84}}{D_{16}}} \quad (2.54)$$

Eq. 2.54 and 2.48 yield identical results. An equation of similar form but with different percentiles was proposed by Trask (1932)

$$s_{g,T} = \sqrt{\frac{D_{75}}{D_{25}}} \quad (2.55)$$

Results of Eqs. 2.54 and 2.55 are different because they are based on different percentiles.

Graphic geometric sorting coefficients computed from percentiles in mm are dimensionless.

***The second moment (arithmetic sorting from a frequency distribution)***

The general form of the equation for the 2nd moment, i.e., the distribution variance, for grouped (or binned) data is

$$s_{frq}^2 = \frac{1}{n-1} \sum_{i=1}^k n_i (\phi_{ci} - \phi_m)^2 \quad (2.56)$$

where  $\phi_{ci}$  is the center of class in  $\phi$ -units of  $i$ th size class,  $n_i$  is the number of particles retained for the  $i$ th size class,  $k$  is the number of size classes in the sample,  $n$  is the total number of particles, and  $\phi_m$  is the arithmetic mean of the distribution in  $\phi$ -units. Eq. 2.56 can likewise be applied to the weight of particles for the  $i$ th size class, in which case  $n_i$  is substituted by the weight of particles in the  $i$ th size class  $m_i$ . If Eq. 2.56 is applied to percent frequencies,  $n_i$  or  $m_i$  are substituted by  $n_{\%i}$  and  $m_{\%i}$ , respectively, and  $m_{tot}$  or  $n$  are set to 100%.

$$s_{frq}^2 = \frac{1}{100-1} \sum_{i=1}^k n_{\%i} (\phi_{ci} - \phi_m)^2 \quad (2.57)$$

For the actual computation of the sorting parameter, the quadratic expressions in Eq. 2.56 or 2.57 need to be solved and rearranged, and the square root needs to be taken because standard deviation is defined as the square root of variance ( $s \equiv \sqrt{s^2}$ ). Eq. 2.58 is the solution of Eq. 2.56. The solution is similar for Eq. 2.57 for which  $n_i$  is substituted by  $n_{\%i}$ , and  $n = 100$ .

$$s_{frq} = \sqrt{\frac{\sum_{i=1}^k (n_i \cdot \phi_{ci}^2) - \left( \frac{\left( \sum_{i=1}^k n_i \cdot \phi_{ci} \right)^2}{n} \right)}{n-1}} = \sqrt{\frac{\sum_{i=1}^k (n_i \cdot \phi_{ci}^2) - n \cdot \phi_m^2}{n-1}} \quad (2.58)$$

***Conversion between standard deviation of the log-transformed and the original data***

If Eqs. 2.56 to 2.58 were applied to particle sizes in mm (exchange all symbols  $\phi$  for  $D$  in Eq. 2.58 and compute as above), the resulting numerical value  $s_{logfrq}$  has no resemblance to the geometric graphic sorting computed for percentiles in mm (Eqs. 2.49 and 2.52 – 2.54). However, it is possible to compute the graphic arithmetic standard deviation for particle sizes in  $\phi$ -units  $s_\phi$  from the  $s_{logfrq}$  (Eqs. 2.56 to 2.58) using the following equation (Church et al. 1987):

$$s_\phi = c \left[ \ln \left( \left( \frac{s_{logfrq}}{D_{gm}} \right)^2 + 1 \right) \right]^{0.5} \quad (2.59)$$

$D_{gm}$  is the geometric distribution mean, and  $c = 1.4427$  when log-transformations are based on  $\phi$ -units (e.g., equations by Inman), or  $c = 0.4343$  for transformations based on the  $\log_{10}$  of particle sizes, and  $c = 1$  for the  $\ln$  of particle sizes. Using the example distribution in Table 2.3 and Fig. 2.12, the logarithmic standard deviation  $s_{logfrq}$  computed for mm sizes using Eqs. 2.56 to 5.58 is 58.13 mm, the distribution mean  $D_{gm}$  (e.g., from

the square root approach in Eq. 2.35 ) is 27.2 mm. Eq. 2.59 computes a standard deviation of  $s_{\phi} = 1.89$  which is similar to the Inman sorting coefficient of  $s_I = 1.94$  (Eq. 2.31), but lower than the standard deviation computed from the second moment of  $s_{freq} = 2.02$  (Eq. 2.58). Equity of results requires a true normal/lognormal distribution.

The graphic arithmetic sorting coefficients computed for particle sizes in  $\phi$ -units ( $s_I$  or  $s_{F\&W}$ ) yields the same numerical value as the standard deviation  $s_{freq}$  computed using equation 2.56 to 2.58 if both distributions are truly normal, and both results are in units of  $\phi$ . Graphic arithmetic sorting coefficients and the standard deviation computed using Eqs. 2.56 to 2.58 produce similar numerical values if the particle-size distribution is not truly normal.

### 2.1.5.5 Skewness

Normal distributions are symmetric around the mean and not skewed towards either side of the distribution. Distributions with negative skewness are skewed towards the low end tail of the distributions, whereas distributions with positive skewness are skewed towards a high end tail (Fig. 2.20). The degree of skewness of a distribution can be seen as a degree of deviation from normality.

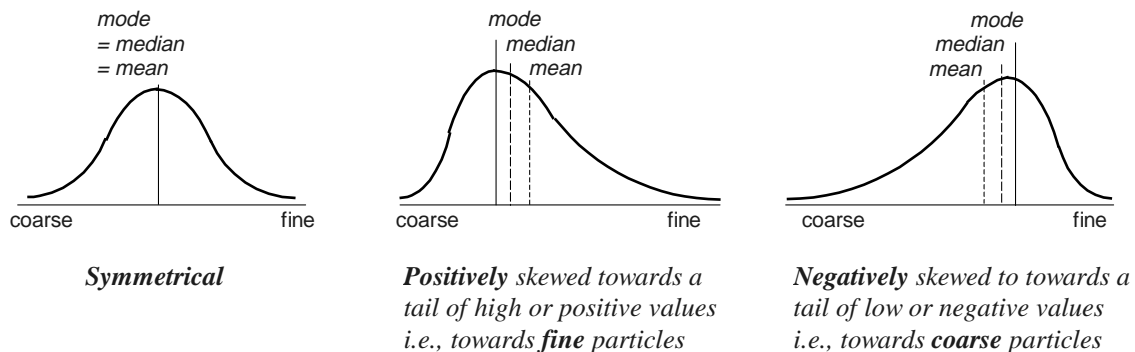


Fig. 2.20: Shape of symmetrical, positively and negatively skewed frequency distributions

When applied to particle-size distributions in  $\phi$ -units, in which the coarsest particles sizes have the smallest numerical values (e.g.,  $-7\phi = 128$  mm,  $-1\phi = 2$  mm,  $+2\phi = 0.25$  mm), the term skewness is reversed: positive skewness is towards a tail of fine particles (high  $\phi$ -values, and negative skewness is towards a tail of coarse particles (low  $\phi$ -values).

Bed-material size distributions in  $\phi$ -units in mountain gravel-bed rivers are often skewed towards a tail of finer gravel and sand (positively skewed), and thus deviate from symmetrical normal distributions. In positively skewed distributions, particle frequency of the largest size classes comprise the bulk of the sample, while finer particles cover a wide

range of sizes, but the frequency per size class is low. Positive skewness of a sample can also be the result of unrepresentative sampling in which a few large clasts comprise 30 to 50% of the total sample weight. When analyzing a particle-size distribution for skewness, samples need to be representative such that the weight of the largest size class does not constitute more than a small percentage of total weight. Church et al. (1987) suggested that the maximum allowable weight of the largest size class was 0.1% of the total weight for  $D_{max} \leq 32$  mm, 1% for  $D_{max} \leq 64$  mm, and 5% for  $D_{max} \leq 128$  mm (Section 5.4.1.1).

Particle-size distributions in  $\phi$ -units that are mostly comprised of sand and fine gravel with a few large gravel particles are skewed towards a coarse tail. Such distributions are negatively skewed.

Skewness may be computed from various modifications of the ratio between distribution mean and sorting. Computations may focus on the central part of the distribution, or include the distribution tails to various degrees. The user should select the computational method that suits the data situation and provides the clearest answer to the study objective. If, for example, little confidence can be placed into the tails of a distribution, they should not be included in the analysis because they might distort the result. However, omitting the tails excludes information that under ideal circumstances should have been included.

### ***Graphic arithmetic skewness***

Graphic arithmetic skewness is computed from several percentiles in  $\phi$ -units. The percentiles need to refer to the percent *coarser* cumulative frequency distribution if positive skewness is to yield positive skewness values and negative skewness negative values. However, the percent *finer* is the more commonly used form of a cumulative frequency distribution for bed-material samples. Thus, if graphic arithmetic skewness is computed from the percent *finer* distribution, skewness values need to be multiplied by -1 to obtain the correct sign.

The computed value for skewness is sensitive to the range of data used for its computation. Inman (1952) computes skewness as the difference between mean and median divided by sorting.

$$sk_{a,II} = \frac{\phi_m - \phi_{50}}{\sigma_\phi} = \frac{\frac{\phi_{16} + \phi_{84}}{2} - \phi_{50}}{\frac{\phi_{84} - \phi_{16}}{2}} = \frac{\phi_{16} + \phi_{84} - 2\phi_{50}}{\phi_{84} - \phi_{16}} \quad (2.60)$$

In order to account for skewness in the distribution tails, Inman (1952) suggested a second computation in which the data range includes the 95<sup>th</sup> and 5<sup>th</sup> percentiles.

$$sk_{a,I2} = \frac{\phi_5 + \phi_{95} - (2 \cdot \phi_{50})}{2 \cdot (\phi_{84} - \phi_{16})} \quad (2.60a)$$

Folk and Ward (1957) combined both of Inman's equations and slightly modified the second one.

$$sk_{a,F+W} = \frac{\phi_{16} + \phi_{84} - (2 \cdot \phi_{50})}{2 \cdot (\phi_{84} - \phi_{16})} + \frac{\phi_5 + \phi_{95} - (2 \cdot \phi_{50})}{2 \cdot (\phi_{95} - \phi_5)} \quad (2.61)$$

Warren (1974) simplified the Folk and Ward equation for skewness into a form that yields a numerical identical result, but is easier to compute.

$$sk_{a,W} = \frac{\phi_{84} - \phi_{50}}{\phi_{84} - \phi_{16}} - \frac{\phi_{50} - \phi_5}{\phi_{95} - \phi_5} \quad (2.61a)$$

The numerical values of skewness computed with Eqs. 2.60 or 2.60a are not identical to those from Eq. 2.61 and 2.61a, but all three equations yield 0 for symmetrical distributions, and -1 and +1 for very negatively and very positively skewed distributions. The Folk and Ward (1957) and the Warren (1974) skewness coefficients can be verbally classified into the following categories (Table 2.11).

Table 2.11: Classification of skewness values (from: Folk and Ward 1957)

Skewness value	Description in terms of:	
	$\phi$ -units	Relative particle size
-0.3 to -1	very negatively skewed	very skewed towards the fine side
-0.1 to -0.3	negatively skewed	skewed towards the fine side
-0.1 to 0.1	nearly symmetrical	nearly symmetrical
0.1 to 0.3	positively skewed	skewed towards the coarse side
0.3 to 1	very positively skewed	very skewed towards the coarse side

Gordon et al. (1992) suggest a computation with a slightly smaller data range, which may be useful when the tails of the distribution are unreliable. Results from Eq. 2.62 and Eqs. 2.61 and 2.61a are not identical.

$$sk_{a,Gor} = \frac{\phi_{84} - \phi_{50}}{\phi_{84} - \phi_{16}} - \frac{\phi_{50} - \phi_{10}}{\phi_{90} - \phi_{10}} \quad (2.62)$$

The quartile skewness coefficient  $sk_{a,quart}$  uses only the central 50 percent of the data and completely neglects the distribution tails.

$$sk_{a,quart} = \frac{(\phi_{75} - \phi_{50}) - (\phi_{50} - \phi_{25})}{\phi_{75} - \phi_{25}} \quad (2.63)$$

Trask (1932) limits his equation to the central 50 percent as well, but uses mm units.

$$sk_{a,T} = \frac{D_{25} \cdot D_{75}}{D_{50}^2} \quad (2.64)$$

***Geometric skewness from the square root approach (Fredle Index)***

As with arithmetic skewness (Eqs. 2.60 – 2.63), geometric skewness is the ratio of the geometric mean to geometric sorting. Recall that the geometric mean and geometric sorting can be computed in a variety of ways. A simple expression for geometric skewness is

$$sk_{g,FI} = \left( \frac{D_{84} \cdot D_{16}}{D_{75}} \right)^{0.5} \cdot \frac{D_{75}}{D_{25}} = \text{Fredle index} \quad (2.65)$$

which is also an expression for the Fredle index that is used by fishery biologists to relate permeability and porosity of spawning gravel (Lotspeich and Everest 1981).

***Geometric skewness from frequency distributions and percentiles***

Platts et al. (1983) compute the Fredle index from:

$$sk_{g,F2} = \frac{(D_{c1}^{m\%_1} \cdot D_{c2}^{m\%_2} \dots D_{ck}^{m\%_k})^{1/100}}{\left( \frac{D_{75}}{D_{25}} \right)} \quad (2.66)$$

The numerator of Eq. 2.66 is identical to the geometric mean computed from frequency distributions (power approach, Eq. 2.38).  $D_{c1}$  to  $D_{ck}$  are the midpoint diameters of particles retained on the  $k$ th sieve class, and  $m_1$  to  $m_k$  are the percentage weight of particles retained on the  $k$ th sieve class. Rice (1995) uses the square root of the denominator, which is the Trask (1932) sorting coefficient (Eq. 2.55).

$$sk_{g,F3} = \frac{(D_{c1}^{m\%_1} \cdot D_{c2}^{m\%_2} \dots D_{ck}^{m\%_k})^{1/100}}{\sqrt{\frac{D_{75}}{D_{25}}}} \quad (2.67)$$

Equations 2.65 and 2.67 yield almost identical results. The Fredle index can only be compared between samples if all size distributions are truncated at a common large particle size, such as at 64 mm (Rice 1995), because the value of this index is affected by the truncation point.

A graphic logarithmic approach to compute skewness is not available. But in analogy to graphic logarithmic mean and sorting, a graphic logarithmic skewness could theoretically be computed from the ratio of mean and sorting

$$sk_{g,log} = \frac{\log(D_{16} \cdot D_{84})}{\log(D_{75}/D_{25})} \quad (2.68)$$

***The third moment (arithmetic skewness from frequency distributions)***

The general form of the equation for the 3rd moment for grouped (binned) data is

$$Sk_{frq} = \frac{\sum_{i=1}^k m_i (\phi_{ci} - \phi_m)^3}{m_{tot} \cdot \sigma^3} \quad (2.69)$$

where  $\phi_{ci}$  is the center of the  $i$ th class,  $\phi_m$  is the distribution mean,  $k$  is the number of classes,  $m_i$  is the particle weight in the  $i$ th class,  $m_{tot}$  is the total weight of particles, and  $\sigma$  is the distribution sorting as computed from the square root of the 2nd moment (see Section 2.1.5.4). Eq. 2.69 needs to be solved before it can be applied to grouped data. Gordon et al. (1992) provide the following solution

$$sk_{frq} = \frac{m_{tot}}{(m_{tot}-1) \cdot (m_{tot}-2)} \cdot \frac{\left( \sum_{i=1}^k \phi_{ci}^3 \cdot m_i \right) - 3\phi_m \left( \sum_{i=1}^k \phi_{ci}^2 \cdot m_i \right) + 2 m_{tot} \cdot \phi_m^3}{s^3} \quad (2.70)$$

Eqs. 2.69 and 2.70 can be applied to number-frequencies of particles as well. In this case,  $m_i$  is substituted by  $n_i$ , the number of particles per size class, and  $m_{tot}$  by  $n$ , the total number of particles per sample. Eqs. 2.69 and 2.70 can also be applied to percent frequencies. In this case,  $m_i$  and  $n_i$  are substituted by  $m_{\%i}$ , and  $m_{\%i}$ , the percentage particle weight and number for the  $i$ th size class, and  $m_{tot}$  and  $n$  are set to 100.

Skewness values computed using the moment method produce positive values for positively skewed distributions, and negative values for negative distributions. However, skewness values from the moment method are not bound to the +1 to -1 interval as is the graphic arithmetic skewness, but may reach values of  $\pm 3$  or  $\pm 4$  or more.

#### 2.1.5.6 Kurtosis

Kurtosis denotes the peakedness or flatness of a distribution in comparison to a normal distribution. This measure is only infrequently used to characterize particle-size distributions in gravel-bed rivers.

##### ***Graphic arithmetic kurtosis***

For particle-size distributions in  $\phi$ -units, Folk and Ward (1957) propose to compute kurtosis using the tails and the quartiles of the distribution.

$$ku_{a,F\&W} = \frac{\phi_{95} - \phi_5}{2.44 \cdot (\phi_{75} - \phi_{25})} \quad (2.71)$$

Kurtosis as computed by the Folk and Ward approach can be verbally classified into five categories (Table 2.12)

Table 2.12: Classification of kurtosis values (from Folk and Ward 1957)

Value	Classification	Explanation
< 0.67	very platykurtic	very flat frequency distribution
0.67 - 0.90	platykurtic	flat
0.90 - 1.11	mesokurtic	not especially peaked, normal
1.11 - 1.50	leptokurtic	highly peaked
> 1.50	very leptokurtic	very highly peaked

The Inman (1952) equation is also based on particle sizes in  $\phi$ -units and focuses on the tails of the distribution

$$ku_{a,I} = \frac{0.5 (\phi_{95} - \phi_5) - \frac{\phi_{84} - \phi_{16}}{2}}{\frac{\phi_{84} - \phi_{16}}{2}} \quad (2.72)$$

When original untransformed particle sizes in mm are used, kurtosis can be computed from the Trask (1932) equation

$$ku_{a,Tr} = \frac{D_{75} - D_{25}}{2 (D_{90} - D_{10})} \quad (2.73)$$

***Graphic geometric kurtosis***

Graphic approaches to compute kurtosis are not available. If kurtosis is regarded as the ratio of two sorting coefficients, kurtosis, in analogy to the square root approach, could hypothetically be computed from

$$ku_{g,sq} = \sqrt{\frac{D_{16}/D_{84}}{D_{75}/D_{25}}} \quad (2.74)$$

Another theoretical computation of kurtosis is analogous to the logarithmic approach

$$ku_{g,log} = \frac{\log (D_{16}/D_{84})}{\log (D_{75}/D_{25})} \quad (2.75)$$

***The fourth moment (arithmetic kurtosis) from frequency distributions***

Kurtosis can also be computed as the fourth moment  $ku_{frq}$ . The general form of the equation is

$$ku_{frq} = \frac{\sum_{i=1}^k m_i (\phi_{ci} - \phi_m)^4}{m_{tot} \cdot \sigma^4} \quad (2.76)$$

where  $\phi_{ci}$  is the center of the  $i$ th class,  $\phi_m$  is the distribution mean,  $k$  is the number of classes,  $m_i$  is the absolute frequency of particle weights or numbers in the  $i$ th class,  $m_{tot}$  is the total weight of particles, and  $\sigma$  is the distribution sorting as computed from the square root of the 2nd moment (see Section 2.1.5.4). Eq. 2.76 can likewise be used for number frequencies ( $m_i \rightarrow n_i$ ;  $m_{tot} \rightarrow n$ ), or for percentage frequencies ( $m_i \rightarrow m_{\%i}$  or  $n_{\%i}$ ;  $m_{tot} \rightarrow 100$ ). Eq. 2.76 becomes rather extensive when solving the term  $m_i (\phi_{ci} - \phi_m)^4$  and will not be shown here since kurtosis is infrequently used to characterize a particle-size distribution.

### 2.1.5.7 Comparison between methods

The four distribution parameters (mean, sorting, skewness and kurtosis) were computed for the example particle-size distribution in Table 2.3 using several methods. The distribution is poorly sorted and skewed towards large particles. The same methods and equations as shown in Table 2.8 were applied. The results of those computations are listed in Table 2.14 for a comparison of methods.

#### **Mean**

Arithmetic and geometric mean are both in units of length and mutually convertible. The arithmetic mean of particle sizes in  $\phi$ -units, converted back into units of mm (Eq. 2.5 or 2.6), equals the geometric mean of particle sizes in mm, if the computations are based on the same percentiles (Table 2.13). Similarly, geometric mean, computed in mm and transformed to  $\phi$ -units using Eq. 2.3 or 2.4 equals the arithmetic mean computed for  $\phi$ -units.

All of the means are smaller than the  $D_{50}$  or  $\phi_{50}$  because the particle-size distribution is skewed towards fine particles. Trask's mean is considerably larger than the distribution  $D_{50}$  in skewed distributions because skewed distributions have a large mm-value of the  $D_{75}$ .

#### **Sorting**

Arithmetic sorting coefficients and the standard deviation computed from the moment approach produce identical values for true normal and symmetrical distributions (Table 2.14). Arithmetic sorting coefficients computed from  $\phi$ -unit for the distribution in Table 2.3 differ somewhat between methods because the distribution is not truly normal, but all values are generally within the same range. Hence, the Inman sorting  $s_I = 1.94$  (Eq. 2.46) and the Folk and Ward sorting  $s_{F\&W} = 1.70$  (Eq. 2.47) are not identical. The difference between  $s_I$  and the 2<sup>nd</sup> moment  $s_{frq} = 2.02$  (Eq. 2.58) may be attributed to truncation of the distribution at the fine end, because the unsieved remainder in the size class smaller than 2 mm was excluded in the moment method, but is included in the computation of percentiles from the cumulative percentage frequency (i.e., the percent finer).

Table 2.13: Equality between various geometric and arithmetic means when computed by different approaches for the same distribution and expressed in the same units. Numbers in parenthesis indicate equation numbers in Section 2.

Geometric mean (computed in mm)	=	Arithmetic mean (comp. in $\phi$ ), expressed in mm		
Geom. mean (computed in mm), expressed in $\phi$	=	Arithmetic mean (computed in $\phi$ )		
Square root appr. (35)	$\sqrt{D_{16} \cdot D_{84}}$	=	Inman appr. (31)	$\frac{\phi_{16} + \phi_{84}}{2}$
Log appr. (37)	$10^{\left(\frac{\log(D_{16} \cdot D_{84})}{2}\right)}$	=	Inman appr. (31)	$\frac{\phi_{16} + \phi_{84}}{2}$
Cube root appr. (36)	$(D_{16} \cdot D_{50} \cdot D_{84})^{1/3}$	=	Folk & Ward appr. (33)	$\frac{\phi_{16} + \phi_{50} + \phi_{84}}{3}$
Power appr. (38)	$(D_{c1}^{m\%1} \cdot D_{c2}^{m\%2} \cdot \dots \cdot D_{ck}^{m\%k})^{1/100}$	=	1 <sup>st</sup> moment (40)	$\frac{1}{100} \sum_{i=1}^k (\phi_{ci} \cdot m_{\%i})$
Log freq. appr. (41)	$10^{\left(\frac{1}{100} \sum_{i=1}^k \{\log(D_{ci}) \cdot m_{\%i}\}\right)}$	=	1 <sup>st</sup> moment (40)	$\frac{1}{100} \sum_{i=1}^k (\phi_{ci} \cdot m_{\%i})$

Table 2.14: Results of distribution parameters computed with several methods for the example particle size-distribution in Table 2.3 (Small numbers in *italics* refer to equation numbers in Section 2).

( $D_5 = 1.8$ ,  $D_{16} = 7.1$ ,  $D_{25} = 12.7$ ,  $D_{50} = 32.0$ ,  $D_{75} = 74.7$ ,  $D_{84} = 104.3$ ,  $D_{95} = 195.8$  mm;  
 $\phi_5 = -0.89$ ,  $\phi_{16} = -2.82$ ,  $\phi_{25} = -3.67$ ,  $\phi_{50} = -5.00$ ,  $\phi_{75} = -6.22$ ,  $\phi_{84} = -6.70$ ,  $\phi_{95} = -7.61$ ).

	Graphic (or percentile) approaches						Freq.distr.appr.		
	Geometric approaches (for mm)			Arithmetic approaches (in $\phi$ )			Inman (1952)	Folk & Ward (1957)	Moment Method*
power appr.	grad. coeff.	square root	log appr.	cube root	Trask (1932)				
Mean ( $\phi$ )	-	-	-	-	-	-	-4.76	-4.84	-4.74
(mm)	26.8	-	27.2	27.2	28.7	43.7	27.2	28.7	26.8
Eq.	38	-	35	37	36	32	31	33	40
Sorting ( $\phi$ )	-	-	-	-	-	-	1.94	1.70	2.02
(mm)	-	-	-	-	-	-	3.84	3.25	4.06
(-)	-	3.88	3.84	3.84	-	2.42	-	-	-
Eq.	-	53	54	49, 52	-	55	46	47	58
Skewness (-)	11.1	-	11.2	3.73	-	19.0	0.12	0.17	0.72
Eq.	66	-	65	68	-	64	60	61	70
Kurtosis (-)	-	-	1.6	1.5	-	0.2	0.7	1.1	-
Eq.	-	-	74	75	-	73	72	71	76

\* Computations for the moment method excluded sediment passing the 2 mm sieve from the analysis.

Geometric sorting coefficients computed from percentiles in mm are dimensionless and only a measure of the logarithmic standard deviation which has units of mm. The square root approach (Eq. 2.54) and the log approach (Eq. 2.49) yield identical results  $s_{g,sq} = s_{g,log} = 3.84$ , which in a true lognormal distribution would be identical to the gradation coefficient  $s_{grad} = 3.88$  (Eq. 2.53) as well. Some of the geometric and arithmetic sorting coefficients are transformable.

The geometric sorting coefficient of the untransformed data in mm  $s_{log,l}$  and Inman's arithmetic sorting coefficient  $s_T$  computed for  $\phi$ -units are convertible using Eqs. 2.51 and 2.52. Similarly, the standard deviation in  $\phi$ -units can be estimated from the standard deviation computed from particle sizes in mm according to the moment method (Eqs. 2.56 – 2.58) by applying Eq. 2.59. The Trask sorting parameter  $s_T$  is not comparable with sorting computed by the other methods because it is based on different percentiles.

The various computations of skewness and kurtosis do not compare well because their computations are too dissimilar.

#### 2.1.5.8 Percent fines

Stream monitoring and fisheries studies are often concerned with the amount of fine sediment (sand and fine gravel) in the streambed because large amounts of fine sediment impair the spawning success of salmonid fish. Depending on the fish species concerned, or on the monitoring objective, fine sediment might comprise medium sand  $< 0.85$  mm, sand  $< 2$  mm, or various sizes of fine gravel  $< 3.36, 4.4, 6.4, \text{ or } 9.5$  mm (Reiser and Bradley 1993; Rice 1995). The amount of fine sediment is usually computed as the cumulative percent frequency finer than a specified particle size and referred to as the “percent fines”. The percent fines is a more sensitive indicator of the amount of fines than the  $D_5$  or  $D_{10}$ , because the size of small percentiles is affected by the coarse part of the distribution.

For a comparison of the percent fines over space or time, Church et al. (1987) recommend that the percent fines be computed for size distributions truncated at a certain large particle size. This is to ensure that the percent fines is not affected by the presence of a few large particles. If, for example, a large cobble was added to one of two otherwise identical gravel samples, and that cobble comprised 20% of the total sample mass, then the percent fines would be smaller in the sample with the cobble than in the sample without the cobble. The cut-off particle size for truncation should be some large gravel size present in all samples, e.g., 45 or 64 mm.

The percentage surface fines computed for a given deposit does not only depend on whether the sample was truncated or not, but also strongly depends on the sampling method. Picking particles off the surface (an areal surface sample) produces a lower percentage surface fines than removing a thin layer of particles from the surface (an armor layer sample). This aspect is further discussed under bimodality in Section 2.1.5.9 because a large percent fines in a gravel bed leads to a bimodal particle-size distribution. See also Sections 4.1.2 and 4.1.3 for the effect of different sampling methods on the resulting

particle-size distribution. The percentage fines in a sample also varies between different methods for identifying the particle to be picked up from the streambed, and is likely to vary between operators (Section 4.1.1.3).

### 2.1.5.9 Bimodality

A bimodal particle-size distribution has two modes, i.e., two distinct peaks in the frequency distribution, one in the finer and one in the coarser fraction. If the percent sand and fine gravel becomes high enough, the distribution becomes bimodal, developing a mode (peak) in the sand range in addition to the other mode (peak) in the gravel range. Bimodality can indicate the presence of two distinct particle-size populations, supplied from a different source, with perhaps different petrology and abrasion resistance, and each population may have had a different transport distance. The recognition and characterization of the degree of bimodality is important for studies of sedimentation and fluvial geomorphology because incipient motion conditions and transport behavior are different in unimodal and bimodal sediment mixtures (Wilcock 1993). Bimodality is also of concern for matters of stream ecology and fish spawning habitat, especially if one of the distribution modes is in the size range of sand to pea-gravel.

#### ***Bimodality parameters***

Wilcock (1993) proposed a parameter  $B$  to characterize the degree of bimodality. The parameter is based on the distance between the two modes, and on the amount of sediment contained in the modes. The distance between the modes is expressed in the equation as the ratio of the particle size in mm of the coarse mode  $D_{cm}$  and the fine mode  $D_{fm}$ . In analogy to the definition of geometric standard deviation, the square root is taken from this ratio. To this ratio is added the proportion of sediment contained in the coarse modes  $P_{cm}$  and in the fine mode  $P_{fm}$ . These proportions are obtained by summing the decimal frequency of four ( $k$ ) contiguous size classes of  $1/4 \phi$ -units that contain the mode.

$$P_{cm} = \sum_{i=1}^k m_{\%cmi} \quad \text{and} \quad P_{fm} = \sum_{i=1}^k m_{fmi} \quad (2.77)$$

For sieving in  $1/2 \phi$ -units,  $k$  becomes 2, comprising the size class of the mode and the largest neighboring size class. For polymodal distributions, Eq. 2.77 is applied to all modes. If all sediment is contained in one of the two modes,  $P_{cm} + P_{fm} = 1$ . This value decreases towards 0 as the degree of bimodality reduces. Bimodality may be computed from (Wilcock 1993):

$$B = \left( \frac{D_{cm}}{D_{fm}} \right)^{0.5} \cdot (P_{cm} + P_{fm}) \quad (2.78)$$

Wilcock (1993) found a threshold value of  $B = 1.7$ , and that gravel is entrained as unimodal sediment if the bed-material bimodality value is low ( $B < 1.7$ ). By contrast, bedload is entrained as bimodal sediment if the bed-material is bimodal ( $B > 1.7$ ). The particle-size distribution in Table 2.3 has a coarse mode in the size class of 45.3 mm. Eq. 2.78 could be applied to test if the increased frequency for the size class of 22.6 mm qualifies for bimodality. The square root of the ratio of the particle-size class of the coarse mode (45.3 mm) and the presumed fine mode (22.6 mm) =  $2^{0.5} = 1.41$ . The decimal frequency of the coarse mode and its largest neighboring size class (64 mm), and the decimal frequency of the presumed fine mode and its largest neighboring size class (16 mm) are summed, yielding  $0.111 + 0.109 + 0.106 + 0.094 = 0.42$ . The product of the two bracketed terms in Eq. 2.78 is 0.6, which is smaller than the threshold value of 1.7. Thus, the particle-size distribution in Table 2.3 is not bimodal.

Sambrook Smith et al. (1997) proposed a slightly different bimodality index ( $B^*$ ). This index accounts for the relative size of the two modes and produces a numerical value that reflects the magnitude of the difference in the particle size of the fine and the coarse mode. The bimodality index is applicable to particle-size distributions in  $\phi$  units.

$$B^* = |\phi_{m2} - \phi_{m1}| \left( \frac{P_{2m}}{P_{1m}} \right) \quad (2.79)$$

$\phi_{1m}$  and  $\phi_{2m}$  are the  $\phi$ -sizes of the primary and the secondary mode, respectively, and  $P_{1m}$  and  $P_{2m}$  are the proportions of sediment contained in the primary and secondary mode. The above index is always positive. Bimodality starts at  $B^* > 1.5 - 2.0$ . Exchanging the absolute signs in Eq. 2.79 for brackets renders  $B^*$  negative for a primary mode in the fine sediment. Applied to the particle-size distribution on Table 2.3, the primary and secondary modes are  $-5.5$  and  $-4.5$   $\phi$ , and contain 11.1 and 10.6% of the sediment, respectively. Thus, Eq. 2.79 yields  $|-5.5 - -4.5| \cdot (11.1/10.6) = 1.0 \cdot 1.05 = 1.05$  and indicates that the distribution is not bimodal.

### ***Surface bimodality and percent fines: effect of different sampling methods***

Bimodality and the percent fines (Section 2.1.5.8) are related, although not by a monotonic function, and both the degree of bimodality and the percent fines are altered depending on how the sediment on the stream surface is sampled. Sambrook Smith et al. (1997) developed a numerical model to show this change. As sand is supplied to a gravel surface, sand first fills the voids between the gravel particles, until, as more sand is added, even the big particles become buried. The entire amount of sand in the experiment adds up to 100 %. For various percentages of sand added, the surface sediment is repeatedly sampled using two different methods: (1) picking individual particles off the surface (areal surface samples), and (2) removing a layer of surface sediment (armor layer sample). Both the percent surface sand and the degree of bimodality were computed for given

percentages of sand added to the streambed, and both parameters varied depending on the sampling method used.

When particles were picked off the surface, the percent sand computed from those areal samples  $S_a$  quickly rose to 80% as the voids between the large clasts started to be filled (20% sand added). The percent sand computed from the volumetric armor layer samples  $S_v$  increased slowly, reaching not even 40% when the entire surface was covered with sand (at  $S_a = 100$ ) (Fig. 2.21).

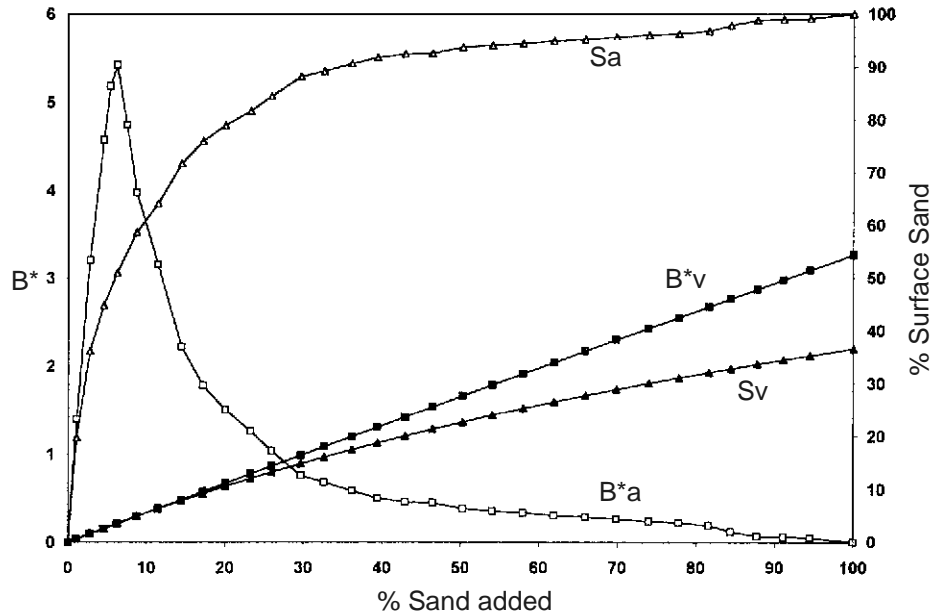


Fig. 2.21: Percent surface sand and degree of bimodality computed for two different sampling methods for increasing amounts of sand.  $S_a$  and  $B^*_a$  are the percent surface sand and degree of bimodality computed for areal surface samples,  $S_v$  and  $B^*_v$  are the percent surface sand and the degree of bimodality computed for an armor layer sample (Reprinted from Sambrook Smith et al. (1997), by permission of the American Geophysical Union).

The degree of bimodality differed even more between the two sampling methods. For the areal samples, bimodality  $B^*_a$ , increased sharply and was most pronounced when about 50% of the surface was covered by sand ( $S_a \approx 50\%$ ). For larger amounts of sand, the degree of bimodality again decreased. When using armor layer samples, bimodality  $B^*_v$  increased slowly as progressively more sand was added to the bed.

## 2.2 Shape analysis

Particle forms are characterized by two factors: shape and angularity. Shape refers to the ratio of the three axes lengths, whereas angularity refers to whether a particle has angular edges as opposed to a rounded surface.

Many parameters for characterizing particle form were developed in the 1930s to 1960s because it was realized that particle form affects the area exposed to forces of flow, drag forces, lift forces, and therefore particle entrainment, transport, and deposition. Thus, two particles of the same weight or the same  $b$ -axis size but with different shapes can respond quite differently to water flow. It is therefore important to consider whether a particular study requires knowledge of the longest, the intermediate, or the shortest axis, or of all axes.

### 2.2.1 Compact, platy, bladed, and elongated particle shapes

Particles are classified into four basic shapes according to the ratios of the three particle axes, where  $a$  is the longest axis,  $b$  is the intermediate axis, and  $c$  is the shortest axis. The length of the particle axes can be measured manually using a ruler, calipers, or a pebble box (Sections 2.1.3.7 – 2.1.3.8). An approximation of particle axes lengths can also be computed from the axes of an ellipse that best fits the planimetrically determined outline of a particle on a photograph (see photosieving, Section 4.1.3.3). The ellipse-approximation eliminates the effects of angularity on particle shape, and thus improves the determination of particle shape for angular particles (Diepenbroek and De Jong 1994).

The particle shape of a disc is characterized by its small  $c$ -axis. The degree of disc-shape is quantified by the axis ratio of  $c/b$  (Krumbein 1941). A sphere-like particle, in turn, has almost identical  $a$ ,  $b$ , and  $c$  axes. A bladed particle is thin and long, i.e., it has small ratios of  $c/b$  and  $b/a$ , whereas a rod-like particle is long, which is quantified by a small  $b/a$  ratio (Fig. 2.22). Fig. 2.23 depicts these particle shapes using blocks for simplicity.

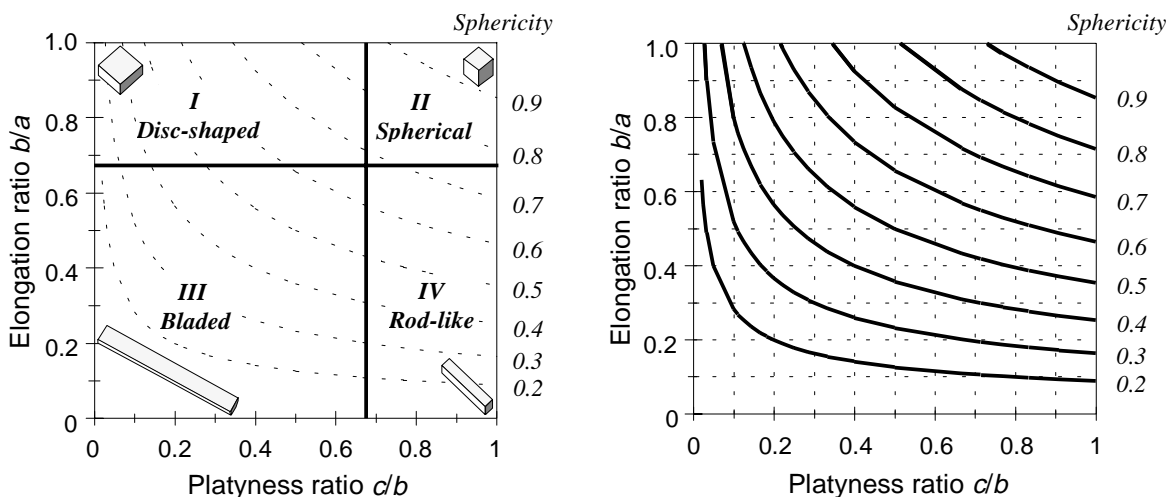


Fig. 2.22: (A) Relation between axes ratios and particle shape (Zingg's classification) (Redrawn from Krumbein (1941), by permission of the Society for Sedimentary Geology). (B) Relation between sphericity and particle shape. Lines of equal sphericity shown as function of the axes ratios  $b/a$  and  $c/b$ . (Redrawn from Krumbein (1941), by permission of the Society for Sedimentary Geology).

Sneed and Folk (1958) classify particle shape in terms of platyness, bladedness, and elongatedness, and compactness (Fig. 2.23). The form factor  $F$  distinguishes between platy (i.e., disc shaped), bladed (i.e., ellipsoid) and elongated (i.e., rod shaped) particles and is computed from

$$F = \frac{a - b}{a - c} \quad (2.80)$$

$F < 0.33$  defines platy particles,  $0.33 < F < 0.67$  defines bladed particles, and  $F > 0.67$  defines elongated particles. The degree of platyness, bladedness, and elongatedness, i.e., the degree of deviation from compactness  $S$ , is defined by the ratio of

$$S = \frac{c}{a} \quad (2.81)$$

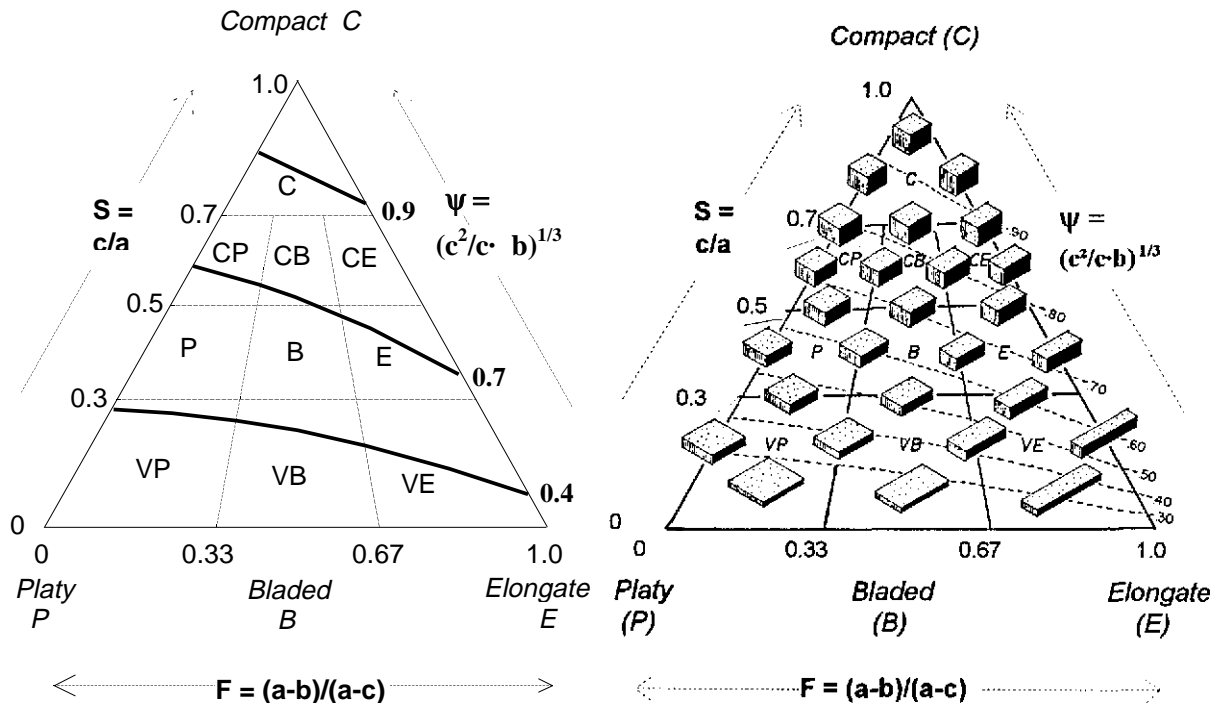


Fig. 2.23: (A) Sphericity-form diagram showing relation between particle shape and sphericity (Redrawn from Sneed and Folk (1958), by permission of the University of Chicago Press). (B) Form triangle with illustration of particle shapes using blocks of the appropriate axes ratios; all blocks have the same volume (Reprinted from Sneed and Folk (1958), by permission of the University of Chicago Press).

Particles are compact (*C*) with a shape close to a sphere if the *S* factor > 0.7. Particles classify as compact *platy*, *bladed*, or *elongated* if  $0.5 < S < 0.7$ , as *platy*, *bladed*, or *elongated* for  $0.3 < S < 0.5$ , and as *very platy*, *bladed*, or *elongated* for  $S < 0.3$ . The four classes for compact, platy, bladed, and elongated, plus the degrees of deviation from sphericity (e.g., compact bladed or very bladed) yield a total of 10 shape categories. The numerical values of the *F* and *S* factors are plotted in a triangular diagram from which the descriptive term of particle shape can be read.

## 2.2.2 Sphericity

Particle sphericity refers to how well a particle of a given shape relates to the transport properties of a sphere, whereas the expression roundness refers to the degree to which the edges of a particle are rounded (Section 2.2.3). Sphericity can be used as an indication of fluvial transport distance (Section 2.2.2.1), as well as a measure of particle suspensibility and transportability, i.e., the ability of a particle to remain in transport once entrained (Section 2.2.2.2). Since both concepts involve different principles, i.e., abrasion versus suspensibility, it is important to use different definitions of sphericity in each case.

### 2.2.2.1 Indication of fluvial transport distance

As particles are transported over long distances, abrasion wears off not only the particle edges (see roundness, Section 2.2.3), but may tend to equalize the three axes lengths as well, thus making a particle more spherical. Wadell (1932) defined this kind of sphericity as the third cube of the ratio of a measure for particle volume to the volume of the sphere circumscribing it. This expression was simplified by Krumbein (1941) and Pye and Pye (1943) who suggested computing sphericity  $\psi$  as

$$\psi = \left( \frac{b \cdot c}{a^2} \right)^{1/3} \quad (2.82)$$

Krumbein's sphericity reaches the value of 1 for perfect spheres and decreases towards 0 for extremely platy or elongated particles. Particles of different shapes can have the same sphericity value. However, platyness and elongatedness do not increase at even rates as the degree of sphericity decreases. For example, a particle with an elongation ratio of  $b/a = 0.6$ , and a platyness ratio of  $c/b = 0.2$  has a sphericity value of  $\psi = 0.42$ , but a particle with an elongation ratio of  $b/a = 0.2$ , and platyness ratio of  $c/b = 0.6$ , has a sphericity value of  $\psi = 0.32$  (Fig. 2.22). This sphericity index acknowledges that as sphericity increases with transport distance, the degree of elongatedness wears off more quickly or pronouncedly during fluvial transport than the degree of platyness.

Particles of different structural properties from different geological parent material have different susceptibilities to becoming sphere-like. Granite tends to break into cubic blocks

and reaches a high degree of sphericity quickly with increasing transport distance, whereas the “layered” structure of schist produces disc-shaped particles that do not necessarily become highly spherical even after long transport distances. Similarly, large basalt particles tend to chip pieces off during transport, thus producing small elongated instead of spherical particles.

Not all researchers agree on the degree to which fluvial or coastal transport affects particle sphericity. Bartolomä (1992) concluded that sphericity and shape are predominantly controlled by the structural properties of the source rock, and barely affected by transport, and that consequently sphericity and roundness (Section 2.2.3) are independent properties.

### 2.2.2.2 Indication of particle transportability

Two definitions of sphericity are commonly used to refer to particle transportability: the Corey (1949) shape factor  $C$ , and the Sneed and Folk (1958) effective settling sphericity  $\psi_r$ . Both definitions are similar and transformable, and both definitions reach the value of 1 for perfect spheres and decrease towards 0 with increasing departure from sphericity.

#### ***Corey shape factor***

The Corey (1949) shape factor is used as a parameter to determine the particle settling velocity which for particles of equal weight is affected by particle shape. The shape factor is computed from (Yang 1996, p.4):

$$C = \frac{c}{(a \cdot b)^{0.5}} \quad (2.83)$$

Ellipsoidal or compact bladed gravel particles with long fluvial transport distances have values around 0.7, whereas bladed particle shapes in mountain streams have values around 0.5.

#### ***Sneed and Folk effective settling sphericity***

Sneed and Folk (1958) define the effective settling sphericity as

$$\psi_r = \left( \frac{c^2}{a \cdot b} \right)^{1/3} \quad (2.84)$$

and provide a diagram to show how effective settling sphericity is related to particle shape: the form factor  $F$  that distinguishes between platy, bladed, and elongated particles (Eq. 2.80) and the degree of compactness  $S$  (Eq. 2.81) (Fig. 2.23).

Lines of equal settling sphericity go diagonally across the diagram, and show that for the same degree of flatness (axis ratio of  $c/a$ ) platy particles offer more resistance to settling than elongated particles. Thus, the same value of  $\psi_r = 0.7$  is obtained for compact platy as well as elongated particles (Fig. 2.23). This definition of settling sphericity indicates the tendency of platy particles to settle relatively slowly. Thus, platy particles easily remain suspended in flow, and once entrained can be transported over long distances.

If lines of equal Corey shape factors were included in the Sneed and Folk diagram (Fig. 2.23), they would plot approximately parallel but below to the lines of equal settling sphericity. Lines of equal values of the Krumbein (1941) sphericity would also plot diagonally across the Sneed and Folk diagram, but point into the opposite direction of the Sneed and Folk sphericity. Compact elongated and platy particles would plot on the same line indicating a similar transport distance. The Krumbein sphericity, referring to transport distance, and the Sneed and Folk sphericity, referring to transportability, intersect and have the same numerical values for particles roughly along the dividing line between bladed and elongated particles with  $F$  values around 0.67.

### 2.2.3 Roundness or angularity: analytical and visual approaches

Roundness describes how well the “edges” of a particle are rounded. Roundness and sphericity are not conceptually related and are largely independent, however, nearly spherical fluvial particles seldom show any sharp edges, whereas particles that are ellipsoidal, bladed, or elongated are much more likely to show sharp edges.

Angular particles tend to wedge into each other and do not roll well. Thus, angularity reduces particle mobility and probability of entrainment. Roundness increases as the edges wear due to abrasion. Thus, high angularity also indicates that a particle has not been transported over a long distance. A number of different roundness indices has been developed and are summarized by Swan (1974).

Wadell (1932) developed a complicated procedure of measuring and computing particle roundness  $P$  that computes the mean size of the radii  $r$  that can be fitted into the number of corners  $n$  that a particle has and divides this number by the radius of the maximum inscribed circle  $R$  so that

$$P = \frac{\sum r_n}{n \cdot R} \quad (2.85)$$

On the basis of Wadell’s results, Krumbein (1941) developed a chart for the visual estimate of particle roundness which has values between 0.1 (for very angular) and 0.9 (for very smooth particles) (Fig. 2.24). Mean roundness  $P_m$  for a deposit is computed by a weighting approach that multiplies the roundness index  $P$  by the number of particles  $n$  that

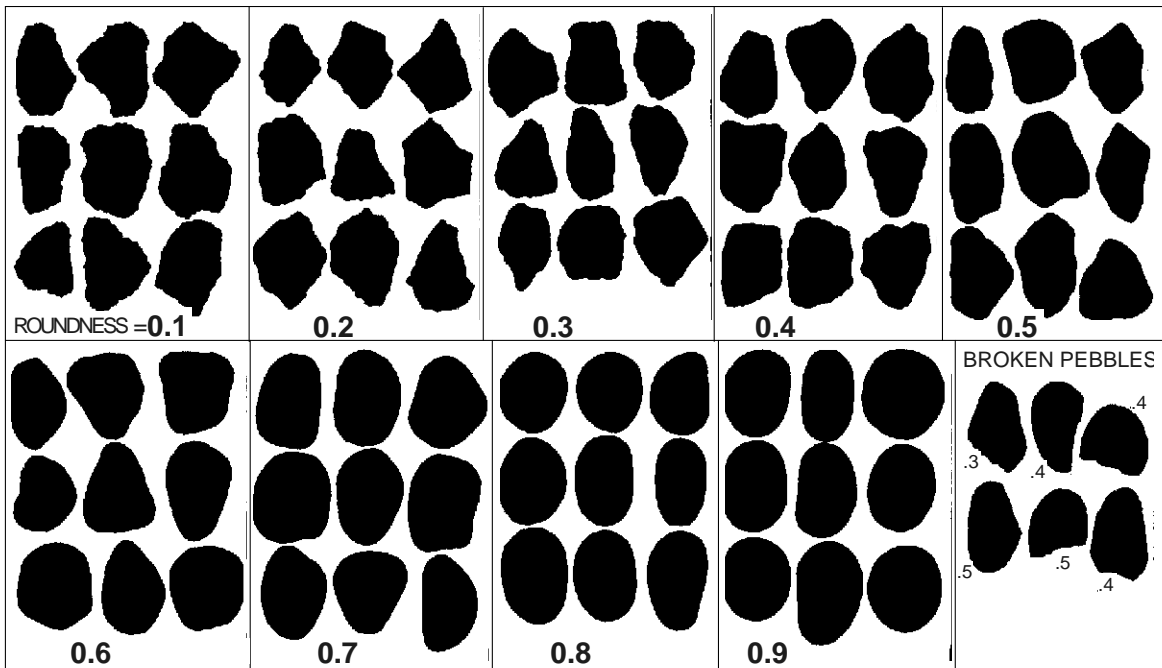


Fig. 2.24: Images for visual analysis of roundness for pebbles 16 - 32 mm. The analysis should be carried out for each particle-size class individually. The chart should be enlarged so that shown particle *b*-axes are of the same length as the particles to be analyzed. (Slightly modified from Krumbein (1941), by permission of the Society for Sedimentary Geology).

have that roundness, sums the  $P_n$  products and divides by the total number of particles in the sample  $\Sigma n$ .

$$P_m = \frac{\Sigma P \cdot n}{\Sigma n} \quad (2.86)$$

Further discussion of conceptual and practical issues regarding particle roundness are provided by Diepenbroek et al. (1992).

#### 2.2.4 Shape/roundness matrix: visual field classification

Some field studies might want to classify particles not only by one, but by two parameters combined, such as particle shape and angularity, in order to differentiate between deposits of different sedimentary origins or depositional processes. Crofts (1974) designed a chart for visual field evaluation of particle shape and angularity (Fig. 2.25). For 50 random particles collected from a 1-m<sup>2</sup> area, the first step of the visual analysis distinguishes between spherical and flat particles. Particles are assigned to one of the 6 shape categories ranging from very spherical to very flat (neglecting the degree of elongatedness). Then

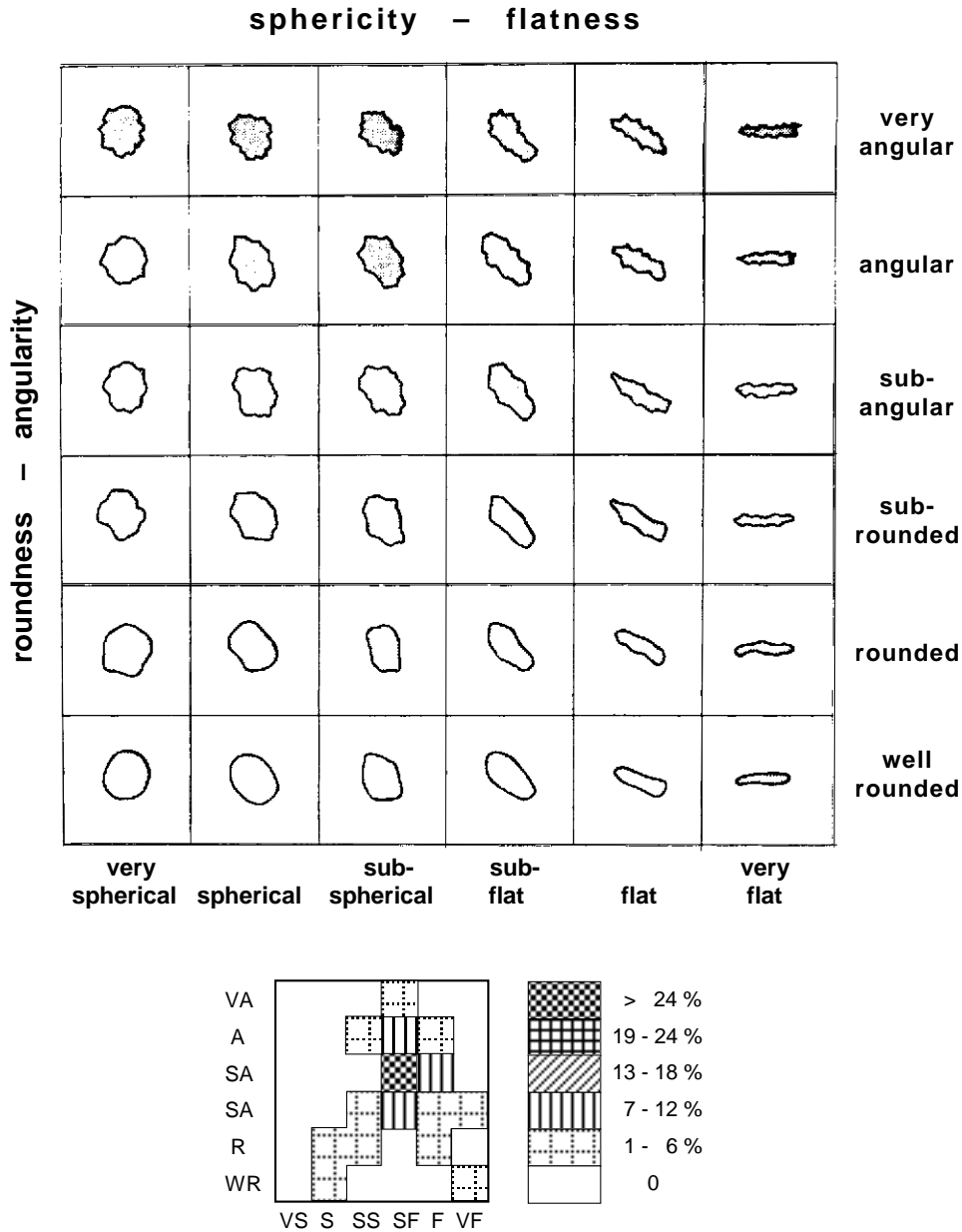


Fig. 2.25: Visual 6-by-6 matrix distinguishing between the degrees of sphericity-to-flatness and roundness-to-angularity (top), and example of plotted results (bottom). (Reprinted from Crofts (1974), by permission of the Society for Sedimentary Geology.)

each particle is sorted into one of the 6 degrees of angularity. The number of particles within each of the potential 36 shape-angularity categories is recorded and may be plotted as a bivariate scattergram. For such a plot, the number of particles per category is grouped into 4 - 6 evenly spaced intervals, and each consecutive interval is assigned an increasing degree of shading or hatching. The visual analysis of 50 particles from one field location takes less than 30 minutes including the time for field plotting the results.

The same approach as outlined above can be applied to any two-particle parameters if their variability can be described in certain visually distinguishable increments. For best results, the visual classification matrix should be larger than 4 by 4, but not exceed 9 by 9 fields. Each study needs to find the optimum matrix size, as well as the optimum sample size, compromising between accuracy and time expenditure.

Visual field classification can also be used to distinguish between three particle parameters. An example in which particle-size mixtures are visually classified into three major and 12 minor size categories, and results are plotted in ternary diagrams, is provided by Buffington and Montgomery (1999a) (Section 4.1.3.5).

### 2.2.5 Pivot angles and their computation

One of the most important applications of particle-shape parameters in sediment transport studies of gravel-bed rivers is the determination of the pivot angle, also called the angle of repose or intergranular friction angle. The pivot angle is the angle  $\Phi$  that a top particle of the diameter  $D$  has to overcome when rolling over a bottom particle with the diameter  $K$  that is partially under and partially in front of it (Fig. 2.26). Thus, pivot angles control the force required for particle motion, and are an integral part of force-balancing equations.

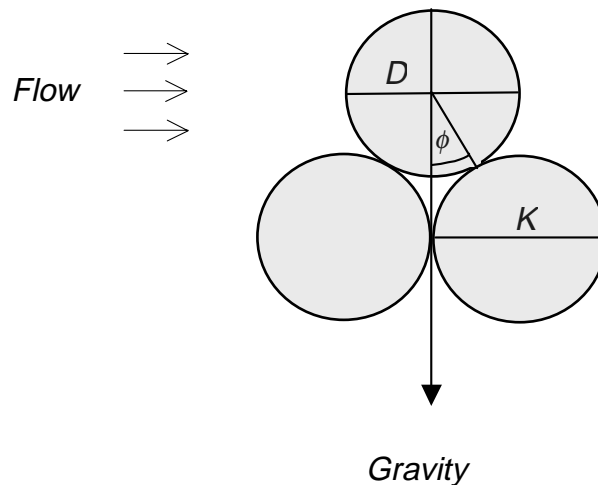


Fig. 2.26: Definition of pivot angle  $\Phi$ , and particle diameters  $D$  (top particle), and  $K$  (bottom particle).

Pivot angles are difficult to measure in the field (Johnston et al. 1998). Measurements are therefore either performed on pieces of reconstructed streambed in a lab (Kirchner et al. 1990) or the pivot angle is estimated from various particle parameters such as:

- particle roundness,
- particle shape,
- packing (base of two, three, or four bottom particles  $K$ ), and
- relative particle size  $D/K$ .

### **Angularity or roundness**

Pivot angles increase with angularity (Fig. 2.27), a reason why riprap is often angular. In order to rotate an even-sized triangle (all inside angles =  $60^\circ$ ) situated on a flat plain over one of its angles, a pivot angle of  $60^\circ$  needs to be overcome. The pivot angle for a square with four angles of  $45^\circ$  is 45. Pivot angles  $\Phi$  for even-sided polygons can be expressed as (Julien 1995):

$$\Phi = \frac{180^\circ}{n} \quad (2.87)$$

where  $n$  is the number of angles within the polygon. For a sphere, the number of inside angles is indefinitely large, thus  $\Phi = 180^\circ/\infty = 0^\circ$ , which means that there is no pivot angle for a sphere on a flat surface. Pivot angles on a streambed may exceed those in Fig. 2.27 because surface particles may be nestled in shallow depressions on top of three or four bottom particles.

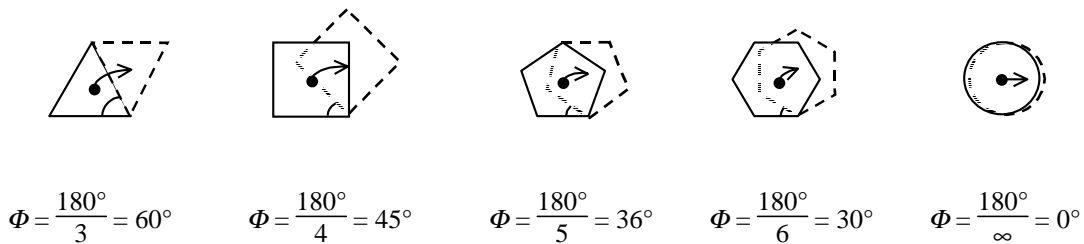


Fig. 2.27: Effect of angularity on pivot angles on a flat surface (Redrawn from Julien (1995), by permission of Cambridge University Press).

### **Particle packing**

Pivot angles vary with packing patterns of the bottom particles. A spherical top particle  $D$  can be nestled on a base of two, three, or four spherical bottom particles  $K$  (Fig. 2.28). Pivot angles described in Fig. 2.28 vary with three parameters: (1) the size ratio  $D/K$ , (2) whether the top particle  $D$  rolls over the top (grain-top rotation) or over the saddle between two spheres  $K$  (saddle-top rotation) and (3) the number of bottom particles  $K$  comprising the base for the top particle  $D$  (Li and Komar 1986; Julien 1995).

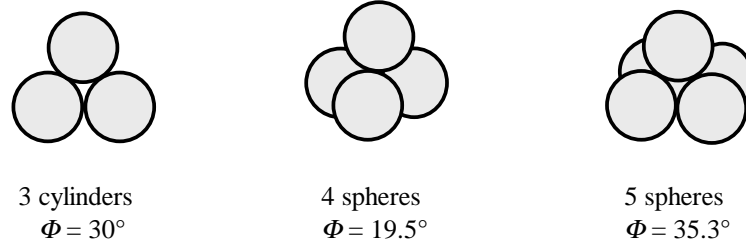


Fig. 2.28: Pivot angles for unisized particles ( $D/K = 1$ ) with different packing: top particles lying on top of two (left), three (center), and four particles (right). (Redrawn from Julien (1995), by permission of Cambridge University Press ).

### ***Particle shape***

Spherical particles have smaller pivot angles than particles with ellipsoidal, elongated, or platy particle shapes. Pivot angles for spheres are approximately  $10^\circ$  lower than those for ellipsoids which are about  $10^\circ$  lower than those for angular particles (Li and Komar 1986).

### ***Relative size***

Miller and Byrne (1966) express the effect of relative particle size  $D/K$  on the pivot angle  $\Phi$  by a negative power function.

$$\Phi = a \left( \frac{D}{K} \right)^b \quad (2.88)$$

Pivot angles for small surface particles  $D$  nestled on top of large bottom particles  $K$  with  $D/K \approx 0.3$  are  $40$ - $50^\circ$  larger than the pivot angles for large surface particles on top of small bottom particles with  $D/K \approx 3$  (Fig. 2.29). This effect of relative size is seen for all particle shapes.

### ***Pivot angles in channel beds***

Kirchner et al. (1990) measured pivot angles on water-worked flume surfaces and concluded that pivot angles obtained from experiments with well sorted and well rounded particles in regular packing are too low, and vary too much with relative size. Kirchner et al. (1990) therefore suggest the following  $a$ -coefficient and  $b$ -exponent for Eq. (2.86) (Fig. 2.30):

$$\Phi_{50} = 55.2 \left( \frac{D}{K_{50}} \right)^{-0.31} \quad (2.89)$$

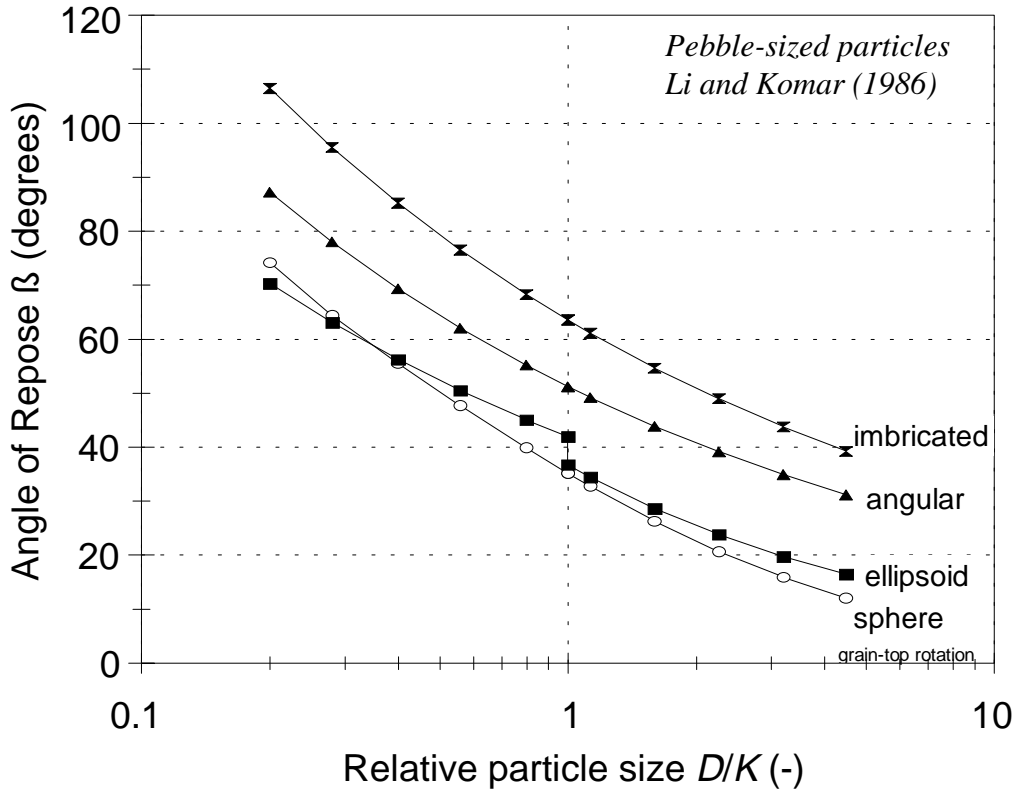


Fig. 2.29: Pivot angles for spherical, ellipsoidal, and angular particle shapes as well as for imbricated deposits as functions of relative particle size, i.e., the ratio of entrained particle size  $D$  to bottom particle size  $K$  (plotted with data from Li and Komar 1986).

where  $\Phi_{50}$  is the median pivot angle, and  $K_{50}$  is the median size of the bottom bed-material particles. Gravel-bed rivers with particles of various dimensions, various relative sizes, shapes, rotation modes, and packing have a wide range of small and large pivot angles (Buffington et al. 1992). Each riverbed is characterized by a unique probability distribution of pivot angles, and the parameters of the distribution (median, skewness, and kurtosis) are a function of various particle parameters.

Buffington et al. (1992) include a term for bed-material sorting  $\sigma$  in their equation and provide the coefficient  $x$  (Eq. 2.90). Adjusting  $x$  facilitates computing the probability distribution of pivot angles.  $\tan\Phi$ , to which critical shear stress  $\tau_c$  is proportional, can vary widely on a given streambed, indicating the differential erodibility of surface particles.

$$\Phi_x = a_x \left( \frac{D}{K_{50}} \right)^{-b_x} \cdot \sigma^{-c_x} \quad (2.90)$$

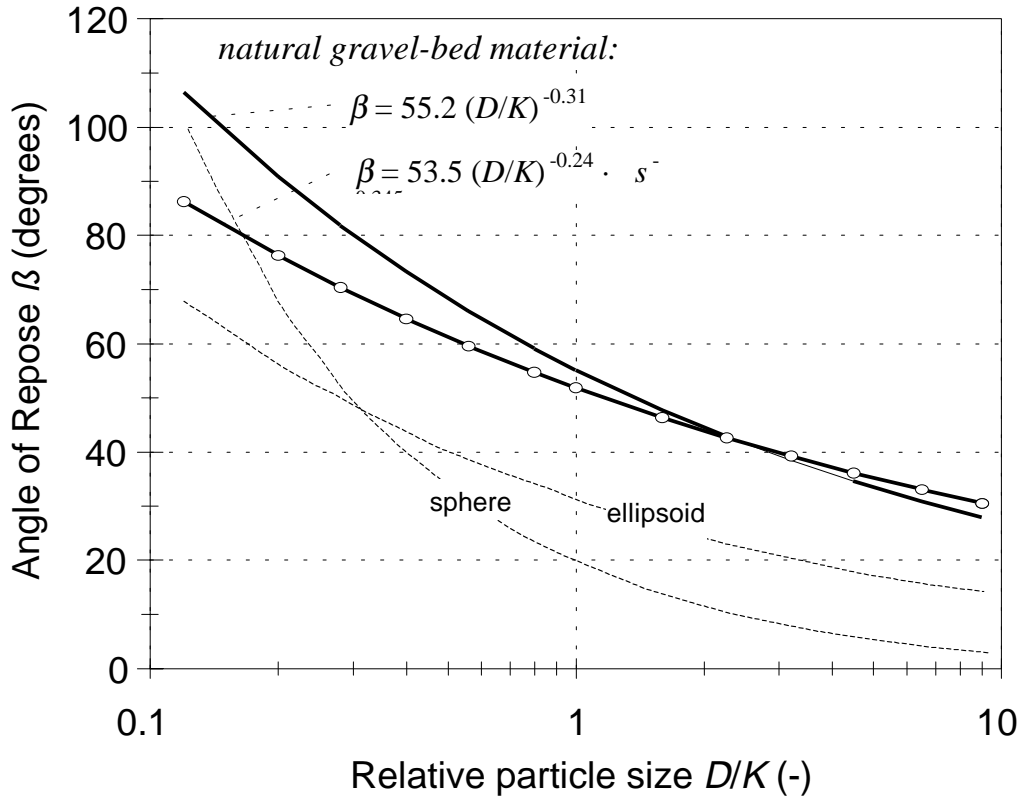


Fig. 2.30: Pivot angles for particles on channel surfaces computed from Eq. 2.89 by Kirchner et al. (1990) (thick line); Median pivot angles computed from Eq. 2.90 by Buffington et al. (1992) (thick line with bullets). For comparison: pivot angles for saddle-top rotation of well sorted spheres and ellipsoids in regular packing, based on results by Li and Komar (1986) (thin hatched lines).

### 2.2.6 Sample size for shape analysis

The number of particles used to establish the dominant bed-material particle shape depends on the variability of the particle shapes found at a site. There also might be several populations of particle shapes corresponding to differences in hardness of the source rock and differences in travel distance. Particles originating from soft rocks, or those traveled farthest are more rounded and more ellipsoidal than hard rocks or bedload supplied to the mainstem stream by a small tributary just upstream. Particles from local rockfall or debris flows are usually angular and deviate from a spherical or ellipsoidal particle shape.

Because the situation can be quite different from stream to stream, pilot studies are recommended. The first step is to visually identify particle-shape populations. Then collect 25 particles from each population, measure the 3 axes, compute the  $S$  and  $F$  form factors (Eqs. 2.80 and 2.81) and plot them in a sphericity-form diagram (Fig. 2.23). If the data for 25 particles do not plot closely together, more particles may need to be analyzed or the criteria for identifying particle shapes need to be changed. Another option is to

apply Student's *t*-statistics to measured particle-shape parameters and to determine the sample size necessary for an acceptable accuracy and a given particle-shape variability (see Section 5 on sample size).

### 2.3 Particle density, specific weight, specific gravity, and submerged specific weight

Many equations for sediment transport or the initiation of particle motion require particle density or the specific particle weight as input. Particle density is particle weight (or mass) (*m*) divided by its volume *V*. Conventionally, particle density is abbreviated by the Greek letter “rho” with the subscript *s* for sediment ( $\rho_s$ ) to distinguish it from the fluid density (in this case water) which is noted by  $\rho_f$ .

$$\rho_s = \frac{m}{V} \quad (2.91)$$

The units of particle density are  $\text{g/cm}^3$ , or  $\text{kg/m}^3$ . Particle mass is measured by weight and particle volume is either measured or estimated from particle shape. To measure particle volume, take a large measuring beaker for large particles, or a graded cylinder for small rocks, fill it about half full with water and record the volume of water. Place the particle into the water (particle must be completely submerged) and record the water volume corresponding to the elevated water level. The difference between the two water volumes in the beaker is the particle volume. When particles are small, or when one wants to know the average density of particles in a mixture, several particles can be analyzed together. To reduce measurement errors, the entire analysis should be repeated several times with new particles.

The density of quartz and feldspar particles is  $2.65 \text{ g/cm}^3$  or  $2,650 \text{ kg/m}^3$ . This value can often be used as a first approximation of particle density because many particles contain a high percentage of quartz and feldspar. Rock density is less than the one for quartz when rocks have pores filled with water or air. Sandstone rocks, for example, have a density of about  $2.2 \text{ g/cm}^3$ . Solid, dark volcanic rocks or those with high metal content have a density of more than  $3 \text{ g/cm}^3$ . Density is to some extent dependent on particle size. Cobble and gravel-sized pieces of vesicular basalt or pumice might have densities between 2 and  $1 \text{ g/cm}^3$ . This value can increase to about  $3 \text{ g/cm}^3$  when vesicular volcanic rock is ground into sand size and the vesicular structure is lost. Table 2.15 presents particle densities for common geological materials.

Table 2.15: Particle densities (g/cm<sup>3</sup>) of various materials\*

Material	Density
humus, pumice	<1.5
sandstone	2.1 - 2.2
limestone, quartz, granite, porphyry	2.7
feldspars (the “white” in granite)	2.5 - 2.8
dolomite, anhydrite	2.9
micas (the flaky, shiny parts of granite)	2.7 - 3.3
apatite	3.1 - 3.3
peridotite, gabbro	>3.2
basalt, diabas	3.3
iron	7.2

\*for comparison: water density at 4°C = 1.00 g/cm<sup>3</sup>

### ***Specific particle weight***

Specific particle weight  $\gamma_s$  is the product of particle density  $\rho_s$  and acceleration due to gravity  $g$ . For most applications in gravel-bed rivers  $g$  can be assumed to take a value of 981 cm/s<sup>2</sup>, or 9.81 m/s<sup>2</sup>.

$$\gamma_s = \rho_s \cdot g = 2.65 \cdot 981 \frac{\text{g} \cdot \text{cm}}{\text{cm}^3 \cdot \text{s}^2} = 2,600 \frac{\text{g}}{\text{cm}^2 \cdot \text{s}^2} \quad (2.92)$$

### ***Specific gravity of sediment and water***

Specific gravity is the dimensionless ratio of specific weights or densities. For quartz particles with a density of 2.65 g/cm<sup>3</sup> and water with a density of 1 g/cm<sup>3</sup>, the specific gravity is

$$G_s = \frac{\gamma_s}{\gamma_w} = \frac{\rho_s}{\rho_w} = \frac{2.65}{1} = 2.65 \quad (2.93)$$

The density of pure water at 4°C ( $\rho_{pw}$ ) is 1 g/cm<sup>3</sup>. River water with suspended sediment concentration and a temperature above 4°C may have a density ( $\rho_{rw}$ ) higher than 1, perhaps 1.005. The specific gravity of river water  $G_{rw}$  is computed from

$$G_{rw} = \frac{\gamma_{rw}}{\gamma_{pw}} = \frac{\rho_{rw}}{\rho_{pw}} = \frac{1.005}{1} = 1.005 \quad (2.94)$$

### ***Submerged specific weight***

The submerged specific weight  $\rho'_s$  of a quartz particle is the difference between the particle density and the fluid density. For clear water, the submerged specific particle weight is

$$\rho'_s = \rho_s - \rho_f = 2.65 - 1 = 1.65 \text{ g/cm}^3. \quad (2.95)$$

For heavily sediment-laden water with a sediment concentration of 100 g/l, fluid density increases to  $1.23 \text{ g/cm}^3$ . Thus, the submerged specific particle weight is reduced to  $1.42 \text{ g/cm}^3$ . This reduction in the specific weight of particles in heavily sediment-laden flow leads to an increase in particle mobility and may even cause boulders to “swim”.

## **2.4 Bulk density, porosity, and void ratio**

Knowledge of sediment bulk density is needed to evaluate the pore space available for aquatic habitat (Milhous 2001). Bulk density  $\rho_b$  is defined as the ratio of the weight of a bulk material  $m_b$  that is contained in a specific bulk volume  $V_b$ .

$$\rho_b = \frac{m_b}{V_b} \quad (2.96)$$

### ***In situ gravel sediment, inundated sediment***

Bulk density of riverbed material should be measured on undisturbed samples in their original packing because the bulk density changes when the natural packing is disturbed by shoveling the sediment. Piston cores also disturb the original packing and are not suitable for measurements of bulk density in gravel deposits.

Milhous (pers. comm. 2000) suggested that bulk density of inundated sediment in gravel-bed rivers may be measured in situ from large freeze cores (Section 4.2.4.8) taken from the substrate below the water surface, so that the sample is completely saturated with water (i.e., all pores filled with water, none with air). The cores are weighed frozen and fully waterlogged ( $m_w$ ), as well as after the ice has melted and the sediment has dried ( $m_s$ ). To compute the bulk density of the sediment in the core, the dry sediment mass is divided by the total core volume which is the volume of the sediment particles  $V_s$  plus the volume of the water in the pores  $V_w$ .

$$\rho_b = \frac{m_s}{V_w + V_s} \quad (2.97)$$

The volume of the sediment particles is calculated from

$$V_s = \frac{m_s}{\rho_{rw} \cdot G_s} \quad (2.98)$$

where  $\rho_{rw}$  is the density of the river water, and  $G_s$  is the specific gravity of the sediment (Section 2.3). The volume of the water contained in the sample is computed from

$$V_w = \frac{m_w}{\rho_{rw} \cdot G_{rw}} \quad (2.99)$$

where  $G_{rw}$  is the specific gravity of the river water (Section 2.3).

### ***In situ gravel sediment, dry surface***

Milhous (2001) suggested the following technique for measuring the bulk density of subsurface sediment in a dry part of the streambed:

#### **Step 1: Measure the volume of water that displaces the surface sediment or the armor layer**

Remove all surface particles from a dry streambed area for a measurement of the subsurface sediment bulk density. Alternatively, remove the armor layer (Sections 4.1.3.1, 4.1.3.2, 4.2.1.2) before measuring the subarmor bulk density. Place a square frame, 0.6 – 0.9 m in length, and 2.5 – 5 cm high onto the area cleared of armor sediment (Fig. 2.31). Place some sediment along the inside of the frame just next to the frame to create a smooth transition between sediment and frame. Smooth out the corners as well. Do not sample or disturb this sediment. Cover the exposed subsurface sediment surface with a plastic sheet, and fit it snugly into all corners within the inside of the frame. Fill the plastic-lined depression with water (river water is fine) and measure the water volume needed until overflow using a large laboratory cylinder. Alternatively, weigh the amount of water needed to fill the plastic sheet and compute the volume using a fluid density of 1,000 kg/m<sup>3</sup> for clear, cold water. Discard the water and remove the plastic sheet (Fig. 2.32 top). Be careful not to disturb the frame or the exposed sediment surface.

#### **Step 2: Measure the volume of water that displaces the subsurface or subarmor sediment**

Take a subsurface bed-material sample with a volume of about 20 liters from inside the area within the frame (See Section 4.2.2 for vertical extent of a subsurface bulk sample). This sample is later dried, weighed, and sieved. When extracting the sample, the operator should try to create a hole with a smooth bottom. The operator should be



Fig. 2.31: Frame for measuring in situ subsurface sediment bulk density (Photo courtesy of R. Milhous).

careful not to disturb the exposed subsurface sediment surface or the position of the frame while taking the subsurface sample. After the subsurface sample is taken, carefully line the hole with plastic sheeting and extend the sheet over the exposed sediment surface within the frame, and the frame itself. Make sure that the plastic sheet fits snugly into the hole and leaves no cavities. Air-filled cavities are especially prone to develop in the bottom of the hole. Make sure the plastic sheet is everywhere in contact with the bottom of the hole. Refill the plastic sheet with water and measure the volume needed until overflow onto the gravel surface (Fig. 2.32 bottom).

The volume displacing the subsurface sample  $V_{sub}$  is the difference between the volume of the second  $V_2$  and the first measurement  $V_1$ .

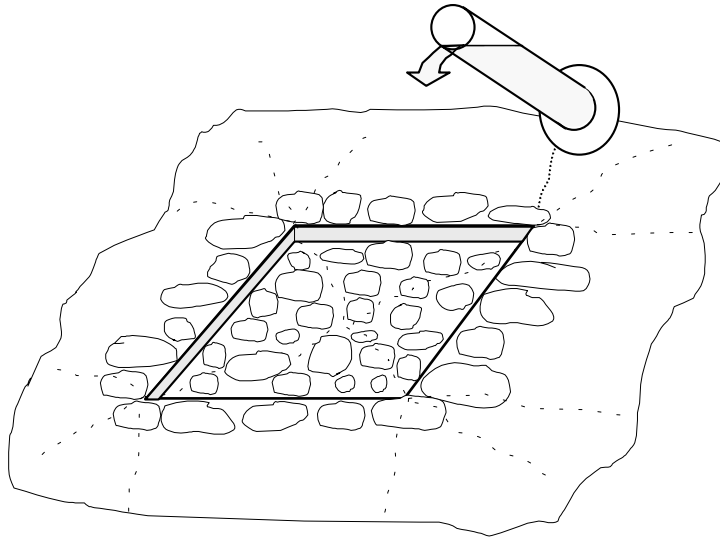
$$V_{sub} = V_2 - V_1 \quad (2.100)$$

The bulk density of the bed material  $\rho_{sub}$  is the ratio of dry weight of the subsurface sediment removed from the hole  $m_{sub}$  to the volume of the subsurface sample  $V_{sub}$ .

$$\rho_{sub} = \frac{m_{sub}}{V_{sub}} \quad (2.101)$$

Bulk density measured this way in several gravel-bed rivers ranged between 1.7 and 2.6 g/cm<sup>3</sup>, with a mean of 2.1 g/cm<sup>3</sup>.

Step 1:



Step 2:

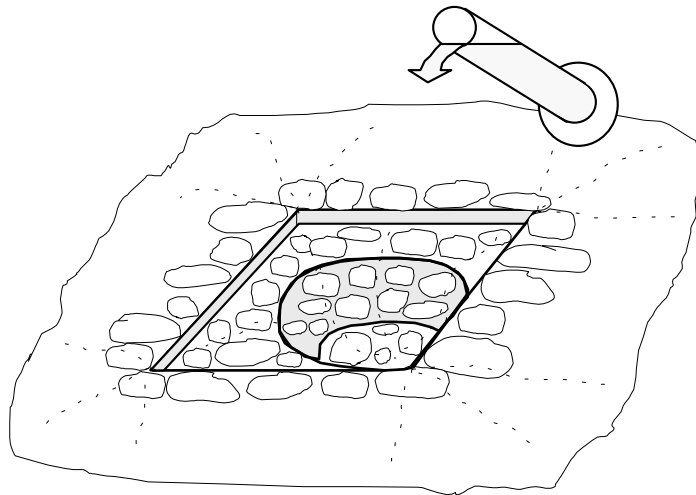


Fig. 2.32: In situ measurements of the subsurface sediment bulk density.

Repeating density measurements to determine a mean value is advisable, because differences in material packing as well as operator errors are likely to produce a range of results. Note also that a 20-liter sample volume yields a sample mass of approximately 10

kg and that several subsamples may be required to obtain the total sample mass necessary for a preset accuracy of the particle-size analysis.

If the sediment porosity  $p$  is known, bulk density may also be computed from

$$\rho_b = \rho_s \cdot (1 - p) \quad (2.102)$$

***Effect of particle packing on bulk density***

Particle packing can significantly affect bulk density. The weight of quartz sand filling a 10 liter pail (1,000 cm<sup>3</sup>; ca. 2.5 gallons) is not 2.65 g/cm<sup>3</sup> times 1,000 cm<sup>3</sup> = 26.5 kg, but considerably less (approximately 20 kg). The exact weight depends on how closely the quartz grains are packed. Particle packing can range between open and dense. The packing is open or cubic when each unisized sphere has a neighbor exactly on top and beneath, on the north, east, south, and the west side. The resulting bulk density for this packing is 1.39 g/cm<sup>3</sup>. In the densest packing (rhombohedral), six spheres are clustered around the center sphere, and have a top sphere in the “pocket” or depressions between the bottom spheres. In this case, the bulk density is 1.96. Assemblages of natural particles are seldom unisized, however. Thus, small particles fit between the voids left by larger particles, and the packing becomes denser the wider the particle-size distribution. Packing also becomes more dense as the deposit becomes more compacted due to pressure or shock waves (e.g., more rice grains can be filled into a jar if one gently hits the bottom of the jar). Bulk densities for various sediments are presented in Table 2.16.

Table 2.16: Bulk density and porosity for various sediments with a particle density of 2.65 g/cm<sup>3</sup>.

Description	Bulk density (g/cm <sup>3</sup> )	Porosity (-)
Unisized spheres in open (cubical) packing ( <i>theoretical</i> )	1.39	0.48
Unisized spheres in closest packing ( <i>theoretical</i> )	1.96	0.26
Clay	1.59 – 1.06	0.40 – 0.60
Silt		
Fine sand		
Coarse sand		
} (Smith and Wheatcraft 1993)		
Surface soil of wet clay	1.12	0.58
Surface soil of loam texture		
Subsoil of sandy texture		
Sandy loam compacted by heavy traffic		
Sandstone		
} (Marshall and Holmes 1988)		
sand-gravel mixture (Carling and Reader 1982, <i>freeze cores</i> )	2.30	0.13
range in several gravel-bed rivers	2.60 - 1.70	0.02 – 0.36
mean of several gravel-bed rivers		
} (Milhous, 2001, <i>volume difference</i> )		

### **Porosity**

Porosity is defined as the ratio of the space taken up by voids to the total volume of sediment. Porosity is a dimensionless number less than 1, and may be expressed as a percentage. Porosity  $p$  can be computed in two ways. One possibility is:

$$p = \frac{V_v}{V_t} = \frac{V_t - V_s}{V_t} = \frac{V_t - \left(\frac{m_s}{\rho_s}\right)}{V_t} \quad (2.103)$$

where  $V_v$  is the volume of the void or pore spaces,  $V_t$  is the total volume of sediment, and  $V_s$  is the volume of the sediment without pores. The dry mass of the sediment is  $m_s$  and particle density is  $\rho_s$ . Alternatively, porosity may be computed from:

$$p = \left(1 - \frac{\rho_b}{\rho_s}\right) \quad (2.104)$$

Eqs. 2.102 and 2.104 show that bulk density of a sediment deposit is inversely related to porosity, and one term can be used to compute the other. Porosity is a measure important for aquatic habitat studies, as well as for assessing the potential amount of fines in a streambed. However, little is known about the spatial and temporal variability of porosity and bulk density in gravel-beds because in-situ measurements of bulk density are time consuming and therefore rare.

### **Void ratio**

The void ratio  $e$  is a parameter similar to sediment porosity, and is computed from the ratio of the volume of voids to the volume of sediment particles:

$$e = \frac{V_v}{V_s} = \frac{V_t - V_s}{V_s} = \frac{V_t - \left(\frac{m_s}{\rho_s}\right)}{\frac{m_s}{\rho_s}} \quad (2.105)$$

Similar to porosity, void ratio also yields values smaller than 1, but the values are somewhat larger.

Example 2.1:

A subsurface sample taken with the water displacement method described in Section 2.4 has a total volume of  $V_t = 0.020 \text{ m}^3$  or 20 liter, and a dry mass of  $m_b = 42 \text{ kg}$ . The parent material is mainly quartz with a particle density of  $\rho_s = 2,650 \text{ kg/m}^3$ .

Bulk density	$\rho_b = m_b/V_t$	$= 42 \text{ kg}/0.02 \text{ m}^3$	$= 2,100 \text{ kg/m}^3$ .
Sed. volume	$V_s = m_b/\rho_s$	$= 42 \text{ kg}/2650 \text{ m}^3$	$= 0.01585 \text{ m}^3$ .
Void volume	$V_v = V_t - V_s$	$= 0.020 \text{ m}^3 - 0.01585 \text{ m}^3$	$= 0.00415 \text{ m}^3$ .
Porosity (1) $p$	$= V_v/V_t$	$= 0.00415 \text{ m}^3/0.020 \text{ m}^3$	$= 0.208$ or 20.8%
Porosity (2) $p$	$= 1-(\rho_b/\rho_s)$	$= 1-(2,100(\text{kg/m}^3)/2,650(\text{kg/m}^3))$	$= 1-0.792 = 0.208$
Void ratio	$e = V_v/V_s$	$= 0.00415 \text{ m}^3/0.01585 \text{ m}^3$	$= 0.2619$

### 3. Spatial variability of bed-material size

---

Bed-material particle sizes may vary along the direction of stream flow (longitudinally), between the stream banks (cross-sectionally), and vertically within the bed. This variability occurs at various spatial scales. The objective of bed-material sampling may be to characterize this variability in detail, or through integration to characterize the streambed at a spatial scale larger than the bed-material variability (Section 6).

Bed-material sampling considers three spatial scales: the stream reach, a stream section, and the local scale. A stream reach is approximately 5 - 10 channel widths long, and the spatial variability of bed-material sizes in the reach scale is mainly tied to large bedforms such as riffles, bars, pools, and steps. A stream section is comprised of a series of several reaches that are either similar in stream type and bed-material composition or feature a shift in stream type and bed-material composition such as downstream fining. The local scale covers streambed areas of a few m<sup>2</sup> or less. Analysis at the local scale focuses on bed-surface structures such as particle clusters, sediment lobes and deposits of fines in pools or backwater areas, as well as local deposits of coarse particles. Patterns of spatial variability of bed-material size and the processes causing it are discussed in Section 3 of this document because spatial variability of bed-material sizes has implications for site selection and sampling schemes (Section 6).

#### 3.1 Downstream fining

##### *Spatial scale and processes*

Downstream fining of the surface sediment is a process resulting in large-scale spatial variability of bed-material sizes. Usually, downstream fining occurs over a stream section several reaches long, but might occur over shorter distances as well. Downstream fining may be attributed to a number of mechanisms including local control of stream gradient, coarse tributary sediment supply, or particle abrasion and breakdown (Surian 2000). Local grade control may be caused by geological uplift, blockage of the valley by mass movement, or man-made dams. A decrease in stream gradient leads to a decrease in the amount and particle size of bedload transport (transport capacity and competence) (Sambrook Smith and Ferguson 1995; Ferguson et al. 1998). Log jams can also act as a local grade control and lead to downstream fining towards the upstream side of the log jam. Bed scour and a lag deposit of coarse bed material on the downstream side of the log jam can exacerbate the downstream fining trend in a series of log jams (Rice and Church 1996a). Coarse tributary sediment supply that can be transported only on rare occasions causes rapid downstream fining between tributaries (Rice and Church 1998). A supply of fluvial sediment that experiences particle abrasion and breakdown easily can cause rapid downstream fining as well (Sambrook Smith and Ferguson 1995).

### ***Implications for sampling***

The usual objective for sampling a stream section in which particle sizes become finer downstream is to demonstrate the degree of downstream fining and to link it to a potential cause. Sampling methods suitable to demonstrate a downstream fining trend vary depending on the situation. Transects selected at even-spaced intervals may be suitable if the cross-sectional variability is not too large. As the lateral variability increases, samples could be taken from a sequence of riffles because riffles tend to be laterally less variable than other cross-sections. Alternatively, one could sample the 30 largest particles within a preset geomorphological unit, e.g., a bar head, or sample all particles contained within a small sampling area, e.g., within 0.5 m<sup>2</sup> at the center of a bar (Sampling Procedures, Section 4). The downstream increase of fine sediment may cause a bimodal particle-size distribution (Section 2.1.5.9) and the development of patches of fine and coarse sediment, with the number and size of fine patches increasing downstream (Seal and Paola 1995; Seal et al. 1998). In this case, gravel and sand patches are sampled independently from patches intersected by a transect or falling within a preset area (Spatial Sampling Schemes, Section 6).

The stream situation determines not only the sampling locations, but also the particle-size parameter that should be analyzed. The  $D_{50}$  particle size may not be well suited to show downstream fining, particularly in bimodal sediment distributions. It might be necessary to analyze both the decrease of coarse (e.g., the  $D_{95}$ , Section 2.1.4.2), and the increase of fine sediment (e.g., the percent fines, Section 2.1.5.8).

## **3.2 Surface bed-material sizes within a reach**

Bed-material sampling projects are often concerned with the spatial variability of bed-material size within the reach scale (about 5 - 10 channel widths long). At this scale, patterns of bed-material size variability are tied to channel morphology. The patterns, such as downbar fining or an alternation of relatively coarse riffles with finer-grained pools are recurring and generally predictable. Off-stream supply of non-transportable large clasts or the presence of large woody debris can disturb systematic patterns.

Patterns of bed-material size, stream morphology, the three-dimensional patterns of flow and bedload-transport processes are interdependent, but their relations may not necessarily be straight forward. The next chapters will first introduce the various geomorphological units of streambeds, and then show the spatial variability of bed-material particle sizes along geomorphological units such as downbar and landward fining on bars, lateral variability across riffles, and differences in riffle and pool sediment size.

### **3.2.1 Morphology of the bar-unit with pools, riffles, and bars**

The longitudinal stream profile along the thalweg of regular riffle-pool sequences is undulating; pools form topographic lows and riffle crests topographic highs (Fig. 3.1). In plan view, the morphological units pools, riffles, and bars are part of a single three-

dimensional bedform called the *pool-riffle-bar triplet* (Church and Jones (1982), or the *bar unit* (Dietrich 1987). The bar unit for a straight, a meandering, and a braided stream is shown in Fig. 3.2. The upstream end of the bar unit is the pool that widens and shoals

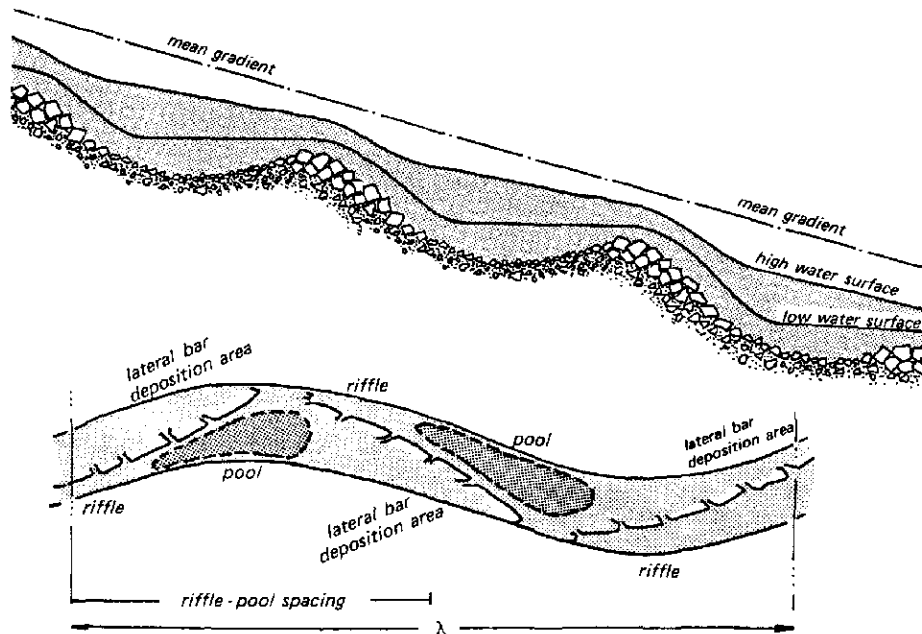


Fig. 3.1: Longitudinal (top) and plan view (bottom) of a riffle-pool sequence. The diagonal front lobe of the bar, the submerged part of which is the riffle. (Slightly modified from Church and Jones (1982), by permission of John Wiley and Sons, Ltd.).

downstream until it terminates in an oblique shallow lobe front that extends diagonally across the stream. The downstream part of this front lobe is usually above the water line during low flows and forms the exposed bar. Farther upstream and towards the other side of the stream, the lobe front becomes inundated. The deepest and submerged part of the lobe front is the riffle crest (Dietrich 1987).

The bar unit extends over the length of two visible bars. Bar patterns that are repeated along opposite banks are called alternate bars in straight streams or riffle bars (Dunne and Leopold 1978), and point bars in meandering streams (Fig. 3.2, top and center).

The relative position of the riffle crest (or the “topographic high”) with respect to the bar depends on whether the stream is meandering or straight, and on the angle with which the riffle-forming bar lobe crosses the stream. In straight streams with alternate bars, the lobe front crosses the stream not perpendicular, but at a rather low angle to the banks. This positions the riffle crest near the upstream end of the bar, or close to the downstream end on the next bar upstream (Fig. 3.2, top). If the lobe front crosses the stream almost perpendicular to the banks, the riffle appears in front of the bar (Fig. 3.3).

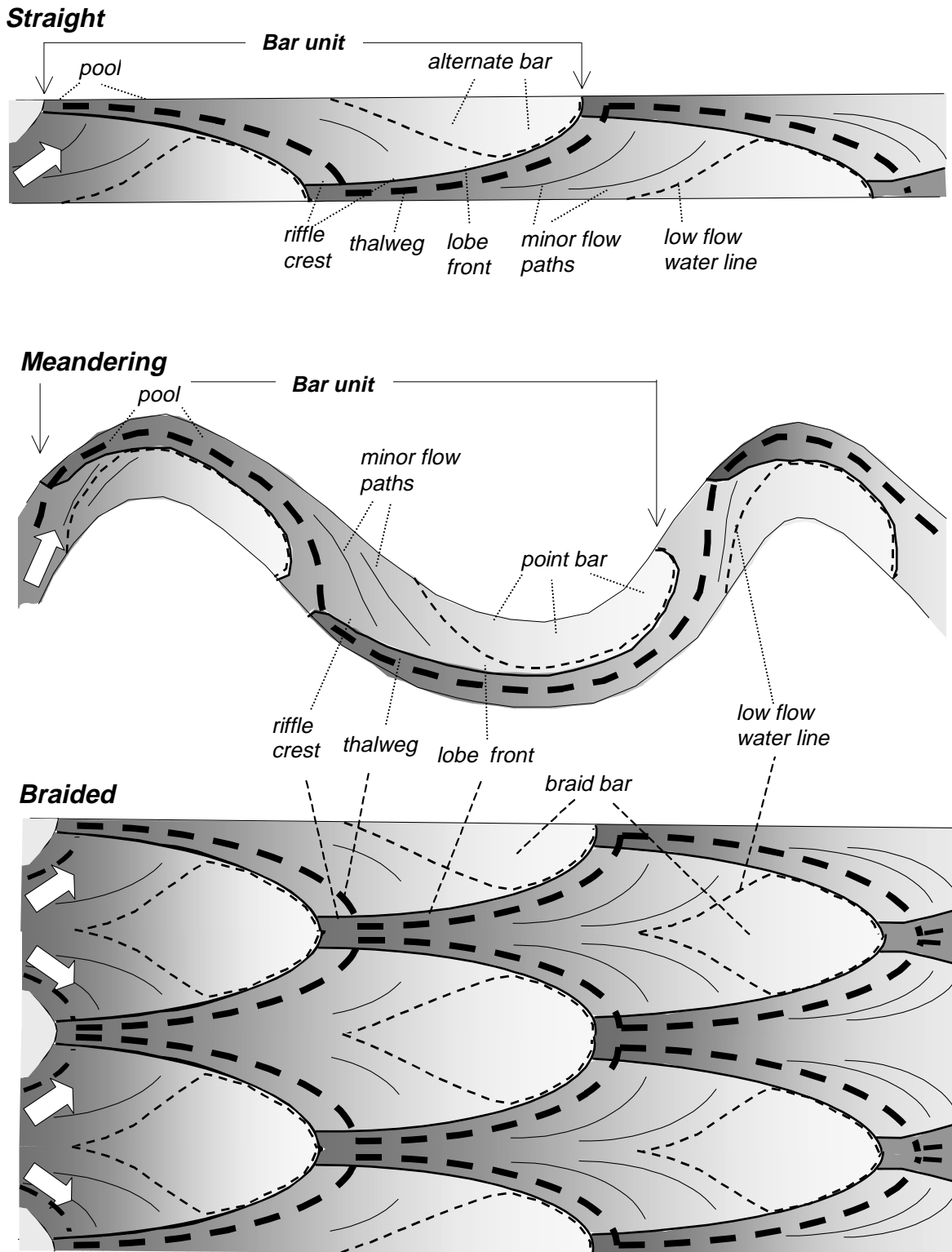


Fig. 3.2: Morphology of a bar unit in straight (top) and meandering (bottom) streams. Water depth is deepest in the areas with darkest shading, while areas of lightest shading are bars that are exposed during low flows. (Adapted after Dietrich (1987), Fujita (1989), and Whiting and Dietrich (1993)).

In meandering streams, the bar wraps around the bend and forms a point bar. The bar unit extends over the length of a complete meander (i.e., two bends) (Fig. 3.2, center). In meandering streams, the riffle is at the crossing of stream curvature between two bars. The pool in a bend is part of the bar unit that extends to the next point bar downstream. Table 3.1 summarizes riffle locations for various bar types in pool-riffle or C-type channels.

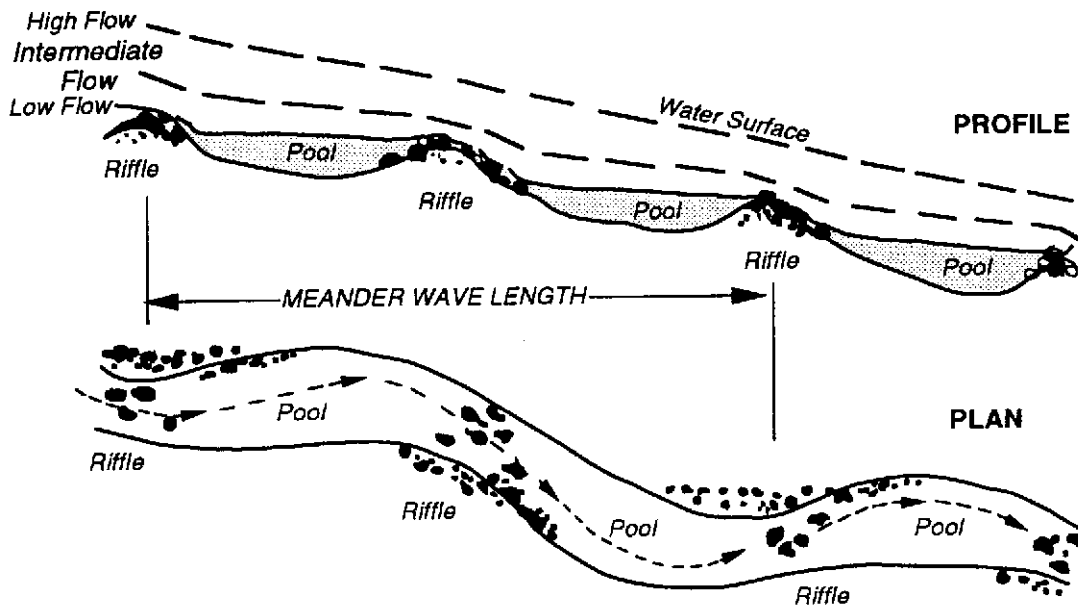


Fig. 3.3: Longitudinal (top) and plan view (bottom) of a riffle-pool sequence. Note that the riffle is located in front of the riffle bar. (Reprinted from Newbury and Gaboury (1993), by permission of Newbury Hydraulics, Ltd.).

Table 3.1: Riffle locations for various bar types in pool-riffle or C-type channels.

Bar type	Position of riffle relative to the bar	Figure providing example
Alternate bars	near the upstream end of a bar or further upstream close to the downstream end of the next bar upstream	Fig. 3.2, top Fig. 3.1, bottom
Riffle bars	near the front or the center of the bar	Fig. 3.3, bottom
Point bars	at the crossing of curvature between two point bars	Fig. 3.2, center

Bars in mountain gravel-bed rivers with low sediment supply are usually poorly developed, small in size or confined to stream reaches with a low gradient or local backwater areas.

As sediment supply increases and stream gradient flattens, bars become more prominent: they increase in size, occupy larger proportions of the streambed and occur more regularly. Within single-thread streams, bars reach their fullest extent as alternate bars.

A further increase in sediment supply leads to a braided stream in which flow divides into several channels separated by bars that tend to shift and change during a high flow event. Bars in streams with high sediment supply and rapidly changing channels can occur at various locations within the streambed and assume a variety of different shapes (Fig. 3.4)

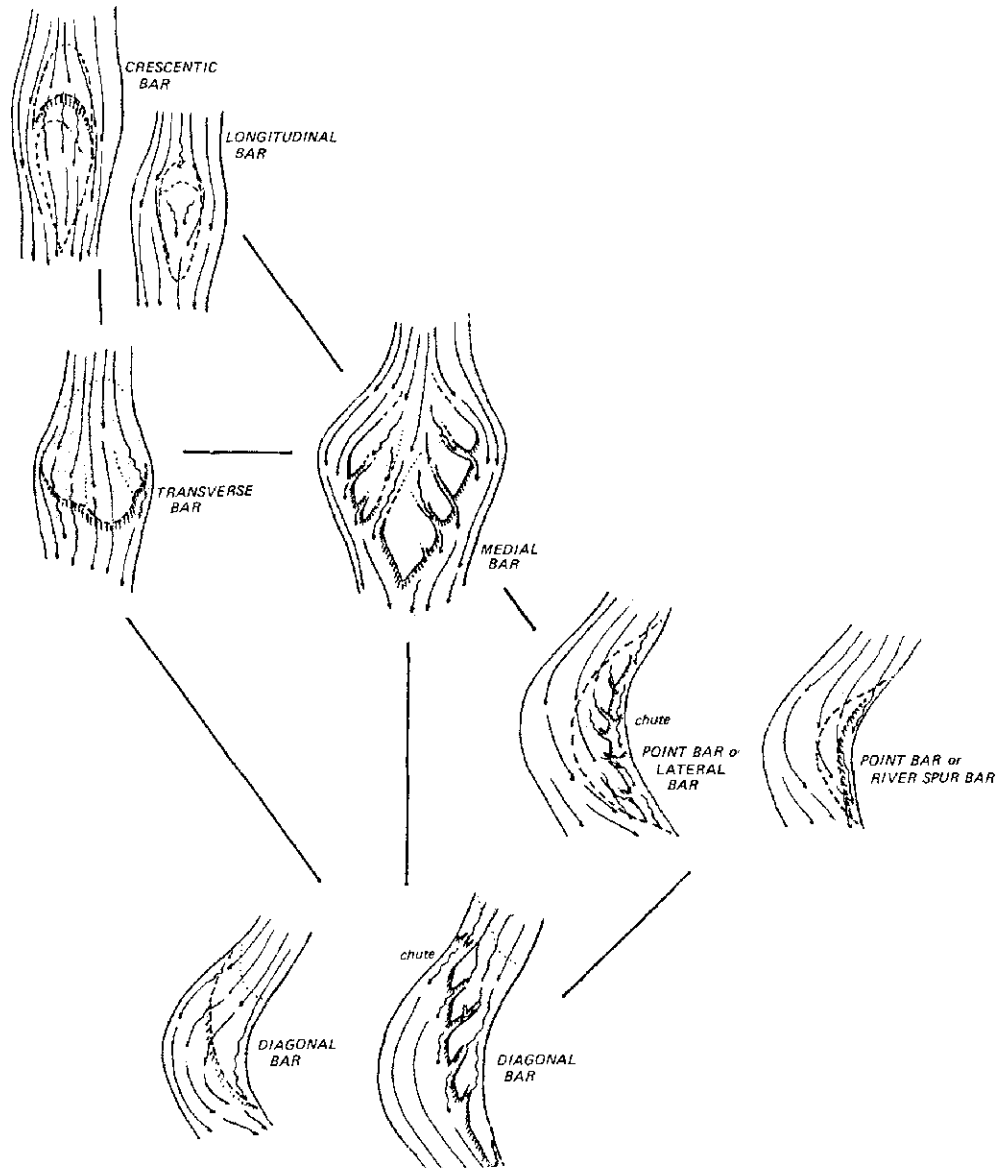


Fig. 3.4: Bar types in braided streams. Stability increases from longitudinal bars to transverse bars to medial bars to point, or lateral bars to diagonal bars. (Modified after Church and Jones (1982), by permission of John Wiley and Sons, Ltd.).

(Church and Jones 1982; Bluck 1982; Ashworth et al. 1992). A braided stream composed of longitudinal or medial bars is shown schematically in Fig. 3.2 (bottom).

### 3.2.2 Bed-material particle-sizes on pools, riffles, and bars

#### 3.2.2.1 Helical flow and bed-material size in a bar unit

The three-dimensional model of helical flow in which surface and bottom flow are at angles to each other (Thompson 1986) can be used to describe longitudinal and lateral variability of bed-material sizes within the reach (Fig. 3.5). On the riffle at the crossover between meander bend curvatures, the near-bottom flow spreads diagonally across the stream, extending from the thalweg to the upstream part of the bar on the opposite side of the stream (Dietrich 1987). Flow traverses the bar head diagonally from the bank towards the thalweg (Fig. 3.6) (Dietrich 1987). The diagonal spread of flow, combined with the relatively low flow depth on riffles and bar heads reduces the flow velocity and leads to deposition of coarse bedload during high flows (Anthony and Harvey 1991). Flow velocities in the pool are high during high flows and can transport all but the largest particles. Thus, in accordance with the zones of highest shear stress, bed material is coarsest in pools, on riffle crests and on the upstream end of bars (Bridge and Jarvis 1982; Dietrich and Smith 1984; Dietrich and Whiting 1989).

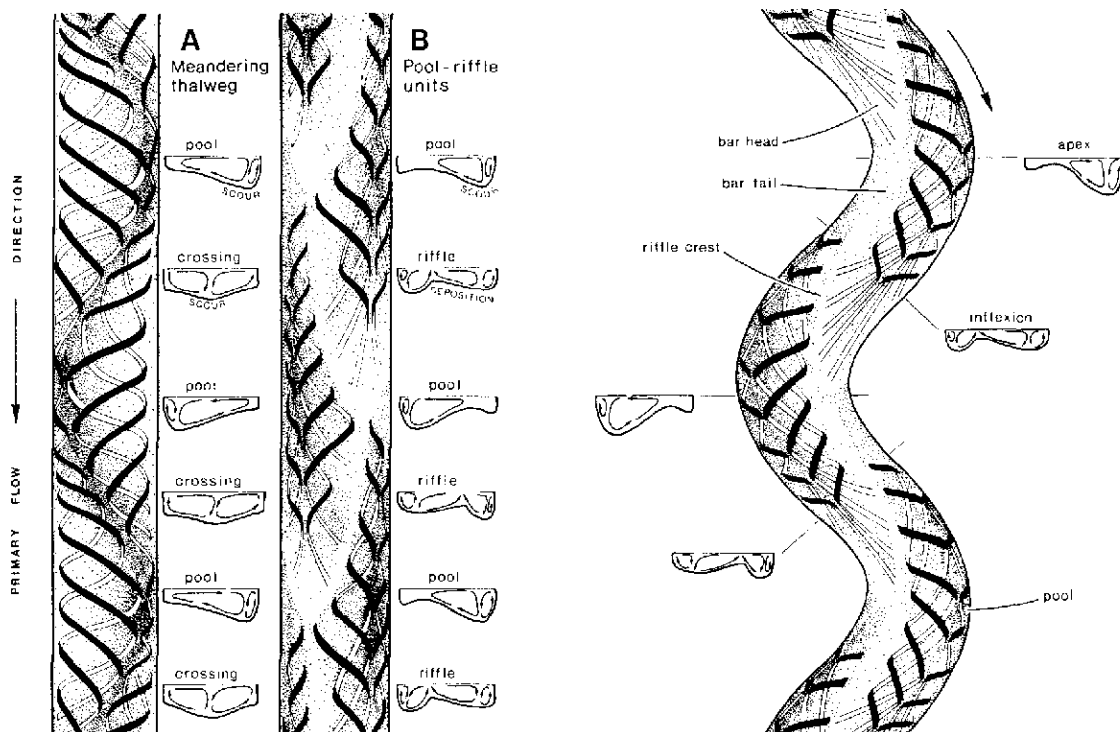


Fig. 3.5: Model of helical flow in a straight stream with a meandering thalweg (left), in a straight stream with riffle-pool units (alternate bars), and in a meandering stream (Reprinted from Thompson (1986), by permission of John Wiley and Sons, Ltd.).

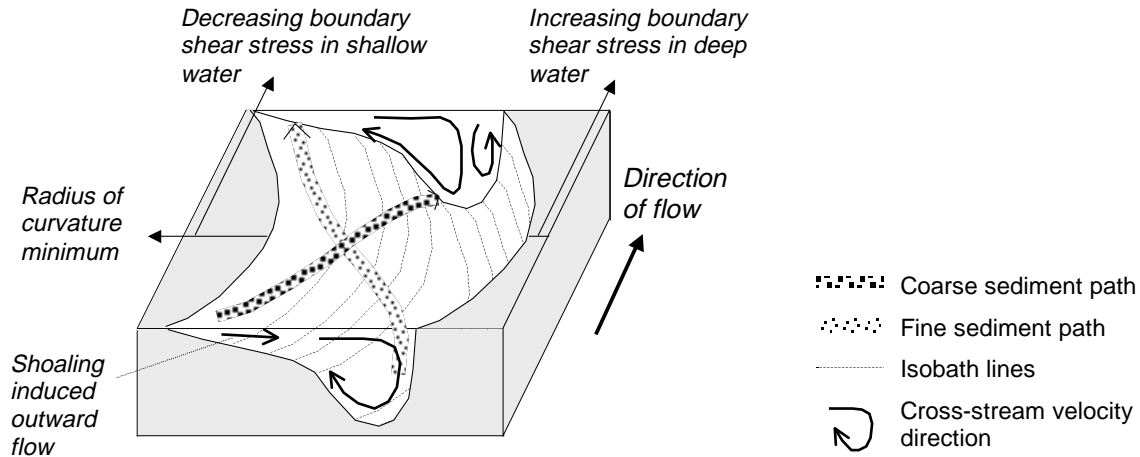


Fig. 3.6: Bottom and surface flow velocities and particle paths for coarse and fine bedload in a meander bend. (Redrawn and slightly modified from Dietrich and Smith (1984), by permission of American Geophysical Union).

At the downstream end of a bar, bottom flow is directed from the thalweg up the bar slope, transporting and depositing fine sediment at the downstream end of the bar. Thus, gravel bars cover the full spectrum of transportable particle sizes, with the coarsest particles on the upstream end, and the finest particles at the downstream end (downbar fining). Downbar fining occurs on basically all free-formed bars, but has been demonstrated in particular detail on large gravel bars in braided rivers (Smith 1974; Bluck 1982, 1987; Church and Jones 1982; Ferguson and Werritty 1983; Mosley and Tindale 1985; Ashworth and Ferguson 1986; Brierley and Hickin 1985, 1991; Brierley 1991; Wolcott and Church 1991; Ashworth et al. 1992). The downbar fining trend is accompanied by a landward fining trend that extends from the bar toe to the bank (e.g., Bridge and Jarvis, 1976, 1982; Keller and Melhorn 1981; Dietrich and Smith 1984; Lisle and Madej 1992).

At first sight, bars may seem to be ideal sampling locations because they are exposed and dry during low flows. However, due to downbar and landward fining, no single bar location is representative of the particle-size distribution of the entire bar, nor is the particle-size distribution on bars necessarily representative of the entire stream reach. In coarse gravel-bed streams with low sediment supply, bar surface sediment tends to be finer than the reach-average bed-material size, especially if the bar is forced by an obstacle to flow. The difference in bar and channel particle size becomes less pronounced as the sediment supply to the stream increases. Another factor that may cause problems for bed-material sampling on bars is that bars may feature small-scale surface structures such as gravel lobes and particle clusters (Section 3.3).

Fig. 3.7 shows the spatial variability of surface bed-material size over morphological units of pools, riffles, and bars. Trends of downbar fining, landward fining, and a generally coarse thalweg occur in alluvial streams with different morphologies.

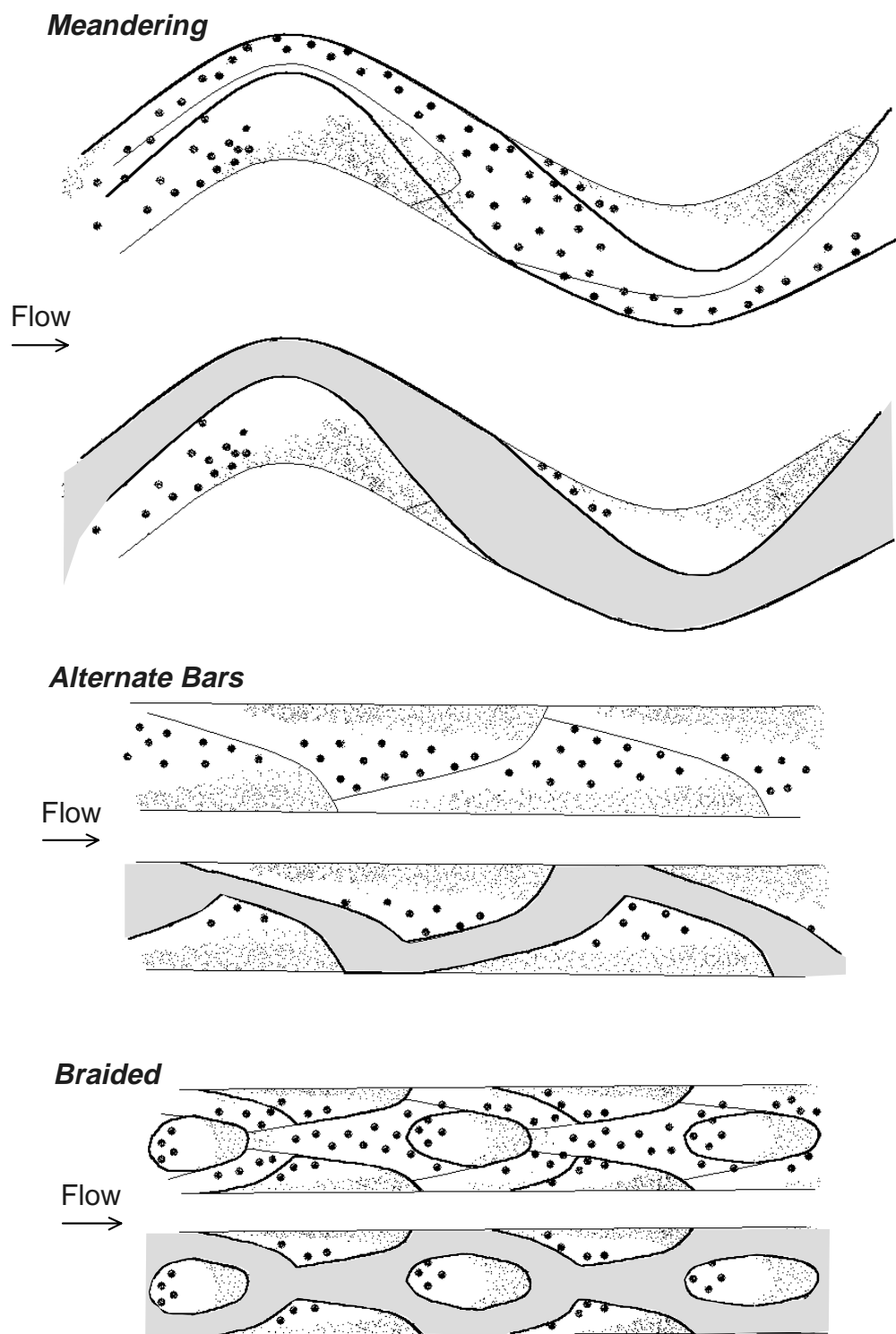


Fig. 3.7: Spatial variability of surface bed-material size on morphological units for meandering, straight, and braided streams. Large dots indicate coarse bed-material size, small dots indicate fine sizes. Top plots for each stream type show an empty streambed and the structure of the bar unit. Bottom plots show the channels during low flow. Comparison with Fig. 3.2 helps identify bar units. (Modified from Whiting (1996), by permission of John Wiley and Sons, Ltd.).

The formation of well developed pool-riffle-bar triplets, or bar units, does not only require a sufficiently large sediment supply and an appropriate stream gradient. It is also important that the interaction between flow and sediment transport is not controlled by the presence of large woody debris (LWD) or large boulders. Effects of LWD and boulders on channel morphology and the spatial distribution of bed-material size are discussed in Sections 3.2.4 and 3.2.5.

### 3.2.2.2 Riffle-related features: rapids, runs, glides, and pool-exit slopes

Riffles and pools, the two major constituents of the inundated part of the reach, can be further segregated into geomorphological (or habitat) units (Fig. 3.8). The form and bed-material size of riffles, and riffle-related features are discussed below. The relation

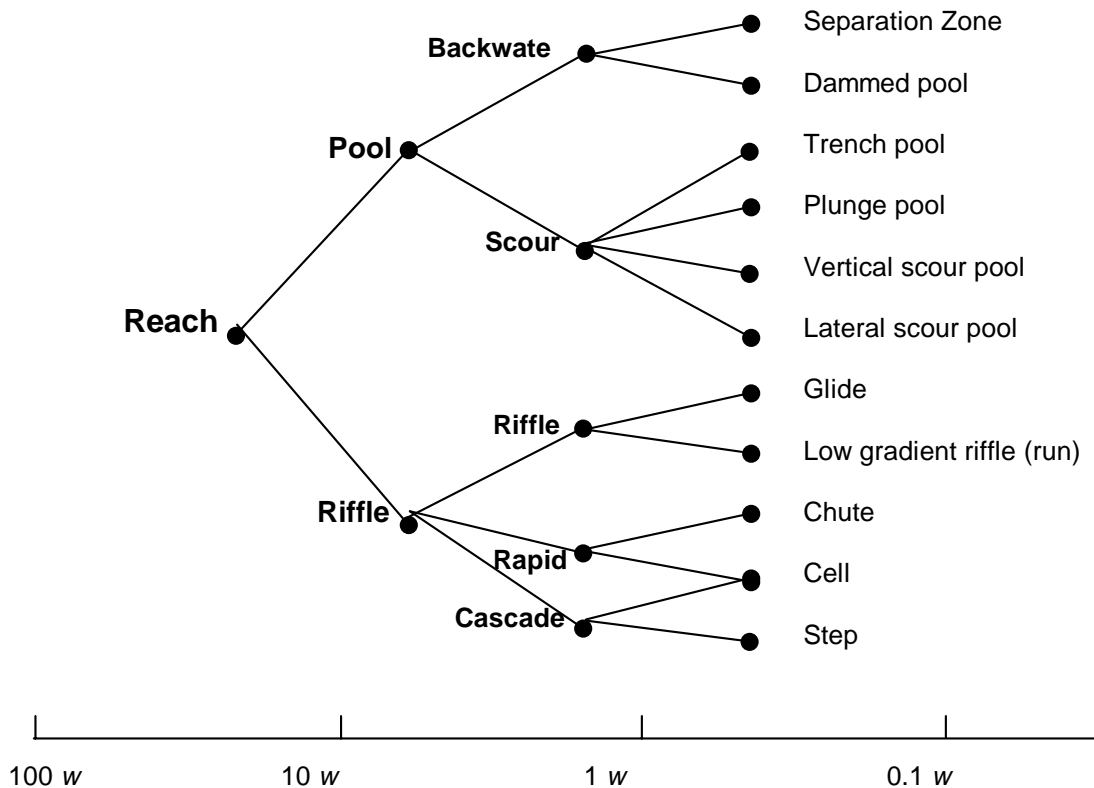


Fig. 3.8: A spatially hierarchical representation of channel morphology units;  $w$  = stream width. (Slightly modified from Church (1992), by permission of Blackwell Science, Ltd.)

between riffle and pool bed-material size is discussed in Section 3.2.2.3. The various pools indicated in Fig. 3.8 are caused by the presence of LWD that effectively controls flow hydraulics and sedimentation within a reach. Pools are therefore discussed in Sections 3.2.4 and 3.2.5.

Riffles, as well as the streambed area between pools and riffles can assume a variety of morphological forms with different flow dynamics and bed-material composition. Fluvial geomorphologists and fishery biologists distinguish between rapids, runs, and glides (e.g., Bisson et al. 1982; Church 1992), however, the terminology describing morphological units may not be entirely identical between authors. The descriptions are summarized below.

*Rapids* are steeper, contain larger particles, and have faster flow than riffles. Flow on riffles is usually subcritical (Froude number  $<1$ ) during low flows, whereas much of the flow over rapids is generally critical, or supercritical (Froude number  $\geq 1$ ). Riffles might include a few untransportable large particles protruding through low flow, but these are not organized into transverse ribs (Section 3.4.1), as they tend to be on rapids. Riffles have local gradients of less than 0.02, while rapids have local gradients of about 0.02-0.04 (Grant et al. 1990; Church 1992). Cascades are steeper than rapids, and are comprised of cobbles and boulders. Small pools are common between large clasts.

*Runs* refer to stream segments with a straight downstream sloping bed surface (Platts et al. 1983) and relatively homogeneous bed material, similar to the plane-bed morphology described by Montgomery and Buffington (1997, 1998), whereas riffles are sections of locally steep gradient in the longitudinal stream profile. Compared to low flow conditions on riffles, runs have deeper flows, and lower flow velocities.

The term *glide* is sometimes used synonymously with run. A glide may refer to the transitional area between the deep part of the pool and the crest of the riffle in which stream width increases while flow depth decreases (Bisson et al. 1981). This transitional zone may be termed *pool-exit-slope* (Thompson et al. 1996), especially if the stream gradient is sloping upward over this area. Bed material on the glide or pool exit slope tends to be less coarse than on the riffle crest. Church (1992) applies the term glide to a former pool that has been completely filled with sediment. If a differentiation is made between runs and glides, glides have deeper flows and lower flow velocities than runs and have a closer resemblance to pools than to riffles (i.e., a nearly horizontal water surface).

### 3.2.2.3 Coarsest parts of the reach: pools, riffles, and bar heads

In alluvial, free-formed streams, pools, riffle crests, and bar heads are generally the coarsest areas in a stream reach. However, the relation of bed-material size between pools and riffles, and riffles and bar heads varies depending on whether erosional or depositional processes are predominant in forming the pool and riffle in a given bar unit.

#### ***Coarse pool sediment due to scour***

During high flows, shear stress is often higher in pools than on riffles and scours all but the coarsest sediment out of pools, leaving a coarse lag deposit behind. If pool scour is the prevailing mechanism, then pools may be the coarsest parts of the streambed.

### ***Coarse riffle deposits and scour of finer gravel***

Field measurements in gravel-bed rivers often show that riffles and not pools are the coarsest locations within a reach (e.g., Keller 1971; Richards 1976; Keller and Melhorn 1978, 1981; Lisle 1979; Hirsch and Abrahams 1981; Campbell and Sidle 1985; Lisle and Madej 1992, Keller and Florsheim 1993). This phenomenon is often attributed to the reversal of velocity, or shear stress, during a high flow event, a concept introduced by Keller (1971). During low flows, flow velocities are highest on riffles, and lowest in pools, owing to the steep gradient and shallow flow depth on riffles, while pools are deep and have a low stream gradient. During rising flows, flow velocity and bottom shear stress increases at a faster rate with discharge in pools than on riffles, so that at a certain high flow of approximately bankfull, flow velocity is higher in pools than on riffles. This high flow velocity scours and transports large particles from the pool, leaving a coarse lag deposit behind. The largest particles removed from pools are likely to be deposited on riffles where the flow velocity and shear stress are lower. As flow begins to wane, flow velocity on riffles is still lower than on pools, and falls below the competence to transport large particles before pools are affected, causing further deposition of coarse particles on riffles. Riffle coarsening is further augmented during low flows because flow velocity and shear stress do not drop as low on riffles as in pools. This allows scouring fines off riffles, leaving only the coarser and most stable particles in place. The finer gravel particles scoured off riffles are then deposited in pools (Bhowmik and Demissie 1982; Yang 1971). Both deposition of coarse particles on riffles and subsequent scour of fines can occur together (Campbell and Sidle 1985) and act on coarsening the riffle while fining the pool.

### ***Riffles are not always coarser than pools***

Field studies have not consistently verified the occurrence of velocity reversal and its sedimentary consequences, (i.e., that riffles are coarser than pools). Velocity reversal may occur at any discharge and is not necessarily limited to high flows around bankfull (e.g., Teleki 1972; Bhowmik and Demissie 1982; Carling 1991). Numerical modeling revealed that velocity reversal requires that pools are hydraulically rougher (i.e., coarser) than riffles, or that riffles are substantially wider than pools. The discharge at which velocity reversal occurs decreased with increasing riffle spacing and increasing stream width. Consequently, wide streams with wide riffle spacing and pools with coarse lag deposits seem to be most likely to experience velocity reversal (Carling and Wood 1994). Detailed measurements of flow patterns by Thompson et al. (1996) suggest that velocity reversal requires the presence of a recirculating eddy in the pool.

### ***Structural stability on riffles***

Clifford (1993) observed that within a series of riffle-pool sequences, some riffles were coarser than pools and some were not. Sear (1996) suggested that riffles do not need to be coarser than pools for purposes of stability, but that riffles maintain their stability by having structural elements, such as clusters, particle interlocking, and imbrication (Fig. 3.9). Clusters dissipate flow energy by creating turbulence, while imbrication and particle interlocking delay sediment entrainment by minimizing the particle area exposed

to flow, and by high pivot angles. The presence of such structural features should therefore be recorded when sampling bed-material (see Section 3.4).

BEDFORM	RIFFLE	POOL-HEAD	MID-POOL	POOL-TAIL	RIFFLE
LONGITUDINAL VIEW					
BED STATE	Congested	Smoothing			Congested
SEDIMENTARY STRUCTURE OF SURFACE	Tightly packed. High frequency of particles in stable structures. Armoured. Open-work	Loosely packed. High frequency of particles in unstable positions in bed. Armoured. Increasing matrix			
SURFACE $D_{50}$					
ENTRAINMENT THRESHOLD	High	Decreasing			Low
DISTRAINMENT OPPORTUNITY	High	Decreasing			Low
BED SLOPE	+ High	Gentle			- ive
PARTICLE MOVEMENT	Short L Low $V_b$	High L High $V_b$			Mod L Mod $V_b$
BEDLOAD BALANCE	Aggrading	Degrading			Aggrading
RELATIVE EXPOSURE $D_{50}$ RIFFLE PARTICLE	Low	Increasing			High

Fig. 3.9: Model of bed material properties and bedload parameters in a riffle-pool sequence. + = very, -ive = negative,  $L$  = particle transport distance,  $V_b$  = particle transport velocity, Relative exposure of  $D_{50}$  particle = within the bed material. (Reprinted from Sear (1996), by permission of John Wiley and Sons, Ltd.).

### Deposition of fines in pools

Pool fining can become quite pronounced in streams with a high supply of sand and silt-sized sediment that is transported at low flow and deposited over the coarse bottom sediment in pools. Riffles are relatively unaffected by low flow sand transport because the higher flow velocities prevent deposition. Pool fines may cover the pool bottom as a thin veneer or fill a substantial portion of the pool volume (Lisle and Hilton 1992, 1999; Hilton and Lisle 1993). Sampling fine sediment in pools is discussed in Section 6.6.2.

### Riffles and bar heads

Riffles and the upstream end of bars may be of similar coarseness if sediment supply is equal to the capacity of the stream to transport it or if sediment supply exceeds the transport capacity. If sediment supply is generally less than transport capacity, coarse gravel particles tend to be scoured off the riffle, leaving only the coarsest particles as a

lag deposit, whereas the bar head sediment remains unchanged. This increases the difference in bed-material size between riffles and bar heads.

### ***Lateral variability on riffles and runs***

Some riffles do not have significant spatial variability of particle sizes; this homogeneity makes riffles preferred sampling locations, in spite of being submerged by flow. However, not all riffles have homogeneous particle size-distributions. The patterns of bottom flow near the bar can also lead to lateral variability of the particle size on riffles, particularly if the downstream spacing between bars is tight. In this case, riffle bed-material tends to be coarse between the thalweg and the side of the riffle that merges into the upstream end of the downstream bar, and finer at the opposite bank close to the next bar upstream.

A common form of lateral variability is bankward fining that may occur in any cross-section with self-formed banks. Bankward fining is not only due to gravel particles becoming finer towards the banks, but also due to the deposition of sand in the area between the low-flow and the high-flow bank line, whereas most of the mid-channel streambed is sandless. Thus, bed-material samples collected between the high-flow water lines of both banks often produce a finer bed-material size than sampling within the borders of the low-flow water line. Careful scrutiny of the sampling objectives should help deciding whether sampling should extend to the low-flow or the high-flow water line.

Table 3.2 summarizes features of bedform morphology, flow, and patterns of bed-material size for riffles, pools, and bars in C-type streams with riffle–pool morphology. Note that the transition between the upstream end of the bar and the riffle, as well as between the downstream end of the pool and the upstream end of the riffle can be smooth without any recognizable morphological boundaries.

An example of the spatial variability of bed-material particle sizes within a riffle-pool reach is provided by Lisle and Madej (1992) (Fig. 3.10). Generally, bed material is coarsest on riffles, and bar heads, both in the aggrading and degrading reach, while pools have deposits of fines. However, irregularities and patchiness in the spatial patterns of bed-material size may obscure underlying schematic spatial patterns of bed-material size.

Table 3.2: Morphological, hydraulic, and sedimentary features characteristic of riffles, pools and bars during low and high flows in C-type streams with riffle-pool morphology

Criterion	Riffles	Pool	Bar
Longitudinal form	ridge, or locally steep	depression, or locally flat	evenly inclined, but less steep than thalweg
Cross-section shape	± symmetrical or asymmetrical	asymmetrical	asymmetrical
<i>Low flow situation</i>			
Flow depth	shallow	deep	mostly exposed
Flow velocity	relatively fast	relatively slow	n/a
Water surface	locally steep and rippled	nearly horizontal, smooth	n/a
Stream width	wide	narrow	n/a
Bed-material size	coarse scour lag	coarse scour lag, or deposit of fines	transition from coarse to fine
Surface fines	not likely	possible	possible
Spatial variability	_____	lateral & longitudinal	_____
Structural elements	clusters, wedging, imbric.	wedging, imbrication	clustering & imbrication
<i>High flow situation</i>			
Flow depth	shallow	deep	shallow
Flow velocity	slow	fast	slow
Water surface	_____	evenly inclined over the reach	_____
Stream width	_____	± even over the reach	_____
Bed-material size	coarse deposit	coarse scour lag	transition from coarse to fine
Surface fines	not likely	not likely	possible

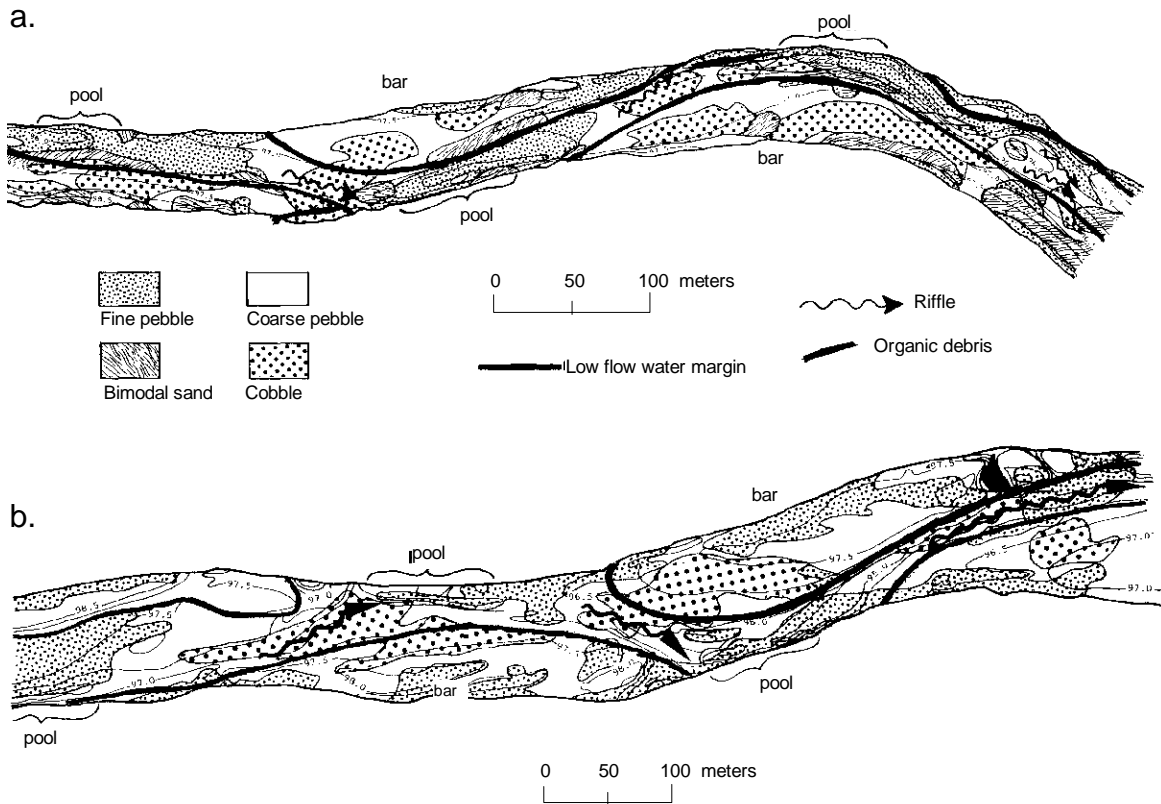


Fig. 3.10: Spatial variability of bed-material sediment sizes in a degrading (a) and aggrading (b) riffle-pool reach of Redwood Creek, northern California. (Reprinted from Lisle and Madej (1992), by permission of John Wiley and Sons, Ltd.).

### 3.2.3 Stream morphology and particle-sizes in B-type and A-type streams

Riffle-pool sequences and bar units typical of C-type streams with riffle-pool morphology (Section 1.3.1 and 1.3.2) and gradients within the range of about 0.001 to 0.02 become less well developed as the stream gradient steepens and stream morphology approaches a plane-bed in B-type streams with gradients of 0.01 or 0.02. Steep C-type streams tend to have only intermittent sequences of riffle-pool units, whereas low-gradient B-type streams tend to have only a few pools interspersed in a plane-bed morphology consisting largely of runs. Gravel bars as sediment storage features are poorly developed, because transport capacity often exceeds sediment supply. The few bars present have irregular forms, are tied to locations of stream widening, and occur isolated and non-sequential. Thus, free-formed pools and bars are rare in plane-bed streams with gradients around 0.01-0.03 (Montgomery and Buffington 1993). Most of the streambed could be classified as a run with little spatial variability in bed-material particle size beyond landward fining towards the bankline. This relative homogeneity in bed-material particle size is a factor that makes bed-material sampling easy in plane-bed streams. However, this ease is counteracted by the difficulty of extracting the large and often wedged particles off the streambed.

The morphology of step-pool or A-type streams (Section 1.3.1 and 1.3.2) is a sequence of steep steps composed of cobbles and boulders that alternate with pools of finer bed material (Montgomery and Buffington 1997; 1998, Church 1992; Section 1.3.1). Thus, step-pool streams have a systematic longitudinal sorting. The lateral variability is mostly random (Fig. 3.11). Bed-material sampling in step-pool streams is difficult for several reasons. Particles comprising steps are often large, tightly wedged, and cannot be extracted from the bed. Large particles also require a large spacing between individual sampling points of pebble counts to avoid serial correlation (Section 4.1.1.4). The requirement for large spacing extends sampling over a long stream distance because most step-pool streams are only a few meters wide. Individual steps or pools are too small to provide an adequately large sample size. Therefore, several steps and pools have to be sampled. Many of the step-forming particles can be transported only by catastrophically large floods. The researcher needs to decide the largest boulder size that should be included in the sample.

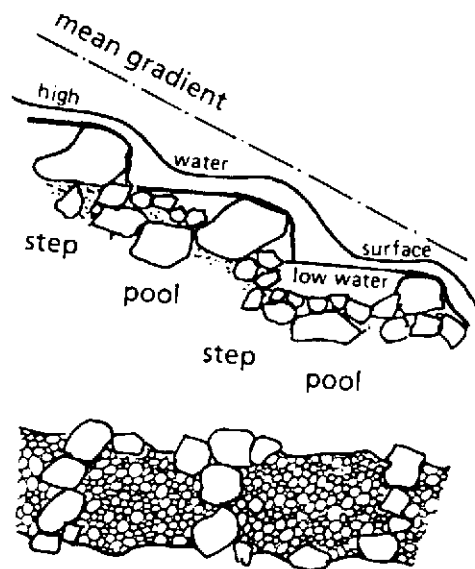


Fig. 3.11: Longitudinal and plan view of a step-pool stream. (Reprinted from Church (1992), by permission of Blackwell Science, Ltd).

### 3.2.4 Effect of large woody debris and other stream blockages on stream morphology and particle sizes

The presence of large woody debris (LWD), debris flow or landslide deposits, and beaver dams in streams affect the sediment-transport dynamics in streams, the channel morphology, and the spatial distribution of sediment size in various spatial scales. LWD or other material can block the downstream bedload conveyance entirely or partially. This may lead to the deposition of coarse sediment upstream of the blockages, of fine sediment in areas of backwater or water ponding, and to coarse lag deposits in scour and plunge pools. Reaches downstream of the obstruction may be cut off from sediment

supply and become degraded. Even isolated pieces of LWD or large boulders may alter the local flow field and affect stream morphology and particle sizes in their vicinity.

***Large-scale effects: upstream sediment wedge and downstream scour***

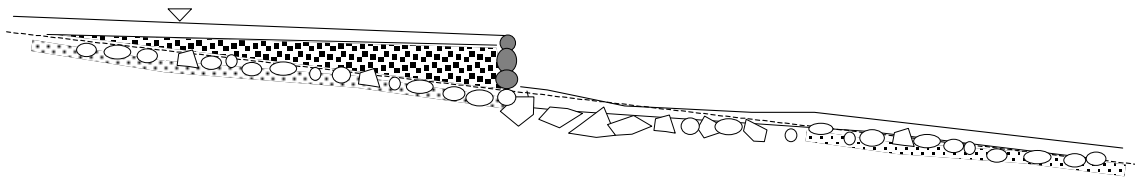
A log jam consisting of several large tree trunks and finer woody debris can effectively block the downstream conveyance of sediment. Blockage causes the deposition of bedload sediment on the upstream side. The alluvial wedge (Fig. 3.12 a) resulting from this deposition may extend over a distance of several 100 m. The channel gradient upstream of the log jam decreases as the alluvial wedge starts to grow, so that particle sizes deposited close to the log jam become finer over time. The downstream side of the log jam receives no sediment from upstream. Thus, excess shear stress winnows sand and gravel particles from the bed until only large particles that are commonly untransportable are left on the bed as a coarse lag deposit or erosion pavement (Rice 1994, 1995; Rice and Church 1996a; Buffington and Montgomery 1999b). Depending on the duration of the log jam, the downstream erosion pavement may extend over a 100 m or more as well. Some log jams are long-lived, and remain in place for decades depending on the rotting resistance of the wood. Eventually, as the log jam begins to deteriorate, it becomes increasingly permeable to sediment. Sediment starts to be scoured off the upstream deposit which then coarsens over time. The downstream bed starts to become finer as the lag deposit is replenished with upstream supply. Not all log jams are long-lived. Some log jams shift annually, causing an annual change in the morphology and particle-size distribution of the streambed.

***Medium-scale morphological and sedimentary effects***

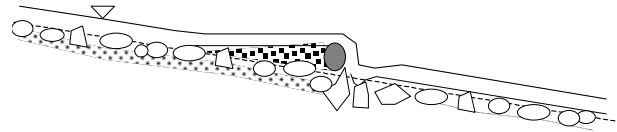
Channel blockage may also affect stream morphology and particle sizes in the medium scale of several meters. One or a few logs blocking a stream may cause upstream deposition of relatively coarse bedload (Fig. 3.12 b). A plunge pool may form at the downstream side if flow overtops the channel obstruction (Thompson 1995; Montgomery et al. 1995; Montgomery and Buffington 1997, 1998). The plunging water is likely to scour all but the largest particles, leaving a coarse erosion pavement. Fine sediment might deposit in the backwater area of plunge pools during low flows, or flow in plunge pools may be continually large enough to winnow all fines. Downstream degradation of the bed does not occur when bedload passes over the obstruction after having filled the upstream void. A closely-spaced sequence of large woody debris pieces extending over the width of the stream may produce a sequence of log steps (forced step-pool channel) (Fig. 3.12 c).

If the stream blockage extends high above the water surface and if the sediment supply from upstream is low, a *dammed* pool may form on the upstream side of log jams (Bisson et al. 1981; Thompson 1995). Dammed pools may have only small deposits of fines or may become filled with sediment given enough time (Fig. 3.12 d).

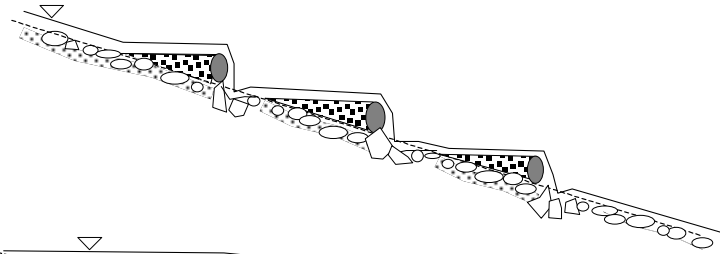
a) Alluvial wedge and degraded stream bed downstream



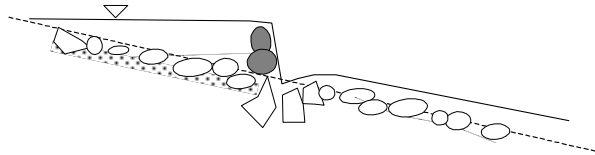
b) Log step with coarse upstream fill and downstream plunge pool



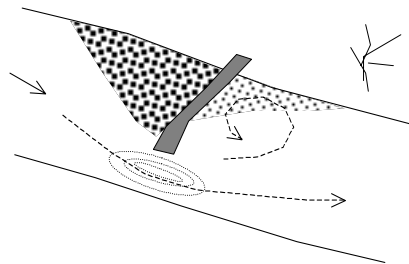
c) Sequence of log steps (forces step-pool stream)



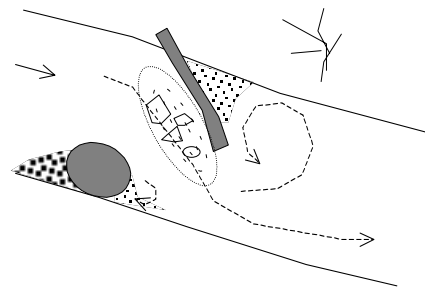
d) Upstream dammed pool with some fines and coarse-bottomed downstream plunge pool



e) Coarse deposit upstream of log, coarse-bottomed scour pool, and deposit of fines downstream



f) Coarse-bottomed scour pool or trench along log, backwater deposit of fines



g) Backwater pool with deposits of fines

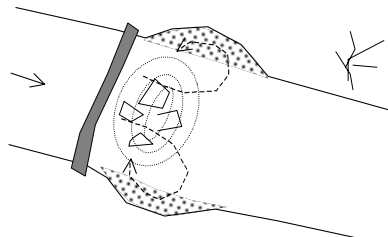


Fig. 3.12: Stream morphology and bed-material size around large woody debris. Deposit of coarse and fine sediment, lag deposit of coarse particles, unaffected streambed, and LWD or other stream obstructions. (a - d) side view, (e - g) plan view.

The stream blockage does not have to be complete to have a pronounced morphological and sedimentary effect on the stream. Partial blockage of the downstream sediment conveyance by individual pieces of large woody debris interrupts the necessary three-dimensional patterns of flow and disturbs the formation of riffle-pool sequences. A piece of LWD extending from the banks partially into the stream may have a deposit of relatively coarse sediment on the upstream side, while finer sediment is deposited in the backwater area on the downstream side (Fig. 3.12 e). A coarse-bottomed scour pool with a coarse lag deposit may develop where a piece of LWD confines or constricts the flow within the cross-section (Fig. 3.12 f, see also Fig. 3.12 e). A *backwater pool* with deposits of fine sediment may be created in the backwater area of a log (Fig. 3.12 g).

### *Chaotic patterns of bed-material size*

The presence of LWD may erase any apparent systematic patterns in spatial variability of bed material size (Buffington and Montgomery 1999b) (Fig. 3.13). The resulting patchy appearance of bed-material size has implications for bed material sampling locations and sampling schemes.

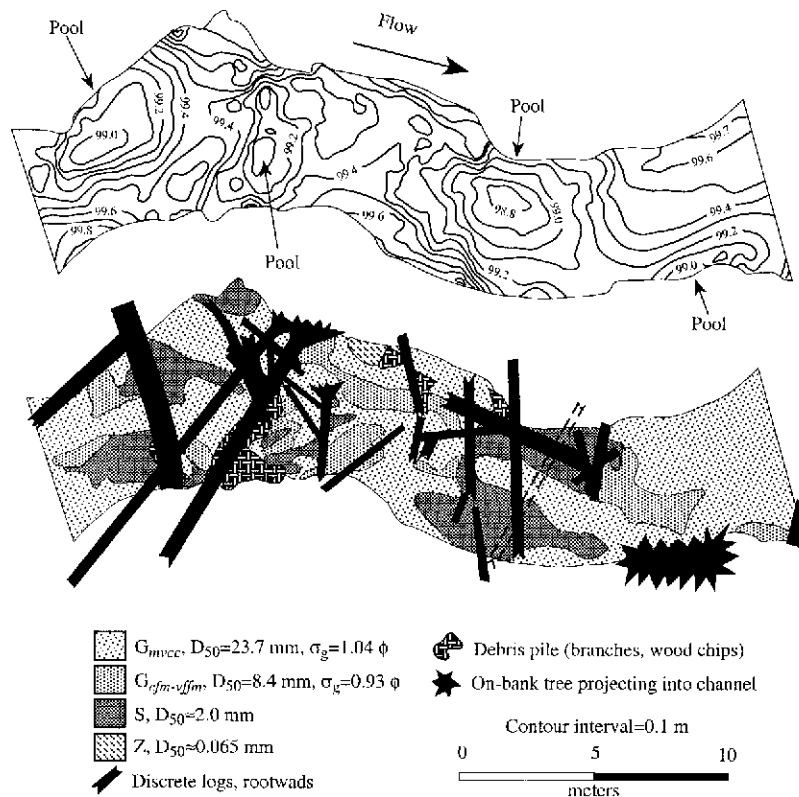


Fig. 3.13: Stream morphology and chaotic patterns of bed-material particle size in a stream containing a large amount of large woody debris. Flow direction is from left to right.  $G$  = gravel (see Section 4.1.3.4 for more detailed definition of facies descriptions),  $S$  = sand, and  $Z$  = silt;  $\sigma_{gs}$  = Inman (1952) sorting coefficient (Section 2.1.5.4). (Reprinted from Buffington and Montgomery (1999b), by permission of the American Geophysical Union).

If possible, reaches with LWD should be avoided when sampling bed-material with the aim of characterizing a reach. A reach that consistently displays a particular stream type with its recurring features of fluvial geomorphology should be selected instead. However, some streams, especially in the Pacific Northwest, consist of a sequence of log jams and are continually loaded with large woody debris. If such streams need to be sampled, it is important to identify the sedimentary processes and the resulting sedimentary units. That knowledge forms the basis for selecting which of the sedimentary units to sample, and for determining how they are to be included in the sampling project.

### **3.2.5 Bed-material particle sizes around boulders**

Isolated boulders supplied from rockfall or unearthed from glacial deposits likewise cause complicated local hydraulic conditions in their vicinity and thus affect the bed morphology and the spatial variability of bed-material size.

Coarse sediment may be deposited on the upstream side of boulders. Coarse-bottomed plunge pools may form where flow overtops logs or boulders. Coarse-bottomed scour pools form if flow is confined vertically or laterally by logs or boulders and scours the adjacent stream bed (Bisson et al. 1981, 1987; Sullivan et al. 1987; Church 1992; Wood-Smith and Buffington 1996). A horse-shoe vortex scour may form at the upstream side of boulders, while fine sediment is deposited in the downstream wake (Section 3.4.4). Boulders or logs may also create backwater in which fine sediment is deposited.

It is important to understand the sedimentary processes in the vicinity of untransportable stream objects. This understanding helps to evaluate whether sediment from the vicinity of boulders is representative or appropriate for sampling. The presence of untransportable large boulders also poses the question of whether or not to include these boulders in a particle-size analysis. The answer depends on the specific questions of the sampling project. If, for example, local channel *form roughness* is to be determined, immobile boulders need to be included.

Flow around immobile boulders dissipates energy which otherwise may have been utilized for transporting coarse bedload. Thus, immobile boulders may also have an effect on the general bed-material size of the reach, causing perhaps less coarse and less armored deposits than would develop were the boulders not present (Buffington and Montgomery 1999b). Immobile boulders might also cause flow confinement and scour, leading to a coarse lag deposit and a bed coarser than if the boulders were absent. Thus, if boulders are expected to cause general bed fining or coarsening, both the mobile and the immobile bed material should be sampled. Immobile boulders are usually not included in a sampling project if the bed-material size analysis is used to compute bedload transport rates.

### 3.3 Vertical variability in bed-material size

Gravel deposits can have a variety of different vertical structures depending on the supply of transportable sediment in the streambed, the bed-material particle-size distribution, and the interaction with the hydraulics of flow. Various processes causing a vertical structure (stratification) in the bed-material of gravel-bed streams are discussed in Section 3.3.1. Implications for sampling are discussed in Section 3.3.2.

#### 3.3.1 Sedimentary processes causing vertical stratification

Three distinct particle-size distributions are commonly observed in gravel-bed rivers: (1) Coarse gravel distributions are often skewed towards fines and have a median particle size of 32 to 64 mm. The median particle size of the coarse part is cobbles, whereas the median size class of the fine part is medium gravel. (2) Cobble distributions without much fine and medium gravel have a median particle size in the cobble range. (3) Fine gravel distributions with mostly medium gravel and sand and only a few coarse gravel particles and cobbles. Even within one stream location, the bed-material particle-size distribution may change over time, owing to a change in sediment supply or hydraulics of flow. These changes are reflected in the vertical profile of the streambed sediment.

The vertical profile of a streambed usually shows that particle-size distributions do not change gradually with depth, but change abruptly in the form of layers (or strata). The particle-size distribution in each layer is the result of an interaction between flow hydraulics and sediment. The strata can therefore be used to obtain information on the amount of sediment supplied to the stream, the sediment particles sizes, and the manner in which the sediment was transported and deposited. Although the interpretation of the sedimentation processes may not always be straight forward in a given strata, an analysis of the sequence of the strata can provide information of the temporal sequence of flow and sediment interactions. An analysis, for example, may show an increase in the fine sediment supply and that result may be important for protecting aquatic habitat or for streambed monitoring of watershed management effects. Implications of stratified sediment for bed-material sampling are discussed in Section 3.3.2.

One example of a sediment strata is the *framework-supported* gravel deposit (Fig. 3.14 a). It forms when fine sediment is relatively scarce so that large, adjunct particles touch. If fines exceed about 20-30% of the sediment volume (which is roughly the volume of the voids between large clasts) large particles no longer touch, and the deposit starts to become *matrix-supported* (Fig. 3.14 d).

A frequently observed stratification feature in gravel-bed rivers is that the surface sediment is coarser than the subsurface sediment (Fig. 3.14 a). Surface coarsening (as opposed to subsurface fining) is attributed to three different processes: (1) selective scour of fines (erosion pavement), (2) selective deposition of large particles, or (3) armoring to facilitate equal mobility transport. These processes are discussed in Section 3.3.1.1.

Another example of stratified bed material is the *filled gravel* (Fig. 3.14 c). The presence of gravel with empty voids in the underlying strata supports the interpretation that fine

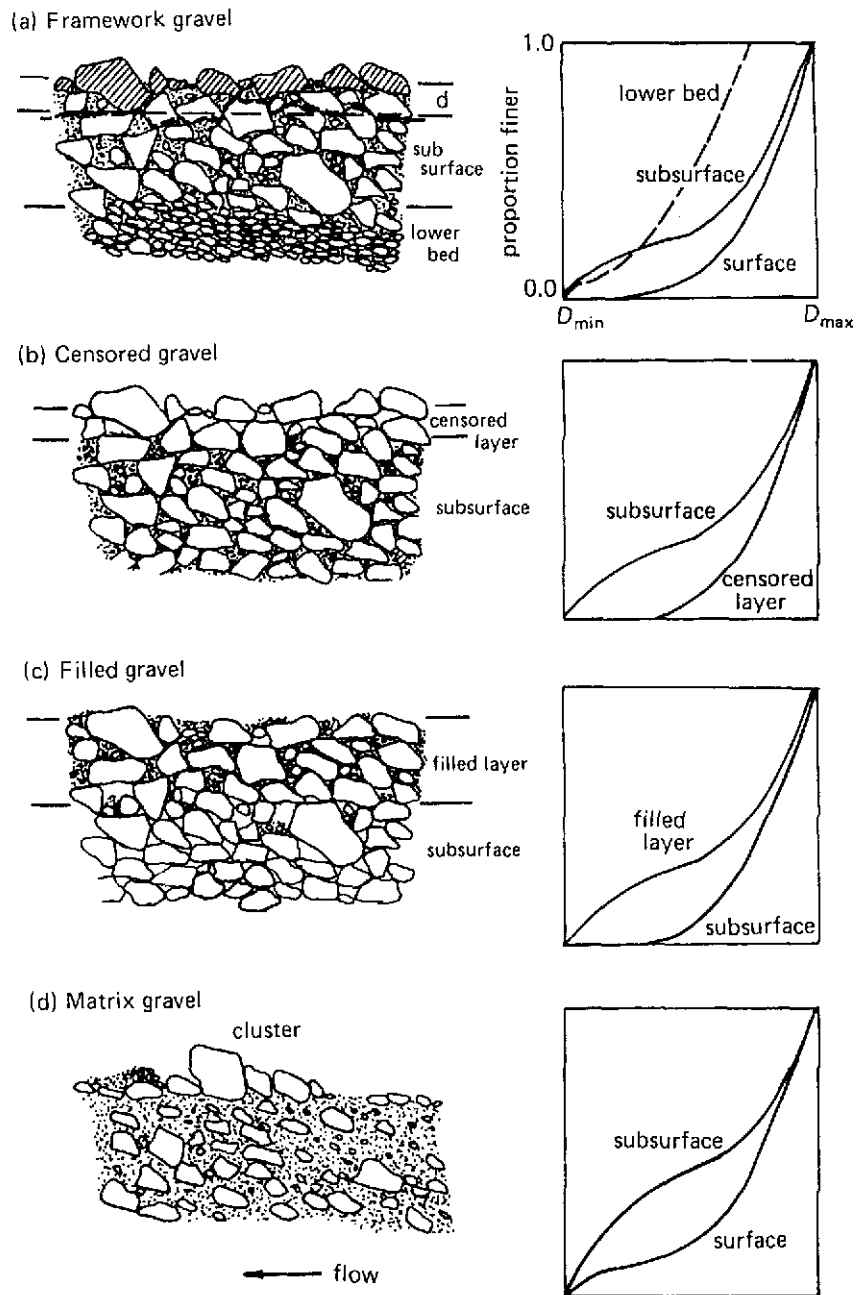


Fig. 3.14: Typical bedding and grain-size distribution curves for fluvial gravel. Note the hatched surface particles in the top figure. Only those particles are part of a *surface* sample. The *armor layer* with a thickness  $d$  in Fig. 3.14 a extends from the surface down to a depth defined by the deepest reaching particle in the sampling area. (Reprinted from Church et al. (1987), by permission of John Wiley and Sons, Ltd).

sediment infiltrated into a deposit of originally coarse gravel. Two main mechanisms have been identified which cause an infiltration of fines into a coarse open framework. These are discussed in Section 3.3.1.2.

Another example of stratification in gravel-beds is a *censored layer* of coarse gravel, one or several particle sizes thick, in which the voids are free of fines (Carling and Reader 1982) (Fig. 3.14 b). The presence of voids filled with fines in the strata below leads to the interpretation of initial scour, followed by either a preferential deposition of coarse particles, or by vertical winnowing (piping) of fines that leaves coarse gravel behind.

### 3.3.1.1 The coarse surface layer: armoring and pavement

Many gravel-bed rivers have surface sediment that is coarser than the subsurface sediment (Fig. 3.14 a). Three processes are attributed to surface coarsening (as opposed to subsurface fining):

- selective scour of fines (erosion pavement),
- selective deposition of large particles, or
- armoring to facilitate equal mobility transport.

#### ***Selective scour of fines***

Selective winnowing of fines from the surface leaves a coarse lag deposit on the surface about one particle diameter thick. The reasons for surface winnowing can be decreased sediment supply, and/or increased flow. Long-term coarsening of the surface occurs in the absence of sediment supply on the downstream side of log jams (Section 3.2.4), in plunge and scour pools, or below reservoir dams (erosion pavement).

#### ***Selective deposition of large particles***

Selective deposition of coarse particles with surface coarsening occurs when waning flows are no longer competent to transport the largest particles - which then begin to settle. The supply of fine particles may be low, at least during flows at which they would settle.

#### ***Armoring to facilitate equal mobility transport***

Another explanation for the formation of a coarse surface armor is that a coarse surface is the prerequisite for *equal mobility* transport of coarse and fine particles (Parker et al. 1982; Andrews and Parker 1987). If the surface was not armored (i.e., surface and subsurface particle size were the same), coarse particles would move less frequently than fine particles. Bedload then has a finer distribution than the bed sediment. The frequently observed similarity between the size distribution of bedload and the subsurface sediment requires that the mobility of coarse particles is increased, while the mobility of small particles is decreased. This mechanism can be facilitated by the presence of a coarse armor layer in which coarse particles are exposed to the surface that provides them

with an increased chance of transport. Fine particles are hidden below the surface where their transport probability is diminished. Thus, the preferential exposure of larger particles in the armor layer acts to equalize the mobility of coarse and fine particles and eliminates most of the differences in the mobility of small and large particle sizes.

A coarse surface layer can be termed *armor* or *pavement*. In the terminology used by Sutherland (1987), armoring refers to episodic surface coarsening when, over the course of commonly occurring high flows, large particles have a chance to be mobile, albeit infrequently. By contrast, pavement refers to static conditions under which the largest particles are immobile given the prevailing flow regime and sediment supply. Andrews and Parker (1987) use the terminology in the opposite way: pavement is the coarse bed that develops to achieve equal mobility, whereas armor denotes a coarse and static lag deposit. Since the terms armor and pavement are not used consistently in the literature, the reader needs to determine the exact meaning of the terms armor or pavement in any given context. This text follows the terminology by Sutherland (1987): armor is mobile and pavement is static.

A surface armor is less developed in streams where transport capacity (i.e., the largest amount of bedload that a given stream reach can transport) equals the amount of sediment supplied to the reach. This is common in braided streams. The particle-size distributions of surface, or armor layer, and subsurface sediment are relatively similar under these conditions. Transport capacity is often larger than sediment supply, and a coarse surface armor becomes prominent. This situation is common in many armored gravel-bed streams. High energy mountain streams usually have high transport capacity but low sediment supply which leads to the formation of an erosion pavement that may only be mobilized by the largest floods.

The degree of armoring may be quantified by the ratio of the  $D_{50}$  surface sediment size to the  $D_{50}$  subsurface sediment size. This ratio approaches a value close to 1 in streams with high sediment supply, whereas streams in which transport capacity exceeds sediment supply, the ratio approaches a factor of approximately 2. The ratio of  $D_{50surf}/D_{50sub}$  may reach values of 3 or more in high-energy mountain streams or when sediment supply is completely shut off and an immobile, coarse lag deposit forms. For example, such conditions are found below reservoir dams. High values in the ratio of  $D_{50surf}/D_{50sub}$  may also be produced by the presence of untransportable, large particles supplied to the stream from non-fluvial sources (rockfall, exhumed boulders), or in the presence of censored layers (Fig. 3.14 d). The surface sediment may also be finer than the subsurface sediment, for example, when a high supply of fine sediment covers the surface. This may decrease the  $D_{50surf}/D_{50sub}$  ratio to values below 1. (See also Sections 6.1.6.2 and 6.5.2 for the ratio surface/subsurface sediment size).

### 3.3.1.2 Mechanisms of fine sediment intrusion into open framework gravel

Research on fish spawning habitat has identified two main mechanisms for fine sediment intrusion into framework gravel with open pores: infiltration based on gravity and intrusion of fine sediment by interstitial flows. In gravity-based infiltration, fine gravel

and sand moving over the bed surface as bedload becomes trapped between large particles and falls into the voids between surface particles. The rate of fine sediment infiltration increases with the supply of fine-sized bedload, and with the number and size of open pores. Fine sediment intrusion is due to downwelling flows that bring fine particles from suspended sediment into the pore space (Alonso 1993). The rate of fine-sediment intrusion increases with the concentration of suspended sediment, the severity of downwelling, the size and number of open pore spaces, and the rate of interstitial flows (Lauck et al. 1993).

Fine sediment intrusion into a non-stratified deposit of coarse gravel can cause different vertical stratification, depending on the intragravel pore sizes and the size of the infiltrating particles. If the infiltrating particles are finer than the intragravel pores, the infiltrating sediment fills the pore space from the bottom up, causing no pronounced vertical variation of infilled particle sizes. If the fine sediment is a mixture of silt, sand and fine gravel, fine gravel can eventually seal the pore spaces near the surface and prevent finer sediment from infiltrating into deeper pores. Depending on how fast the near-surface pore space is sealed, there can be a gradually upward coarsening of the infiltrated fines, or a layer below the surface that is free of infilled fines.

### **3.3.2 Implications of vertical stratification for bed-material sampling**

When sampling bed material that is vertically stratified, it is important to distinguish between different strata because each stratum represents different channel-bed processes. Sampling and analyzing each strata individually is not only important for analyzing sedimentation processes, but also for analyzing the habitat of aquatic ecosystems (Bjornn and Reiser 1991; Montgomery et al. 1996) or for monitoring a change in fine sediment supplied to the stream following a change in watershed management.

The question arises whether sediment strata have a fixed thickness and to what thickness strata should be sampled. The short answer is that some strata have a relatively fixed thickness, while the thickness of other strata is variable.

Surface coarsening (Fig. 3.14 a and Section 3.3.1.1) affects not only the immediate sediment surface, but the armor layer that extends from the surface down to approximately the depth of some large surface-particle size, e.g., the  $D_{90}$  size. Thus, one could sample surface particles (pebble counts, Section 4.1.1; areal samples, Section 4.1.3) or take a volumetric sample of the armor layer (Section 4.2.1). The depth to which surface fining extends downward into the bed (Fig. 3.14 c) depends on how deeply the fines have infiltrated the bed (Section 3.3.1.2). Similarly, the thickness of censored gravel (Fig. 3.14 b) depends on the duration and magnitude of the sedimentary processes. The exact depth of sediment strata can only be determined by digging gravel pits or by taking core samples. All sediment layers below the surface are sampled volumetrically (Section 4.2.2 - 4.2.4).

### 3.4 Bed-surface structures

Bed surface-structures are arrangements of particles into groups of various sizes or arrangements of particles into a particular packing, or a combination of both. These arrangements are caused by the interaction between flow hydraulics and particles. Bed surface-structures may either cause small-scale or local variations of bed-material size, or form beds with little variation in particle size.

Bed-surface structures may cause problems for bed-material sampling. Surface structures require a large spacing between sampling points, and extracting a particle out of a surface structure may be difficult. Particles involved in surface structures are partially hidden from view, which complicates visual and photographic methods of bed-material size analysis. The presence of any bed-surface structures should be recorded in the sampling notes because bed-surface structures can either increase or decrease erosion thresholds and hydraulic roughness.

Bed-surface structures may have a transverse or longitudinal orientation in the stream. They may cover much of a reach, or occur spatially isolated. Various forms of bed-surface structures are introduced in Section 3.4.1 – 3.4.6. Implications for bed-material sampling are discussed in Section 3.4.7.

#### 3.4.1 Transverse and longitudinal bedforms

Large particles transported in a relatively steep stream during a major flood event with high sediment supply produce several kinds of bedforms during deposition. The general mechanism is that the largest particles settle first and control the deposition of other large and small particles in their vicinity.

**Transverse clast dams** have a lobate front of large, loosely fitted and well-sorted clasts. After the coarse lobe front is deposited, finer sediment deposits on the upstream end of the dam (backfill) (Bluck 1987; Krumbein 1940, 1942). Clast dams may vary in size. They may be up to 1 m high or more, and several m or even several 10 m wide and long. The largest particles in the clast dam may reach cobble and boulder size. Height, width, the largest particles, and length of the dam (or spacing between dams) are related. The dam length is approximately equal to the dam width, about 5 times longer than the dam height, and 5 - 7 times the diameter of the largest clast in the dam. Dam width is approximately 5 times the dam height, and the height is 2 to 0.8 times the largest clast size. Height and width of the dam fronts increase with the magnitude of the flood event. The backfill that consists of finer sediment than the coarse clast dam typically coarsens towards the dam. Fines at the upstream end of the backfill can form as a wake deposit from the next front upstream (Fig. 3.15). The largest particle within a lobe is usually not found in the lobe front, but in the backfill. Large particles may destroy the front while passing over it. The height and length of transverse clast dams typically decrease in a downstream direction, and the decrease is more pronounced in steeper channels. Transverse clast dams are found in streams with gradients larger than 1%.

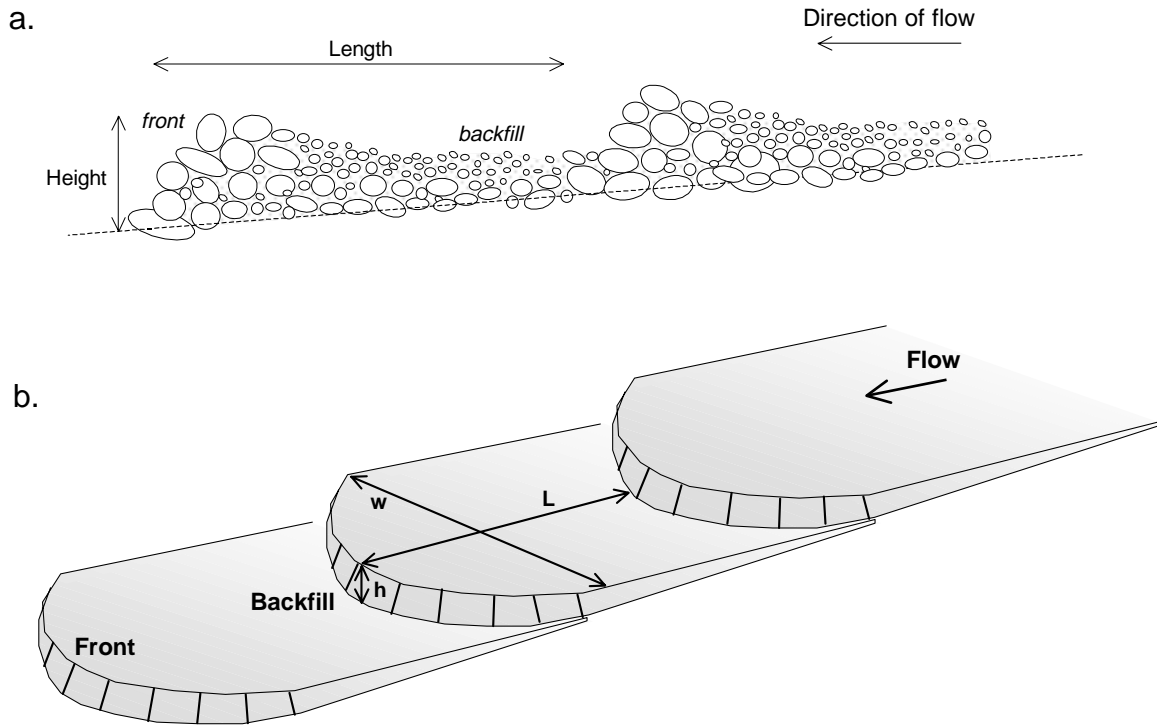


Fig. 3.15: Side view (a) and oblique view (b) of a transverse clast dam.  $h$  is the height of the bedform,  $w$  is the width, and  $l$  is the length.

**Transverse ribs** are sequences of regularly spaced ridge-like deposits of coarse particles that are transverse to flow (McDonald and Banerjee 1971; Boothroyd and Ashley, 1975; Koster 1978) (Fig. 3.16). Particles that form the ribs are oriented with their  $a$ -axes perpendicular to flow, and dip upstream along the  $a$ - $b$  particle plane (Fig. 3.16). The coarsest particles within ribs are on the downstream side, and individual particles are often imbricated (Section 3.4.2). Height, width, length and particle size of transverse ridges are related. The rib height equals about one large particle, the width is 2 - 4 large particles, and the length 5 - 10 large particles. Width and length decrease with stream gradient. The area between the ribs contains finer sediment and sometimes fine sand. This difference in particle sizes makes the presence of the ribs recognizable. Transverse ribs are not restricted to steep channels, but can form on any locally steep depositional surfaces with shallow but high-energy flow. Koster (1978) suggests that transverse ribs form when flow over standing and upstream braking waves starts to wane and interprets transverse ribs as relict antidunes.

**Longitudinal clast ribs** are elongated ribs that form in steep channel sections when large particles are arranged parallel to flow (Bluck 1978). Longitudinal clast ribs may be several meters long and up to 1 m high. Particles in longitudinal clast ribs are well sorted, imbricated, and not longitudinally graded.

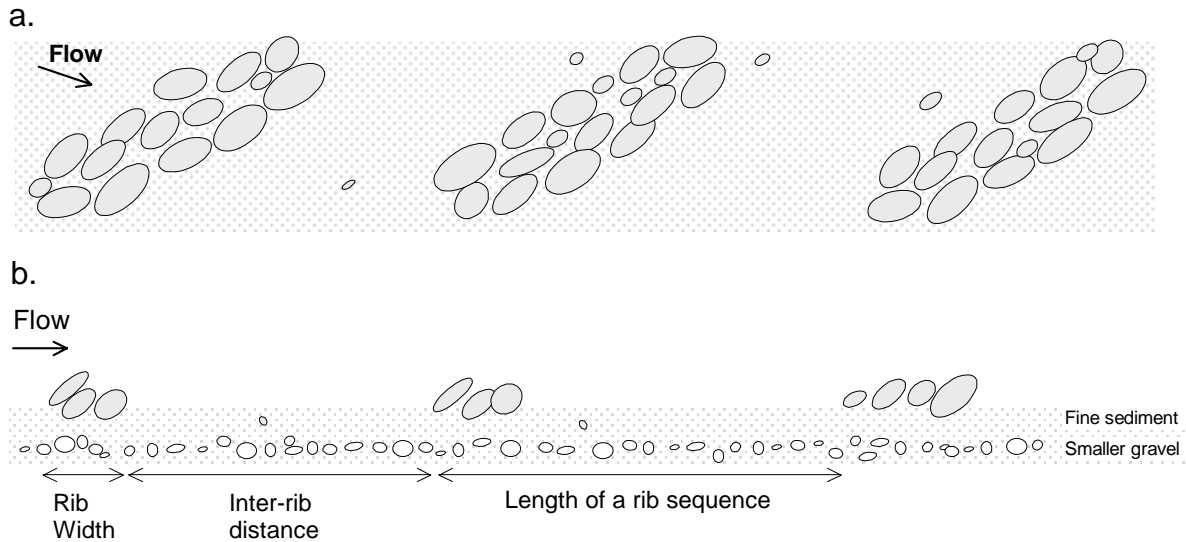


Fig. 3.16: Sequence of transverse ribs in (a) oblique view, and (b) side view.

**Boulder and cobble berms** are elongated deposits in the direction of flow, often curved, and commonly found in wide bends following a more constricted channel upstream. Boulder and cobble berms may form parallel ridges and contain negligible amounts of fine sediment. Boulder and cobble berms develop during turbulent overbank flow with high Froude numbers<sup>1</sup> and a large supply of coarse sediment when part of the flow turns upstream near the stream bank (Carling 1989).

**Bedload or gravel sheets** are a layer of particles with a thickness of 1 – 2 coarse particles. Bedload or gravel sheets travel downstream during flow events with high sediment supply. Coarse particles form the leading edge of this bedform that is much longer than it is high, and fine particles trail behind. Bedload sheets require a proper mixture of fine and coarse gravel. The formation of bedload sheets starts when several large bedload particles come to rest on a rough bed surface. Fine sediment passes over the accumulation of coarse particles, and fills interstices in front of the deposited coarse particles. The smooth surface of fines decreases roughness and increases drag on the coarse particles. This action remobilizes the coarse particles which then travel downstream over a surface of fine particles until coming to rest on the next rough bed-surface downstream (Iseya and Ikeda 1987; Whiting et al. 1988). Migrating bedload sheets travel in sequences and form a bed surface with alternately coarse and fine strips that may extend over much of the stream width. If bedload sheets are preserved during low flow, the alternate strips of coarse and fine sediment form a pattern of longitudinal

<sup>1</sup> Froude number  $F = \frac{v}{\sqrt{g \cdot d}}$ ,  $v$  = flow velocity,  $g$  = acceleration due to gravity, and  $d$  = depth of flow.  $F > 1$  = supercritical flow.

sorting on the bed (Fig. 3.17). Bedload transport rates measured during the passage of a bedload sheet are very high.

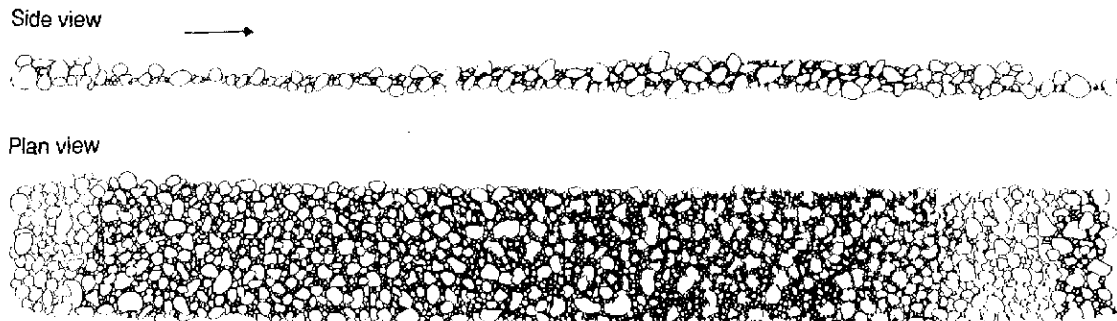


Fig. 3.17: Deposit from a bedload sheet with coarse front and fining towards the tail. Flow is from left to right. The downstream distance of the bedload sheet is about 0.8 m. (Reprinted from Whiting et al. (1988), by permission of the Geological Society of America).

**Stone cells** are bed-material patterns that may form in streams with relatively low bedload supply as a means of bed stability (Church et al. 1998). Stone cells are curved ridges of large particles. The ridges are transversely oriented and may face upstream or downstream, giving the impression of a coarse-grained ring around a cell filled by finer sediment. The development of a stone cell begins with the random deposition of the largest particles. Other large particles are then deposited in their vicinity.

### 3.4.2 Imbrication

Another form of bed-surface structure refers to the packing of particles of similar sizes. Imbrication is a shingle-like deposit in which the upstream particle partially overlaps its downstream neighbor. Flat particles of similar size are most susceptible to form imbricated surfaces. Imbrication can be limited to a few particles within a cluster (see below), be part of linear features such as longitudinal clast ribs (see above), or cover large streambed areas. Imbrication can be classified by the position of the three particle axes in relation to flow (Todd 1996). Particles set in motion by fluid forces roll about their *a*-axis (longest axis) in contact with the bed and are arrested by the particle in front. The *a*-axis is transverse to the flow, and imbrication occurs along the *b*-axis (Fig. 3.18). The thickness of the imbricated layer comprises 1 - 2 particles. Imbrication along the *b*-axis is characteristic of relatively low transport rates.

In streams with high bedload transport rates associated with traction carpets or debris flows, imbrication occurs along the particle *a*-axis, and the *a*-axis is parallel to flow (Fig. 3.18). This indicates that particles move by sliding and with grain-to-grain contact. Particles imbricated along the *a*-axis are separated from each other by finer matrix sediment. Both imbrication structures pose a high erosion threshold.

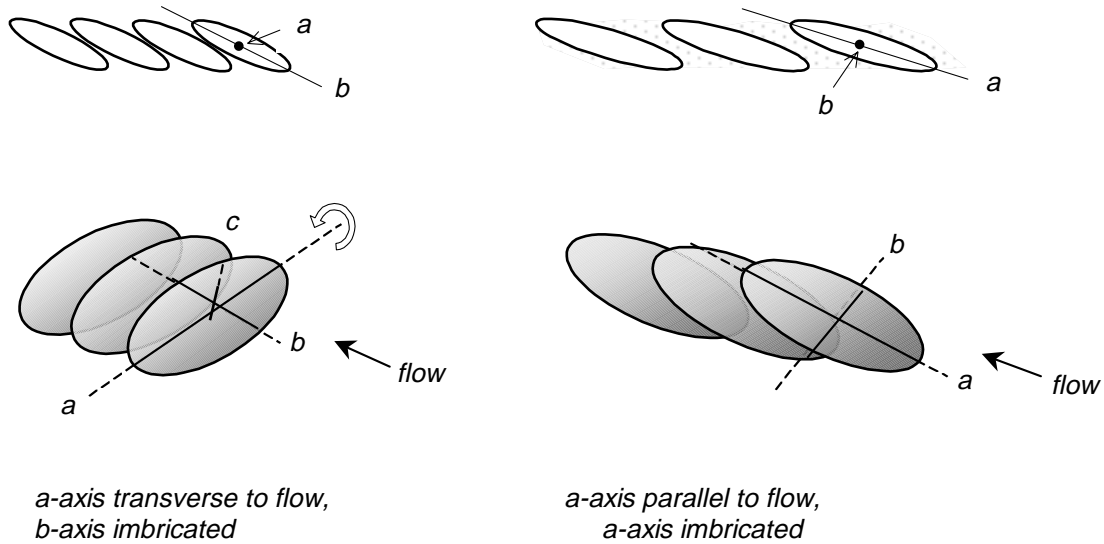


Fig. 3.18: Imbrication along the  $b$ -axis with the  $a$ -axis transverse to flow, characteristic of individual particle movement in fluid flows and low to moderate bedload transport rates (left); imbrication along the  $a$ -axis with the  $a$ -axis parallel to flow, characteristic of grain-to-grain interaction during high intensity sediment transport such as traction carpets and debris flows (right). Side views (top), and oblique views (bottom). (Redrawn from Todd (1996), by permission of John Wiley and Sons, Ltd.).

### 3.4.3 Clustering

A particle cluster is an accumulation of a few coarse particles on the upstream side of a large particle and is formed when a large obstacle clast comes to rest and one or more particles lean against the upstream side of it. Finer particles often accumulate in the wake downstream of the obstacle clast due to the inward-curling eddies of the flow separation zone (Brayshaw, 1984; Naden and Brayshaw 1987; Reid et al. 1992) (Fig. 3.19 a and b). Clusters with stoss and wake deposit are called complete clusters. The length of the wake deposit increases with the size of the obstacle clast. However, the wake deposit may be absent if the obstacle clast has a pointed shape or is aligned parallel to the direction of flow (De Jong 1992) (Fig. 3.19 c). Clusters without wake deposits are called incomplete clusters.

Clusters can be comprised of two or more particles, be one or more particles wide, and form one or several distinct rows of particles. Clusters can be solitary features, or form ribs that extend transversely, diagonally, or in lobate orientation across the stream. Clusters can also cover the streambed or parts of it in rhombic patterns (De Jong and Ergenzinger 1995).

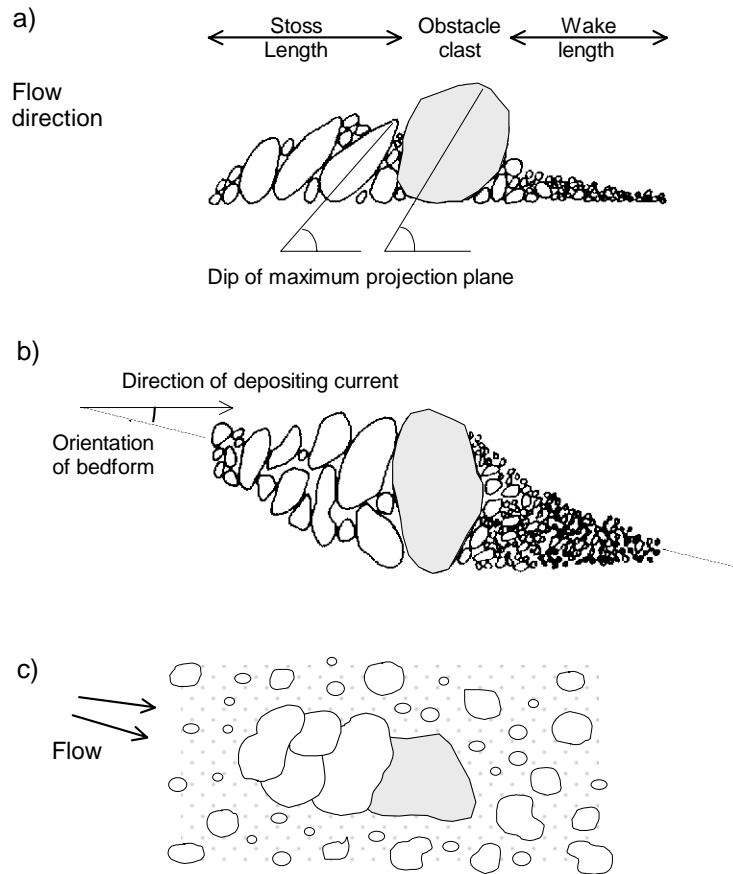


Fig. 3.19: Cross-sectional (a) and plan view (b) of a complete particle cluster with stoss and wake deposit. Flowlines form inward-curling eddies in the wake of the obstacle clast where fine sediment is deposited. (Reprinted from Brayshaw (1984), by permission of the Canadian Society of Petroleum Geologists). Incomplete cluster without wake deposit of fines (c).

### 3.4.4 Horseshoe vortex scour

Horseshoe vortex scour is scour around the upstream side of an immobile object and deposition of the scoured sediment at the downstream side. This form of scour is usually associated with scour around bridge piers, but it also develops around any large immobile obstacle surrounded by erodible finer sediment. As flow increases above a threshold, a helical vortex develops at the upstream side of the object and scours a semicircular trench. Fine sediment scoured from the trench as well as sediment from upstream that is transported through the scour trench is deposited by the inward-curling wake eddy on the downstream side of the obstacle (Fig. 3.20) (Bunte and Poesen 1994). Although horseshoe vortex scour is most prominent in sandy environments (e.g., around pebbles on a sandy streambed or sea shells on a sandy beach), it can also occur around boulders in a gravel streambed.

Horseshoe vortex scour increases particle mobility, because particles begin to be scoured from the vortex at flows much lower than needed for particles entrainment from the bed in the absence of horseshoe vortex erosion.

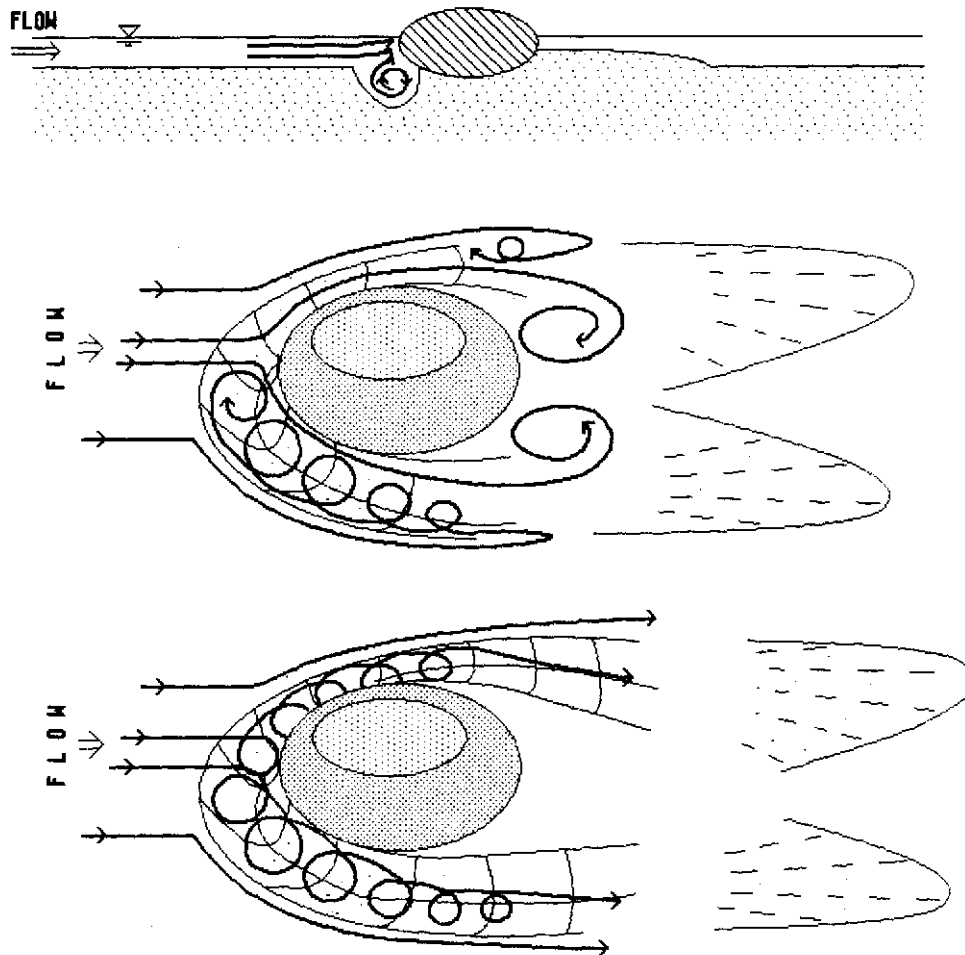


Fig. 3.20: Horseshoe vortex scour around a pebble in a sandy matrix: profile view and moderate flow intensity (top); plan view and moderate flow intensity (center); plan view and high flow intensity (bottom). (Reprinted from Bunte and Poesen (1994), by permission of John Wiley and Sons, Ltd.).

The sizes of particles in wake deposits are affected by the intensity of the local hydraulics around the obstacle. Sand transported over the bed during low flows may be deposited in the boulder wake, whereas during higher flows the material scoured in the vortex is deposited.

### 3.4.5 Cobble embeddedness and protrusion

Embeddedness refers to the position of a large particle relative to the plane of the bed. A large particle that is partially buried in finer sediment is said to be embedded. The degree to which a particle is embedded is called embeddedness. Embeddedness is a parameter used particularly by fisheries biologists to quantify the abundance of fine sediment in a streambed. The particle sizes that constitute large and fine sediment depend on the study objective and the channelbed conditions. According to Burns and

Edwards (1985), embedded particles typically have *a*-axes lengths of 45 to 300 mm, whereas the size of the finer sediment in which large particles are embedded is smaller than 6.3 mm. Embeddedness can occur throughout a reach of concern or be restricted to areas where local hydraulics lead to local deposition of fines.

Several methods may be employed to describe the degree of cobble embeddedness (MacDonald et al. 1991). *Embeddedness* ( $E$ ) is the ratio of total vertical extent of a particle  $D_t$  to the vertical extent of the particle below the bed surface, i.e., the embedded portion of the particle  $D_e$ , so that  $E = D_t/D_e$  (Fig. 3.21 a).

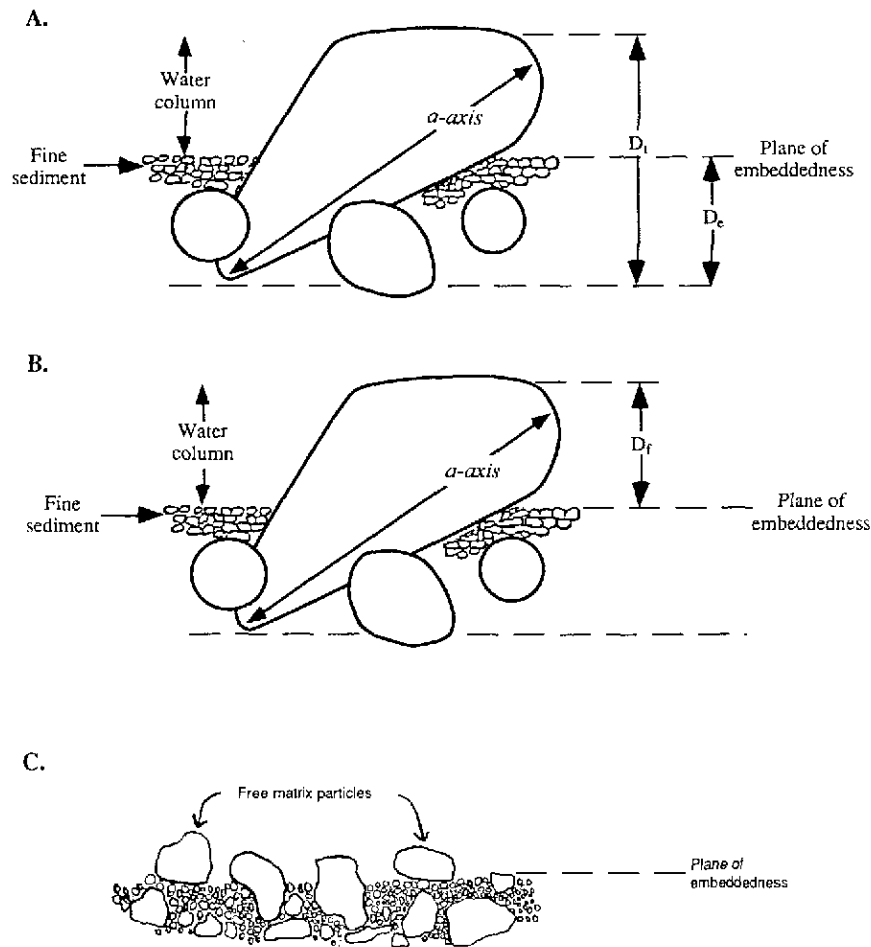


Fig. 3.21 a-c: Three methods of quantifying cobble embeddedness: **Embeddedness**  $E = D_t/D_e$  where  $D_t$  = total vertical extent of a particle, and  $D_e$  = embedded vertical extent of a particle (a); **Free particle space** where  $D_f$  is the height of particle protrusion above the bed (b); **Percentage of free matrix particles** (c). (Slightly modified from MacDonald et al. (1991); source: Burns and Edwards (1985)).

Alternatively, *free particle space*, or *protrusion*  $D_f$  is the height by which a particle extends above the bed surface. Embeddedness and free particle space are related by  $D_f =$

$D_t - D_e$  (Fig. 3.21 b). Free particle space can also be expressed as an *interstitial space index* by computing  $\Sigma D_f/A$ , where  $A$  is the sampling area. To account for the high variability of individual measurements, the index can be computed by summing measured protrusion heights  $D_f$  and dividing by the sampled area, which is typically a circle with a diameter of 60 cm. The *percentage free matrix particles* for a given area is the ratio of the number of particles  $n_{exp}$  freely exposed on top of the bed to the number of particles of similar sizes  $n_{emb}$  that are embedded (Fig. 3.21 c). The percentage of free matrix particles  $n\%_{exp} = 100 \cdot n_{exp}/n_{emb}$  closely corresponds to percent embeddedness  $E\%$ .

Besides direct measurements of free particle space, the degree of protrusion by a particle with the size  $D$  can also be expressed by the ratio of  $D/D_{50}$ . A particle is protruding above the median particle size of the bed if  $D/D_{50} > 1$ , and hiding if  $D/D_{50} < 1$ .

To characterize a streambed, particle embeddedness should be measured on at least 100 particles. A sample size equation (Section 5.2.1) should be consulted to determine the exact relation between sample size and error for a specific sample site. A more intensive sampling scheme is to measure embeddedness within circles of 60 cm in diameter outlined by hoops. Percent cobble embeddedness  $E\%$  for each hoop is  $100 \cdot \Sigma D_e/\Sigma D_t$ . Approximately 25 - 35 particles are measured within each hoop, and approximately 20 hoops (with a total of 500 - 700 particles) are needed to characterize  $E\%$  for a reach.

### 3.4.6 Gravel sheltered in pockets

In contrast to horseshoe vortex erosion that increases gravel mobility, gravel particles hidden in pockets between immobile boulders or other obstacles are sheltered from flow and have a pronouncedly lower mobility. Barta et al. (1993) suggested that pocket gravel is mobilized during flood events with a two-year recurrence interval. Mobilization of pocket gravel required total shear stresses 2 to 20 times larger than those needed if boulders were not present, and the required total shear stress increased with the height of obstructions (Barta et al. 1994). Thus, when sampling bed material for a flow competence analysis in boulder-bed streams, the population of transportable gravel needs to be analyzed separately from immobile boulders.

### 3.4.7 Implications of bed-surface structures for bed-material sampling

Bed-surface structures affect the mobility of particles on the bed. Imbricated, embedded, wedged, sheltered, and clustered particles have higher erosion thresholds than particles of the same size not contained in these surface structures (Brayshaw et al. 1983; Brayshaw 1985, Naden and Brayshaw 1987). Conversely, particles subjected to horseshoe vortex scour are moved by flows much lower than the threshold flow needed for particle motion from a plane bed without obstacles (Bunte and Poesen 1993, 1994). Thus, if bed material is sampled for analysis of forces exerted onto the streambed, initial motion studies, flow competence and bedload transport prediction, it is important to recognize and note particle packing and the presence of structures (Dunkerley 1994). Bed-surface structures also affect the hydraulic roughness of the stream. Imbricated beds and embedded particle

structures have a lower roughness than one would assume from particle size alone, whereas the presence of clusters increases bed roughness beyond that expected for large particle sizes.

Surface structures may cause difficulties when sampling bed material. The presence of clusters or horseshoe vortex erosion requires that the spacing between sample points exceeds the size of the bed-structure. Taking more than one particle from local accumulations of coarse or fine particles (clusters or wakes) causes serial correlation in the sample and should be avoided (Section 4.1.1.4). Similarly, clusters or wakes should be avoided when trying to estimate the average particle size within the sample area. Avoiding bed-material structures is important when collecting all particles contained within a small sampling area (areal sample, Section 4.1.3).

Imbricated and embedded bed surfaces may also cause problems for visual particle-size analysis or when measuring the size of surface particles from a photograph. Imbrication and embeddedness does not pose so much a problem for measurements of the *b*-axis, but for measurements of the *a*- and *c*-axes which are partially hidden from view (Section 4.1.2.2 and 4.1.3.3). Photographs of the streambed surface, however, are quite suitable to map bed-surface structures. The orientation of individual particles can be analyzed from large-scale photographs that cover 0.1 – 1 m<sup>2</sup> of streambed. Areal overview photographs that cover 100 m<sup>2</sup> or more can be taken from a camera suspended 10 - 30 m above ground by a crane or helium balloon and are suitable to analyze the spatial distribution of bed-surface structures within a reach (Section 4.1.3.4).

## 4. Sampling procedures and equipment

---

Bed material in gravel and cobble-bed streams can be sampled by two different methods:

1. **Surface sampling:** samples a preselected number of surface particles from a predefined sampling area, and
2. **Volumetric sampling:** samples a preselected sediment volume from a predefined sedimentary layer.

The study objective determines whether to sample the surface sediment or a particular sedimentary layer. Fig. 4.1 presents the basic four stratigraphic units that are common in armored gravel-bed rivers and that are commonly sampled.

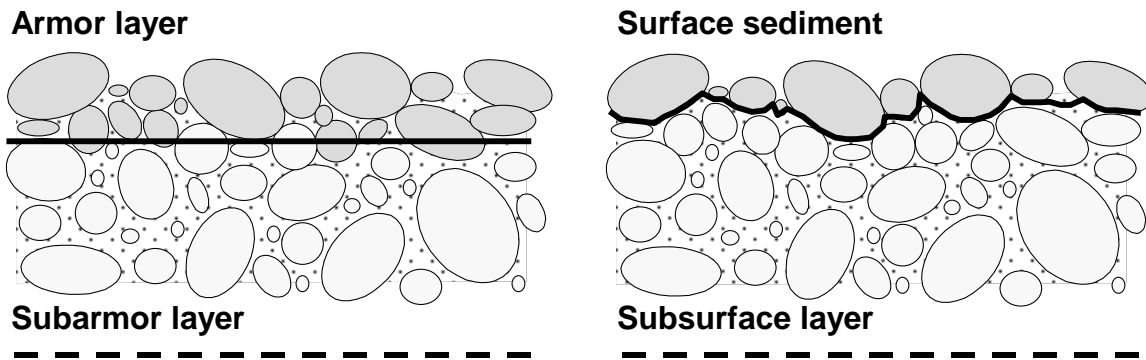


Fig. 4.1: Stratigraphy of an armored bed distinguishing between armor layer, subarmor layer, surface sediment, and subsurface layer.

Surface particles can only be sampled using surface sampling techniques (Section 4.1). Bed-material layers, such as the armor, subarmor, and subsurface layer, which may be infilled and censored (Section 3.3.1), have a specific thickness, and can therefore only be sampled by taking a volumetric sample (Section 4.2).

The procedural details with which a selected method is then performed depends on natural factors such as stream size, stream morphology, flow conditions, and the bed-material particle-size distribution. For example, sampling equipment and procedures must be suitable for the bed-material particle sizes, which in mountain streams may range from sand to boulders. Limited road access in remote areas dictates that equipment must be portable, and pristine conditions in sensitive environments may require sampling the bed in a non-destructive way. Sampling in submerged conditions must address poor

visibility of the bed under water, and the tendency of fine particles to be washed away by the flow.

Man-made factors also play an important role in the selection of sampling procedures. A study might not be able to afford a great deal of field time, but may instead have lab time to analyze samples or photographs taken of the streambed. The study objective or the streambed conditions may require using several different sampling methods or procedures, which then need to be selected to facilitate a comparison or combination of sampling results. A limited budget forces project managers to reduce the extent of the study or to opt for fast and simplistic field techniques performed by minimally-trained seasonal field crews, both of which might compromise the study objective.

The user must also consider the form of particle-size analysis applied to the sample. Particles per size class can be either counted or weighed, and size distributions may be explained in terms of frequency-by-number or frequency-by weight (Section 2.1.4.1). However, number- or weight-based particle-size analyses yield different results.

The user must also consider that different sampling procedures yield different particle-size distributions. A pebble count and an areal sample collected from the same surface yield different particle-size distributions even when the same method of particle-size analysis was used for both samples. In order to compare or combine particle-size distributions from pebble counts and from areal samples, the distribution of areal samples should first be converted (Section 4.3.3). However, the numerical value of conversion factors depends on the exact procedure with which the areal sample was taken (Section 4.3.2).

## 4.1 Surface sampling

Surface sampling collects bed-surface particles that are exposed on top of the streambed whether the bed is dry or submerged. The vertical extent of the surface sediment is equal to the diameter of one particle, i.e., the particle that is exposed on the surface at any given point (Fig. 4.1). Lacking a distinct vertical dimension, surface sediment can only be sampled by surface sampling methods, but not by methods that collect a volume of sediment. Although most surface particles are easy to identify, problems arise when small particles are surrounded by large particles, and when particles are partially exposed only, or partially hidden under neighboring particles (e.g., when the surface is imbricated or clustered (Sections 3.4.2 and 3.4.3)). At some point the question arises as to how much of a particle needs to be actually visible at the surface to qualify as a surface particle.

Bed-surface sediment can be sampled by three methods:

- ***pebble counts:*** (line counts) select and hand-pick a preset number of surface particles at even-spaced increments along transects that may be parallel and span a relatively large sampling area ( $\approx 100 \text{ m}^2$ ) (Section 4.1.1.);

- **grid counts:** select particles at a preset number of even-spaced grid points that span a relatively small sampling area ( $\approx 1-10 \text{ m}^2$ ), hand-picking particles or measuring particle sizes on photographs (Section 4.1.2), and
- **areal samples:** include *all* surface particles contained within a small preset area ( $\approx 0.1 -1 \text{ m}^2$ ) of the streambed, often using adhesives to ensure that small particles are included representatively in the sample (Section 4.1.3).

The three sampling methods differ in several points including the spacing between sampled particles, the size of the sampling area covered, suitability for small and large particle sizes, field time vs. lab time, and the comparability of sampling results. These factors should be taken into account when selecting a sampling method. Differences between the three surface sampling methods are summarized in Table 4.1.

Table 4.1: Comparison between pebble counts, grid counts, and areal samples

<b>Pebble counts</b>	<b>Grid counts</b>	<b>Areal samples</b>
Sample a <i>preset number</i> of particles in wide and approximately even-spaced increments of at least $D_{max}$ size	Sample a <i>preset number</i> of particles under a grid of approximately $D_{max}$ size	Sample <i>all</i> surface particles within a small <i>predefined</i> sampling area
Cover a large sampling area	Sample several small areas within a reach or cover small areas of homogeneous sediment (facies patch)	Focus on point locations and require several samples to be taken within the sampling area
Suitable for gravel and cobbles, not for sand	Suitable for gravel, not for sand	Suitable for sand to medium gravel not for coarse gravel or cobbles
Long field time, no lab time	<i>Hand-picking</i> : long field time no lab time; <i>Photographs</i> : short field time, long lab time	Both field time and lab time
Sampled particle sizes comparable and combinable with particle sizes from grid counts and volumetric samples	Sampled particle sizes comparable and combinable with particle sizes from pebble counts and volumetric samples	Sampled particle sizes not directly comparable and combinable with particle sizes from pebble or grid counts, or volumetric samples

Pebble counts focus on mid-sized and large particles, while neglecting fines and are suitable for covering large sampling areas by parallel transects. Pebble counts take between 0.5 and 2 hours per sample, depending on the number of particles to be collected and the difficulty involved in dislodging particles from the bed; however, no further laboratory time is needed. Grid counts performed in the field select particles under a grid. The grid may consist of elastic bands stretched over a rigid frame. Grid counts are

usually conducted on small sampling areas. Surface sampling of small areas lends itself to using photographs on which grids can be superimposed for later analysis.

Photographing a sediment surface takes very little field time per sample, but analyzing the photographs requires a relatively large amount of laboratory time (Sections 4.1.2.2 and 4.1.3.3). Areal samples require both field time for taking the sample, and lab time for sieve analysis. Areal samples are suitable for gravel sediment that contains a relatively large amount of sand and fine gravel, because areal samples, which focus on a small sampling area, are capable of including these fines, whereas pebble counts and grid counts tend to neglect them.

Particle-size distributions obtained from pebble counts and grid samples are mutually comparable and combinable. Both distributions are also comparable and combinable with distributions obtained from volumetric samples (Section 4.3). Particle-size distributions of areal samples need to be converted into an equivalent volumetric or grid distribution before making a comparison or combination with size distributions from pebble counts or volumetric samples (Sections 4.3 and 4.4).

#### **4.1.1 Pebble counts along transects**

Pebble counts are used to determine the particle-size characteristics of gravel and cobble surface sediment and can be performed on dry beds as well as on inundated beds, as long as the streams are wadable. Percentile values of the cumulative particle-size frequency distribution and the percent fines are used for many applications including computations of incipient bedload motion, channel-bed roughness, stream morphology studies, cumulative watershed effects analysis, and stream habitat evaluation.

##### **4.1.1.1 Heel-to-toe walks and sampling along a measuring tape**

A pebble count samples a *preset number of particles in even-spaced increments along transects*. Two methods are usually used to determine the transect locations, the spacing between selected particles, and identification of the particle to be selected: a heel-to-toe walk and sampling at even-spaced marks along a measuring tape. The main differences between these two methods are summarized in Table 4.2.

##### ***Wolman pebble count with heel-to-toe walk***

Two techniques of particle selection are commonly used for pebble counts. The first technique was proposed by Wolman (1954). An operator traverses a gravel surface along a grid pattern. The grid may be established by pacing or laid out by lines or a tape. A particle is collected in the vicinity of each grid point. Wolman (1954) emphasizes that the particle to be included in the sample must be selected at random. As a means to achieve this randomness, he proposes to pick up the particle from beneath the tip of the boot while looking away. The spacing between selected particles is determined by the size of the grid needed to cover the sampling area with 100 grid points (Wolman 1954). Wolman's methodology is often interpreted as traversing a sampling area with heel-to-toe

steps, paces, strides, or several steps at a time and picking up the particle first touched by a pointed vertical finger, eyes averted, under the tip of the boot (e.g., Leopold 1970; Hey and Thorne 1983; Fripp and Diplas 1993; Potyondy and Hardy 1994; Kondolf 1997a; Marcus et al. 1995; Bevenger and King 1995). The method is most popular because no specific field equipment is required to lay out the grid. The step-spacing can be adjusted to the size of the area to be covered or the size of particles in the stream, and the procedure can be done in wadable flows (Yuzyk 1986).

***Systematic sampling at even-spaced marks along a measuring tape***

A more systematic way of sampling surface bed-material with pebble counts is to stretch a measuring tape in several transects across the sampling area. Particles are selected at intersections with even-spaced marks along the edge of the tape, for example at marks in 1 foot or 0.5 m intervals (e.g., Wohl et al. 1996) or exactly under the grid points of the established measuring grid (Hey and Thorne 1983; Yuzyk and Winkler 1991). The spacing between particles depends on the bed-material particle size and is set to a value larger than the  $b$ -axis of the  $D_{max}$  particle size of concern. This spacing is necessary in order to prevent double counting of large particles, which should be avoided because it causes a serially correlated sample and bias towards large particle sizes (Section 4.1.1.4).

Table 4.2: Overview of differences between heel-to-toe sampling and systematic sampling along a measuring tape and potential operator bias and variability in poorly sorted gravel and cobble-bed streams.

	<b>Heel-to-toe steps</b>	<b>Systematic sampling along a tape</b>
Step spacing:	1 - 2 paces (0.3 - 0.6 m), regardless of bed material size	1 - 2 times the $D_{max}$ particle size, in accordance with bed material size
Particle selection on dry surfaces:	Blind touch at the tip of the boot	Visual correspondence with even-spaced marks on measuring tape
Possible improvements:	Keep finger straight to avoid touching neighboring particles	Use pin or awl for more precise identification of particle to select
Particle selection under water:	Blind touch at the tip of the boot	Visual correspondence with even-spaced marks on a measuring tape as best as possible; otherwise blind touch
Sampling path:	Along an imaginary line at operator's discretion	Along a tape, strictly predetermined
Possibility for operator bias:		
- against fines	Higher	Lower
- against cobbles & boulders	Higher	Lower
Variability between:		
- samples	Higher	Lower
- operators	Higher	Lower

Results of pebble counts can vary greatly between the two methods. The traditional Wolman pebble count with its blind touch, heel-to-toe steps, and walking along imaginary lines allows the operator more latitude in particle selection, the spacing between particles, and the sampling path than sampling at preset intervals along a measuring tape stretched in transects across the reach. This methodological difference and its effects are discussed in more detail in Sections 4.1.1.3 – 4.1.1.5. Data recording and analysis is the same for all pebble count methods (Section 4.1.1.7).

#### 4.1.1.2 Sources of errors in pebble counts

Particle-size distributions obtained from pebble counts must be accurate in order to be useful for a study objective. Estimates of bedload transport rates, for example, vary significantly if the bed-material percentile particle-size used for the computation varies slightly (Gessler et al. 1993; Bunte 1994). Particle-size distributions recorded from pebble counts also need to be accurate for streambed monitoring that compares bed-material size parameters between reaches or over time (Potyondy and Hardy 1994; Bevenger and King 1995; MacDonald et al. 1997; Schnackenberg and MacDonald 1998). The detection of small changes in a percentile of concern or the percent fines is important for a prompt onset of remedial actions. However, pebble counts, which appear to be simple and straight forward on first view, provide many opportunities for sampling errors. Pebble counts are usually subject to operator error and statistical error which are summarized below and discussed in greater detail in the following sections.

##### ***Operator error***

Particles to be included in a sample must not be affected by operator preferences. However, operators are likely to introduce errors into pebble counts by favoring mid-sized and handy particles, while avoiding very small and very large particles that are difficult to pick up (Section 4.1.1.3 and 4.1.1.4). These preferences may be voluntary or involuntary, creating biased and non-random samples. The practice of double counting large particles produces serial correlation (Section 4.1.1.5) and bias towards large particles. Operators also introduce sampling scheme errors by sampling areas that have a systematic spatial variation in particle sizes, or by favoring easily accessed stream locations, while neglecting poorly accessible ones. Spatially non-random sampling again creates bias and non-random samples. Different sampling schemes for pebble counts are discussed in Sections 6.2 and 6.3. Operators also introduce errors into pebble counts when particles sizes are not measured correctly (Section 2.1.3.6). The use of templates largely addresses this problem.

Operator error adds to the statistical error of a sample. However, unlike statistical errors, operator errors do not improve with sample size, but become relatively more important as sample size increases (Hey and Thorne 1983).

### ***Statistical error***

Sample size and precision for number-based particle-size analysis are discussed in detail in Section 5.2. A 100-particle pebble count might determine the  $D_{50}$  to  $D_{84}$  particle sizes to within tolerable levels of precision in a moderately-well sorted gravel bed (no sand, no boulders). However, the precision of a 100-particle pebble count is usually too low to compare particle-size distributions from different sites or over time, nor does a 100-particle sample suffice in poorly sorted gravel beds comprised of sand and boulders. Generally, a fourfold increase in sample size to 400 particles is required to halve the sampling error. Much larger sample sizes are needed to accurately determine distribution parameters such as sorting, skewness and kurtosis (Sections 2.1.5.4 – 2.1.5.6). Most computations of statistical error do not include operator error, except for the statistical procedure of two-stage sampling (Section 5.2.2.1).

#### **4.1.1.3 Operator bias against small particles**

Pebble counts are widely used to determine the proportion of fine sediment on a streambed, such as the  $D_5$  or  $D_{16}$ , or the percent fines. However, it is usually not realized that the computation of the fine part of a cumulative particle-size distribution is not only burdened with a statistical error that is more than twice as large as that for a  $D_{50}$  or  $D_{84}$ , but also with an operator error that again is larger than the operator error associated with the  $D_{50}$  or  $D_{84}$ .

The sampling component of pebble counts consists of two steps: identifying the particle to be included in the sample from among neighboring particles, and the actual lifting or retrieval of the particle from the streambed. Particle identification may be based on touch, i.e., the particle first touched by the pointed finger, eyes averted, is included in the sample. This is the method used in heel-to-toe sampling. Alternatively, particle identification can be visual, i.e., by correspondence of a particle with intersections of even-spaced marks along a measuring tape. Fingertips, or the whole hand are used for particle retrieval.

Both particle identification and retrieval may be problematic when sampling particles of fine gravel or coarse sand. Sampling in a bed of similar-sized, small particles, touching cannot discriminate between neighboring small particles, and retrieving one specific particle may be difficult. Errors in particle identification and retrieval are of negligible consequence when all neighboring particles fall into the same size category and the operator can select any one particle from a pinch of sediment taken from the streambed.

The pinch-approach is not appropriate if small particles are surrounded by neighboring coarser particles, because in the presence of particles of mixed sizes, the operator has to identify and pick one particle. Identifying a small particle amidst larger ones is difficult because the tip of the finger is more likely to touch larger neighboring particles before touching a small particle in their middle. The probability of first touching neighboring large particles increases with the size of the large particles and the tightness of interstitial spaces, and an increasing difference in particle sizes makes the touch method increasingly

prone to sampling error. Similarly, the retrieval of small particles becomes more difficult as the surrounding particles become larger and more tightly spaced.

***Factors exacerbating touch-identification of small particles and their retrieval***

Problems of identifying small particles by touch and retrieving them can be exacerbated by many factors. Long fingernails may reduce the ability to feel the streambed with the fingertips. Not keeping the pointed finger in an exactly vertical position reduces the chance of touching a fine particle (Ramos 1996). Submergence by flow makes it more difficult for the operator to keep the pointed finger steady, which is important when identifying small particles by touch. Cold water can make the fingers numb and too clumsy to feel and pick up a small particle, and a particle just picked up can be washed out the operator's hand by the flow. The cold water problem is most pronounced in mountain streams in late fall or before the spring snow melt. Thus, to improve sampling accuracy, mountain streams should be sampled in later summer when the water is less cold. Gloves can be useful for under-water pebble counts. Simple rubber household gloves tied at the wrists with rubber bands are often a workable compromise between cold protection and retaining some feeling for small particles. Neoprene gloves are usually not suitable for retrieving fine particles from the bed.

***Visual identification most useful on dry beds***

On dry beds, a small particle to be included in the sample can be more accurately identified *visually* at the intersection with even-spaced marks on a measuring tape stretched across the sampling area than by *touch*. The accuracy of visual particle identification on dry beds can be further improved if the operator gets close to the tape and uses a fine pin, or an awl, to pinpoint the exact particle to be included in the sample. If the approach is followed carefully, particles as small as 2 mm can be sampled representatively. The precision of visual particle identification on a dry bed does not necessarily have to decrease as the size of surrounding larger particles increases, provided the operator looks straight (vertically) down, so that small particles are not hidden from view as they would be when viewed obliquely. Thus, whenever possible, pebble counts should be performed on dry beds where particles can be visually identified.

Visual identification becomes problematic for small particles on submerged beds. Rocks need to be placed onto the tape to hold it down on the streambed and this disrupts the bed beyond the disruption associated the actual sampling process (a lead-filled measuring tape might be appropriate). The largest problem is that the visual image becomes distorted under water, which makes it impossible to visually identify small particles, particularly in deeper or faster flows.

***Sampling poorly accessible stream locations or irretrievable particles***

Small particles are not only difficult to identify and retrieve, but are also often deposited in deep or otherwise poorly accessible stream locations. If the sampling objective is to collect particles from the entire reach, then those areas need to be included in the sample.

Operators, for understandable reasons, tend to avoid locations too deep for wading, or poorly accessible areas, such as under overhanging branches or behind logs (Ramos 1996). Thus, fine sediment, which is likely to be encountered in these locations, is less likely to be included in the pebble count and therefore underrepresented. The operator error arising from avoiding streambed areas of poor accessibility can be reduced if the sampling path is predetermined, such as by sampling at even-spaced marks along a measuring tape stretched across the sampling area at even distances. The size class of particles that are irretrievable or in inaccessible sampling locations must be estimated in order to maintain the randomness of the sample. The 0.5  $\phi$  size class of an irretrievable particle can usually be estimated, if the particle to be selected can be seen or touched. If the particle size cannot be estimated, then that location cannot be part of the sampling area.

#### ***Small particles between the low and the high-flow water line***

Unless a sampling protocol clearly determines the stream width to be sampled, fine particles on the exposed bank between the low and high-flow water line may or may not be included representatively in the sample. Lack of a sampling protocol leaves the operator with no guidelines as to how far to sample the banks and may introduce a high variability in the proportion of fine sediment between samples or between operators. The decision of whether the sampling area covers the bankfull width of the stream, or remains within the low flow bed, depends on the sampling objective. A study which focuses on the supply of fine sediment, for example, should sample the bankfull width, whereas sampling for a computation of stream roughness is usually restricted to the low flow bed.

#### ***Results of operator bias: small particles underrepresented and variable***

Operators are more likely to neglect small particles and instead select mid-sized, handy particles (Marcus et al. 1995). This propensity is due to the difficulty of touching small particles first before touching neighboring large particles, of seeing small particles among large ones in a bed submerged by flow, of selecting small particles off the bed, and of loosing small particles in the flow. Some operators are conscious of this problem and try to avoid bias against small particles. Other operators may even overcorrect and introduce a new bias (Marcus et al. 1995). Often, operators are not consistent in their effort to representatively include small particles in the sample, and may include small particles within fine sediment but not small particles in between large ones. Together with the tendency of small particles to accumulate in poorly accessible areas, and a poorly defined stream width to be sampled, the number of small particles tends to be underrepresented in a sample. Between operators, small particle sampling is quite variable. Bias against small particles coarsens a particle-size distribution on its fine end, whereas a variability in the number of fines leads to variability in the percentile particle-size of the  $D_5$  and  $D_{16}$ , or the percentage fines, such as particles smaller than 4 or 16 mm.

### ***Quantification of variability in fines due to operator error***

A good quantification of operator error in pebble counts is currently not available. The magnitude of operator error for pebble counts in gravel-bed streams can be estimated by comparing the total error (operator and statistical) of heel-to-toe pebble counts with the purely statistical error of a surface sample. Ideally, the difference between the total error and the statistical error indicates the magnitude of the operator error.

The purely statistical error around the various particle-size percentiles of a surface sample can be computed using a bootstrap approach in which a computer re-samples a large sample entered into the computer. This was performed by Rice and Church (1996b) for a surface sample of more than 3500 particles collected from the gravel bed of the Mamquam River. The size distribution had a standard deviation of  $1.17 \phi$  and was slightly skewed towards a tail of fines, typical of particle-size distributions in coarse gravel beds. A sample size of 400 particles yielded a statistical percent error around the  $D_5$  (in mm) of approximately  $\pm 20\%$ , which is roughly equivalent to an absolute error of  $\pm 0.3 \phi$  for the  $\phi_5^1$  (Fig. 4.2). The percent error around the  $D_{50}$ ,  $D_{75}$  or the  $D_{84}$  was approximately  $\pm 8\%$ , which is roughly equivalent to an absolute error of  $\pm 0.12 \phi$  (see Section 5.2.2.3 for details). Note that these errors pertain to the statistical error only and that the collected particles are assumed to be statistically independent.

The combined statistical and operator error was computed for a set of 7 heel-to-toe pebble count samples obtained by the authors in several gravel and cobble-bed rivers. The samples had bed-material sorting coefficients  $s_f$  between 1.0 and 1.6, and sample sizes  $n$  between 201 and 537. The mean  $s_f$  for all samples was 1.24, and the mean sample size was 451. Thus, standard deviations and sample size were generally similar to the standard deviation and the 400-particle sample size for the sample from the Mamquam River. Each of the 7 samples was split in two: subsample  $a$  comprised the 1<sup>st</sup>, 3<sup>rd</sup>, 5<sup>th</sup>, ... recorded particle size for each transect, whereas subsample  $b$  comprised the 2<sup>nd</sup>, 4<sup>th</sup>, 6<sup>th</sup>, ... recorded particle size. The percent error  $e_{\%D_p}$  around several percentiles in mm between the two subsamples was computed using a standard sample size equation  $e_{\%D_p} = (1.96 \cdot s/\mu_p)/\sqrt{n}$  (Section 5.2.1), where  $\mu_p$  is the mean of the two subsample percentiles analyzed, e.g.,  $(D_{5(a)} + D_{5(b)})/2$ .

The mean total errors around the  $D_{25}$ ,  $D_{50}$ ,  $D_{75}$ , and  $D_{84}$  for the 7 heel-to-toe samples were roughly within the range of the statistical errors determined by Rice and Church (1996b) (Fig. 4.2). This indicates that the variability between samples due to operator error is of no large concern for central and high percentiles. However, the between-sample variability was quite pronounced for small percentiles. The total relative error (operator and statistical error combined) around the  $D_5$  was  $\pm 50\%$  for the heel-to-toe samples, which is 2.5 times larger than the purely statistical sample error determined for the  $D_5$  from the bootstrap approach by Rice and Church (1996b). The corresponding total

---

<sup>1</sup> The absolute error in  $\phi$  units is not precisely convertible to the percent error in mm because the percent error in mm is not evenly distributed around a percentile (Section 5.2.2.3, Fig. 5.8). However, this imprecision is negligible for small errors. The numerical value of an absolute error in  $\phi$  units can be converted to the percent error in mm by the following rule of thumb:  $e_{\pm\phi} \cdot 70 \approx e_{\%mm}$  or  $e_{\%mm}/70 \approx e_{\pm\phi}$ . For example, an absolute error of  $\pm 0.1 \phi$  is approximately equal to a 7% error in mm ( $e_{\pm\phi m} \cdot 70 \approx e_{\%Dm}$ ).

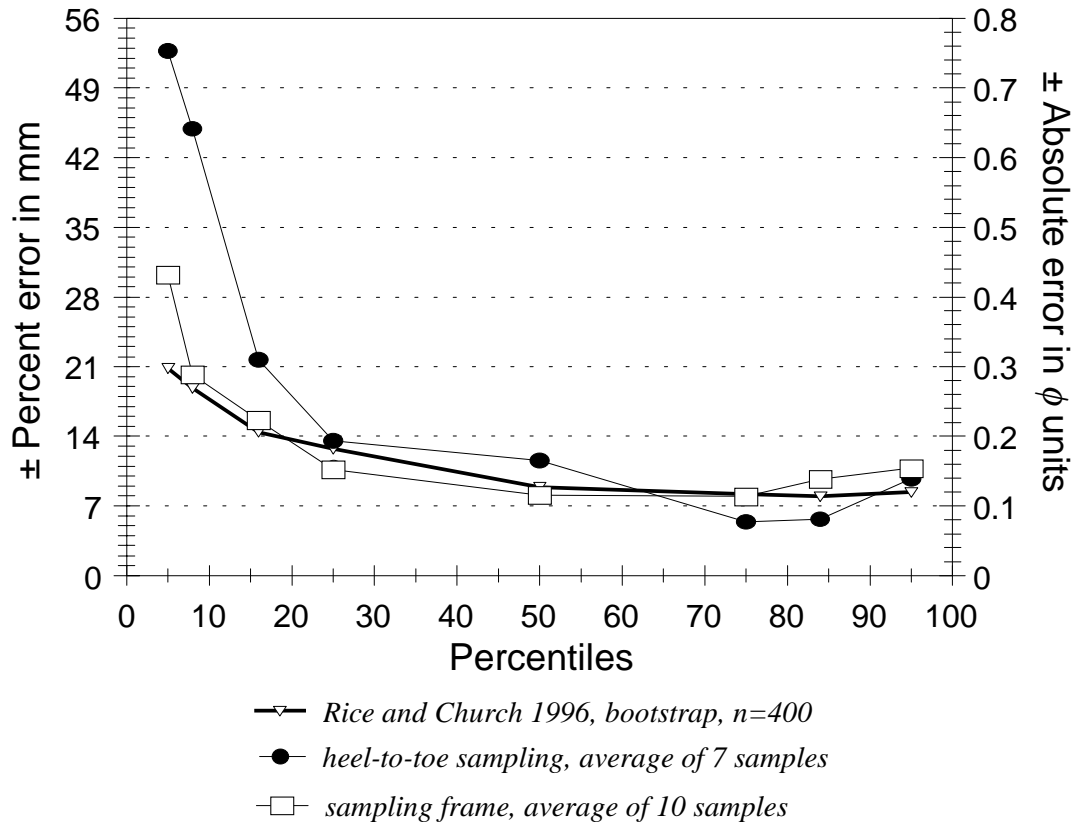


Fig. 4.2: Statistical error computed for a bed-material sample with a standard deviation of 1.17 and a sample size of 400 using a bootstrap approach (—▽—) by Rice and Church (1996b) = R&C '96 (see Section 5.2.3.3 for details). Mean percent error observed for heel-to-toe sampling (—●—), and for samples taken with the sampling frame (—□—) (Section 4.1.1.6).

absolute error around the  $D_5$  for the heel-to-toe samples was  $\pm 0.75 \phi$  units, which is one and a half standard sieve classes. This high error for small percentiles suggests that heel-to-toe pebble counts in coarse gravel- and cobble-bed streams should only be used for determining the  $D_{50}$ ,  $D_{75}$ , and  $D_{84}$  of a distribution, but not for small percentiles or for determining the percent fines.

***Truncation of the underrepresented and variable fine end of size distributions***

The exact particle size at which a bias against small particles in heel-to-toe sampling begins to show depends on the streambed conditions. Rice (1995), for example, found that particles finer than 8 mm are underrepresented in underwater pebble counts, whereas Fripp and Diplas (1993) suggest that particles finer than 15 mm cannot be sampled representatively in heel-to-toe pebble counts. As a statistical measure to address this problem, Rice (1995) suggested exclusion of particles finer than 8 mm from the size analysis, thus truncating the cumulative distribution curve at 8 mm. Truncation at the fine end coarsens the low percentiles of the distribution, while large percentiles are less

affected. Thus, truncation at the fine end of the sample should be restricted to studies in which low percentile particle-sizes, such as the  $D_5$  or  $D_{16}$  are of no concern.

Another, less drastic approach to deal with bias against fines is to tally all small particles in one joint particle-size class, for example, as finer than 8, or 16 mm. (Generally, pebble counts tally particles smaller than 2 mm jointly in the  $< 2$  mm category). This approach assumes that the sampling difficulty lies in the distinction of small particles between neighboring small particle sizes, but does not address the difficulty of reliably identifying and selecting a small particle from between neighboring large particles. The advantage of joint tallying as opposed to truncation is that it does not affect the size distribution of larger particles.

If the correct characterization of small particle sizes is the study goal, Diplas and Fripp (1992) and Fripp and Diplas (1993) suggest taking areal samples (with clay as an adhesive) (Section 4.1.3.1). Note that particle-size distributions from areal samples need to be converted into the equivalent volumetric or grid-by-number distribution before they can be compared to particle-size distributions from pebble counts (Section 4.3.1 and 4.3.2).

#### 4.1.1.4 Operator bias against and towards cobbles and boulders

Heel-to-toe walks were invented for sampling streambeds of mid-sized gravel, but not for sampling beds with cobbles and boulders or streams with bed surface-structures (e.g., clusters and wake deposits). If applied to such beds, heel-to-toe sampling may bring about bias both for and against large clasts.

##### ***Operators avoid stepping onto cobbles and boulders***

One reason for operator bias against cobbles and boulders in heel-to toe samples arises from the practice of determining the sampling location by foot placement. Operators are understandably reluctant to place their feet onto an exposed and slippery cobble or boulder for risk of insecure footing and falling. Consequently, if particle identification is based on foot placement, operators (even unconsciously) tend to avoid cobbles and boulders in heel-to-toe pebble counts. An operator's reluctance to step onto a cobble or boulder is likely to increase with increasing slipperiness, size, and protrusion of cobbles and boulders, the coldness of the water, swiftness of flow, remoteness of the site, or other factors that decrease an operator's readiness for taking a risk. Physical shape of the operator can also play a role in the variability of sampling results between operators in heel-to-toe pebble counts. Bunte and Abt (2001) compared sampling results obtained from heel-to-toe walks in a cobble-bed stream ( $D_{50} = 69$  mm,  $D_{max} > 720$  mm, sorting coefficient  $s_f = 1.7 \phi$ ) between two operators of different size. The operator with a small boot size (Operator B) was more prone to avoiding cobbles and boulders, and produced particle-size distributions with fewer coarse particles than the operator with a large boot size (Fig. 4.3). Operator B also extended the sample further onto the banks and counted more small particles than Operator A (Section 4.1.1.3).

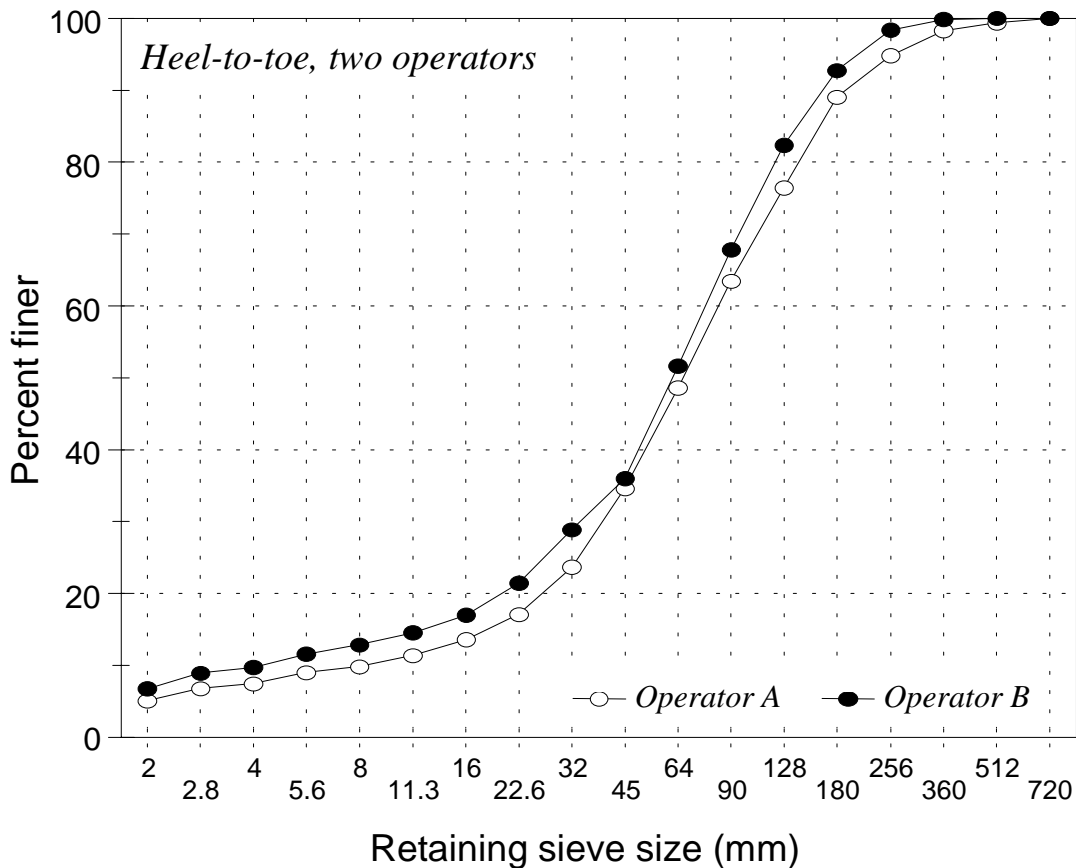


Fig. 4.3: Different cumulative frequency distributions obtained by operator A (large boot size) and operator B (small boot size) sampling with heel-to-toe steps in a cobble-bed stream.

***Operators avoid cobbles and boulders in their sampling paths***

Cobbles and boulders are not only risky to step upon, but also heavy, often wedged, and difficult to dislodge from the bed. Heel-to-toe walks make it easy for operators to avoid such particles; it only requires a slight change in foot position in the last one or two steps. Operators might also change their previously pursued sampling path if a streambed area lies ahead that has particularly unappealing-looking cobbles and boulders or that seems poorly accessible. Again, avoiding cobble and boulders produces a particle size-distribution that, compared to an unbiased sample, is too fine in its coarse part.

The tendency to avoid, and thus bias against cobbles and boulders can be corrected by sampling systematically, such as at even-spaced intersection along a measuring tape stretched at even increments across the sampling area. Systematic sampling along a measuring tape renders the operator's stepping position irrelevant. If an irretrievable particle is encountered, randomness of the sample can be maintained by estimating the particle-size class. The  $0.5 \phi$  size-class of a particle can usually be estimated to within  $\pm$  one size class if the particle to be selected can be seen or touched. If the particle size-class cannot be estimated, then that location must be explicitly excluded from the sampling area.

### ***Inherent bias versus overrepresenting coarse particles by double counting***

Pebble counts have an inherent bias towards coarse particles, because sampling at even-spaced intervals gives coarse particles a larger *statistical* chance of being included in the sample than smaller particles. This inherent statistical bias makes the number frequency of a pebble-count size-distribution directly comparable to the weight frequency of a volumetric sample from the same location, provided the bed is not armored (see conversion of sample distributions, Sections 4.3.1 – 4.3.2). Inherent statistical bias should not be confused with an operator bias towards cobbles and boulders due to the practice of double counting.

Counting the size of cobbles and boulders as frequently as the preset spacing (e.g., one boot length) is statistically not correct because it produces a serially correlated sample that is not random. The step spacing of pebble counts must be wide enough to allot only one count per each cobble or boulder. Yuzyk and Winkler (1991) suggest that the spacing should be twice as large as the largest particle diameter to ensure that each particle receives only one count. Double counting due to proximity should not be confused with double counting that may result from random sampling with replacement.

Double counting of cobbles and boulders overrepresents the presence of large particles and produces particle size-distributions that are too coarse in their coarse part. The effect on the  $D_{50}$  percentile particle-size is small if double counting occurs infrequently, but the effect on the  $D_{95}$  can be quite pronounced if many large particles are counted double or multiple times. This is illustrated by the following example for a poorly sorted cobble bed ( $s_f = 1.7$ ) with a  $D_{50}$  particle size of 69 mm and a  $D_{max}$  particle size class of 720-1024 mm (particle-size distribution for Operator B in Fig. 4.8). If cobbles larger than 180 mm and boulders were allotted double or multiple counts so that the total sample size increased by 1, 2, and 3% (e.g., by 5, 10, and 15 particles in a 469 particle pebble count), the  $D_{50}$  particle size would increase by 1, 3, and 4%, respectively. The  $D_{84}$  would increase by 3, 5, and 8%, and the  $D_{95}$  particle size by 4, 7, and 22%. Although double counting and cobble avoidance introduce biases in opposite directions, and their effects act towards canceling each other, one inaccurate procedure must not be used as a corrective means for another inaccurate procedure.

Another form of spatial correlation is introduced if several particles from within the coarse or fine part of bed surface-structures (Section 3.4.1) are included in the sample. A random sample series should only contain independently deposited particles, whereas the position and size of particles within a cluster or wake deposit are influenced by the size and position of neighboring particles. Thus, in order to avoid multiple counts of large particles within a cluster, or of small particles within a wake deposit, the sample point spacing needs to be larger than the diameter of bed surface-structures.

#### **4.1.1.5 Statistical detectability of operator bias**

Heel-to-toe sampling in gravel-bed streams tends to undersample both very fine gravel as well as the cobble/boulder fraction. Consequently, mid-sized, handy particles are oversampled. Double counting due to small sampling-point spacing oversamples cobbles

and boulders. The bias against fines has the most pronounced effect on the cumulative particle-size distribution if the bed contains a large number of difficult-to-sample fines and thus presents a large opportunity for neglecting fines. Similarly, the tendency of avoiding cobbles and boulders has the most pronounced effect on the cumulative particle-size distribution in beds containing a large number of difficult-to-sample cobbles and boulders. Fig. 4.4 shows the expected effect of operator bias on particle-size distributions in heel-to-toe samples compared to unbiased sampling.

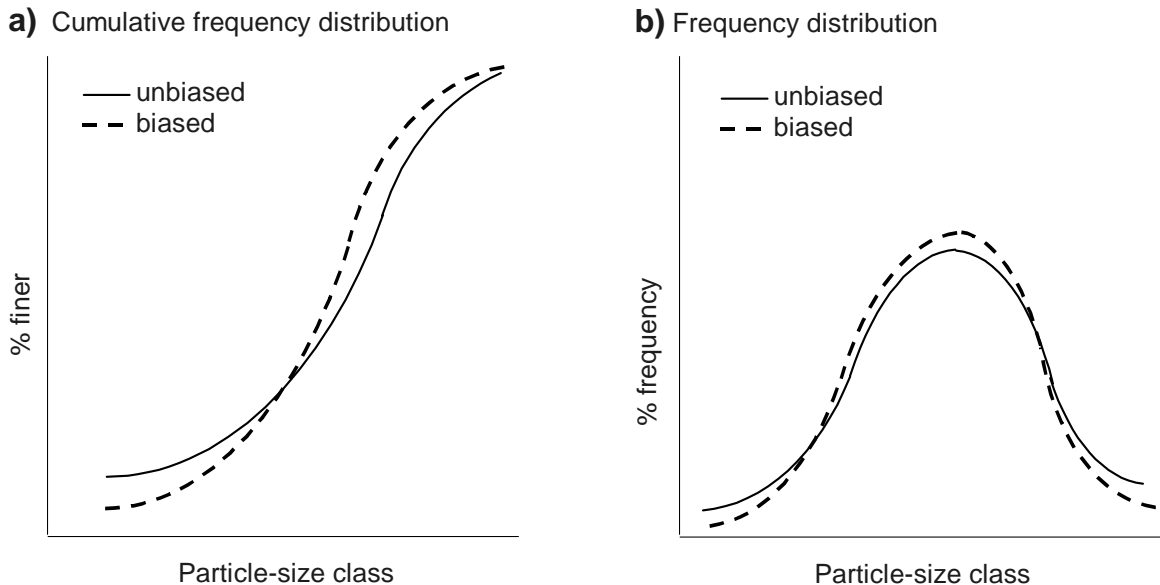


Fig. 4.4: Cumulative distribution (a) and frequency distribution (b) of an unbiased pebble count ( — ) and a pebble count biased against small and large particles ( - - ) typical of heel-to-toe sampling in gravel- and cobble-bed streams.

The bias that heel-to-toe sampling introduces against the fine gravel fraction and the cobble/boulder fraction is not detectable by standard statistical procedures, for example when samples are compared using ANOVA, or F-tests (Wohl et al. 1996). This is because each percentile is associated with a large error due to the relatively large standard deviation on poorly-sorted beds and the statistically small sample size of 100 – 400 particles. The difference between two size distributions, each with a large error, must be quite large before it becomes statistically detectable. For example, the statistical error around the mean particle size of an approximately normal distributed 100-particle pebble count with a sorting coefficient of 1.6 is  $\pm 0.32 \phi^{(2)}$ , or approximately  $\pm 22\%$  for particle sizes in mm<sup>(3)</sup>. Thus, the means of two such 100-particle pebble counts would have to

<sup>2</sup> An absolute error of  $e_{\text{app}} = 0.32 \phi$  was estimated for an assumed normal distribution of particle sizes in  $\phi$  units from  $e_{\phi} = t_{1-\alpha/2, n-1} \cdot s/n^{0.5}$ .  $t_{1-\alpha/2, n-1}$  was set to 1.987,  $\alpha=0.05$ ,  $s$  is the sample sorting coefficient, and  $n$  the sample size. Refer to Section 5.2.1 for further detail.

<sup>3</sup> See footnote 1 in Section 4.1.1.3.

differ by more than 22% before their difference is statistically significant. If one pebble count had a mean of 50 mm, the other pebble-count mean would have to be larger than 61 or less than 39 mm before the difference is statistically significant. Stream studies, however, may be concerned about differences between sample means considerably smaller than 20%, or may require results with an error of much less than 20%.

The absence of a statistically significant difference between two samples from poorly sorted streambeds also gives a false sense of precision and does not mean that there is no difference. Differences between two samples can usually be better presented by simply plotting parallel samples. The user can then decide from the plots whether the observed difference between samples is acceptable for the study.

The study by Wohl et al. (1996) provides an example of inter-sample difference that is observable from plotted data, but not indicated as statistically significant by standard statistics. Wohl et al. (1996) compared samples obtained from heel-to-toe sampling and sampling along a tape on mainly dry beds of several gravel- and cobbles-bed streams. They found that both sampling methods produced statistically indistinguishable results. However, when data were plotted, the ratio of the same percentile particle-sizes between heel-to-toe samples and sampling along a tape showed a systematic decrease with bed-material particle size (Fig. 4.5) (Bunte and Abt 2001). On fine gravel beds, heel-to-toe samples had coarser  $D_{16}$ ,  $D_{50}$  and  $D_{84}$  particle sizes than sampling along a tape. By contrast, heel-to-toe sampling in coarse gravel and cobbles beds had smaller  $D_{50}$  and  $D_{84}$  particle sizes than sampling along a measuring tape (Fig. 4.5). Both results correspond to the findings of observer bias.

#### 4.1.1.6 Sampling frame for bias reduction in particle identification

A measuring tape, which is a useful sampling tool for preventing operator bias against fine and coarse particles on dry beds, is difficult to use when the streambed is submerged by flow, particularly when the flow is fast. The marks on the tape are difficult to see and relocating a large number of rocks to hold the tape down on the bed creates an extra bed disturbance beyond that induced by the actual sampling process. Operators performing pebble counts in mountain gravel-bed streams are often faced with submerged beds and swift flow, however, and need a device that overcomes the shortcomings of a measuring tape in underwater pebble counts and that mitigates the typical sampling errors associated with heel-to-toe walks. For this reason, Bunte and Abt (2001) developed a sampling frame, following a suggestion made earlier by Marcus et al. (1995).

##### ***Construction of the sampling frame***

The sampling frame consists of four aluminum bars that are connected to form a square with an inside diameter of 60 by 60 cm (Fig. 4.6 a). The four aluminum bars are 0.63 cm thick (0.25 inch), 3.81 cm (1.5 inch) wide, and 65.4 cm long, cut in a miter joint and held together by corner pieces. The corner pieces have threaded pins that fit through borings at the ends of the aluminum bars. Wing nuts ensure easy set-up of the frame. The frame is sturdy and can be stepped upon to hold it down on the stream bottom in fast flow. In

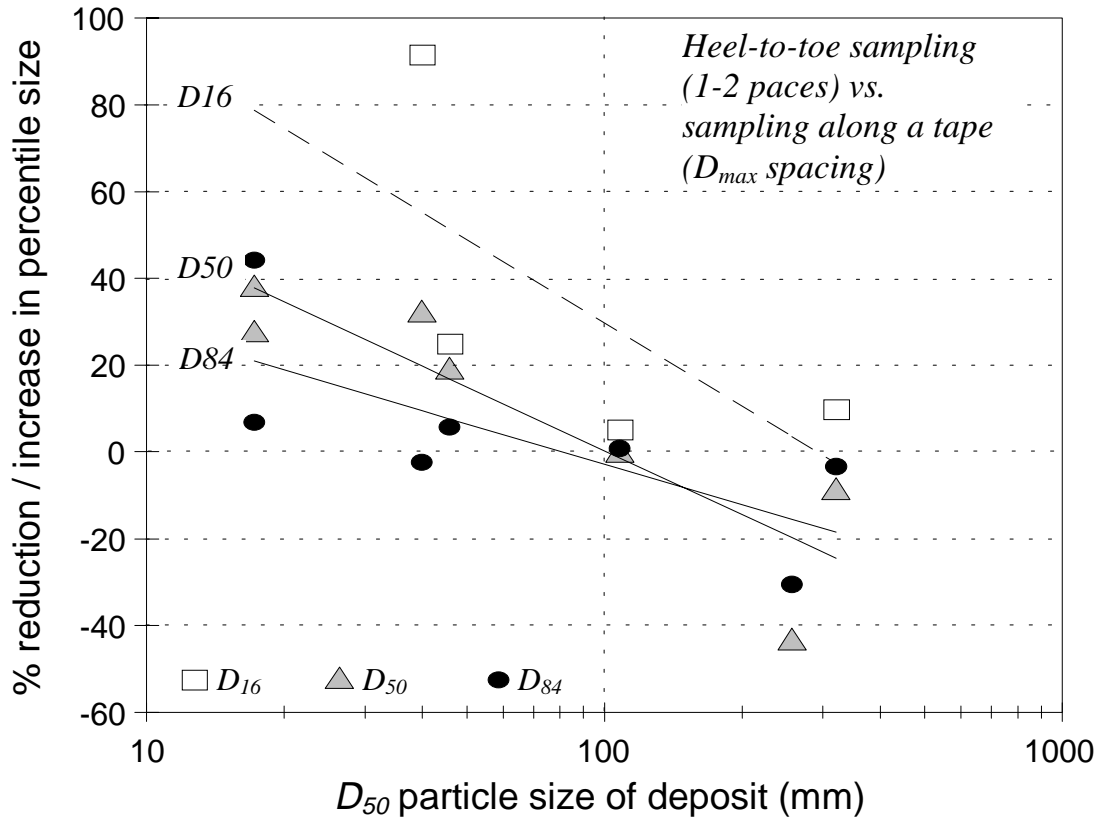


Fig. 4.5: Coarsening of the  $D_{16}$ ,  $D_{50}$  and  $D_{84}$  on fine gravel beds and fining of the  $D_{50}$  and  $D_{84}$  on cobble beds for heel-to-toe sampling compared to sampling along a measuring tape with a spacing of the  $D_{max}$  particle size  $b$ -axis length. Stippled lines indicate best-fit regression lines. Data from Wohl et al. (1996).

order to make the frame easier to assemble and to transport, the parts can be reduced to a length of 35 cm, yielding 8 pieces that snap together with a spring and bolt mechanism (Bunte and Abt 2001) (Fig. 4.6 b).

Small slots cut in 5 cm increments along the outside edges of the frame hold thin white elastic bands in place that are stretched horizontally across the frame. Together with elastic bands stretched in a vertical direction, a grid with four or more cross-points is defined. The spacing of the grid points is adjusted to a size equal to or larger than the  $D_{max}$  particle size.

#### ***Using the sampling frame***

To use the sampling frame in the stream, a tape measure is stretched from bank to bank. The sampling frame is placed onto the stream bottom so that one of the corners aligns with even-spaced marks on the tape, e.g., every three feet or one meter. Grid points derived by the elastic bands are used to visually define the particle to be selected. If the flow is deep and fast, and vision is blurred, looking at the grid intersection can help identify the particle to be included in the sample. If, for example, the grid intersection

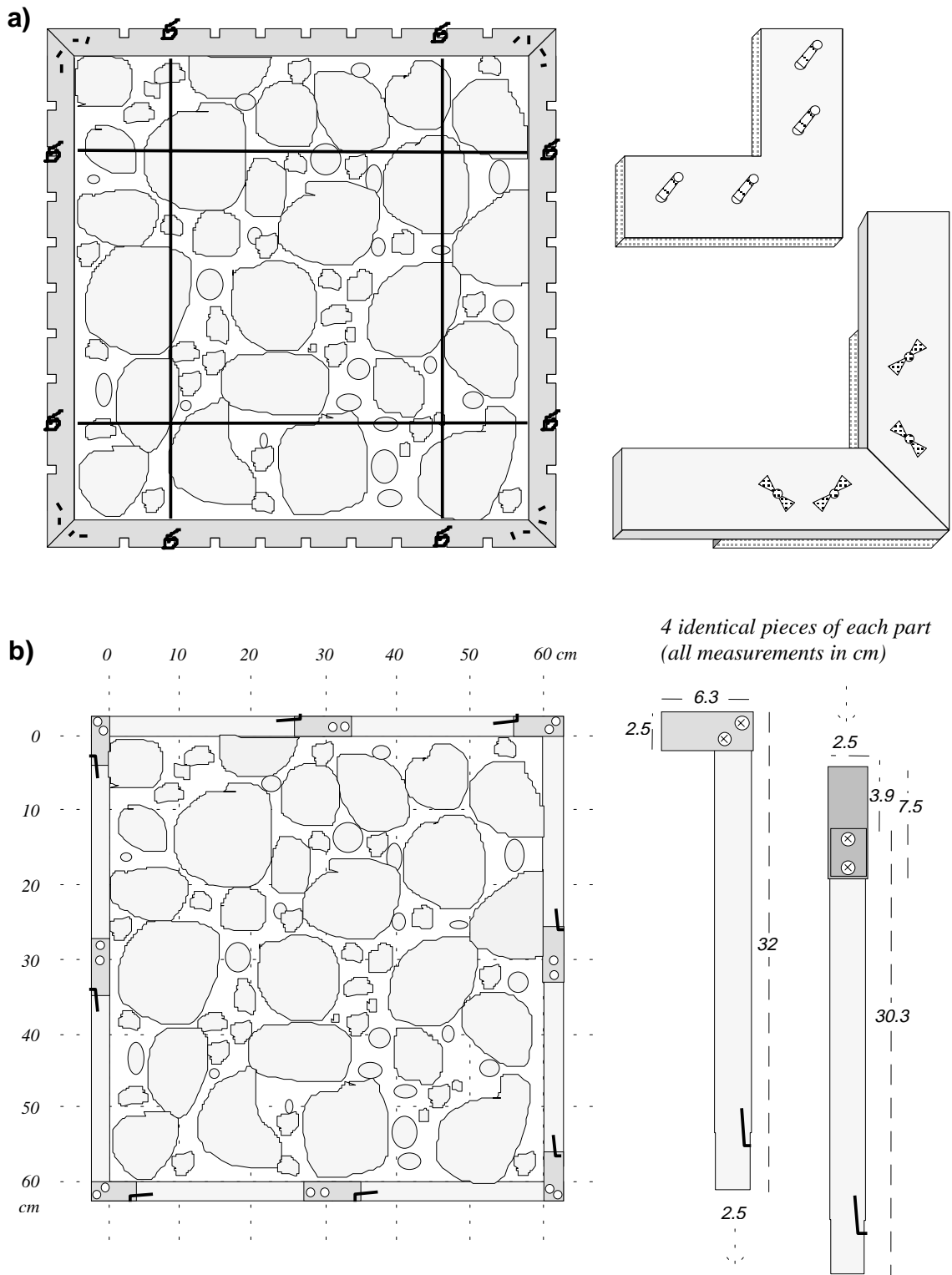


Fig. 4.6 (a): Four-piece sampling frame 60 by 60 cm with an adjustable grid of elastic bands (left). Detail of the corner piece with mounted threaded pins is shown and the joining using corner pieces and the wing nuts (right). (b): Eight-piece sampling frame modified for easy assembly and transport (left). Detail of pieces that snap together with a spring and bolt mechanism (right).

is between two cobbles, the operator knows that a small interstitial particle should be selected, but neither of the cobbles.

If flow is too deep or too fast to see the particle under the grid intersection, the particle to be included in the sample has to be identified by touch. A pointed index finger is placed in a corner of the grid intersection, and vertically lowered onto the sediment surface. The grid intersection serves as a guide for the position of the finger as it is lowered to the bed surface. Using the grid intersection as a reference point as opposed to the tip of the boot helps the operator select a particle more representatively because the operator works in a more comfortable posture when bending down to the sampling frame as opposed to bending down to the tip of the boot. The elastic bands in the sampling frame do not hinder the removal of a particle from the streambed. Particles are collected from under all four grid points, measured with a template, and placed back approximately into the same position from which they were taken. The frame is then moved to the next position along the tape. For many coarse gravel-bed rivers, a 30-cm grid within a 60 by 60 cm frame placed at 1 m, or 3 feet increments along the tape will be adequate. The sampling frame can be used on both sides of a transect. Individual transects should be 3 - 4 m apart to avoid overlap between sampled areas.

#### ***Comparison of sampling results between sampling frame and heel-to-toe walks***

Particle-size distributions obtained from using the sampling frame and from sampling with heel-to-toe walks were compared in samples obtained on a poorly sorted cobble-bed stream ( $s = 1.7 \phi$ ) with a  $D_{50}$  of 69 mm (Bunte and Abt 2001). Each of two experienced operators performed two pebble counts over the same river reach, one pebble count using the sampling frame and one collecting a heel-to-toe sample. Sample size ranged between 470 and 570 particles per sample.

A comparison of the frequency distribution for both sampling methods shows that samples from the sampling frame contained a larger number of cobbles than samples from heel-to-toe walks (Fig. 4.7). The heel-to-toe samples comprised a large number of mid-sized gravel in the size class 45 and 64 mm and generally fewer cobbles. This difference clearly demonstrates an operator bias against cobbles and boulders in heel-to-toe samples, while large, handy particles were favored instead. For inexperienced operators, the difference is expected to be even more pronounced.

#### ***Sampling frame reduces variability between operators***

Two operators sampling the same transect using the heel-to-toe method are very likely to produce different particle-size distributions, especially if the operators are of different stature (Fig. 4.7). Using the sampling frame largely reduced the variability between operators, because it eliminates operator decision on the selection of cobbles and boulders and equalizes the sampled stream width, as well as the number of particles sampled by both operators. Consequently, both operators who had markedly different distributions in heel-to-toe samples (Fig. 4.7), produced very similar particle-size distributions when using the sampling frame (Fig. 4.8). The percentile particle-sizes of the  $D_{50}$  to  $D_{95}$

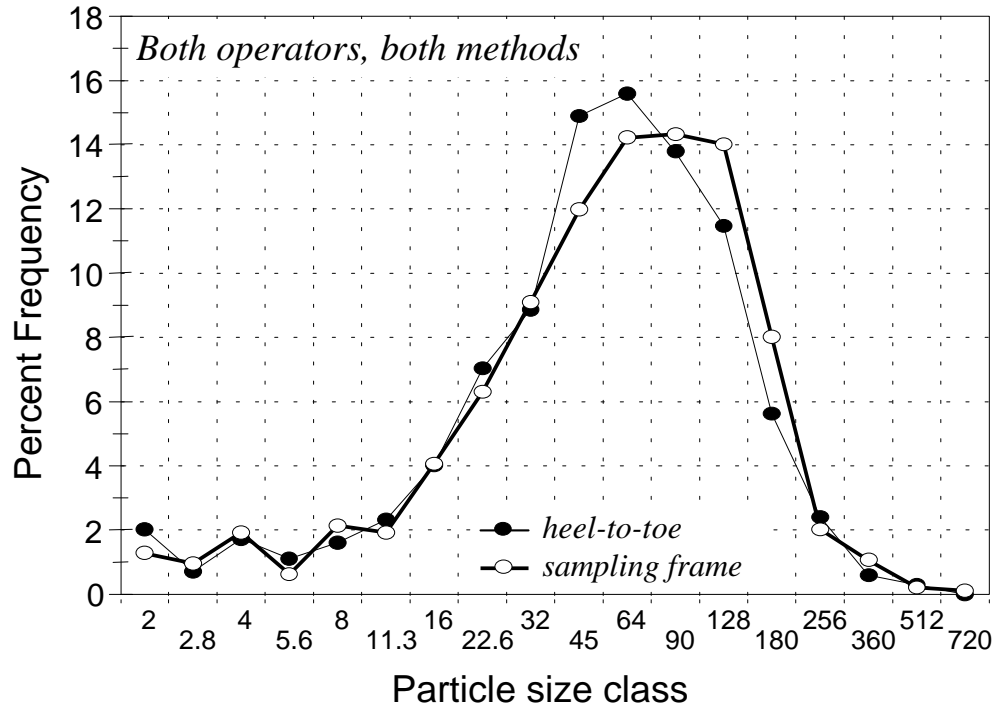


Fig. 4.7: Difference in frequency distributions obtained for heel-to-toe sampling and the sampling frame (both operators). The size class < 2 mm is not included in the analysis.

differed by less than 5% between operators, whereas the percentile difference for the  $D_{50}$  to  $D_{95}$  ranged from 7 to 22% when both operators sampled with heel-to-toe walks (Fig. 4.9).

***Quantification of sample variability due to operator error***

In order to estimate the magnitude of the operator error when using the sampling frame, the total error incurred in samples from the sampling frame was compared to the statistical error computed by Rice and Church (1996) for a large sample from gravel-bed river sample in Section 4.1.1.3 (Fig. 4.2). A set of 10 samples collected by the authors of this study in several gravel- and cobble-bed streams using the sampling frame was available for this comparison. The sorting coefficient  $s_I$  for the 10 samples ranged between 0.97 and 1.64, and sample sizes  $n$  between 309 and 469. The mean sorting coefficient of  $s_I = 1.26$  of these 10 samples was similar to the standard deviation of the Mamquam River for which Rice and Church (1996b) computed the relation between sample size and statistical error with a bootstrap approach. Likewise, the mean sample size of 426 was similar to the sample size of 400 for which the statistical error around various percentiles is shown in Fig. 5.10 and 5.11.

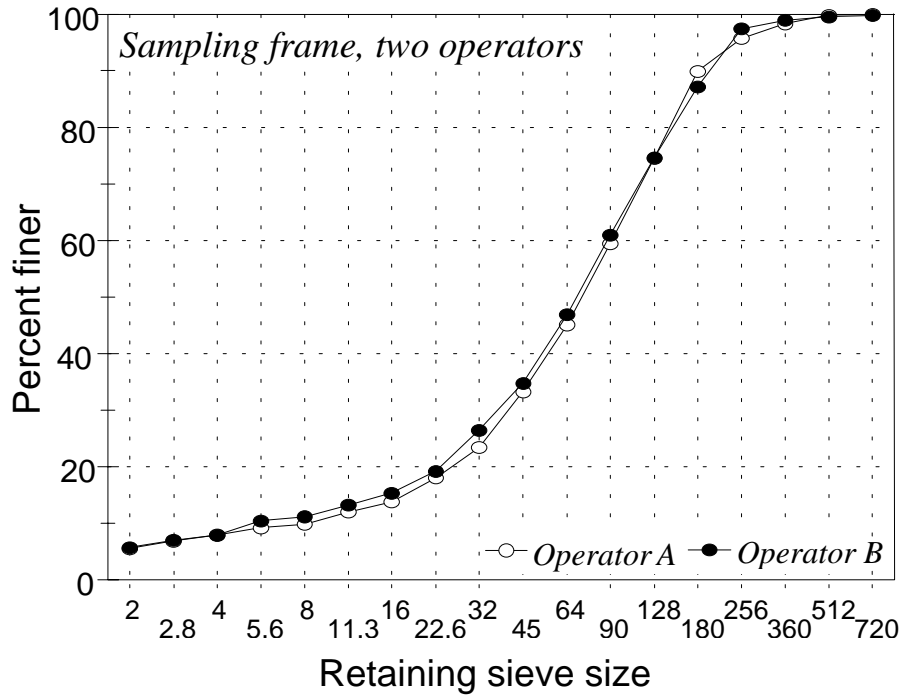


Fig. 4.8: Almost identical cumulative frequency distributions obtained by operators A and B when using the sampling frame in a cobble-bed stream.

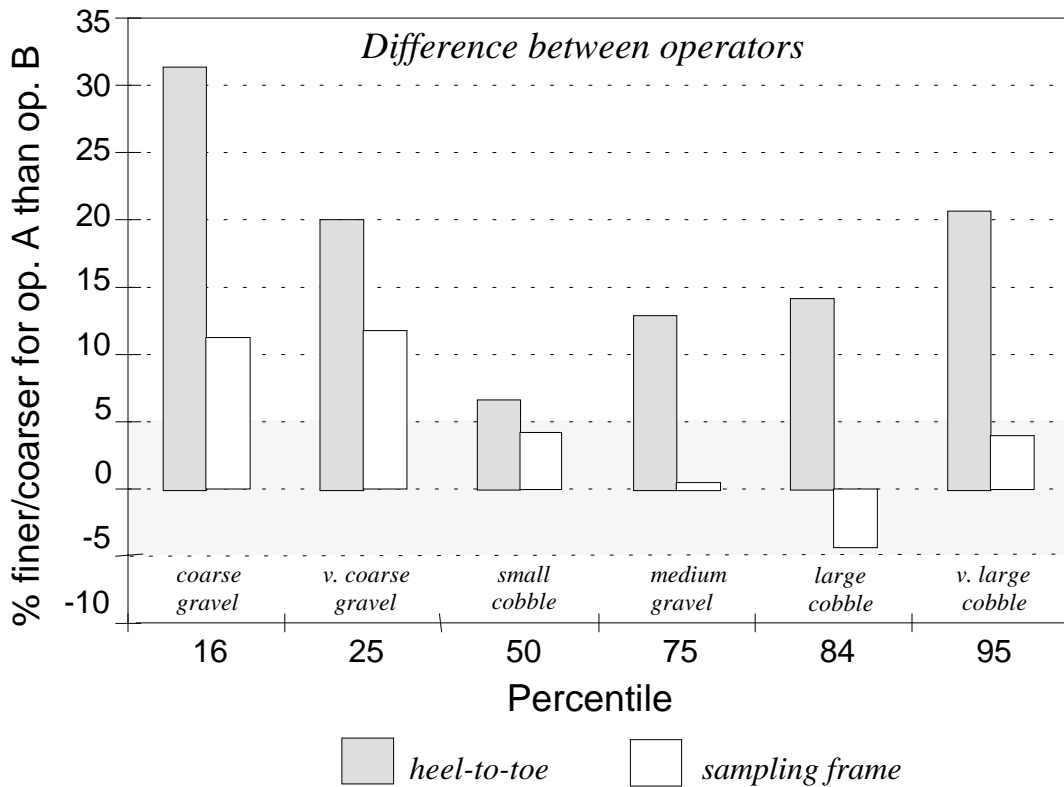


Fig. 4.9: Percentage difference in percentile particle-size obtained by operator A and by operator B. The gray band indicates the range of up to  $\pm 5\%$  difference.

In order to compute the operator error for each sample collected with the sampling frame, each of the 10 samples was split in two: subsample *a* comprised the 1<sup>st</sup>, 3<sup>rd</sup>, 5<sup>th</sup>, ... recorded particle size for each transect, while subsample *b* comprised the 2<sup>nd</sup>, 4<sup>th</sup>, 6<sup>th</sup>, ... recorded particle size. The percent error  $e_{\%Dp}$  around percentiles was computed using a standard sample-size equation  $e_{\%Dp} = (1.96 \cdot s/\mu)/\sqrt{n}$  (Section 5.2.1), where  $\mu$  is the mean of the two subsample percentiles analyzed, e.g.,  $(D_{5(a)} + D_{5(b)})/2$ .

Sampling with the frame yielded an average relative error around the  $D_5$  of  $\pm 30\%$  between samples (Fig. 4.2). This is still higher than the statistical error of  $\pm 20\%$ , but a considerable improvement over the high variability of  $\pm 50\%$  error or more for the  $D_5$  obtained from heel-to-toe sampling. The reduced error for the  $D_5$  suggests that the sampling frame indeed reduces operator variability in the identification of small particles. Using the sampling frame cannot completely eliminate operator error because frame does not prevent inaccurate particle retrieval. For all other percentiles, the operator error computed for the sampling frame samples is similar to the purely statistical error computed by Rice and Church (1996b), suggesting that the sampling frame does largely eliminate operator errors and thus inter-sample variability in all but the smallest particle sizes.

#### 4.1.1.7 Measuring, recording and analyzing pebble count data

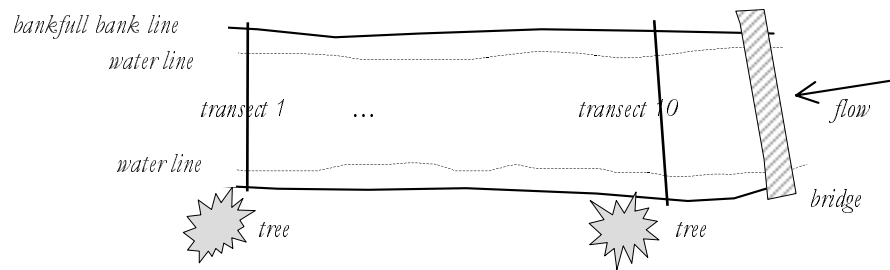
Pebble counts are usually a two-person operation: one person selects and picks up a particle from the streambed, measures its *b*-axis, preferably with a template (Section 2.1.3.6) and places the particle back onto the streambed in the location where it was taken. The second person records the particle size in a notebook. Voice activated tape recorders may be an option for data recording if a person works alone. However, the background noise from the water flow in mountain gravel-bed streams is too loud to allow a recorder shut-off and thus causes a lengthy record.

For many purposes, particle sizes in pebble counts are best measured with a template (Section 2.1.3.6) that has a 0.5  $\phi$  gradation (Section 2.1.2). Smaller or larger  $\phi$  gradations may be appropriate in some studies or stream situations. Particles finer than 2 mm are usually not differentiated in size, but tallied together as a single size-class finer than 2 mm. Some studies use a ruler or caliper to measure particle axes to the nearest mm (Section 2.1.3.7). This should only be done if the range of measured particle sizes is small, if a near-normal distribution of particle sizes in terms of  $\phi$  units cannot be assumed, or if all particle axes are measured (Section 2.1.3.7). Measuring the particle *b*-axis with a ruler is not recommended as a substitute for template measurements. Using templates not only reduces the variability in particle-size measurements between operators, but also ensures comparability of the measurements with data obtained from using standard square-hole sieve sets.

When the measured particle sizes are recorded, the note taker should use a separate column for each transect in order to allow tracing back the approximate location of each recorded particle size (Table 4.3). This can be helpful in identifying systematic spatial variability of particle sizes. Information can be lost when recording particle sizes as tick

Table 4.3: Example of a sampling form for pebble counts

Stream: Squaw Creek Reach: 100-150 m downstream of Spire Rock Campground Bridge  
 Date: July 8, 1996 Person sampling: Jack Brown Person recording: Jill White  
 Particle size measurements: Template in 0.5  $\phi$  gradation; Calipers (yes/no); Ruler (yes/no)  
 Select one: x Largest size class (mm) through which particle cannot pass (larger than)  
 \_\_\_ Smallest size class (mm) through which particle can pass (smaller than)  
 Stream morphology: mostly plane bed, small plunge pools, some riffles and rapids  
 Banks within reach: LB steep, ca. 0.5 m incised into meadow; RB gentle sloping, sandy Bed material  
 structure and packing: large particles wedged, some clusters, little imbrication  
 Particle shape: mostly ellipsoid, some discs, subrounded; cobbles and boulders mostly angular  
 Lithology: 70% andesite and other volcanic rocks, 20% sedimentary, 10% gneiss  
 Remarks: used sampling frame with grid spacing of 0.3 m  
 Sketch of sampling site:



Location of 1<sup>st</sup> transect: 150 m downstream of bridge

Transect number:	1	2	3	...	k
Dist. upstream from 1 <sup>st</sup> transect (m):	0	5	10	...	j
Left Bank	5.6	11.3	8		4
	16	8	5.6 WL		11.3
WL = waterline	32 WL	22.6	45		16
	45	64 WL	90		128 WL
	⋮	⋮	⋮		⋮
	90	45	32		64
	16	11.3 WL	8		22.6
	2.8	5.6	4 WL		16
	4 WL	<2	2		2.8
Right Bank	2		5.6		

marks in the respective size class of a sampling form. A sequential data record is also necessary if a sample is to be split for a statistical error analysis (Section 5.2.1 and 5.2.2). Mention of the water line and whether a particle was collected bankward or waterward from the water line is important because it facilitates the decision to either include or exclude fine particles near banks from the analysis, an option that depends on the study objective. Field forms and field books are further discussed in Section 4.5.

Particle sizes are analyzed based on the frequency-by-number of particles per size class. A cumulative percentage frequency distribution is computed from the measured particle sizes, and particle-size percentiles, such as the  $D_{50}$  or  $D_{84}$  (Sections 2.1.4.1 and 2.1.4.2), or the % fines smaller than 2, or 8 mm (Section 2.1.5.8) are determined. Particle-size parameters may be computed from the frequency distribution or from percentiles of the cumulative frequency distribution (Section 2.1.5).

### **4.1.2 Grid sampling**

In grid sampling, particles are measured from under a *preselected number of grid points* that cover a predefined sampling area. Particles can be physically picked up from under a grid laid directly on the streambed surface, and in this case, a grid count is actually a pebble count. Pebble count procedures are described in Section 4.1.1. Another form of grid count is to take vertical photographs of the sediment surface, and measure particle sizes under a grid superimposed on the photograph. Both physical grid counts (pebble counts) and photographic grid counts can be performed at a variety of different spatial scales.

#### **4.1.2.1 Grid sizes and spatial scale**

Grid counts can cover sampling areas of any shape as long as the grid is evenly spaced. The spatial scale of grid counts is flexible. The smallest grid unit is determined by the coarsest particles on the sediment surface. Grid spaces should be at least as large as the  $D_{max}$  particle size, or even better twice the  $D_{max}$ , in order to avoid double counting and serial correlation (Section 4.1.1.2). A gravel surface with a  $D_{max}$  of 100 mm requires at least a 0.1-m grid. A grid of this size can be set up by rubber bands spanned across the sampling frame (Section 4.1.1.6, Fig. 4.6). Minimum sampling area for a sample size of 400 particles for this grid spacing is 4 m<sup>2</sup>. A cobble surface with a  $D_{max}$  of 256 mm requires at least a 0.25-m grid, and the minimum area for sampling 400 particles is 10 m<sup>2</sup>. At this scale, grid points can be marked by parallel transects along a measuring tape. The largest extent for a grid count is an areal overview that extends over a reach of several 100 m<sup>2</sup> in.

#### **4.1.2.2 Photographic grid counts**

A grid count can be performed on a photograph taken vertically over the sediment surface. The photograph is superimposed with a grid, and the projected *b*-axis length of particles under the grid points is measured with a ruler or planimetrically (Section

4.1.3.3). The measurements are converted to the natural scale of the particles by an appropriate scale factor before a particle-size analysis is done.

Scales of photographic grid counts vary with the desired resolution of the photograph, the coverage for each photograph, and the coarseness of the bed. Each scale facilitates analyzing a certain range of particle sizes. If a broad particle-size spectrum is to be analyzed, areal photographs need to be taken at various scales.

#### ***Scale, resolution, and areal coverage of the photograph***

A photograph with a side ratio of 1:1.5 covers an area of approximately 0.5 m by 0.75 m = 0.35 m<sup>2</sup>, if taken by a standing person at a distance of about 1.3 m, when using 24 by 36 mm negatives, and a standard 50-mm camera lens. The smallest distinguishable particle size of such photographs is about 2 mm (Bunte and Poesen 1993). Coverage of larger areas is desirable on coarse gravel surfaces. This can be obtained by cameras with lenses that have wider angles (e.g., 35 mm), or by creating a larger distance between camera and the ground. A 35-mm lens leads to distortion at the edges of the photograph, but is a compromise to the otherwise greater camera height required for a larger areal coverage. With a 35-mm lens, camera height equals the natural length of the longest side of the photograph. For example, to cover areas of 0.9 by 1.4 m, 1.33 by 2 m, or of 2 by 3 m on a photograph, camera height needs to be 1.4, 2, and 3 m, respectively (Ibbeken and Schleyer 1986). The smallest distinguishable particle size for a coverage of 1.33 by 2 m is approximately 10 mm, but the resolution depends on the quality of the photograph (see discussion below). Several photographic scales may have to be used to analyze all particle sizes within a reach.

For camera heights of 1.4 m or more, the camera can be mounted either to the underside of a wide legged tripod, or the underside of a pyramid-shaped frame especially designed for this purpose. The bottom part of the pyramid is connected to a rectangular frame (ground frame) that outlines exactly the area covered by the photograph. A cm scale, preferably in black and white stripes like on a surveyor's rod, is attached or painted to the bottom part of the ground frame to serve as a scale in each photograph. Each photograph requires some form of identification. An electronic or mechanical remote control is needed to operate the camera shutter if the camera is mounted out of reach and the film is advanced with an automatic winder.

If an entire stream reach is to be photographed on a scale so that each photograph covers approximately 1 m<sup>2</sup>, consecutive photographs should not overlap, but be exactly adjacent so that particles at the edge of photos are neither excluded from the analysis nor counted twice. The correct position required for neighboring ground frames can be determined with a tape measure and small pins or flags that mark the corner positions of the ground frame.

Photography experience is essential to produce usable pictures under poor light conditions. Single-lens reflex cameras with adjustable aperture and speed tend to produce better pictures than fully automatic "point and shoot" cameras. A high speed

film (400 ASA) that facilitates a short exposure time to prevent blurring in hand-held photography is not unconditionally recommended because of its graininess. 100 or 200 ASA films are less grainy, and these films are ideal for sunny weather when short exposure times of 1/125 s can be used or for mounted cameras. Photographs should be taken around mid-day to minimize shadows around large particles in which small particles could be undetectable. Dark conditions, such as under forest canopy, require long exposure times of perhaps 1/8 of a second, and a camera stand to avoid blurring. Prints should be developed with low contrast to span a large range of gray tones or color shades, and be enlarged to about 18 by 24 cm.

### ***Grid setting***

A grid may be placed directly onto the sediment surface before the photo is taken (Kellerhals and Bray 1971), but this is not recommended because the physical grid may obscure small particles from view. A better alternative is to take a slide photograph of the sediment surface and project the slide onto a screen with grid lines. Such a “screen” can be a letter-sized or larger piece of paper with grid lines printed on it. The slide is then projected onto this screen from a close distance (Bunte and Poesen 1993). The grid line spacing should match the  $D_{max}$  particle size in the selected projection scale to avoid serial correlation and double counting (Section 4.1.1.2). If, for example, the largest particle in the projection is 2 cm, then the grid spacing should be at least 2 cm as well. A letter-sized piece of paper has about 13 by 10 = 130 grid points in a 2 cm grid.

### ***b-axes measurements on photographs***

If particles lie flat with the  $b$ -axis plane parallel to the photographic plane, the short particle axis visible on photographs is the particle  $b$ -axis. The simplest way to measure  $b$ -axis lengths of particles under grid points is with a ruler. Ruler measurements are suitable if the number of photographs to be analyzed is relatively small. If particle sizes span a narrow range only, or if measured  $b$ -axis lengths are not tallied in  $\phi$  units,  $b$ -axis lengths are measured to the nearest mm. If particle sizes are to be tallied in 0.5  $\phi$  units, ruler-measurements can be simplified if the mm equivalent of all size classes in 0.5  $\phi$  units (larger or smaller class sizes for some studies) is computed based on the scale of the photograph. Once the mm-equivalent for 0.5  $\phi$  size classes is known, ruler measurements only need to determine the 0.5  $\phi$  size class into which a  $b$ -axis length falls. Ruler measurements of  $b$ -axes on photographs correspond to sieve results from round-hole sieves and need to be converted before they can be compared to standard sieve results from square-hole sieves (Section 2.1.3.4 and 2.1.3.5).

A particle-size analysis from a photographic grid count produces a grid-by-number (i.e., frequency-by-number) particle-size distribution. Measuring the  $b$ -axes of *all* particles on the photograph constitutes an areal sample, which is a different sampling technique and results in a different particle-size distribution. Areal sampling is discussed in Section 4.1.3.3.

Errors from misreading the ruler, or from miscomputing measurements can be avoided by using an optical particle-size analyzer (Ritter and Helley 1969) to measure particle  $b$ -axes. This instrument projects an adjustable circle of light onto the photograph of a gravel surface. The size of the light spot is adjusted to match the apparent  $b$ -axis of a particle. An activated foot switch then registers the diameter of the circle in the instrument and marks the particle just analyzed. After all particles have been measured, a size distribution is computed.

Errors in  $b$ -axes measurements resulting from particles that are partially hidden from view, or when the  $b$ -axis plane is not parallel to the photographic plane can be mitigated when measuring particle  $b$ -axes planimetrically using computer digitizing equipment (Ibbeken and Schleyer 1987). This technique is described in Section 4.1.3.3.

#### ***Potential errors of photographic $b$ -axes measurements***

If all particle  $b$ -axes on the photograph are fully visible and parallel to the photographic plane, the photographic distribution is similar to the distribution obtained by physically measuring the  $b$ -axes of all surface particles of the deposit with a ruler. However, neither the photograph, nor the sedimentary structure is always ideal for photographic analysis, and the farther conditions are from ideal, the larger the deviation between photographic and physical  $b$ -axes measurements.

The particle  $b$ -axes lengths measured on a photograph and converted to their natural size using the appropriate scale factor tend to be smaller than  $b$ -axes lengths measured on the actual particles. This is due to several factors: the  $b$ -axes length may not be fully visible on the photograph when particles are embedded or partially hidden by other particles. The projected  $b$ -axis is also shorter than the natural  $b$ -axis if the particle does not lie flat ( $b$ -axis plane not parallel to photographic plane). Thus, photographic grid counts are problematic on imbricated and clustered surfaces.

The question of whether this discrepancy is dependent on particle size has been debated and probably depends on the shape and orientation of the particles on the sediment surface. Kellerhals and Bray (1971) found that the mean particle size on photographic analyses was 5 mm smaller than that obtained by sieving. This discrepancy could be corrected by adding 5 mm to all photographically determined particle sizes. A constant difference of a few mm for all particle sizes could be conceivable for a surface on which particles are bladed and lying flat.

Adams (1979) found that the discrepancy between photographic analysis and sieving with square-hole sieves becomes larger with particle size. Therefore, the correction factor to be applied for conversion of photographic  $b$ -axes and photographic percentiles into an equivalent sieve size should be a constant fraction of a  $\phi$  unit. Excluding particles finer than 8 mm from both photographic and sieve analysis, Adams (1979) suggested that  $0.1 \phi$  should be subtracted (or  $0.1 \psi$  be added) to make photographic grid counts comparable to results from square-hole sieves. For analysis in mm units, the correction factor is

multiplication of the photographic  $b$ -axes lengths by a constant factor of 1.07 (Adams 1979).

In some deposits, the  $a$ -axis is easier to identify on photographs than the particle  $b$ -axis. For such surfaces, Adams (1979) suggested computing a particle-size distribution of  $a$ -axes lengths. This distribution is then converted into an equivalent distribution that would have been obtained had the particles been sieved using square-hole sieves by adding 0.45  $\phi$  units (or subtracting 0.45  $\psi$  units) to all photographic particle-size percentiles. Such a procedure is only recommended if the axis ratio  $a/b$  is constant within and between particle-size classes.

Both manual pebble counts and small-scale photographic grid counts covering approximately 1 m<sup>2</sup> per photograph are prone to bias against fines. The resolution of the photograph may not be sufficient to identify particles as fine as 2 mm, and some of the small particles might be overlooked on the photograph because they are located in shadows between large particles. Both factors cause bias against fines and a particle-size distribution that is coarser, particularly at the fine end, than the true distribution. In order to avoid bias against invisible fines, it might be necessary to exclude particles finer than 10 or 20 mm from the analysis, depending on the scale and the quality of the photograph.

In summary, photographic grid counts facilitate non-destructive sampling of gravel- and cobble beds and substantially reduce field time. Thus, photographic grid counts are a good choice if field time must be short, although time is needed for analyzing the photographs. A disadvantage of photographic grid counts is that the lengths of the scale-adjusted  $a$ - and  $b$ -axes measured on the photograph tend to be smaller than the actual particle  $a$ - and  $b$ -axes, and that fines tend to be overlooked. This is due to non-horizontal particle orientation and shadows on the photograph. Numerical factors correcting for these discrepancies vary depending on the shape and orientation of particles on the sediment surface. Thus, photographic grid counts are best applied when particles are lying flat and are fully visible, when high-quality photographs can be obtained, and when the fine part of the particle-size distribution may be neglected in the study.

### **4.1.3 Areal sampling**

#### ***Definition, sample area, sample size and number of samples***

For areal surface samples, the operator collects *all* particles exposed on the surface within a *predefined* area, which is typically an area of about 0.1 - 1 m<sup>2</sup>. Sampling *all* surface particles without including any subsurface particles can be problematic. Not only is it conceptually difficult to determine how much hiding is tolerable for a surface particle, but it is also physically difficult to retrieve all surface particles without leaving some surface particles unsampled and without starting to sample subsurface particles. This sampling problem becomes more pronounced as the range of particle sizes increases, and as the particle packing deviates from a simple side-by-side arrangement with  $b$ -axes planes parallel to the bed surface.

A variety of methods have been proposed for particle retrieval in areal samples:

- Manual picking, lifting, and scraping,
- Adhesives (contact and penetrating), and
- Non-destructive methods (photo sieving, visual estimate, and wax imprints).

These methods are discussed in greater detail in the following sections. Some of the techniques are more suitable for fine gravel, others are better suited for coarse gravel. Sampling results from different areal sampling procedures can vary greatly. This is because gravel bed-material usually has a coarse surface layer overlying a deposit richer in fines, and each of the areal procedures collects surface particles down to a slightly different depth. Consequently, each method includes a different percentage of small particles partially hidden between large clasts.

Areal samples typically cover an area of 0.1 – 1 m<sup>2</sup> per sample. The number of particles, or the sample volume obtained from areal samples of that size, may provide sufficient material for a meaningful particle-size analysis if the bed is comprised of fine gravel, but not for a bed of coarse gravel (see Section 5.3 and 5.4 for size of an individual sample). In coarse beds, areal samples should be repeated several times within an area of homogeneous bed material until a sufficiently large amount of sediment has been collected for a statistically meaningful size analysis. Note that even if one areal sample provided sufficient material for a statistically meaningful size analysis, one sample only characterizes a reach if the bed material within the reach is spatially homogeneous. This is rarely the case. Several samples are required if the bed-material size is spatially inhomogeneous. The number of samples necessary to characterize a reach increases with the degree of spatial variability of the bed-material size and may be determined using a two-stage sampling approach (Section 5.3.2)

Areal samples may be analyzed either on a weight- or as a number-based frequency. Both particle-size distributions, area-by-weight or area-by-number, are different from weight frequencies obtained in volumetric samples (volume-by-weight) or the number frequencies obtained in pebble counts (grid-by-number). To be comparable with pebble counts or volumetric samples, particle-size distributions of areal samples need to be converted to a volume-by-weight or grid-by-number sample. Conversion is also necessary to compare areal samples obtained by different methodologies, and even to compare areal samples obtained by the same methodology (Diplas 1992a). Sample conversion is discussed in Sections 4.3.1 and 4.3.2.

#### 4.1.3.1 Manual sampling

##### ***Hand picking on coarse gravel surfaces***

Hand-picking is the method of choice for areal sampling on coarse gravel beds. The operator outlines the sampling area with a frame (e.g., lawn edging) and hand-picks all surface particles within the area (Billi and Paris 1992). The smallest particles are most difficult to assign to either the surface or the subsurface sediment, particularly when small particles are difficult to see and to retrieve in between large clasts or are partially hidden.

Although small partially hidden surface particles can only be seen and retrieved after large surface particles have been removed, generally the smallest particle should be picked first. This procedure may leave some hidden surface particles unsampled, but if large particles are removed first, it is almost impossible to determine whether remaining small particles belong to the surface or whether they lay under a large particle already removed and thus belong to the subsurface. Picking the smallest particles first and then continuing with progressively larger particles ensures that only exposed surface particles are included in the sample (D. Rosgen, pers. comm.).

Lane and Carlson (1953) suggested differentiating surface from subsurface particles by marking surface particles with spray paint. Church et al. (1987), however, note that spray paint does not unequivocally identify surface particles because the paint might run down the side of rocks and infiltrate into the subsurface sediment.

The strict distinction between surface and subsurface particles becomes even more problematic when hand-picking particles in areal samples under water because one can only feel but not see the sediment surface. A bias towards large particles ensues when only undisputed, large surface particles are picked. Scraping all surface particles in an effort not to overlook the finer particles is likely to include fine subsurface particles and may cause a bias towards fines.

#### ***Surfaces with fine gravel and sand***

Fine gravel and sand cannot be hand picked. Surface particles could be scraped, which is a rather indiscriminate procedure, or individual particles could be picked up with tweezers. A less tedious method is to coat surface particles with *magnetic paint* (spray paint with magnetite dust) and then lift all coated surface particles with a strong hand-held magnet (Wilcock and Stull 1989). Usually, adhesive methods are used for fine gravel.

#### **4.1.3.2 Adhesive sampling**

Adhesive methods may be used for areal samples of gravel surfaces that contain particle sizes between sand and coarse gravel. Adhesive methods are particularly recommended for surfaces that contain relatively large amounts of sand and fine gravel. The general procedure for areal adhesive sampling is that a board covered with an adhesive is pressed onto the gravel surface. The adhesive penetrates the sediment surface and touches all surface particles, both large and small. When the board is lifted off the surface, surface particles adhere to the adhesive. For a size analysis, sampled particles are separated from the adhesive, by dispersing or dissolving the adhesive, or by brushing and scraping particles off. Cured epoxy makes an inseparable bond with the particles and requires a thin section analysis.

A variety of substances have been used as adhesive, including all-purpose glue, epoxy resin, mud, clay, soap, grease, wax, putty and flour paste (e.g., Little and Mayer 1976; Gomez 1979; Ettema 1984; Diplas and Sutherland 1988; Diplas 1992a; Diplas and Fripp

1992; Gessler 1992; Marion and Fraccarollo 1997). The selection of an adhesive depends on several factors which include the depth of penetration required for a deposit of a given particle size and sorting, whether the sample is to be wet-sieved right at the stream site, whether the sample needs to remain undisturbed during transport, or whether it is to be analyzed by thin-section analysis. Most adhesives stick only to dry surfaces. Gomez (1983a) used a freeze technique whereby the surface particles froze to plastic wrap cooled by liquid nitrogen. This technique could be used on wet and slightly inundated river beds.

The requirement of areal samples to sample *all* surface particles, and to sample surface particles exclusively can lead to the following dilemma. Adhesives that barely penetrate the surface ensure that only surface particles are sampled, however, by not reaching the bed-surface plane, small interstitial surface particles are probably not sampled in their entirety and are underrepresented in the sample (Fig. 4.10, a, b and c). By contrast, adhesives that penetrate the surface sediment deeply ensure that all surface particles are sampled, but subsurface particles may falsely be included in the sample as well (Fig. 4.10, e), resulting in a semi-volumetric sample. Accurate areal samples require that the adhesive penetrates the surface to the appropriate depth (Fig. 4.10 d), which is the bed-surface plane. Deep penetration of the adhesive is required to reach the bed-surface plane in coarse and poorly sorted gravel beds, while less or slight penetration suffices in fine and well sorted beds.

#### ***Obtaining the right penetration depth for a given sediment***

The appropriate penetration of the adhesive to the bed-surface plane can be obtained in two ways: by selecting an adhesive with an appropriate viscosity and plasticity, and by controlling the penetration depth through the method with which the adhesive is applied. The degree of viscosity determines the flow rate of the adhesive (that may range from thin glue to stiff pottery clay). The degree of plasticity determines how well the adhesive is pliable to the surface particles (that may range from very soft grease to putty). In order to control the depth of penetration, an operator may vary the thickness of the adhesive coating, the pressure exerted when bringing adhesive and sediment into contact, and the flexibility or rigidity of the background onto which the adhesive coating is spread.

Penetration of the adhesive can be deepened by using thin or soft adhesives, and by applying thick coatings of adhesive with moderately high pressure from a flexible background. Penetration depth can be lessened by using a somewhat less pliable adhesive, and by applying thin coatings with slight pressure from a rigid background. The same adhesive applied in the same manner to bed material of different sizes and sorting coefficients leads to different sampling results.

Fig. 4.11 combines the three variables of adhesive properties, sedimentary properties, and mode of application, and suggests how adhesives of different penetration properties can be combined with application modes that result in different penetration depths in order to achieve the right penetration depth required for accurate areal samples in deposits of different particle sizes and sorting coefficients.

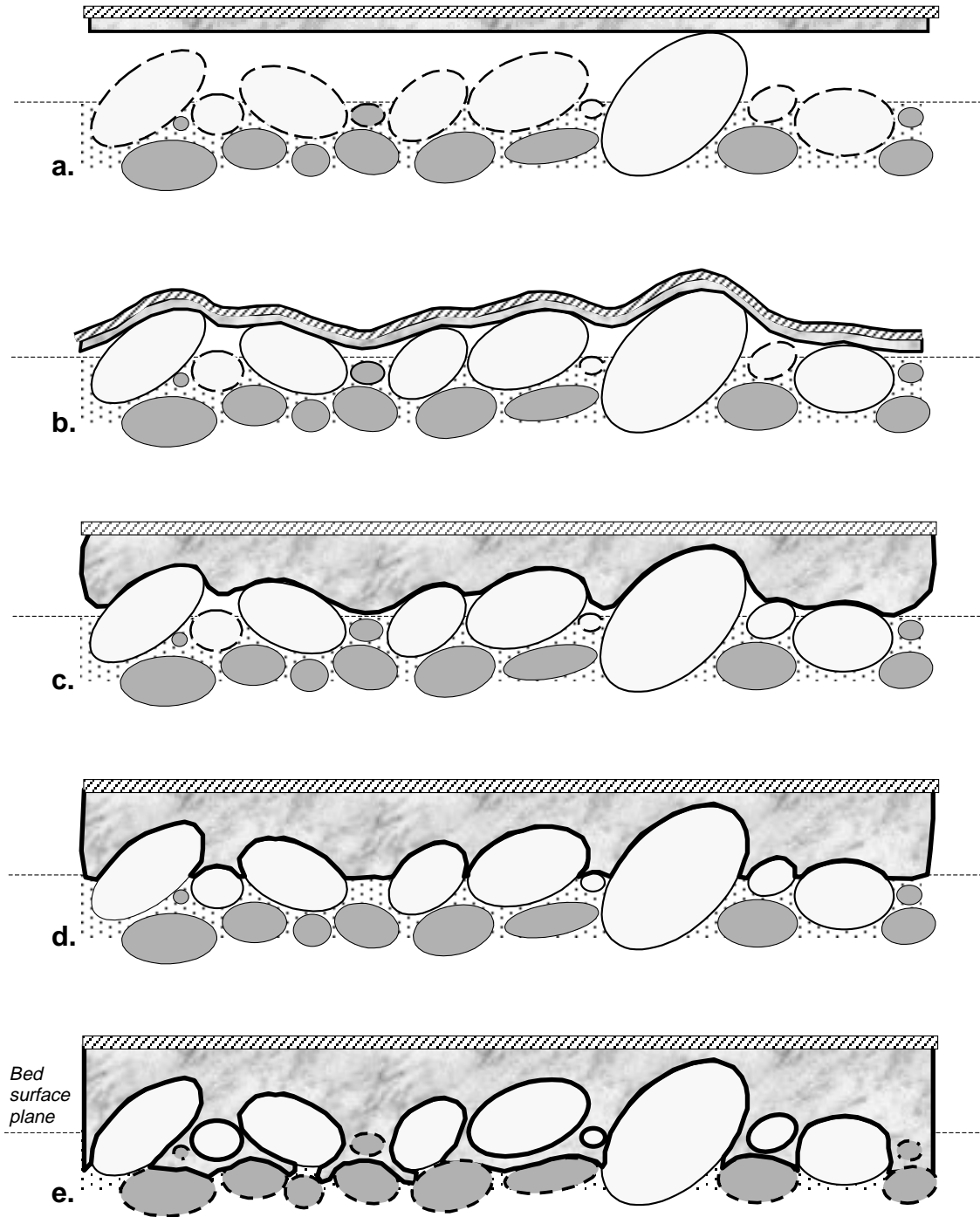


Fig. 4.10: Sampling properties of adhesives with coatings of different thickness, applied to different backgrounds, their viscosity, and different sampling properties on a poorly sorted bed that includes sand and gravel. ○ Sampled surface particles; ○ Wrongly unsampled surface particles; ● Subsurface particles; ● Wrongly sampled subsurface particles; ■ Adhesive; ▨ Backing. Insufficiently thin coating of adhesive applied to a board (a) and a textile (b); Thick coating of adhesive, but too little penetration (c); appropriate penetration (d); too much penetration (e).

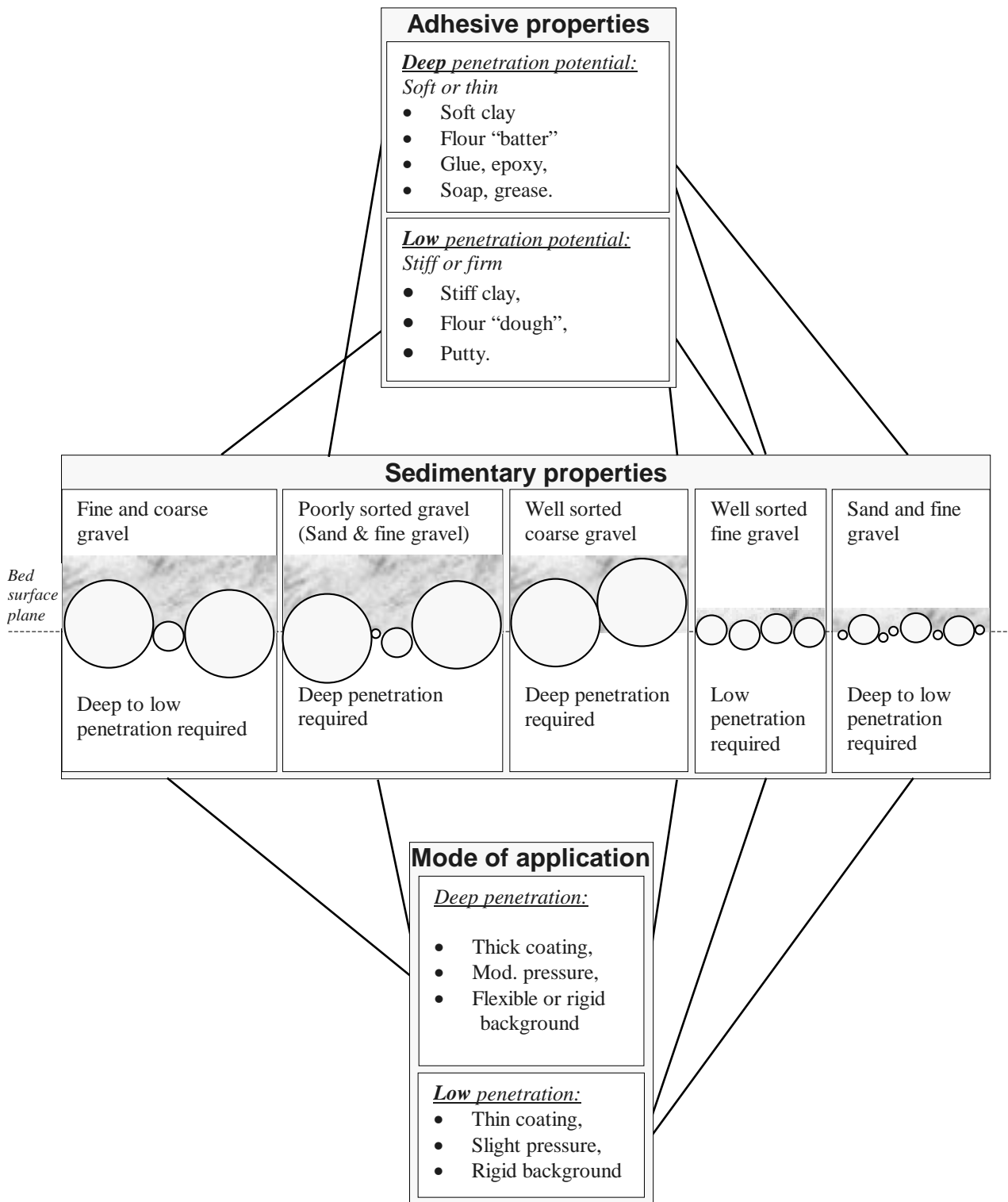


Fig. 4.11: Interrelation between adhesive properties and their potential depth of penetration, the mode of application, the resulting depth of penetration, and the sedimentary properties with their required penetration depths. Note that modifiers such as soft, stiff, deep, low, thin, and thick are relative.

### ***Testing***

The accuracy of a sampling procedure obtained from the combination of a particular adhesive and the particular mode of application should be tested before it is used for a study project. This could be accomplished by carefully coloring the surface particles with an appropriate paint. All colored particles should adhere to the adhesive, while none should remain on the streambed. The adhesive and/or the application technique should be modified until all surface particles can be accurately sampled.

A sampling error on the fine sediment end (missing surface fines or wrongly including subsurface fines) is more difficult to determine and to correct than errors that result when large particles fall off as the adhesive is lifted off the surface. When in doubt, select an adhesive and an application technique that is most suitable for sampling the fine surface particles in voids between large particles. If the sampling area contains a few disproportionately large particles or narrow voids, it might be helpful to do some preparation work. An application of adhesive material around large particles or into small voids before the adhesive is generally applied to the sample area makes small particles in voids between large particles more accessible to the adhesive.

### ***Operator variability***

Areal samples are highly prone to variability between operators, because each operator has a slightly different way of adhesive preparation, or in application technique. Thus, one operator should do all the adhesive preparation, while another operator takes all the samples. Variability between operators should be tested and minimized before multiple operators take areal samples within the same study.

### ***Separation of sampled particles from the adhesive***

Properties of the adhesives determine how sediment and adhesive are separated after the sample is taken. Adhesives may be dispersible or soluble in water, or in solvent. Adhesives may remain largely inert, harden over time, or cure. This requires different methods of separating the sampled particles from the adhesive, and different methods of particle-size analysis. An overview of these factors is presented in Table 4.4.

Soft clay, and flour batter are dispersible in water. The dispersion is discarded through a sieve with a mesh size smaller than the smallest sampled particle size. A similar procedure can be applied to water-soluble, uncured all-purpose glue and to solvent-soluble grease. If stiffer clay, and flour “dough” is used as an adhesive, sampled particles can mostly be brushed away. If a little scraping is necessary, the sample needs to be washed or wet-sieved to eliminate the clay or the flour from the sample.

The clay, or the flour dough, can be reused for another sample if a moist wrap keeps the clay or flour dough from drying. If no future use is planned for the adhesive, or if samples cannot be processed soon after the field work, the clay and flour dough adhesives can be allowed to harden. Sampled particles from hardened clay or dough are retrieved by brushing and scraping. A thin-section technique is required for particle-size analysis

Table 4.4: Adhesives and their properties, method of particle separation from the adhesive, adhesive reusability, and method of particle-size analysis

Adhesive	Adhesive Property	Method of separation	Reusability of adhesive	Method of particle-size analysis
soft clay, flour “batter”, uncured glue	sticky, runny, dispersible, water soluble	disperse or dissolve adhesive in water	not intended	wet or dry sieving
grease	sticky, solvent soluble	dissolve adhesive in solvent	none	wet or dry sieving
stiffer clay*, flour “dough”**, putty, wax	firm, inert *in moist wrap	brush and scrape off sampled particles	reusable	wet or dry sieving
stiffer clay, flour “dough”	hardens without moist wrap	brush and scrape off sampled particles	not intended	wet or dry sieving
epoxy resin, all-purpose glue	curable	visual separation only	none	thin section analysis

of areal samples obtained by epoxy resin or glue that was allowed to cure. The plane of the cut should be exactly at the bed-surface plane, otherwise surface particles are wrongly excluded, or subsurface particles are wrongly included in the analysis.

#### ***Advantages of clay and flour paste as adhesive***

Using clay (Diplas and Fripp 1992) or flour paste (Gessler 1992) as adhesive has several advantages besides being affordable, generally available, and non-toxic for the operator. Flour dough or batter can be mixed with water to obtain a desired degree of viscosity and plasticity. The mixing result is basically reproducible (write down exact proportions of wet and dry ingredients, and manufacturer), although the consistency may vary slightly with air humidity. Since flour dough or batter can be prepared in the field, it can be prepared to the appropriate consistency for a given deposit. Mixing clay from powder, or changing the moisture content of moist clay in order to change its viscosity and plasticity takes more time, so ready-to-use clay of different consistencies should be brought to the field site. The possibility of mixing flour dough or batter to the right consistency, or using clay of just the right consistency for a given deposit provides a good chance of producing accurate and unbiased sampling results.

Clay and flour paste are two of the few substances that adhere to wet surfaces. Clay can be used for under water sampling. For multiple use, the clay surface needs to be well scraped between samples to provide a fresh surface for the next sample. Clay and flour paste provide two options for separating the sampled particles from the adhesive. The adhesive matrix can be dissolved and the sampled particles wet-sieved, or particles can be mechanically brushed off the clay surface and collected (see above). Both methods can

be performed at the field site. Dispersion has the advantage that no clay or flour batter needs to be hauled back to the lab. However, dispersed clay or flour should not be discarded into a stream as it may clog interstitial spaces and impair streambed habitat. Brushing particles from the clay or dough slab and reconstituting the adhesive surface for a new sample saves material and has the advantage that only the material for a few samples needs to be carried to the stream site. Clay or flour dough that is kept in a moist wrap can be reused for sampling at a later time. To delay or prevent flour dough from getting moldy with time, substitute water with vinegar, or freeze the dough.

#### 4.1.3.3 Photographic areal sampling

For photographic areal sampling, a photograph is taken of a sediment surface and the size of *all* particles visible on the photograph is measured, either with a ruler or planimetrically (Section 4.1.2.2). Like manual or adhesive samples, particle-size distributions obtained from photographic areal samples need to be converted before comparison with other samples (Sections 4.3.1 and 4.3.2). Photographic techniques for analyzing particle sizes off photographs are described in Section 4.1.2.2. Three different methods of particle-size analysis can be used for photographic areal sampling:

- Measuring the *b*-axes of all particles,
- Planimetric particle-size measurements and analysis (photo sieving), and
- Empirical relation between the number of particles per photograph and a pebble count  $D_{50}$  size.

#### ***Measuring *b*-axes of all particles on the photograph***

The techniques of *b*-axes measurements with a ruler or an optical particle-size analyzer are discussed in Section 4.1.2.2. However, in contrast to grid samples that measure the *b*-axes of particles under grid points only, *areal* samples measure the *b*-axes of *all* particles visible on the photograph. Measuring all particle *b*-axes provides an *area-by-number* distribution, i.e., the number-frequency of *all* particles contained within the sample area, and this distribution is different from the grid-by-number distribution obtained from photographic grid counts (Section 4.1.2.2). See Section 4.3 for conversion of distributions obtained by different methods of sampling and analysis.

#### ***Planimetric particle-size measurements and analysis: Photo sieving***

*b*-axes measurements on photographs with a ruler or an optical particle-size analyzer become relatively inaccurate if particle *b*-axes are partially hidden from view or not parallel to the photographic plane (Section 4.1.2.2). Ibbeken and Schleyer (1986) largely overcame this problem by developing a photographic particle-size analysis that attempts to restore the third dimension of the particle lost in the projection from actual particle to its photographic image. Particle shapes are assumed to be generally ellipsoidal for this technique, and the best-fit ellipsoidal body is fitted into the outline of the particle shape on the digitized photograph. This procedure improves the size determination of particles partially hidden from view or with particle *b*-axes not parallel to the photographic plane.

Computed particle volumes are converted to weight. Since this photographic procedure produces a particle-size analysis in terms of frequency-by-weight similar to a sieving result, it is called photo sieving.

Photo sieving was developed for analyzing the areal surface particle-size distribution of open framework gravel with empty voids between large particles. Ibbeken and Schleyer (1986) used low contrast prints 18 by 24 cm, obtained from 24- by 36-mm negatives taken with a 35-mm camera lens from 2 m above ground. Each photograph covered an area 1.33 by 2 m, and was large enough to identify particles as small as 10 mm.

A flow chart shows the various steps involved in photo sieving (Fig. 4.12). The first step in approximating particle volume is to outline the perimeter of each particle on the photograph using a digitizer connected to a computer. A computer program fits the longest possible axis  $L$  into the outlined particle area on the photograph and computes the subaxes  $S_1$  and  $S_2$  that extend at right angles from both sides of  $L$ , so that the short axis on the photographed particle is  $S = S_1$  and  $S_2$  (Fig. 4.13). An ellipsoidal shape is assumed for all particles. The true particle  $b$ - and  $c$ -axes are not known, so the projected  $S$ -axis is squared.  $S^2$  is close to the product of  $b \cdot c$ , because  $S$  is likely to be smaller than the particle  $b$ -axis, but larger than the  $c$ -axis. Particle mass  $m_p$  is computed from

$$m_p = V_p \cdot \rho_s = \frac{\pi}{6} L \cdot S^2 \cdot \rho_s \quad (4.1)$$

where  $V_p$  is the particle volume, and  $\rho_s$  is the particle density.

Ibbeken and Schleyer (1986) used samples from various gravel surfaces to compare photo-sieving results to results obtained from mechanical sieving with square-hole sieves. All surface particles  $> 20$  mm were painted or numbered in situ before a photograph was taken. All painted or numbered particles were picked off the surface before the photo was taken and sieved with a square-hole sieve set. For particles that were fully visible and had compact shapes in the Sneed and Folk form-sphericity diagram (Fig. 2.23, Section 2.2), photo sieving correctly predicted the true particle weight. Photo sieving tended to overpredict the true particle weight when particles were platy and bladed, and underpredicted the true particle weight of particles that were partially hidden on the photograph (Ibbeken and Schleyer 1986). Particles that were allotted to different size classes by photo sieving and mechanical sieving did not have different particle shapes, thus particle shape has no effect on the assigned grain-size class. Consequently, overprediction of the particle frequency of a specific size class is attributed to the effects of particle position (i.e., the angle from which a particle is seen on a photograph). Particle hiding causes an underprediction of the frequency of particle sizes in that size class. However, when analyzing an entire photograph, many of these errors cancel each other.

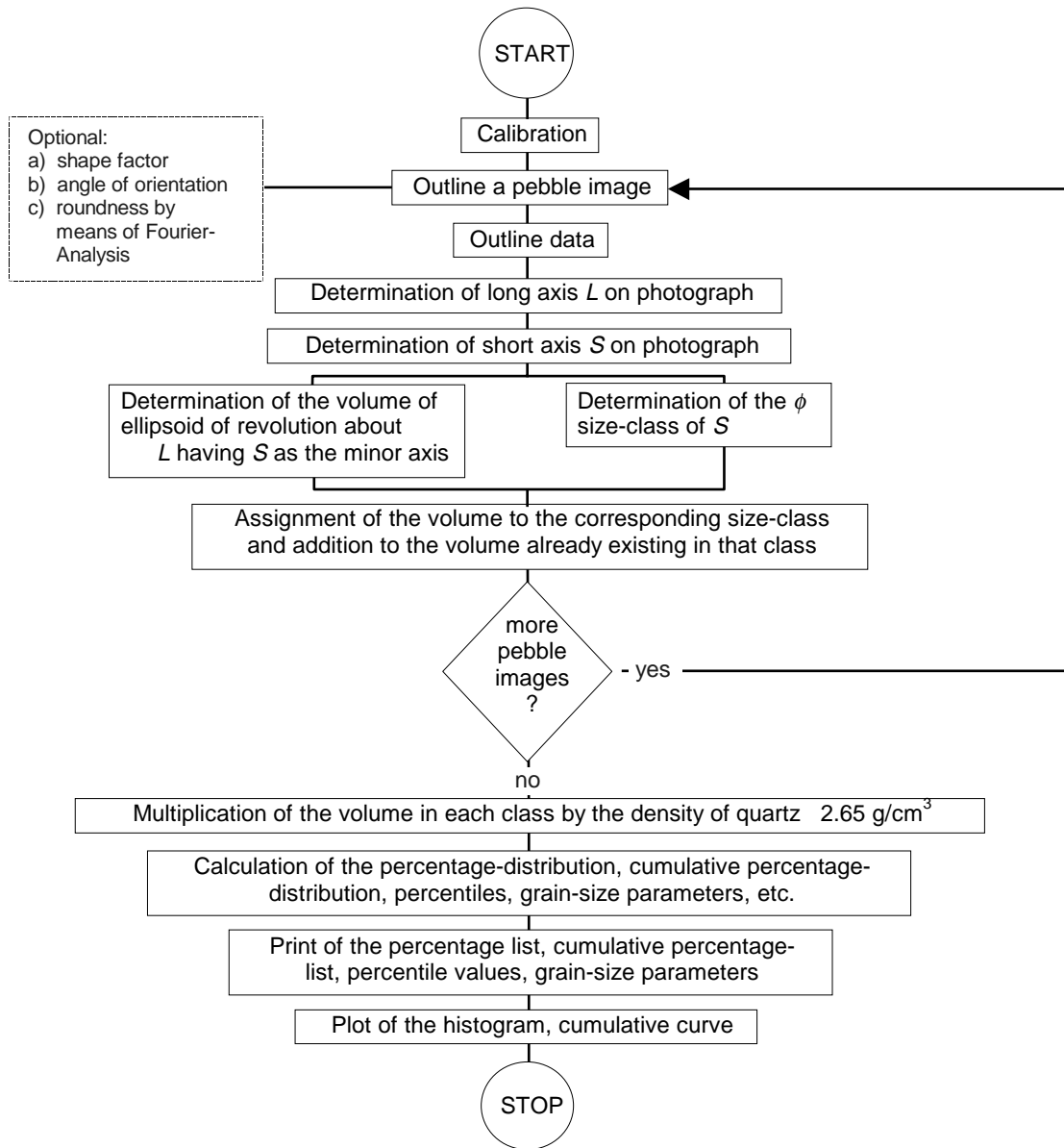


Fig. 4.12: Flow chart for photo sieving analysis. (Redrawn from Ibbeken and Schleyer (1986), by permission of John Wiley and Son. Ltd.).



Fig. 4.13: Axes  $L$ ,  $S_1$  and  $S_2$  fitted by computer into the outlined and digitized particle shape (a); Computer-fitted ellipsoidal reference particle shape for computation of particle volume (b). (Redrawn from Ibbeken and Schleyer (1986), by permission of John Wiley and Sons, Ltd.).

A comparison between percentile particle sizes obtained from photo sieving and mechanical sieving showed a good correlation between the two sieving methods but did have a systematic bias. Percentile particle sizes obtained from photo sieving were about 0.1  $\phi$  units coarser than percentile particle sizes obtained from mechanical sieving (only visible particles larger than 20 mm were included in this analysis).

Over- and underprediction of particle weight or frequency per size class can be mitigated in two ways. Particle shape, position, and degree of hiding can be measured in the field and this information may then be incorporated into the algorithm that computes particle volume. Another approach is to develop an empirical factor from a regression function that relates the percentile particle size of both sampling methods to each other. This factor can then be used to fine-tune the correspondence between true particle weight and the weight predicted from photo sieving.

As photo sieving outlines the particle shape and computes particle axes lengths, the procedure can also be used to analyze particle-shape parameters such as roundness, and sphericity. Photo sieving is also suitable to analyze bed-surface structures such as clusters, as well as particle orientation within a rose diagram (Diepenbroek and De Jong 1994). Photo sieving is not well suited for fine sediment (sand and fine gravel) (Harvey 1987), unless photographs are taken from a close distance.

Photographs usable for photo sieving can be obtained from gravel beds deeply submerged by water if an underwater camera is used (Ibbeken and Schleyer 1986). However, photo sieving is not suitable for wadable streams, because taking a usable picture through the water surface is difficult due to reflections on the water surface. A glass-bottom box may be used when the water is deeper than 0.6 m and allows the investigator to photograph an area of about 0.1 m<sup>2</sup> with a camera having a 50-mm lens.

Compared to field sampling and sieving, photo sieving reduces field time substantially and is suitable for beds containing medium gravel, cobbles, and boulders. The effective use of field time in photo sieving allows the study to sample a large number of field sites, and the decision on sampling location and sample size can be made by an experienced person. However, a digitizer is needed for the planimetric analysis of particle shape, and special programs need to be written. Once the system is set up, digitizing the photographs is the only time consuming part of the analysis (approximately 1 hour per photograph covering 1.33 m by 2 m). Fully automated and correct particle recognition is conceivable as the techniques required for improved particle boundary identification (gray scale thresholding, edge growing and particle segmentation) are being developed (Butler et al. 2000).

#### ***Counting the number of particles per photograph and conversion to pebble count $D_{50}$***

A simple and fast, but relatively crude way of obtaining information on the bed-material particle size from a photograph is to count the number of particles contained on the photograph. The larger the number of particles (that exceed a preset threshold size) that can be counted, the smaller the particle size of the photographed deposit. For a

quantitative analysis, the number of particles on the photograph needs to be calibrated against some field determined particle-size parameter that characterizes the average surface particle size, such as a pebble count  $D_{50}$ . The calibration function is then used to predict the  $D_{50}$  particle size from the number of particles countable on the photograph.

The counting method avoids any complications posed to photographic particle-size analysis by irregular particle shapes, particle position, and partial burial. Rice (1995) applied this method when analyzing downstream change in particle size over long stream distances. For small streams in the Pacific Northwest, the best fit relationship ( $r^2 = 0.99$ ) between the pebble count  $D_{50}$  of particles in the range of 20 - 200 mm and the number of particles  $n_{ph}$  contained within a photographed area of  $0.25 \text{ m}^2$  was obtained by a logarithmic function:

$$D_{50} = 396 - 62 \ln (n_{ph}), \quad (4.2)$$

The parameters of the function vary with particle embeddedness and particle shape which need to be the same for all photographs. The scatter of the data decreases as particle shape and degree of hiding become more uniform. As many as 30 analyzed photographs may be needed to define the calibration function. Therefore, the counting approach only becomes economical if the study involves a large number of field sites. Results of this photographic analysis are, in principle, comparable to results of pebble counts, because the photographic analysis is calibrated against pebble counts.

#### 4.1.3.4 Photographic (areal) analyses in other scales

Intermediate scales of about  $1 \text{ m}^2$  bed-area per print are not the only scale used for photographic analyses. Close-up photographs covering about  $0.1 \text{ m}^2$  can be used to analyze detailed sedimentary structures, such as particle packing or the vertical structure of bed material in a photograph of the sediment face. By contrast, areal overviews cover about  $100 \text{ m}^2$  and may be useful for analyzing bed-surface structures as well as for streambed monitoring.

#### ***Photographic analysis of vertical sediment structure***

Fraccarollo and Marion (1993) used photographic areal sampling techniques to analyze the vertical structure of the sediment, such as vertical armor development and infiltration of fines. A container deeper than the armor layer was placed into the bed of a flume and filled with the same material as the bed. It was assumed that the sedimentary structures that develop during a flow event (armoring or infiltration of fines) are the same inside as well as outside the container. After the armor layer development has started, the flow is stopped. The container is retrieved, frozen, and the sediment block is vertically broken in half. The plane of rupture is photographed for a qualitative or quantitative analysis before the two halves are reassembled, and placed back into the original channel-bed location. After the sediment is thawed, the flume experiment can continue. The

container is again retrieved for sediment analysis after the armor layer development or the infiltration has progressed further. In this way it is possible to obtain information on the vertical sediment structure during various phases of the armor development during a single flume experiment.

### ***Reach-spanning areal overview***

An areal overview of a river reach can be obtained if an auto focus camera with a 32-mm lens is elevated 10 – 15 m above the riverbed surface using a crane, or a helium-filled balloon (Fig. 4.14), (Ergenzinger et al. 1999; Kozłowski and Ergenzinger 1999). The



Fig. 4.14: Areal view of a step-pool reach at the Schmedlaine, Bavaria (FRG) taken with a 35-mm camera mounted to a tethered helium balloon. Balloon height is about 15 m. Length of surveyor's rod is 3 m. Flow direction is from upper left to lower right. (Photograph courtesy of B. Kozłowski and P. Ergenzinger, Dept. of Physical Geography, Free University of Berlin, Germany).

area covered by one photograph in the format of 1:1.5 is 110 - 160 m<sup>2</sup> (about 9 by 12 m to 11 by 15 m). The smallest particles distinguishable on such photographs are cobbles of about 100 mm in diameter. Besides an analysis of cobble and boulder particle sizes, and of bed surface structures, areal views provide a good opportunity to monitor change within a river reach. This can be a change in the bank line, change in patterns of scour and fill, the displacement of individually marked large particles, or change in the size of the area covered by gravel-sized and finer particles. Church et al. (1998) used elevations of about 30 m to analyze bed surface structures such as stone cells. Their photographs had a resolution of about 150 mm.

Areal overviews should be taken with ample lateral overlap to account for lateral distortion, as well as for the fact that the exact position of the photographed area cannot be determined before the photograph is taken. Unfortunately, particles submerged by flow are poorly or not at all visible, unless the water depth is very shallow, or light conditions are ideal. Thus, areal view photographs are restricted to analyses of the dry portions of the streambed.

#### ***Summary and evaluation of photographic methods***

- Photographic methods facilitate non-destructive sampling of the bed.
- Photographic methods minimize field time.
- Photographic methods can be conducted at any spatial scale by changing the camera height. Close-up photographs are used to evaluate small sedimentary structures (particle packing and orientation), while photographs covering about 1 m<sup>2</sup> in size are used for bed-material particle-size analysis. Areal overviews that cover an entire reach are used to analyze large bed-surface structures or to monitor streambed change (4.1.3.4). This makes photographic methods a versatile tool for analysis of bed-material structures, documentation, monitoring, and historical records.
- Photographic methods can be applied to obtain information on surface particle sizes in the form of grid counts (Section 4.1.2.2), as areal samples (Section 4.1.3.3) and as a relation between the number of particles on the photograph and a pebble count  $D_{50}$ .
- Photographic analysis through the water surface is usually impossible, but underwater photography can be used when the water depth exceeds about 2 m.
- Photographic analysis often requires field calibration. Photographic measurements of particle  $b$ -axes tend to underestimate ruler-measured  $b$ -axes in the field because partially buried or hidden particle axes cannot be measured in their full length on photographs.
- The photo-sieving method (Ibbeken and Schleyer 1986) improves the accuracy of photographic particle-size measurements in deposits with partially hidden particles and when the  $b$ -axis plane is not parallel to the photographic plane.
- Photo sieving tends to overpredict the weight of angular, platy and bladed particles, and to underpredict the weight of partially hidden particles. Both errors tend to cancel each other when analyzing large streambed areas.

#### **4.1.3.5 Visual particle-size estimates**

The fastest way to assess the local particle-size distribution is a visual particle-size estimate. Several different techniques have been used for visual estimates.

### ***Percentage of surface area covered by particles of various size classes***

Fisheries studies often estimate the percent area covered by particles of various size classes. The size classes used for this analysis are usually larger than the 0.5  $\phi$ -size classes. Platts et al. (1983), for example, differentiated between larger boulders (> 610 mm), small boulders (> 305 mm), cobbles (> 76 mm), gravel (> 4.8 mm), large fines (> 0.83 mm), and small fines (< 0.83 mm). A dominant size class was assigned to each 1-foot section along a transect by visually estimating the particle-size class that covers the largest proportion within that one-foot long section. The estimation process is aided by visually arranging the particles of different size classes within the 1-foot section into strips and estimating the strip length for each size class. The dominant size classes along the transects are summed and expressed as percentages of the stream width.

Visual particle-size estimates require operator training and skill, and untrained operators can easily introduce a bias. Trained operators can be quite proficient and accurate (Shirazi and Seim 1981) in estimating bed-material sizes, particularly for bed material within the gravel range (Platts et al. 1983). By contrast, Kondolf and Li (1992) found that visual estimates as described above tend to overemphasize the frequency of fine gravel if the deposit consists mainly of fine gravel. Similarly, visual estimates overemphasize the frequency of coarse particles in deposits that consist mainly of coarse gravel. Thus, visual estimates described above seem to have their best use for reconnaissance sampling, such as when walking the stream to become familiar with the stream site, or for a delineation of streambed areas with similar bed-material size (patches) that are subsequently sampled by more stringent methods. Visual estimates are probably not the right tool for monitoring bed-material size, as that requires detecting small changes in particle size over time or space.

### ***Estimate of particle percentile size***

Visual estimates are also used for delineating areas of homogeneous particle sizes (patches or facies) when using a spatially segregated sampling scheme (Lisle and Madej 1992; Lisle and Hilton 1998, pers. comm.) (Section 6.3.2.1). For this purpose, particle sizes of one (e.g.,  $D_{75}$ ) or two percentiles (e.g.,  $D_{50}$  and  $D_{90}$ ) are visually estimated and facies types are differentiated based on the particle percentile size.

### ***Estimate of percentage of three main particle-size classes with further specification of the major size class***

Buffington and Montgomery (1999a) devised a two-level visual particle-size classification that refers to both the mean particle size and the sorting when distinguishing between different facies. The method is statistically meaningful in that deposits with statistically similar pebble counts were also visually identified as the same facies, whereas deposits with statistically different pebble counts also had different visually identified facies.

Level 1 of the visual classification procedure estimates the relative abundance of the three main constituents of a particle-size distribution. A gravel bed, for example, may be

comprised of the three major constituents of sand, gravel, and cobbles. Their percentages may be 10% sand, 60% gravel, 30% cobble. This composition classifies the facies as sandy, **cobbly Gravel**, abbreviated as **scG**. Gravel is the primary constituent, cobbles the secondary, and sand the tertiary. Similarly, a bed comprising 50% **Gravel**, 30% **cobble** and 20% **boulders** is a **bouldery, cobbly Gravel** facies, abbreviated to **bcG**.

The appropriate facies terminology can also be derived by plotting the frequency of the three major constituents in a triaxial diagram, or ternary. The appropriate facies terminology is obtained from the name of the field onto which data are plotted. Fig. 4.15 (top) is an example of a triaxial diagram for deposits that have sand, gravel, and cobbles as their major constituents. For facies with other major constituents, the user must rename the corner points. Copies of the spare template in Fig. 4.15 (center), or commercially available triaxial graph paper can be used for this purpose. Plotting is not necessarily required for determining the appropriate terminology of a deposit, but is recommended to aid in the grouping process. The fields outlined in Fig. 4.15 are somewhat arbitrary, and can be changed if sediment from a facies delineated in the stream plots in a cluster and falls onto the border of two neighboring facies types on the triaxial diagram. The circled group of data points in Fig. 4.15 (top), for example, plots on the border of a **gsC** and a **sgC** facies. A more appropriate characterization for this cobble facies might be a relative abundance of more than 50% cobbles, less than 30% gravel, and 15-30% sand.

A Level 2 classification further distinguishes the subsample of the major constituent that had been described in broad terms only in the Level 1 classification. For example, the composition of the cobble size in a cobble facies can be specified according to the percent frequency of very coarse (180 - 256 mm), coarse (128 - 180 mm), and medium (90 - 128 mm) cobbles. If the visual estimate determined 25% very coarse, 12% coarse, and 62% medium sized cobbles, the cobble portion of that deposit classifies as coarse, very coarse, **medium cobbles**, abbreviated as  $C_{cvcem}$  (Fig. 4.15, bottom). Similarly, for a Level 2 classification of relatively fine gravel, the corner points of a triaxial diagram need to be termed very fine, fine, and medium. The unlabeled diagram can be used for this purpose.

Although not specified by the authors, the Level 2 classification could probably be applied not only to the major constituent, but to the secondary, or tertiary constituent instead, if those particle sizes were of most concern for the study.

Buffington and Montgomery (1999a) found that an increase in the number of fields per triangular diagram did not significantly improve the accuracy of the visual method. Adding the Level 2 analysis to the Level 1 analysis, however, greatly improved the ability of the visual analysis to identify statistically similar particle-size distributions.

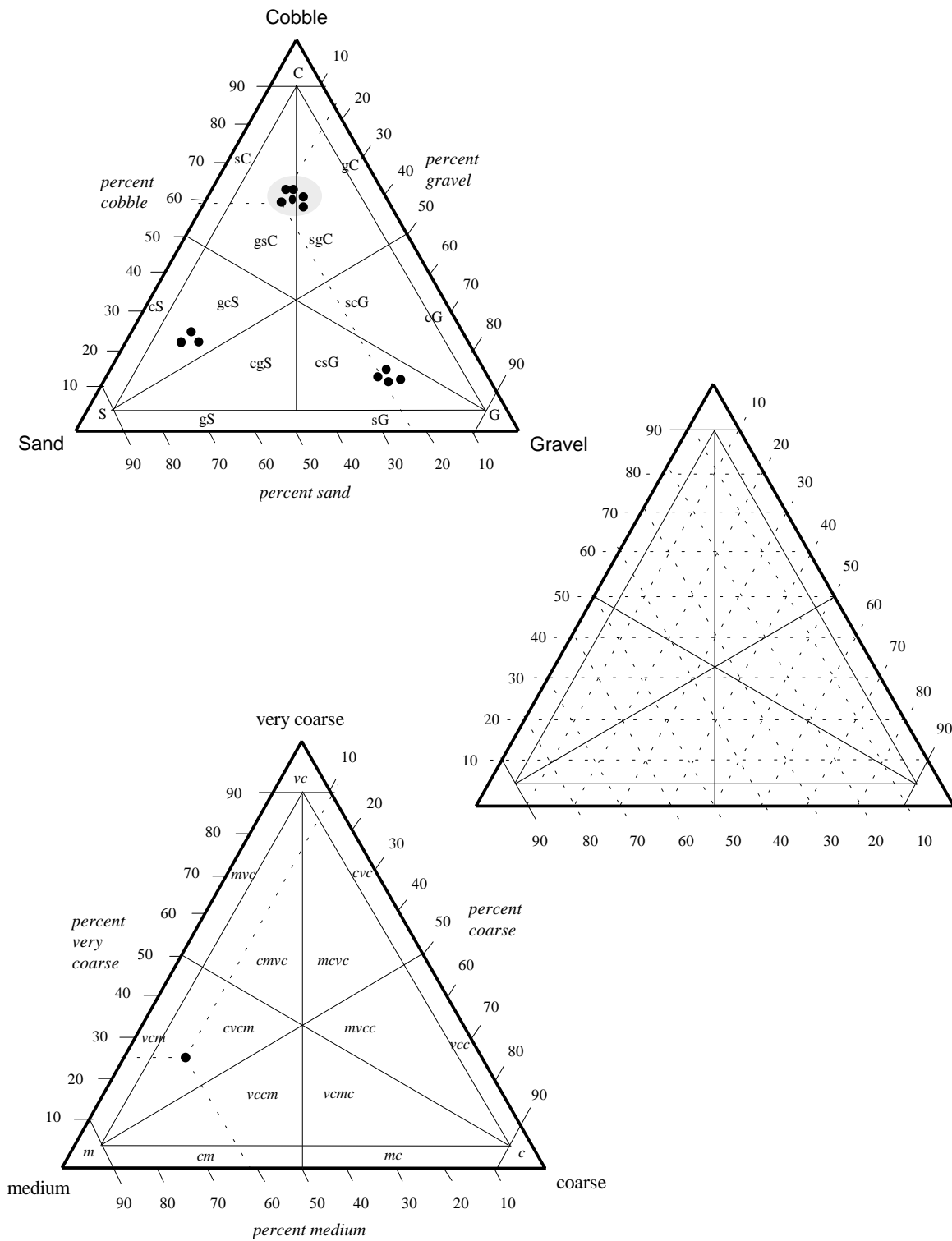


Fig. 4.15: Example triangular diagram for Level 1 classification: visually estimated percent frequency of the major three constituents of a deposit (top); Triangular diagram for user-specified use (center); Example triangular diagram for Level 2 classification: visually estimated percent frequency of the three major size breaks within a size class (bottom). (Slightly modified from Buffington and Montgomery (1999a), by permission of the American Geophysical Union).

## 4.2 Volumetric sampling

Volumetric samples extract a *predefined volume, or mass* of sediment from the bed. Volumetric samples are three-dimensional and may be taken from various strata of the sediment column: the armor layer, the subarmor and subsurface sediment, and the unstratified bulk sediment (Fig. 4.1). The surface sediment, which has two-dimensional properties, cannot be sampled volumetrically.

### 4.2.1 Armor layer

#### 4.2.1.1 Definition and description

Several mechanisms have been proposed to explain the cause of surface coarsening and the development of an armor layer (Fig. 4.1). These include winnowing of surface fines, selective deposition of large particles, and increased availability of coarse surface particles as part of equal mobility transport (Section 3.3.1.2). A difference between the particle-size distribution of surface and subsurface layer can also be caused by an infiltration of fines into an open framework subsurface sediment (Section 3.3.1.1). Armor layers are poorly developed in streams with high sediment supply or in well sorted sediment.

Samples of the armor layer are used to characterize the streambed for many purposes including streambed monitoring and sediment transport analysis. The degree of armoring can be determined by comparing the particle-size distribution or the  $D_{50}$  of the armor layer with the  $D_{50}$  particle size of the subarmor sediment. The larger the ratio, the larger the degree of armoring. A change in the degree of armoring is used as an indication of a change in sediment supply or in flow regime.

The armor layer is three-dimensional and can only be sampled volumetrically. By contrast, an areal surface sample is two-dimensional. It collects only surface particles (Section 4.1.3), and cannot be used to describe the armor layer. In the presence of a coarse armor layer, volumetric armor-layer samples and areal surface samples describe different particle populations, and thus have different particle-size distributions. The particle-size distributions of volumetric armor-layer samples and areal surface-samples are even different in non-stratified deposits, and both distributions cannot be compared without prior application of an appropriate conversion factor (Section 4.3.1 and 4.3.2).

#### 4.2.1.2 Thickness and sampling depth of the armor layer

The thickness of the armor layer is commonly described as extending from the bed-surface plane down to the bottom side of the largest ( $D_{max}$ ) or a frequently occurring large surface particle size ( $D_{dom}$ ) (Fig. 4.1). A sample of the armor layer should extend over the entire thickness of the armor layer. If the sample is not sufficiently deep, it misses the fine particles under the coarse surface particles and produces a size distribution that is too coarse. An armor-layer sample that extends too deeply into the bed includes subsurface sediment which is finer than the armor layer and thus produces a sample that is too fine.

In order to sample the strata accurately, the thickness of the armor and subarmor layer needs to be known. One possible way to obtain this information is to dig a pilot pit and examine the vertical extent of the respective strata. This approach is a labor and time intensive undertaking and is impeded by the fact that the thickness of sedimentary layers is spatially variable, which would require multiple pits. In order to avoid this procedure (which should not be completely dismissed), and considering the fact that the thickness of the armor- and subarmor-layer increases with the general coarseness of the surface sediment, several suggestions have been proposed to predict the thickness of the armor layer. All procedures are based on some characteristic of large surface particles. Armor thickness is approximated by:

- the  $c$ -axis of the  $D_{max}$  particle of the surface (Ettema 1984),
- the  $b$ -axis of the  $D_{max}$  particle size (Diplas 1992 a);
- 2 times the  $b$ -axis of the  $D_{90}$  surface particle size (Simons and Sentürk 1992, p.654),
- the embedded depth of the reach-average  $D_{dom}$  particle size (Winema National Forest (1998), and
- the embedded depth of the local  $D_{max}$  particle size.

The five prediction criteria listed above result in different armor-layer depths when applied to the same deposit. This is demonstrated in Fig. 4.16. Assume a deposit from a coarse gravel or cobble-bed stream with a  $D_{max}$  particle size of 200 mm, and a  $D_{dom}$  of 150 mm which is about equal to the  $D_{90}$  particle size. All particles are ellipsoidal in shape. The  $a$ -axis of embedded particles is inclined by an angle of  $45^\circ$  and particles are embedded with approximately 80% of their volume.

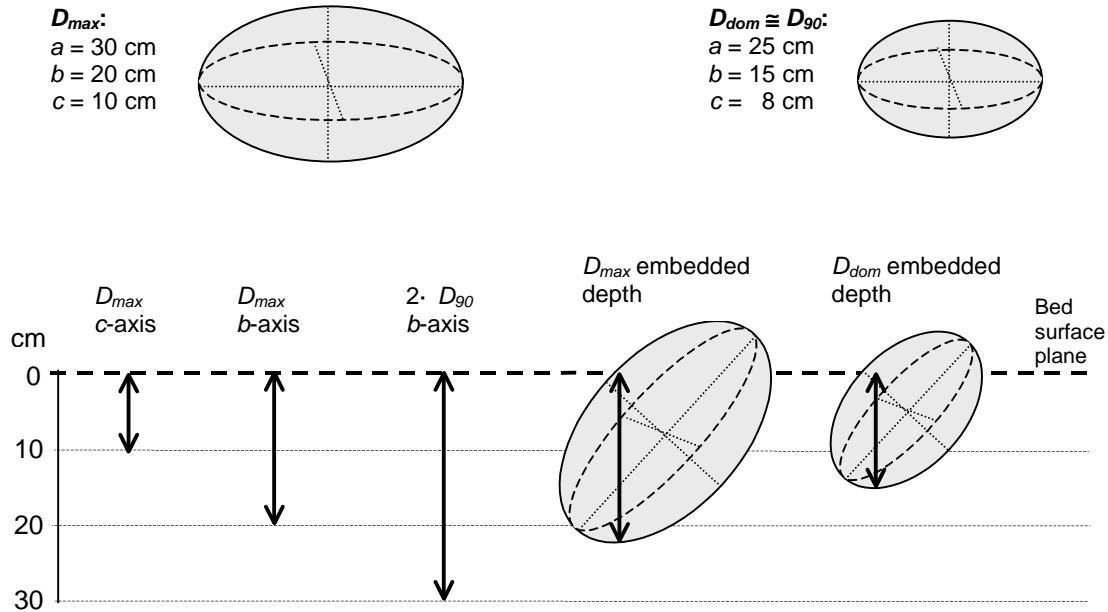


Fig. 4.16: Differences in armor-layer thickness determined for the same deposit using various prediction criteria.

The embedded depth  $D_e$  is the vertical depth to which the bottom side of a large particle ( $D_{max}$  or  $D_{dom}$ ) extends downward into the channel bed (Figs. 3.21a and 4.17). Its exact extent depends on particle position and shape. A particle in a near horizontal position typical of disc-shaped particles does not extend deeply into the bed, and in this case, embedded depth is equivalent to the  $c$ -axis of a large particle and determines a relatively thin armor-layer sampling depth. By contrast, a particle in a vertical position extends deeply into the bed, particularly if the particle has an elongated shape. In this case, the embedded depth and the predicted armor layer thickness is equal to the particle  $a$ -axis.

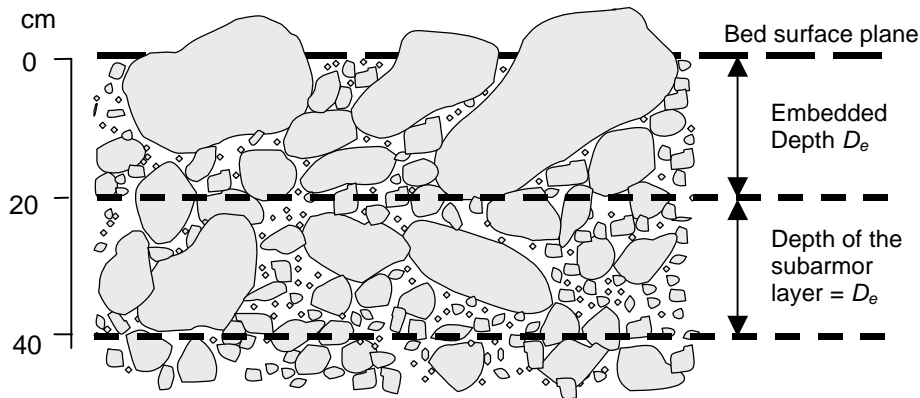


Fig. 4.17: Sampling depth of armor layer and subarmor layer adjusted to the embedded depth of a large particle ( $D_{max}$  or  $D_{dom}$ ). (Figure courtesy of Winema National Forest, Klamath Falls, OR; slightly altered).

Specific stream situations and study objectives might require case-specific criteria for determining the armor-layer sampling depth. The embedded depth of the  $D_{max}$  particle is only representative of the armor layer thickness, if the  $D_{max}$  particle is involved in fluvial transport (in large but relative frequent floods). In this case, the armor layer depth may be determined based on the  $D_{max}$  particle size within the sampling area.

If  $D_{max}$  particles are too large to be involved in fluvial transport, the armor-layer depth should be predicted from large particles more representative of the reach and the bedload transporting flow regime. A possibility is the mean dominant large particle size  $D_{dom}$  which is a reach-averaged measure of large particle sizes and determined as the mean  $b$ - or  $c$ -axis measured on about 30 large, but not the largest, particles.  $D_{dom}$  could also be substituted by a large particle-size percentile, e.g., the  $D_{90}$ .

The criterion of 2 times the  $D_{90}$  particle size  $b$ -axis length also predicts a relatively thick armor layer. Sampling the armor layer to a large depth risks including subarmor sediment in the armor sample. Mixing armor and subarmor sediment should be avoided when comparing the sediment size of the two strata because contamination makes a difference between the armor and subarmor layer less detectable. The mean  $b$ -axis size of  $D_{dom}$  within the sedimentary unit of concern, or the  $D_{dom}$  embedded depth, seems to be

an appropriate criterion for determining the sampling depth if armor- and subarmor layers are to be compared. Some large particles may reach farther into the bed than the embedded depth of  $D_{dom}$ . These particles should be included in the armor layer sample.

If the study objective is to characterize the armor layer within a sedimentary unit (facies), all samples within that unit should be collected to the same depth, since an equal sampling depth allows one to combine or compare individual armor-layer samples. For a comparison of armor-layer samples between sedimentary units, or to determine the area-weighted average armor-particle size for a larger reach, armor layers should be sampled to the depth appropriate for each of the sedimentary units within the reach. This discussion shows that the sampling depth for the armor layer cannot be easily expressed by a general equation. A reasonable armor-layer sampling depth must be determined for each study objective and should be identified in the field. This is best accomplished with a pit dug in a dry bed.

***Surface coarsening: ratio of pebble count  $D_{50}$  to the  $D_{50}$  of a volumetric subsurface or subarmor sample***

An armor-layer sample may not be required to determine the degree of armoring. The degree of armoring may be quantified by collecting a surface pebble count and a volumetric subsurface sample instead. Taking a surface pebble count instead of a volumetric armor layer sample for this analysis has several advantages. A pebble count circumvents the problems of defining and sampling the appropriate armor-layer depth. Besides, the size distribution of the armor layer and the bed surface are directly related. Another advantage is the spatial flexibility. A pebble count can be laid out to span a few m<sup>2</sup> or hundreds of m<sup>2</sup>. A volumetric armor-layer sample covers a small area only and requires taking multiple samples to cover the reach. Collecting numerous volumetric samples with a sufficiently large total sample mass and the ensuing sieve analysis makes armor-layer sampling considerably more labor and time intensive than pebble counts. A caveat of this substitution is that the assumed equality between the size distribution of a pebble count and a volumetric sample may not be warranted in every situation.

## **4.2.2 Subsurface, subarmor, and unstratified bed material**

### **4.2.2.1 Definition and description**

Subsurface sediment is the sediment under the streambed surface, and subarmor is the sediment under the armor layer (Fig. 4.1). Subsurface and subarmor sediments are usually finer than surface or armor sediments, respectively, unless the stream is aggrading or has received a veneer of surface fines. Particle-size distributions of subsurface and subarmor sediments are basically the same, thus the term subsurface is often applied to both subsurface and subarmor sediments. The subsurface sediment size is controlled by the supply of fine sediment to the stream, by a lack of winnowing flows, and by local hydraulics that favor deposition of fines.

In order to sample subsurface or subarmor sediment, the overlying surface sediment or armor layer, respectively, first needs to be removed. This can be performed by taking an

areal surface sample that exposes subsurface particles, or by a volumetric armor-layer sample that exposes the subarmor layer. The overlying sediment needs to be removed entirely in order to prevent contamination of the subsurface or subarmor sediments by surface or armor sediments. Thus, Church et al. (1987) suggest removal of the armor layer to the bottom side of the largest particle in the sample area. Thorough removal of the armor layer (Section 4.2.1.2) is an easier technique than removing all surface particles by taking an areal sample (4.1.3.1 and 4.1.3.2).

Subsurface or subarmor sediments should be sampled to at least the same thickness as the armor-layer thickness, and possibly to a somewhat larger thickness to compensate for the usually conic shape of the excavation hole. This suggestion implies that there is no lower border to the subsurface or subarmor sediment limiting the thickness. Subsurface sediment can be limited in its thickness in recently aggraded stream locations where a thin layer of sediment was deposited on top of a former surface with a different particle-size distribution.

#### ***Unstratified bed-material samples***

Unstratified volumetric samples of the bed material include both armor and subarmor, or surface and subsurface sediments, respectively. Unstratified bed-material samples are useful only when the bed material is either non-stratified, i.e., non-armored and no veneer of surface fines, or when stratification is negligible or of no concern for the study result.

#### **4.2.2.2 Sampling depth to avoid bias against large particles**

The sampling depth of unstratified deposits does not usually have a lower boundary. This offers the opportunity to take a sample sufficiently deep to avoid bias against large particle sizes. The three criteria presented below can be used to compute sample depth

#### ***Cobble surfaces: $2 D_{max}$***

For coarse beds with a  $D_{max}$  in the cobble range, Diplas and Fripp (1992) and Simons and Sentürk (1992) suggest that volumetric sampling of unstratified sediment should extend to a minimum depth ( $d_{Smin}$ ) of  $2 D_{max}$ , e.g., to 36 cm for a  $D_{max}$  of 180 mm (Fig. 4.18).

$$d_{Smin} = 2 D_{max} \quad (4.3)$$

Using 0.5  $\phi$  sieve classes, the value of  $2 D_{max}$  (i.e., the size class of the  $D_{max}$  particle) is equal to or slightly smaller than the common multiple of the largest two sieve sizes, which are also the common multiple of all other smaller sieve sizes (Fig. 4.19). For example, the sampling depth of  $2 D_{max} = 16$  mm computed for a  $D_{max}$  particle size of 8 mm equals  $2 \cdot 8$  mm, and is close to  $3 \cdot 5.67$  mm. Similarly, 16 equals  $4 \cdot 4$  mm which is close to  $5 \cdot 3.36$  mm,  $6 \cdot 2.8$  mm, and  $7 \cdot 2.38$  mm. Thus, if an idealized deposit with a

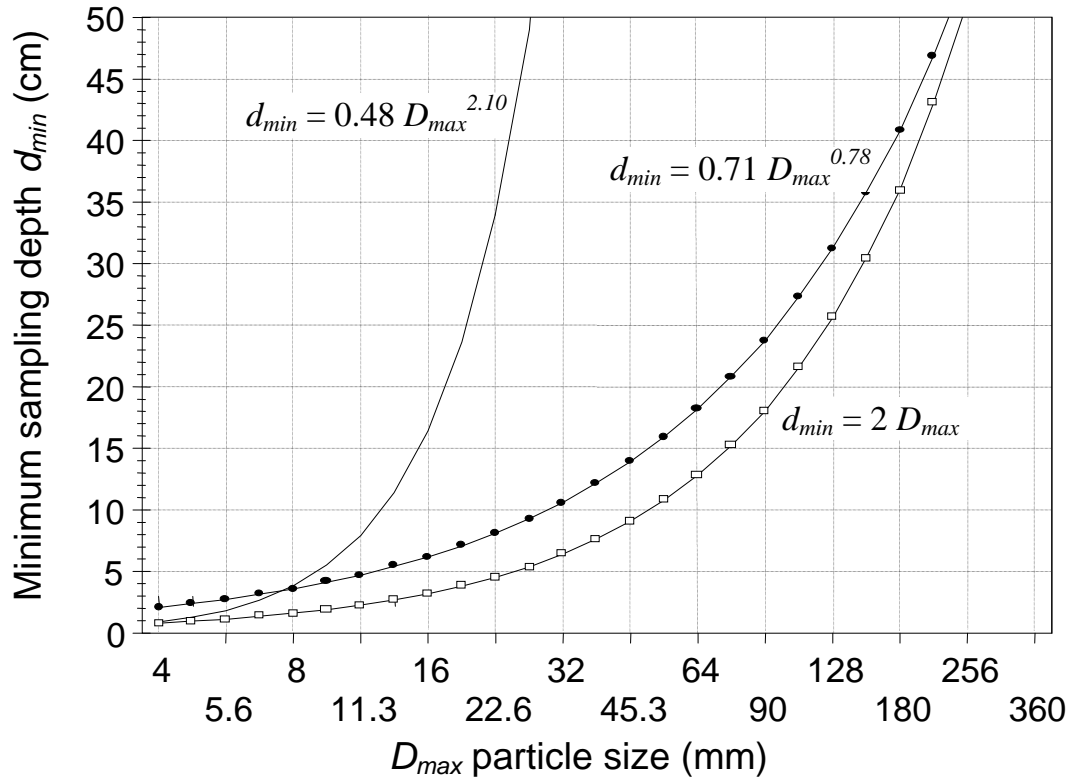


Fig. 4.18: Three functions to calculate minimum sampling depth  $d_{Smin}$  (in cm) from the  $D_{max}$  particle size (in mm).

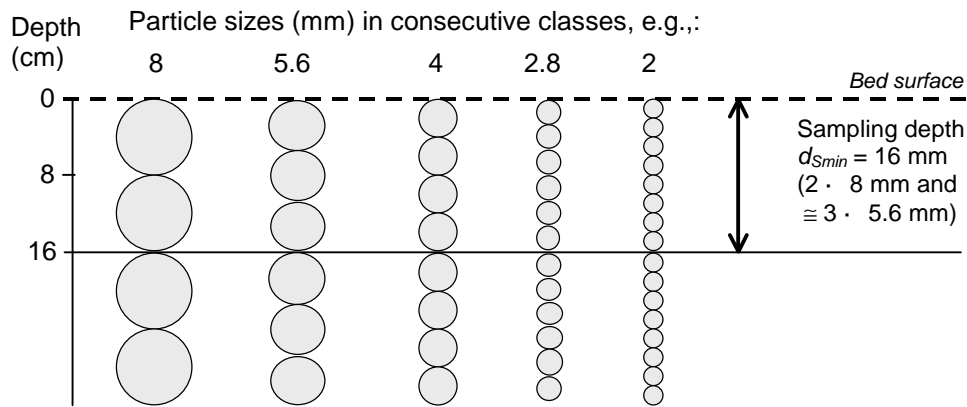


Fig. 4.19: Idealized sediment deposit showing the minimum sampling depth for volumetric samples. (Redrawn from Diplas and Fripp (1992), by permission of the American Society of Civil Engineers).

systematic packing of spheres is assumed (Fig. 4.19), a sampling depth of  $2 D_{max}$  would representatively include large particles. However, a sampling depth of  $2 D_{max}$  may not guarantee that large particles in natural deposits are representatively included in the sample. A bias against large particles appears as particle shapes become more elongated,

and as particle orientation approaches the vertical, i.e.,  $a$ -axes are at a right angle to the bed surface.

***Lowest common multiple of the largest two sieve sizes***

To avoid the bias against large particles in volumetric bulk samples, Diplas and Fripp (1991, 1992) proposed computing the minimum sampling depth as the lowest common multiple of the integer value of the largest two size classes. For example, the two sieve sizes of 4.8 and 6.7 mm ( $\phi = -2.25$  and  $\phi = -2.75$ ) are rounded down to 4 and 6 mm. Their lowest common multiple is computed from  $4 = 2 \cdot 2$ , and  $6 = 2 \cdot 3$ , and results in  $2 \cdot 2 \cdot 3 = 12$  mm. For the two size classes 5.67 and 4 mm, the lowest common multiple is 20, and 88 for the two size classes of 11.3 and 8 mm. The lowest common multiples increase steeply with increasing  $D_{max}$  particle size, but the data points scatter. The best fit power regression function fitted to the values expresses the relationship between minimum sampling depth  $d_{Smin}$  and  $D_{max}$  as

$$d_{Smin} = 0.48 D_{max}^{2.10} \tag{4.4}$$

with  $d_{Smin}$  in cm and  $D_{max}$  in mm (Fig. 4.18). Eq. 4.4 is not designed for use in coarse gravel and cobble beds. The ratio between the computed  $d_{Smin}$  and  $D_{max}$  increases strongly with increasing  $D_{max}$  particle size. For fine gravel with a  $D_{max}$  of 4 mm, Eq. 4.4 computes a  $d_{Smin}$  of 8 mm (i.e.,  $2 D_{max}$ ). For a  $D_{max}$  of 64 mm Eq. 4.4 computes a  $d_{Smin}$  of about 3 m, a sampling depth that is 47 times larger than the  $D_{max}$ .

***Variable multiples of  $D_{max}$***

Sampling depths computed with Eq. 4.4 become disproportionately and unmanageably large for medium and large gravel, whereas the sampling depth for fine gravel is manageably small. In order to increase sampling depth for small particles, but maintain a feasible sampling depth for large particles, the authors suggest computing sampling depths as variable multiples of  $D_{max}$ . The depth can be set to exceed  $D_{max}$  by a factor of 2 for cobbles, such as in Eq. 4.3., but be allowed to increase for finer beds. For example, factors of 2, 3, 4, and 5 might be assigned to particle sizes of 256, 64, 16 and 4 mm. A power regression function expresses this criterion for sample depth as

$$d_{Smin} = 0.71 D_{max}^{0.78} \tag{4.5}$$

with  $d_{Smin}$  in cm, and  $D_{max}$  in mm (Fig. 4.18).

### 4.2.3 Procedures and sampling dimensions for dry beds

Sampling bed material in dry beds has the advantage that no special sampling equipment is needed. Also, problems arising from sampling under water do not need to be considered (e.g., poor visual control, slumping walls in the sampling pit, potential for losing fines, working with your hands in cold water). Thus, bed material should generally be sampled during lowest flows when much of the bed is exposed.

However, the relative ease of volumetric bed-material sampling under dry conditions should not be abused by selecting only dry locations when sampling in partially inundated streambeds. Dry streambed areas are most likely bars, and particle sizes on bars, both surface and the subsurface, tend to be finer than bed material in other parts of the streambed. Thus, unless the study objective focuses on the investigation of bars, representative sampling for characterizing a reach requires sampling all areas of the reach, wet and dry (see sampling schemes, Sections 6.4 and 6.5).

#### 4.2.3.1 Tools for shoveled samples

A sturdy shovel often suffices as a tool for sampling bed material on dry beds. A pick, or a pry bar can be useful to pry loose cobbles and boulders. A trowel is handy for separating armor and subarmor sediment and for working in finer gravel. A metal bowl is convenient for scooping sediment out of a narrow pit.

The sampling area should to be outlined by a frame, preferably one that is round and adjustable, e.g., lawn edging. The walls of the pit should remain as straight as possible because a conic-shaped hole has different proportions of sediment from the top and the bottom of the pit. The advantage of shoveled samples is that they do not limit the sample size, as freeze-cores or pipe samplers do (Sections 4.2.4.8 and 4.2.4.5). In addition, a shovel is relatively inexpensive and easy to use and to transport.

If samples from dry and inundated locations are to be compared, the same technique should be used for both locations to prevent a methodological bias between samples. Sampling procedures and equipment used for volumetric sampling under water (Section 4.2.4) are generally usable for dry conditions as well.

#### 4.2.3.2 Sample dimensions for shoveled samples in unstratified bed material

Volumetric samples must have a predefined sample volume. This volume is determined from sample-mass criteria. Some of the sample mass criteria are empirically based and compute sample mass as a function of the  $D_{max}$  particle size (Section 5.4.1), whereas others are analytically based and determine sample mass on the basis of a preset precision for a sediment deposit of a given coarseness and sediment sorting (Sections 5.4.2 and 5.4.3). Sampling dry beds has the advantage that the dimensions of the sampling pit can be made sufficiently large to match the appropriate sample volume and sample depth, i.e., sampling equipment does not pose a limitation on sample size.

**Minimum sample mass and volume**

Sections 5.4.1 and 5.4.2 discuss a variety of sample-mass equations from which the user can choose. The discussion below uses a simple function that determines sample mass for particles with a  $D_{max} > 32$  mm by

$$m = (2.87 \cdot D_{max} - 44.8) \tag{4.6}$$

where sample mass  $m$  is in kg and  $D_{max}$  in mm. Eq. 4.6 is plotted in Fig. 4.20 and derived from the three sample mass criteria proposed by Church et al. (1987) for bed material of different  $D_{max}$  particle sizes (Section 5.4.1.1). Sample volume is obtained by multiplying

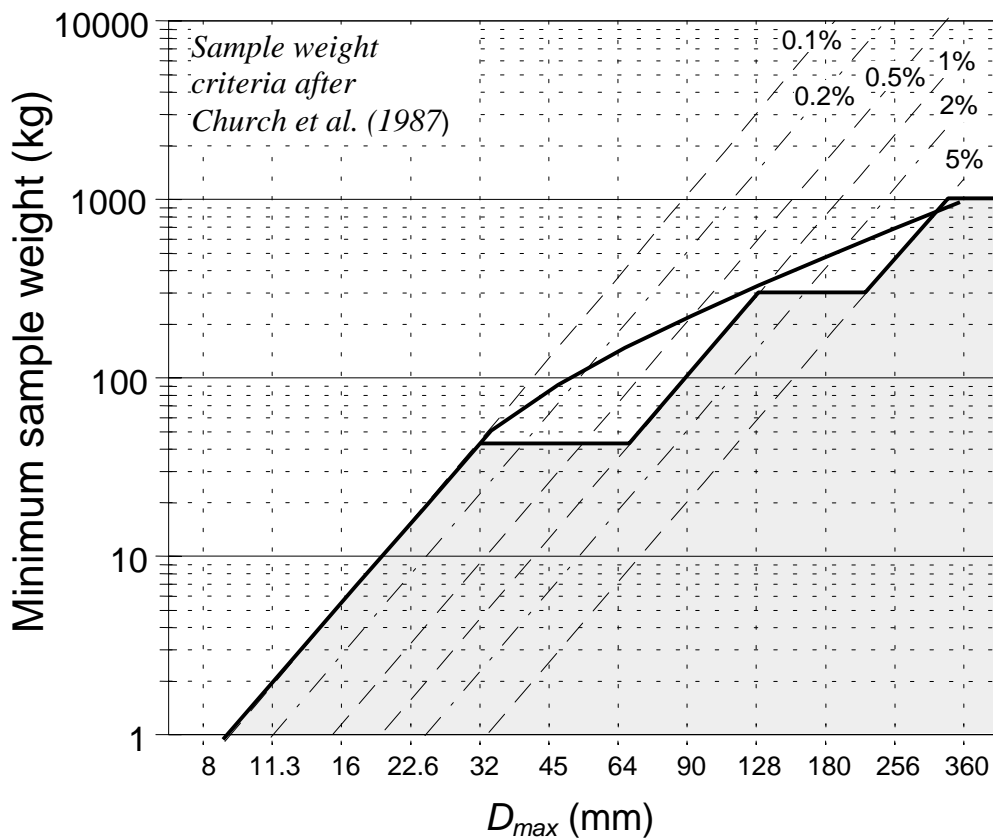


Fig. 4.20: Minimum sample weight for sediment with different  $D_{max}$  sizes ( $D_{max} = 0.1\% m$  for a  $D_{max} < 32$  mm,  $D_{max} = 1\% m$  for a  $D_{max} < 128$  mm, and  $D_{max} = 5\% m$  for  $D_{max} > 128$  mm) (after Church et al. 1987). The thick line represents a linear regression function fitted through the “corner points” of the stair-case function derived from the three sample-mass criteria by Church et al. (1987).

sample mass and sediment bulk density. Bulk density for shoveled gravelly sediment is approximately  $1.500 \text{ kg/m}^3$ , while *in situ* bulk density may range between  $1.700$  and  $2.600 \text{ kg/m}^3$  (Section 2.4).

### ***Minimum sample dimensions***

Once minimum sample mass and volume, as well as an appropriate sampling depth (Section 4.2.2.2) are determined, the quotient of volume to depth provides an estimate of the areal extent of the sample. This area can be allotted to a circle which should have a diameter at least as large as the sampling depth to ensure representative sampling of large particles.

The example below can be used to visualize the size of the pit required for sampling in medium and coarse gravel beds.

#### Example 4.1:

Sample mass for a deposit with a  $D_{max}$  of 45 mm is about 84 kg (Eq. 4.6). Tightly packed, this mass is about 42,000 cm<sup>3</sup> or 4.2 household pails in volume if a bulk density of about 2 g/cm<sup>3</sup> is assumed. Sampling depth for a deposit with a  $D_{max}$  of 45 mm is 9 cm (Eq. 4.3,  $2 D_{max}$ ), or 14 cm (Eq. 4.5, variable multiples of  $D_{max}$ ). Eq. 4.4 (common multiple method) is not applicable to particles larger than 22 mm because it computes unreasonably large sampling depths (Fig. 4.18). A sampling depth of 9 cm ( $2 D_{max}$ ) requires a round pit with a diameter of 77 cm. For a sampling depth of 14 cm, the pit has to be 60 cm in diameter.

In a coarse gravel-bed river with a  $D_{max}$  particle size of 180 mm, sampling depth is 36 cm (Eq. 4.3), or 40 cm (Eq. 4.5). Taking the average of 38 cm, the sample volume of 236,000 cm<sup>3</sup> (about 24 household pails) requires a pit of 89 cm in diameter. The user might consider allocating the required sample volume to several smaller pits excavated at several sampling sites (Wolcott and Church 1991; Rood and Church 1994 (Section 6.4.4).

A calculation analogous to the one above can be used to compute the areal extent for volumetric armor-layer samples.

#### 4.2.3.3 Surface pebble count on subsurface sediment

Based on the equivalence of particle-size distributions determined from volume-by-weight and grid-by-number samples proposed by Kellerhals and Bray (1971) on non-stratified deposits (see Section 4.3.1), Buffington (1996) developed a technique that uses pebble counts to sample the subsurface sediment. The first step of the procedure is to remove surface particles by hand from an area of about 1 m<sup>2</sup> in order to expose the subsurface sediment. Sand and fine gravel particles which often accumulate just below the surface are usually not completely removed by manual picking of surface particles (Section 4.1.3.1) and would produce a sample that is biased towards fines. In order to prevent this potential bias, these fines are mixed into the subsurface sediment prior to sampling. The depth of mixing should be slightly deeper than the sampling depth that would be required for a volumetric sample, which depends on the  $D_{max}$  particle size and

the number of samples taken. Mixing to the depth of one shovel blade length is a practical criterion. The necessity for mixing becomes apparent by Buffington's test analyses: without mixing, only 2 out of 5 of the subsurface pebble counts corresponded ( $\alpha = 0.05$ ) to a volume-by-weight analysis of samples of the same sediment. The mixing procedure produced a statistical correspondence between subsurface pebble counts and volume-by-weight analyses in 4 of 5 samples.

Buffington (1996) suggested that particles included in the pebble count should be selected at random by pointing at a particle with a pencil tip, eyes averted. Bias against fines or large particles is probably not much of a concern under these circumstances (Sections 4.1.1.2 - 4.1.1.6). However, an operator kneeling or crouching besides the pit may involuntarily favor the center or some other easily reached part of the sampling area, thus introducing a spatial bias. A sampling frame that covers the 1 m<sup>2</sup> surface with a small-scale grid of 10 by 10 cm or smaller (Section 4.1.1.6) can be used in the absence of cobbles and ensures that particles are sampled systematically from the entire sample area.

Another concern regarding this method is that an area of 1 m<sup>2</sup> might not provide ample space to collect a sufficient number of particles in coarse bed material without counting some particles twice. Counting 400 particles is required to determine the particle sizes of the  $D_{50}$  and  $D_{95}$  to within about 0.1 - 0.15  $\phi$ -units, and the  $D_5$  to within about 0.3  $\phi$ -units (Rice and Church 1996b, Section 5.2.2.3) in a deposit with a standard deviation of 1.17  $\phi$ . If the spacing between grid points equals the  $D_{max}$  particle size, and the  $D_{max}$  particle size is 180 mm, the sampling area needs to be 13 m<sup>2</sup> ( $400 D_{max}^2$ ) which may be met with a square 3.6 by 3.6 m in size. A sampling area of 1 m<sup>2</sup> can accommodate a 100 particle count if the  $D_{max}$  particle size is 100 mm, or a 400 particle count if the  $D_{max}$  particle size is 50 mm. Thus, several pits may have to be sampled in order to obtain enough sampling points for a representative pebble count on subsurface sediment that contains cobbles.

#### **4.2.4 Procedures and equipment for submerged conditions**

Although dry gravel bars are convenient for volumetric sampling, samples need to be taken from all parts of the streambed for a reach-averaged analysis of sediment size, or from riffles for tasks such as an analysis of fish spawning habitats, or the ratio of surface to subsurface particle size. Thus, armor, subsurface, and unstratified volumetric samples frequently have to be obtained under water. Several procedures and equipment for taking volumetric samples under water are described below. These include:

- shovels, scoops and clams,
- pipe and McNeil samplers,
- barrel samplers,
- freeze-core samplers and resin cores, and
- hybrid pipe freeze-core samplers.

An extensive comparison of various sampling procedures for unstratified bed material is summarized by Ramos (1996). His literature review compares equipment needed, the sampling procedure, advantages and disadvantages, as well as a description of the

accuracy and precision expected from five sampling devices: single probe, and multiprobe freeze-cores, McNeil samplers, shovels, and the hybrid pipe-freeze-core sampler. Not all samplers are equally well suited for a specified study objective. The user needs to select a sampling procedure appropriate for the particular bed-material characteristics, sample-size requirements, and the remoteness of the site.

In addition to taking samples under submerged conditions, volumetric bed-material sampling in mountain gravel-bed rivers has to overcome several other problems:

- Armoring is usually well developed, in which case many study objectives require stratification of the bed material into surface and subsurface or armor and subarmor,
- Stream-bed particle sizes that range from silt and boulders are difficult to sample with one method,
- Large sample sizes of 100 kg and more are required for representative particle-size analysis, and
- Fast flow velocities that wash away fines dislodged when the bed is disturbed by the sampling process.

Most procedures for underwater volumetric sampling employ sampling devices that have fixed sample volumes. The volume of one sample may be much smaller than what is required for the total sample mass. Because of this, several subsamples may need to be combined to obtain the required total sample mass (Sections 6.4.4; Wolcott and Church 1991; Rood and Church 1994).

#### 4.2.4.1 Shovels

When sampling subsurface sediment under water, the operator needs to ensure that fine sediment remains in the sample and is not swept away by the flow. A shovel sample taken from the riverbed under water loses these fines and causes an unrepresentative sample that is biased against fines. The loss of fines increases with the increasing velocity of flow. Billi and Paris (1992) and Billi (1994) caution against using shovels in submerged conditions, unless the water is still, and an underwater storage box with a mesh-bag cover is available for depositing the sampled sediment.

#### ***Comparison of shovel methods with the McNeil sampler***

Schuett-Hames et al. (1996) compared the results of three methods of collecting shoveled samples with results obtained with the McNeil sampler (Section 4.2.4.5), a sampler that is commonly used on beds of fine and medium gravel. The three shovel methods used were a standard shovel, a standard shovel used within a stilling well that shields the sampling site from moving flow, and a special shovel with elevated sides to minimize the loss of fine sediment over the sides of the shovel. Paired samples were taken with the McNeil sampler and one of the shovel methods at several riffles on two streams with relatively fine gravel beds. Sampling protocols were followed carefully, and the data were analyzed by several statistical tests.

At one of the streams, samples taken with a standard shovel within a stilling well and with a McNeil sampler produced similar geometric mean particle sizes and a similar percent fines (particles less than 0.85 mm). The other two shovel methods had 2.9 - 4.7 % less fines than the McNeil sampler, and geometric mean particle sizes were on average 20% larger. This suggests that a standard shovel used within a stilling well can be a suitable alternative to the McNeil sampler. Shovels and a stilling well are convenient to use in the field and have the advantage of providing a larger sample mass than the McNeil sampler.

All of the shovel methods produced a similar percent of coarse sand (0.85 - 2 mm) as did the McNeil sampler. But only the McNeil sampler collected sediment less than 0.1 mm (fine sand and silt) representatively. Material of this size is transported in suspension when the bed is disturbed during sampling. Regression functions between methods had low coefficients of determination and could not be used to predict the observed discrepancies in the percent of sediment finer than 0.85 mm or in the geometric mean particle sizes.

In the other stream, all shovel methods produced geometric means that were coarser by 9 - 18 % than the geometric means produced by the McNeil sampler, and had a slightly higher percentage of fines. Water depth and flow velocity in the two streams could not explain the difference in the results between the two streams. However, pooled data from both streams indicated a significant relation between the percentage of sediment larger than 3.35 mm and the difference in the percent fines between any shovel method and the McNeil sampler. Shovel methods produced less percent fines than the McNeil sampler in streambeds with more than 70% coarse sediment, and more percent fines than the McNeil sampler in streambeds with less than 70% coarse sediment.

Differences in the percent fines between the McNeil sampler and various shovel sampling methods appear to be the product of streambed characteristics, and further analysis of this dependency is necessary. However, sampling methods should be consistent within a study, particularly if results are to be compared over time or among locations.

#### 4.2.4.2 Mesh-bag scoop

A mesh-bag scoop is a useful tool for sampling armor and subarmor sediment in streambeds consisting mostly of sand and fine gravel (Forest Service, Klamath Falls, OR, pers. communication). A mesh-bag scoop has a metal frame that is of the same dimensions as the back side of a 3 by 3 inch Helley-Smith bedload sampler (20.3 by 12.1 cm). The frame is constructed of V-profiles, so that a standard Helley-Smith sampling bag (0.25 mm mesh width) can be slipped into the notch of the profile. A handle is attached to the top of the metal frame (Fig. 4.21).

The mesh-bag scoop may be used in conjunction with a stilling well or a plywood shield that encloses three sides of a sampling area 0.6 by 0.6 m in size (Section 4.2.4.7). The mesh-bag scoop is especially useful when sampling armor layer and subarmor sediments in fine-grained beds. After the armor layer depth is determined, the mesh-bag scoop is

pulled through the bed material along the lower border of the armor layer, scraping the armor layer sediment into the mesh bag. With the free hand, the operator ensures that dislodged armor layer particles are not pushed to the side, but enter the sampler.

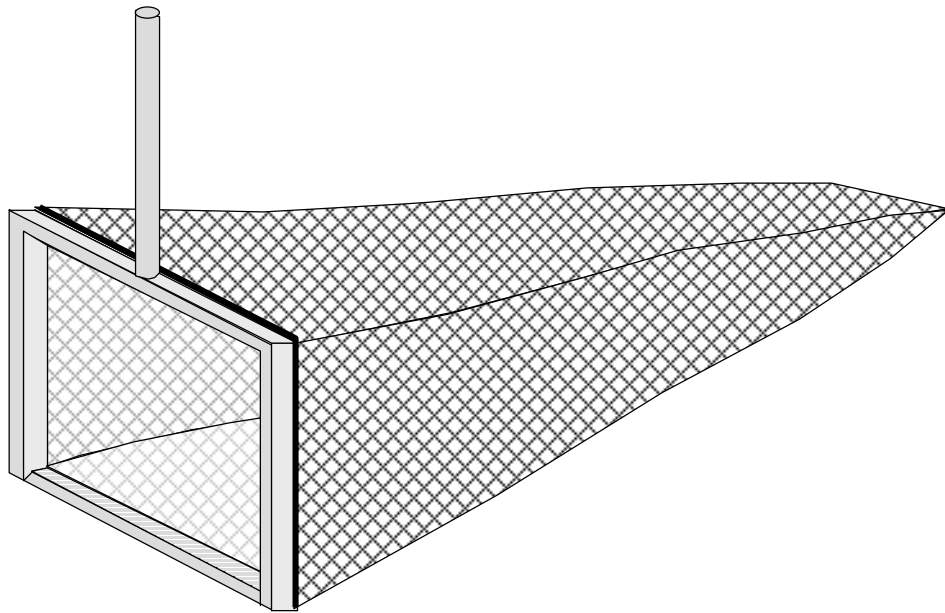


Fig. 4.21: Mesh-bag scoop with attached Helley-Smith sampling bag for sampling armor layer and subarmor sediment in fine and medium gravel-bed streams.

Sampling patterns follow parallel paths to ensure that the sampling area is sampled entirely, and that no places are sampled twice. The sampled sediment in the mesh bag is frequently emptied into a bucket. After all the armor layer sediment is removed, the mesh-bag scoop can be used to collect the subsurface sample. This sampling method works well in streambeds with predominantly fine gravel and produces about 1 - 2 household pails of armor layer sediment. However, this method has not yet been validated by peer review.

#### 4.2.4.3 Grab samples (US RBMH-80)

A grab sampler collects as much sediment as can be held in the jaws of the sampling device. Fines are retained if the jaws close properly. Grab samplers have been developed for sand-bedded streams, but can be used in beds of fine gravel as well, provided no gravel particles become wedged in the jaws and inhibit the closing mechanism. The newest grab sampler developed by the Federal Interagency

Sedimentation Project<sup>4</sup> is the hand held rotary scoop sampler US RBMH-80 (Fig. 4.22). An older version of this sampler is described in Edwards and Glysson (1988). A cylindrical bucket 20 cm wide houses the rotary scoop. The bucket is mounted at the end of a rod. The total length of the sampler 1.42 m.

The sampler can be operated under water in wadable streams. To obtain a sample, the opened sampler is placed onto the streambed and firmly held down. A wire mechanism, operated by a lever, opens and closes the rotary scoop. The sampler can collect approximately 175 cm<sup>3</sup> of unstratified bed material, from a maximum depth of 4.5 cm. After the sample is collected, the sampler is lifted from the bed, and the sample is emptied into a bucket.

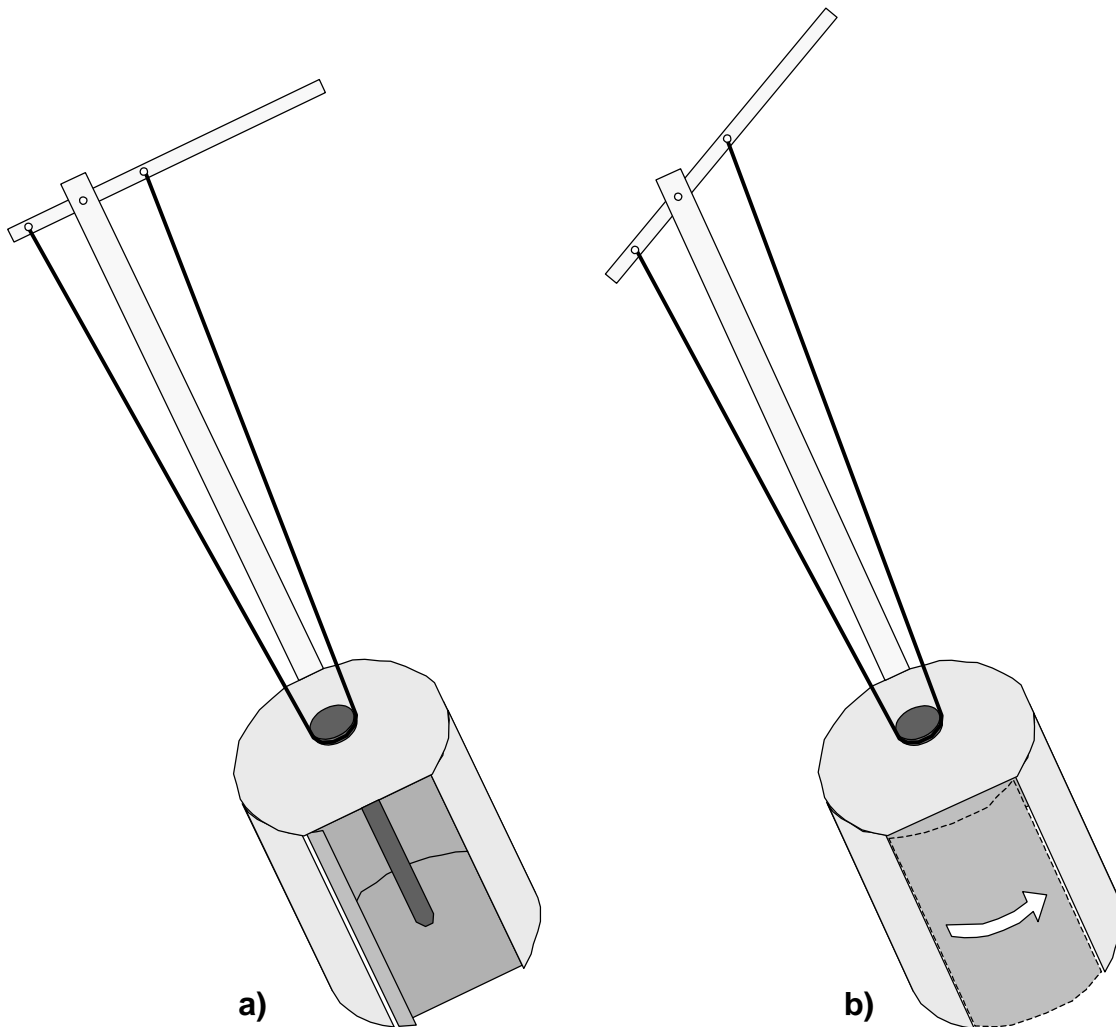


Fig. 4.22: Schematic diagram of US RBMH-80 hand-held, rotary-scoop bed material sampler developed by the Federal Interagency Sedimentation Project. a) Rotary scoop open; b) Rotary scoop closed.

---

<sup>4</sup> The US RBMH-80 sample can be viewed and ordered from the Federal Interagency Sedimentation Project web site <http://fisp.wes.army.mil/>.

The advantage of the rotary-scoop sampler is that a large number of samples can easily be taken over the entire sampling area, which may be a facies patch or a relatively homogeneous reach of the stream. Samples can then be commingled for a composite analysis (Sections 6.4.4; Wolcott and Church 1991; Rood and Church 1994). The disadvantage is that the sampler is not suitable for large gravel, and that the sampler may not close properly and will lose its fines if a pebble becomes lodged in the mechanism.

#### 4.2.4.4 Backhoe

In wide alluvial gravel-bed rivers where bed material is mobilized during one or several flood events annually and tread damage is of little concern, a backhoe can be an efficient tool for sampling large amounts of unstratified sediment. However, in small and often incised mountain gravel-bed streams, backhoes may damage riparian areas and should be used with great care. Also, when digging into an inundated streambed with a backhoe, fines are likely to be washed away and will be underrepresented in the sample. However, backhoes and boom trucks parked on a bridge with the shovel (bucket) lowered to the stream can be helpful for lifting equipment and heavy sediment samples collected by other means from the streambed.

#### 4.2.4.5 Pipe samplers and the McNeil sampler

Pipe samplers and the McNeil sampler (McNeil and Ahnell 1964) were developed for fish habitat studies primarily concerned with the amount of fine sediment in spawning gravels. Pipe and McNeil samplers have also been used to monitor the amount of fines for cumulative watershed effects analyses. Depending on the fish species of concern, or the size of fine sediment supplied to the stream from watershed disturbances, the term “fines” can refer to any particle size between fine sand (< 0.1 mm) to pea-sized gravel (< 8 mm). Therefore, the term fines needs to be specified in a given study.

Pipe and McNeil samplers consist of a stainless steel pipe 0.1 – 0.2 m in diameter that extends through the bottom of a cylinder with a diameter 2 - 3 times larger than that of the inner pipe (Fig. 4.23 a-c). Designs of pipe and McNeil samplers vary in the diameters of the inner and the outer pipe, and in the angle at which the outer pipe attaches to the inner pipe. These differences should not affect sampling performance. However, when bed-material particle sizes approach the dimensions of the sampler opening i.e., the inner pipe, the physical size of the sampler may artificially truncate the sampled particle-size distribution. Thus, the sampler opening should be large enough to easily accommodate the largest particles to be sampled. An opening size of  $2 D_{max}$  is suggested.

Pipe and McNeil samplers are designed for wadable flows with depths of less than 0.5 m and relatively slow flow velocities. The end of the small pipe is worked into the submerged river bed, usually to a depth of about 15 cm. The sediment inside the pipe is excavated by hand and temporarily stored in the built-in storage basin. The water inside the large pipe may contain fine sediment brought into suspension during sampling. This fine sediment may be sampled by swirling the water within the sampler and taking a suspended sediment sample for lab analysis (Fig. 4.23 a and b). To retain nearly all of

the fine-grained bed-material for analysis, the inside opening of the small pipe is capped before the sampler is removed from the streambed (Fig. 4.23 c). The quantity of suspended sediment can be determined directly in the field using an Imhoff cone. Failure to sample or retain the fines may significantly underestimate their presence in the substrate.

Separating surface or armor sediment from subsurface or subarmor sediment may be somewhat difficult when using pipe or McNeil samplers with small sampler openings. This is particularly true if the sampler is used underwater and the differentiation between strata has to be accomplished by feel alone. Therefore, pipe and McNeil samplers are usually used to collect an unstratified volumetric sample. The percent fines is then determined for the unstratified sample. Note that the percent fines in an unstratified sample is smaller than the percent fines in a subsurface sample. This is because the unstratified sample contains more large particles (i.e., those from the surface) than the subsurface sediment. The difference between the percent fines of the unstratified sediment and the subsurface sediment may be largely eliminated if the sample is truncated at a commonly occurring large particle size before the percent fines is computed.

Sample mass collected by McNeil samplers varies with sampler dimensions, but commonly ranges between 6 and 15 kg (Rood and Church 1994). Such sample sizes are small when the stream contains large gravel, and require taking several samples if a particle-size analysis is to be obtained for particles larger than 35 to 48 mm according to the 1% criterion by Church et al. (1987) (Section 5.4.1.1). A 0.2-m diameter McNeil sampler can be used for determining the percent fines if cobbles (coarser than 64 mm) are discarded. Discarding particles larger than some preset size is also suggested by Rice (1995) as a means to decrease the effect of large particles on the computed percent fines. Truncation improves the comparability of the percent fines between samples provided the selected truncation size is equal for all samples included in the comparison.

Pipe and McNeil samplers can be fabricated in various dimensions to best suit a particular stream-bed situation. Pipe samplers are relatively quick and easy to use, and are light enough to be transported to remote areas. However, Rood and Church (1994) caution that it takes considerable operator skill to representatively sample the fine sediment collected by the McNeil sampler. Evaluations of how representative results from McNeil samplers are with respect to fine sediment vary among studies. NCASI (1986) found that the McNeil sampler minimizes the loss of fines, but Rood and Church (1994) caution that the sampler underrepresents the fine sediment in the sample. Further information on sampling results of pipe and McNeil samplers are summarized by Ramos (1996) who compared samples of the McNeil sampler with freeze-core and other samplers. Schuett-Hames et al. (1996) compared samples from the McNeil sampler to samples obtained by various shovels (Section 4.2.4.1).

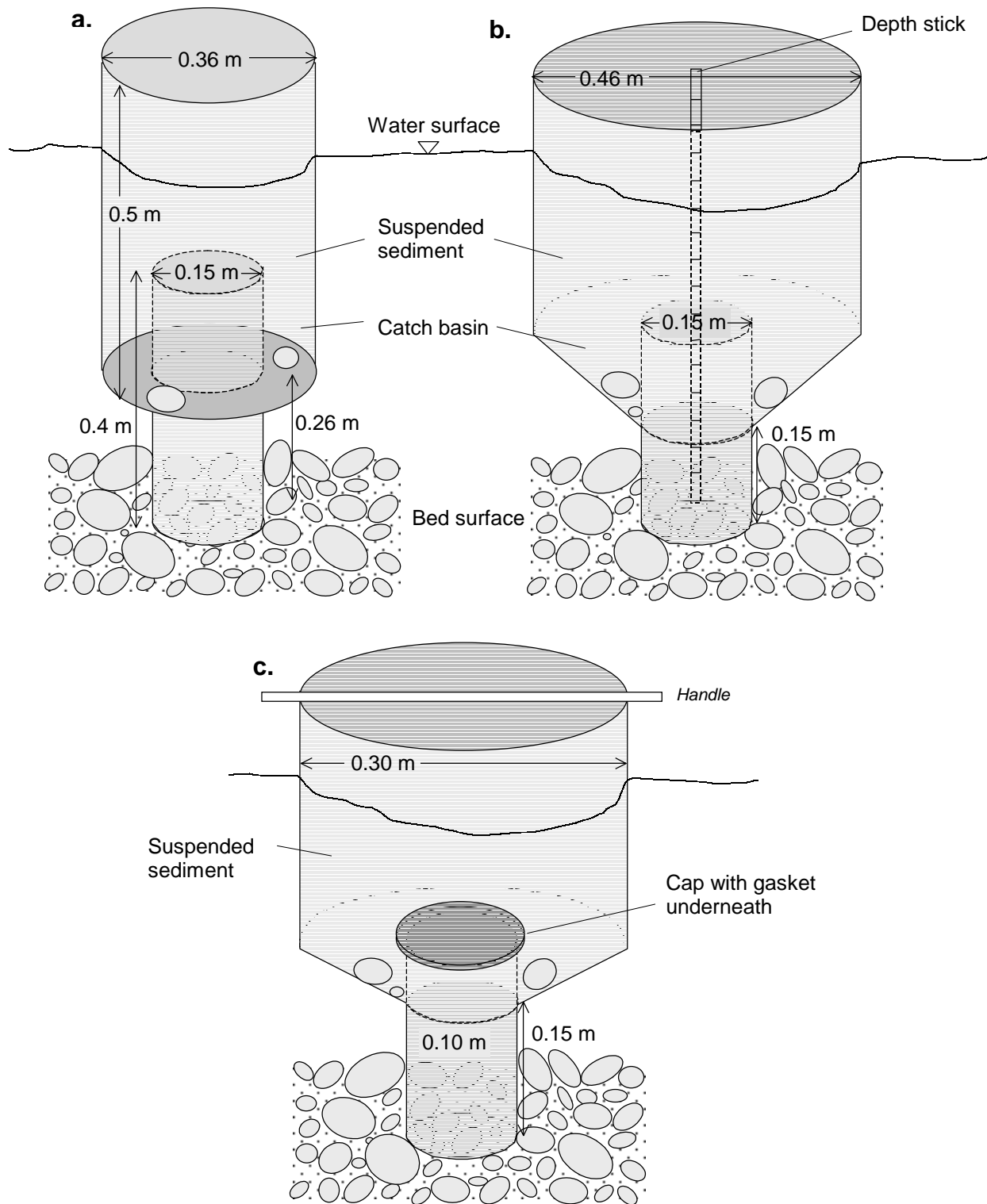


Fig. 4.23 a - c: Pipe and McNeil samplers: (a) Pipe sampler. Adapted from Yuzyk (1986); (b) McNeil sampler. Adapted from Hamilton and Bergersen (1984), source: Shepard and Graham (1983); (c) McNeil sampler. Adapted from Hogan et al. (1993), source: McNeil and Ahnell (1964).

#### 4.2.4.6 Barrel samplers

Barrel samplers were developed specifically to accommodate the tasks and problems of collecting volumetric bed-material samples in gravel-bed rivers. Because of their large size, barrel samplers allow sampling over a wide range of particle sizes, and relatively large sample volumes. Barrel samplers retain suspended fines that can be sampled separately, and can be used under submerged conditions. Two different barrel samplers are described below.

##### *Cookie-cutter sampler*

The “cookie-cutter” or gravel-cutter sampler was developed by Klingeman and Emmett (1982) for use in coarse gravel- and cobble bed streams. The cookie-cutter sampler has an opening large enough to sample cobbles and small boulders, and facilitates large sample sizes that can better represent the percentage of gravel and cobbles than samples from the smaller pipe and McNeil samplers. The cookie-cutter sampler consists of an open 55-gallon drum that is cut in half. The resulting cylinder is about 0.4 m high and 0.5 m in diameter (Fig. 4.24). Two operators are required to use this device. The barrel is fitted with handles. Teeth are cut into the bottom of the barrel so that it can be worked a few cm into the streambed. When the sampler is used in shallow water that does not overtop the barrel, armor- and later subarmor-layer sediment is scooped out of the barrel and poured into buckets. Under submerged conditions, the sampled sediment is temporarily stored in a rectangular sample box that attaches to the barrel and is held by one of the operators. The sample box is 0.7 m long by 0.3 m high by 0.4 m wide. One end of the sample box is open, the other end has a fine mesh wire of 0.2 mm to retain

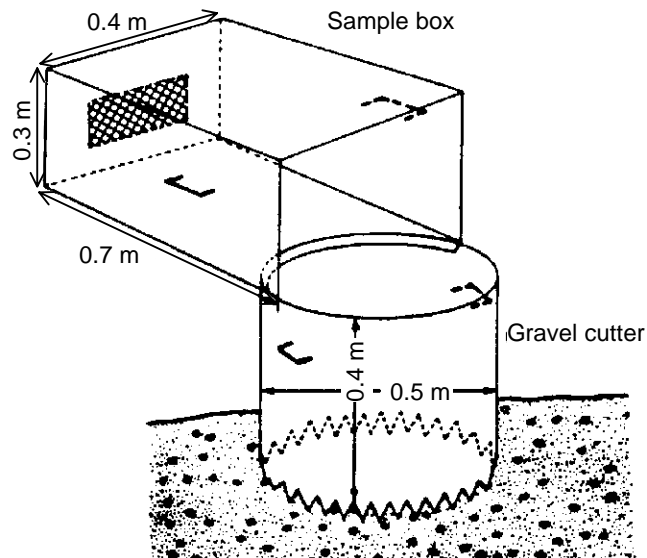


Fig. 4.24: Cookie-cutter sampler developed by Klingeman and Emmett (1982). (Reprinted from Yuzyk (1986)).

finer. The sample box is placed on the downstream side of the sampler so that the current that flows through the sample box carries the fines into the box. After sampling, the sample box is lifted out of the water and emptied. The gravel-cutter sampler can be used in deep, unswimmable water if divers and a support boat are used.

### ***CSU barrel sampler***

The CSU-barrel sampler developed by Hogan et al. (1993) and Milhous et al. (1995) is a simplified alternative to the cookie-cutter sampler. To prevent the loss of suspended fines, the CSU-barrel sampler uses a taller barrel than the cookie-cutter sampler. The CSU sampler is 0.6 m high and 0.46 m in diameter, made from a 30-gallon drum that is cut open on both ends (Fig. 4.25).

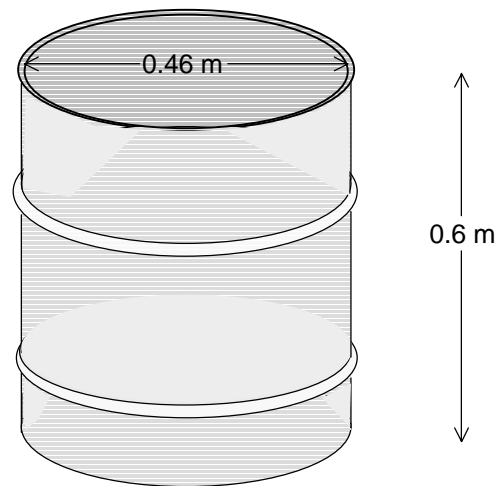


Fig. 4.25: CSU barrel sampler.

At the selected sampling location, the barrel is slightly inserted into the bed material. For a subsurface sample, surface particles must be removed first. For this task, the operator has to rely mainly on feeling the particles, because visibility on the barrel bottom is poor primarily due to suspended fines. Distinguishing between surface and subsurface particles by feel is difficult in cold water when neoprene gloves are needed. Working systematically from one side to the other helps ensure that no large surface particles are overlooked. However, small surface particles cannot be removed representatively. Also, it is not possible to distinguish between surface and armor layer when using the barrel sampler in coarse gravel beds. Particles that are under the edge of the barrel are always removed, but only included in the sample if more than half of the particle volume protrudes into the barrel. Removing surface particles from under the edge of the barrel allows the barrel to be moved deeper into the bed.

After the surface particles have been removed, the subsurface is sampled by collecting all particles within the barrel until the pit has reached a predefined depth. Particles are picked by hand, or scooped with small trowels and bowls, and put into large buckets (Fig. 4.26) that are held by an assistant who also hauls filled buckets back to the bank. An old screwdriver may be needed to pry loose large particles that are wedged in the bed.

Suspended particles (fine sand and silt) can be sampled by swirling the water around in the barrel and then taking a suspended sediment sample. To retain fines even under completely submerged conditions in chest deep water, a cloth hood can be secured over the top of the barrel. The operator wears a diving mask and a snorkel and reaches the sediment in the bottom of the barrel through a slit in the cloth.

Compared to freeze-core samplers, barrel samplers provide a low-tech method for sampling unstratified subsurface sediment under submerged conditions in gravel-bed rivers. Barrel samplers are inexpensive and relatively easy to use. The comparatively large dimension of barrel samplers provides a sample mass of about 60 - 70 kg per barrel, and makes barrel samplers suitable for cobble beds. The disadvantage of the barrel sampler is that it is difficult to carry over long distances and therefore not suitable for use at remote sites. Tall barrel samplers are also difficult to use by small persons, particularly in deep flow.



Fig. 4.26: Taking a barrel sample, South Fork Cache la Poudre Creek, Colorado. (Photograph by K. Bunte).

#### 4.2.4.7 Three-sided plywood shield

Armor and subarmor layer in submerged conditions can be sampled more effectively and more comfortably for the operator if the sample area is enclosed by a three-sided plywood shield. The operator collects the sample from the open downstream side. The enclosure consists of three plywood sheets, each 0.6 by 0.9 m or 0.9 by 0.9 m in size, that are joined on their long sides by piano hinges. The plywood shield has a tarpaulin skirt along the outside. The tarpaulin is fastened near the bottom of the plywood sheets and extends about 0.5 m beyond the plywood (Fig. 4.27). This sampling device was developed by the Winema National Forest, Klamath Falls, OR.

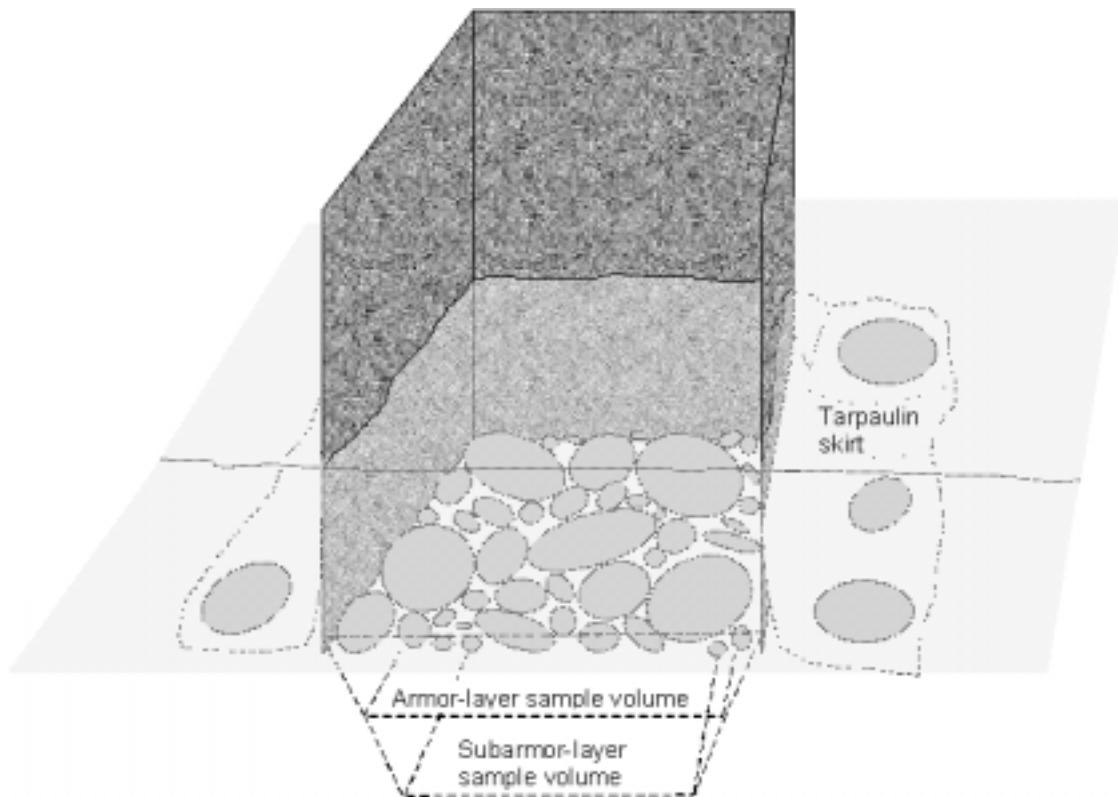


Fig. 4.27: Plywood shield to provide a three-sided enclosure of the sampling area.

Set-up of the plywood shield requires two persons. The plywood shield is unfolded and set at the appropriate location on the streambed, the open side facing downstream. The bottom side of the plywood is shoved slightly into the bed. The skirt is spread along the outside of the shield and rocks are placed along the edge of the skirt to hold it down. The set-up should be performed quickly to minimize the water flow through openings below the plywood enclosure or through the hinge area as it may scour fines from the bed. Any

leaks should be minimized by squeezing rocks, rags, and plastic shopping bags into openings until the water inside the plywood shield is relatively stagnant.

The operator wears chest waders and while kneeling or crouching at the open side, removes the armor layer to a predetermined depth. In coarse gravel- and cobble-bed streams, the operator collects the armor-layer material using a trowel and a medium-sized metal bowl (approximately 1 liter capacity), and perhaps a pry bar to pry loose particles that are wedged into the bed. A mesh-bag scoop (Section 4.2.4.2) is a suitable tool for collecting armor-layer sediment in fine and medium gravel beds. The nearly stagnant water within the shielded sampling area minimizes the amount of fines swept out of the sampling area. All collected sediment is saved in buckets. After the armor layer is removed, the subarmor layer is sampled to a predetermined depth.

Working with the plywood enclosure has two advantages: it improves the access for the operator while sampling and provides a larger sampling area ( $0.36 - 0.81 \text{ m}^2$ ) than a barrel ( $0.14 - 0.20 \text{ m}^2$ ). An armor-layer sample in a coarse gravel or cobble-bed stream may yield 70 – 130 kg depending on the sampling depth. If the subarmor sample is sampled to the same thickness as the armor-layer sample, the sample mass is smaller due to the conic shape of the excavation and may yield 40 – 80 kg. Thus, if the study objective is solely the subarmor sediment, a thin armor layer should be removed in order to increase the amount of subarmor sediment that can be sampled. Even though sample mass of an individual sample from within the plywood shield is larger than that obtained with any other sampling method, several samples are needed to obtain a total sample mass that is sufficient for a statistically meaningful particle-size analysis (Section 5.4).

#### 4.2.4.8 Freeze-cores

Freeze-core samplers collect all particles that are frozen to one or several hollow rods pounded into the streambed. The sample extends from the surface into the subsurface and leaves the stratification intact.

Freeze-core sampling was developed for aquatic habitat studies for which the distinction between surface and subsurface sediment size and the percentage of fine sediment is important. The advantage of freeze-core samples is that the bed-material stratification is visible in the sample. Also, freeze-cores can be collected in flows deeper and faster than those appropriate for McNeil and pipe samplers. Freeze-core sampling is discussed by Walcotten (1973, 1976), Adams and Beschta (1980), Everest et al. (1980), Lotspeich and Reid (1980), Carling and Reader (1981, 1982), Platts et al. (1983), Thomas and Rand (1991), Young et al. (1991), Thoms (1992), Hogan et al. (1993), Rood and Church (1994), and Milhous et al. (1995).

A single-tube freeze-core sampler consists of a pointed hollow rod with a 2 cm inside diameter. The rod is driven approximately 0.2 m into the streambed. A cooling agent, such as liquid nitrogen or liquid carbon dioxide, is injected into the rod and escapes through a series of nozzles at the lower end so that the pore water in the sediment adjacent to the rod freezes (Fig. 4.28). The size of the frozen core depends on the amount

of cooling agent used, the temperature of the streambed, the velocity of the stream flow, the pore water movement, and the pore space. The frozen core is then dug out or extracted by a hoist and thawed for particle analysis. Typically, freeze-cores are 0.1 – 0.15 m in diameter and weigh about 1 - 5 kg. Sample mass can be increased to 10 - 15 kg if liquid nitrogen is used as the cooling agent (Rood and Church 1994). The sediment stratigraphy remains intact when the frozen core is retrieved, and, if the core is thawed over a slotted box (Fig. 4.29 b), the stratigraphy can be analyzed incrementally. Problems with freeze-core sampling stem from the difficulty of pounding a rod into a streambed, disruption of the bed stratification due to pounding, the extensive amount of equipment, and the cost (several thousand dollars).

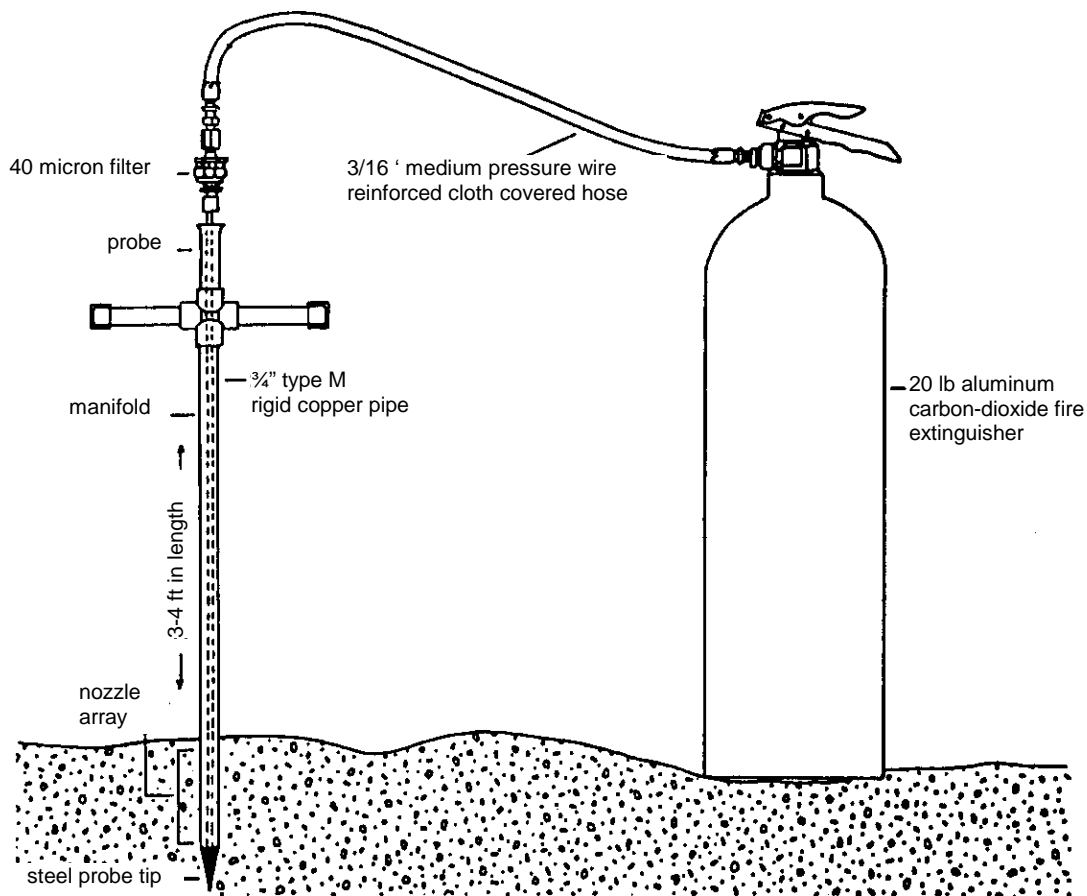


Fig. 4.28: Freeze-core samplers: Single-tube freeze-core sampler with a fire extinguisher as the source for liquid CO<sub>2</sub>. (Reprinted from NCASI (1986), source Walcotten (1976), by permission of the National Council of the Paper Industry for Air and Stream Improvements).

In order to enlarge the freeze-core, and include larger particles in the sample, Lotspeich and Reid (1980), and Everest et al. (1980) developed the tri-tube freeze sampler. Three rods are arranged in a triangular fashion and driven into the streambed through templates at the upper end of tubes to ensure that the distance of the tubes relative to each other remains constant between 3.8 and 7.6 cm (Fig. 4.29 a). A tripod and winch are used to extract the core.

Sample mass for tri-tube samples is 10 - 20 kg (about 0.5 - 1 bucket full), which is approximately 2 - 4 times more than the mass of single-rod freeze-cores. A sample mass of 10 kg satisfies the 0.1% sample mass criterion by Church et al. (1987) for a  $D_{max}$  smaller than 20 mm (i.e., the  $D_{max}$  particle comprises 0.1% of the total sample weight,

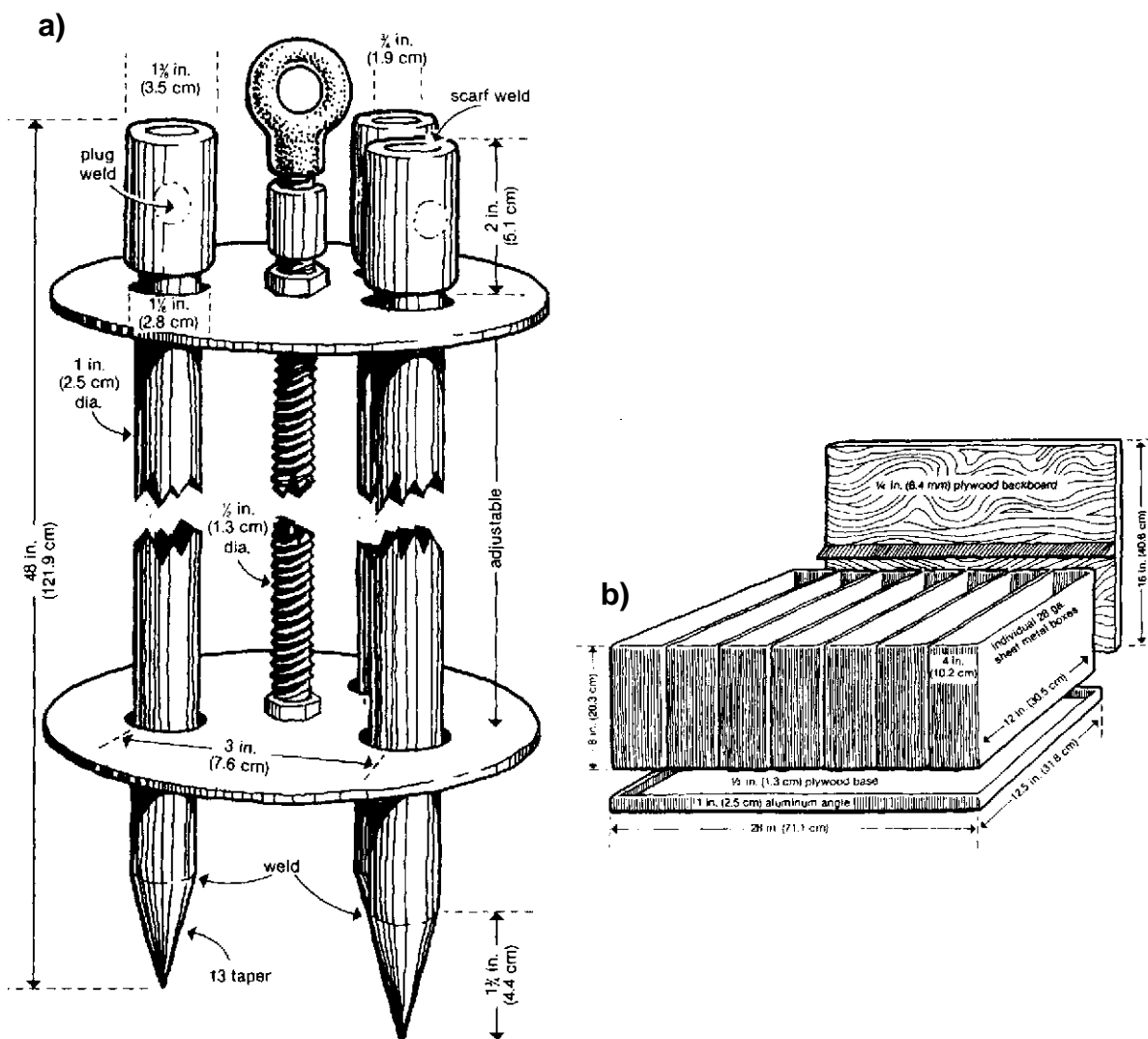


Fig. 4.29 a and b: (a) Tri-tube freeze-core sampler with templates to keep an even distance between the tubes (Reprinted from Platts et al. (1983)); (b) A slotted sheet metal box for subsampling and analysis of the sediment stratigraphy (Reprinted from Platts et al. (1983)).

Section 5.4.1.1), or if the 1% criterion is applied, for particles smaller than 40 mm. Repeated samples have to be taken to analyze the size distribution of larger particles, unless the study aim justifies a truncation of the particle-size distribution, as is often necessary when determining the percent fines.

Freeze-core samples have irregular shapes that depend on how far the freezing advanced outward from the rod. Irregular core shapes can cause an unrepresentative particle-size distribution of the sample. Large particles that are only partially frozen to the core might be lost during retrieval. Because large particles occur most frequently near the bed surface, but are likely to be lost during the sample retrieval, freeze-core samples tend to underrepresent the coarse particles of the armor layer. Conversely, a few large particles frozen to the core can dominate the sample mass and underrepresent the amount of fine sediment (Rood and Church 1994). However, Thoms (1992) found that freeze-core samples are more representative of the true bed-material particle-size than grab samples. A comparative study by NCASI (1986) found that tri-tube samples underestimate the percent fines smaller 4 mm to a lesser extent than single-tube freeze-cores. Repeated tri-tube samples also have a lower variability in measured percent fines than single-tube samples. Ramos (1996) summarizes various studies comparing freeze-core samples with samples from the McNeil and other samplers.

#### 4.2.4.9 Resin cores

Resin cores of sediment are obtained by pouring liquid resin into a small vertical hole that is created by forcing and retrieving a rod into the bed material. The hole may be approximately 1 m deep. Due to its viscosity, resin penetrates farther into the sediment when pore spaces are large, thus collecting large volumes of porous sediment layers and small volumes of tightly packed sediment layers. Resin cores can only be granulometrically analyzed by cutting the hardened core and applying thin section techniques used for sandstone or conglomerates (Adams 1979; Neumann-Mahlkau 1967). Resin cores, however, provide an excellent visual image of the bed stratigraphy.

#### 4.2.4.10 Hybrid samplers: combined pipe and freeze-core sampler, or excavated freeze-cores

Rood and Church (1994) developed a hybrid sampler that combines the advantages of a McNeil and a freeze-core sampler: it produces a predefined sample volume contained within a pipe and a core that can be analyzed stratigraphically. The hybrid sampler has two major components: (1) a toothed pipe, or core barrel, 0.2 m in diameter with an upward extension pipe 1 m long and 0.065 m in diameter, and (2) a freeze-core probe 1.5 m long, and 0.05 m in diameter with a hardened tip (Fig. 4.30).

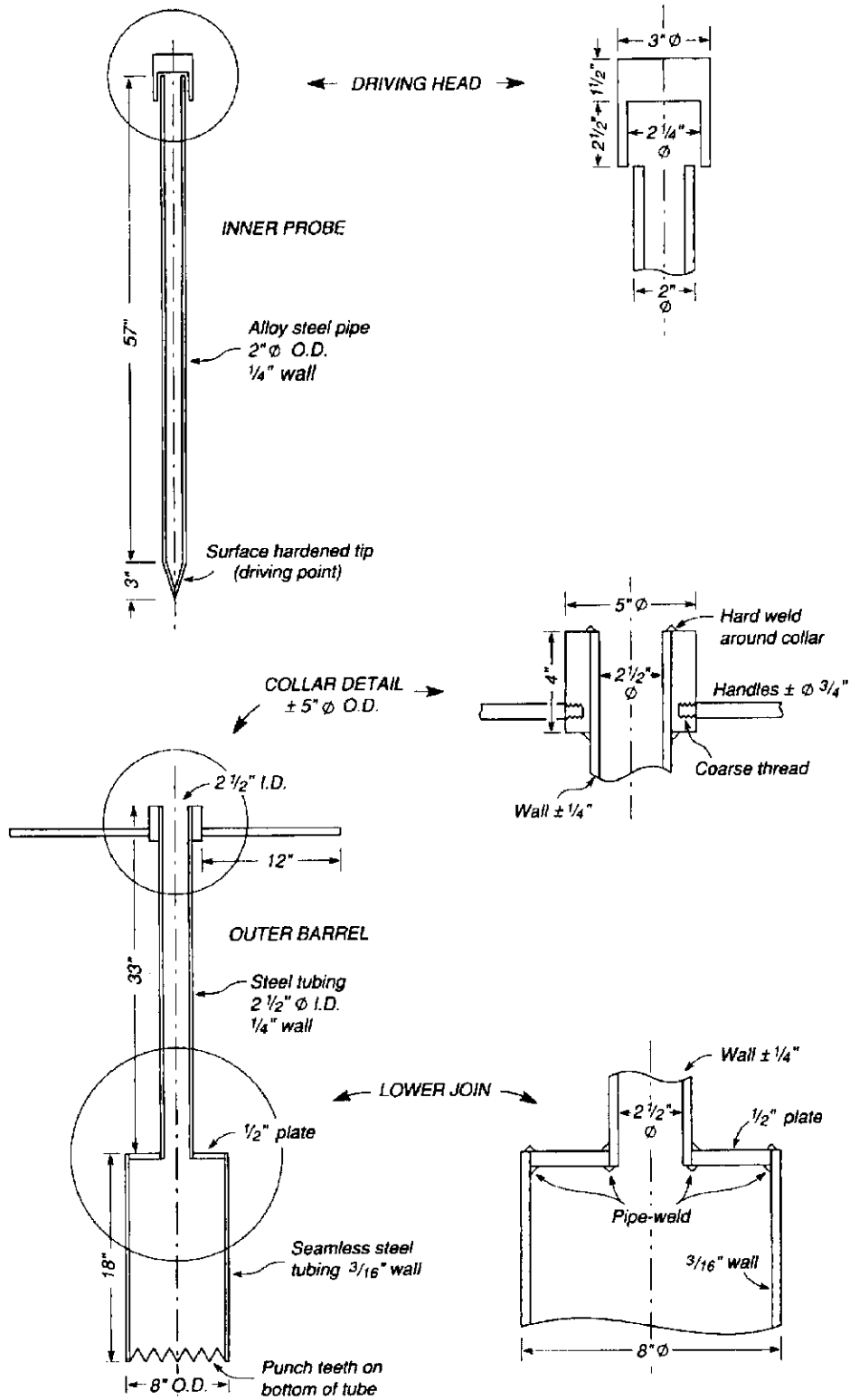


Fig. 4.30: Hybrid sampler. Manufacturing drawings for the outer barrel and the inner probe of the freeze-corer. Some lines in the drawing have been shortened for compact presentation. (Reprinted from Rood and Church (1994), by permission of the American Fisheries Society.)

The hybrid sampler is designed for use in gravel beds and is particularly useful for analyzing spawning gravel that contain no cobbles. Two people work the core barrel into the gravel bed to a minimum depth of 0.3 m, the depth of redds built by spawning salmonid fish. The freeze-core probe is placed inside the extension pipe and driven into the bed with a sledgehammer, until the tip of the probe extends below the bottom of the core barrel. 6 - 8 liters of liquid nitrogen are poured into the freeze-core probe. After approximately 5 minutes the sample is frozen. The core barrel is twisted to break the freezing at the bottom of the core and then lifted out of the bed by one or two people. A small inflatable raft is useful for transporting the core to the bank. The frozen core is removed from the core barrel, and particles frozen to the freeze-core probe are either chipped off with a hammer or the entire sample is left to thaw. The sample can be split into several layers before bagging.

Maximum sample volume of the hybrid sampler is approximately 10 liters or the volume of a household pail. Maximum sample mass is about 13.5 kg. Repeated samples are necessary to obtain a sample mass sufficiently large to analyze a particle-size distribution that extends into the cobble range. The hybrid sampler can be used in any wadable flow, but is restricted to gravel beds with particles smaller than 128 mm. Due to the heavy equipment and the large amount of liquid nitrogen needed for repeated sampling, road access to the sampling site is desirable.

#### **4.2.5 Volumetric sampling in deep water**

If water becomes too deep for wading, bed material can either be sampled by one of the methods described in Section 4.2.4 using trained divers, or an attempt can be made to sample bed material using towed dredges (Burrows et al. 1981). Dredges are pipes or boxes with a cutting edge or teeth at the front and a mesh screen or a mesh bag at the back end (Fig. 4.31). As the dredge is pulled over the stream bottom, the cutting edge cuts a few cm into the bed material while the forward motion accumulates the sediment inside the dredge. Water moves through the dredge and out the screen at the tail end. Dredges are best used for sampling relatively fine and unstratified sediment. Hilton and Lisle (1993) and Lisle and Hilton (1999), for example, used a pipe dredge to sample fine sediment accumulated in pools (Section 6.6.2).

It is difficult to obtain representative samples with dredges in deep streams with coarse beds. Pipe dredges must be sufficiently heavy to dig into the bed and large enough to accommodate the largest bed-material particles. Towed box dredges must have a properly adjusted cable length to maintain a horizontal position. Surface and subsurface sediment is mixed in a dredged sample, so that the percent surface or subsurface sediment contained in the sample is unknown. The maximum particle size that can be sampled depends on the dredge opening. The likelihood of collecting a particle with a diameter close to that of the dredge opening is rather small. Sample volume depends on the size of the dredge, which in turn depends on whether the dredge is operated by hand or by machinery. Another drawback is that sediment collected with towed dredges can not be designated to a specific streambed location, and the rate of fill can vary as the dredge is towed.

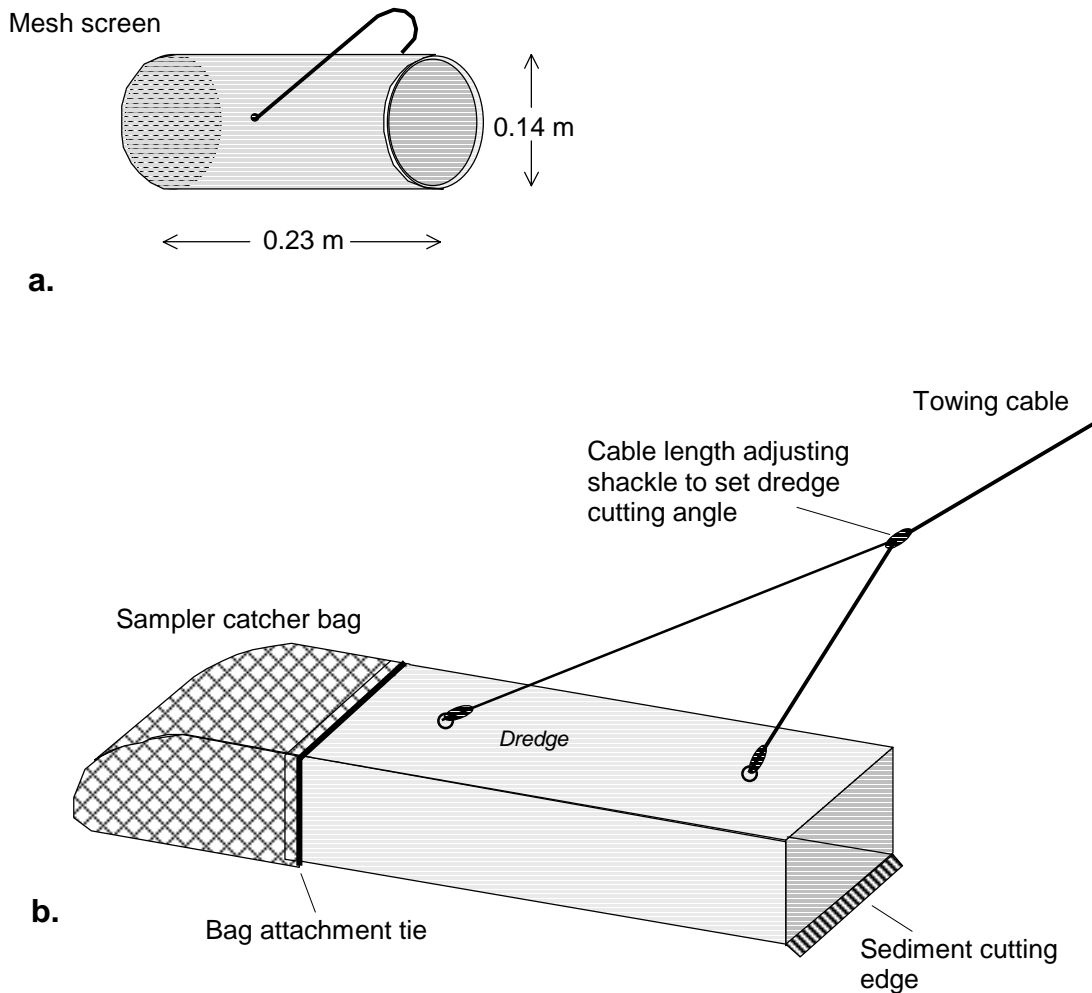


Fig. 4.31: (a) Pipe dredge for gravel sediment; (Redrawn from Yuzyk (1986)). (b) Box dredge; (Redrawn from Lewis and McConchie (1994), by permission of Chapman and Hall).

If the surface sediment size is a concern in streams with coarse beds, underwater photos taken by divers and analyzed by the photo-sieving method (Section 4.1.3.3) (Ibbeken and Schleyer 1986) is an alternative to dredging. Underwater photo sieving requires clear water and a water depth of more than 2 m.

### 4.3 Conversion of sample distributions: grid - areal - volume, and number - weight

Bed-material samples may be obtained by three different techniques: grid samples (i.e. pebble counts) (Sections 4.1.1 and 4.1.2), areal samples (Section 4.1.3), and volumetric samples (Section 4.2.1). Particle-size distributions can be analyzed by a number frequency of particles per size class (by-number), or a frequency-by-weight (by-weight). The three methods of sampling (grid, areal, and volumetric) and two methods of particle-

size analysis (by number and by weight) may be combined to six possible ways of sampling and analyzing bed-material. The terminology describing the methods of both sampling and analysis is as follows: a grid-by-number sample refers to a grid sample analyzed by a number frequency (abbreviated by g-n); an area-by-weight sample refers to an areal sample analyzed by its weight frequency (a-w). The terminology for the other combinations of sampling and analysis follows the same pattern. Analyzing a volumetric sample by a number-frequency (volume-by-number) is theoretically possible, but usually not very practical, and therefore not further discussed.

If streambeds span a wide range of particle sizes, several methods of sampling or analysis may have to be employed to representatively sample all particle sizes at one site, an approach called hybrid sampling. Boulders, for example, can only be included in a surface sample if a widely spaced pebble count is used, whereas representative sampling of fine surface sediment requires an areal sample. Another example is the comparison of surface and subsurface sediment. The surface may be sampled with an areal sample, while the subsurface is sampled volumetrically. Meta-studies that analyze bed-material samples from previous studies in a new context are likewise faced with samples taken or analyzed by different techniques.

Different methods of sampling and analysis applied to the same deposit produce different particle-size distributions. Area-by-weight samples, for example, have coarser distributions than volume-by-weight samples from the same deposit. Thus, before samples derived from different sampling methods can be combined or compared (Section 4.4), their size distributions have to be transformed into the size distribution of the same sample and analysis category.

Several methods have been proposed for conversion of particle-size distributions between different categories of sampling and analysis. Kellerhals and Bray (1971) introduced the voidless cube model as a means to explain the different particle-size distribution that may result from the five categories of sampling and analysis. They proposed factors for the conversion of a particle-size distribution obtained by one method of sampling and analysis into the distribution obtained by another method of sampling and analysis. Diplas and Fripp (1992) introduced the modified cube model to explain that differences between observed and computed conversions between areal and volumetric samples are due to sediment characteristics and the penetration depth of the adhesive used for areal sampling. Fraccarollo and Marion (1995) argued that the assumed similarity between grid-by-number and volume-by-weight samples does not hold when a more realistic model of surface particles is applied (split plane surface model). Also, because it is difficult to make the adhesive penetrate to exactly a specific depth, Marion and Fraccarollo (1997) based the conversion between areal and volumetric samples on a computed penetration depth of the adhesive.

### 4.3.1 Voidless cube model

Kellerhals and Bray (1971) used a model deposit comprised of a mixture of three cube sizes packed without voids (voidless cube model) (Fig. 4.32) to determine conversion factors between the various combinations of sampling method and sample analysis. The cube model represents an idealized deposit of spheres in a systematic and loose, but voidless packing. The cubes have the three sizes of  $D_1 = 1$ ,  $D_2 = 2$ , and  $D_3 = 4$  (any linear unit, e.g., cm). The surface area  $A$  taken up by particles with a size of  $D_1$ ,  $D_2$ , and  $D_3$  is  $A = D^2$  and yields  $A_1 = 1$ ,  $A_2 = 4$ , and  $A_3 = 16$  (e.g.,  $\text{cm}^2$ ), respectively. Particle volume is computed by  $V = D^3$  and yields  $V_1 = 1$ ,  $V_2 = 8$ , and  $V_3 = 64$  (e.g.,  $\text{cm}^3$ ). Cubes of each size class take up the same portion of the total volume, i.e., 33.33%. A particle density of 1 is assumed, so that volume equals weight. The number of particles of the sizes  $D_1$ ,  $D_2$ , and  $D_3$  contained in the total sediment volume is  $n_1 = 4608$ ,  $n_2 = 576$ , and  $n_3 = 72$ . The number of surface particles  $n_{surf,1} = 192$ ,  $n_{surf,2} = 48$ ,  $n_{surf,3} = 12$  (Table 4.5 a and b).

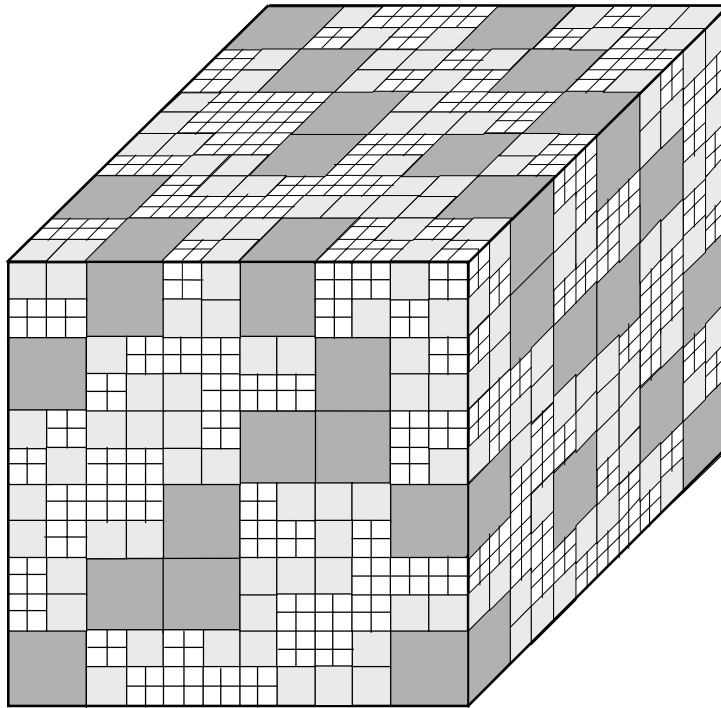


Fig. 4.32: Model of densely packed cubes (voidless cube model) developed by Kellerhals and Bray (1971). (Redrawn from Kellerhals and Bray (1971), by permission of the American Society of Civil Engineers).

Tables 4.6 a and b demonstrate the different particle-size distributions that are obtained if particles from a deposit mimicked by the voidless cube model are sampled and analyzed by different methods. The particle-size distribution of an area-by-weight sample, for example, is simulated by multiplying the number of surface particles per size class with

their respective volume. The resulting values are then expressed as percent frequencies (Table 4.5 a). A grid-by-number sample is simulated by multiplying the number of surface particles per size class by their area (Table 4.5.b).

The cumulative frequency distributions obtained by sampling the voidless cube model with grid, areal, and volumetric methods analyzed by a weight and a number frequency are plotted in Fig. 4.33. The voidless cube model yields the same particle-size distribution for volume-by-weight and grid-by-number samples. Area-by-weight and grid-by-weight samples are coarser than volume-by-weight or grid-by-number samples, whereas area-by-number and volume-by-number samples are considerably finer. The  $D_{50}$  of the area-by-number sample is smaller than the  $D_{50}$  of the volume-by-weight and grid-by-number sample by a factor of 1.5, whereas the  $D_{50}$  of the area-by-weight sample is a factor of 1.5 coarser.

Table 4.5 a: Particle-size distributions obtained from collecting volumetric, areal and grid samples from the voidless cube model and analyzing the samples by a weight frequency (i.e., volume-by-weight, area-by-weight, and grid-by-weight samples).

$D$	(vol.-by-number)			<u>vol.-by-weight</u>		$n_{surf}$	<u>area-by-weight</u>		<u>grid-by-weight</u>	
	$A=D^2$	$V=D^3$	$n$	$n \cdot V$	%		$n_{surf} \cdot V$	%	$n_{surf} \cdot A \cdot V$	%
1	1	1	4608	4608	33.3	192	192	14.3	192	1.4
2	4	8	576	4608	33.3	48	384	28.6	1536	11.0
4	16	64	72	4608	33.3	12	768	57.1	12288	87.7
$\Sigma$			5256	13824	100.0	252	1344	100.0	14016	100.0

$D$  = particle size, e.g., in cm;  $A$  = particle area;  $V$  = particle volume which equals weight if a particle density of 1 is assumed;  $n$  = number of the particles per size class; % = percent frequency;  $n_{surf}$  = number of surface particles per size class.

Table 4.5 b: Particle-size distributions derived by collecting areal and grid samples from the voidless cube model and analyzing the samples by a number frequency (i.e., area-by-number, and grid-by-number samples). The volume-by-weight sample is shown for comparison.

$D$	$A=D^2$	$V=D^3$	$n$	<u>vol.-by-weight</u>		<u>area-by-number</u>		<u>grid-by-number</u>	
				$n \cdot V$	%	$n_{surf}$	%	$n_{surf} \cdot A$	%
1	1	1	4608	4608	33.3	192	76.2	192	33.3
2	4	8	576	4608	33.3	48	19.0	192	33.3
4	16	64	72	4608	33.3	12	4.8	192	33.3
$\Sigma$			5256	13824	100.0	252	100.0	576	100.0

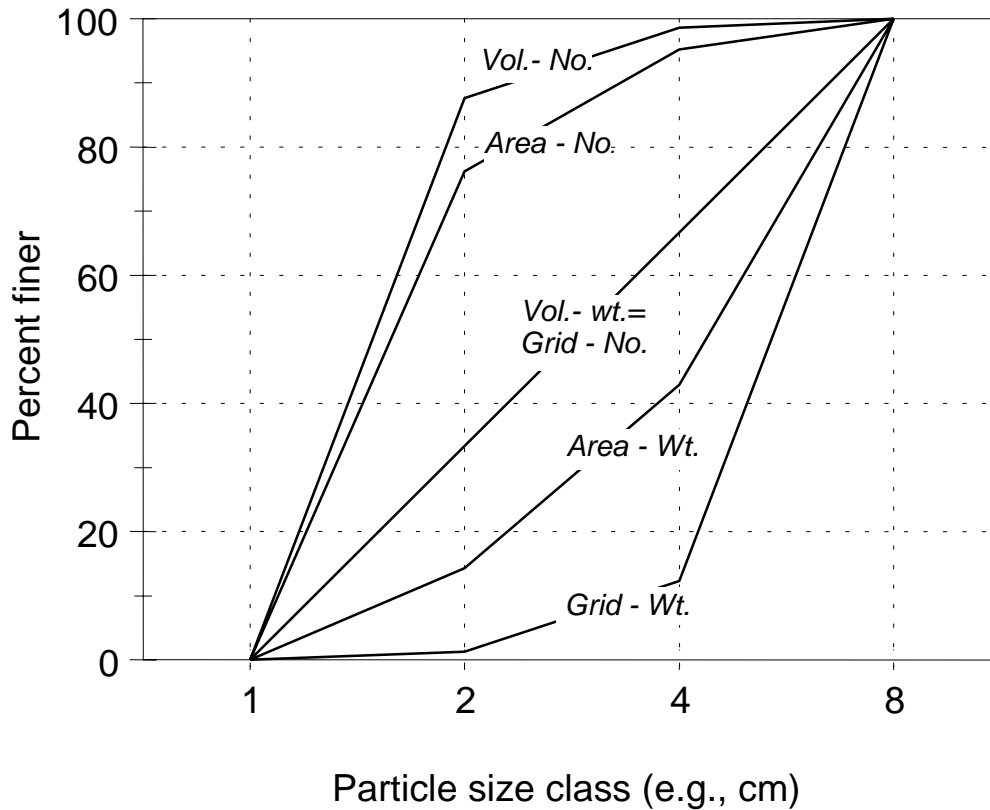


Fig. 4.33: Cumulative frequency distributions obtained for various sample and analysis methods of particles from the voidless cube model by Kellerhals and Bray (1971). Vol. - No. = volume-by-number sample, Area - wt. = area-by-weight sample; other abbreviations are likewise derived.

### Conversion factors

Conversion factors consist of two parts: the conversion between methods of particle-size analyses (weight or number frequency), and the conversion between the various sampling methods (grid, areal, and volumetric). Table 4.5 a and b show that the difference between a by-number and by-weight sample is the factor  $V$  (particle volume) or  $D^3$ . Thus, converting a number frequency to a weight frequency requires multiplying the weight frequency of particles per size class by the particle size cubed ( $D^3$ ). Conversely, multiplying the weight frequency of particles per size class by the reciprocal of their cubed particle size ( $1/D^3$ ) yields the distribution in terms of frequency-by-number.

The conversion system is similar between samples that are analyzed alike, but sampled with different methods. Table 4.5 a and b show that the difference between volume and grid samples is a factor of  $V$  or  $D^3$ . Thus, a particle-size distribution of a volumetric sample yields the particle-size distribution of a grid sample when the frequency of all particle-size classes is multiplied by  $D^3$ , whereas multiplication by the factor  $1/D^3$  converts a grid sample to a volumetric sample. Converting a volumetric sample to an areal sample requires multiplication by the factor  $D$ , whereas the conversion from an areal sample to a volumetric one requires multiplication by  $1/D$ . Finally, a factor of  $D^2$  converts an areal sample into a grid sample, and  $1/D^2$  converts a grid sample into an

areal sample, assuming the same method of analysis in both cases. Table 4.6 summarizes these factors. Conversion factors assume spherical particles for which the sieve diameter  $D$  approaches the nominal diameter  $D_n$  (Eq. 2.1 in Section 2.1.2), a voidless particle packing, and the same density for all particles. In a strict sense, the conversion factors in Table 4.6 apply only to these conditions. If used for deposits with other properties, the conversion factors yield only an approximation.

Table 4.6: Conversion between samples analyzed or sampled by different methods.

Conversion from → to:	Factor
<u>Different methods of analysis:</u>	
weight frequency → number frequency . . .	$1/D^3$
number frequency → weight frequency . . .	$D^3$
<u>Different sampling methods:</u>	
volume → grid . . . . .	$D^3$
grid → volume . . . . .	$1/D^3$
volume → area . . . . .	$D$
area → volume . . . . .	$1/D$
area → grid . . . . .	$D^2$
grid → area . . . . .	$1/D^2$

The two parts of a conversion factor, one that accounts for converting sampling methods, and one that accounts for converting different methods of analysis, need to be applied together when converting particle-size distributions obtained by different methods of sampling *and* by different analysis. For example, to convert a volumetric sample analyzed on the basis of weight frequency (volume-by-weight) to an areal sample analyzed on the basis of a number frequency (area-by-number), the frequency distribution needs to be multiplied by the product of  $D \cdot 1/D^3$  ( $D$  for conversion of volume → area) and  $1/D^3$  for conversion of weight → number-frequency. The product  $D \cdot 1/D^3$  is then simplified to  $1/D^2$ . Similarly, the conversion of a volume-by-weight sample to a grid-by-number sample is obtained by applying the factor  $D^3 \cdot 1/D^3 = 1$ , which means that both particle-size distributions are identical and do not require any conversion in order to be compared or combined. Table 4.7 lists the conversion factors used for the various combinations of sample methods and methods of analysis.

Conversion factors are also expressed in terms of the exponent that  $D$  takes in the conversion factor. A conversion factor of  $1/D^2 = D^{-2}$  is then referred to as using an exponent of -2 for the conversion.

Table 4.7: Conversion factors for samples collected by various methods (from Kellerhals and Bray 1971). Numbers in the gray bars express the conversion factor as the exponent of  $D$ .

Conversion from	Conversion to				
	Volume-by-weight	Grid-by number	Grid-by weight	Area-by number	Area-by weight
Volume-by-weight	1 0	1 0	$D^3$ 3	$1/D^2$ -2	$D$ 1
Grid-by number	1 0	1 0	$D^3$ 3	$1/D^2$ -2	$D$ 1
Grid-by weight	$1/D^3$ -3	$1/D^3$ -3	1 0	$1/D^5$ -5	$1/D^2$ -2
Area-by number	$D^2$ 2	$D^2$ 2	$D^5$ 5	1 0	$D^3$ 3
Area-by weight	$1/D$ -1	$1/D$ -1	$D^2$ 2	$1/D^3$ -3	1 0

### Converting a particle-size distribution

Table 4.8 shows how a particle-size distribution is transformed, using the example of an area-by-weight sample that is converted to a grid-by-number sample. To apply the conversion factors (Table 4.7) to a particle-size distribution (Table 4.8), particle size  $D$  is

Table 4.8: Conversion of an areal sample expressed as weight frequency (area-by-weight) to a surface grid sample expressed as number frequency (grid-by-number) (slightly modified from Kellerhals and Bray 1971).

Size class $D_i$ (mm)	area-by-weight			Center of class $D_{ic}$ (mm)	grid-by-number		
	Freq. (%)	Cum freq. (%)			adj. to 100%	Freq. (%)	Cum. Freq. (%)
2.8	2	0		3.3	0.60	11.7	0.0
4	1	2		4.8	0.21	4.1	11.7
5.67	2	3		6.7	0.30	5.8	15.8
8	5	5		9.5	0.53	10.3	21.6
11.3	13	10		13.4	0.97	18.9	31.9
16	17	23		19.0	0.89	17.5	50.8
22.6	19	40		26.9	0.71	13.8	68.3
32	22	59		38.1	0.58	11.3	82.1
45.3	16	81		53.8	0.30	5.8	93.4
64	3	97		76.1	0.04	0.8	99.2
90.6	0	100		0.0			100.0
total:	100				5.11	100.0	

expressed by the center of class  $D_{ic}$  which is computed from the geometric mean particle size (Section 2.1.5.3) of the size fraction (equal to the logarithmic mean of particle sizes in mm, or arithmetic mean of particle sizes in  $\phi$ -units). The cumulative frequency distributions of the area-by-weight sample converted into a grid-by-number sample are shown in Fig. 4.34.

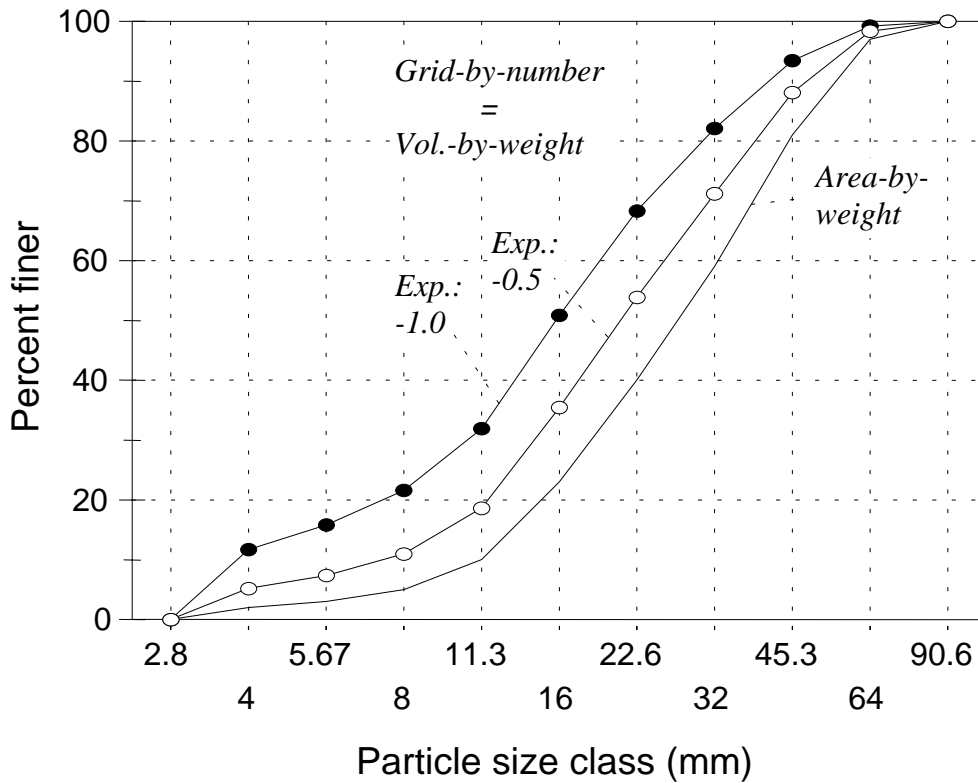


Fig. 4.34: Particle-size distribution of the area-by-weight sample in Table 4.8 converted into a grid-by-number sample (or volume-by-weight sample) using a conversion factor of  $1/D$  ( $= -1.0$ ) (after Kellerhals and Bray 1971) and using a conversion factor of  $-0.5$  as proposed by Parker (1987).  $D_{50}$  particle sizes are 27.6 mm for the area-by-weight sample, 15.7 mm for the grid-by-number and volume-by-weight samples using a conversion factor of  $-1.0$ , and 20.6 mm for a conversion factor of  $-0.5$ .

The geometrically-based conversion factors obtained from the voidless cube model yielded perfect results in the mutual conversion of a grid-by-weight to a grid-by-number frequency and confirmed earlier results by Sahu (1964) and Leopold (1970). Kellerhals and Bray (1971) concluded that their conversion factors should be applicable to any sediment and that grid-by-number and volume-by-weight analysis should yield identical results when applied to non-stratified gravel beds. The convertibility of the two methods was confirmed by Church et. al. (1987) who used different sampling methods on a gravel mixture that was shaken in a closed box to form a random, non-stratified, homogeneous deposit. Even when tested on bed material taken from various Alberta streams, the conversion factors yielded acceptable results. Note, however, that most gravel-bed

rivers, and especially mountain streams, are vertically stratified (Section 3.2); surface sediment is coarser than subsurface sediment. Consequently, surface pebble counts correctly indicate a coarser particle size-distribution than the volumetric sample of the subsurface sediment.

### ***Controversies about conversion factors***

Several studies have observed that the conversion factors proposed by Kellerhals and Bray (1971), particularly the conversion between areal and volumetric samples, do not apply under all circumstances. The observed incompatibility has been attributed to the over-simplified description of bed-material surfaces by the voidless cube model.

### **4.3.2 Modified cube model**

The voidless cube model by Kellerhals and Bray (1971) indicates a factor of  $1/D$  (i.e., an exponent of  $D$  of -1) for converting an area-by-weight sample into a volume-by-weight sample for homogeneous material. However, when applied to gravels from stratified and armored deposits, researchers found that the conversion factor exponent of -1 yielded grain-size distributions that are too fine (Ettema 1984). Gomez (1983), Anastasi (1984), Parker (1987), Diplas and Sutherland (1988), and Diplas (1989) proposed substituting the exponent with a value of approximately -0.4 to -0.5. An exponent of -0.5 refers to a conversion factor of  $1/D^{-0.5}$ . Fig. 4.34 shows that a conversion factor of  $1/D^{-0.5}$  (i.e., and exponent of -0.5) provides a less fine distribution of the area-by-weight sample converted to volume-by-weight or grid-by-number sample than an exponent of -1.

The necessity of raising the exponent from -1 to approximately -0.5 is a result of an opposing sampling bias for fine sediment in surface grid counts and areal samples. Surface grid samples or pebble counts easily neglect fine particles in voids, whereas in areal samples a deep penetration of the adhesive into subsurface sediment may collect more fines than present in the surface layer. The inclusion of surface fines by adhesive areal samples produces a finer surface-size distribution than surface grid samples. Based on this observation, Diplas and Sutherland (1988) developed the hypothesis that the exponent needed in the conversion factor of area-by-weight to volume-by-weight depends on the depth to which surface particles are actually included into the areal sample. To illustrate their point, they modified the voidless cube model used by Kellerhals and Bray (1971) (Fig. 4.32) into a void-containing cube model, in which voids take the same size and volume as the size and volume of the smallest particle-size class. This resulted in a cube model with 33% porosity, a value typical of fluvial deposits.

An adhesive areal sample of a deposit with surface voids is likely to include small particles from the next layer under a surface void. These small particles would not have been extracted by a sampling method such as adhesive tape that is truly restricted to surface particles only. Modeling adhesive areal samples from the modified porous cube model, Diplas and Sutherland (1988) and Diplas (1989) obtained finer particle-size distributions for an areal sample than predicted by the voidless cube model of Kellerhals and Bray (1971). Diplas and Sutherland (1988) and Diplas (1989) determined that an

exponent of -0.42 was an appropriate conversion factor for areal samples obtained using adhesives. The general validity of a conversion exponent of -0.4 to -0.5 was confirmed in subsequent laboratory experiments.

***Effect of porosity, sediment size, sorting, and sampling depth on the conversion exponent***

Based on previous findings which suggested that the exponent might shift from -1.0 to -0.5 for sediment that is more porous, finer in particle size, and better sorted, Diplas and Fripp (1991) conducted a study to specifically address these issues. The void-containing cube model determined a pronounced decrease of conversion exponents from 0 to -0.5 for very-well sorted deposits with a ratio of  $D_{90}/D_{10}$  smaller than 2.5, whereas poorly sorted deposits with a ratio of  $D_{90}/D_{10}$  larger than 8 required conversion factors of -0.8 to -0.9. However, the dependency on sediment sorting was less pronounced in laboratory experiments.

A series of experiments by Diplas and Fripp (1992) showed that the depth (and thus the conversion factor) at which an areal sample becomes volumetric depends on several factors of the particle-size distribution for the sediment used in the experiments. Areal wax samples were taken from different mixtures of framework-supported (sand content < 20 or 25%) and matrix-supported gravels (sand content > 30%) (see Fig. 3.14 a and 3.14 d). The abundance of fine sediment in matrix-supported gravels prevented the deep penetration of the wax, rendering the sample a true surface sample for which the conversion factor exponent of -1, established by Kellerhals and Bray (1971), is generally valid. Similarly, if an adhesive tape that only picks up true surface particles was used for sampling, the conversion exponent should be -1, as predicted by Kellerhals and Bray (1971). Laboratory experiments confirmed these results with exponents ranging from -0.9 to -1.19.

For framework-supported gravels, the penetration of wax was generally deeper, but depended on the overall particle size of the mixture. In coarse framework-supported sediment mixtures, areal wax samples required a conversion factor exponent of -0.5, while for generally fine framework-supported gravels, the conversion factor exponent varied between -0.5 and +0.5, with an average of 0.

An exponent of -1 should be appropriate for converting area-by-weight particle-size distribution produced from photo-sieving into a grid-by-number (e.g., for comparison with pebble counts) or volume-by-weight distribution. Particles smaller than 10 mm, which could potentially be part of the subsurface and require a conversion factor larger than -1.0 (i.e., towards -0.5) are explicitly excluded from a photo sieving analysis. Table 4.9 summarizes the results of the findings.

Table 4.9: Approximate value of the conversion factor exponent required for converting the particle-size distribution of an area-by-weight sample into a volume-by-weight sample in deposits of different characteristics, based on results of several studies.

Approximate value of the conversion factor exponent		
-1.0	-0.5	→ 0
Determined from voidless cube model (Kellerhals and Bray 1971)	Determined from void-containing cube model (Diplas and Sutherland 1988)	
Coarse and fine matrix-supported gravel with high sand content	Frame-work supported gravel, esp. coarse gravel deposits	Fine frame-work gravels
Deposits of low porosity	Deposits of high porosity	
Coarse gravel deposits	Deposits of fine gravel and sand	
No depth penetration of adhesive e.g., adhesive tape	Deep penetration of adhesive into subsurface sediment	
Poorly sorted gravel deposits	Well-sorted gravel deposits	Very-well sorted gravel
Photo-sieving		

### 4.3.3 Conversion based on computed penetration depth

Many applications require a particle-size distribution in terms of volume-by-weight, but surface sediment can only be sampled by a surface grid sample (i.e., pebble count) (fine - coarse gravel) or an areal sample (sand - fine gravel). Conversion of an area-by-weight to a volume-by-weight particle-size distribution is problematic, because the exponents for the conversion vary with the adhesive penetration depth which in turn depends on factors such as sorting, particle-size, porosity, and on the adhesive viscosity (Section 4.3.2). The combination of these factors makes it difficult to control the exact penetration depth.

To avoid these problems, Marion and Fraccarollo (1997) developed a conversion procedure in which the exact depth of penetration is irrelevant. The conversion algorithm computes the adhesive penetration depth  $d_p$  which is then used to compute the particle-size distribution of the corresponding volume-by-weight distribution for each size class ( $p_{i,0}$ ). The algorithm is applicable over a range of penetration depths and can account for the case in which the adhesive penetrates so deeply that the presumed areal sample is in fact volumetric. In this case, the conversion procedure does not produce a different distribution.

The penetration depth  $d_p$  of the adhesive is computed from

$$m_{tot} = \sum_{j=1}^k m_j = \frac{\rho_s A_s (1 - p_{v,0})}{\sum_{j=1}^k p_{j;a-w} / (d_p + D_i/2)} \quad (4.7)$$

$m_{tot}$  is the total weight of the sample,  $k$  is the number of size classes,  $m_j$  is the weight of the  $j$ th size class,  $\rho_s$  is sediment density,  $A_s$  is the sampling area covered by the areal sample,  $p_{v,0}$  is the porosity and set to a value within the range 0.3 – 0.4,  $p_{j;a-w}$  is the weight fraction of the  $j$ th size class for the area-by-weight sample ( $m_j/m_{tot}$ ),  $d_p$  is the adhesive penetration depth, and  $D_i$  is the particle size of the  $i$ th size class.

Eq. 4.7 is solved iteratively, using the size of the  $D_{50}$  particle as a starting value for  $d_p$ . The denominator is solved for all size classes and summed. The numerator is solved next and is constant for all size classes. The total weight of the sample  $m_{tot}$  computed from Eq. 4.7 is compared with the actual measured sample weight.  $d_p$  is then adjusted until the computed  $m_{tot}$  matches the measured  $m_{tot}$ . The resulting value of  $d_p$  is the penetration depth and usually corresponds to a particle size between the  $D_{20}$  and the  $D_{80}$ . The percentage of total volume occupied by particles of the  $i$ th size fraction,  $p_{i,0}$  is computed from Eq. 4.8.

$$p_{i,0} = \frac{p_{i;a-w} (1 - p_{v,0})}{(d_p + D_i/2) \sum_{j=1}^k p_{j;a-w} / (d_p + D_j/2)} \quad (4.8)$$

An example computation is provided in Table 4.10. The three particle-size distributions of the original area-by-weight sample, the converted volume-by-weight sample, and an actual volume-by-weight sample taken from the deposit (last column of Table 4.10) are plotted in Fig. 4.35.

#### 4.3.4 Split plane surface model

The voidless cube model used by Kellerhals and Bray (1971) for conversion between different methods of sampling and analysis determined that grid-by-number and volume-by weight samples of unstratified deposits have the same distribution and are therefore directly comparable. However, Fraccarollo and Marion (1995) caution that a voidless cube model is a poor representation of a real sediment deposit and not generally applicable. They proposed that if voids were properly accounted for both in a modeled sediment surface as well as in the sampling process, grid-by-number samples would have finer distributions than volume-by-weight samples. Consequently, the correspondence between grid-by-number and volume-by-weight samples may be considered a sampling artifact, caused by neglecting the presence of voids in the voidless cube model, as well as by neglecting to sample particles in voids when doing pebble counts.

Table 4.10: Example computation of the adhesive penetration depth  $d_p$  and the particle-size distribution of the converted volume-by-weight sample  $p_{i,0}$ , using the parameter listed below.

$\rho_s$ (g/mm <sup>2</sup> ):		0.00265		$d_p$ (mm) comp., (start with $D_{50}$ ):		4.0		
$A_s$ (mm <sup>2</sup> ):		14,000		$m_{tot}$ (computed from Eq. 4.7) (g):		146.2		
$p_{v,0}$ (-):		0.32						
$D_i$ (mm)	Area-by-weight sample				Converted vol.-by-weight sample			Vol. sample
	$m_i$ (g)	$P_{i,a-w}$ (-)	$P_{i,a-w}$ (% finer)	$P_{j,a-w}/(d_p+D_i/2)$ (Eq. 4.7, denominator) (1/mm)	$P_{i,0}$ (Eq. 4.8) (-)	$P_{i,0}$ (%)	$P_{i,0}$ (% finer)	$P_{i,v-w}$ (for comparison) (% finer)
0.18	5.8	0.040	0.0	0.010	0.037	5.7	0.0	0.0
0.25	4.4	0.030	4.0	0.007	0.027	4.2	5.7	5.0
0.35	3.0	0.020	7.0	0.005	0.018	2.8	9.9	10.0
0.5	3.0	0.020	9.0	0.005	0.018	2.8	12.7	14.0
0.7	2.9	0.020	11.0	0.005	0.017	2.7	15.4	17.5
1	2.2	0.015	13.1	0.003	0.013	2.0	18.1	20.0
1.4	5.1	0.035	14.6	0.007	0.028	4.3	20.1	22.5
2	6.6	0.045	18.1	0.009	0.034	5.2	24.4	26.0
2.8	28.5	0.019	22.6	0.036	0.136	21.0	29.7	33.0
4	39.4	0.027	42.1	0.044	0.169	26.1	50.6	54.0
5.6	21.9	0.150	69.1	0.022	0.082	12.8	76.7	78.5
8	13.1	0.090	84.1	0.011	0.042	6.5	89.4	90.0
11.3	8.7	0.059	93.1	0.006	0.023	3.6	95.9	94.0
16	1.5	0.010	99.0	0.001	0.003	0.5	99.5	98.0
22.6	<u>0.0</u>	<u>0.000</u>	100.0	<u>0.000</u>	<u>0.000</u>	<u>0.0</u>	100.0	100.0
total:	146.1	1.000		0.673	0.650	100.0		

Fraccarollo and Marion (1995) suggest that a more realistic model of a sediment surface is obtained by a sediment model consisting of a block of sediment with irregularly-shaped particles of various sizes that is split apart along a plane (imagine a split block of frozen sediment). In the model of the split plane, particles on the split line are assigned to that part of the split block in which their center of gravity is located (Fig. 4.36). The area under a large particle that was assigned to the other part of the block is likely to contain particles that are smaller than the large particle that was lost to the other side, especially in matrix-supported gravel. Sampling such a split surface by a grid-by-number sample includes a larger proportion of fines than a volume-by-weight sample and makes the grid-by-number sample similar to an area-by-number distribution of particle sizes.

The model of surface-particle sizes proposed by Fraccarollo and Marion (1995) has fine surface particles in very exposed positions directly at the surface. This particle arrangement is not representative of armored beds in which fine surface particles are generally scarce and are not found exposed, but hidden between large particles. The model proposed by Fraccarollo and Marion (1995) is more likely to represent surfaces in aggrading streams with ample fines between large particles. In such streams, surface grid-by-number counts may be finer than volume-by-weight samples. The proposed finer distributions of grid-by-number than volume-by-weight samples are also contingent upon

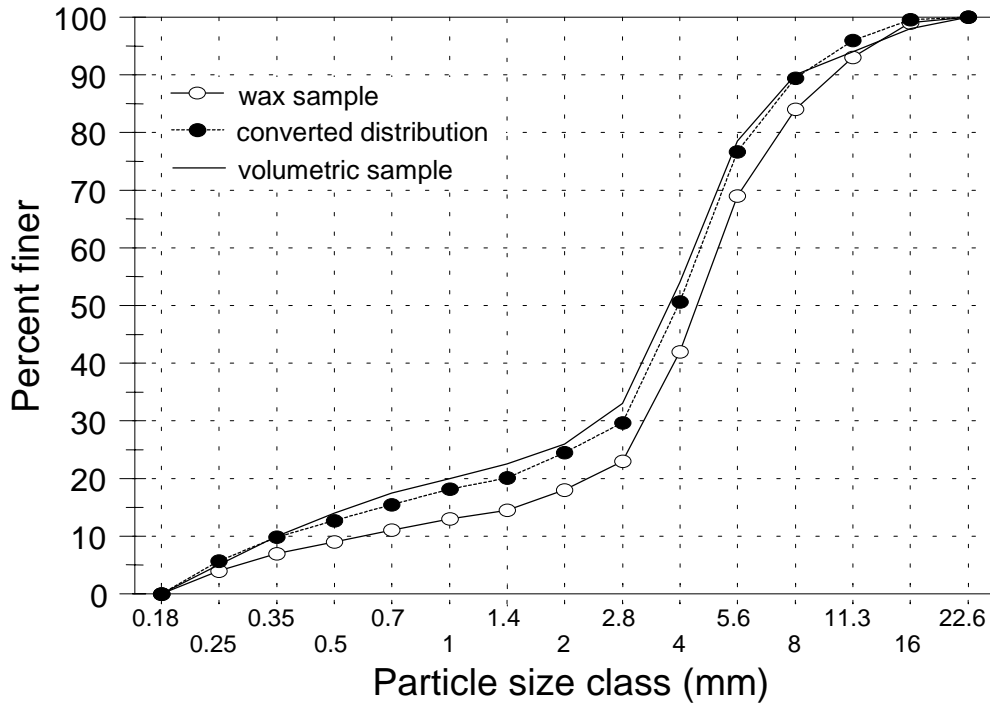


Fig. 4.35: Particle-size distribution of an area-by-weight sample collected from a surface comprised of sand and fine gravel ( $D_{50} \approx 4$  mm), and its conversion to a volume-by-weight equivalent. The distribution of a volume-by-weight sample is shown for comparison (based on data by Marion and Fraccarollo 1997).

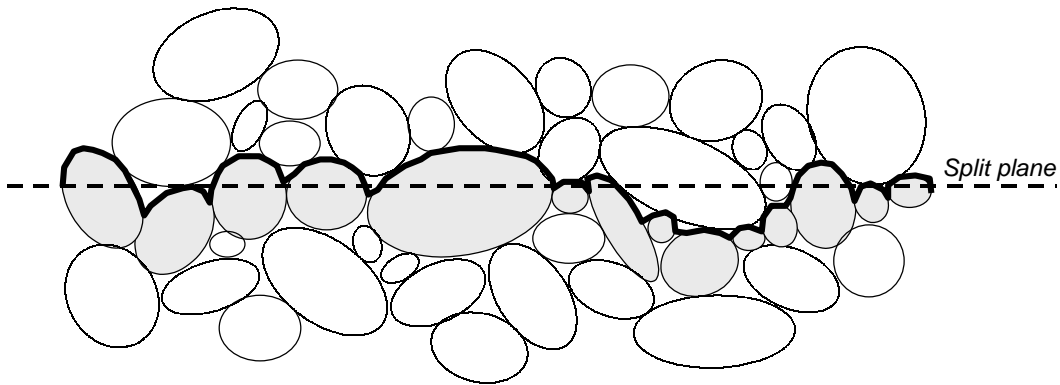


Fig. 4.36: Schematic of surface (gray particles) generated by split plane; Bold line indicates surface profile. (Redrawn from Fraccarollo and Marion (1995), by permission of the American Society of Civil Engineers.

accurate sampling of fine particles in interstitial voids. However, pebble counts on armored coarse gravel or cobble beds can not practically include interstitial fines to their full extent, especially not when the sample must be collected under water or under adverse conditions (Section 4.1.1.3). Thus, fines are underrepresented due to practical

restrictions of pebble counts or grid samples, and it seems that this underrepresentation brings grid-by-number samples into a relatively close correspondence with volume-by-weight distributions.

#### 4.4 Combination of two particle-size distributions

Fluvial deposits with wide particle-size distributions ranging from sand to boulders often require several sampling methods in order to sample all particle sizes present in the reach. Most sampling methods, however, sample only a portion of the bed-material particle-size distribution in a representative way. A surface pebble count (Section 4.1.1), for example, can representatively sample particle sizes between medium gravel and small boulders. However, pebble counts may not accurately characterize the sediment finer than 8, or 2 mm, depending on the sampling conditions. Areal samples, on the other hand, can accurately determine the fine part smaller than 40 mm of a sample, particularly if clay is used as an adhesive to collect the sample (Section 4.1.3.2). However, coarse gravels and cobbles cannot be sampled by areal methods. Thus, in order to characterize the entire bed-material surface distribution within a reach, a grid-by-number pebble count and several areal samples, which have been converted to equivalent distributions of grid-by-number samples before, (Section 4.3) need to be combined.

Several methods are available for combining two particle-size distributions:

- Rigid combination,
- Flexible combination, and
- Adjustment of frequency distributions.

##### 4.4.1 Rigid combination

If the coarse portion of a pebble count size-distribution is considered representative for a reach, only the fine part of a pebble count needs to be adjusted to the fine part of an areal sample (converted to a grid-by-number sample beforehand) to obtain a distribution representative of all particle sizes. The rigid combination method presented by Anastasi (1984) and Fehr (1987) facilitates this adjustment. The method uses the percentile ratio between an areal sample and a pebble count at the lower and upper border of one selected particle-size class to create a new cumulative frequency distribution for the fine part for the pebble count.

Within the range of particle sizes common in both samples, one particle-size class is sought in which the ratios between the lower and an upper percentiles of the areal sample,  $p_{A\ low}$  and  $p_{A\ up}$ , and the lower and upper percentiles of the pebble count,  $p_{P\ low}$  and  $p_{P\ up}$ , are as similar as possible (see Eq. 4.9 and gray bars in Fig. 4.37 a - c). Note that all percentiles are used as decimals (e.g., 0.23 instead of 23 % finer).

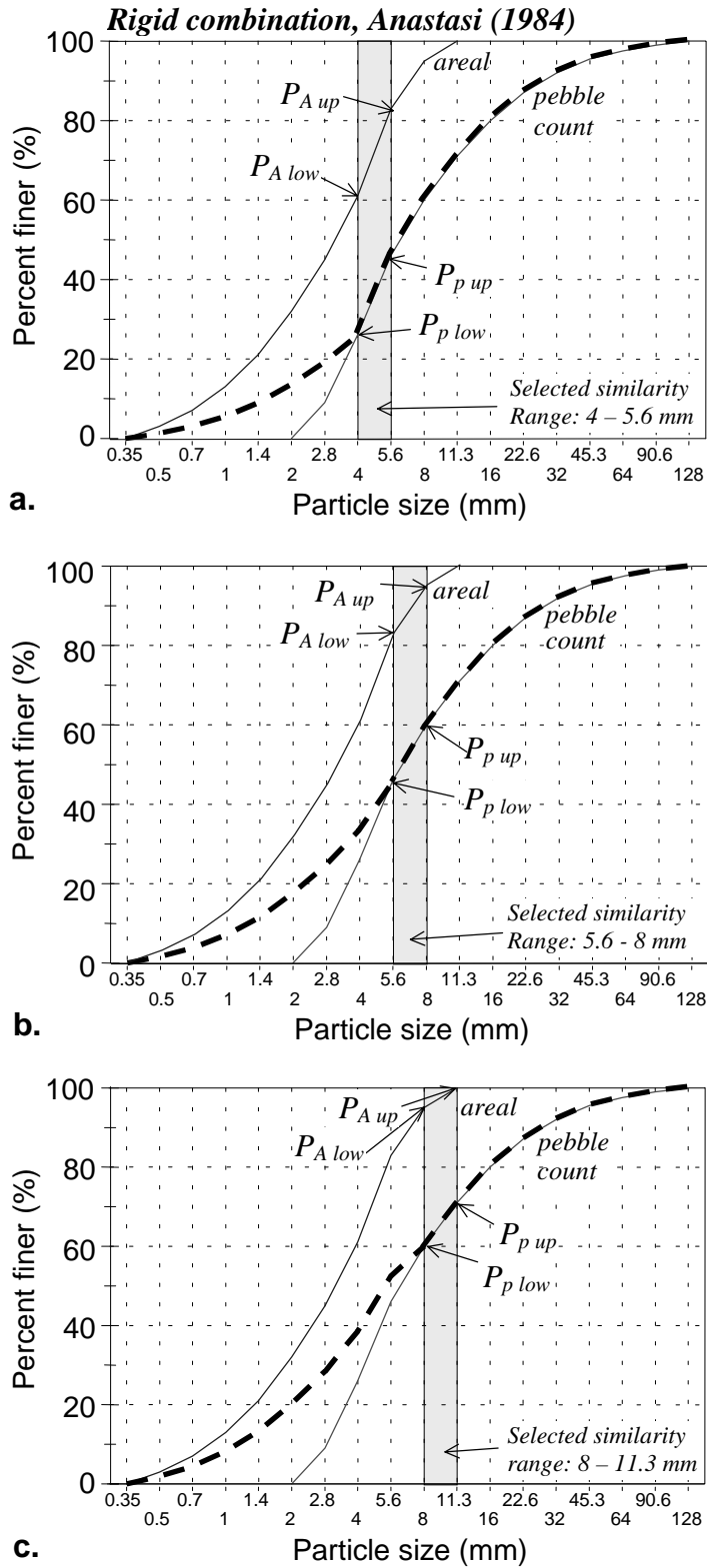


Fig. 4.37: Rigid combination (— —) between an areal sample and a pebble count to form a new fine part of the pebble count size distribution, using three different particle-size ranges of similarity (gray bars): 4 – 5.6 mm (a), 5.6 – 8 mm (b), and 8 – 11.3 mm (c). The cumulative percent finer was computed as decimals, but plotted as percentage.

$$\frac{p_{A\ low}}{p_{A\ up}} \approx \frac{p_{P\ low}}{p_{P\ up}} \quad (4.9)$$

The rigid combination methods computes the percentiles  $p_{r\ i}$  (subscript  $r$  for rigid) for each particle size  $D_i$  of the fine part of the combined pebble count size-distribution from:

$$p_{r\ i} = p_{A\ i} \cdot \frac{p_{P\ low}}{p_{A\ low}} \quad (4.10)$$

**Example 4.2:**

Table 4.11 provides an example computation for a rigid combination of two particle-size distributions. The particle-size range 5.6 – 8 mm was considered to be similar for the areal sample and the pebble count. The percentiles of the areal sample and the pebble count at the upper and lower border of the selected similarity range, i.e., at 5.6 and 8 mm, were read as  $p_{P\ up} = 0.60$ ,  $p_{P\ low} = 0.46$ ,  $p_{A\ up} = 0.95$ , and  $p_{A\ low} = 0.83$ . The similarity ratio in

Table 4.11: Computation of a rigid combination between an areal sample and a pebble count. The selected particle-size range of similarity is between 5.6 and 8 mm.

$D_i$ (mm)	Cumulative size distribution $\Sigma_n\%d_i$		
	Areal sample = $p_{A_i}$ ( $\Sigma$ )	Pebble count = $p_{P_i}$ ( $\Sigma$ )	Rigid combination = $p_{r_i}$ ( $\Sigma\%$ )
0.35	0.00		0.000
0.5	0.03		0.017
0.7	0.07		0.039
1.0	0.13		0.072
1.4	0.21		0.116
2.0	0.32	0.00	0.177
2.8	0.45	0.09	0.249
4.0	0.61	0.260	0.338
5.6	0.83 = $p_{A\ low}$	<b>0.46 = <math>p_{P\ low}</math></b>	<b>0.460</b>
8.0	0.95 = $p_{A\ up}$	0.60 = $p_{P\ up}$	
11.3	1.00	0.71	
16.0		0.80	
22.6		0.87	
32.0		0.92	
45.3		0.955	
64.0		0.975	
90.6		0.99	
128.0		1.00	

Eq. 4.9 is  $0.77 \approx 0.87$ . For the particle size  $D_i = 2.8$  mm, for example, the percentiles of the adjusted fine part of the pebble count are computed as  $p_{r\ 2.8} = 0.45 \cdot 0.554 = 0.249 = 24.9\%$  (Eq. 4.10)

Results of the rigid combination vary depending on the particle-size range that is selected for similarity. Fig. 4.37 shows rigid combinations that adjust the fine (unrepresentative) portion of a pebble count to an areal sample for three different particle-size ranges selected for similarity. Only the selected range of similarity in Fig. 4.37 b yields a smooth adjustment. This variability makes it necessary to repeat computations for several similar size ranges and to select a result that best fits the study objective.

#### 4.4.2 Flexible combination

A flexible combination (Anastasi 1984; Fehr 1987) generates a completely new particle-size distribution, combined from the distribution of a pebble count and an areal sample (converted to a grid-by-number sampler beforehand) (Fig. 4.38). The distribution obtained from a flexible combination resembles a hand-drawn adjustment curve that extends from the coarse end of the pebble count distribution to the fine end of the areal sample.

Following the same approach as with the rigid combination in Section 4.4.1 (Eq. 4.9), a particle-size class is sought for which the frequency is similar in both samples (similarity range), so that

$$\frac{p_{A\ low}}{p_{A\ up}} \approx \frac{p_{P\ low}}{p_{P\ up}} \quad (\text{see Eq. 4.9})$$

$p_{A\ low}$  and  $p_{A\ up}$  are the lower and an upper percentiles of the areal sample, and  $p_{P\ low}$  and  $p_{P\ up}$  are the lower and upper percentiles of the pebble count. All percentiles are used as decimals. The fine part of the new distribution below  $p_{f\ low}$  (subscript  $f$  for flexible) and the coarse part above  $p_{f\ up}$  are each generated using a different equation. The fine portion of  $p_{fi(fine)}$  is computed from

$$p_{fi(fine)} = p_{A\ i} \cdot \frac{p_{f\ low}}{p_{A\ low}} \quad (4.11)$$

$p_{A\ i}$  is the percentile of the areal distribution for the  $i$ th size class.  $p_{f\ low}$  is the percentile of the flexible combination at the lower border of the similarity range and is computed from

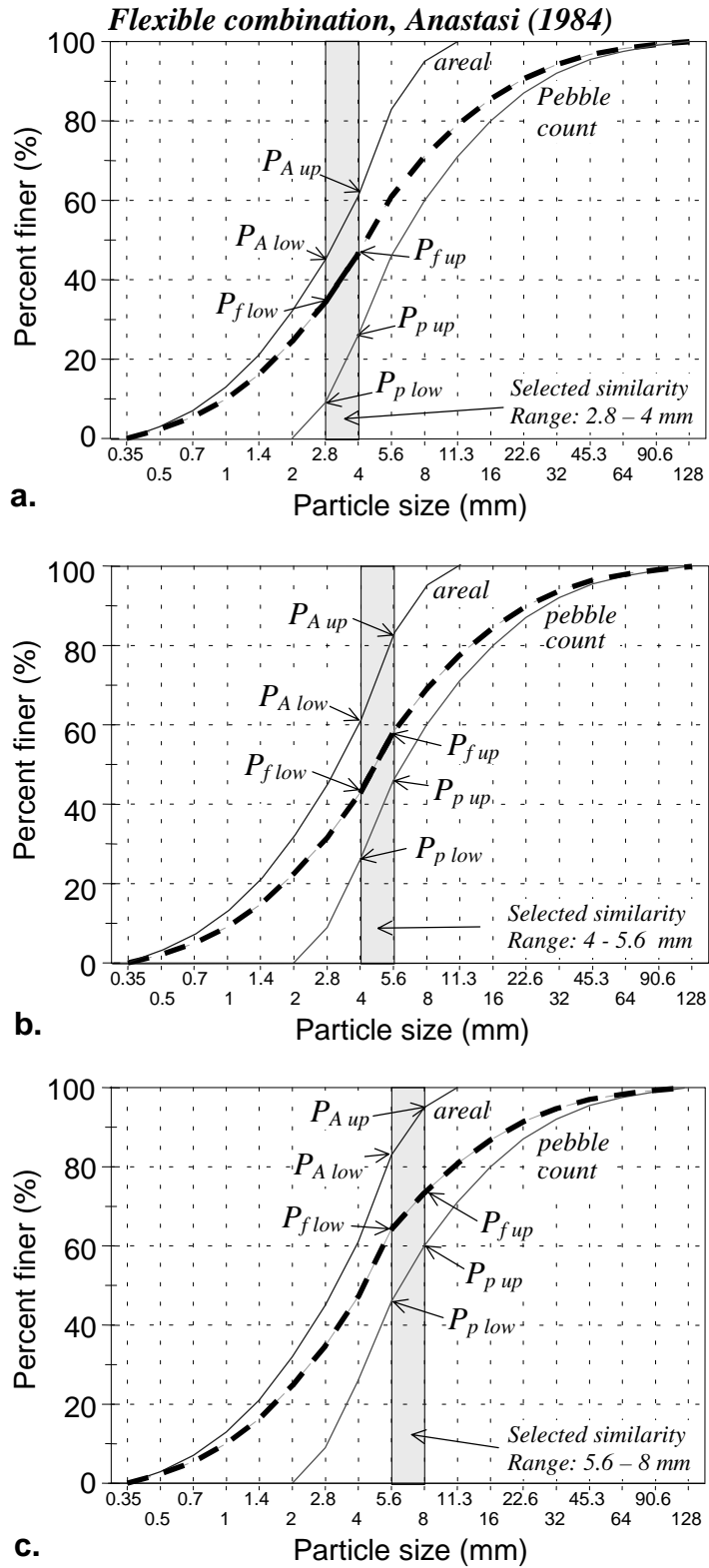


Fig. 4.38: Flexible combination (—) between an areal sample and a pebble count, for three different particle-size ranges of similarity (gray bars): 2.8 – 4 mm (a), 4 – 5.6 mm (b), and 5.6 – 8 mm (c). Results show minimal variations between different selected ranges of similarity.

$$p_{f\ low} = \frac{(1 - p_{P\ low}) - (1 - p_{P\ up})}{\frac{p_{A\ up}}{p_{A\ low}} \cdot (1 - p_{P\ low}) - (1 - p_{P\ up})} \quad (4.12)$$

$p_{p\ low}$  and  $p_{p\ up}$  are the percentiles of the pebble count at the lower and upper border of the similarity range. The coarse portion of  $p_{fi(coarse)}$  above the upper border of the similarity range  $p_{f\ up}$  is computed from

$$p_{fi(coarse)} = \frac{1 - p_{p\ i}}{1 - p_{p\ low}} \cdot (p_{f\ low} - 1) + 1 \quad (4.13)$$

The percentile of the flexible combination  $p_{f\ up}$  at the upper border of the similarity range is

$$p_{f\ up} = p_{f\ low} \cdot \frac{p_{A\ up}}{p_{A\ low}} \quad (4.14)$$

Example 4.3:

Table 4.12 provides an example computation for the flexible combination of two particle-size distributions. The particle-size range of 4 – 5.6 mm was considered to be similar for the areal sample and the pebble count (grid sample).

The percentile of the flexible combination at the lower border of the similarity range at 4 mm is (Eq. 4.12):

$$\begin{aligned} p_{f\ low} &= \frac{(1-0.26) - (1-0.46)}{(0.83/0.61) \cdot (1-0.26) - (1-0.46)} \\ &= \frac{0.2}{(1.36 \cdot 0.74) - 0.54} = \frac{0.2}{0.467} = 0.428 \text{ or } 42.8\% \end{aligned}$$

The percentiles of the areal sample and the pebble count at the upper and lower border of the similar range, i.e., at 4 and 5.6 mm, were read as  $p_{A\ low} = 0.61$ ,  $p_{A\ up} = 0.83$ ,  $p_{P\ low} = 0.26$ , and  $p_{P\ up} = 0.46$ . The similarity ratios in Eq. 4.9 were  $0.61/0.83 = 0.57$  and  $0.26/0.76 = 0.73$ .

Table 4.12: Computation of a flexible combination between an areal sample and a pebble count. The selected particle-size range of similarity is between 4 and 5.6 mm (see gray band).

$D_i$ (mm)	Cumulative size distribution $\Sigma_{n\%i}$			
	Areal sample	Pebble count	Flexible combination	
	$p_{Ai}$ ( $\Sigma$ )	$p_{Pi}$ ( $\Sigma$ )	$p_{fi}$ (fine) ( $\Sigma$ )	$p_{fi}$ (coarse) ( $\Sigma$ )
0.35	0.00		0.000	
0.5	0.03		0.021	
0.7	0.07		0.049	
1.0	0.13		0.091	
1.4	0.21		0.147	
2.0	0.32	0.00	0.225	
2.8	0.45	0.09	0.316	
4.0	0.61 = $p_{A\ low}$	0.26 = $p_{P\ low}$	<b>0.428</b> = <b>0.428</b>	= $p_{f\ low}$
5.6	0.83 = $p_{A\ up}$	0.46 = $p_{P\ up}$	<b>0.583</b> = <b>0.583</b>	= $p_{f\ up}$
8.0	0.95	0.60		0.691
11.3	1.00	0.71		0.776
16.0		0.80		0.846
22.6		0.870		0.900
32.0		0.920		0.938
45.3		0.955		0.965
64.0		0.975		0.981
90.6		0.990		0.992
128.0		1.000		1.000

The percentile of the flexible combination at the upper border of the similarity range at 5.6 mm is (Eq. 4.14):

$$p_{f\ up} = \frac{0.428 \cdot 0.83}{0.61} = 0.583 \text{ or } 58.3\%.$$

For the particle-size class of  $D_i = 2.8$  mm, the adjusted fine part of the size distribution has a percentile of  $p_{f2.8} = 0.45 \cdot 0.43/0.26 = 0.691$  or 69.1% (Eq. 4.11). For the particle size class of  $D_i = 8$  mm, the adjusted coarse part of size distribution has a percentile of  $p_{f8} = (1-0.60)/(1-0.26) \cdot (0.43-1)+1 = 0.691$  or 69.1% (Eq. 4.13).

Flexible combinations were computed for three selected size ranges of similarity: 2.8 – 4 mm (a), 4 – 5.6 mm (b), and 5.6 – 8 mm (c) (Fig. 4.38). Computations of the flexible combination vary only moderately between different selected ranges of similarity, if the two original distributions (areal sample and pebble count) have only a few particle-size classes in common, which is the case in Fig. 4.38. However, the combined distribution curves become more varied between different similarity ranges as the two original

distributions share a larger range of common particle-size classes and span a wider range of particle sizes.

#### 4.4.3 Adjusting frequency distributions

Fripp and Diplas (1993) present a method for combining two frequency distributions that is computationally different from the flexible combination in Section 4.4.2, but yields the same result. The combination method by Fripp and Diplas (1993) uses two original percent frequency distributions (e.g., from an areal sample that has been converted to a grid-by-number distribution beforehand and from a pebble count). The number-frequency distributions of both samples are adjusted to create a new, combined frequency distribution. An example computation is provided in Table 4.13.

Table 4.13: Combining frequency distributions of two samples to yield a combined sample. The percent frequency of the particle-size class 4 – 5.6 mm (bold print) is selected as the similar size class for both samples (after Fripp and Diplas 1993)

$D_i$ (mm)	Areal sample		Original Pebble count		Adjusted Pebble count	Combined Areal sample + pebble count		
	$n_{\%A_i}$ (%)	$\Sigma n_{\%A_i}$ ( $\Sigma\%$ )	$n_{\%P_i}$ (%)	$\Sigma n_{\%P_i}$ ( $\Sigma\%$ )	$n_{Padji}$ (-)	$n_{ci}$ (-)	$n_{\%ci}$ (%)	$\Sigma n_{\%ci}$ ( $\Sigma\%$ )
(1)	(2)	(3)	(4)	(5)	(6)	(7)	(8)	(9)
0.35	0.0	0.0	-	-	-	0.0	0.0	0.0
0.5	3.0	3.0	-	-	-	3.0	2.3	2.3
0.7	4.0	7.0	-	-	-	4.0	3.1	5.4
1.0	6.0	13.0	-	-	-	6.0	4.6	10.0
1.4	8.0	21.0	-	-	-	8.0	6.1	16.1
2.0	11.0	32.0	0.0	0.0	0.0	11.0	8.4	24.5
2.8	13.0	45.0	8.0	9.0	7.5	13.0	10.0	34.4
<b>4.0</b>	<b>16.0</b>	61.0	<b>17.0</b>	26.0	<b>16.0</b>	16.0	12.2	46.7
5.6	22.0	83.0	20.0	46.0	18.8	18.8	14.4	61.1
8.0	12.0	95.0	14.0	60.0	13.2	13.2	10.1	71.2
11.3	4.0	100.0	11.0	71.0	10.4	10.4	7.9	79.1
16.0	0.0	-	9.0	80.0	8.5	8.5	6.5	85.6
22.6	-	-	7.0	87.0	6.6	6.6	5.0	90.6
32.0	-	-	5.0	92.0	4.7	4.7	3.6	94.2
45.3	-	-	3.5	95.5	3.3	3.3	2.5	96.8
64.0	-	-	2.0	97.5	1.9	1.9	1.4	98.2
90.6	-	-	1.5	99.0	1.4	1.4	1.1	99.3
128.0	-	-	<u>1.0</u>	100.0	<u>0.9</u>	<u>0.9</u>	<u>0.7</u>	100.0
	100.0		100.0			142.4	100.0	

For all particle size classes  $D_i$  (column 1 in Table 4.13) the percent frequency (by number) is listed for the converted areal sample  $n_{\%A_i}$  (column 2) and the pebble count  $n_{\%P_i}$  (column 4). From the size classes  $D_i$  present in both samples, one size class is selected for which the percent frequencies are most similar for the areal sample  $n_{\%A}$  and the pebble count  $n_{\%P}$  (“the common size class”). These were the frequencies of 16 and

17% for the size class 4 – 5.6 mm in Table 4.13 (bold print in column 2 and 4). A scaling factor  $F$  is then computed that makes it possible to equate the percent frequencies of both samples for the one selected (common) size class  $i$  so that

$$n_{\%Pi} = n_{\%Ai} + (F \cdot n_{\%Pi}) \quad (4.15)$$

Solving for  $F$  yields

$$F = \frac{n_{\%Pi} - n_{\%Ai}}{n_{\%Pi}} \quad (4.16)$$

$F$  is expressed as a percentage  $F\%$  and subtracted from the percent frequency of the original pebble count  $n_{\%pi}$  for all size classes below the size class selected as similar for both samples to yield  $n_{Padj i}$  (column 6).

$$n_{Padj i} = n_{\%pi} - F\% \quad (4.17)$$

The frequency of one size class,  $n_{\%p adj,4}$  in this example, is now identical for the areal sample and the adjusted pebble count. The adjusted pebble count frequencies  $n_{Padj i}$  for all size classes  $D_i \leq 4$  mm (shaded part of column 6) and the percent frequency of the areal sample  $n_{\%Ai}$  for all size classes  $D_i > 4$  mm (shaded part of column 2) are presented in column 7 and summed. The sum of column 7 does not add to 100 and is readjusted to 100% by dividing each value in column 7 by the sum of column 7 (i.e., 142.4) and multiplying by 100 (column 8). The cumulative frequency distribution in column 9 is the new particle-size distribution for the combined sample.

Histograms of the original areal sample and the pebble count are shown in Fig. 4.39. The two samples have similar particle-size frequencies for three size classes: 4 – 5.6 mm, 5.6 – 8 mm, and 8 – 11.3 mm (i.e., three “common size classes”). Using one of these three particle-size frequencies at a time, three combined particle-size distributions were computed and produced the three combined curves in Fig. 4.40. Results vary slightly between the three computations (see also Fig. 4.38). However, variability of the result increases as the difference in (common) particle-size frequency for the areal and the grid sample increases. Thus, computations should be repeated using several similar percent frequencies (i.e., common size classes), and the combined distribution that best fits the study objective should be selected.

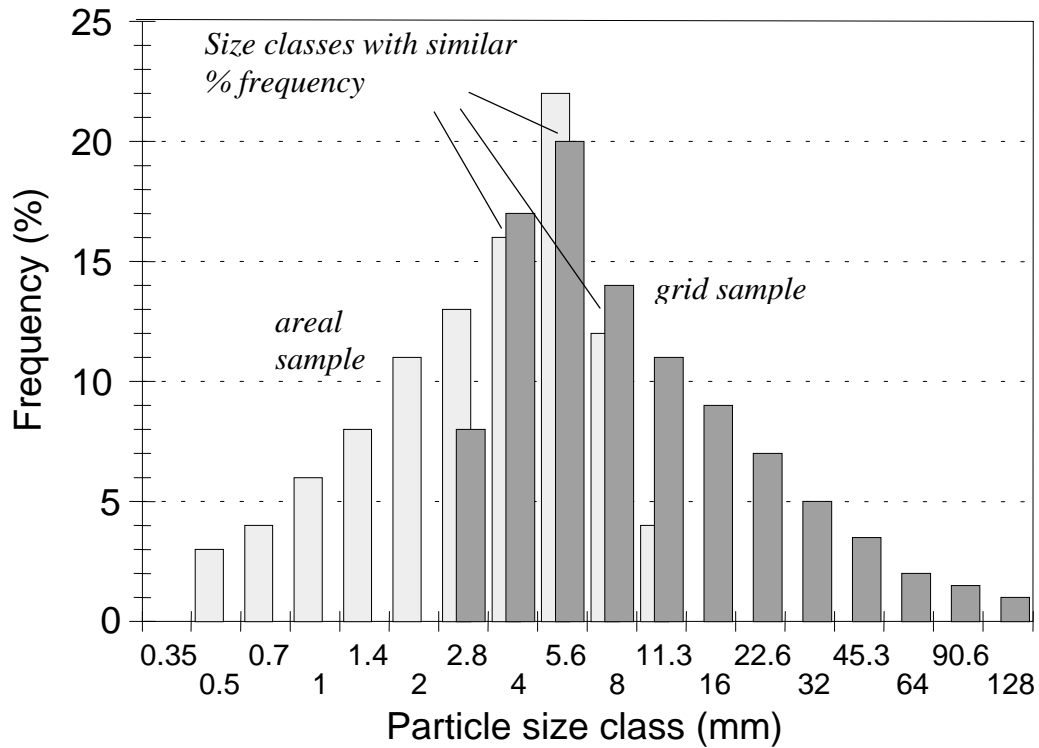


Fig. 4.39: Histogram of an areal sample and a pebble-count

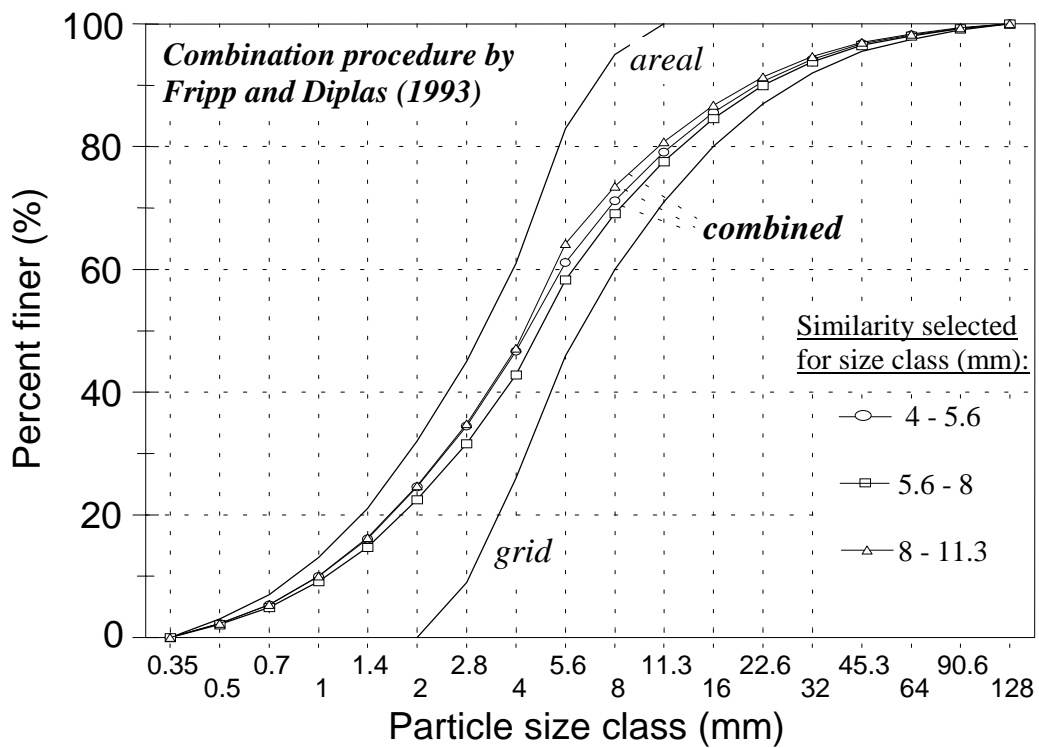


Fig. 4.40: Cumulative frequency distributions of an areal sample and a pebble-count, and the three combined samples obtained from using the percent frequencies of different particle-size classes.

## 4.5 Recording field results

Sampling results need to be recorded in the field. Either a field book or sampling forms developed prior to the field work may be used for this purpose. Both methods have advantages and disadvantages. Ready-made forms are useful when sampling yields information that is similar for all sites. Sampling forms are also useful to maintain a preset standard of data recording if different people are involved in the field work. One of the greatest advantages of using sampling forms is that the process of developing the forms requires visualizing and anticipating the sampling process. This “homework” helps to organize the field work as it prompts the form developer to consider all the information to be recorded, the order of measurements, all the equipment needed, and other information useful to record. Thus, developing sampling forms may be time well spent, even if the field forms are ultimately not used.

The disadvantage is that forms used during field work get dirty, become illegible when wet, and tend to get lost. Single forms are prone to being swept away by the current or the wind, or to becoming buried in the equipment. A rain-proof field book used for one site or for one study only tends to better “weather” the field season and is more suitable when different kinds of observations are recorded. A compromise between a field book and sampling forms is to print field forms on water-resistant paper, and assemble them with a spiral binding, a plastic cover, and a hard back. Personal choice and the type of field work ultimately determine whether to use a field book or field forms, or a combination of both. Both the field book and sampling forms should be photocopied frequently between days of field work, and copies should be stored in a safe place.

## 5. Sample size

---

One of the most common objectives of bed-material sampling is the characterization of the distribution of particle sizes present in a given stream channel. The ideal way to describe the particle-size distribution of a streambed would be to count and measure every particle within the reach. This is essentially impossible, and therefore one must rely on taking samples of the bed material and use the sample results to estimate the general characteristics of the sampling area.

The question is, how many particles or how much sediment should be sampled? The answer is a compromise between sampling precision and sampling effort. As the number of particles collected increases, the precision with which the bed material can be described increases as well. The precision obtained in the sample must be sufficient to measure the effects being investigated by the project goals (e.g., Is there a significant increase or decrease in streambed fines? Has the armor layer changed, etc.?). If the sampling program is not sufficient to meet these goals, the validity of the field results must be called into question. As the sample sizes collected increase, the costs and effort associated with the field work also increase and will eventually become prohibitively large. Another factor to consider is that the increased precision obtained by collecting ever larger sample sizes does not follow a linear relationship. The benefit obtained from collecting an additional 10 particles is much greater when the existing sample size is 20 as opposed to when the sample size is 200.

The characteristics of the bed material being sampled is also an important factor in determining sample size. When there is little variability in the material, i.e., when the bed is well sorted, smaller samples will suffice to precisely describe the bed. With greater variability, i.e., poorer sorting, the sample sizes must be increased to obtain the same precision. Similarly, a smaller sample size suffices if the bed is homogeneous, which means that the particle-size distribution is more or less the same throughout the sampling area.

Because sample size determines both the cost and the benefits of field measurements, careful attention should be paid to this aspect before going out into the field. The minimum sample size necessary to ensure a specific sampling precision should be calculated beforehand and then be evaluated for cost requirements. However, in order to estimate the minimum sample size for some preset precision, one must have at least an approximate estimation of the bed-material standard deviation or sorting – which in itself requires sampling. This circularity may be resolved by performing a pilot data-collection study or through estimation based on experience with streams that have bed-material characteristics similar to the stream being studied.

Various methods for computing a relationship between sample size and precision for bed-material samples are described in the literature. The methods fall into three groups:

- Empirical recommendations,
- Computations based on an assumed normal distribution, and
- Computations that do not assume any underlying distribution type.

Older literature on sediment sampling often has empirical recommendations of sample size that are based on the  $D_{max}$  particle size and developed for particular bed-material properties. These recommendations usually do not assign a certain level of precision to a certain sample size and are not generally applicable. More recent literature bases sample-size computation on an assumed normal distribution of the bed-material particle size. These procedures are generally applicable if the assumptions of a normal distribution holds, but the descriptions can be highly technical and difficult to understand without background knowledge of statistics. Other sample-size recommendations do not assume an underlying distribution type and are generally applicable. This document compiles a variety of sample-size computations, explains their application, and compares the results. This chapter provides the user with background information that assists in selecting a sample-size procedure suitable for a specific study objective.

Methods used to compute minimum sample size are different for number-based sampling (Section 4.1.1 and 4.1.2), areal sampling (Section 4.1.3), and volume-based sampling (Section 4.2). For this reason, sample-size computations are discussed separately for each sampling method.

## 5.1 Factors affecting sample size

The computation of sample size is affected by a variety of factors which include:

- Assumptions made about the underlying distribution type of the bed-material particle-size (approximately normal, log-normal, or no assumptions are made regarding the distribution type (Section 2.1.4.3)) and these assumptions determine which statistics need to be used;
- Bed-material characteristics:
  - standard deviation  $s$  of the particle-size distribution (typically estimated by the Inman sorting coefficient  $s_I$  or by the moment method  $s_{frq}$ ),
  - heterogeneity of bed material within the reach (variability among samples),
  - limited parent population size ( $N$ ) in relation to sample size ( $n$ ) in a small sampling area;
- Acceptable error of measurements which may relate to:
  - absolute, percentage, or standard error,
  - particle sizes in  $\phi$  or mm units,

- the distribution mean or any percentiles (e.g.,  $D_5$ ,  $D_{50}$ , or  $D_{95}$ ), and
  - be affected by the number of operators involved;
- Acceptable chance that the computed result is wrong
    - expressed by a predetermined confidence level  $\alpha$ ;
  - Bias (systematic deviation of sampling results from population characteristics) due to:
    - unrepresentative particle selection (operator bias),
    - unrepresentative sampling from heterogeneous deposits (sampling bias),
    - unrepresentative presence of particles from the largest size class (statistical bias).

***Assumptions made about the underlying distribution type***

Assumptions made regarding the population distribution type of the bed material sampled determine the kind of statistics used for sample-size computations. Traditionally, it is assumed that unimodal, log-transformed bed-material particle-size distributions derived from a sufficiently large sample size approach a normal distribution in  $\phi$ -units. Assuming an approximately normal distribution has the advantage that commonly available sample-size statistics can be used which are based on normal distributions (Section 5.2.2). Bed-material samples, however, rarely have a true normal or Gaussian distribution (Kothyari 1995). The user needs to evaluate whether the goodness-of-fit to a Gaussian distribution is close enough to warrant the assumption of approximate normality (Section 2.1.4.3). Church et al. (1987) and Rice and Church (1996b) cautioned that true Gaussian distributions for log-transformed particle-size distributions are unlikely for gravel-bed streams. The user could either use an empirical approach to determine a “sufficient” sample size, or use a bootstrap (resampling) approach (Section 5.2.3.4) that provides a relation between sample size and error. Sample size – error relations computed from a bootstrap approach are independent of an underlying distribution type and may differ substantially from similar relations computed using Gaussian-based statistics.

***Bed-material characteristics***

For a specified accuracy and precision, sample size  $n$  should increase as the variability of the parent population increases, i.e., as the sorting of the bed material becomes poorer or the standard deviation becomes larger. If the bed-material composition is spatially heterogeneous and varies markedly between different locations of the sampling reach, samples collected from the reaches are likely to be highly variable as well. The large standard deviation between individual samples necessitates collecting a large number of samples for a desired accuracy and precision. Small mountain streams with large particles might have only a limited number of particles available for sampling. In this situation, the population size  $N$  is limited in relation to sample size  $n$ . This limitation takes a statistical effect as  $N$  becomes less than about 100 times the necessary number of particles  $n$  and causes a decrease in the sample size necessary for a specific precision. Bed-material characteristics further affect the relationship between sample size and accuracy when

operators tend to favor mid-size particles while neglecting fines and large cobbles in poorly sorted bed material.

### ***Accuracy and precision***

Usually when samples are taken, the user wants to know the accuracy and precision of a sample. Accuracy refers to the size of the deviations from the true value. The accuracy of bed-material sampling may never be known because the true distribution of bed-material particles in the reach could only be determined by collecting every particle in the reach. Using the example of target practice (Fig. 5.1), with the target being the representative description of the particle-size distribution of a deposit, accuracy is the closeness of the shots to the target center (Fig. 5.1 d). Precision refers to the size of deviations from the mean value obtained by repeated applications of the sampling procedure, i.e., the ability to repeatedly hit the same area (hopefully the center) of the target (Fig. 5.1c and d).

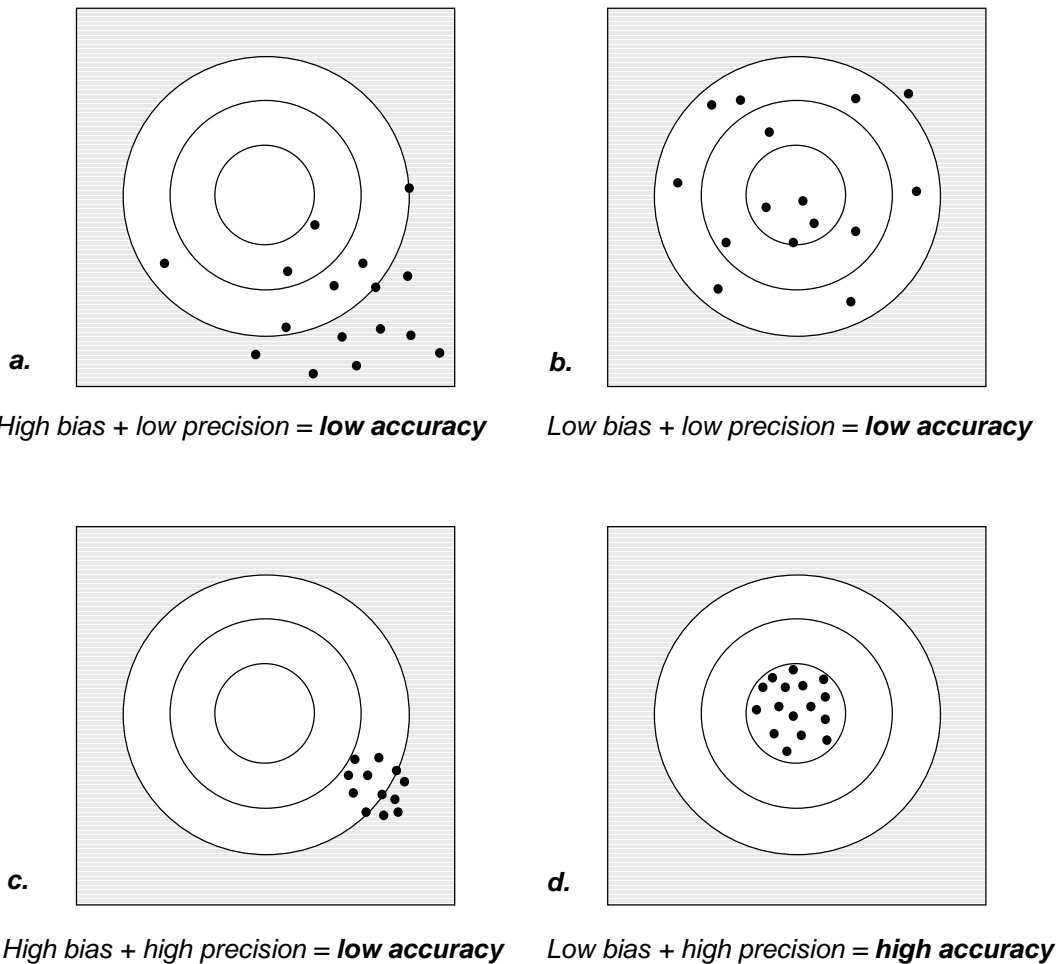


Fig. 5.1: Patterns of shots at a target. (Redrawn from Gilbert (1987), by permission of John Wiley and Sons, Ltd.).

Precision describes how dispersed or tightly bunched the shots are (Fig. 5.1 a and b) and indicates the inter-sample variability (i.e., standard deviation between samples). Precision is used to quantify how many repeated samples are needed to arrive at a stable sampling result. Accuracy and precision are interrelated. Samples of low precision also have a low accuracy (Fig. 5.1 a and b). Samples of high precision are not necessarily accurate if all samples are off set from the true result by some constant amount, i.e., by bias. Precise samples can only be accurate in the absence of bias (Fig. 5.1 d).

### ***Bias***

Bias is the systematic deviation of a sampling result from the true population characteristics (Fig. 5.1 a and c). Bias can stem from a variety of sources. *Operator* bias results when the operator selects mid-sized, “handy” particles and excludes “inconveniently” small, or large particles, or particles from poorly accessible streambed locations. Operator bias can be ameliorated by training and using an appropriate sampling methodology (Sections 4.1.1.3 – 4.1.1.6, 5.2.2.8), but since it cannot be eliminated, operator bias increases with the number of operators and with sample size. *Statistical* bias is caused by sampling too few particles from the largest size class and is ameliorated by a large sample size (Sections 5.4.1.1, 5.4.1.3, 5.4.1.4). *Sampling* bias means to sample particle distributions not representative of the parent distribution in the reach and may result from sampling spatially heterogeneous beds in an unrepresentative way. This can be avoided by using spatially segregated sampling schemes (Sections 6.3 and 6.5).

## **5.2 Pebble counts: number-based sample-size recommendations**

### **5.2.1 General form of number-based sample-size equations**

For approximately Gaussian shaped particle-size distributions that are not very skewed, mean and median are similar. In this case, a one-step procedure can be applied to estimate the sample size necessary to obtain a desired precision of the sample mean particle size  $\phi_m$  or  $D_m$ . The general form of a sample-size equation is:

$$n = \left( \frac{t \cdot \sigma}{e} \right)^2 \quad (5.1)$$

$n$  is the sample size, i.e., the number of particles to be sampled,  $t$  is a statistical numerical value,  $\sigma$  is the population standard deviation, and  $e$  is the acceptable error around the mean. These terms will be described in more detail.

### ***Standard deviation***

The population standard deviation  $\sigma$  describes how wide the range of values is within the population, specifically the range of values comprised within the central 68% of all data

(Section 2.1.5.4). However, the population standard deviation is rarely known, and must therefore be substituted by an estimate of standard deviation that is derived from the sample.  $\sigma$  may be estimated from the sample standard deviation  $s \equiv \sqrt{s^2}$ , where  $s^2$  is the sample variance. The sample standard deviation  $s$  is computed from the absolute or percent frequencies of the particle number frequency-distribution

$$s = \sqrt{s^2} = \sqrt{\frac{1}{n-1} \sum_{i=1}^k n_i (\phi_{ci} - \phi_m)^2} \quad (\text{see Eq. 2.56})$$

where  $n$  is the total number of particles (or 100 %),  $k$  is the number of size classes,  $n_i$  is the number of particles per size class (or the percentage),  $\phi_{ci}$  is the center of class in  $\phi$ -units of the  $i$ th size class, and  $\phi_m$  is the arithmetic mean particle size in  $\phi$ -units. This computation of standard deviation is also called the “second moment” method. The expression becomes complicated for grouped data such as particle-size distributions (see Eq. 2.58) and is therefore commonly substituted by the Inman sorting coefficient  $s_I$  that describes the range of particle sizes contained within the central 68% of all data (Eq. 2.46, Section 2.1.5.4).

$$s_I = \frac{|\phi_{84} - \phi_{16}|}{2} \quad (\text{see Eq. 2.46})$$

Numerical values of standard deviation and the Inman sorting coefficient are identical for true Gaussian distributions, but deviate somewhat if the particle-size distribution is not exactly normal (see Table 2.14).

The sample standard deviation or the Inman sorting coefficient is usually not known before the sampling project starts, and need to be obtained from a pilot study. A preliminary value of sample size is then computed for a preset precision using the estimated value of  $s$  or  $s_I$  and a sample of the computed size is collected. The standard deviation  $s$  or  $s_I$  is computed for the collected sample, and sample size is recalculated. If sample sizes based on the pilot study and on the actual sample are different, the process of computing and comparing sample-size requirements needs to be repeated until the difference in required and collected sample size is insignificant.

### **Error**

The error around the mean can be expressed in absolute or in percentage terms. The user may specify an acceptable error for the sample mean, e.g.,  $\pm 0.15 \phi$  around the mean in  $\phi$ -units ( $\phi_m$ ) or  $\pm 10\%$  around the mean in mm ( $D_m$ ), and compute the sample size necessary to attain this goal. Similarly, the error associated with a given sample size may be

calculated by solving sample-size equations for the error  $e$ . The inverse square relation between  $n$  and  $e$  is such that a fourfold increase in sample size reduces the error by half, whereas allowing for twice the error reduces the sample size by a factor of 4. Other possibilities to express sampling errors include standard errors and errors around percentiles in terms of mm,  $\phi$ , % or in terms of a percentile range (Section 5.2.3).

**Sample statistics**

The term  $t$  in Eq. 5.1 is a statistical numerical value known as Student’s  $t$ . For bed-material sampling studies, Student’s  $t$  is preferred over other statistics because the population  $\sigma$  is usually not known and approximated by  $s$ , the sample standard deviation. The  $t$ -variate cuts off  $(100 \alpha/2)\%$  of the upper tail of a  $t$ -distribution with  $n-1$  degrees of freedom. The numerical value of Student’s  $t$  depends on two parameters: confidence level: and sample size. The confidence level  $\alpha$  describes the certainty (or the percent of all cases) in which a specified precision will be obtained by sampling the required sample size. A value typically chosen is  $\alpha = 0.05$  which pertains to a 95% confidence level which means that the particle size of interest will be within a predetermined limit in 95% of all cases. Table 5.1 shows the relation between percent confidence,  $\alpha$ -levels, and the resulting value for  $t_{1-\alpha/2, n-1}$  for large  $n$ . Note that for large  $n$ , values of  $t_{1-\alpha/2, n-1}$  are identical

Table 5.1: Relation between precision (expressed in terms of confidence levels, or percent chance that error is exceeded), the corresponding  $\alpha$ -levels, and values of  $t_{1-\alpha/2}$  or  $Z_{1-\alpha/2}$  for  $n \rightarrow \infty$ .

% confidence that error is not exceeded $1-\alpha$ (%)	% chance that error is exceeded $\alpha$ %	$\alpha$ -level $\alpha$	Percentile of normal distribution $1-\alpha/2$	Distance betw. median and percentile in terms of standard deviation $t_{1-\alpha/2, n \rightarrow \infty}$ or $Z_{1-\alpha/2}$
0	100	1.0	0.5	0.0
30	70	0.7	0.65	0.385
50	50	0.5	0.75	0.675
68.2	31.8	0.318	0.841	1.000
80	20	0.20	0.90	1.280
85	15	0.15	0.925	1.440
90	10	0.1	0.95	1.645
91	9	0.09	0.955	1.695
92	8	0.08	0.96	1.750
93	7	0.07	0.965	1.810
94	6	0.06	0.97	1.880
<b>95</b>	<b>5</b>	<b>0.05</b>	<b>0.975</b>	<b>1.960</b>
98	2	0.02	0.99	2.327
99	1	0.01	0.995	2.576
99.5	0.5	0.005	0.9975	2.810
99.9	0.1	0.001	0.9995	3.270
99.96	0.04	0.0004	0.9998	3.490
99.99	0.01	0.0001	0.99995	3.603

to the values of  $Z_{1-\alpha/2}$  which is the standard normal deviate that cuts off  $(100 \alpha/2)\%$  of the upper tail of a standard normal distribution. Values of  $Z_{1-\alpha/2}$  are used instead of  $t_{1-\alpha/2, n-1}$  if the population standard deviation  $\sigma$  is known and  $n$  is larger than 100.

For a specified confidence level, the relationship between  $t$  and sample size  $n$  is not linear. For sample size larger than 200,  $t$  takes a constant value of 1.96 for a 95% confidence level (for  $\alpha = 0.05$ ,  $t_{1-\alpha/2, n-1} = t_{0.975, n-1} = 1.96$ ). But for small sample sizes,  $t$  changes significantly with sample size. For a sample size of 5 which allows  $n-1 = 4$  degrees of freedom,  $t_{0.975, n-1} = 2.776$ , and increases to 12.7 for a sample size of 2. Table 5.2 provides  $t$ -values for various degrees of freedom which are equal to  $n-1$ , and a 95% confidence level for which  $t_{1-\alpha/2} = t_{0.975}$ . Values for  $t$  for other confidence levels and samples sizes can be obtained from statistical tables available in standard statistics books (e.g., Gilbert 1987).

Table 5.2: Values for Student's  $t$  for various degrees of freedom ( $n-1$ ) and a 95% confidence level ( $\alpha = 0.05$ ) with  $t_{1-\alpha/2} = t_{0.975}$

$n-1$	$t_{1-\alpha/2, n-1}$	$n-1$	$t_{1-\alpha/2, n-1}$						
1	12.706	11	2.201	21	2.080	35	2.032	85	1.991
2	4.303	12	2.179	22	2.074	40	2.021	90	1.990
3	3.182	13	2.160	23	2.069	45	2.015	95	1.988
4	2.776	14	2.145	24	2.064	50	2.010	100	1.987
5	2.571	15	2.131	25	2.060	55	2.005	105	1.985
6	2.447	16	2.120	26	2.056	60	2.000	110	1.983
7	2.365	17	2.110	27	2.052	65	1.998	115	1.981
8	2.306	18	2.101	28	2.048	70	1.996	120	1.980
9	2.262	19	2.093	29	2.045	75	1.995		
10	2.226	20	2.086	30	2.042	80	1.993	$\infty$	1.96

### Sample size

The necessary sample size  $n$  may have to be computed iteratively if  $n$  is smaller than approximately 200 because the value of  $t$  depends on sample size (Table 5.2). This is not a concern for pebble counts which comprise more than 200 particles. However, when using the general sample-size equation Eq. 5.1 to compute the number of subsamples required for a specified precision (two-stage sampling, Section 5.2.3.1),  $n$  may be smaller than 10, and  $t$  varies pronouncedly with  $n$  when  $n$  is small (Table 5.1).

The calculated sample size refers to the confidence level specified by the  $t$  value. If a  $t$ -value for a 95% confidence level is used, i.e.,  $t_{1-\alpha/2, n-1} = t_{0.975, n-1}$ , a sample size is computed for which there is a 95% chance that the absolute difference (positive or negative) between the estimated sample mean and the true population mean is less than the specified acceptable error.

The computed sample size is usually rounded to the next higher integer value, because sample sizes are whole numbers, not decimals. Either 7 or 8 samples are collected, but not 7.3. It is left at the user's discretion of whether a sample size of 13.1 is rounded to 13 or 14. Rounding is denoted by the symbol  $\cong$  in this document.

## 5.2.2 Prespecified error around the mean

The variables in the right-hand term of the general sample-size equation (Eq. 5.1) can be slightly altered, so that Eq. 5.1 can be used to compute the sample size around the mean for a variety of different applications. Sample errors around the mean may be specified as absolute error  $e_{\pm\phi m}$  in  $\phi$ -units, as percent error  $e_{\%Dm}$  around the mean in mm, and as percent error  $e_{\%\phi m}$  around the mean in  $\phi$ -units (Sections 5.2.2.1 – 5.2.2.3). The confidence level may be changed, and consequently the numerical value of  $t$ . In all example computations provided in this section, sample sizes are computed for a 95% confidence level ( $\alpha = 0.05$ ), a value that is commonly selected. However, some study objectives may specify a different confidence level. A normal distribution of bed-material is assumed when using Eq. 5.1, but a slight variation of the error term makes it possible to use the equation for logarithmically distributed samples (Section 5.2.2.4). Another assumption for Eq. 5.1 is an unlimited supply of particles to be sampled. Again, a slight modification of Eq. 5.1 allows the user to compute sample size when the number of particles that may be sampled is limited, for example, in a small sampling area (Section 5.2.2.5). All variations of Eq. 5.1 used in Section 5.2.2.1 to 5.2.2.5 are listed in Table 5.5 in Section 5.2.2.6. Example computations are performed with all equations introduced in Sections 5.2.2.1 - 5.2.2.5 for the same particle-size distributions so that computed samples sizes may be compared (Section 5.2.2.6).

### 5.2.2.1 Absolute error around the mean in $\phi$ -units

The sample size for a specified absolute error around the mean particle size of a sample in terms of  $\phi$ -units (e.g.,  $e_{\pm\phi m} = \pm 0.2 \phi$ -units) is computed from:

$$n = \left( \frac{t_{1-\alpha/2;n-1}}{e_{\pm\phi m}} \cdot s_I \right)^2 \quad (5.2)$$

$n$  is the sample size for which there is a small (e.g., 5%) chance only ( $\alpha = 0.05$ ) that the absolute difference (positive or negative) between the estimated sample mean and the true population mean is larger than or equal to the acceptable absolute error  $e_{\pm\phi m}$ .

#### Example 5.1:

Given is the particle-size distribution from Table 2.3 and Fig. 2.12 in Section 2.1.4.1:

$$\begin{array}{lll}
D_{84} = 104 \text{ mm} & \phi_{84} = -6.70 & s_I = |\phi_{84} - \phi_{16}|/2 = 1.94 \\
D_{50} = 32 \text{ mm} & \phi_{50} = -5.00 & \\
D_{16} = 7 \text{ mm} & \phi_{16} = -2.82 & \\
D_m = 27.2 \text{ mm} & \phi_m = -4.76 & 
\end{array}$$

If the user has no idea about the approximate value of  $n$ , the  $t$ -value for an indefinitely large sample size  $n \rightarrow \infty$  is used in a first trial. For  $\alpha = 0.05$ ,  $t_{0.975, n-1} = 1.96$ , and sample size  $n$  for an acceptable absolute error  $e = \pm 0.2 \phi$ -units becomes:

$$n = \left( \frac{1.96}{0.2} \cdot 1.94 \right)^2 = 361.5 \cong 362.$$

If the acceptable error is increased to  $e_{\pm\phi m} = \pm 0.5 \phi$ ,  $n$  becomes 57.8, rounded up to 58. In this case, a  $t$ -value of 1.96 would not be appropriate and computations need to be repeated with a  $t$ -value for  $n-1 = 57$ , which is close to 2.00 (Table 5.2). Using  $t_{0.975, n-1} = 2.00$ ,  $n = 60.2$ , and is rounded to 61. This computed  $n$  is almost similar to the  $n$  for which the  $t$ -value was selected. Usually, about three iterations are required to reach this convergence.

Eq. 5.2 indicates that a pebble count in a poorly sorted streambed ( $s_I \approx 2$ ) requires almost 400 particles for a 95% certainty that the mean of the sample is by no more than  $\pm 0.2 \phi$ -units different from the population mean. An error of  $\pm 0.2 \phi$  means that in 95% of all samples, the sampled mean can be expected to be within the range of -4.56 to -4.96  $\phi$  (i.e., between 23.6 and 31.1 mm) of the true mean of -4.76  $\phi$  (i.e., 27.2 mm).

Fig. 5.2 shows relations between sample size and the absolute error  $e_{\pm\phi m}$  in  $\phi$  units around the mean using  $t$ -statistics and a 95% confidence level for samples with various sorting coefficients. These curves may be used to estimate the number of particles required for a desired precision in pebble counts in streams with different sorting coefficients. Sample size in Fig. 5.2 was calculated iteratively to account for the variation of  $t_{1-\alpha/2, n-1} = t_{0.975, n-1}$  with  $n$ .

### 5.2.2.2 Percent error around the mean in mm

Eq. 5.2 can be adjusted to apply to particle sizes in mm (ISO 1992). In this case, sorting is expressed as the logarithmic geometric standard deviation  $s_{g:sq}$  (see Eq. 2.54, Sect. 2.1.5.4), and the error is expressed in terms of the log of the percentage error around the  $D_m$  in mm added to 1.

$$n = \left( \frac{t_{1-\alpha/2; n-1}}{\log(1 + e\%D_m)} \cdot s_{g:sq} \right)^2 \quad (5.3)$$

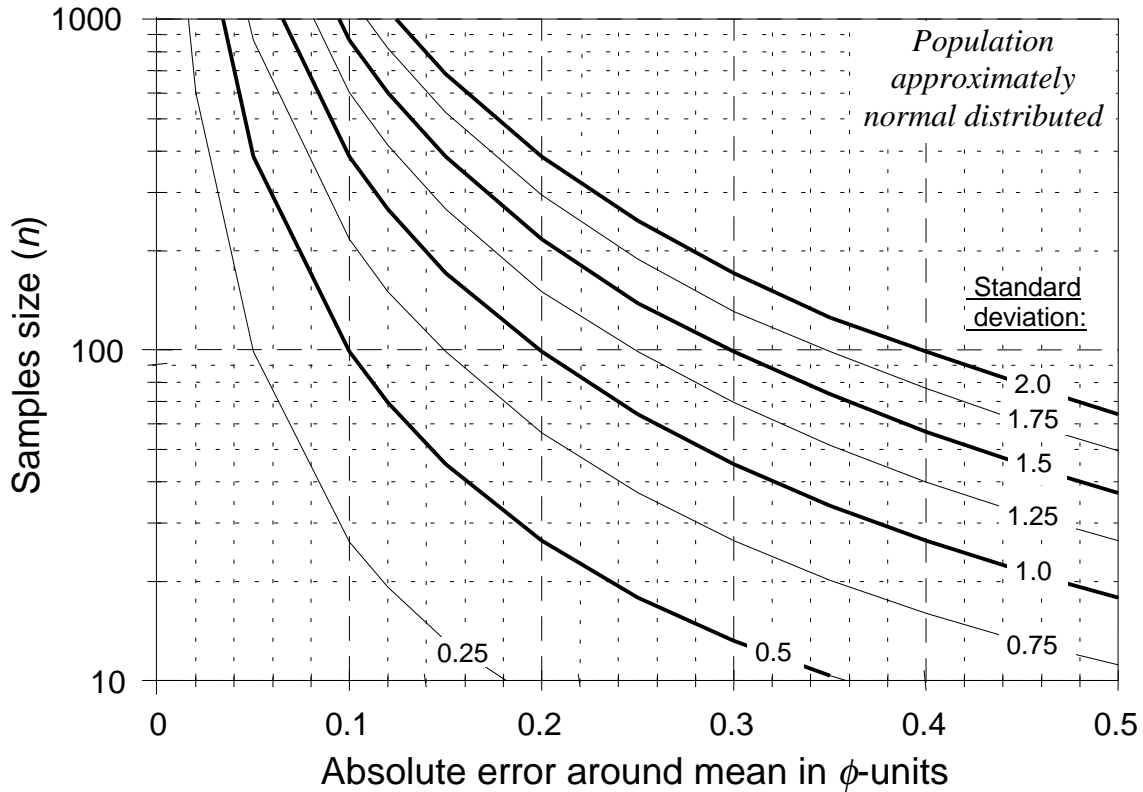


Fig. 5.2: Relation between sample size  $n$  and absolute error  $e_{\pm\phi_m}$  around the mean in  $\phi$ -units based on Student's  $t$ -values for approximately normal distributed bed material for various sorting coefficients, and  $\alpha = 0.05$ . Sample size  $n$  was computed iteratively to adjust for the variability of  $t_{0.975, n-1}$  with sample size.

**Example 5.2:**

A pilot study estimates  $D_{84} = 104$  mm, and  $D_{16} = 7$  mm. The logarithmic geometric standard deviation (Sect. 2.1.5.4) is  $s_{g:sq} = 0.5 \log(D_{84}/D_{16}) = 0.586$ .

The absolute error of  $\pm 0.2 \phi$  in Eq. 5.2 corresponds approximately to a  $\pm 13.9\%$  error around the  $D_m$  of 27.2 mm (see below) which was chosen as the tolerable error. In log units, an error of  $\pm 13.9\%$  is expressed as  $\log(1+0.139)$ .  $n$  is computed by solving the equation:

$$n = \left( \frac{1.96}{\log 1.139} \cdot 0.586 \right)^2 = 415.7 \approx 416$$

**Comparison of absolute error in  $\phi$  and percent error in mm**

Sample-size computations in  $\phi$  units and in the corresponding units of mm are not truly equivalent, because an error that is symmetrical around a mean in  $\phi$  units is not

symmetrical around the mean in mm, and vice versa. For example, an absolute error of  $\pm 0.2 \phi$  units around a mean particle size of  $\phi_m = -5.0 \phi$  encompasses the range of -4.8 to -5.2  $\phi$ . The equivalent range in mm is 27.9 to 36.8. The percent difference between 27.9 mm and the mean particles size  $D_m$  of 32 mm is  $(27.9 - 32) \cdot 100/32 = -12.8\%$ , whereas the percent difference between 36.8 mm and the  $D_m$  of 32 mm is  $(37.7 - 32) \cdot 100/32 = 15.0\%$ . This asymmetry may be negligible for relatively small errors, but becomes quite pronounced as the absolute error in  $\phi$  increases. An error of  $\pm 1.0 \phi$  around a  $\phi_m$  of  $-5.0 \phi$  (=percentage error of 20%) encompasses the size range of -4 to -6  $\phi$  that is equivalent to the range of 16 to 64 mm, and describes an error of -50 to +100% around the  $D_m$  of 32 mm (see Fig. 5.9 in Section 5.2.3.4).

### 5.2.2.3 Percent error around the mean in $\phi$ -units

The percent error  $e_{\% \phi_m}$  around the mean in  $\phi$ -units is the absolute error divided by the mean and computed from  $e_{\% \phi_m} = e_{\pm \phi_m} / \phi_m$ . Sample size for a percent error  $e_{\% \phi_m}$  with a 5% chance ( $\alpha = 0.05$ ) that the difference between sample  $\phi_m$  and population mean  $\phi_m$  is smaller than the prespecified percent error may be computed from

$$n = \left( \frac{t_{1-\alpha/2; n-1}}{e_{\% \phi_m}} \cdot \frac{s_I}{\phi_m} \right)^2 = \left( \frac{t_{1-\alpha/2; n-1}}{e_{\% \phi_m}} \cdot CV \right)^2 \quad (5.4)$$

Note that sample standard deviation (or sediment sorting) is divided by  $\phi_m$  as well.  $s/\phi_m$  defines the coefficient of variation  $CV$ , also termed the relative standard deviation. Using the Inman sorting coefficient  $s_I$  to describe the standard deviation  $s$ ,  $CV$  may be computed from:

$$CV = \frac{s}{\phi_m} = \frac{\frac{|\phi_{84} - \phi_{16}|}{2}}{\phi_m} = \frac{|\phi_{84} - \phi_{16}|}{2\phi_m} \quad (5.4a)$$

Estimates of  $\phi_{84}$ ,  $\phi_{50}$ , and  $\phi_{16}$  may be obtained from a pilot study of a 100-particle pebble count. Table 5.3 presents coefficients of variation ( $CV$ ) for bed material of different sorting coefficients and different mean particle sizes.

#### Example 5.3:

From Example 5.1,  $s_I$  is taken as 1.94, and sample  $\phi_m$  is  $-4.76 \phi$ .

An absolute error of  $\pm 0.2 \phi$ -units (Example 5.1) becomes a percent error  $e_{\% \phi_m} = \pm 0.2 / -4.76 = 0.042$  or 4.2%.  $n$  is computed from:

$$n = \left( \frac{1.96}{0.042} \cdot \frac{1.94}{-4.76} \right)^2 = (46.67 \cdot 0.408)^2 = 361.7 \cong 362$$

The sample size calculated by Eq. 5.4 is equal to the sample size calculated by Eq. 5.2.

Table 5.3: Values of CV for poorly sorted bed material with various sorting coefficients and various mean particle sizes

$D_m$ (mm)	$\phi_m$ ( $\phi$ -units)	Sorting coefficient $s_f$		
		1.0	1.5	2.0
16	-4.0	0.25	0.38	0.50
22.6	-4.5	0.22	0.33	0.44
32	-5.0	0.20	0.30	0.40
45	-5.5	0.18	0.27	0.36
64	-6.0	0.17	0.25	0.33

#### 5.2.2.4 Percent error in $\phi$ and mm for approximate lognormal distributions

Although particle-size distributions in  $\phi$  units tend to roughly approach normal distributions, it is conceivable that a particular particle-size distribution might obtain a better fit to a log-normal distribution than a normal distribution. In this case, Eq. 5.5 may be used to estimate the sample size for a prespecified percent error around the mean (Gilbert 1987).

$$n = \frac{t_{1-\alpha/2;n-1}^2 \cdot s_f^2}{\ln(e^{\% \phi_m} + 1)} \quad (5.5)$$

#### Example 5.4:

In accordance to Example 5.3, an absolute error of  $\pm 0.2 \phi$ -units around the mean of  $-4.76 \phi$  becomes a percent error of 0.042 or 4.2%. Sample size is computed from:

$$n = \frac{1.96^2 \cdot 1.94^2}{\ln(0.042+1)} = \frac{3.84 \cdot 3.76}{0.041} = 351.4 \cong 352$$

A similar form of Equation 5.5 may be applied if particle sizes in mm units approached a lognormal distribution. The graphic geometric standard deviation  $s_{g;sq} = (D_{84}/D_{16})^{0.5}$  is used in this case and has the value of 3.85 for  $D_{84} = 104$ , and  $D_{16} = 7$  mm (Eq. 2.54 in Section 2.1.5.4). A percentage error of 0.042 (4.2%) in terms of  $\phi$ -units (see above) is approximately similar to a percent error of 13.9% in mm-units for the particle-size distribution in the example.

$$n = \frac{t_{1-\alpha/2;n-1}^2 \cdot s_{g;sq}^2}{\ln(e^{\%Dm} + 1)} \quad (5.6)$$

Example 5.5:

$$n = \frac{1.96^2 \cdot 3.85^2}{\ln(0.139+1)} = \frac{3.84 \cdot 14.83}{0.129} = 438.9 \cong 439$$

#### 5.2.2.5 Limited number of particles available for sampling ( $N \neq \infty$ )

When sampling small geomorphological units (e.g., bars and riffles), or sedimentary units (areas of homogeneous bed-material composition) there may be a shortage of particles that can be sampled. The number of particles present on the particular geomorphological or sedimentary unit (the population size  $N$ ) might not be much larger, or even smaller than the sample size  $n$  computed with Eqs. 5.2 - 5.6. In this case, sample size  $n$  needs to be adjusted for limited population size  $N$ . This is accomplished by dividing the equation for unlimited sample size by  $1 +$  the quotient of the original sample-size equation and population size  $N$ . Equations that include a term for limited population size  $N$  provide virtually the same results as equations for unlimited  $N$ , if  $N$  exceeds  $n$  by a factor of 1000 or more. If  $N = 100 n$ ,  $n$  is reduced by less than 1% compared to the  $n$  computed without adjustment for  $N$ , and if  $N = 10 n$ ,  $n$  reduces by 10%. Thus, as  $N$  decreases, sample size  $n$  also decreases.

#### ***Absolute error around mean in $\phi$ -units***

For a prespecified absolute error  $e_{\pm\phi m}$  in  $\phi$ -units, and a limited number of particles  $N$  in the target population available for sampling,  $n$  is computed from (Gilbert 1987)

$$n = \frac{\left( \frac{t_{1-\alpha/2;n-1}}{e_{\pm\phi m}} \cdot s_I \right)^2}{1 + \left( \left( \frac{t_{1-\alpha/2;n-1}}{e_{\pm\phi m}} \cdot s_I \right)^2 / N \right)} \quad (5.7)$$

Example 5.6:

A grid count is done on a small bar with an area  $A_b = 2 \text{ m} \cdot 2.6 \text{ m} = 5.2 \text{ m}^2$ . Almost all surface particles are within the size range of 35 - 45 mm. If the mean particle  $b$ -axis size is 45 mm, and particles are mostly ellipsoid ( $a$ -axis = 1.5  $b$ -axis) and flat lying, the area covered by one particle  $A_p$  can be approximated by  $A_p = \pi (0.045/2 \cdot 0.068/2) = 0.0024 \text{ m}^2$ . Thus, the number of surface particles on this bar is estimated to be  $N = A_b/A_p = 2164$ .

$$n = \frac{\left(\frac{1.96}{0.2} \cdot 1.94\right)^2}{1 + \left(\frac{1.96}{0.2} \cdot 1.94\right)^2 / 2164} = \frac{361}{1 + (361/2164)} = 309.4 \cong 310$$

Equation 5.2 (for unlimited population size) produced a sample size of 362. Because of the limited number of particles in the population, Eq. 5.7 calculates a lower sample size of  $n = 310$ . The effect of population size  $N$  on sample size becomes negligible as  $N$  exceeds 100  $n$  (ca. 50,000), and  $n$  increases to 359. For the example above, this occurs as the sampling area reaches 119 m<sup>2</sup> (Table 5.4).

Table 5.4: Example of change in sample size  $n$  with a change in population size  $N$ .

$N$	Sampling Area (m <sup>2</sup> )	Side length for square (m)	$n$
100	0.24	0.5	78
500	1.2	1.1	210
1,000	2.4	1.5	265
5,000	12	3.5	337
10,000	24	5	349
50,000	119	11	359
100,000	238	15	360
500,000	1190	35	361

#### ***Percentage error around the mean in mm***

If the adjustment for limited population size is applied to Eq. 5.3, the sample size required for a specified percentage error around the  $D_m$  (in mm) is computed from:

$$n = \frac{\left(\frac{t_{1-\alpha/2;n-1} \cdot S_{gl}}{\log(1+e\%D_m)}\right)^2}{1 + \left(\frac{t_{1-\alpha/2;n-1} \cdot S_{gl}}{\log(1+e\%D_m)}\right)^2 / N} \quad (5.8)$$

#### ***Percent error around the mean in $\phi$ -units***

Similar to Eq. 5.4, sample size for a specified percent error around the mean in a limited population size and an approximately normal distribution of particle sizes in  $\phi$ -units is estimated from:

$$n = \frac{\left( \frac{t_{1-\alpha/2;n-1}}{e_{\% \phi m}} \cdot \frac{s}{\phi_m} \right)^2}{1 + \left( \left( \frac{t_{1-\alpha/2;n-1}}{e_{\% \phi m}} \cdot \frac{s}{\phi_m} \right)^2 / N \right)} \quad (5.9)$$

***Percent error around the mean in  $\phi$ -units, approximate lognormal distribution assumed***

Parallel to Eq. 5.5, sample size for a specified percent error around the mean of an approximately lognormal distribution of particle sizes in  $\phi$ -units and a limited population size is obtained from:

$$n = \frac{t_{1-\alpha/2;n-1}^2 \cdot s^2}{[\ln(e_{\% \phi m} + 1)] + \left( \frac{t_{1-\alpha/2;n-1}^2 \cdot s^2}{N} \right)} \quad (5.10)$$

***Percent error around the mean in mm, approximate lognormal distribution assumed***

As in Eq. 5.6, sample size for a specified percent error around the mean of an approximately lognormal distribution of particle sizes in mm and a limited population size is obtained from:

$$n = \frac{t_{1-\alpha/2;n-1}^2 \cdot s^2}{[\ln(e_{\% Dm} + 1)] + \left( \frac{t_{1-\alpha/2;n-1}^2 \cdot S_{g:sg}^2}{N} \right)} \quad (5.11)$$

**5.2.2.6 Comparison between sample-size equations for errors around the mean**

Equations introduced in this section are summarized in Table 5.5. When applied to the same particle-size distribution, all equations compute sample sizes between 352 to 439 for an absolute error around the mean of  $\pm 0.2 \phi$ , which is equivalent to a 4.2 % error (around the mean in  $\phi$ ), and approximately equal to an error of  $\pm 13.9$  % around the mean in mm. To compare the results of the five equations (5.2 to 5.6) over a wide range of errors, sample sizes were computed for errors between  $\pm 0.1$  and  $1.0 \phi$ , and plotted in Fig. 5.3. Eqs. 5.2 ( $e_{\pm \phi m}$ ) and 5.3 ( $e_{\% \phi m}$ ) yield identical relations between sample size and error, while sample size computed for a corresponding percent error in mm units, ( $e_{\% Dm}$ ) (Eq. 5.3) is slightly higher. The sample size – error relations have a somewhat different shape if the particle-size distribution is assumed to approach a lognormal distribution instead of a normal one.

Table 5.5: Variations of the standard sample-size equation for computing absolute or percent errors around the mean particle-size in mm ( $D_m$ ) or  $\phi$ -units ( $\phi_m$ ) for approximately normal and lognormal distributions, and for unlimited and limited population particle numbers. Numbers in parentheses refer to equation numbers in the document.

Particle size units	Particle-size distribution type	Error around the mean	Unlimited population Size ( $N > 100n$ )	Limited population Size ( $N < 100n$ )
$\phi$	approx. lognormal	absolute	$\left(\frac{t \cdot s_I}{e_{\pm\phi m}}\right)^2$ (eq. 5.2)	$\frac{\left(\frac{t}{e_{\pm\phi m}} \cdot s_I\right)^2}{1 + \left(\left(\frac{t}{e_{\pm\phi m}} \cdot s_I\right)^2 / N\right)}$ (eq. 5.7)
mm	approx. lognormal	percent	$\left(\frac{t \cdot s_{g:sq}}{\log(1+e_{\%Dm})}\right)^2$ (eq. 5.3)	$\frac{\left(\frac{t \cdot s_{g:sq}}{\log(1+e_{\%Dm})}\right)^2}{1 + \left(\frac{t \cdot s_{g:sq}}{\log(1+e_{\%Dm})}\right)^2 / N}$ (eq. 5.8)
$\phi$	approx. normal	percent	$\left(\frac{t \cdot s_I}{e_{\%\phi m} \cdot \phi_m}\right)^2$ (eq. 5.4)	$\frac{\left(\frac{t}{e_{\%\phi m}} \cdot \frac{s_I}{\phi_m}\right)^2}{1 + \left(\left(\frac{t}{e_{\%\phi m}} \cdot \frac{s_I}{\phi_m}\right)^2 / N\right)}$ (eq. 5.9)
$\phi$	approx. lognormal	percent	$\frac{t^2 \cdot s_I^2}{\ln(1+e_{\%\phi m})}$ (eq. 5.5)	$\frac{t^2 \cdot s_I^2}{\ln(1+e_{\%\phi m}) + \left(\frac{t^2 \cdot s_I^2}{N}\right)}$ (eq. 5.10)
mm	approx. lognormal	percent	$\frac{t^2 \cdot s_{g:sq}^2}{\ln(1+e_{\%Dm})}$ (eq. 5.6)	$\frac{t^2 \cdot s_{g:sq}^2}{\ln(1+e_{\%Dm}) + \left(\frac{t^2 \cdot s_{g:sq}^2}{N}\right)}$ (eq. 5.11)

$t$  = values for Student's  $t$  statistic, =  $t_{1-\alpha/2; n-1}$ ;  $s_I$  = Inman's sorting coefficient;  $s_{g:sq}$  = geometric standard deviation, square-root approach;  $e_{\pm\phi m}$  = absolute error around the mean particle-size computed in  $\phi$ -units.  $e_{\%Dm}$  = percent error around the mean particle-size;  $e_{\%\phi m}$  = percent error around the mean particle-size computed in  $\phi$ -units.

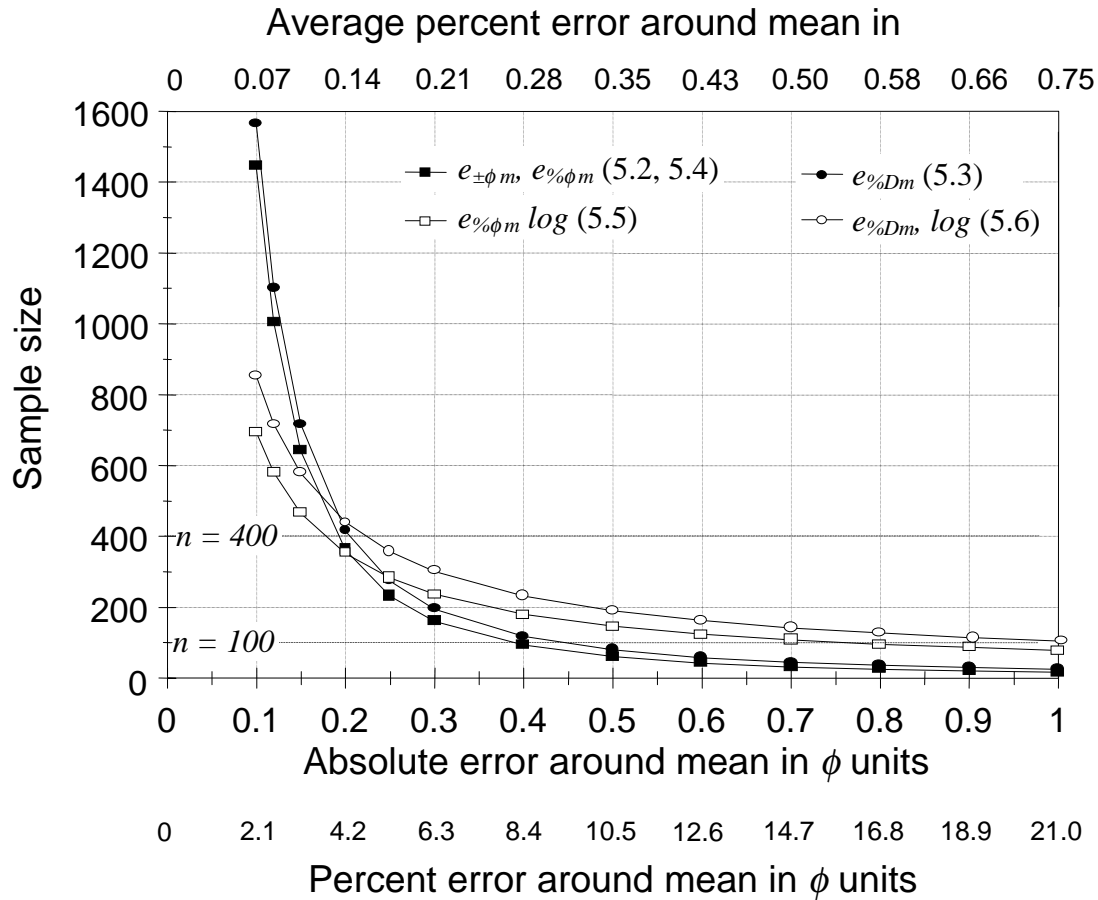


Fig. 5.3: Relation between sample size and error around the mean computed for the example particle-size distribution ( $D_{50} = 32$  mm,  $s = 1.94$ ; Table 2.3, Fig. 2.12) with five sample-size equations (Eq. 5.2 – 5.6). Equation numbers are indicated in brackets. The  $x$ -axis scale “Absolute error around the mean in  $\phi$ -units” refers to Eqs. 5.2 and 5.4. The  $x$ -axis scale “Percent error around the mean in  $\phi$ -units” refers to Eq. 5.5, whereas the  $x$ -axis scale “Average percent error around the mean in mm-units” refers to Eqs. 5.3 and 5.6.

### 5.2.2.7 Effect of bed-material sorting and error on sample size

The effects of bed-material sorting and acceptable error on sample-size requirements are quite pronounced (Fig. 5.2). Bed-material sorting typically ranges between 0.5 (well sorted lowland gravel-bed rivers) and 2.5 (poorly sorted headwater streams). Acceptable errors typically range between 5 and 50%. The numerical value for Student’s  $t$  varies by no more than 1% for sample sizes larger 25. Assume that a well sorted ( $s_I = 0.5$ ) lowland stream requires a sample size of 25 particles for an acceptable error around the mean. Sample size for the same mean particle size and the same acceptable error increases by a factor of 4 to 100 particles in a moderate to poorly sorted streambed ( $s_I = 1$ ), and again by a factor of 4 to 400 particles in a poorly to very poorly sorted ( $s_I = 2$ ) mountain gravel-bed stream. Similarly, for the same particle-size distribution, an increase of acceptable error from 10, to 20, to 40% decreases the sample-size requirement from 400, to 100, to 25

particles, respectively. Either a doubling in sorting, or halving of the acceptable error leads to a fourfold increase in sample size. These numerical examples demonstrate that statements of sample-size requirements cannot be taken out of context, but must be evaluated in light of streambed sorting and the acceptable error.

#### 5.2.2.8 Influence of multiple operators on sampling accuracy

None of the sample-size recommendations presented so far account for errors introduced by operators. Operator errors may be attributed to two main factors: (1) incorrect measurement of particle size (Section 2.1.3.6), and (2) biased particle selection among operators (Section 4.1.1.3 – 4.1.1.6). Both factors increase the variability of the sample (i.e., standard deviation) and consequently increase the sample-size requirement or reduce the accuracy. In contrast to the statistical error, the operator error becomes relatively more important as sample size increases. This is because the statistical error decreases with sample size, but operator error is the same for all sample sizes (Hey and Thorne 1983). Since sampling accuracy is comprised of the errors made by all operators involved, sampling accuracy decreases as more operators are involved in the sampling.

Prompted by observed operator errors, Marcus et al. (1995) compared results of five replicate samples each obtained by eight different operators at two different sites with five replicate samples each from a single operator. They found that when multiple operators took the samples, the standard deviation around a given particle size increased at a rate about twice as high with particle size than standard deviations of replicate samples from a single operator (Fig. 5.4). For a particle size of 2 mm, samples collected by the single operator had a standard deviation of  $\pm 2.6$  mm. This value increased to  $\pm 4.2$  mm when the replicate samples were collected by several operators. Likewise, particles with a 250 mm diameter had a standard deviation of  $\pm 30$  mm for a single operator. The value nearly doubled to  $\pm 54$  mm for multiple operators. This difference shows that it is more problematic to detect a change in bed-material size over time or between sites when several operators are involved.

As the standard deviation for multiple-operator samples exceeds the standard deviation for samples from a single operator (Marcus et al. 1995) by a factor of 1.8, the sample size needs to be larger by a factor of  $1.8^2 = 3.2$  when multiple operators are employed. Consequently, using two or more operators in the belief that the larger sample will provide a more accurate estimate of the population characteristics has the opposite effect: it increases the sample size necessary for the sample level of accuracy. The maximum benefit of intensive sampling is achieved *only* if *all* samples are collected by a single operator, unless operator bias can be substantially reduced (e.g., by training and using a sampling frame), or be eliminated altogether.

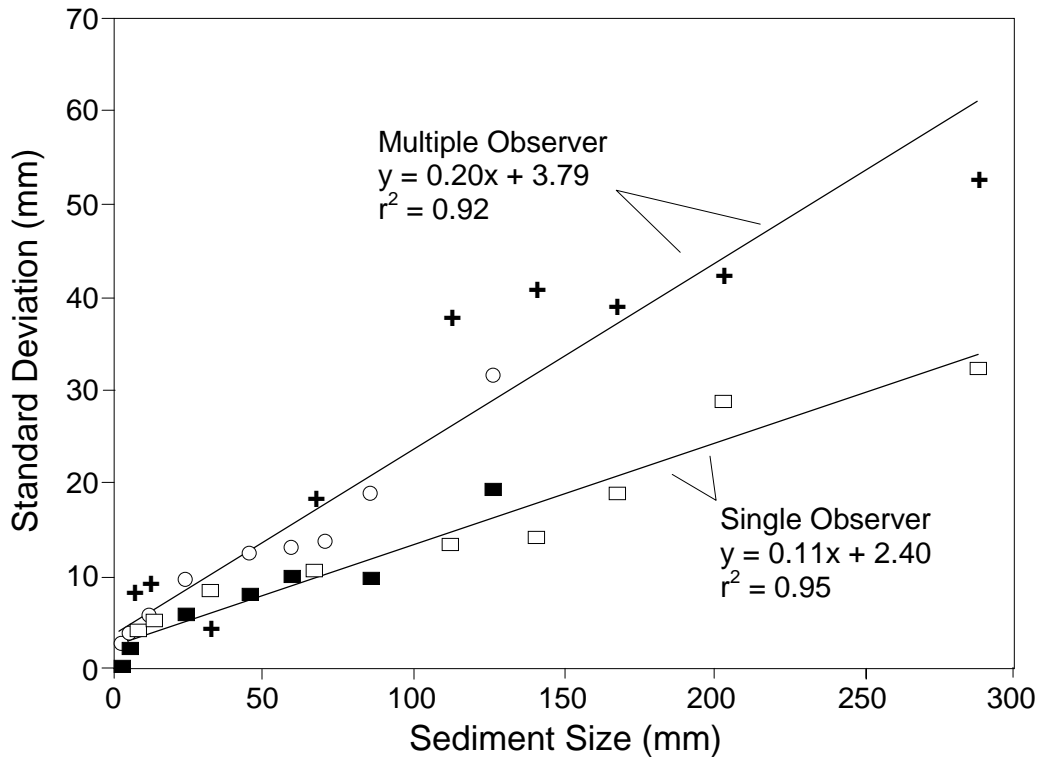


Fig. 5.4: Relation of mean size of 10 percentiles ( $D_{min}$ ,  $D_5$ ,  $D_{10}$ ,  $D_{25}$ ,  $D_{50}$ ,  $D_{75}$ ,  $D_{84}$ ,  $D_{90}$ ,  $D_{95}$ ,  $D_{max}$ ) to standard deviation for replicate samples collected by one (■, □) and by multiple observers (○, +). ■ and ○ refer to one sampling site, □ and + to another. (Redrawn from Marcus et al. (1995), by permission of the American Geophysical Union).

#### 5.2.2.9 Computation of sample size and error in the field

A study site may not be close to the office, and it might be inconvenient, if not unfeasible, to return to the study site at a later time to augment a sample size that is too small. Thus, it is recommended to compute the relation between sample size and error around the mean in the field. A laptop computer is needed and a prepared spreadsheet that computes a cumulative frequency distribution, the  $\phi_{16}$  and  $\phi_{84}$ , the Inman sorting coefficient, and the absolute error around the mean for a given sample size (Fig. 5.5). The spreadsheet should likewise be set up to compute the sample standard deviation using the moment method (Section 2.1.5.4).

As particles are added to the frequency distribution of the sample ( $n_i$ ), sample size, the particle size of the percentiles of interest, the sorting coefficient, and the currently obtained absolute error are automatically updated. Particles need to be added to the sample until the computed error is less than a specified value, for example  $\pm 0.2 \phi$ .

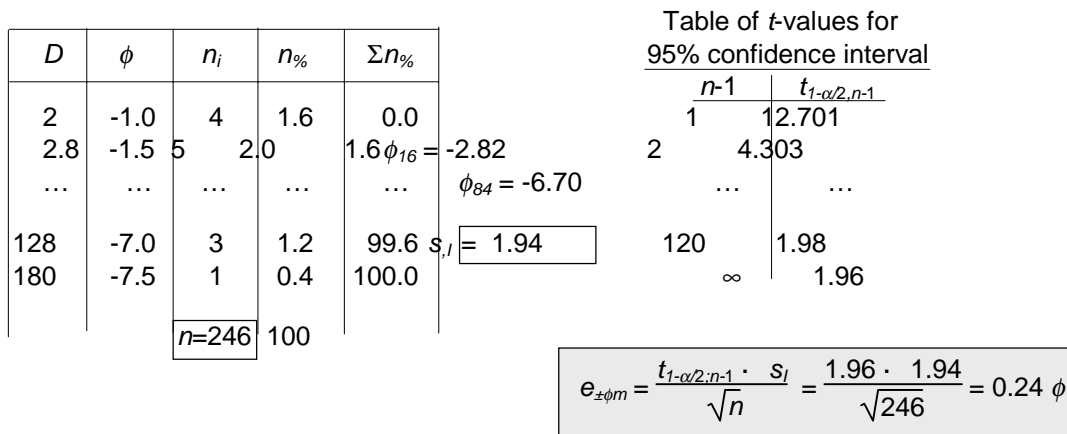


Fig. 5.5: Schematic presentation of a spreadsheet that could be used to compute the absolute error around the mean particle size in  $\phi$ -units directly in the field.

### 5.2.3 Specified error for all percentiles

The equations presented in the previous sections determine the sample size required for estimating the error between the sample and the population mean. However, the user might need to know the error associated with specific percentiles or with all percentiles of the distribution. A two-step sampling procedure (Section 5.2.3.1) can be used to compute the relation between sample size and precision for the median or percentiles close to the median. A binomial approach (Section 5.2.3.2) can be used for specific percentiles (e.g.,  $D_{10}$ ,  $D_{90}$ ), while a multinomial approach (Section 5.2.3.3) is used for computing the precision of the entire distribution. A bootstrapping approach (Section 5.2.3.4) can be used to compute the precision around specified percentiles through a resampling procedure.

#### 5.2.3.1 Two-stage sampling approach (ISO 1992)

Two-stage sampling is a procedure for bed-material sampling proposed by the International Organization of Standards (ISO 1992). The first step of the procedure involves collecting several subsamples (e.g., 5) each of equal size (e.g., 50 or 100 particles each). The median or, a percentile close to it, is computed for all subsamples as well as the standard deviation. In the second step a common sample-size equation (e.g., Eq. 5.2 in Section 5.2.2.1) is used to determine the number of subsamples needed to ensure that the difference between the computed median particle-size and the population median particle-size does not exceed a specified error value. The total number of sampled particles is the number of subsamples times the number of particles per subsample.

#### *Computation for particle sizes in mm*

Following the general steps previously described, a number of subsamples ( $q$ ) are taken from a homogeneous deposit, each sample containing  $n$  particles. For each of the  $q$  subsamples, the particle size of the median is determined, either graphically from

cumulative distribution curves, or by logarithmic interpolation between percentiles (Section 2.1.4.2). ISO (1992) proposes to compute the  $D_{50}$  in units of mm (although  $\phi$  units are preferable, see below). It is assumed that the  $q$  values of  $D_{50}$  are approximately normal distributed. The standard deviation  $s_{50}$  of the  $q$  values of  $D_{50}$  is determined from:

$$s_{50} = \sqrt{\frac{\sum_{i=1}^q (D_{50} - D_{50m})^2}{q-1}} \quad (5.12)$$

where  $D_{50m}$  is the arithmetic mean particle size in mm of the  $D_{50}$  obtained from the  $q$  subsamples.

The number of subsamples  $q$ , each with the same sample size  $n$ , required for a 5% chance (if  $\alpha = 0.05$ ) that the absolute difference (positive or negative) between the sampled median  $D_{50}$  and the population median (i.e., the mean median established from the subsamples) is larger or equal to the acceptable absolute error  $e_{\pm D_{50}}$  is computed using Eq. 5.13. The sample size  $q$  is likely to be rather small, perhaps less than 10. The value for  $t$  varies markedly with sample size as long as samples sizes are small. It is therefore important to use an appropriate value for  $t_{1-\alpha/2, q-1}$  (Table 5.2). The appropriate value for  $t$  is found by iteratively solving Eq. 5.13 until  $q$  equals the subsample size  $q$ .

$$q = \left( \frac{t_{1-\alpha/2, q-1}}{e_{\pm D_{50}}} \cdot s \right)^2 \quad (5.13)$$

The total number of particles to be sampled is the number of particles in each subsample  $n$ , multiplied by the number of  $q$  subsamples.

**Example 5.7:**

Eq. 5.13 is solved iteratively because the number of subsamples is typically smaller than 30 in bed-material samples, and the value for  $t_{1-\alpha/2, q-1}$  varies especially for small sample sizes. Assume that five subsamples had  $D_{50}$  particle sizes of 45, 64, 76, 90, and 108 mm, with a mean  $D_{50}$  of 77 mm, and a standard deviation  $s_{50}$  of 24.1 mm. The tolerable absolute error around the  $D_{50}$  is  $\pm 10$  mm. In the absence of an *a priori* estimate of the appropriate sample size for a  $\pm 10$  mm error, a value of  $q = 20$  subsamples is selected in the first trial of solving Eq. 5.13 (any other value would have been fine, too) and yields a subsample size of  $q = 26$ . The estimated subsample size ( $q_{est}=20$ ) and the computed subsample size ( $q_{comp}=26$ ) do not match after the first trial. The second trial uses

the estimated subsample size  $q = 26$  to estimate the appropriate value of  $t$ . The newly computed subsample size is  $q = 25$ . Using the  $t$ -value for  $q = 25$ , the value computed for  $q$  is 25. Equivalence is reached between the estimated and computed  $q$  for a subsample size of 25 after the third trail.

Trial	$q_{est}$	$q-1$	$t_{1-\alpha/2; q-1}$	$q_{comp}$
1	20	19	2.093	$25.4 \cong 26$ .
2	26	25	2.060	$24.7 \cong 25$
3	25	24	2.064	$24.7 \cong 25$ .

A total of 1,250 particles, i.e., 25 subsamples of 50 particles each, have to be sampled to ensure that the  $D_{50}$  particle size is within  $\pm 10$  mm of the true  $D_{50}$  particle size.

### **Computations in units of $\phi$**

It is recommended to apply the two-stage approach to particle-sizes in units of  $\phi$ , rather than to units of mm. The term  $D_{50}$  in Eqs. 5.12 and 5.13 is then substituted by values of  $\phi_{50}$ . The advantage of computations in  $\phi$  units is that the medians in  $\phi$  obtained from several subsamples approximate a normal distribution better than median values  $D_{50}$  in mm. For a normal distribution, sample means will be normally distributed for any subsample size  $n$ , whereas for lognormal or skewed distributions, sample means attain a normal distribution only for subsample sizes of 30 and larger (Triola 1995, p. 252-257).

#### Example 5.8:

The  $\phi_{50}$  particle sizes of four subsamples of 50 particles each are -5.2, -5.1, -5.0, and -4.8  $\phi$ . The standard deviation  $s$  of the four values of  $\phi_{50}$  is 0.171  $\phi$ . For an acceptable absolute error of  $\pm 0.2$   $\phi$ , Eq. 5.13 yields

$$q = \left( \frac{3.182}{0.2} \cdot 0.171 \right)^2 = 7.4 \cong 8$$

$q = 8$  subsamples (of 50 particles each, = 400 particles total) are required for an acceptable error around the  $\phi_{50}$  of  $\pm 0.2$   $\phi$ -units.

The two-step sampling method is most suitable when estimating the required sample size for a specified error around the median in the field. For sample sizes of 100 or 50, the median particle size can be quickly calculated on paper. Sample standard deviation is a preprogrammed function of many scientific calculators. Prepared forms or spreadsheets may be helpful when computing the sample size necessary for a specified error in the field.

### 5.2.3.2 Binomial distribution approach (Fripp and Diplas 1993)

The one-step methods compute the absolute error in mm or  $\phi$ -units, or the percentage error around the mean, whereas the two-step methods compute the absolute or percent error around a specified percentile. For both procedures it was assumed that either the entire distribution approximated a normal distribution, or that the percentile values from the various subsamples approached normal distributions. A binomial and a multinomial approach (Section 5.2.3.3) can be used for computing the error around a given percentile in terms of a percentile range. For example, a percentile error of  $\pm 10\%$  means that the particle size of the  $D_{75}$  may be within the particle size range of the  $D_{65}$  and  $D_{85}$  of the population. Binomial and multinomial approaches assume no specific underlying distribution type.

The binomial approach presented by Fripp and Diplas (1993) is based on the binomial probabilities of the percent finer or percent coarser cumulative particle-size distribution (i.e., the grain-size curve). The approach is used for computing the percentile error around a given percentile  $e_{\pm p}$ . The computed sample size  $n$  ensures that the particle size of a given percentile  $p$  is within a specified error range between two percentiles that are  $\pm$  some percentage larger and smaller than the percentile  $p$ .  $n$  is calculated from:

$$n = \frac{(Z_{1-\alpha/2})^2 \cdot p \cdot (1-p)}{e_{\pm p}^2} \quad (5.14)$$

$Z$  is the standard normal deviate that cuts off  $(100 \alpha/2) \%$  of the upper tail of a standard normal distribution.  $Z$ -values for various values of  $1-\alpha/2$  can be obtained from statistical tables provided in general statistics books. The value of  $Z_{1-\alpha/2}$  for the commonly chosen 95% confidence interval with  $\alpha = 0.05$  is 1.96 (see Table 5.1 for the relation between confidence interval,  $\alpha$ -levels, and corresponding values for  $Z_{1-\alpha/2}$ ).  $p$  is used as a decimal value of the percentile of interest (i.e., 0.5 for  $D_{50}$ ), and the subscript  $p$  refers to a specified percentile.

#### Example 5.9:

The sample size required to remain below a  $\pm 10\%$  percentile error around the  $D_{16}$ , i.e., the  $D_{16}$  particle size is to be within the range of the sample  $D_6$  to  $D_{26}$ , is

$$n = \frac{1.96^2 \cdot 0.16 \cdot (1 - 0.16)}{0.1^2} = 51.6 \cong 52$$

Eq. 5.14 can be solved for the error term and be used to compute the error associated with a given sample size. The error around the 50<sup>th</sup> percentile of a distribution of particle-sizes in mm ( $D_{50}$ ) for a sample size of  $n = 100$  is

$$e_{\pm p} = 1.96 \cdot \sqrt{\frac{0.5 \cdot (1 - 0.5)}{100}} = 0.098 = 9.8\%$$

An error of  $e_{\pm p} \approx 10\%$  indicates that the particle size of the sample  $D_{50}$  is within the  $D_{60}$  and the  $D_{40}$  of the population distribution

The binomial approach calculates independent confidence intervals, one at a time, for each particle size-class and can therefore not be used to represent the entire distribution. A multinomial approach is needed to compute error bands around an entire particle-size distribution.

### 5.2.3.3 Multinomial distribution approach (Petrie and Diplas 2000)

To overcome the limitations of a binomial approach, Petrie and Diplas (2000) presented a multinomial approach which can be used for placing confidence intervals around all particle-size classes in a cumulative frequency distribution curve of a pebble count sample. The population cumulative frequency distribution (i.e., the percent finer or percent coarser curve) can then be expected to be within the confidence interval in a specified percentage of all cases (e.g., in 90% of all cases for a 90% confidence interval). Similar to a binomial approach, a multinomial approach does not assume a specific underlying distribution type.

#### ***Relation between sample size and error***

The number of particles  $n$  necessary to ensure that a percentile of interest  $p$  is within an allowable confidence interval,  $e_{\pm p}$  (i.e., percentile error) is computed from:

$$n = \frac{(e_{\pm p} + p) \cdot (1 - e_{\pm p} - p) \cdot \chi^2_{\alpha/k;1}}{e_{\pm p}^2} \quad (5.15)$$

$e_{\pm p}$  is the error in percentage points around the percentile  $p$  of a particle-size distribution. An error of  $\pm 10$  percent around the  $D_{50}$  ( $e_{\%p50} = 0.1$ ), for example, means that the particle size of the sample  $D_{50}$  may be within the  $D_{40}$  and the  $D_{60}$  of the population distribution.  $\chi^2_{\alpha/k;1}$  is the upper  $(1-\alpha/k) \cdot 100$  percentage point of the chi-square distribution for one degree of freedom and can be obtained from standard statistical tables.  $\alpha$  is the confidence coefficient and  $k$  is the number of size classes of the particle-size distribution. If table values are not available, the value for  $\chi^2_{\alpha/k;1}$  can be approximated using a regression function that relates published values of  $\chi^2_{\alpha/k;1}$  to  $\alpha/k$  and yields ( $r^2 = 0.99$ ):

$$\chi^2_{\alpha/k;1} = -1.435 (-1.755 \cdot \ln(\alpha/k)) \quad (5.16)$$

**Example 5.10:**

$D_{50}$  is the percentile of interest  $p$ . The tolerable error  $e_{\pm p}$  between the sample estimate of  $D_{50}$  and the confidence interval around the  $D_{50}$  is  $\pm 10$  percent, i.e.,  $e_{\pm p} = 0.1$ . This means that the particle size of the sample  $D_{50}$  could be within the particle size of the  $D_{40}$  and the  $D_{60}$  of the population distribution. The desired confidence level is  $\alpha = 0.05$ , and the distribution has 10 size classes so that  $\alpha/k = 0.005$ . The table value of  $\chi^2_{\alpha/k;1}$  for one degree of freedom and  $\alpha/k = 0.005$  is 7.88. Eq. 5.16 computes  $\chi^2_{\alpha/k;1}$  as 7.86. Using the value 7.88, the necessary sample size is (Eq. 5.15)

$$n = \frac{(0.1 + 0.5) \cdot (1 - 0.1 - 0.5) \cdot 7.88}{0.1^2}$$

$$= \frac{0.6 \cdot 0.4 \cdot 7.88}{0.01} = 189.1 \cong 190.$$

The relation between sample size and percentile errors around the  $D_{50}$  is plotted in Fig. 5.6 for different numbers of particle size-classes  $k$ . A pebble count particle-size distribution from a coarse gravel or cobble-bed stream typically has 15 to 20 size classes when particle sizes are measured in  $0.5 \phi$  intervals. According to Eq. 5.15, a 100-particle sample with 15 size classes has a percentile error  $e_{\pm p50}$  of  $\pm 16\%$  and can only ensure that the  $D_{50}$  particle

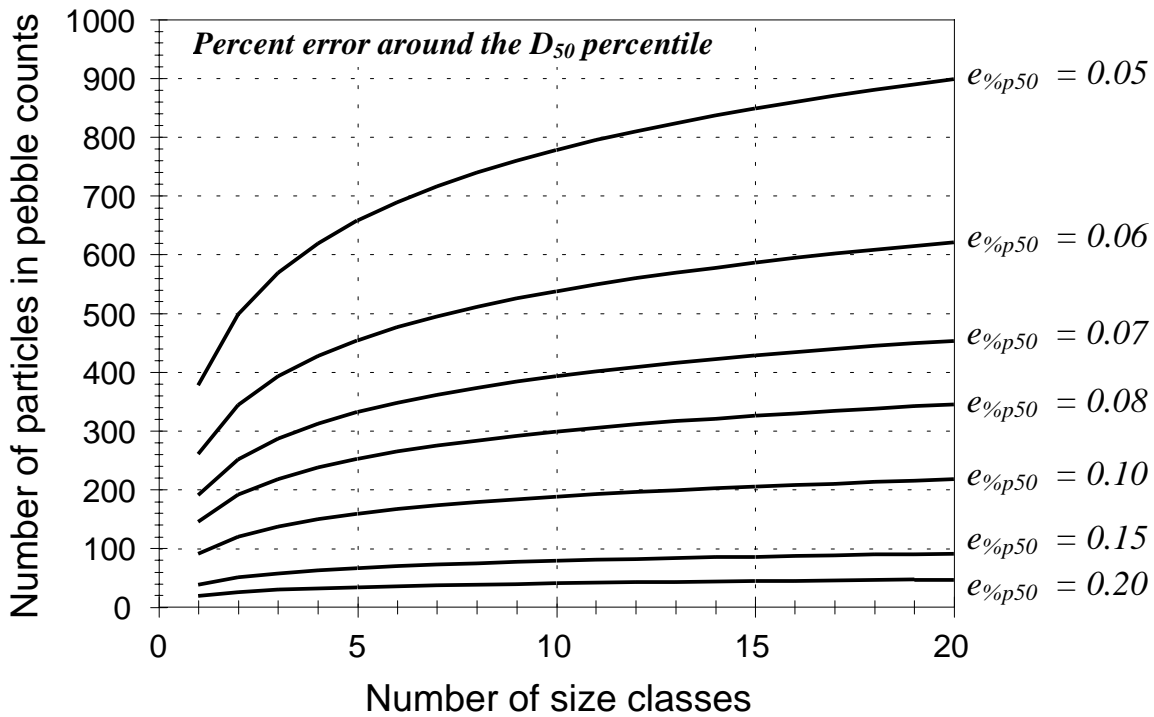


Fig. 5.6: Sample size necessary for various percentage errors around the  $D_{50}$  for different numbers of particle size-classes  $k$  of a particle-size distribution.

size is within the range of the population  $D_{34}$  to  $D_{66}$ . A 400-particle sample reduces this error to about  $\pm 7\%$ , narrowing the range of the  $D_{50}$  particle size of the sample to within a range between the  $D_{43}$  and the  $D_{57}$  population particle-size.

### Confidence bands

Confidence bands can be plotted around a distribution using the equation

$$e_{\pm p} = \sqrt{\frac{\chi^2_{\alpha/k;1} \cdot p_i \cdot (1 - p_i)}{n}} \quad (5.17)$$

The absolute percentile error around a given percentile varies only with the number of size classes  $k$  and the selected  $\alpha$ -value, and is the same for any particle-size distribution as long as the values of  $\alpha$  and  $k$  are identical. Fig. 5.7 plots error bands for a 95% confidence

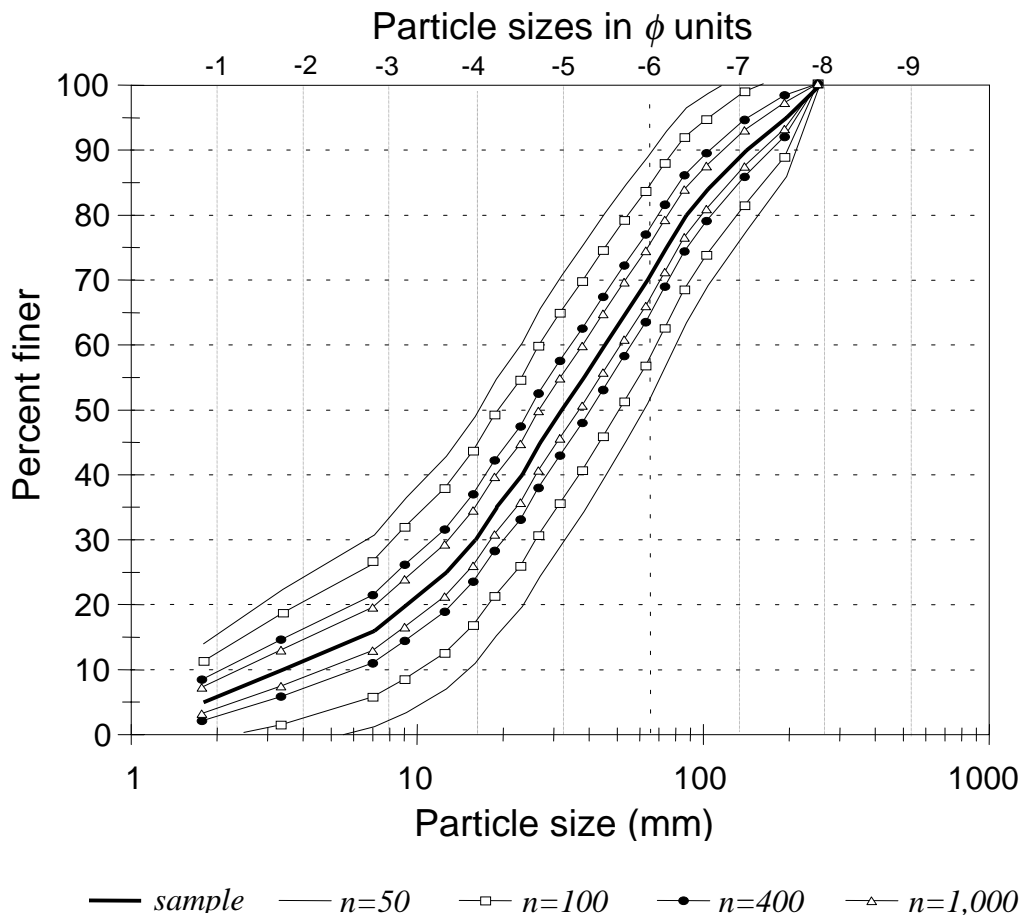


Fig. 5.7: Error bands ( $e_{\pm p_i}$ ) for a 95% confidence level around the example particle-size distribution given in Section 2.1.4.1 with 15 size classes ( $\alpha/k = 0.05/15 = 0.0033$ ;  $\chi^2_{\alpha/k;1} = 8.57$ ). Vertical lines indicate particle size classes in 1.0  $\phi$ -units.

level around the example particle-size distribution with 15 size classes presented in Section 2.1.4.1. Error bands are not entirely symmetrical around the distribution. For the example distribution used in Fig. 5.7, a sample size of  $n = 100$  produces a percentile error around the  $D_{80}$  of  $\pm 11.7\%$ , i.e., the  $D_{80}$  particle size could fall between the  $D_{92}$  and the  $D_{68}$  particle size. The percentile error around the  $D_{16}$  is  $\pm 10.5\%$ , meaning that the  $D_{16}$  particle size may fall between the  $D_{5.5}$  and the  $D_{26.5}$  population particle size.

#### 5.2.3.4 Bootstrap approach: no assumed distribution type (Rice and Church 1996b)

Rice and Church (1996b) proposed a computer sampling, or “bootstrap” method for determining the sample size required for a prespecified error (standard error or error in  $\phi$  units) around a given percentile. Bootstrapping determines the relation between error and sample size from repetitive computer sampling of a parent distribution that constitutes several thousands of actually measured bed-material particle  $b$ -axes. Bootstrapping, like the binomial and multinomial approaches (Section 5.2.3.2 and 5.2.3.3), does not require assumptions about the underlying parent distribution type. Computations are therefore free of any error introduced by assuming an inappropriate underlying distribution type and have the advantage that the computed sample-size requirements are tailored to a specific bed-material composition found at a specific sampling site.

#### ***Computation of the bootstrap percentile standard error and the absolute percentile precision***

A measurement of 3,500 particle  $b$ -axes provides a data base that is sufficiently large to be a good approximation of the population distributions. A large number of replicate samples  $r$ , e.g.,  $r = 200$  is drawn, each with the sample size  $n$  (sampling without replacement for each individual sample). A particle-size frequency distribution and a probability density function are constructed for each sample, and all percentiles of interest are determined. Thus, for each sample size  $n$  there are 200 repeated samples for a given bootstrap percentile  $D_{pb}$  (subscript  $b$  refers to bootstrap analyses), e.g., 200 values of  $D_{16b}$  established for a sample size of  $n = 50, 100, 500$ , etc. particles. The 200 replicates define a distribution of  $D_{pb,r=200}$  - values with an arithmetic mean  $D_{pmb,r=200}$  and a standard deviation  $s_{pb,r=200}$ . The standard deviation is the bootstrap percentile standard error  $s_{pb}$  for the bootstrap percentile  $D_{pb}$  and is computed from (Rice and Church 1996b):

$$s_{pb} = \frac{\sum^r (D_{pb} - D_{pmb})^2}{r - 1} \quad (5.18)$$

where  $D_{pmb}$  is the mean particle size of a specified percentile  $p$  in the bootstrap analysis. The procedure is repeated for each percentile of interest for various sample sizes. Once

the bootstrap standard error around a given percentile is known for various sample sizes, a power regression function can be established between  $s_{pb}$  and sample size  $n$

$$s_{pb} = a_p \cdot \sigma n^c \quad (5.19)$$

for each percentile.  $\sigma$  is the population bed-material standard deviation,  $a_p$  and  $c$  are coefficients obtained from the regression function.

For a *known* distribution, a percentile standard error  $s_p$  can be computed from:

$$s_p = \frac{\sqrt{p \cdot (1-p)}}{y_p} \cdot \frac{\sigma}{\sqrt{n}} \quad (5.20)$$

The index  $p$  refers to the specified percentile,  $p$  is the decimal value of the percentile (i.e., 0.5 for  $D_{50}$ ),  $y_p$  is the ordinate (y-value) of the population probability density function at the given percentile.  $y_p$  is not known if the distribution is not known, which makes it impossible to use Eq. 5.20 without prior knowledge of the particle-size frequency distribution. However, the first term of Eq. 5.20

$$\frac{\sqrt{p \cdot (1-p)}}{y_p} = a_p = \text{constant} \quad (5.21)$$

assumes a constant value  $a_p$  for each percentile for all sample sizes. The value  $a_p$  can be obtained from the least-square regression function of the relation between standard error and sample size (Eq. 5.19) computed from the bootstrap results. Substituting the first term of Eq. 5.20 with  $a_p$  allows the computation of the standard error around a percentile in an unknown distribution:

$$s_p = a_p \cdot \frac{\sigma}{\sqrt{n}} \quad (5.22)$$

In order to adjust computer sampling without replacement to a finite population from which the samples are drawn, a correction factor needs to be applied to the percentile standard error for a preset sample size  $n$  and population size  $N$ . This adjustment modifies Eq. 5.20 to

$$s_p' = \frac{\sqrt{p \cdot (1-p)}}{y_p} \cdot \frac{\sigma}{\sqrt{n}} \cdot \sqrt{\frac{N-n}{N-1}} \quad (5.23)$$

The standard percentile error corrected for finite population size is then computed from

$$s_p' = a_p \cdot \frac{\sigma}{\sqrt{n}} \cdot \sqrt{\frac{N-n}{N-1}} \quad (5.24)$$

For a population sample size  $N$  of 100  $n$  or more, the last term approaches 1 and can be omitted.

Rice and Church (1996b) used the bootstrap approach to compute the relation between sample size and error for various particle-size percentiles of a gravel-bed river in Canada (Mamquam River, Fig. 5.8). The particle-size distribution has a standard deviation of  $s = 1.17 \phi$  and is slightly skewed towards a tail of fine particles ( $sk_{aF\&W} = 0.165$  (Eq. 2.61);  $sk_{freq} = 0.55$  (Eq. 2.70)), a characteristic common to many gravel beds. The graphs showing the relationship between sample size and standard error (Fig. 5.10 and 5.11) are

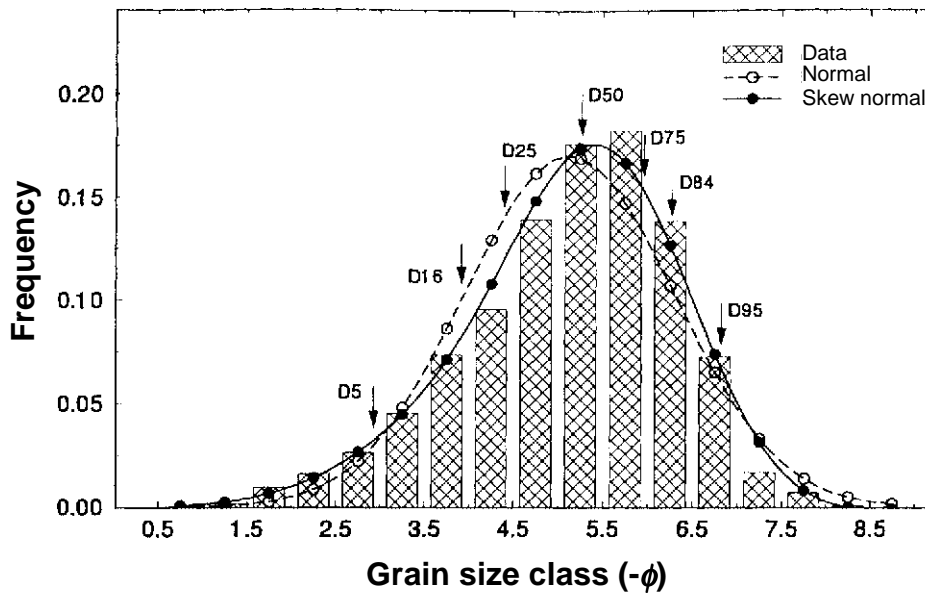


Fig. 5.8: Particle-size distribution for a sample from a bar head in the Mamquam River, British Columbia; mean annual flood is  $152 \text{ m}^3/\text{s}$ .  $D_{95} = 111 \text{ mm}$  ( $-6.8\phi$ ),  $D_{84} = 79 \text{ mm}$  ( $-6.29\phi$ ),  $D_{50} = 38 \text{ mm}$  ( $-5.25\phi$ ),  $D_{16} = 15 \text{ mm}$  ( $-3.91\phi$ ), and  $D_5 = 7.5 \text{ mm}$  ( $-2.91\phi$ );  $\sigma = 1.17\phi$ , skewness =  $0.165$  ( $sk_{aF\&W}$ ) or  $0.55$  ( $sk_{freq}$ ). According to a Kolmogorov-Smirnov test there is a less than 1% chance ( $\alpha = 0.01$ ) that the distribution is Gaussian. (Reprinted from Rice and Church (1996b), by permission of the Society for Sedimentary Geology).

discussed in the following section where the statistical (bootstrap) bootstrap error will be compared to statistical errors computed by assuming an underlying distribution type. The standard error computed from Eq. 5.24 can be converted into an absolute error in  $\phi$ -units by

$$s_p = \frac{e_{\pm\phi p}}{t_{(1-\alpha/2, n-1)}} \quad \text{and vice versa} \quad e_{\pm\phi p} = s_p \cdot t_{(1-\alpha/2, n-1)} \quad (5.25)$$

Values of  $t_{(1-\alpha/2, n-1)}$  for various samples sizes are listed in Table 5.2. Table 5.6 presents absolute errors in  $\phi$  obtained by converting the bootstrap standard errors for sample sizes 50, 100, 400, and 1000 particles and a 95% confidence level. Error values in Table 5.6 may be used as a general estimate of absolute errors expectable around various percentiles for bed material that is slightly skewed towards a tail of fine particles and that has a sorting coefficient close to 1.17.

Table 5.6: Absolute error  $e_{\pm\phi p}$  in  $\pm \phi$ -units for a 95% confidence level for percentile estimates of the Mamquam River, with a distribution slightly skewed towards a tail of fine particles and a standard deviation of  $s = 1.17 \phi$  (from Rice and Church 1996b).

Sample size	$D_5$	$D_{16}$	$D_{25}$	$D_{50}$	$D_{75}$	$D_{84}$	$D_{95}$
50	0.89	0.61	0.52	0.37	0.33	0.35	0.44
100	0.62	0.40	0.36	0.26	0.23	0.25	0.30
400	0.30	0.21	0.19	0.12	0.11	0.11	0.12
1000	0.19	0.13	0.12	0.07	0.07	0.06	0.07

Note that the computed bootstrap error is purely statistical. It does not include errors stemming from unrepresentative sampling by operators. The (statistical) bootstrap error around the seven percentiles between  $D_5$  and  $D_{95}$  for a sample size of  $n = 400$  (gray shaded box in Table 5.6) is plotted in Fig. 4.2 (Section 4.1.1.3) and compared to the total error observed in parallel pebble counts in mountain streams.

Standard and absolute errors in  $\phi$ -units can be converted into percent errors in mm-units. Fig. 5.9 may be used for these conversions.

***Percentile standard errors: bootstrap computation versus computations with assumed distribution types***

In symmetrical Gaussian distributions, standard percentile errors  $s_p$  and absolute errors in  $\phi$ -units  $e_{\pm\phi p}$  around percentiles have two properties: (1) they are paired such that errors around the  $\phi_{95}$  and the  $\phi_5$ , and errors around the  $\phi_{84}$  and  $\phi_{16}$ , etc. are equal; and (2) the tails of the distribution ( $\phi_5$  and  $\phi_{95}$ ) have higher errors than the mean ( $\phi_{50}$ ).

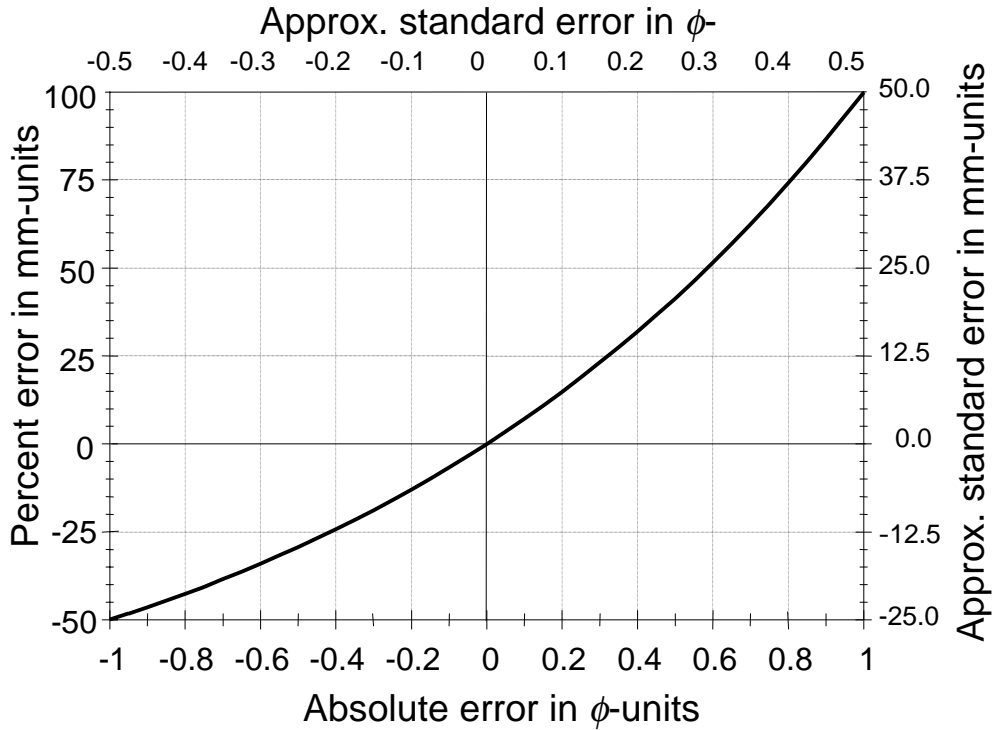


Fig. 5.9: Conversion of absolute and standard errors, in  $\phi$ -units to percent error in mm-units.  $t_{1-\alpha/2, n-1}$ , or  $Z_{1-\alpha/2}$  were approximated by the numerical value of 2.

The distribution of bed-material particle sizes in gravel-bed rivers is rarely symmetrical, not even when large sample sizes with smooth frequency distributions are collected in large streams (Fig. 5.8). Coarse gravel beds are usually slightly skewed towards a tail of fines particles. Therefore, standard or absolute errors are usually not paired, nor is the standard error of any percentile identical to the one computed when an underlying Gaussian distribution is assumed. In bed-material size distributions that are skewed towards a fine tail, the computed bootstrap error around the  $\phi_{84}$  is smaller than the error around the  $D_{84}$  computed from an assumed symmetrical normal distribution (Fig. 5.10). By contrast, the bootstrap error around the  $\phi_{16}$  is larger than the error around the  $\phi_{16}$  computed for an assumed Gaussian distribution. The more asymmetrical the particle-size population, the larger the difference between the error of paired percentiles, e.g., the  $D_{16}$  and  $D_{84}$ .

Similarly, the more asymmetrical the particle-size population the larger the difference between the standard or absolute errors for given percentiles obtained by bootstrapping compared to those obtained by assuming an underlying Gaussian distribution.

Note however, that the absolute error  $e_{\pm\phi_{50}}$  obtained from the bootstrap approach for the  $D_{50}$  particle size at the Mamquam River is similar to the absolute error around the mean  $e_{\pm\phi_m}$  computed by the general sample-size equation (Eq. 5.2).

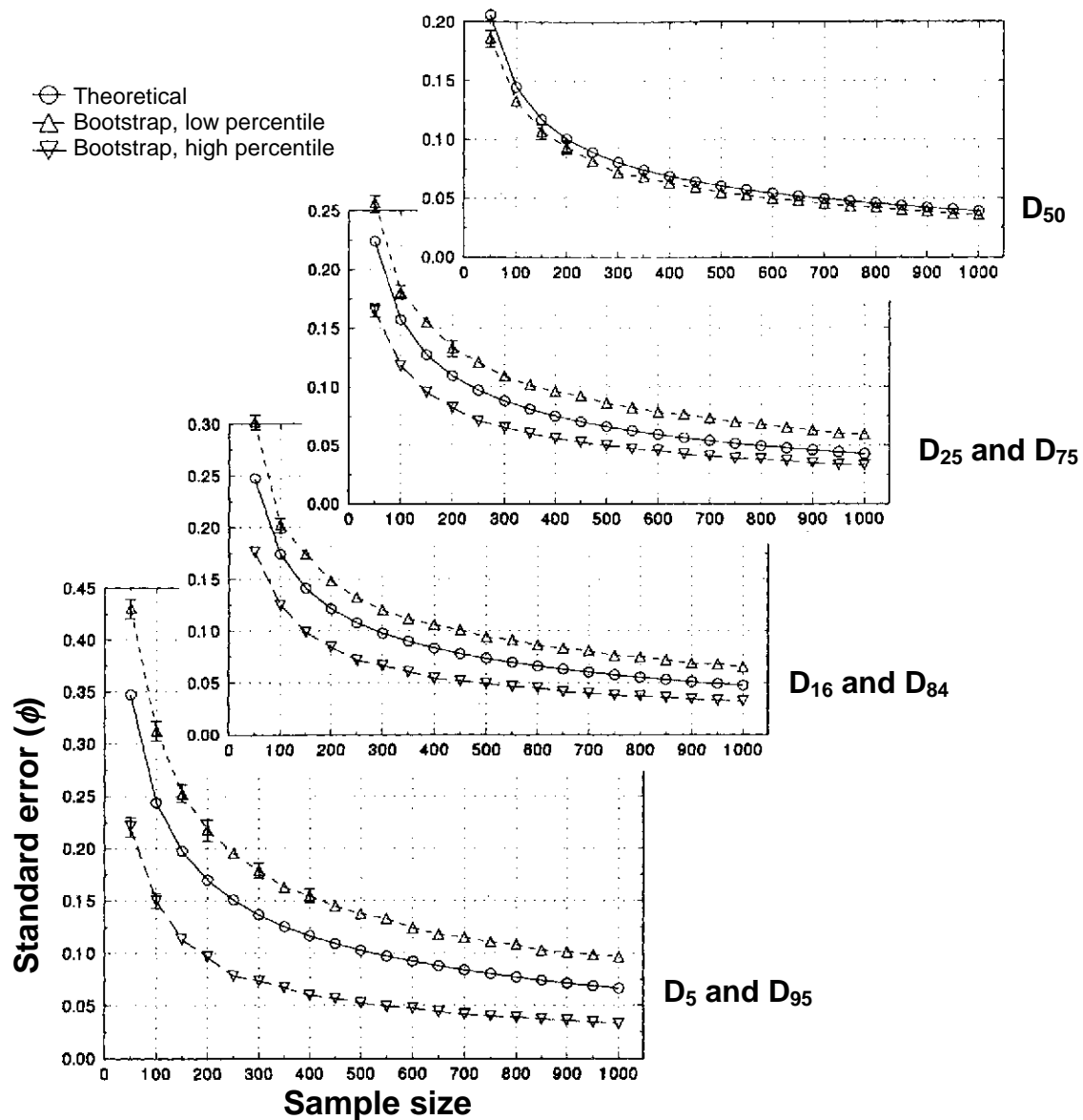


Fig. 5.10: Percentile standard errors for various sample sizes obtained from bootstrapping and from assuming an unskewed Gaussian distribution. (Reprinted from Rice and Church (1996b), by permission of the Society for Sedimentary Geology).

Rice and Church (1996b) compared not only the bootstrap percentile errors with the percentile errors computed for an assumed normal distribution, but also for a skewed normal distribution. The question was whether fitting a skewed normal distribution to the parent population would remove the difference between the bootstrap error and the error computed analytically for a best-fit skewed normal distribution. The assumption of a skewed normal distribution did not achieve a better agreement between bootstrap error and analytical error (Fig. 5.11). Particularly disconcerting was the unreliability of the

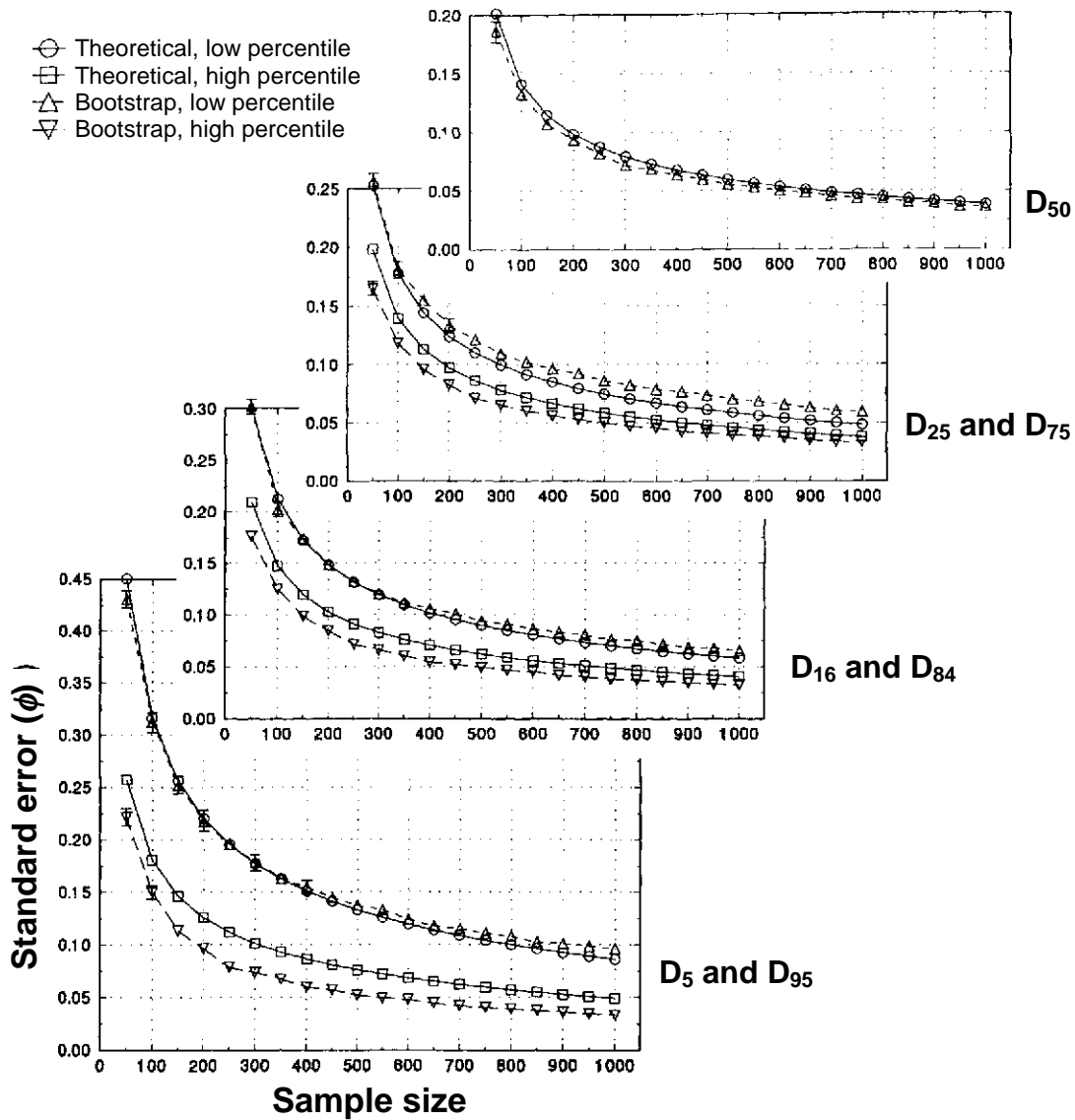


Fig. 5.11: Percentile standard errors for variable sample size obtained from bootstrapping and from assuming a skewed normal distribution. (Reprinted from Rice and Church (1996b), by permission of the Society for Sedimentary Geology).

improvements: while errors around some percentiles were well predicted when assuming a underlying skewed normal distribution, errors around other percentiles were greatly over- or underpredicted (Fig. 5.11). The only percentile for which there is relatively little difference between sample-size requirements from a bootstrap approach and those computed from assuming an underlying symmetrical or skewed Gaussian distribution is the  $\phi_{50}$ . This similarity indicates that bootstrapping is not necessary if the percentile in question is the  $D_{50}$ , or if a pilot study indicates that surface bed-material sizes could be approximated by a Gaussian distribution. If the distribution does not approach a normal distribution, and the percentile of interest is a high or low percentile, then bootstrapping or

a multinomial approach should be used. Alternatively, a two-step approach for percentiles in  $\phi$ -units may be used (Section 5.2.3.1). Bootstrapping becomes particularly useful for skewed and bimodal distributions, since the latter has no formal sample-size criteria (Rice and Church 1996b).

Software that includes bootstrapping procedures is commercially available, such as the program “Resampling Stats” from Resampling Stats Inc<sup>1</sup>, which has an add-in version for the spreadsheet program Microsoft Excel.

### ***Collecting the large sample necessary for bootstrapping is problematic in mountain streams***

A thorough bootstrapping analysis requires taking a large field sample to characterize the parent population. Rice and Church (1996b) used a sample of more than 3,500 particles. Sample sizes that large may be possible to obtain only in the beds of large streams that have large areas of homogeneous particle-size mixtures. Sampling several thousand particles is a problem in mountain gravel bed-rivers. If, for example, a stream is 10 m wide, and four particles are sampled per 1-m section along a transect using the sampling frame (Section 4.1.1.6), 40 particles can be sampled per transect. Almost 90 transects would have to be sampled to obtain 3,500 particles such as in the study by Rice and Church (1996b). If transects were spaced at about 2 m intervals, a homogeneous reach almost 200 m long would have to be sampled. Homogeneity over a 200 m stream segment could perhaps be expected in a plane-bed stream, but not in a riffle-pool stream that, if 10 m wide, has about 4 riffle-pool sequences over a 200 m distance. However, even though a bootstrap approach may not be feasible in a mountain gravel-bed river, the knowledge gained from the bootstrap study by Rice and Church (1996b) about percentile errors in skewed distributions as opposed to symmetrical ones is quite valuable and should be considered when estimating errors around high or low percentiles in skewed distributions.

### **5.2.3.5 Summary: the relation between sample size and error**

#### ***Beneficial effect of sampling tapers off for large sample sizes***

Sampling precision increases as the reciprocal of the square root of sample size  $n$  (standard error  $s_p \approx 1/\sqrt{n}$ ). Thus, sampling precision improves dramatically as  $n$  increases at small values of  $n$ , but the improvement becomes insignificant for high values of  $n$ . For the bed material of the Mamquam River with  $\sigma = 1.17 \phi$ , Rice and Church (1996b) determined the cutoff point beyond which further sampling does not significantly improve sampling precision is at a sample size of 400 particles.

#### ***Relation between sample size, sorting, and error***

The relation between sample size, sorting, and error  $n = (t \cdot s/e)^2$  is such that halving the acceptable error margin  $e$ , or doubling of bed-material sorting  $s$  leads to approximately a

---

<sup>1</sup> Resampling Stats, Inc., 612 N/ Jackson St., Arlington, VA 22101; Web-page: <http://www.resample.com>;

fourfold increase in sample size  $n$ , and a doubling in sorting doubles the error for a given sample size (Section 5.2.2.7). The relation between sample size, sorting, and error around the mean is visible in Fig. 5.2. A 400-particle surface sample in moderately-sorted bed material ( $s = 1 \phi$ ) yields an approximate absolute error of  $\pm 0.1 \phi$  around the mean, whereas sampling only 100 particles increases the absolute error margin to approximately  $\pm 0.2 \phi$ . In more poorly sorted bed material with  $s = 2 \phi$ , sampling 400 particles leads to an absolute error around the mean of  $\pm 0.2 \phi$ , and 100 particles to an error of  $\pm 0.4 \phi$ .

### ***Comparison: one-step and bootstrap approach***

The relation between sample size, sorting, and error around the mean is similar to the relation between sample size, sorting, and error around the  $D_{50}$  established by Rice and Church (1996b) in a bootstrap approach. For the Mamquam River with a standard deviation of  $1.17 \phi$ , a sample size of 400 particles resulted in an absolute error around the  $D_{50}$  of  $\pm 0.122 \phi$ , whereas an absolute error of  $\pm 0.115 \phi$  around the mean particle size  $\phi_m$  was computed for a 400-particle sample by the general sample size equation (Eq. 5.2).

For percentiles other than the  $D_{50}$ , results from the bootstrap approach and an assumed normal distribution differ and the difference increases towards the tails of the distribution. The bootstrap approach indicates that for distributions skewed towards a tail of fine particles, sample error is significantly lower for high percentiles than for low percentiles. Consequently, it takes a considerably larger sample size to accurately characterize low percentiles ( $D_5, D_{16}$ ) than high percentiles ( $D_{84}, D_{95}$ ) in distributions skewed towards a fine tail. Percentiles between  $D_{50}$  and  $D_{95}$  require nearly the same sample size for a given precision (Table 5.6 and Fig. 4.2 in Section 4.1.1.3).

The poor precision of low percentiles for a given sample size in distributions skewed towards a fine tail results from the relative scarcity of fine gravel particles in coarse gravel and cobble-bed streams. In a 100-particle pebble count from a coarse gravel bed, the number of counts per size class typically varies between 0 and 5 for each of the finest 5 or 8 size classes (excluding sand). However, each of the coarsest 4 or 5 size classes (except the very largest size class) might have 10 or 20 counts. The addition of one more count in any of the fine size classes cause more change in the percentile particle size of that size class than the addition of one more count to a coarse size class that has already 10 or 20 counts. This results in more uncertainty in the quantification of the low percentiles.

### ***Comparison: bootstrap and empirical results***

Results from the bootstrap analysis compare well with results from empirical studies conducted in mountain gravel-bed streams (Section 4.1.1.3, Fig. 4.2) with distributions skewed towards fines and sorting coefficients of  $\approx 1.2 \phi$ . When a sampling frame (Section 4.1.1.6) was used to reduce operator bias in particle selection in pebble counts, repeated pebble counts on riffles in various streams had total absolute errors  $e_{\pm\phi}$  of  $\pm 0.1$  to  $\pm 0.15 \phi$  around all percentiles between the  $D_{50}$  and  $D_{95}$ . This range of total absolute errors is quite similar to the bootstrap errors established for the slightly skewed distribution from the

Mamquam River and suggests when sampling large gravel and cobbles, operator errors do not significantly contribute to the total error.

The absolute error of  $\pm 0.42 \phi$  obtained for the  $D_5$  particle size of pebble counts in mountain streams exceeded the bootstrap error around the  $D_5$  of  $\pm 0.30 \phi$ . The poor accuracy for samples of small particles in pebble counts is attributable to the (inconsistent) operator bias against small particles and should be disconcerting for studies concerned with the amount of surface fines. Sampling accuracy for small particles requires not only larger sample sizes than are required for large percentiles, but requires sample sizes even larger than predicted from appropriate sample-size statistics to account for operator bias against fines.

#### ***Comparison: One-step and bootstrap with multinomial approach***

Fig. 5.7 illustrates error bands computed around the example distribution presented in Section 2.1.4.1 ( $s = 1.94 \phi$ ,  $sk_{aF\&W} = 0.17$ ,  $sk_{fq} = 0.72$ ) for various sample sizes using the multinomial approach. An absolute error in mm around a given percentile can be obtained from Fig. 5.7 as the horizontal distance between the error band and the sample distribution. The absolute error around the  $D_{50}$  is approximately  $\pm 0.4 \phi$  units for a sample size of 400 and increases to nearly  $\pm 0.8 \phi$  for a sample size of 100. Therefore, the absolute error predicted for the  $D_{50}$  from the multinomial approach is approximately twice as large as the absolute error around the mean computed from the one-step approach (Eq. 5.2).

The error bands computed with the multinomial approach for the skewed distribution described in Section 2.1.4.1 indicate a larger absolute error for small percentiles than for large percentiles. These figures are similar to the bootstrap results for the skewed distribution from the Mamquam River.

#### **5.2.4 Detectability of change in percent fines (Bevenger and King 1995)**

Natural or anthropogenic disturbances in the watershed or the riparian area may lead to elevated amounts of fine sediment in a streambed. The amount of fine sediment that impairs aquatic habitat depends on the species of concern, the benthic community, and bed-material properties. Monitoring fine sediment can be used to observe and evaluate the effects of change in the natural conditions of the watershed or in watershed management.

Fine sediment supplied to a mountain gravel-bed stream accumulates primarily in the interstitial spaces of the subsurface sediment and in backwater areas. Accumulations of fines in the surface sediment of the general streambed are relatively scarce. Taking volumetric samples of the subsurface is time and labor consuming, however. To simplify and accelerate the sampling process, Bevenger and King (1995) proposed sampling and analyzing the amount of surface fines in the bed using a (zigzag<sup>2</sup>) pebble-count procedure.

---

<sup>2</sup> The operator walks a zigzag course from bank to bank picking pebbles from the streambed at intervals spaced about 7 feet apart, and covers about a hundred meters of stream section (Bevenger and King 1995), (Section 6.2.2.1). The 7-foot interval was chosen to reduce serial correlation in the samples particles and more closely adhere to the statistical independence assumptions of the analysis.

The statistical error associated with small percentiles is usually relatively large (Section 4.1.1.3). Bevenger and King (1995) therefore specified the sample size necessary for detecting differences in the percent fines obtained from two pebble counts using a 2 x 2 contingency table analysis. One of the pebble counts is carried out in a *reference* reach, which means before the reach was impaired or in an unimpaired reference reach that serves as “background”. The second pebble count is performed in the *study* reach, which means in the reach in which the percent fines may have changed over time. The sample size necessary to detect a change in the percent fines of the study reach depends on four factors:

- Sample size at the reference site  
Sample size at the study site has to be larger if the sample size at the reference site is small, and can be smaller, if a large sample was taken at the reference site.
- Percent of fines at the reference site  
A larger sample must be taken at the study reach if the reference reach has a high percentage of fines (i.e., sandy gravel-bed streams). A smaller sample can be taken when the percent fines at the reference site is small (i.e., gravel beds with little sand).
- The minimum difference in the percent fines to be detected between the reference and study site  
Detecting a small difference in the percent fines between study and reference sites requires a larger sample size than is needed to detect a larger change in the percent fines.
- Acceptable risk levels in terms of Type I and Type II error  
Type I error is the risk of falsely concluding a significant difference between the two samples and is typically set at  $\alpha = 0.05$ . Type II error is the risk of falsely concluding that there is no difference and is typically set to  $\beta = 4\alpha = 0.20$ . Type I and Type II errors are inversely proportional for a given sample size. That is, a decrease in one necessarily results in an increase of the other. If the occurrence of a difference in the grain-size distribution is as important as the occurrence of no difference, then both  $\alpha$  and  $\beta$  are set to 0.05.

#### 5.2.4.1 Sample-size determination from diagrams

The required sample size depends on combinations of the four factors mentioned above. Thus, Bevenger and King (1995) provided multiple plots with several curves each (Figs. 5.12 and 5.13) to specify the sample size at the study site for different values of the four factors. The following five steps are taken to determine sample size from the diagrams:

1. Determine the risk levels for Type I and Type II error and select the appropriate figure (Fig. 5.12 or 5.13).

- Determine the percent fines at the reference site and select the appropriate plot from Fig. 5.12 or 5.13. For 10% fines at the reference site ( $p_r = 0.10$ ), select the plot “10% fines at reference site” in Fig. 5.12 or 5.13.
- Determine the detrimental percent fines at the study site. For example, 19% fines at the study site ( $p_s = 0.19$ ) may be a threshold value for impairing aquatic habitat. The necessary minimum detectable difference between study and reference site must then be  $p_s - p_r = 0.19 - 0.1 = 0.09$  or 9%.
- Determine the sample size taken or to be taken at the reference site and select the corresponding graph for 100, 150, 300, 450, or 600 particles on the diagram.
- On the appropriate diagram in Figs. 5.12 or 5.13 locate a minimum detectable difference of 0.09 on the vertical axis, and determine the sample size at the study-site at the intersection of a minimum detectable difference of 0.09 with the respective graph for reference-site sample size.

For example, the plot for 10% fines at the reference site in Fig. 5.12 indicates that a 300-particle sample (stippled line) at the reference site requires another 160 particles to be

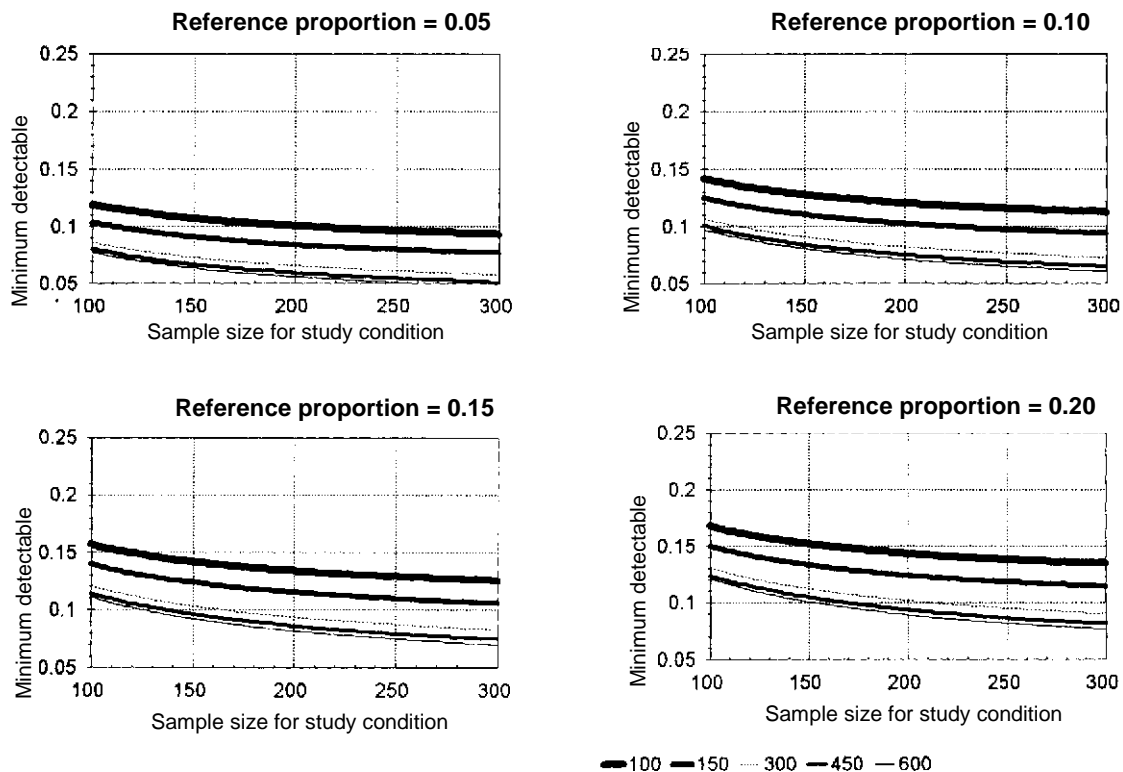


Fig. 5.12: Sample size necessary at the study site to detect a minimum difference in percent fines between the study and the reference site  $p_s - p_r$  for various reference-site sample sizes and risk levels. Risk levels for type I and type II errors are set to  $\alpha = 0.05$  and  $\beta = 0.20$ . (Reprinted from Bevinger and King (1995)).

collected at the study site. A 600- particle sample at the reference site reduces the sample size at the study site to 120. Likewise, if 150-particle had been sampled at the reference site, a little over 300 particles have to be sampled at the study site.

If the tolerable percent fines at the study site was 12% ( $p_s = 0.12$ ), and the reference site had 5% fines, the required minimum percent difference that needs to be detectable between study and reference site is  $p_s - p_r = 0.07$ . In this case, the plot for 5% fines at the reference site in Fig. 5.12 indicates that at 300-particle sample at the reference site requires at least 170 particles to be sampled at the study site.

Fig. 5.13 is used if both the Type I and Type II error are set to a confidence level of 95% ( $\alpha$  and  $\beta = 0.05$ ). If there are 10% fines at the reference site, and the tolerable percent fines at the study site is 20%, the minimum difference to be detected is  $p_s - p_r = 0.10$ . The plot for 10% fines at the reference site in Fig. 5.13 indicates that about 290 particles need to be sampled at the study site, if 300 particles had been sampled at the reference site.

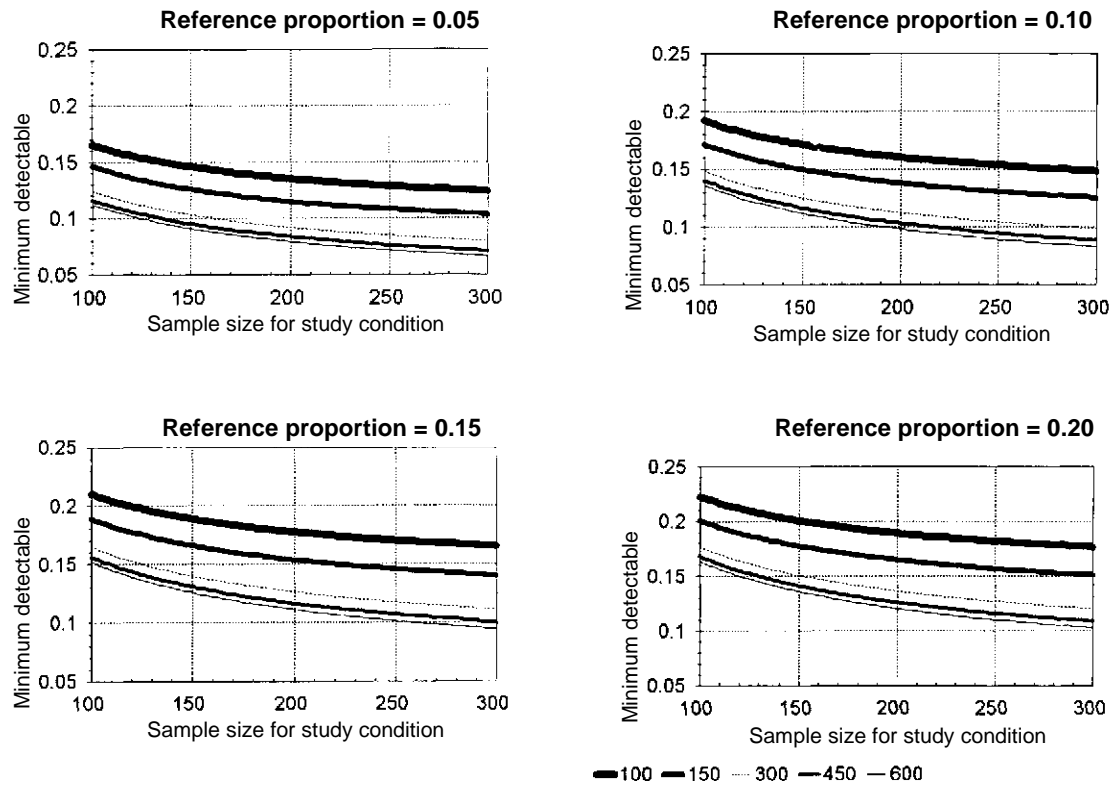


Fig. 5.13: Sample size necessary at the study site to detect a minimum difference in the percent fines between the study and the reference site  $p_s - p_r$  for various reference-site sample sizes and risk levels. Risk levels for Type I and Type II errors are set to  $\alpha = 0.05$  and  $\beta = 0.05$ . (Reprinted from Bevenger and King (1995)).

This yields a total sampling effort of 590 particles. If 600 particles had been collected at the reference site, 195 particles would have to be collected at the study site, and this increases the total sample size to 795 particles. If 100 particles were sampled at the reference site, an extrapolation of the graph for 100 particles would intersect the line for a minimum detectable difference of 0.1 at more than 1,000 particles for the study site and result in a total sample size of more than 1,100. Little information about a change in the percent fines is gained when small samples are collected both at the reference and the study site. If 100 particles were sampled at each site, the minimum detectable difference is only 0.18. Given 9% fines at the reference site, a 100-particle pebble count can at best detect a doubling of the percent fines at the study site (Potyondy and Hardy 1994; King and Potyondy 1993).

The total sampling effort can be minimized if the same number of particles are sampled at both sites. Table 5.7 indicates, for  $\alpha$  and  $\beta = 0.05$ , that sampling 293 particles at both sites results in the smallest total sample size (586 particles). In order to optimize the study effort and to find the smallest total sample size that will detect a given difference pilot studies should be conducted to estimate the percent fines at both the reference and the study sites. The result can then be used for estimating the optimum sample size.

Table 5.7: Equal and unequal sample sizes for  $p_r = 0.10$  and  $p_s = 0.20$ , and preselected values of  $\alpha$  and  $\beta$  (from Bevenger and King 1995).

$\beta$	Equal sample Size			Unequal sample Size					
	$\alpha$			$\alpha$					
	0.01	0.05	0.10	0.01	0.05		0.10		
	$n_r, n_s$	$n_r, n_s$	$n_r, n_s$	$n_r$	$n_s$	$n_r$	$n_s$	$n_r$	$n_s$
0.01	566	417	347	848	424	635	318	534	267
0.05	419	293	236	617	309	439	220	357	179
0.10	349	236	185	510	255	350	175	278	139
0.20	275	177	134	394	197	257	129	197	99

#### 5.2.4.2 Sample-size computation

The statistical background for the procedure presented by Bevenger and King (1995) is provided by Fleiss (1981). Sample size for a tolerable risk level is based on the acceptance or rejection of the null hypotheses that the difference between the proportion of the percent fines at the reference site  $p_r$  and the study site  $p_s$  is either 0 (no difference), or  $> 0$  (i.e., there is a difference). Minimum sample size  $n_s$  for the pebble count at the study site can be calculated from Equations 5.26 and 5.27 (Fleiss 1981). If sample size at the reference site  $n_r$  is negotiable, and if there is no reason for different sample sizes between the two sites, an equal sample size should be selected for the reference and study sites as it results in the smallest combined sample size  $n_s + n_r$ . The smallest sample size for both the study and reference site can be computed from:

$$n_s = \frac{n'}{4} \left( 1 + \sqrt{1 + \frac{4}{n' \cdot |p_s - p_r|}} \right)^2 \quad (5.26)$$

with

$$n' = \frac{\left( z_\alpha \sqrt{p_r + p_s \cdot \left( 1 - \frac{p_r + p_s}{2} \right)} - z_{1-\beta} \sqrt{p_r \cdot (1 - p_r) + p_s \cdot (1 - p_s)} \right)^2}{(p_s - p_r)^2} \quad (5.27)$$

where  $z_\alpha$  and  $z_{1-\beta}$  refer to the ordinates of the standard normal distribution, and the subscripts  $\alpha$  and  $\beta$  refer to the risk levels of the error Type I and II. Commonly used values for  $z_\alpha$  and  $z_{1-\beta}$  are:

$\alpha$ or $\beta$	:	0.01	0.05	0.10	0.20
$z_\alpha$ (neg. values); $z_{1-\beta}$ (pos. values):	(-)	2.327	1.645	1.282	0.842

**Example 5.11:**

If the reference site has 10% fines < 8 mm ( $p_r = 0.10$ ), and it is desirable to detect an increase in the percent fines to 20% or more at the study site ( $p_s = 0.20$ ), with acceptable risk levels of  $\alpha = 0.05$  and  $\beta = 0.20$ , sample size at the study site is computed from Eq. 5.26 and 5.27:

$$n' = \frac{\left( -1.645 \sqrt{0.1 + 0.2 \cdot \left( 1 - \frac{0.1+0.2}{2} \right)} - 0.842 \cdot \sqrt{0.1 \cdot (1 - 0.1) + 0.2 \cdot (1 - 0.2)} \right)^2}{(0.2 - 0.1)^2}$$

$$n' = \frac{(-1.645 \cdot \sqrt{0.3 \cdot 0.85} - 0.842 \cdot \sqrt{0.1 \cdot 0.9 + 0.2 \cdot 0.8})^2}{0.1^2}$$

$$n' = \left( \frac{-0.831 - 0.421}{0.1} \right)^2 = 157$$

and

$$n_s = \frac{157}{4} \cdot \left( 1 + \sqrt{1 + \frac{4}{157 \cdot |0.2 - 0.1|}} \right)^2$$

$$n_s = 39.2 \cdot (1 + \sqrt{1.255})^2 = 177$$

Modified forms of Eqs. 5.26 and 5.27 are used if the sample size for the reference and study site are different; however, the ratio of sample size at the reference site and the study site needs to be known prior to the computation. The reader is referred to the source literature by Bevenger and King (1995) and Fleiss (1981) for this case.

#### 5.2.4.3 Operator error in the percent fines adds to the statistical error

Statistical computations of sample size, including the computation of sample size by (Bevenger and King 1995) refer to the *statistical* error associated with a certain sample. Computation of sample size, including the computation of sample size by Bevenger and King (1995) only refer to the sample size needed to avoid a statistical error. However, the user must keep in mind that operators introduce further sampling errors that are not included in the computed statistical sampling error but nevertheless add to it. Operators commonly bias against fine particles (Section 4.1.1.3), because fine particles may be partially hidden between large particles, and because large particles are more likely to be touched and selected in a pebble count than fine particles. Fine particles also tend to accumulate in locations of the streambed that are poorly accessible, such as in pools or under overhanging branches near the banks. Inaccessibility makes fine particles less likely to be included in a pebble count. Operator errors and bias against fines are not included in a computed relation between sample size and statistically detectable error in the percent fines. The actual minimum detectable error in the percent fines is therefore smaller than computed from the statistical analysis. To account for this neglect, a sample size larger than predicted is required to detect a given change in the percent fines. Operator bias against fines as well as the variability of sampling results between operators can be reduced by using a sampling frame (Bunte and Abt 2001) (Section 4.1.1.6). Sampling the streambed in a systematic pattern along even-spaced transects spanning the full bankfull width of the stream further assists in reducing operator errors with respect to sampling fines.

### **5.3 Areal sampling: area-based sample-size recommendations**

In contrast to pebble counts or grid samples that collect a predetermined number of particles from a transect or a grid, areal samples collect all surface particles contained in a specified (small) sampling area (Section 4.1.3). Thus, sample size may be described in terms of the size of the area that needs to be sampled. The size of the sampling area may be based on geometrical consideration, such as a multiple of the area covered by the  $D_{max}$  particle size. Alternatively, a two-stage sampling approach may be applied to specify the

number of subsamples needed from a homogeneous deposit to attain a specified sampling precision for the median particle size (Section 5.3.2). A multinomial approach may be used to compute the percentile error for the entire distribution (Section 5.3.3)

### 5.3.1 $D_{max}$ and geometrical considerations

Diplas (1992a) and Diplas and Fripp (1992) suggested that an areal sample should cover a sampling area equal to at least 100 times the area of the  $D_{max}$  particle size in order to provide a relatively high precision for all percentiles. Fripp and Diplas (1993) increased this sample-size recommendation to 400 times the area of the  $D_{max}$  particle. This increase ensured that the volume of the sample would satisfy De Vries' (1970) "low precision" criterion with a relative error of 10% (Sect. 5.4.1.1).

The area of one individual areal sample is usually small (about  $0.1 \text{ m}^2$ ) and several individual areal samples need to be combined for the total sample. The total sampling area  $A_{tot}$  can be estimated from a multiple of the exposed area of the largest particle(s)

$$A_{tot} = 400 D_{max}^2 \quad (5.28)$$

#### Example 5.12:

The  $D_{max}$  particle size of a deposit is estimated at 40 mm, the upper range of particle sizes suitable for adhesive sampling (Section 4.1.3.2). If a spherical particle shape is assumed, the area covered by an individual particle  $A_p$  with a 40 mm  $b$ -axis size is

$$A_p = \pi \cdot \left(\frac{b}{2}\right)^2 = \pi \cdot \left(\frac{0.04 \text{ m}}{2}\right)^2 = 0.00126 \text{ m}^2$$

If an ellipsoidal particle shape with the  $a$ -axis 1.5 times the  $b$ -axis is assumed, the area covered by one particle increases to

$$A_p = \pi \cdot \left(\frac{a \cdot b}{4}\right) = \pi \cdot \left(\frac{0.06 \text{ m} \cdot 0.04 \text{ m}}{4}\right) = 0.00189 \text{ m}^2$$

An intermediate particle area of  $0.00160 \text{ m}^2$  is obtained if a square particle shape is assumed with  $A_p = b^2$ . Using  $A_p = b^2$ , the total sampling area  $A_{tot} = 400 \cdot 0.0016 \text{ m}^2 = 0.64 \text{ m}^2$ , which is an area of 0.8 by 0.8 m.

If one areal sample covers approximately  $0.1 \text{ m}^2$ , Eq. 5.28 suggests that 6 – 7 of those areal samples should be collected in order to sample an area of sufficient size and to gain sufficient material for a particle-size analysis.

### 5.3.2 Two-stage sampling: specified error around the median

ISO (1992) proposes a two-stage approach for defining the minimum sampling area. ISO (1992) advises that the minimum sampling area for each individual sample  $A_s$  must be larger than 8 times the area of the  $D_{max}$  particle size in order to avoid bias towards the largest particles. For a  $D_{max}$  particle size of 40 mm, each individual areal sample should be at least 0.11 by 0.12 m = 0.013 m<sup>2</sup> in size.

#### *Computation in mm units*

A two-stage approach can be used to determine the relation between sample size and absolute error around central percentiles of the distribution (Section 5.2.3.1). A number of  $q$  areal subsamples are collected, and the median particle size is computed for each of the  $q$  subsamples, either graphically from cumulative distribution curves, or by linear interpolation between percentiles (Section 2.1.4.2). ISO (1992) suggests using the median particle size  $D_{50}$  in units of mm, assuming that the  $q$  values of  $D_{50}$  are approximately normally distributed. This guideline document recommend using the median particle size  $\phi_{50}$  in units of  $\phi$  (see below).

The sample standard deviation  $s_{50}$  of the  $q$  values for  $D_{50}$  is determined from

$$s_p = \sqrt{\frac{\sum_{i=1}^q (D_{50} - D_{50m})^2}{q-1}} \quad (5.29)$$

$D_{50m}$  is the arithmetic mean particle size in mm of the  $D_{50}$  values obtained from the  $q$  samples. An appropriate value for  $t_{1-\alpha/2; q-1}$  is selected from Table 5.2. Eq. 5.30 can then be used to calculate the number of subsamples  $q$  so that there is only a 5% chance (at  $\alpha = 0.05$ ) that the absolute difference (positive or negative) between the estimated values of the percentile in question  $D_{50}$  and the true population  $D_{50}$  is larger or equal to the acceptable absolute error  $e_{\pm D_{50}}$ . The absolute error is the difference (in mm) between the sample and the population  $D_{50}$ . Note that Eq. 5.30 may have to be solved iteratively (see Example 5.13)

$$q = \left( \frac{t_{1-\alpha/2; q-1}}{e_{\pm D_{50}}} \cdot s_{50} \right)^2 \quad (5.30)$$

The total sampling area for one complete areal sample is  $A_{tot} = A_s \cdot q$ .

Example 5.13:

$D_{max}$  is estimated as 40 mm and  $D_{50}$  is the percentile of interest. Sample area  $A_s$  required for avoiding bias against large particles in a subsample is  $8 \cdot 0.04^2 \text{ m}^2 = 0.0128 \text{ m}^2$ . Five subsamples were collected with five closely-spaced values for  $D_{50}$  of 22, 25, 27, 30, and 32 mm. From Eq. 5.29, the sample standard deviation  $s$  for the  $D_{50}$  percentile is computed to be 3.96 mm. The acceptable error around the  $D_{50}$  particle size is 5 mm.

Eq. 5.30 needs to be solved iteratively when  $t$ -statistics are used. An arbitrary sample size of 10 subsamples is selected in the first trial of Eq. 5.30 and yields a sample size of 3.2. Estimated and computed subsample size  $q$  do not yet correspond. After four subsequent trails, correspondence is reached for a subsample size of 5.

Trial	$q_{est}$	$q-1$	$t_{1-\alpha/2; q-1}$	$q_{comp}$
1	10	9	2.262	$3.2 \cong 4$
2	4	3	3.182	$6.4 \cong 7$
3	7	6	2.447	$3.7 \cong 4$
4	5	4	2.776	$4.8 \cong 5$

Taking 5 subsamples from a total area of  $A_{tot} = 5 \cdot 0.013 \text{ m}^2 = 0.065 \text{ m}^2$  (about 0.25 by 0.26 m) provides a 95% probability that the sample  $D_{50}$  size is within  $\pm 5$  mm of the population  $D_{50}$ . This is a sampling area about 10 times less than predicted from Eq. 5.28.

If the 5 subsamples were more different and had  $D_{50}$  sizes of 14, 19, 27, 33 and 39 mm, and a standard deviation of 10.139, the iterative solution of Eq. 5.30 yields  $(2.101 \cdot 10.139/5)^2 = 18.15$  which is rounded up to 19. The total area covered by the subsamples is  $A_s = 19 \cdot 0.013 \text{ m}^2 = 0.247 \text{ m}^2$  (about 0.49 m by 0.50 m). The total sampling area in this example is much larger than in the previous example because the spread (variance) of the 5 values of  $D_{50}$  is much larger. Nevertheless, the sampling area computed from Eqs. 5.29 and 5.30 is still less than half the total sampling area computed from Eq. 5.28.

Note that the two-stage approach computes only the precision for the particular set of subsamples used in the computation. The precision associated with a given sample size would have to be computed numerous times, each time with a newly collected set of subsamples, in order to compute the mean precision associated with a specified subsample size in a specified sampling area. This topic is discussed in more detail in Section 5.4.2.1.

### *Computations in units of $\phi$*

It is recommended to apply the two-stage approach to median particle-sizes in units of  $\phi$ , rather than the median in mm, because values of  $\phi_{50}$  from several subsamples approximate a normal distribution better than the values of  $D_{50}$  (Triola 1995; Section 5.2.3.1).  $D_{50}$  in Eq. 5.29 is then substituted by values of  $\phi_{50}$ .

### **5.3.3 Multinomial approach**

Sample sizes computed from simple geometric approximations such as sampling area  $A = 100$  or  $400 D_{max}^2$  (Eq. 5.28) yield relatively large sample sizes in order to provide a relatively high precision for all percentiles. However, a concrete relation between sample size and error around a given percentile and selected confidence level is not obtained from Eq. 5.28. In order to specify a relation between sample size and error, Petrie and Diplas (2000) suggest a multinomial approach to compute the size of the sampling area. The multinomial approach is applied in two steps. The first step computes the number of particles needed for a grid sample (Section 5.2.3.3). The second step converts this number of particles to the size of a sampling area. A factor is needed for this conversion, and its numerical value depends on the packing of surface particles and the proportion of surface voids. For a voidless surface, the Kellerhals and Bray (1971) conversion coefficients (Section 4.3.1), may be used. Other conversion factors may be needed for other surface conditions (Sections 4.3.2 and 4.3.3). The reader is referred to the original literature by Petrie and Diplas (2000) for details.

## 5.4 Volumetric sampling: mass-based sample-size recommendations

Sample mass required for representative volumetric samples can be computed by three methods:

- As an empirical function of the  $D_{max}$  particle size,
- By computing the number of subsamples required (two-stage approach), and
- By analytical means based on an assumed underlying distribution type.

A large number of empirical equations exist in which sample mass is expressed as a function of the  $D_{max}$  particle size (Sect. 5.4.1). These equations are simple to apply, but different equations predict greatly different sample sizes. Sample-mass recommendations based on the  $D_{max}$  particle size do not require assumptions about an underlying frequency distribution type. Sample sizes predicted from empirical functions of  $D_{max}$  are generally large, but they do not provide information about the relationship between sample mass and error. Therefore, the precision of a sample remains unknown.

If the precision of a sample needs to be known, sample-mass equations should be employed that provide information on the relation between sample mass and precision. One possibility is a two-stage sampling approach in which a number of subsamples is collected (Section 5.4.2.1). Based on the central limit theorem, the precision of any percentile<sup>3</sup> in a distribution can be computed for various samples sizes. However, the precision obtained for a specific sample size, e.g., three subsamples, is not the same for any set of three subsamples from a deposit because each subsample is (slightly) different. Therefore, many sets of three subsamples would have to be collected to obtain the mean precision for a subsample size of three. The requirement for collecting a specified number of subsamples repeatedly can be bypassed by plotting the precision for various (unrepeated) subsample sizes. The data will scatter, but fitting a power- or exponential function through data points provides a surrogate relation between sample size and precision for a given percentile in a given deposit (Section 5.4.2.2).

A large physical sampling effort can be reduced by using a bootstrap procedure. Bootstrapping is a technique that collects repeated samples (by computer) from a parent population. The parent distribution might be generated by a computer based on specifications of the actual deposits (standard deviation and mean) that are obtained from a pilot study and an assumed distribution type (Section 5.4.3). The computational effort of bootstrapping is rather large and may require using a resampling program. The main drawback is that the computer-generated sample cannot be a perfect surrogate for a large sample from a distinct parent distribution. Bootstrapping may also be applied to a parent distribution of an actual bed-material sample (5.2.3.4) that is entered into the computer. The sample needs to be (usually prohibitively) large in order to accurately describe the parent population and all particles must be collected independently of each other.

---

<sup>3</sup> Two-stage approach is better suited for central percentiles. Peripheral percentiles require a larger sample size to reach normality.

### 5.4.1 Sample mass as a function of largest particle size

#### *Why use the $D_{max}$ particle size?*

Sample-size statistics that assume an underlying normal distribution indicate that a larger sample size is required to accurately describe the distribution tails than the central parts of the distribution. Consequently, a sample size that is sufficiently large to describe the distribution tails will also suffice to accurately describe the entire particle-size distribution.

The coarse tails of bed-material samples from gravel- and cobble bed streams are comprised of only a few large particles per size class which nevertheless contribute a rather large proportion of the total sample weight. Presence or absence of one or a few large particles in the distribution tail influences not only the percentiles of the coarse tail, but central and fine percentiles as well. Therefore, a volumetric sample needs to be sufficiently large so that coarse particles are representatively included in the sample. Because representatively sampling the coarse tail ensures accuracy for the entire distribution, sample mass is determined as a function of the  $D_{max}$  particle size. Because particle mass is a function of the third power of particle size, sample-size equations for volumetric samples are (usually) a function of the third power of  $D_{max}$ , i.e.,  $D_{max}^3$ .

#### *Defining the $D_{max}$ particle size*

The  $D_{max}$  particle size used for determining the mass of volumetric samples does not necessarily have to be the largest particle found in the sampling reach, but should be the size of the largest particles to be represented in the sample. The largest particle sizes to be represented in a sample depend on the study objective. When determining the  $D_{50}$  or another percentile for computations of bedload transport rates in a given streambed, untransportably large particles, e.g., boulders: unearthed from glacial deposits, or supplied from rock fall, should not be included in the sample. If the study objective is to compute the stream roughness, untransportably large boulders should be included in the analysis.

The largest particle size of concern that should be representatively included in bed-material samples for bedload studies is often the dominant, large particle size  $D_{dom}$ . In mountain streams with occasional supply of non-fluvial supply of large particles, the particle size of  $D_{dom}$  is roughly equivalent to the  $D_{90}$  particle size.  $D_{dom}$  is approximately the largest particle size transportable during frequently occurring large floods (e.g., bankfull flow or a flood with a two-year recurrence interval). The size of  $D_{dom}$  can be estimated from the mean  $b$ -axis size of about 30 large (except the very largest) particles deposited on the upstream end of gravel bars or on other fresh depositional surfaces that are not affected by backwater or wake hydraulics. Absence of alga cover and negligible embeddedness may be interpreted as signs of recent transport. Those indicators can be misleading and indicate particle sizes too large for  $D_{dom}$ , if the last flood greatly exceeded the commonly largest bankfull or biennial flood and deposited either extraordinarily large clasts, or buried the streambed with finer sediment. In this case, a tractive force diagram (Lane 1955; Leopold 1992, p. 194) may be used to estimate the size of  $D_{dom}$  for flow properties of commonly occurring floods.

In uncoupled streams, the  $D_{max}$  particle size may be transportable during the floods of concern. Sample-mass: equations may then be based on the center of class of the largest fluvially transported size class  $D_{max,c}$ , or the  $D_{95}$  particle size. The term  $D_{max}$  is used as the largest transportable size class in the discussion of sample mass in the following section, and not as the absolute largest particle size found in a reach.

#### 5.4.1.1 Sample mass as cubic functions of $D_{max}$

Several sample-mass recommendations are available that predict sample mass as a function of  $D_{max}^3$ ; (e.g., ISO (1977) following De Vries (1970), Neumann-Mahlkau 1967), Church et al. (1987), Diplas (1992a), Diplas and Fripp (1992), Fripp and Diplas (1993). However, these cubic sample-mass equations are based on different criteria which include:

- Effect that adding or omitting the largest particle(s) has on the total sample mass,
- Error acceptable for the particle size of a large size fraction,
- Constant coefficient of variation for the sizes of individual particles within a size class over neighboring large size classes,
- Number of particles that should be contained in the largest size class, and
- Feasibility of obtaining a statistically required sample volume.

The different criteria produce different cubic sample-mass equations. To facilitate a better comparison of the numerical results, all cubic sample-mass equations are expressed in the same form of

$$m_s = a \cdot D_{max}^3 \cdot \rho_s = b \cdot D_{max}^3 \quad (5.31)$$

where  $m_s$  is sample mass and usually expressed in units of kg unless otherwise specified.  $a$  and  $b$  are coefficients, and  $\rho_s$  is the particle density. The unit of the  $D_{max}$  particle size is in meters for the equations in Section 5.4.1.1, however in Fig. 5.14,  $D_{max}$  is indicated in units of mm for familiarity. For simplicity, all particles are assumed to be spheres or ellipsoids<sup>4</sup>, and the term  $\pi/6$  is incorporated in the  $a$  coefficient. A particle density  $\rho_s$  of 2,650 kg/m<sup>3</sup> is assumed for particles and the numerical value is incorporated into the  $b$  coefficient. All cubic sample-mass equations are plotted in Fig. 5.14 (the numbers on graphs refer to equation numbers in Section 5) and listed in Table 5.8. Sample masses predicted by these equations for a specified  $D_{max}$  particle size range over three orders of magnitude, i.e., the percentage weight of the  $D_{max}$  particle size of total sample mass ranges between roughly 0.01 and 10%.

---

<sup>4</sup> The volume of an ellipsoid with an axis ratio  $a:b:c$  of 3/2:1:2/3 is equal to the volume of a sphere with a diameter of 1. See Eq. 5.64 in Section 5.4.5.

### ***Percent error in total sample mass incurred by the largest particle***

One of the criteria used to establish an appropriate sample mass is the amount of error produced by the unrepresentative presence or absence of the largest particle in the total sample mass. In small samples from poorly sorted deposits, the largest particle can account for a substantial fraction of the total sample weight. The arbitrary presence or absence of the largest particle thus substantially affects the weight of the total sample mass. If the resulting error in sample mass is not to exceed 1%, sample mass must be larger than 100 times the mass of the  $D_{max}$  particle. A regression function fitted to the graph provided by Neumann-Mahlkau (1967) determined the relationship between sample mass and  $D_{max}$  particle size to be

$$m_s = 138,000 D_{n,max}^3 \quad (5.32)$$

where  $D_{n,max}$  is the nominal diameter (in m) of the  $D_{max}$  particle size (Section 2.1.2), and  $m$  is sample mass (in kg). For spheres, or ellipsoidal particles with axes ratios of  $a = 3/2 b$ ,  $b = D_{max}$ , and  $c = 2/3 b$ , the particle weight of  $D_{max}$  is equal to the weight of a particle with a nominal diameter of  $D_{max}$  ( $D_{(n)max}$ ). If the potential error introduced by the largest particle is allowed to increase to 10% (i.e., the  $D_{max}$  particle size is allowed to assume 10% of the total sample mass), the regression function becomes (same units as above)

$$m_s = 13,800 D_{n,max}^3 \quad (5.33)$$

Both functions are plotted in Fig. 5.14 and labeled 32 and 33.

### ***Relative error***

The sample-mass recommendation by De Vries (1970) is based on an analysis of the relative error  $e_{\%pi}$  of the  $i$ th size fraction. The relation can be computed from:

$$e_{\%pi}^2 = \frac{D_i^3 \cdot \beta \cdot \rho_s}{p_i \cdot m_s} \quad (5.34)$$

where  $p_i$  is the probability by mass of the  $i$ th size fraction and  $\beta$  is a constant. Laboratory experiments using sand and small gravel < 14 mm estimated a mean value of  $\beta = 0.8$ . De Vries (1970) considered the  $D_{84}$  as characteristic of the large particle-size fraction. Thus, sample mass  $m_s$  as a function of the  $D_{84}$  particle size can be computed from:

$$m_s = \frac{D_{84}^3 \cdot 0.8 \cdot \rho_s}{e_{\%pi}^2 \cdot p_i} \quad (5.35)$$

De Vries (1970) suggests setting  $p_i = 10\%$ . For a relative error  $e_{\%pi}$  of 1% (“high precision”), the denominator in Eq. 5.35 is  $10^{-5}$ . The sample size for various degrees of precision is

$$m_s = \frac{D_{84}^3 \cdot 0.8 \cdot \rho_s}{0.01^2 \cdot 0.1} = \frac{D_{84}^3 \cdot 0.8 \cdot \rho_s}{10^{-5}} = 0.8 \cdot 10^x \cdot D_{84}^3 \cdot \rho_s \quad (5.36)$$

with units in meters and kg. The exponent  $x$  equals 5 for a “high” precision of 1%, 4 for a “normal” precision of 3%, and 3 for a “low” precision of 10%.

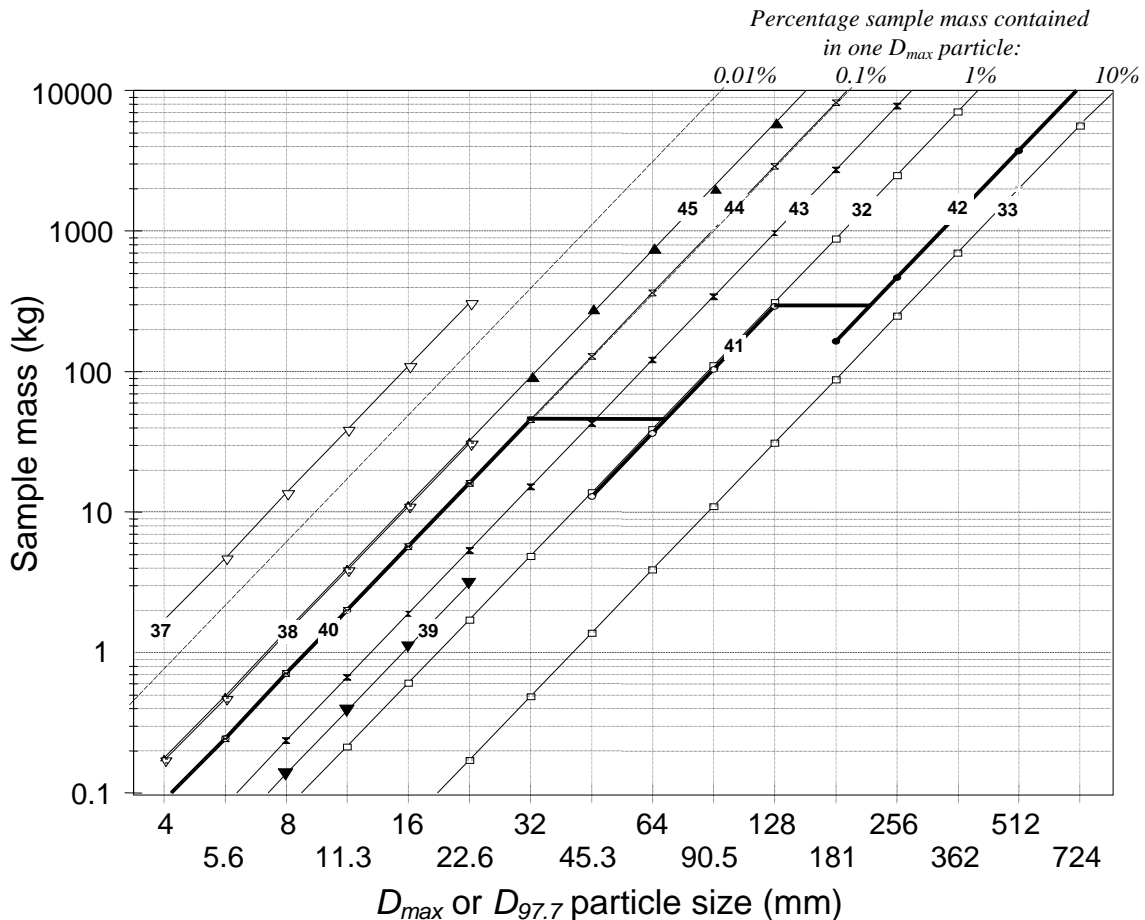


Fig. 5.14: Comparison of various sample-mass recommendations (kg) for gravel and cobble bed material based on cubic functions of  $D_{max}$ . The numbers on the graphs refer to the equation numbers in Section 5. The four lines labeled 0.01, 0.1, 1 and 10 refer to the percent sample mass contained in the mass of the  $D_{max}$  particle.

The sample-mass recommendations by De Vries (1970) were developed for sand and fine gravel. If De Vries' recommendations are applied to medium and large gravel particles and cobbles, the sample mass becomes very large. The International Organization of Standardization (ISO 1977) adopted the De Vries (1970) sample-size recommendations.

In order to compare the sample-mass recommendations by De Vries (1970) and ISO (1977) that use the  $D_{84}$  particle size with those that are based on  $D_{max}$ , the recommendations based on the  $D_{84}$  needs to be modified. If the  $D_{max}$  particle size is assumed to be equal to the  $D_{97.7}$ , and the sample standard deviation is  $1.0\phi$ , then the  $D_{97.7}$  particle size is approximately  $1.0\phi$ -units larger than the  $D_{84}$  (i.e., twice as large) (Fig. 2.19 in Section 2.1.5.4). The sample mass required for a  $D_{84}$  particle 8 mm in size in the original plot by De Vries (1970) is therefore assigned to a  $D_{97.7}$  or  $D_{max}$  particle size of 16 mm in Fig. 5.14. The sample mass (kg) for high, normal, and low, precision recommended by De Vries (1970) (Eq. 5.36) can then be expressed as cubic functions of the  $D_{97.7}$  particle size (m)

$$m_s = 26,500,000 D_{97.7}^3 \quad \text{for "high precision"} \quad (5.37)$$

$$m_s = 2,650,000 D_{97.7}^3 \quad \text{for "normal precision"} \quad (5.38)$$

$$m_s = 265,000 D_{97.7}^3 \quad \text{for "low precision"} \quad (5.39)$$

***Constant variability of particle sizes per size class over all size classes***

Church et al. (1987) presented a sample-mass criterion that is independent of an assumed underlying distribution type. Church et al. (1987) found that the coefficient of variation  $CV$  of particle sizes within a  $0.5\phi$ -size class is approximately 10% if the size class contains more than 100 particles. To ensure a constant  $CV$  of 10% for all sizes classes including the largest, Church et al. (1987) empirically determined that the mass of the largest particle in the sample should not exceed 0.1% of the total sample mass. Consequently, the sample mass  $m_s$  (kg) should be 1,000 times the mass of the  $D_{max}$  particle size. This recommendation can be mathematically expressed as

$$m_s = 1,000 \frac{\pi}{6} D_{max}^3 \cdot \rho_s = 524 \cdot D_{max}^3 \cdot \rho_s = 1,388,000 D_{max}^3 \quad (5.40)$$

with  $D_{max}$  in m, and a particle density  $\rho_s$  of  $2,650 \text{ kg/m}^3$  (see graph labeled 40 in Fig. 5.14). Similar to the "normal" precision criterion by De Vries (1970), Eq. 5.40 yields unmanageably large sample masses when applied to particle sizes larger than 32 mm. For coarse gravel with a  $D_{max}$  of 32 to 128 mm, Church et al. (1987) therefore suggest a less stringent criterion in which the mass of a  $D_{max}$  particle accounts for 1% of the total sample mass. This can be expressed by:

$$m_s = 100 \frac{\pi}{6} D_{max}^3 \cdot \rho_s = 52.4 \cdot D_{max}^3 \cdot \rho_s = 138,000 D_{max}^3 \quad (5.41)$$

Equation 5.41 (graph 41 in Fig. 5.14) is identical to the sample-mass equation by Neumann-Mahlkau (1967) for the 1% precision criterion (Eq. 5.33, graph 33 in Fig. 5.14). As particle sizes exceed 128 mm, sample masses again become so large that Church et al. (1987) lowered the criterion to  $D_{max} = 5\%$  of the total sample weight.

$$m_s = 20 \frac{\pi}{6} D_{max}^3 \cdot \rho_s = 10.47 \cdot D_{max}^3 \cdot \rho_s = 27,751 D_{max}^3 \quad (5.42)$$

The three sample-mass criteria by Church et al. (1987) plot as parallel graphs in Fig. 5.14. In order to obtain one function applicable to all particle sizes, the three functions can be united by a staircase function which, in a second step, can be smoothed by a power regression function that is fitted through the corner points of the staircase functions. This procedure and the resulting sample-mass equation is discussed further under “Canadian standards” in Section 5.4.1.2.

### ***Volumetric considerations***

Diplas (1992a) and Diplas and Fripp (1992) based their sample-mass recommendation for volumetric samples on the following considerations: If 100 particles are sufficient for a line or a grid sample, and if a particle with the diameter  $D$  occupies an area larger than  $D^2$ , then the minimum area for an areal sample is  $A_{min} = 100 \cdot D^2$ . For an entire particle-size distribution, total sampling area could be defined as  $A_{tot} = 100 D_{max}^2$ . If the minimum depth of a volumetric sample is set to  $2 D_{max}$  (Sect. 4.2.2.2), sample mass  $m$  (kg) becomes

$$m_s = 200 D_{max}^3 \cdot \rho_b = 460,000 D_{max}^3 \quad (5.43)$$

where  $D_{max}$  is in meters and  $\rho_b$  is the sediment bulk density assumed to be  $2,300 \text{ kg/m}^3$  (Table 2.16 in Section 2.5). Subsequent computations of precision and sample size prompted Fripp and Diplas (1993) to increase the minimum number of particles for a pebble count to 200 - 400 particles. Total sample area  $A_{tot}$  then increases to 200 or 400  $D_{max}^2$  (Eq. 5.28), with a sample mass of

$$m_s = 400 \text{ to } 800 D_{max}^3 \cdot \rho_b = 1,380,000 D_{max}^3 \quad (5.44)$$

if a multiplier of 600 is selected. Note that sample-mass recommendations in Eq. 5.44 are nearly identical to those proposed by Church et al. (1987) in their 0.1% criterion (Eq. 5.40).

***Sampling until 5  $D_{max}$  particles are contained in the sample***

A simple field criterion for estimating the necessary sample mass that does not require monitoring sample weight is proposed by Ibbeken (1974). He suggests continuing to sample until at least 5 particles of the  $D_{max}$  size class are contained in the sample. This approach implies that the spatial distribution of  $D_{max}$  particles within a sediment deposit is truly random, and that there is no user bias towards or against sampling large clasts. In order to compare Ibbeken's criterion with those discussed above, a percentage weight needs to be assumed for  $D_{max}$  particles in the total deposit. If the percentage is set to 1%, and the  $D_{max}$  particle-size class is 180 mm with an average  $D_{max}$  particle weight of 8 kg, Ibbeken's sample-mass criterion yields  $5 \cdot 8 \text{ kg} \cdot 100 = 4,000 \text{ kg}$ . In this sample of 4 metric tons, the mass of one  $D_{max}$  particle  $m_{D_{max}}$  comprises 0.2% of the total sample weight. In terms of the notations used above, Ibbeken's sample-mass criterion can be rewritten as:

$$m_s = 2000 \cdot m_{D_{max}} = 2000 \cdot \frac{\pi}{6} D_{max}^3 \cdot \rho_s = 2775,073 D_{max}^3 \quad (5.45)$$

If it is assumed that  $D_{max}$  particles make up 5% of the deposit, Ibbeken's sample-mass criterion yields  $5 \cdot 8 \text{ kg} \cdot 20 = 800 \text{ kg}$  and the mass of one  $D_{max}$  particle  $m_{D_{max}}$  would comprise 1% of the total sample weight. This result is identical to the sample mass criterion in Eq. 5.41.

**5.4.1.2 National standards: non-cubic functions of  $D_{max}$  particle size**

It is conceptually evident that sample mass should increase as a *cubic* function of particle size. Nevertheless, the resulting steep increase of sample mass with particle size leads to large and often unmanageable sample sizes for cobble-sized bed material. Most national standards therefore propose sample-mass recommendations that require a relatively high sample mass for small  $D_{max}$  sizes, but the increase of sample mass with particle size then continues at a lesser rate than it does with a cubic function. Regression functions fitted to the relations between sample mass and particle size yield either power functions with exponents between 1 and 1.5, or linear functions. Note that these relations are empirical and units on both sides of the equations do not necessarily match.

***British, German, and American table value standards***

Some of the national sample-mass recommendations are provided as table values only. Examples are the British BS 812, I standards (cited by Mosley and Tindale 1985), the German recommendations (DVWK 1988), and the American ASTM D75-71 standards

(cited by Mosley and Tindale (1985)). The British and German sample-mass recommendations are limited to particle sizes smaller than 60 mm, whereas the American ASTM D75-71 standards apply to particles smaller than 90 mm. For a visual comparison of sample mass, tabulated values and computed sample mass are plotted in Fig. 5.15.

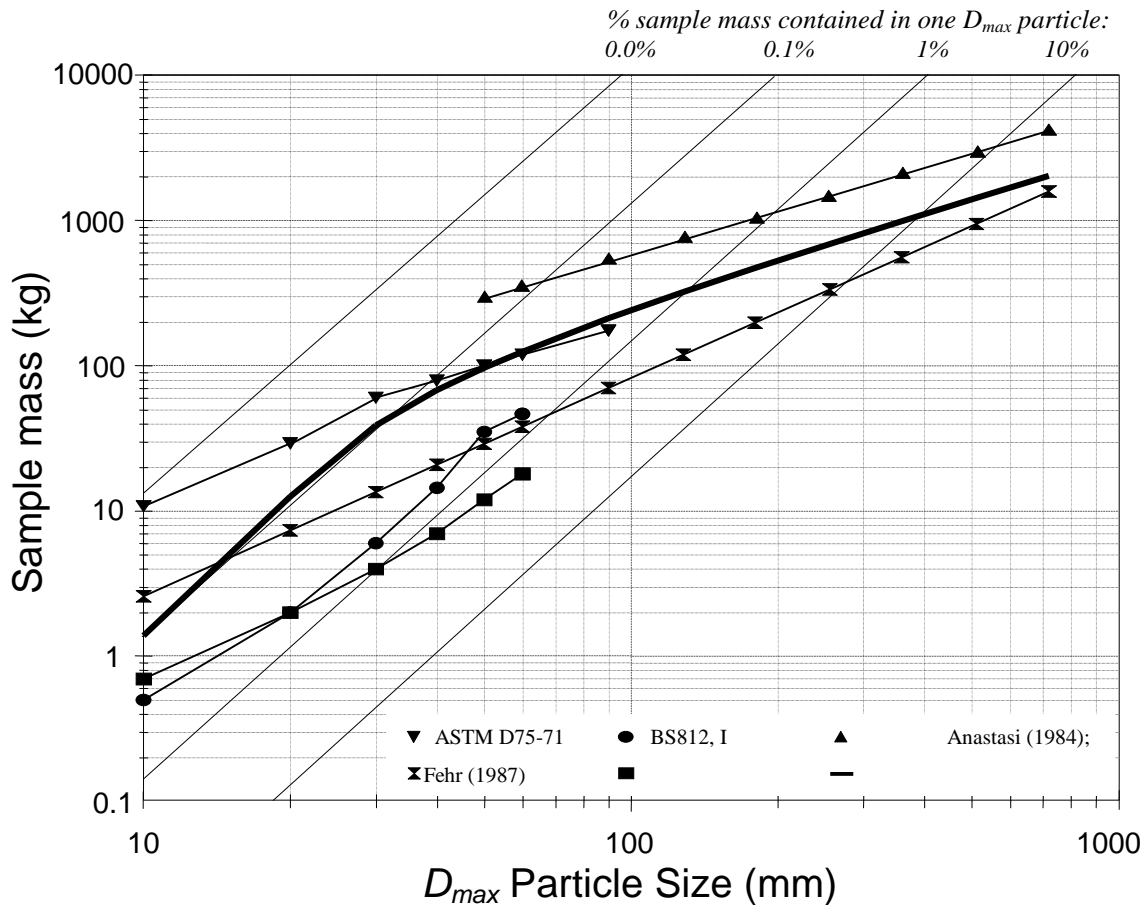


Fig. 5.15: Empirical sample-mass recommendations for gravel and cobbles expressed as power and linear functions of  $D_{max}$  (combined from various sources). The four lines indicate the percentages of 0.01, 0.0, 1, and 10 % of the total sample mass comprised in the mass of the  $D_{max}$  particle size (see Fig. 5.14).

### American standards

Sample mass (kg) recommended by the ASTM D75-71 standards for particles smaller than 90 mm can be expressed by a linear regression equation

$$m_s = 2,069 D_{max} - 6.7 \quad (5.46)$$

with  $D_{max}$  expressed in units of m (Fig. 5.15). The American ASTM C136-71 standard (cited by Church et al. 1987) has no restriction on particle size and determines sample mass  $m$  (kg) as

$$m_s = 2,596 D_{n,max}^{1.5} \quad (5.47)$$

where  $D_{n,max}$  (in m) is the nominal diameter (Section 2.1.2) of the particles retained on the largest sieve size (Fig. 5.15).

### ***German standards***

Sample-mass recommendations published by the Deutscher Verband für Wasserbau und Kulturtechnik (DVWK 1988) extend to particle sizes up to 60 mm and can be expressed by a power regression function (with  $m$  in kg, and  $D_{max}$  in m; Fig. 5.15)

$$m_s = 712.4 D_{max}^{1.43} \quad (5.48)$$

### ***Swiss standards***

The empirical Swiss recommendations for sample mass in gravel-bed rivers are based on sample volume ( $V$ ) (Anastasi 1984; Fehr 1987)

$$V_s = 2.5 D_{max} \quad (5.49)$$

with  $V$  in  $m^3$  and  $D_{max}$  in m. The mass of sediment contained in this sample volume varies with the bulk density  $\rho_b$  which is affected by the sorting and packing of the particles in the sample. Bulk density for gravel deposits ranges between 1,700 and 2,600  $kg/m^3$  (Table 2.16 in Section 2.5). For comparison with other sample-mass equations,  $\rho_b$  was set to 2,300  $kg/m^3$ , a value proposed for gravel-sand mixtures by Carling and Reader (1982). Sample mass ( $m$ ) in kg is then

$$m_s = 2.5 D_{max} \cdot \rho_b = 5,750 D_{max} \quad (5.50)$$

### ***Canadian standards***

Church et al. (1987) proposed using three sample-mass criteria depending on the  $D_{max}$  particle size (Section 5.4.1.1). However, use of three criteria can lead to confusion in samples-mass estimates. Sample-mass requirements for particles of 32 mm is 45 kg if the 0.1% criterion is applied (Eq. 5.40), whereas sample mass for 45 mm particles is only 13 kg, if a less stringent criterion of 1% is used (Eq. 5.41) (Fig. 5.14). The Canadian standards described by Yuzyk (1986), Yuzyk and Winkler (1991), and Zrymiak (in press) fitted a staircase function through the three graphs by Church et al. (1987) to unite the three criteria in a monotonic function. Another possibility to unite the three sample-mass criteria in one strictly monotonic function is to fit a power regression function through the

corner points of the staircase function (Fig. 4.20 in Section 4.2.3.2), yielding the sample-mass equation ( $r^2=0.999$ ):

$$m_s = 2,881.6 D_{max} - 47.56 \quad (5.51)$$

with  $m$  in kg, and  $D_{max}$  in m. The adjusted sample-mass equation for Church et al. (1987) falls midway between the range of the other non-cubic sample-mass equations (Fig. 5.15).

### **Summary**

Sample-mass recommendations that are based on the size of the  $D_{max}$  particle vary over several orders of magnitude for a specified  $D_{max}$  particle size (Fig. 5.14. and 5.15). This variability is shown in Table 5.8 that presents cubic and non-cubic regression equations for sample-mass recommendations and compares sample-mass requirements for  $D_{max}$  particle sizes of 16 and 180 mm.

None of these recommendations have been formally adopted as the standard for sampling bed material in gravel-bed streams in the United States. The empirical sample-mass recommendations most frequently used and referenced are those by Church et al. (1987). The adjusted and strict-monotonic sample-mass equation for Church et al. (1987) describes the center of the range proposed by cubic and non-cubic sample-mass equations.

#### **5.4.1.3 Error of the entire particle-size distribution due to the presence or absence of particles from the largest size class**

Presence or absence of large particles not only affects total sample mass, but also alters the particle-size distribution in general. The presence of a statistically non-representative large particle is less likely than an absence, but has a disproportionate effect on the sampled particle-size distribution. The presence of an unrepresentative large  $D_{max}$  particle, that comprises a large percentage of the total sample mass, considerably coarsens the entire particle-size distribution compared to a parent population in which large particles are not overrepresented. This can be illustrated with Fig. 5.16, which is described in a different context below. Assuming the heavy black line in Fig. 5.16 represents the parent particle-size distribution of the deposit, the line termed “biased” indicates a sample distribution in which the largest particle comprises 30% of the total mass. Compared to the parent population, the  $D_{50}$  particle size is more than doubled, and the  $D_{75}$  size is even quadrupled in the sample in which large particles are overrepresented.

Chance absence of particles from the largest size class causes a sample particle-size distribution that is finer than the parent population. This effect is less pronounced than a chance overrepresentation, but it occurs statistically more often. The effect of chance absence of the  $D_{max}$  particle on the sample particle-size distribution is discussed in more detail in Section 5.4.1.4.

Table 5.8: Comparison of cubic and non-cubic regression functions for sample mass as a function of the  $D_{max}$  particle size (sample mass in kg and  $D_{max}$  particles size in m). Sample mass in parentheses indicates that the  $D_{max}$  particle size is beyond the intended range of the equation. See text for assumptions and units.

Regression Function	Author, <i>Criterion</i>	Equation Number	Sample Mass (kg) for $D_{max}$ of:	
			16 mm	180 mm
<i>Cubic sample-mass equations:</i>				
$m_s = 26,500,000 D_{max}^3$	De Vries (1970), ISO (1977), <i>high prec.</i>	5.37	108	(154,550)
$m_s = 2,775,073 D_{max}^3$	Ibbeken (1974), <i>5 <math>D_{max}</math> particles</i>	5.45	11.4	16,180
$m_s = 2,650,000 D_{max}^3$	De Vries (1970), ISO (1977), <i>norm. prec.</i>	5.38	10.9	(15,450)
$m_s = 1,388,000 D_{max}^3$	Church et al. (1987), $D_{max} = 0.1\% m_s$	5.40	5.7	8,090
$m_s = 1,380,000 D_{max}^3$	Fripp and Diplas (1993), <i>400 particles</i>	5.44	5.7	8,050
$m_s = 460,000 D_{max}^3$	Diplas and Fripp (1992), <i>100 particles</i>	5.43	1.9	2,680
$m_s = 265,000 D_{max}^3$	De Vries (1970), ISO (1977), <i>low prec.</i>	5.39	1.1	(1,550)
$m_s = 138,800 D_{max}^3$	Church et al. (1987), $D_{max} = 1\% m_s$	5.41	(0.60)	810
$m_s = 138,000 D_{max}^3$	Neumann-Mahlkau (1967), $m_s = 100 D_n$	5.32	0.57	805
$m_s = 27,751 D_{max}^3$	Church et al. (1987), $D_{max} = 5\% m_s$	5.42	(0.11)	160
$m_s = 13,800 D_{max}^3$	Neumann-Mahlkau (1967), $m_s = 10 D_n$	5.33	0.06	80
<i>Non-cubic sample-mass equations:</i>				
$m_s = 5,750 D_{max}$	Anastasi (1984); Fehr (1987)	5.50	(92)	1030
$m_s = 2,069 D_{max} - 6.7$	ASTM D75-71	5.46	26	(370)
$m_s = 2,882 D_{max} - 47.6$	Church et al. (1987), <i>adjusted</i>	5.51	1.1	472
$m_s = 2,596 D_{max}^{1.5}$	ASTM C136-71	5.47	5.2	200
$m_s = 712.4 D_{max}^{1.43}$	DVWK (1988)	5.48	1.9	(61)

#### 5.4.1.4 Sample-mass reduction: truncation and readjustment at the coarse end

All cubic, and even some of the non-cubic sample-mass equations recommend sample masses ranging from several metric tons to several hundreds of metric tons for bed material containing large cobbles and boulders. Such sample masses are not only unmanageably large, but would severely disturb the streambed as a consequence of their collection.

Church et al. (1987) recommend truncating volumetric samples in coarse beds and excluding from the sample particles larger than 256 mm, which typically weigh more than about 23 kg a piece. Particles larger than 256 mm are difficult, if not unsafe, to pick up for most persons and are therefore not likely to be representatively included in a volumetric sample, anyway. However, the presence of particles larger than the largest sampled size-class in the streambed should be recorded in the field notes. Any inadvertently collected large particle may then be discarded and only sufficient sediment is retained for an unbiased sample of the largest particle size present in the truncated sample.

The truncation and readjustment method of estimating the coarsest part of a cumulative frequency distribution is based on the assumption that the percent frequency of the largest one or two particles size classes is typically small in very large and representative samples from coarse gravel-bed streams. To obtain a smooth shape of the upper end of the cumulative distribution curve, the truncated sample needs to be extended to its relevant or full (pre-truncation) particle-size spectrum. This is accomplished by assigning small percentage frequencies to the truncated size classes (Fig. 5.16). The added percentages decrease for consecutively larger particle sizes. Estimates for those small percentages can

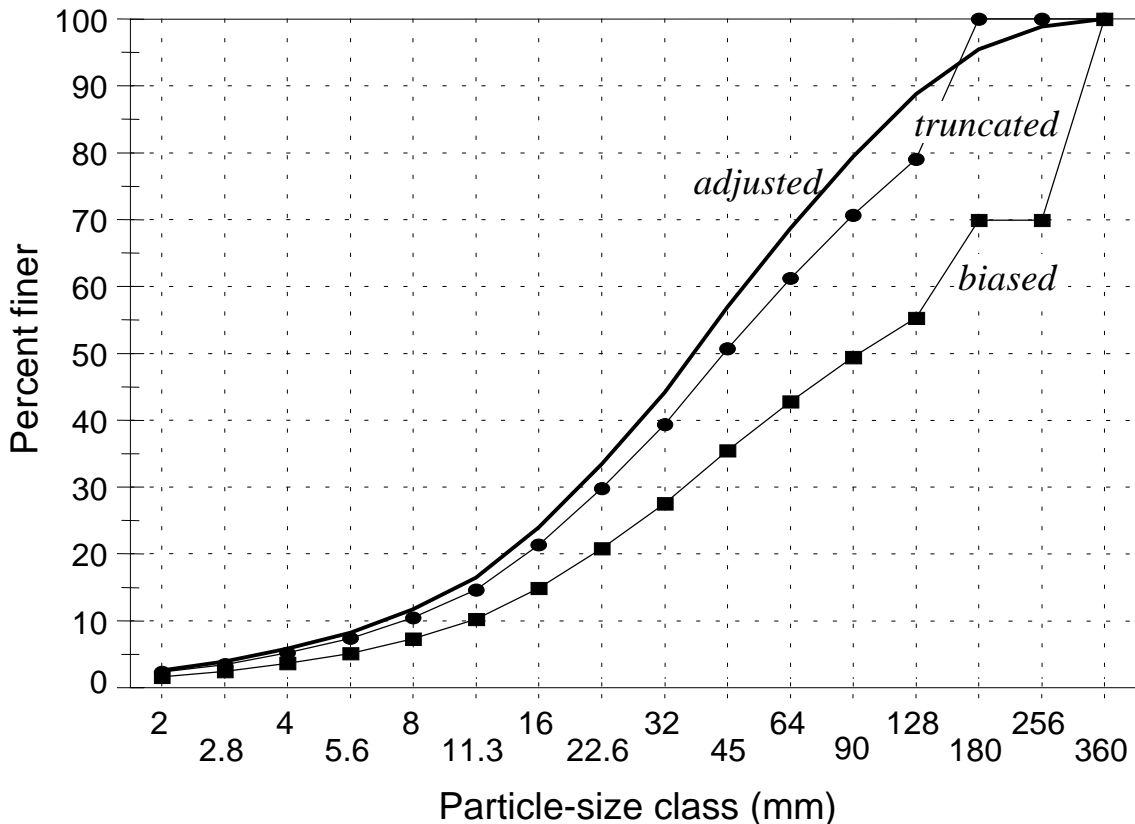


Fig. 5.16: Example of a biased sample from a deposit with a  $D_{max}$  size class of 256 mm. The sample was truncated by two size classes at 128 mm and then readjusted to its original  $D_{max}$  particle-size class of 256 mm.

be obtained by handfitting a smooth upper part of the cumulative distribution curve. The total percent frequency needs to be reset to 100% to compute the new cumulative frequency distribution.

If the assumption that large particles in unbiased samples account for only a small percentage of the total distribution mass is valid for a given sampling situation, truncation and readjustment can provide a more accurate approximation of the true bed-material size distribution than in small samples in which 20% or more of the sample weight is due to a single large particle, or in which the largest particles are not accounted for at all.

Truncation and readjustment is not applicable if there is reason to believe that the paucity or abundance of large particles in the sample is a result of fluvial processes, for example, a recent change in the local sediment budget. An abundance of large particles in subsurface sediment, or a scarcity of large particles in the surface sediment, may result from the burial of a former armor surface by a local deposition of mid-sized particles.

#### 5.4.2 Sample mass as a function of acceptable percentile errors

Sample-mass considerations in previous sections are primarily aimed at avoiding bias due to the unrepresentative presence or absence of a single large particle. The resulting empirical sample mass equations do not provide information regarding sampling precision. If a relationship between sample mass and sampling precision is needed, it may be computed from a two-step approach. A two-step approach computes the number of subsamples necessary for a specified sampling precision around the median particle size based on the central limit theorem. The particle size of the means or medians (or of percentiles close to the median) in subsamples are approximately normal distributed). Sections 5.2.3.1 and 5.3.2 described two-stage sampling for pebble counts with number-based sample-size statistics and for areal samples. Section 5.4.2.1 describes how a two-stage approach is used to estimate the precision of volumetric weight-based samples.

##### 5.4.2.1 Two-stage sampling approach (ISO 1992)

Individual volumetric samples taken with one of the sampling devices described in Section 4.2.3 are not likely to contain sufficient sediment for an acceptable level of precision in a size-distribution analysis. Therefore, ISO (1992) suggests collecting several subsamples. The mass of the largest particle  $D_{max}$  (in m) per subsample should be less than 3% of the subsample mass  $m_{ss}$  in order to avoid sample bias towards the larger fraction. This criterion for subsample mass  $m_{ss}$  (in kg) can be expressed by the function:

$$m_{ss} = 33.3 \frac{\pi}{6} D_{max}^3 \cdot \rho_s = 46,205 D_{max}^3 \quad (5.52)$$

where  $\rho_s$  is particle density of 2,650 kg/m<sup>3</sup>.

### Computation in units of mm

Similar to the two-stage sampling approaches proposed by ISO (1992) for grid and areal sampling (Sections 5.2.3.1 and 5.3.2), a number ( $q$ ) of volumetric samples are collected from a homogeneous deposit. For each individual sample, the particle size of the median or a percentile close to it is computed, either graphically from cumulative distribution curves or by logarithmic interpolation between percentiles (Section 2.1.4.2). ISO (1992) proposes to compute the median  $D_{50}$  in units of mm. It is assumed that the  $q$  values of  $D_{50}$  are approximately normally distributed. This guideline document recommends performing the computations in  $\phi$ -units (see below).

The sample standard deviation  $s_{50}$  of the  $q$  values of  $D_{50}$  is determined from:

$$s_{50} = \sqrt{\frac{\sum_{i=1}^q (D_{50} - D_{50m})^2}{q-1}} \quad (5.53)$$

$D_{50m}$  is the arithmetic mean particle size in mm of the median  $D_{50}$  obtained from the  $q$  samples. Equation 5.53 for sample standard deviation is preprogrammed in most scientific pocket calculators and spreadsheet programs. For two subsamples,  $s_{50}$  is computed by

$$s_{50} = \frac{D_1 - D_2}{\sqrt{2}} \quad (5.54)$$

Eq. 5.55 can be used to determine the number of weight-based subsamples  $q$  required to remain below a 5% chance ( $\alpha = 0.05$ ) that the absolute difference (positive or negative) between the estimated values of the  $D_{50}$  and the true population  $D_{50}$  is larger than or equal to the acceptable absolute error  $e_{\pm D_{50}}$ . The absolute error is the difference (in mm) between the  $D_{50}$  in the sample and in the population. Using an appropriate value for Student's  $t$  from Table 5.2, the number of subsamples  $q$  is

$$q = \left( \frac{t_{1-\alpha/2; q-1}}{e_{\pm D_{50}}} \cdot s_{50} \right)^2 \quad (5.55)$$

Total sample mass  $m_{tot}$  is the mass contained in each subsample  $m_{ss}$  multiplied by the number of  $q$  subsamples.

**Example 5.14:**

The  $D_{max}$  particle size of a deposit is estimated as 64 mm. Sample size  $m_{ss}$  for each subsample is 12 kg according to Eq. 5.52. Five subsamples were collected and have  $D_{50}$  particle sizes of 23, 29, 32, 38, and 44 mm. From Eq. 5.53, the standard deviation  $s_{50}$  for the  $D_{50}$  is 8.1 mm. An absolute error of  $e_{\pm D_{50}} = 5$  mm around the  $D_{50}$  particle size is considered acceptable. Eq. 5.55 needs to be solved iteratively when  $t$ -statistics are used (see Table 5.2 in Section 5.2.1 for  $t$ -values). An arbitrary sample size of 20 subsamples is selected in the first trial of Eq. 5.55. The subsample size  $q_{est} = 20$  is not equal to the computed subsample size  $q_{comp} = 12$  after the first trial.

Trial	$q_{est}$	$q-1$	$t_{1-\alpha/2; q-1}$	$q_{comp}$
1	20	19	2.093	$11.5 \cong 12$
2	12	11	2.201	$12.7 \cong 13$
3	13	12	2.179	$12.5 \cong 13$

After the third trial, the subsample size  $q_{est}$  for which the  $t$ -value was selected has converged with the computed subsample size  $q_{comp} = 13$ . The total sample mass of 13 subsamples of 12 kg each = 156 kg has a 95% probability that the sample  $D_{50}$  size is approximately within  $\pm 5$  mm of the size of the population  $D_{50}$ .

Note that one physical sample, i.e., the amount of sediment that is collected by using a sampling device once, might not have a sufficient mass for an unbiased representation of large particles. For  $D_{max}$  particle sizes larger than 90 mm, the 3% criterion in Eq. 5.52 requires a subsample mass of 34 kg. Therefore, for large  $D_{max}$  sizes, it may be necessary to combine several physical samples into one subsample in order to reduce bias incurred by the statistically unrepresentative presence or absence of large particles. Combined subsamples are then used for the two-stage sampling approach.

**Computations in units of  $\phi$**

It is recommended applying the two-stage approach to median particle sizes in units of  $\phi$  rather than to units of mm. Values of  $\phi_{50}$  from several subsamples are expected to approximate a normal distribution better than the values of  $D_{50}$  (in mm) and should therefore be preferred over computations in units of mm (Triola 1995) (Section 5.2.3.1).  $D_{50}$  in Eqs. 5.53 and 5.54 is then substituted by values of  $\phi_{50}$ .

**Precision from two-stage approach is not general but refers to analyzed samples only**

Each set of subsamples has a unique precision. For example, one set of three subsamples may have three  $D_{50}$  particle sizes of 45, 50, and 55 mm, while another set of three subsamples has the three  $D_{50}$  sizes of 43, 49, and 54 mm. Sample standard deviations will be slightly different for each set of subsamples, e.g., 5.0 in the first set of subsamples, and

5.5 in the second. Consequently, the computed sampling error (or precision) is different as well, yielding an absolute error of 12.4 mm around the  $D_{50}$  for the first, and of 13.7 mm for the second set of three subsamples.

The variability between individual subsamples increases due to bed-material heterogeneity in the sampling area or due to operator errors. The mean precision for a specified number of subsamples within a sampling area (e.g., three subsamples) is obtained if sets of three subsamples are collected repeatedly and precision is computed for each set. The precision is then averaged over all subsets of three samples and the result is the mean precision expected for a sample size of three. The same procedure is repeated for all sample sizes. The resulting data provide a description of the relationship between sample size and precision for a given percentile in a given deposit. The precision of this relationship increases with the number of subsamples over which precision is averaged for each subsample size. However, the repeated computation of precision for a large number of samples of the same sample size is a (prohibitively) large sampling effort.

Sampling efforts can be reduced by two procedures: One is using a regression function to determine the relationship between sample size and precision in a scatter plot. The second is a computer re-sampling procedure from a parent distribution for which the measured particle sizes are entered into a computer. Hogan et al. (1993) combined both procedures and developed a computerized two-stage sampling methodology (Section 5.4.2.2).

#### 5.4.2.2 Computerized two-stage sampling (Hogan et al. 1993)

The first step for computerized two-stage sampling is to obtain a large bed-material sample (parent sample) that may be derived from combining several subsamples taken from within a homogeneous deposit. The parent sample serves as a population surrogate and should be as large as possible, because the larger the mass of the parent sample, the more accurate the surrogate. The sample is sieved, and the sizes of all particles are entered into a computer data file. No assumptions about the distribution type of the parent population need to be made. The computer then selects random particles from the parent distribution with replacement to create subsamples to which particles are added until a specified mass (e.g.,  $m_{ss} = 50$  kg) is exceeded. The subsample mass needs to be large enough to avoid bias against or towards large particles in the sample (sample size for bias avoidance: Section 5.4.2.1, Eq. 5.52, and Section 5.4.3.1, Eq. 5.60 and Fig. 5.20).

##### ***Sampling with no replication***

The smallest subsample size ( $q = 2$ ) collected from the parent population consists of two subsamples, each with a sample mass of  $m_{ss} \geq 50$  kg and a total sample mass of  $2 m_{ss} \geq 100$  kg. The largest sample size might comprise 30 subsamples ( $q = 30$ ) with a mass of  $30 m_{ss} \geq 1,500$  kg. The particle sizes of all percentiles of concern  $D_p$  are computed for each subsample, for example the seven percentiles  $D_5$ ,  $D_{16}$ ,  $D_{25}$ ,  $D_{50}$ ,  $D_{75}$ ,  $D_{84}$ , and  $D_{95}$ . The smallest subsample comprises two values for each percentile  $D_p$ , whereas the largest subsample comprises 30 values for each  $D_p$ . Although Hogan et al. (1993) used mm-units,

these guidelines recommend that the analyses be performed in units of  $\phi$ , because percentiles in  $\phi$  approach normality better than percentiles in mm.

The next step in the two-stage procedure is to compute the sample standard deviation  $s_{pq}$  for the  $q$  percentile values  $D_p$ , assuming that the  $q$  values for the percentile particle size  $D_p$  approximate a normal distribution. Either Eq. 5.53 or a preprogrammed function in a spreadsheet program may be used to compute the sample standard deviation. The absolute error  $e_{\pm D_p}$  (in mm) around a percentile  $D_{pq}$  is computed from:

$$e_{\pm D_p; q} = \frac{t_{1-\alpha/2; q-1}}{\sqrt{q}} \cdot s_{pq} \quad (5.56)$$

which is the general sample-size equation Eq. 5.55 or 5.2 solved for the error term. Table 5.2 provides values of Student's  $t$ . Alternatively, the absolute error  $e_{\pm D_p}$  added or subtracted from the *population* percentile value  $D_{p\mu}$  could be computed. If the study requires a result in terms a percent error, the percent error  $e_{\%D_p}$  around a percentile  $D_p$  is computed from

$$e_{\%D_p} = \frac{e_{\pm D_p}}{D_{p\mu}} \cdot 100 \quad (5.57)$$

### ***Best-fit regression function for visualizing the data trend***

For all percentiles of concern, the error computed for each sample size (Eq. 5.56) is plotted against that sample size. Data plotted from these computations may scatter considerably (due to the lack of sample replications, Section 5.4.2.1). An example of such scatter can be observed in Fig. 6.18 (Section 6.4.3.1). In order to visualize the trend of the data, a best-fit regression function is fitted through the points (Fig. 5.17). Knowing that the trend of the curves describes a decrease of sampling error  $e$  with  $1/\sqrt{q}$ , the regression function may have the form of  $e = a \cdot q^{-0.5}$ .

The resulting graphs for positive, as well as negative errors, approach the  $x$ -axis asymptotically from both sides (“trumpet curve”) (Fig. 5.17). Graphs as these can be established for all percentiles of concern. Graphical visualization of the relationship between sample size and error is useful when determining where to make the compromise between tolerable error, sample size, and expendable effort and costs. Note, however, that the smoothed graphs imply an unduly high precision of the computed relationship between sample size and precision. A further caveat of this methodology is that two-stage approach used for the computations is not designed to determine errors around low and high percentiles, which may not approach normality for low sample sizes. Thus, the true precision may differ from the computed precision. However, the computations are relatively easy and may suit as a first approximation of sampling precision.

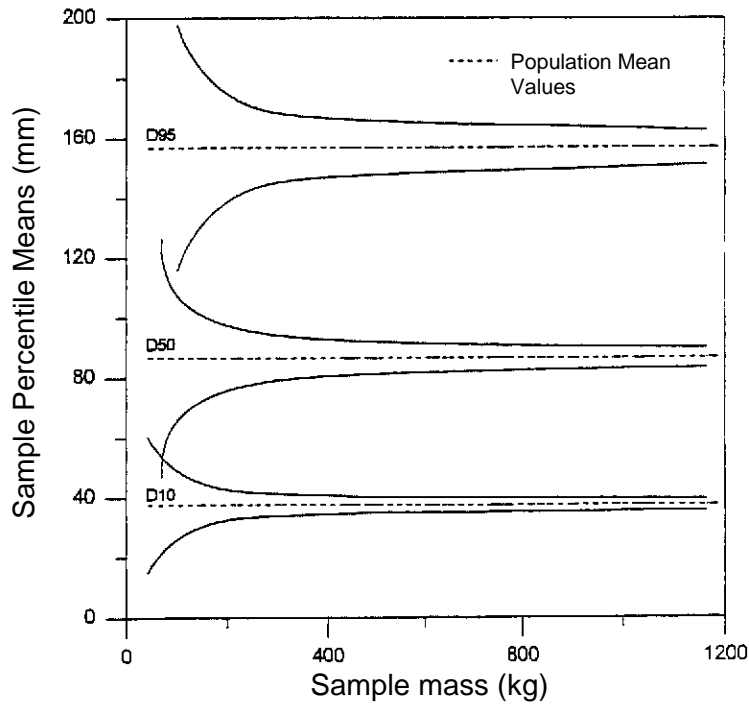
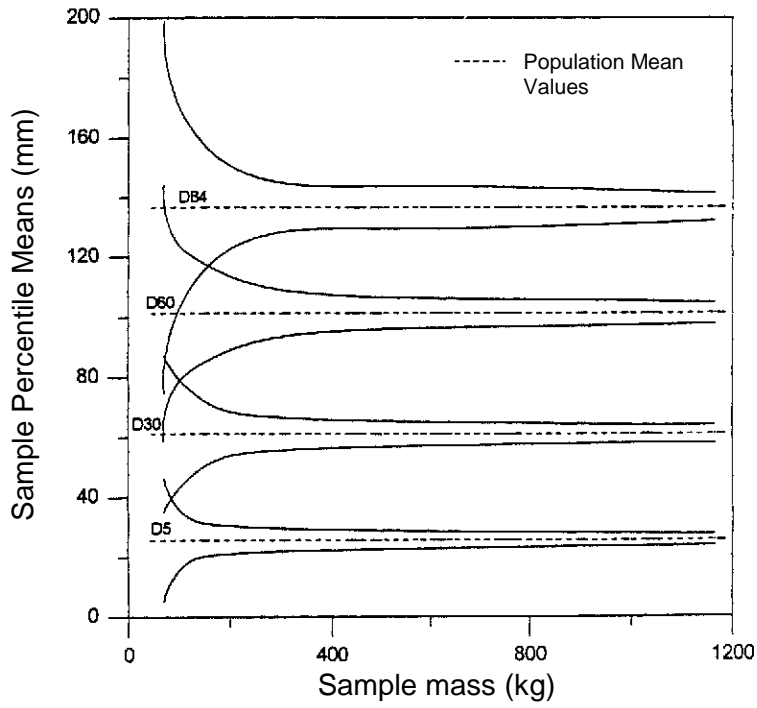


Fig. 5.17: Results of two-stage computer sampling with no replications for a bed-material sample from the Cache la Poudre River, Colorado. Relation between absolute error (in mm) around percentile particle sizes of the  $D_5$ ,  $D_{30}$ ,  $D_{60}$ , and  $D_{84}$  (top), and  $D_{10}$ ,  $D_{50}$ , and  $D_{95}$  (bottom) added and subtracted from the population percentile particle-size and sample mass. The error curves have been smoothed by fitting a regression function (from Hogan et al. 1993).

### ***Error-curves***

The error is at a maximum when sample size is small (or mass in this case) and becomes smaller as sample size increases. At some point, a further increase in sample size contributes only insignificantly to a further decrease in sampling error (see also Figs. 5.10 and 5.11 in Section 5.2.3.4). The absolute error around a percentile in units of mm for a given sample size is smallest for small percentiles and increases for larger percentiles (Fig. 5.17). However, a more interesting result from the study by Hogan et al. (1993) is that the percent error for a specified sample size is not symmetrically distributed around paired percentiles. For a fixed sample size, the percent error is largest around the  $D_5$ , strongly decreases towards the  $D_{10}$ , is lowest for the  $D_{84}$  and increases slightly for the  $D_{95}$ . This result can be expected for the bed-material from the South Fork Cache la Poudre which is a coarse gravel or cobble distribution slightly skewed towards fines. This finding is also in agreement with the results obtained by Rice and Church (1996b) for their bootstrap analysis of a large sample from the Mamquam River (Section 5.2.3.4).

For the bed-material sample analyzed in Fig. 5.17, a sample mass of 200 kg determines the  $D_{10}$  particle size to within  $\pm 5$  mm of the population  $D_{10}$  particle size of 38 mm. More than 500 kg are needed to define the  $D_{50}$  to the same absolute precision of  $\pm 5$  mm. The increase in the absolute error for higher percentiles for a given sample size (or mass) is a result of using mm-units for the analysis. It is recommended that the analysis be performed in  $\phi$ -units if the underlying distribution approaches normality in  $\phi$ -units. The error would then be highest for low and high percentiles and lowest around central percentiles. The distribution of errors around low and high percentiles for a specified sample size is discussed in Section 5.4.4.

### ***Replicate sampling***

Scatter in the data points can be reduced if precision is computed repeatedly for different sets of samples of the same subsample size, and if the mean precision for a given subsample size is plotted. The more sets of subsamples collected and analyzed, the higher the precision of the relationship between sample size and certainty of the result.

Replicate sampling reduces the scatter in the plots of sampling precision versus sample size. The number of replicates needed to produce smooth error curves increases as the sorting of the parent distribution becomes poorer, and as subsamples with smaller mass are taken. Rice and Church (1996b) recommend that about 200 replicates be performed for each sample size. Ferguson and Paola (1997) even used 500 replicates. Because this might exceed the capacity of user-developed spreadsheets, the use of commercially available bootstrapping programs may be required (e.g., Resampling Stats, available as an add-in program to Microsoft Excel, Section 5.2.3.4).

For 200 replications, each sample size  $q$  is represented by 200 replicates  $r_1, r_2, \dots, r_{200}$ . Each of the 200 replicates has a slightly different composition of particle sizes. Thus, the particle size of the  $D_{50}$  and all other percentiles is slightly different for each of the 200 replicates constituting the sample size  $q$ . The variability is reduced when the  $D_{50}$  particle

size associated with the sample size  $q$  is taken as the arithmetic mean of the 200 individually computed  $D_{50}$  particle sizes ( $D_{50,q,200}$ ). Likewise, the  $D_{84}$  particle size computed for the sample size  $q = 3$  is the arithmetic mean of all the  $D_{84}$  values obtained from 200 repetitions with a sample size 3 ( $D_{84,3,200}$ ).

The actual two-stage sampling procedure is the same as described in Section 5.4.2.1, with the exception that each particle-size percentile represents the arithmetic mean of 200 replicates. A diagram explaining the resampling procedure for two-stage sampling is provided in Fig. 5.18, for a preset subsample mass of 50 kg, two subsample sizes  $q = 2$  with  $m_2=100$  kg, and  $q = 3$  and  $m_3=150$  kg, and with  $D_{16}$  as the percentile of concern.

### 5.4.3 Analytical computation of sample mass (Ferguson and Paola 1997)

Sample size necessary to obtain a specified precision is influenced by a variety of factors (Section 5.1), but volumetric sample-size equations discussed thus far have not addressed many of those factors. The empirical recommendations that determine sample mass as a function of  $D_{max}$  were developed for various sampling goals and physical settings. Thus, sample-mass requirements vary widely between different equations (Section 5.4.1). None of the  $D_{max}$ -based sample-mass recommendations provides information on percentile errors. The two-stage approach (Section 5.4.2.1) can be used to indicate the error around the sample mean or median for a specific set of subsamples. A computerized two-stage resampling approach provides a surrogate for percentile errors (Section 5.4.2.2). A bootstrap approach that re-samples a large parent distribution repeatedly (e.g., 200 times) can reliably quantify percentile errors (Section 5.2.3.4) once a large sample is collected.

However, a methodology is needed that allows the user to make a reliable estimate of the sample mass required for a tolerable error around a specified percentile for a given stream setting before the sample is collected, and to compute the sampling precision for a collected sample. With this task in mind, Ferguson and Paola (1997) developed sample-mass equations with the following properties: the equations (1) allow the user to compute the sample mass necessary for avoiding bias; (2) are suitable for computing the relationship between sample-size and error for any percentile(s) of concern, and (3) can be applied to bed-material of any standard deviation or sorting coefficient. However, a pilot study is needed to estimate the bed material  $D_{50}$  and the standard deviation (sorting). A drawback of the approach is that the computations are based on an assumed normal distribution, and results are correct only if an underlying normal distribution in  $\phi$ -units can be assumed for the deposit, which strictly speaking is rarely the case.

The sample-mass equations determined by Ferguson and Paola (1997) were derived from three large computer-generated particle-size populations with standard deviations or sorting coefficients of 0.5, 1.0, and 1.5  $\sigma$ . The samples were generated based on an underlying lognormal distribution of particle mass per size class for particle sizes in mm-units (equivalent to a normal distribution in terms of  $\phi$ -units). Random samples with replacement were drawn by computer from these parent populations until samples of

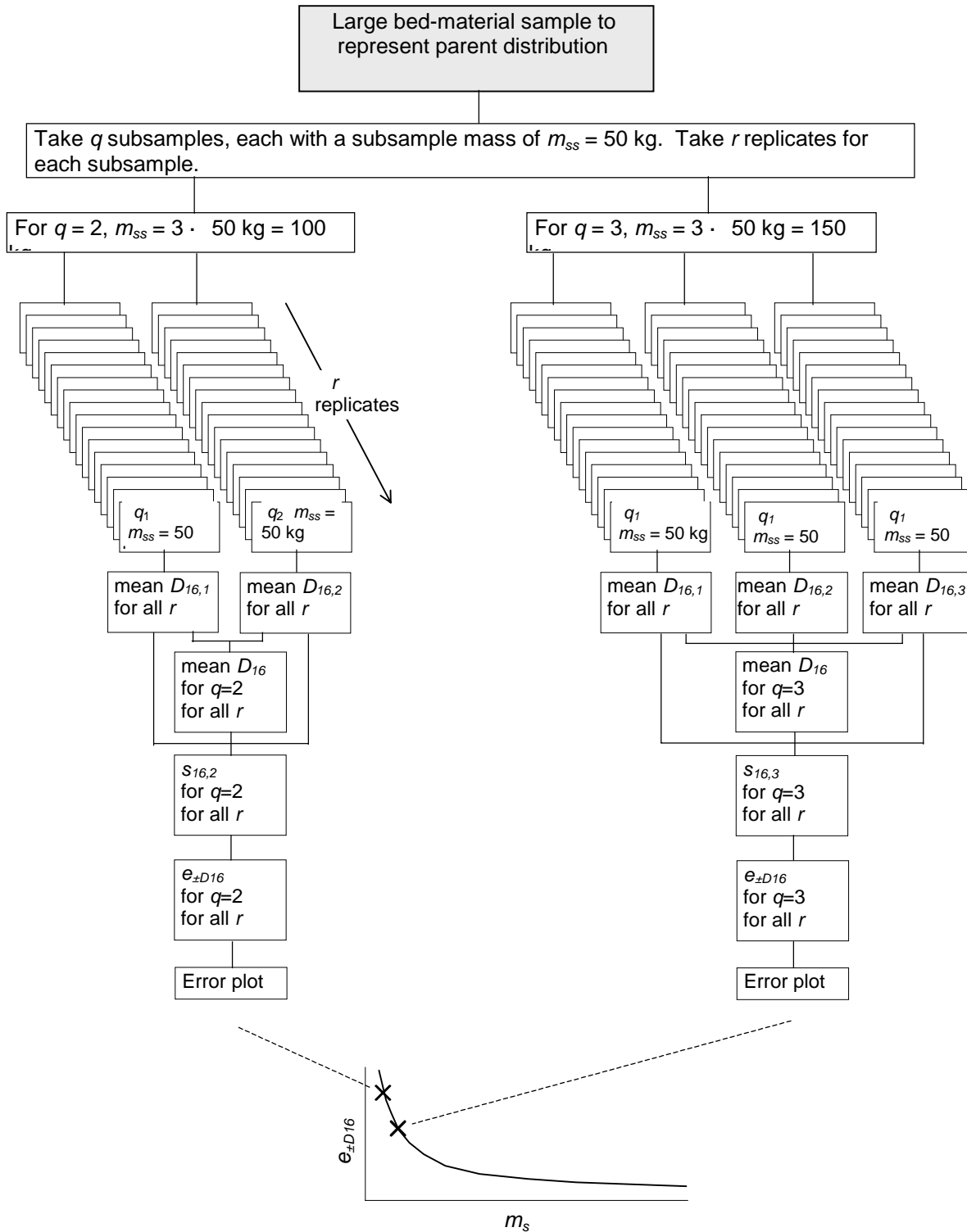


Fig. 5.18: Diagram explaining a resampling procedure with replicates for the example of a preset subsample mass of 50 kg, with subsample sizes  $q = 2$  and  $m_{q2}=100$  kg, and  $q = 3$  and  $m_{q3}=150$  kg, and with  $D_{16}$  being the percentile of concern.  $s_{16,2}$  and  $s_{16,3}$  are the standard deviation of the  $D_{16}$  particle sizes of the 2 or 3 subsamples, respectively.

specified volumes were reached. Each sample size was represented by 500 replicate samples to ensure a high precision of the computed relationship between sample size and error.

***Computation of relative sample volume and absolute sample mass***

In order to develop graphs that are applicable to all particle sizes, Ferguson and Paola (1997) expressed sample size as the ratio of the total sample volume  $V$  and the volume of the  $D_{50}$  particle size  $V_{50}$ . A spherical or ellipsoidal  $D_{50}$  particle of 32 mm, for example has a volume of  $\pi/6 D_{50}^3 = 17.16 \text{ cm}^3$ . A relative sample volume of  $V/V_{50} = 1$  corresponds to a volume of  $17.16 \text{ cm}^3$ , and a sample mass of  $V \cdot \rho_s = 17.16 \text{ cm}^3 \cdot 2.65 \text{ g/cm}^3 = 45 \text{ g}$  or  $0.045 \text{ kg}$ , where  $\rho_s$  is the particle density. Similarly, relative sample volumes ( $V/V_{50}$ ) of 10, 100, 1,000, and 10,000 correspond to absolute sample masses of 0.45, 4.5, 45, and 455 kg, respectively. For a  $D_{50}$  particle of 16 mm, the corresponding sample masses are 0.006, 0.057, 0.57, 5.7, and 57 kg, respectively (see Figs. 5.19 a-c, 5.21 a-c and 5.22 a-c). Thus, to compute sample mass in absolute terms, the  $D_{50}$  particle size needs to be known.

***Estimation of the  $D_{50}$  particle size from one other percentile and the distribution sorting***

If the only percentile known from a distribution is the  $D_{84}$ , for example, then the user can determine the respective  $D_{50}$  particle size if the distribution sorting is known, and if a normal distribution in terms of  $\phi$ -units can be assumed. The  $D_{50}$  particle size can then be determined graphically (Fig. 2.19 in Section 2.1.5.4) or analytically. Fig. 2.19 can be used to identify the  $D_{50}$  if the distribution sorting  $s_I$  is close to the values of 0.5, 1, or 1.5. The curve with the appropriate sorting coefficient is shifted to the right or left until the curve passes through the one known percentile value, e.g.,  $D_{84} = -6.5 \phi$ . The  $D_{50}$  particle size can then be read from the shifted curve. The  $\phi_{50}$  percentile particle size can be estimated analytically if the sample standard deviation and one other percentile size is known (Gilbert 1987):

$$\phi_{50} = \phi_p + (Z_p \cdot s) \quad \text{for } \phi_p > \phi_{50} \tag{5.58}$$

or

$$\phi_{50} = \phi_p - (Z_p \cdot s) \quad \text{for } \phi_p < \phi_{50} \tag{5.59}$$

where  $\phi_p$  is the particle size of the known percentile, and  $Z_p$  indicates the distance between the percentile  $p$  and the median (i.e.,  $\phi_{50}$ ) in terms of standard deviation.  $Z_p$  can be obtained from standard statistics tables (e.g., Gilbert 1987, p. 254, Table A1). Values for  $Z_p$  for frequently used percentiles are provided in Tables 5.9 and 5.1.

Table 5.9: Values for  $Z_p$  for various percentiles (See Table 5.1 for more values)

Percentiles:	50	65	75	84	90	95	97.5	99
		35	25	16	10	5	2.5	1
$Z_p$	0	0.385	0.675	0.995	1.282	1.645	1.96	2.327

**Example 5.15:**

From a previous study it is known that the  $D_{75} = 68$  mm, and the sample sorting  $s = 1.67$ . Convert the  $D_{75}$  percentile size into  $\phi$ -units:  $\phi_{75} = -3.3219 \log(68) = -6.09 \phi$ . Compute  $\phi_{50}$  using Eq. 5.58:  $\phi_{50} = -6.09 + (0.675 \cdot 1.67) = -6.09 + 1.13 = -4.96 \phi$ . Converting back to mm yields:  $D_{50} = 2^{4.96} = 31.1$  mm

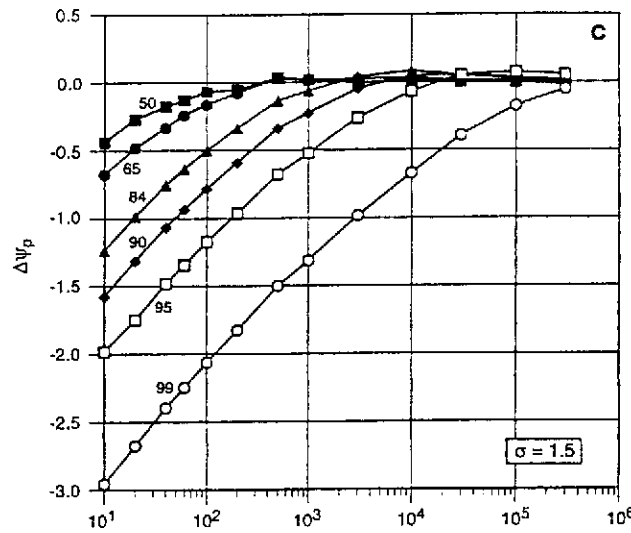
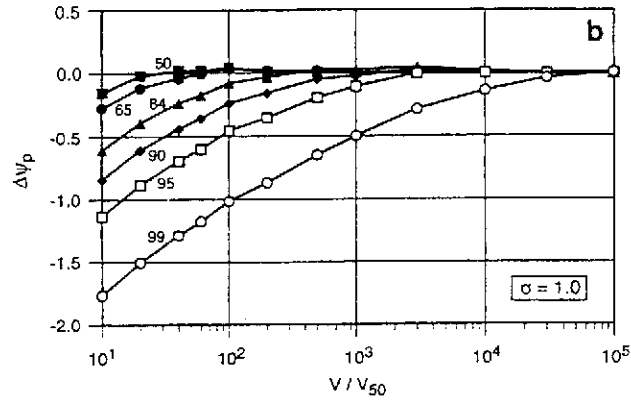
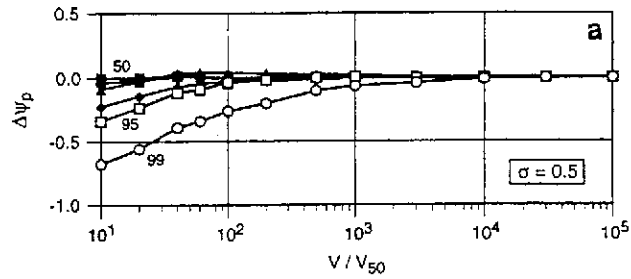
**5.4.3.1 Sample mass for bias avoidance**

The analysis by Ferguson and Paola (1997) indicated that small samples are systematically biased towards the fine fraction (Fig. 5.19 a-c). This becomes evident as the number of large particles is relatively small in a given sample volume. Thus, there is a less than average chance for large particles to be included in a small sample. Consequently, the sample particle-size distribution is finer than the population size distribution. Bias due to the chance *presence* of an overly large particle in an individual sample is not addressed in this computation, because particles larger than the parent distribution cannot be drawn from the parent population by the computer. But the occurrence of bias in an individual sample may introduce a pronounced error into the resulting particle-size distribution (Sect. 5.4.1.4).

Figs. 5.19 a-c indicate that bias is more pronounced for poorly sorted rather than for well sorted sediment. Fig. 5.15 also shows that the relative sample mass required for avoiding bias for the  $D_{95}$  particle size is approximately two orders of magnitude larger than the sample mass for avoiding bias in the  $D_{50}$ . On the basis of these results, Ferguson and Paola (1997) propose a dimensionless equation for determining the bias-avoiding sample volume  $V_b$ .  $V_b$  is a relative sample volume scaled by the volume of the  $D_{50}$  particle  $V_{50}$ :

$$\log \left( \frac{V_b}{V_{50}} \right) = 1.3 + \log(\sigma) + 0.9 \sigma \cdot Z_p \tag{5.60}$$

$Z_p$  describes the distance between the percentile  $p$  and the median in terms of the standard deviation of a normal distribution (Table 5.9). Eq. 5.60 can be used for any percentile. The percentile for which bias is avoided is specified through the selection of an appropriate value of  $Z_p$ . To apply to the  $D_{84}$ ,  $Z_p$  is selected as 0.995 from Table 5.9 or Table 5.1.



$D_{50}$ (mm)	}	<b>11.3:</b>	0.020	0.20	2.0	20.0	200	2,002	} Sample mass (kg)
		<b>16:</b>	0.057	0.57	5.7	56.8	568	5,683	
		<b>22.6:</b>	0.160	1.60	16.0	160.0	1,600	16,017	
		<b>32:</b>	0.455	4.55	45.5	454.7	4,547	45,467	
		<b>45:</b>	1.264	12.64	126.4	1,264.4	12,644	126,439	
		<b>64:</b>	3.637	36.37	363.7	3,637.3	36,373	363,734	
		10	100	1,000	10,000	100,000	1,000,000		
		$V/V_{50}$							

Fig. 5.19 a-c: Relation between bias in terms of  $\phi$ -units ( $\Delta\psi_p$ ) and relative sample volume  $V/V_{50}$  for given percentiles between  $D_{50}$  and  $D_{99}$ , and standard deviation of  $\sigma = 0.5 \phi$  (a),  $\sigma = 1.0 \phi$  (b), and  $\sigma = 1.5 \phi$  (c). Numbers on the curves indicate percentiles. Bias is the difference (continued on next page)

between the sample mean particle size of a given percentile in  $\phi$ -units, averaged over 500 replicate samples, and the particle size of that percentile in the population. A negative difference indicates the sample percentile is finer than the population percentile. Sample size is a multiple of the volume  $V_{50}$  of the population median particle-diameter. (Reprinted from Ferguson and Paola (1997), by permission of John Wiley and Sons, Ltd.). Discrete values of sample mass (kg) are given for various  $D_{50}$  particle sizes (mm) at the bottom of the plot. The numbers on the bottom of the plots indicate sample mass values in kg for  $10^1$ ,  $10^2$ ,  $10^3$ ,  $10^4$ ,  $10^5$ , and  $10^6 V/V_{50}$  for various  $D_{50}$  particle sizes.

Example 5.16:

Assume the bed-material sample in  $\phi$ -units approaches a normal distribution and has a standard deviation of  $s = 1.5 \phi$ . Relative sample volume  $V_b/V_{50}$  for avoiding bias in the estimation of the  $D_{84}$  particle size is computed from Eq. 5.60:

$$\begin{aligned} \frac{V_b}{V_{50}} &= 10^{(1.3 + \log(1.5) + 0.9 \cdot 1.5 \cdot 0.995)} \\ &= 10^{(1.3 + 0.176 + 1.343)} = 10^{2.819} = 659 \end{aligned}$$

For a  $D_{84}$  particle size of 90 mm, and a sorting of  $s = 1.5 \phi$ ,  $D_{50}$  is 32 mm (see Fig. 2.19 or Eq. 5.58). Sample volume without pore space is

$$V_b = 659 \cdot (\pi/6) \cdot D_{50}^3 = 659 \cdot 17.16 \text{ cm}^3 = 11,307 \text{ cm}^3$$

Multiplication by particle density  $\rho_s = 2.65 \text{ g/cm}^3$  provides sample mass

$$m_b = 11,307 \cdot 2.65 = 29,963 \text{ g} = 30 \text{ kg}$$

Dividing by an assumed bulk density of  $1,500 \text{ kg/m}^3$  for shoveled gravel gives the sample volume of  $0.02 \text{ m}^3$  which is about 2 household buckets of 10 liters each.

Relative sample volume in terms of  $V/V_{50}$  for bias avoidance was computed with Eq. 5.60 and plotted against sediment standard deviation  $\sigma$  for various percentiles between  $D_{50}$  and  $D_{99}$  in Fig. 5.20. Fig. 5.20 indicates that a relative sample volume of  $V/V_{50} = 30$  is required for avoiding bias in the  $D_{50}$  particle size in a distribution with a standard deviation of  $1.5 \sigma$ . The numbers on the side of the plot present the absolute sample mass in kg for relative sample volumes of 10, 100, 1,000, etc. If the  $D_{50}$  particle size of the deposit was 32 mm, the column under 32 mm is used to interpolate between 4.5 and 45 kg. A relative sample volume of  $659 V/V_{50}$  is approximately  $6.6 \cdot 4.5 \text{ kg} \approx 30 \text{ kg}$ .

Sample mass for bias avoidance can become very large for high percentiles in poorly sorted river beds. A relative sample volume of 35,000  $V/V_{50}$  is needed to avoid bias around the  $D_{95}$  in a poorly sorted distribution with  $s = 2 \phi$ . If the distribution has a  $D_{50}$  particle size of 64 mm, an absolute sample mass of  $3.5 \cdot 3640 \text{ kg} = 12.7$  metric tons is needed.

The widely used sample-mass requirements by Church et al. (1987) suggest that the mass of a particle of the  $D_{max}$  size should comprise 0.1, 1, and 10% of the sample mass (Section 5.4.1.1). For comparison, these criteria are also plotted in Fig. 5.20. Fig. 5.20 shows that even the 10% criterion suffices to prevent bias in all but the 99th percentile.

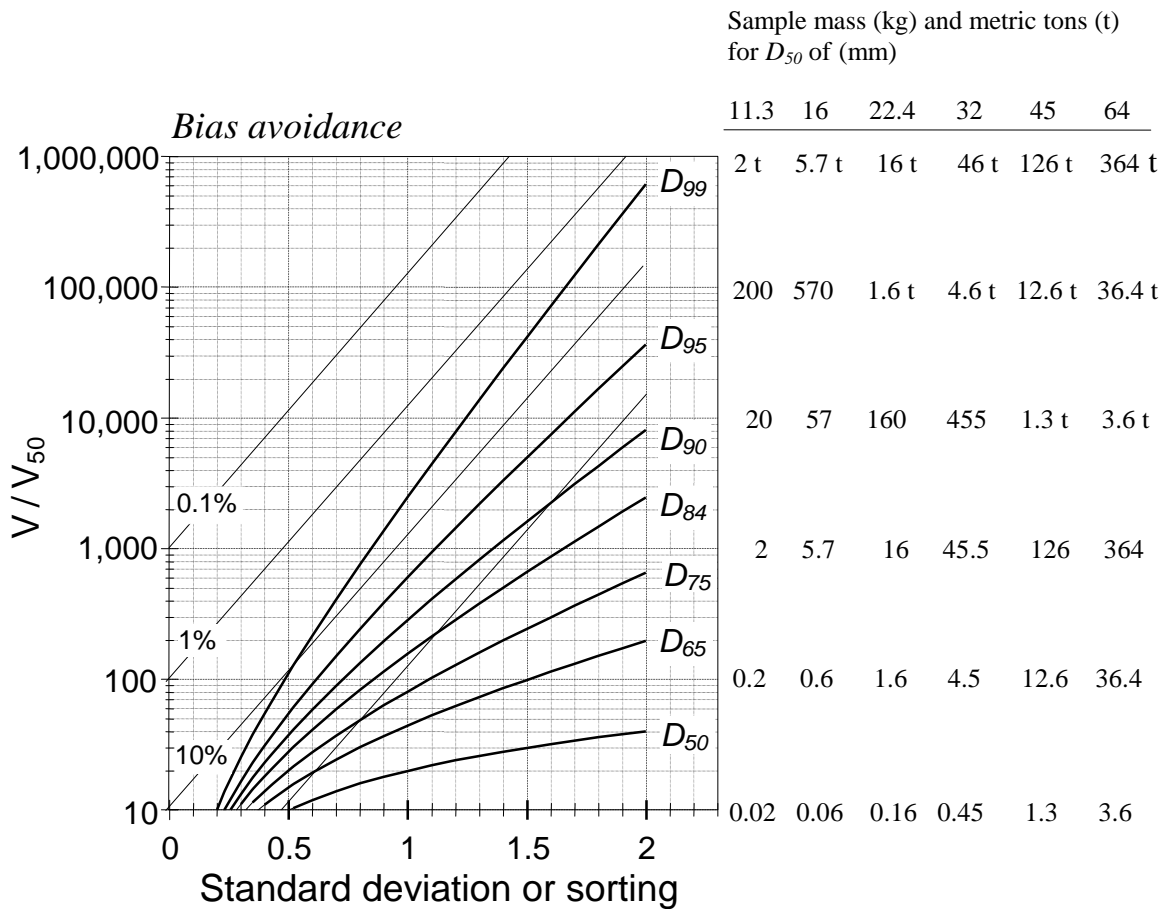


Fig. 5.20: Relation between relative sample volume ( $V/V_{50}$ ) for bias avoidance and sediment sorting for various percentiles between  $D_{50}$  and  $D_{99}$ . Sample sizes for paired percentiles (e.g.,  $D_{10}$  and  $D_{90}$ ) are identical. The numbers on the right side of the plot indicate sample-mass values in kg and metric tons for  $10^2$ ,  $10^3$ ,  $10^4$ ,  $10^5$ ,  $10^6$ , and  $10^7$   $V/V_{50}$  for various particle sizes of  $D_{50}$ . (Modified from Ferguson and Paola (1997), by permission of John Wiley and Sons, Ltd.).

### 5.4.3.2 Sample mass for specified acceptable error

Sampling precision can be quantified by means of the percentile standard error  $s_p$  in  $\phi$ -units between replicate samples. In unbiased samples,  $s_p$  is computed from Eq. 5.53. The percentile standard error  $s_p$  relates to the absolute error  $e_{\pm\phi p}$  around a percentile in  $\phi$ -units by

$$e_{\pm\phi p} = Z_{1-\alpha/2} \cdot s_p \quad (5.61)$$

where  $Z_{1-\alpha/2}$  is 1.96 for a 95% confidence limit (Table 5.1). Thus, a percentile standard error  $s_p$  of  $\pm 0.15$   $\phi$ -units is equivalent to an absolute error  $e_{\pm\phi p}$  of almost  $\pm 0.3$   $\phi$ -units, which, in turn, corresponds to a percentage error in mm-units  $e_{\%Dp}$  of -18 to +23%, and a percentage standard error in mm-units  $s_{p,\%D}$  of -9 to +12% (Fig. 5.8 in Section 5.2.3.4).

The results of the bootstrap procedure by Ferguson and Paola (1997) in Fig. 5.21 a-c illustrate a similar trend to the results by Rice and Church (1996b; Figs. 5.10 and 5.11) and by Hogan et al. (1993; Fig. 5.17). The error decreases with sample size or sample volume as a function of  $1/\sqrt{n}$  or  $1/\sqrt{V}$ , respectively. For volume-based sampling, it appears that the error decreases only after a threshold sample volume has been exceeded, but this phenomenon may be due to the logarithmic scale of sample size along the  $x$ -axis.

Results by Ferguson and Paola (1997) clearly show the relationship between standard deviation, sample mass, and sampling error. Sample mass for a specified standard error is orders of magnitude larger for poorly sorted sediment than for well-sorted sediment. Sample mass for a specified error is also larger for the  $D_{95}$  percentile size than for the  $D_{50}$ . On the basis of this analysis, Ferguson and Paola (1997) developed a dimensionless equation that facilitates computing sample volume  $V_g$  necessary to obtain a specified percentile standard error  $s_p$  when sampling a population with a standard deviation  $\sigma$ :

$$\log\left(\frac{V_g}{V_{50}}\right) = 1.4 + 4.2 \log(\sigma) + 0.9 \sigma \cdot Z_p - 2 \log(s_p) \quad (5.62)$$

where  $Z_p$  is the  $p$ th percentile variate of the unit normal distribution (Tables 5.9 and 5.1). For a preset percentile standard error  $s_p = 0.15$   $\phi$ -units, the last term in Eq. 5.62 yields the numerical value of -1.65 and simplifies to

$$\log\left(\frac{V_g}{V_{50}}\right) = 3.0 + 4.2 \log(\sigma) + 0.9 \sigma \cdot Z_p \quad (5.63)$$

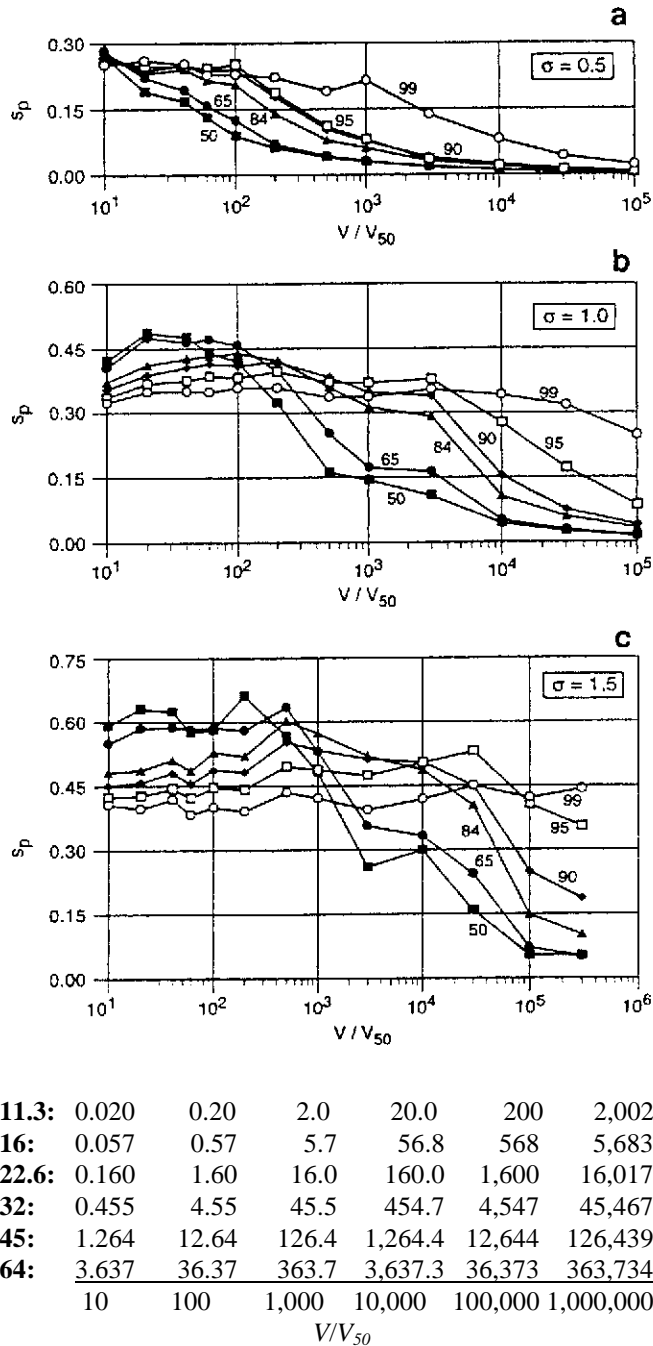


Fig. 5.21 a-c: Results from the bootstrap analysis: Relation between percentile standard error  $s_p$  and relative sample volume  $V/V_{50}$  for given percentiles between  $D_{50}$  and  $D_{99}$ , and population standard deviation of  $\sigma = 0.5 \phi$  (a),  $\sigma = 1.0 \phi$  (b), and  $\sigma = 1.5 \phi$  (c). Numbers on curves indicate percentiles. Note that the bottom plot (c) covers one more log cycle of sample size than plots a and b (Reprinted from Ferguson and Paola 1997, by permission of John Wiley and Sons, Ltd.). The numbers on the bottom of the plots indicate sample-mass values in kg for  $10^1$ ,  $10^2$ ,  $10^3$ ,  $10^4$ ,  $10^5$ , and  $10^6$   $V/V_{50}$  for various sizes of  $D_{50}$ .

If the error around the  $D_{50}$  is of concern, the last term of Eq. 5.63 can be omitted since the numerical value of  $Z_p$  becomes 0.

Example 5.17:

For a deposit that can be assumed to approach a normal distribution and has a sorting of  $s = 1.2$ , the relative sample volume  $V_g/V_{50}$  required for estimating the  $D_{95}$  particle size to within a standard error of  $\pm 0.15 \phi$ -units is (Eq. 5.62) is

$$\begin{aligned} \frac{V_g}{V_{50}} &= 10^{(1.4 + 4.2 \log(1.2) + 0.9 \cdot 1.2 \cdot 1.645 - 2 \log(0.15))} \\ &= 10^{(1.4 + 0.33 + 1.78 - (-1.65))} = 10^{5.16} = 144,544. \end{aligned}$$

If the bed material  $D_{95}$  particle size is 200 mm, the  $D_{50}$  particle size can be computed from Fig. 2.19, or Eqs. 5.58 and 5.59 and is 50.9 mm. The absolute sample volume  $V_s$  can then be computed from

$$\begin{aligned} V_s &= 144,544 \cdot (\pi/6) \cdot D_{50}^3 = 144,544 \cdot 69.05 \text{ cm}^3 \\ &= 9,980,494 \text{ cm}^3 \approx 10 \text{ m}^3. \end{aligned}$$

Multiplication by particle density  $\rho_s = 2650 \text{ kg/m}^3$  provides the sample mass

$$m_s = 10 \text{ m}^3 \cdot 2650 \text{ kg/m}^3 = 26,500 \text{ kg} = 26.5 \text{ metric tons.}$$

Dividing by a bulk density of  $1.5 \text{ kg/m}^3$  for shoveled gravel, sample bulk volume is  $17.7 \text{ m}^3$  (approximately the volume of a small office).

Relative sample volume in terms of  $V/V_{50}$  for sample precision of  $\pm 0.1$ ,  $\pm 0.15$ , and  $\pm 0.2 \phi$  standard errors was computed with Eq. 5.63 and plotted versus the sediment sorting for various percentiles between  $D_{50}$  and  $D_{99}$  in Figs. 5.22 a -c. The graphs indicate that relative sample volume, and thus sample mass, strongly increases with sediment sorting and with an increase in the percentile size being addressed. Because the parent distribution was Gaussian in terms of  $\phi$ -units, sample mass for a preset error and sorting are symmetrically distributed around the mean, and thus identical for paired percentiles such as the  $D_{10}$  and the  $D_{90}$ .

Fig. 5.22 is used similar to Fig. 5.20. The first step is to select the plot with the appropriate error (plot a, b, or c). If, for example, the task is to estimate the sample size necessary to remain below an absolute error of  $\pm 0.2 \phi$  around the  $D_{75}$  in a gravel bed with a standard deviation of  $s = 1.5 \phi$ , select Fig. 5.22 a. A relative sample volume of  $V/V_{50} = 12,000$  is obtained from the graph for  $D_{75}$  in Fig. 5.22 a. If the bed-material  $D_{50}$  particle size is 64 mm, the absolute sample mass may be read on the right side of the plot as  $1.2 \cdot$

36.4 t = 43.5 metric tons. This example is somewhat extreme because the accurate determination of the  $D_{95}$  subsurface particle-size in gravel-bed streams is usually not the task of volumetric sampling. Sample mass is orders of magnitude smaller if the  $D_{50}$  is the percentile of interest, and if the bed-material is better sorted. A relative sample volume of  $V/V_{50} = 2,500$  suffices for estimating the  $D_{50}$  to within an absolute error of  $\pm 0.2 \phi$  if the bed material sorting is  $1\phi$ . For a  $D_{50}$  particle size of 22.6 mm, sample mass on the right side of the plot can be read as  $2.5 \cdot 16 \text{ kg} = 40 \text{ kg}$ .

The user may be frequently surprised by the large sample sizes necessary for volumetric samples in coarse gravel and cobble-bed streams. Sample masses larger than a few 100 kg are usually not feasible to collect in mountain streams. It may become necessary to reduce the tolerable error for the study, or to restrict precision requirements to central percentiles.

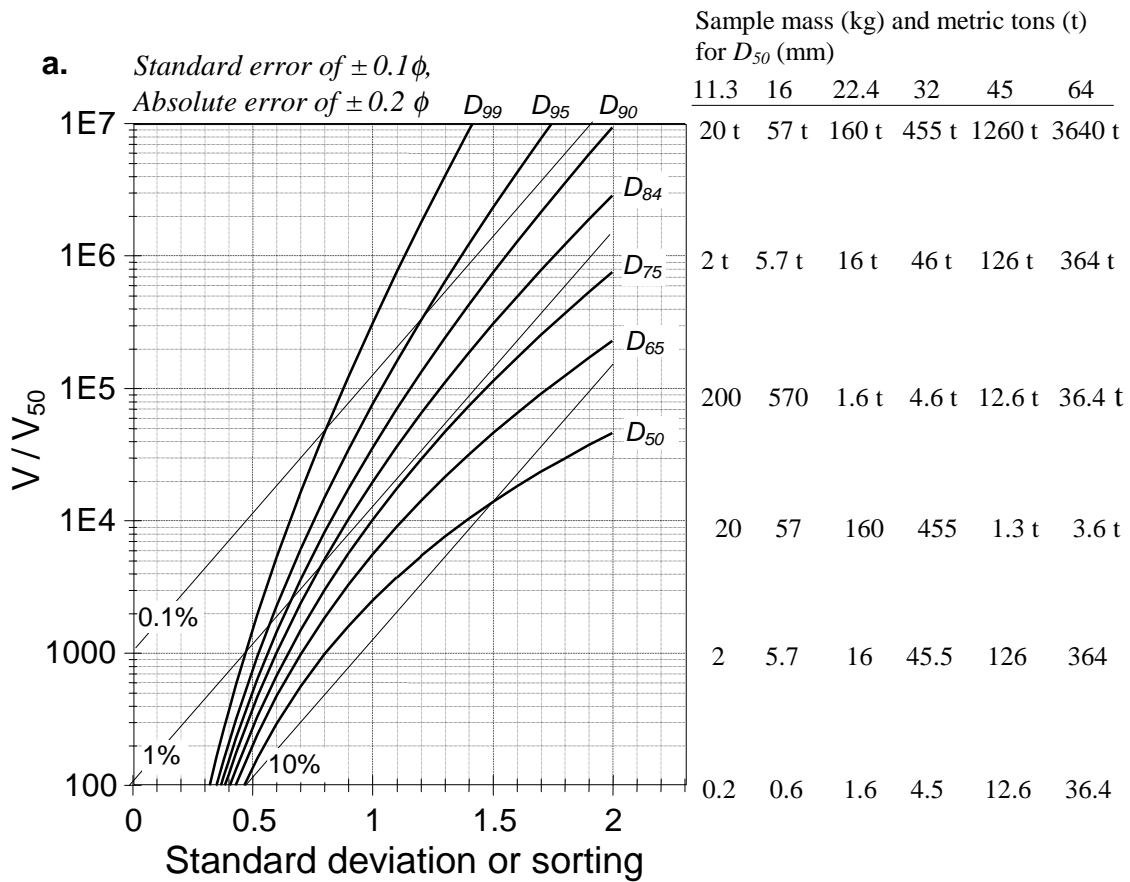
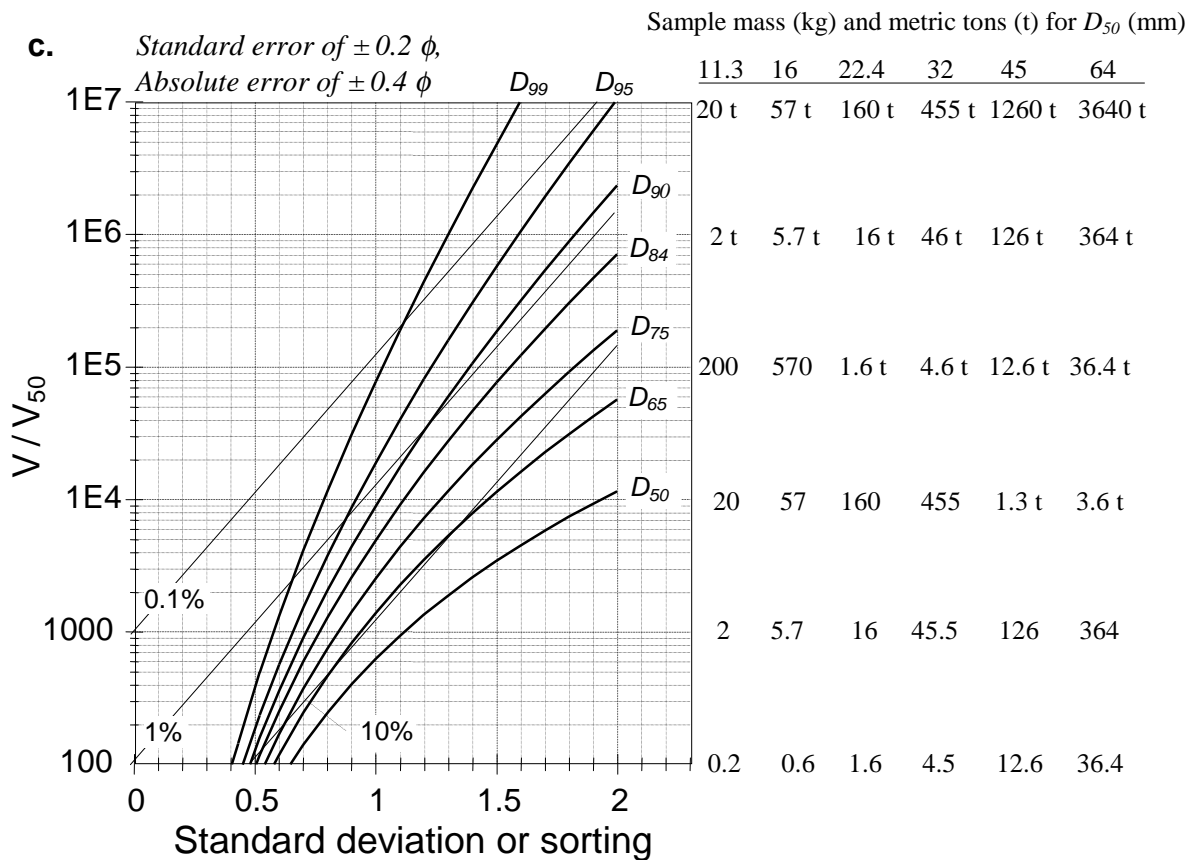
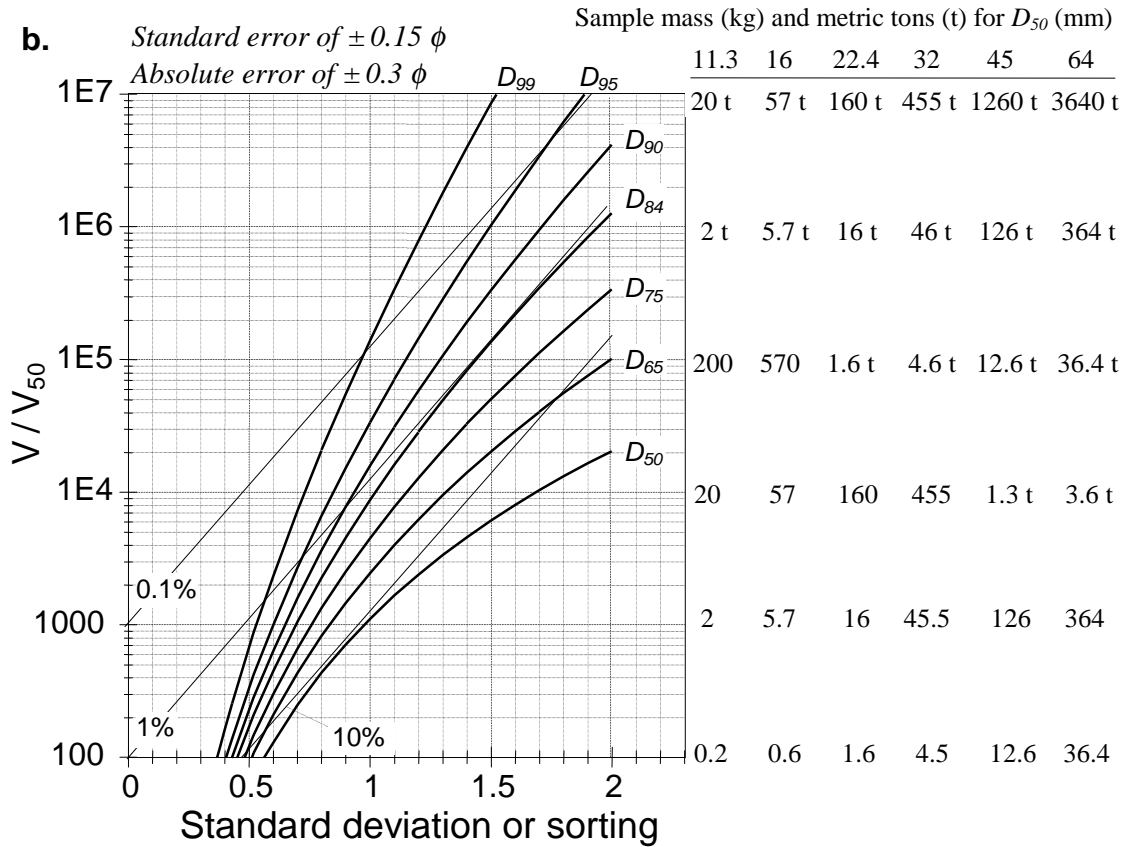


Fig. 5.22 a-c: Relative sample volume  $V/V_{50}$  as a function of sediment sorting for various percentiles between  $D_{50}$  and  $D_{99}$  for specified standard errors of  $\pm 0.1 \phi$ -units (b),  $\pm 0.15 \phi$ -units (c), and of  $\pm 0.2 \phi$ -units (d). Absolute sample mass is a multiple of the volume  $V_{50}$  of the median-sized particle. The 0.1, 1, and 10% sample-mass criteria by Church et al. (1987) are included for comparison. (Modified from Ferguson and Paola (1997), by permission of John Wiley and Sons, Ltd.). The numbers on the right side of the plots indicate sample mass values in kg and metric tons for  $10^2, 10^3, 10^4, 10^5, 10^6,$  and  $10^7 V/V_{50}$  or various sizes of  $D_{50}$ . (continued on next page)



The widely used sample-mass criteria by Church et al. (1987), i.e., the mass of a particle of the  $D_{max}$  size comprises 0.1, 1, and 10% of the sample mass (Fig. 5.14, Section 5.4.1.1) are plotted in Fig. 5.22 for comparison. The 1% criterion ( $D_{max} < 1\%$  of sample mass) is sufficient to determine the  $D_{84}$  and all smaller percentiles with an absolute error of  $\pm 0.3 \phi$ -units in bed material with a sorting coefficient between 1 and 2. In fact, the sample requirement could be an order of magnitude or two less than the 1% criterion for determining the  $D_{50}$  particle size to within an acceptable absolute error of  $\pm 0.3 \phi$ -units. However, the 0.1 % criterion needs to be applied for large percentiles  $> D_{84}$ , or if more stringent error criteria are used.

#### 5.4.4 Comparison of error curves for low, central, and higher percentiles

The general shape of the error curve, i.e., the relationship between precision and sample size  $e = f(1/\sqrt{n})$  is similar for all percentiles, irrespective of the manner in which the error was computed, and irrespective of any assumptions made about the parent distribution. However, sampling error is not automatically smallest for the smallest percentile (e.g., the  $D_5$ ), but is controlled by the way in which the sampling error was computed. The error can be lowest for either the  $D_5$ ,  $D_{50}$ , or the  $D_{95}$  within a specified gravel population depending on whether the error was computed:

- as absolute or percent error,
- in terms of mm or  $\phi$ -units, and
- from an assumed symmetrical, or asymmetrical underlying size distribution.

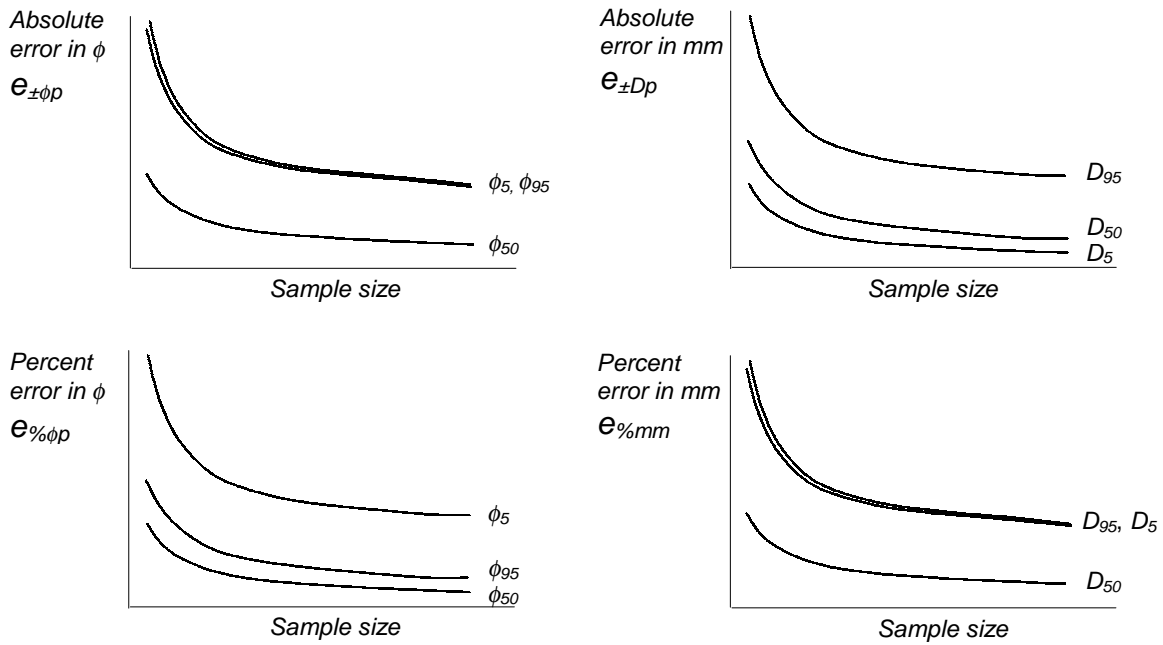
Consequently, comparisons of errors around different percentiles need to specify exactly how the error was computed and which assumptions were made about the underlying distributions.

##### 5.4.4.1 Symmetrical parent distributions

###### ***Absolute error in units of $\phi$ and mm***

In symmetrical, unskewed parent distributions, absolute errors in  $\phi$ -units for a given sample size are paired around the mean. Thus, error curves are identical for the  $\phi_5$  and  $\phi_{95}$  percentiles, and the  $\phi_{16}$  and  $\phi_{84}$  percentiles. The errors are highest for the distribution tails, i.e., the  $\phi_5$  and  $\phi_{95}$  percentiles, and lowest for the  $\phi_{50}$ . The error curves for a theoretical Gaussian distribution provided by Rice and Church (1996b) in Fig. 5.10 are an example for the systematical distribution of errors. If the same degree of precision is desired for each percentile, a smaller sample size suffices to determine the error around the mean or some central percentile than for the fine or the coarse tail. If the error analysis is performed in mm-units, the absolute mm-errors are highest around high percentiles (e.g.,  $D_{95}$ ), and lowest around small percentiles ( $D_5$ ). The error curves by Hogan et al. (1993) in Fig. 5.17 are an example. The relative positions of error curves are sketched for particle sizes in  $\phi$ - and mm-units, absolute and relative errors, for symmetrical, unskewed, as well as for asymmetrical, skewed distributions in Fig. 5.23.

### A: Symmetrical parent distribution



### B: Parent distribution skewed towards a fine tail

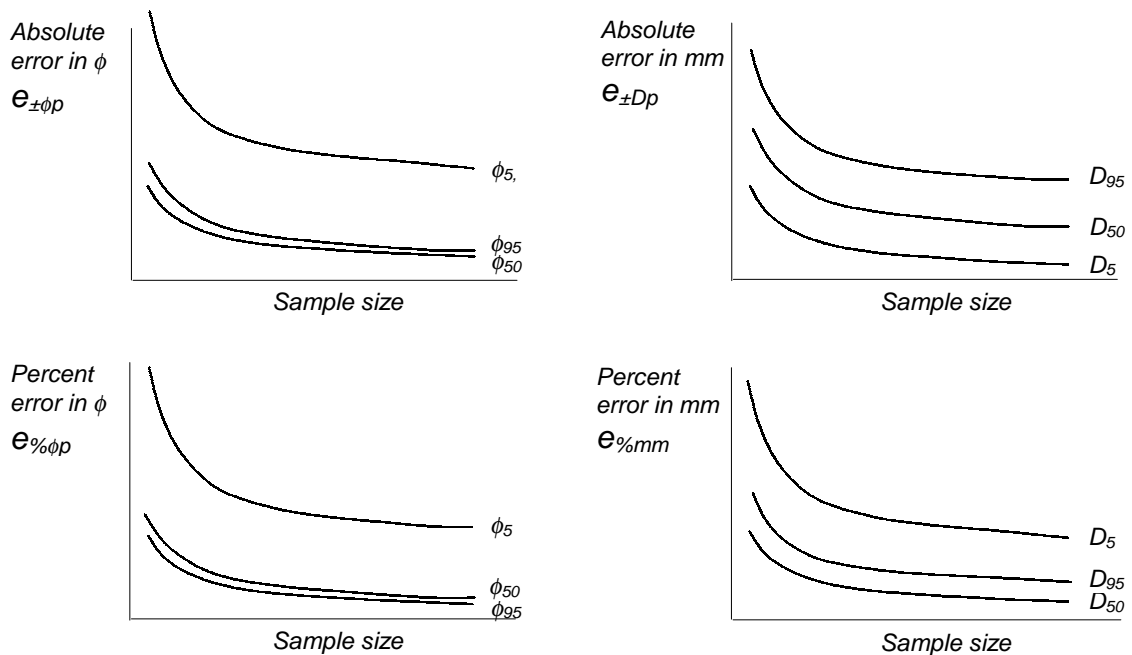


Fig. 5.23: Comparison of error curves around the  $D_5$ ,  $D_{50}$ , and  $D_{95}$  percentile for different computations of error (absolute, percent,  $\phi$ -units and mm). All computations are for the same gravel deposit. A normal and symmetrical parent distribution was assumed in (A), and an asymmetrical distribution positively skewed towards a tail of fines was assumed in (B).

#### ***Percent error in units of $\phi$ and mm***

The percent error around percentiles in  $\phi$ -units is lowest for the  $\phi_{50}$ , higher for the  $\phi_{95}$ , and significantly higher for the  $\phi_5$ . The relative error around percentiles in mm-units is paired, with the lowest error for the  $D_{50}$ , and equally high errors for the  $D_5$  and  $D_{95}$  (Fig. 5.23).

#### **5.4.4.2 Asymmetrical parent distributions skewed towards a fine tail**

##### ***Absolute error in units of $\phi$ and mm***

Particle-size distributions, even when analyzed in  $\phi$ -units, are rarely symmetrical in coarse gravel-bed streams, but are often positively skewed towards a tail of fine particles. The position of the error curves for the  $\phi_5$ ,  $\phi_{50}$ , and  $\phi_{95}$  is different for symmetrical and asymmetrical parent distributions.

For asymmetrical parent distributions that are skewed towards a fine tail, absolute errors around percentiles in  $\phi$ -units for a given sample size are highest around the  $\phi_5$ , lowest for the  $\phi_{50}$ , and only slightly higher around the  $\phi_{95}$  than around the  $\phi_{50}$ . The error curves provided by Rice and Church (1996b) for the bootstrap analysis in Fig. 5.11 are an example. If the same degree of precision is desired for each percentile, nearly the same sample size that suffices to determine the  $D_{50}$  of the distribution is sufficient for the  $D_{95}$  as well. However, a huge sample mass is required to estimate the  $D_5$  to within the same precision. An error analysis in mm-units results in absolute mm-errors being highest around the  $D_{95}$ , and lowest around the  $D_5$ . See the error curves by Hogan et al. (1993) in Figs. 5.17 a and b for an example. Fig. 5.23 b compares error curves for absolute and relative errors in  $\phi$  and mm for skewed distributions. The position of the  $\phi_5$  and  $\phi_{95}$  curves are switched if the distributions are negatively skewed towards a tail of coarse particles (e.g., beds comprising mostly sand and a few larger gravel particles).

##### ***Percent error for units in $\phi$ and mm***

The percent error around percentiles in  $\phi$ -units is approximately equally low for the  $D_{50}$  and the  $D_{95}$ , and highest for the  $D_5$ . The relative error around percentiles in mm-units is lowest for the  $D_{50}$ , higher for the  $D_{95}$ , and highest for the  $D_5$  (Fig. 5.23 b).

## 6. Spatial sampling schemes

---

Spatial sampling schemes refer to the spatial patterns by which individual particles (in pebble counts) or groups of particles (in areal or volumetric samples) are gathered from the streambed to provide a sample. Sampling schemes affect the outcome of a sample and different sampling schemes may produce different results when used in the same stream reach (Mosley and Tindale 1985). No sampling scheme is genuinely superior to others. The appropriateness is case-specific and depends on several factors including:

- *spatial scale* of the investigation, that is, whether sampling is to represent bed material from a long reach (ca. 20 stream widths), a single riffle-pool unit, an individual geomorphological or sedimentary unit, or a small-scale location;
- degree of spatial *homogeneity or heterogeneity* of particle-size patterns within the reach of concern,
- desired sampling *precision* or tolerable *error*;
- restrictions imposed by keeping the sampled volume *manageable*;
- necessity to keep streambed *destruction at a minimum*; and
- the *specifics* of a given study.

Information presented in this section is designed to assist the reader to understand sampling schemes and select an appropriate sampling scheme for a specific situation.

Three main spatial sampling schemes are discussed in this document:

1. ***Spatially integrated***  
= ***unstratified sampling***      Covers the entire reach with the same sampling pattern, and ignores sedimentary<sup>1</sup> or geomorphological units<sup>2</sup>. A reach-averaged bed-material size is obtained (Sections 6.2 and 6.4);
2. ***Spatially segregated***  
= ***stratified sampling***      Distinguishes between geomorphological or sedimentary units and may use a separate sampling pattern for each unit (Sections 6.3 and 6.5);
3. ***Spatially focused sampling***      Focuses on a small area of interest, such as near a hydraulic structure, or fines deposited in a pool (Section 6.6).

---

<sup>1</sup> **Sedimentary units** are streambed areas with uniform particle-size distributions. A sedimentary unit may comprise part of one or several geomorphological units. Sedimentary units are also referred to as textural units, facies, or as patches, when areas of similar particle-size distributions appear to be "patchy". A coarse facies, for example, may cover the upstream part of a bar and extend into the adjacent riffle upstream.

<sup>2</sup> **Geomorphological units** are areas within the streambed that are part of the same geomorphological feature, such as a riffle, pool, bar, rapid, run, or glide (see Section 3.2.1 for descriptions of stream morphology). Particle-size distributions can vary greatly within a geomorphological unit. Bars, for example, display downbar and landward fining.

Statistical analyses of bed-material samples assume that samples are collected at random locations. Randomization of sampling locations is obtained by several sampling patterns:

- Complete random – samples are collected at random locations within the sampling area;
- Systematic grid – samples are collected at the intersections of a systematic grid with a random starting point;
- Overlapping grid systems – subsamples are collected each at a separate grid system, overlaying the other ones,
- Random within systematic cells – samples are collected at random locations within grid cells that have a random starting point.

Combining these four sampling patterns with integrated (unstratified) or segregated (stratified) sampling yields eight different sampling schemes that are commonly applied to gravel-bed streams. An overview of these eight sampling schemes is presented in Fig. 6.1. The terms “strata” and “stratified” in this document refer to sedimentary or geomorpho-gical units. This terminology departs from some texts on sampling schemes where *strata* and *stratified* refer to a segregation of the sampling area into artificial equally-sized strata, which are referred to as cells in this document.

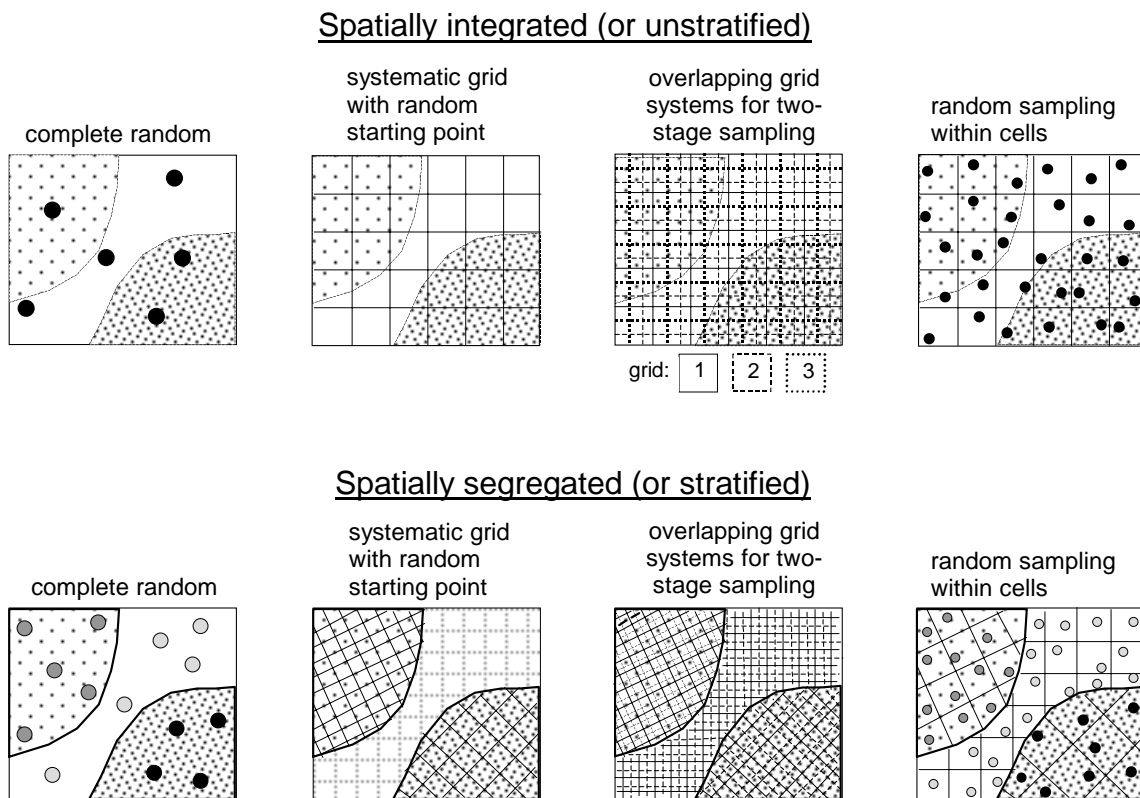


Fig. 6.1: Sampling schemes commonly used for bed-material sampling in gravel-bed streams.  
  Bed unit 1,   Bed unit 2,   and Bed unit 3.

These sampling schemes can be applied to all sampling procedures, such as surface pebble counts, volumetric sampling, and areal sampling. The various sampling procedures have been presented in Sections 4.1 and 4.2.

## **6.1 Terminology and sampling principles**

Before various aspects of spatial sampling schemes are discussed, some terms regarding stream types, stream morphology, reach length, as well as spatial homogeneity and heterogeneity, should be clarified. Furthermore, this introductory section addresses pilot studies and briefly recalls important aspects of pebble counts and volumetric samples.

### **6.1.1 Stream types and stream morphology**

Stream types and stream morphology refer to the stream type classification by Rosgen (1994, 1996), and the stream morphologies as classified by Montgomery and Buffington (1993, 1997). Both classification schemes are discussed in Sections 1.3.1 - 1.3.3.

### **6.1.2 Length of the sampling reach**

The length of the sampling reach is determined by the spatial extent of the sampling goal. For local studies, a sampling reach often comprises the length of one sequence of recurring elements of stream morphology. In C-type streams (Rosgen 1994, 1996) with riffle-pool morphology (Montgomery and Buffington 1993, 1997), this sequence may include a riffle and a pool and extend over approximately 5-7 times the bankfull stream width. In meandering streams, a riffle-pool sequence covers one meander bend. In B-type streams with rather featureless plane-bed morphology, the sampling reach may be one in which there are no visible changes in the streambed composition. In A-type streams with step-pool morphology, a reach could be one, or a few, similar-looking step-pool units.

For a more general characterization of the streambed material, Rosgen (1996) proposes sampling a stream section consisting of at least four consecutive riffle-pool sequences, equaling four meander bends (= two meander wavelengths), or a reach length of 20-30 bankfull stream widths. Bevenger and King (1995) extend the length of the reach sampled by a zigzag pebble count over several hundred meters, covering a reach length on the order of 100 stream widths (Section 6.2.2). Long sampling reaches of 20 stream widths or more in length are especially important for spatially segregated sampling when particle sizes of groups of sedimentary units are combined for a reach-average value (Lisle and Hilton, personal comm.). Similarly, for a comparison of particle sizes of geomorphological units, such as riffles and pools, sampling should extend over several riffle-pool units to average any local effects. In this document, the term *reach* usually refers to the stream length of one riffle-pool sequence or about 5 - 7 stream widths, unless otherwise specified.

### 6.1.3 Homogeneous versus heterogeneous gravel deposits

Gravel surfaces are *homogeneous* when they consist of a mixture of particle sizes, but have no spatial variability in the composition of the particle mixture. Particle-size distributions are then similar in all stream locations. Entire reaches of truly homogeneous gravel beds are rare.

*Near-homogeneity* of gravel-beds may be found in large lowland gravel-bed rivers, or in mountain B-type streams with cobble and gravel beds. B-type streams have a plane-bed morphology with long, rather featureless stream sections characterized as runs. Infrequent pools, typically forced by channel obstructions (LWD, boulders, or bank projections) may occur in these channels and are interrupted by infrequent rapids (Section 6.2.2). The classification of a reach as *near-homogeneous* as opposed to heterogeneous is subjective, since there are no standards defining the degree of spatial homogeneity or heterogeneity in fluvial deposits.

Many mountain gravel-bed rivers have *heterogeneous* bed material in which the composition of the gravel bed varies between different locations of the reach. In C-type streams gravel- and cobble beds are composed of sequences of geomorphological units encompassing bars, riffles, pools, rapids, runs, and glides. Those geomorphological units often have a characteristic spatial variability of particle sizes, such as downbar and landward fining on bars (Section 3.2.2). In the longitudinal direction, bed-material size is commonly finer in pools (particularly when fine sediment deposits in pools) and coarser on riffles. Graphic examples of spatial variability of bed-material size in C-type streams are provided by the detailed field measurements of Lisle and Madej (1992) (Fig. 3.10). A-type streams with a step-pool morphology have steps composed of cobbles and boulders that are only mobile during very large floods. Smaller cobbles or gravel that are annually mobile can be deposited in pools, or occasionally on midstream deposits, while fine gravel and sand are primarily found near the banks. Streams containing large woody debris often have heterogeneous beds because the debris causes spatially varied flow hydraulics with local scour in one location and deposition in the next. An example of a heterogeneous bed in the presence of large woody debris is presented in Fig. 3.12.

### 6.1.4 Pilot studies

A pilot study prior to the main sampling project is useful for several reasons (Sections 2.1.5.4, 4.2.3 and 4.2.4). It allows the investigator to become familiar with the sampling reach, to determine the length of the sampling reach, and to assess the degree of spatial variability of bed-material size. The categorization of the reach into homogeneous or heterogeneous is required for selecting an appropriate sampling scheme. Pilot studies may involve collecting actual samples. Information on a particular particle-size percentile and the sediment sorting coefficient derived from a pilot sample, or the variability between pilot samples, can be used to estimate the sample size needed for a desired precision of the study. The pilot study should include a sketch map of the reach and its delineated geomorphological or sedimentary units. This sketch map, based on quick visual

assessments, should also include bed surface parameters such as the mean and maximum particle size, the percent fines, bed surface structures, the presence of large woody debris, or any other parameters of concern.

### **6.1.5 Spatial aspects of pebble counts**

Sampling procedures for pebble counts and number-based sample size recommendations, are discussed extensively in Sections 4.1.1 and 5.2. However, reiteration of the spatial aspects of the various sampling procedures, sample-size recommendations, as well as particle measurements and data recording seems useful.

#### **6.1.5.1 Minimum sampling point spacing**

Sampling points of pebble counts should be spaced at least the length of the  $D_{max}$  particle size, or twice the  $D_{max}$  particle size, in order to avoid serial correlation due to double-counting large particles. Serial correlation and overrepresentation of large particles also occurs when the sampling path coincides with the longitudinal direction of clusters or transverse ribs (Section 4.1.1.2). A large spacing between sampling points can prevent this overrepresentation.

#### **6.1.5.2 Number of sampling points**

The number of particles that should be sampled is largely determined by statistical considerations. Spatial factors considered in sample-size determinations are minimum sampling point spacing and the size of the stream reach to be covered by one pebble count. A detailed analysis of sample size needed to define the  $D_{50}$  and other percentiles within a specified precision for a given standard deviation or sediment sorting is presented in Section 5.2.2 - 5.2.4. Major findings are summarized below.

Although traditionally 100 particles were counted in a pebble count, recent analysis of sample size indicates that it is advisable to count at least 400 particles (Rice and Church 1996b, Diplas and Lohani 1997). The gravel deposit for which Rice and Church (1996b) provided a detailed analysis of the relationship between sample size and precision can be considered representative for many gravel beds. Sediment sizes ranged from sand to large cobbles, and size frequencies were not exactly, but approximately normally distributed (in terms of  $\phi$ -units), with a slight skewness towards a tail of fine particles, and a standard deviation of  $1.2 \phi^3$ . A 400-particle sample estimated the  $D_{50}$  to within  $\pm 0.15 \phi^4$ , which is approximately equivalent to an error of  $\pm 10\%$  in terms of mm-units. Such a precision is often desirable in particle-size assessments, although an acceptable level of precision needs to be selected for each study individually.

---

<sup>3</sup> This value is on the low side for mountain gravel-bed streams that tend to have standard deviations (or sorting coefficients (Inman 1952)) of 1.5 or higher if the particle-size distribution comprises large boulders. A sorting coefficient of 1.2 - 1.5 may be obtained if large boulders not transportable by frequently occurring floods are excluded from the analysis.

<sup>4</sup> See Section 2.1.2.2 for conversion between mm and  $\phi$ -units.

The sample size needed to estimate the tails of the distribution (e.g., the  $D_5$  or the  $D_{95}$ ) to within  $\pm 0.15 \phi$  is larger than the sample size needed to estimate the  $D_{50}$  to the same precision. If the underlying distribution of the bed material is symmetrical and normal, and has a sorting coefficient of  $1.2 \phi$ , the sample size for estimating the  $D_5$  and  $D_{95}$  is a factor of approximately 2.6 larger than the sample size needed for the  $D_{50}$  (Fig. 5.10). Thus, if 400 particles are required to estimate the  $D_{50}$  to within  $\pm 0.15 \phi$ , more than 1,000 particles are needed to estimate the  $D_5$  or  $D_{95}$  with the same precision.

Many gravel deposits are not symmetrical and normal, but have particle-size distributions (in  $\phi$ -units) that are skewed towards a fine tail. This deviation from a standard normal distribution does not significantly alter the required sample size for the  $D_{50}$  particle-size estimate. However, the sample size needed to estimate the  $D_5$  particle size is more than 4 times larger than the one for the  $D_{50}$  particle size. Thus, if 400 particles were needed to estimate the  $D_{50}$  to within  $\pm 0.15 \phi$ , 1,600 particles would be needed to estimate the  $D_5$  to the same precision in distributions skewed towards a fine tail. No pronounced increase in sample size is necessary to estimate the  $D_{95}$  to within the same precision as the  $D_{50}$  particle size (Fig. 5.11).

Sample sizes larger than indicated in the paragraph above are needed if precision criteria become more stringent, and if particle-size distributions become less well sorted. Note that these sample-size considerations do not account for spatial heterogeneity, but are only valid for homogeneous sampling reaches, such as sedimentary units. For heterogeneous reaches, sample sizes are likely to be larger. A two-stage approach should be used to determine the relation between sample size and precision (Sections 5.2.3.1, 6.3.1.2 and 6.4.4.4). Heterogeneous reaches can be sampled most efficiently if the reach is delineated into sedimentary (homogeneous) units that are sampled separately (Section 6.3.2).

### 6.1.5.3 Minimum sampling area

For a sample size of 400 particles, a pebble count (Section 6.2 and 6.3) requires a minimum sampling area of 400 times the square of the relevant  $D_{max}$  particle size. The necessary sampling area increases rapidly with the  $D_{max}$  particle size. For  $D_{max}$  particle sizes of 64 and 360 mm, the minimum sampling areas are 1.6 and 52 m<sup>2</sup>, respectively (see also Table 6.4). For a more generous particle spacing of  $2 D_{max}$ , minimum sampling area increases fourfold to 6.6 and 207 m<sup>2</sup>, respectively.

### 6.1.5.4 Measurement of particle sizes in pebble counts

The sizes of particles picked up from the streambed during a pebble count are usually measured in half  $\phi$ -units using a template and recorded in 0.5  $\phi$ -unit particle-size classes (e.g., 22.6 - <32 mm). Binning into  $\phi$  classes is useful when comparing pebble count data with sieve data, and using a template reduces errors in particle size measurements. However, binning into  $\phi$  classes assumes an underlying normal distribution of particle sizes, an assumption which may be useful in many, but not in all cases.

If particle sizes in a sampling area are obviously not normally or Gaussian distributed (in  $\phi$ -units), particle axes should be measured with a caliper and recorded in mm, which allows more possibilities for later particle-size analysis. However, caliper or ruler measurements are subject to operator error and not directly comparable to sieve data (see Section 2.1.3.2 for comparison between ruler and template measurements).

#### 6.1.5.5 Recording pebble count data

Particle sizes from pebble counts should always be recorded in a systematic manner, so that the approximate location of each counted particle can be traced. To achieve this, all transects should start on the same side of the stream, beginning at the downstream end of the reach and working upstream. All particle-size data from one transect should be recorded sequentially in one column (or row). Additional information to be recorded are distance from downstream end of the sampling reach, major geomorphological features of the transects (e.g., riffle, run, pool-bar), and the water line position (Table 4.3, Section 4.1.1.7). The same applies to zigzag pebble counts (Section 6.2.2) which can be considered as diagonal transects.

A spatially systematic particle-size record has several advantages. It permits the user to analyze whether particle sizes vary in a longitudinal direction by comparing individual transects, or sets of adjacent transects. Lateral particle-size variability can be estimated from moving averages over 5 to 9 consecutively counted particle sizes. Spatial patterns in particle size determined from the record may not have been obvious prior to sampling. A spatially systematic particle size record can also be used to delineate sedimentary or even geomorphological units retroactively. The delineation can be made visually (looking at the numbers) or by applying a *moving window* technique for a statistical delineation (Crowder and Diplas 1997) (Section 6.3.2.3). Particle-size data can then be consolidated for each sedimentary unit (Section 6.3.2.1). Thus, a crude spatially segregated bed-material size analysis can be obtained after the fact from a spatially integrated sampling scheme.

#### **6.1.6 Spatial aspects of volumetric sampling**

Spatial aspects of sampling schemes for volumetric samples are literally multi-layered and more complex than those for pebble counts.

##### 6.1.6.1 Layers to be sampled

Gravel beds are often vertically stratified. Stratification of gravel beds is described in Section 3.3, and sedimentary layers are described in Fig. 4.1, Section 4, and Section 4.2. Volumetric samples can be obtained from different layers that have different particle sizes. The exact delineation of the sampled layer is crucial to the sampling success. Layers or strata that can be sampled by volumetric samples are:

- the coarse *armor* layer (1-2 times the *b*- or *c*-axis of the  $D_{max}$  particle thick),
- the finer *subarmor* layer,
- the *subsurface* layer below the particles immediately exposed on the bed surface, and
- the *unstratified* bed material.

The surface sediment, i.e., particles exposed to the surface, cannot be sampled volumetrically because conceptually, there is no thickness associated with the sediment surface.

Volumetric sampling of the armor layer in coarse gravel and cobble beds has several problems: (1) A stringent criterion defining the depth of the armor layer is not available, and each study needs to define its own criteria. (2) Taking a volumetric armor-layer sample down to a specified depth is feasible in bed material of fine gravel where the armor-layer sediment can be scraped off the subarmor sediment, but becomes difficult in coarse gravel and cobble beds. (3) For practical reasons, an armor-layer sample is limited in areal extent to approximately 0.1 - 1 m<sup>2</sup>. The sediment mass contained in such armor-layer samples is often too small to be accurate (Section 5.4) and requires taking several subsamples. (4) Volumetric armor-layer samples and surface pebble-counts yield different particle-size distributions in armored gravel-bed rivers because volumetric armor-layer samples contain fine subsurface sediment that is not part of the surface sediment and not sampled by pebble counts.

The subsurface (surface layer removed) and the subarmor layer (armor layer removed) are conceptually similar in particle size, and both are usually finer than the armor layer sediment. This document uses the term *subsurface* sediment for the sediment from both below the surface and below the armor layer unless a specification is necessary.

#### 6.1.6.2 Relation between surface and subsurface sediment size

The spatial variability of the surface sediment is visible, and a sampling scheme can be selected that is appropriate for the specified degree of spatial variability and the study objectives. Subsurface or subarmor sediment is hidden from view and only inferences about its spatial variability are possible based on principles of the relation between surface and subsurface sediment. Buffington and Montgomery (1999a and b), and Lisle (pers. comm.) found a linear relation between percentiles of the surface and subsurface sediment-size distribution for a sediment patch (facies)<sup>5</sup>. Although the subsurface sediment is often finer than the surface sediment, the exact relation varies between facies. Thus, the spatial variability of the surface sediment may be used as a first approximation of the spatial variability of the subsurface sediment, and an appropriate sampling scheme may be selected accordingly (also see Section 6.5.2).

However, the surface sediment size is not always an indication of the subsurface sediment size. For example, a veneer of fine sediment or a lobe of coarse sediment may be

---

<sup>5</sup> *Facies or patches are homogeneous streambed areas with no systematic spatial variation of bed-material size.*

deposited on the surface after the subsurface sediment was formed during the last flood event. In this case, the spatial variability of facies units on the surface is likewise not indicative of the subsurface facies and a sampling scheme selected on the basis of the surface facies may be inappropriate for sampling the subsurface sediment.

#### 6.1.6.3 Feasibility and the statistical relationship between mass of subsamples, total sample mass, and number of sampling locations

An individual volumetric sample describes the bed material at a specified sampling location. Several volumetric samples need to be obtained at various locations to characterize the bed-material size within a reach. Sampling schemes for volumetric samples need to consider three factors:

1. number and mass of individual samples,
2. total sample mass, and
3. spatial allocation of sampling locations within the sampling area of concern.

In moderately sorted fine gravel beds, the three factors can be considered statistically interdependent. A preset sampling precision determines the total sample mass from a sample mass - error relation (Fig. 5.22 a - c), or from a two-step approach (Section 5.4.2.1). Sample mass for individual volumetric samples can be estimated from sample mass equations for bias avoidance (Section 5.4.3.1), or empirically from the percentage mass of the  $D_{max}$  particle size (Sections 5.4.1 and 5.4.1.2). Total sample mass divided by the mass necessary for bias avoidance in individual samples yields the number of sampling locations that need to be allocated in a strict or randomized grid pattern over the reach or sampling area of concern.

A strict statistical approach is not feasible in coarse gravel-bed mountain streams because allotting several hundreds of samples over a reach leads to sample masses of several hundreds or thousands of kg. The coarseness of the bed material and the sampling objectives determine the sampling equipment and the mass of individual samples, although several subsamples can be combined to form an individual sample. Pipe samplers (Section 4.2.4.5) appropriate for fine gravel-bed rivers collect a few kg of sediment. Barrel samplers (Section 4.2.4.6) and plywood sheets (Section 4.2.4.7) are more appropriate for coarse gravel- and cobble-bed rivers and collect about 50 kg per sample.

When using a spatially integrated sampling scheme to sample the reach (Sections 6.4.1. and 6.4.2), the number of samples needed depends on the size of the reach and how spatially variable particle-size distributions are within the reach. When sampling is spatially segregated (Section 6.5), the size of a sedimentary or geomorphological unit determines the number of samples that can reasonably be collected from the sampling area. Collecting 100 barrel samples of 50 kg each may satisfy a preset sampling precision, but doing so on a riffle 10 m by 10 m in size destroys the site. Two to four barrel samples may be justifiable from an ecological standpoint. If a pipe sampler is used in a fine gravel bed, ten or more samples may be appropriate for a 100 m<sup>2</sup> riffle.

The selection of a sampling scheme and the total sample mass for volumetric sampling are often governed by practicality, particularly in coarse mountain gravel-bed streams. Both sampling scheme and sample mass may be a compromise between desired sample precision, the specifics of a given study goal, the particulars of a sampling site, funding, and logistics. The *reasonable* number of sampling locations in a small reach or on a sedimentary unit in mountain gravel-bed rivers may not suffice to cover the spatial variability, and the precision obtained from a small total sample mass may not allow more than a rough estimate of the  $D_{50}$  particle size. However, thoughtful planning of the statistical analysis and the field work may assist obtaining the maximum information possible out of a restricted sampling condition (Section 5.4.1.4, 6.4.3 and 6.4.4).

## **6.2 Spatially integrated or unstratified pebble counts (reach-averaged sampling)**

Spatially integrated pebble counts cover the reach evenly with a preset sampling pattern. The resulting particle-size information is reach-averaged, unless a spatially distinct record permits spatial segregation of the data at a later time (Sections 6.1.5.5 and 6.3.2.3). Reach-averaged information on bed-material particle size may be used for a variety of purposes which include the computation of reach-averaged bedload transport rates, a comparison of bed-material sizes between reaches, or to detect a change over time when sediment supply to the reach has been altered (Lisle et al. 1993). A comparison of the reach-averaged surface  $D_{50}$  size with the  $D_{50}$  particle size of bedload (Lisle 1995), of the subsurface  $D_{50}$  (Dietrich et al. 1989), or the  $D_{50}$  size that the stream is competent to transport (Buffington and Montgomery 1999c) may be used to evaluate whether transport is supply or transport limited.

### ***Sampling patterns for different degrees of reach homogeneity or heterogeneity***

The tightness of sampling patterns used in spatially integrated sampling schemes should reflect the degree of spatial variability of bed-material size, i.e., the degree of reach homogeneity or heterogeneity. For streambeds with moderate spatial variability in bed-material size, i.e., relatively homogeneous beds, widely-spaced sampling patterns are appropriate. As the degree of spatial variability of particle sizes over the reach increases or becomes more complex, the sampling patterns covering the reach must become more tightly spaced in order to sample all sedimentary units of the reach in a representative manner (Table 6.1).

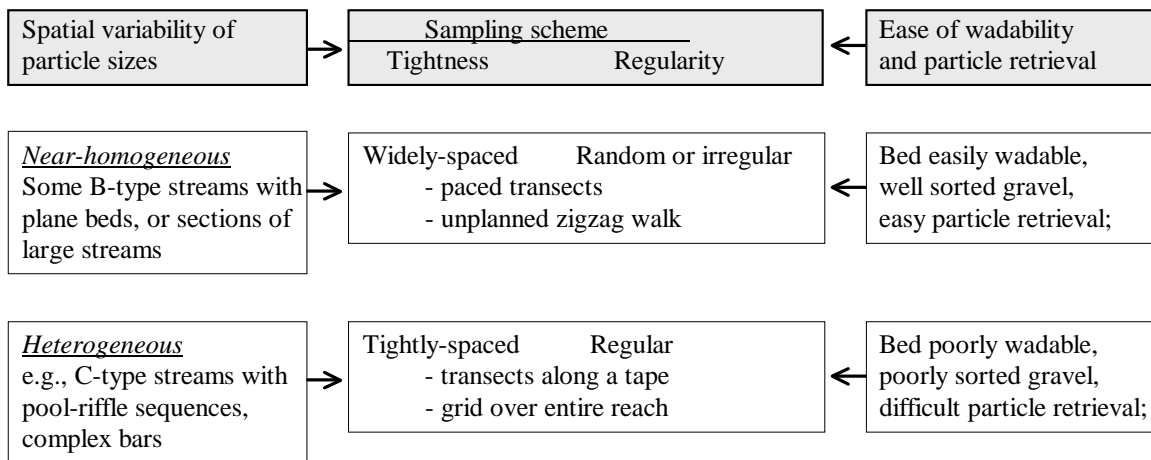
### ***Sampling patterns for different ease of wadability and particle retrieval***

The regularity of the sampling patterns should be selected considering how well all streambed locations are accessible to the wading person and the ease of particle identification and retrieval. Easily wadable and well-sorted gravel beds may be sampled by paced transects or unplanned zigzag courses. Both sampling schemes allow the operator some latitude in deciding the sampling path. Regular and pre-determined sampling

schemes, such as parallel transects along measuring tapes or sampling at grid points are required in beds in which wading and particle retrieval are difficult. Operators may be tempted to avoid sampling in deep spots or behind obstacles and to avoid retrieving interstitial fines and wedged particles (Sections 4.1.1.1 - 4.1.1.4).

The ideal sampling scheme for a reach should reflect both the degree of homogeneity/heterogeneity and the ease of sampling, i.e., the ease of wadability, particle selection and particle retrieval. If homogeneity of the reach is paired with well sorted gravel beds and easy wadability, sampling may use a pattern that is widely-spaced and completely random or unsystematic. Examples are widely-spaced paced transects and unplanned zigzag walks (Table 6.1). If heterogeneity of the reach is paired with poor sediment sorting and difficult particle retrieval, a tightly-spaced grid pattern should be used.

Table 6.1: Suggested spatially integrative sampling schemes for surface samples in reaches with different degrees of spatial variability of particle sizes, ease of wadability and particle retrieval



### 6.2.1 Near-homogeneous reaches: paced transects, transects along measuring tapes, and an unplanned zigzag course

Easily wadable and well-sorted gravel beds in near-homogeneous reaches are most likely to occur on sections of large dry gravel bars. Beds in such reaches can be sampled by picking up particles from paced transects (Wolman 1954) or by following an unplanned upstream zigzag course across the reach. However, these two sampling schemes are not suitable if deep water, obstacles, mud, rapids, fast flow or protruding rocks affect the sampling path of the pacing person, and if interstitial fines and wedging make particles difficult to retrieve from the bed. Difficult wading and particle retrieval may tempt the operator to consciously or unconsciously avoid sampling at those locations, thus creating a bias against particles in poorly accessible locations (Sections 4.1.1.3 and 4.1.1.4). Parallel transects (Leopold 1970) placed along measuring tapes, or sampling in a premeditated zigzag course allows sampling the reach in a more systematic pattern and reduces the possibility for operator subjectivity. The most even coverage of an

approximately homogeneous reach is attained by performing pebble counts in a systematic grid pattern established by transects along a measuring tape.

The reach-averaged particle-size distribution in a homogeneous reach is estimated from a combined sample of all particles sampled within the reach. No information is obtained on the spatial variability of the particle sizes.

### **6.2.2 Long and relatively homogeneous stream sections: planned zigzag course**

B-type streams with plane-bed morphology are representative of streams with relatively homogeneous beds. Long runs with a few pools forced by large rocks or large woody debris are separated from each other by occasional rapids. Paced transects and *unplanned* zigzag walks may be appropriate here. However, these sampling patterns are not appropriate where pools, rapids or large woody debris causes spatial variability in particle size and where poorly sorted gravel beds make wading and particle retrieval difficult. The unpremeditated sampling paths of both sampling patterns are guided by convenience and caution and cause irreproducible sampling results (Kondolf 1997 b). In order to avoid operator bias in selecting sampling locations and particle retrieval, the sampling pattern should become more systematic and provide less opportunity for operator subjectivity. Zigzag pebble counts with a *premeditated, systematic* course, and parallel transects along a measuring tape are often suitable in B-type streams with plane-bed morphology.

#### ***Systematic zigzag sampling path***

A planned, symmetric, bank-to-bank zigzag course may be viewed as a sequence of diagonal transects that integrate over both lateral and longitudinal bed-material variability. When a long stretch of river is sampled by a zigzag course, it is important that the sampling path is premeditated and based on stream dimensions and intended sample size (Fig. 6.2). Bank contact points must be spaced *evenly* and *independent* of any stream features to ensure statistical reliability of the sample. Unpremeditated sampling paths are subjective and do not provide statistical reliability in non-homogeneous stream reaches. “Eye-balled” zigzag sampling paths should be reserved for quick reconnaissance sampling. Bevenger and King (1995) proposed that the ratio of thalweg length to the length of the zigzag course walked by the operator should be about 0.9. This value is obtained when bank contact points for zigzag sampling are spaced at intervals of two stream widths. However, a tighter or wider zigzag course may be needed to obtain the necessary number of sample points (i.e., sample size) and to obtain the necessary sample point spacing within the reach of interest.

Recall that sample size should be at least 400 particles to determine the  $D_{50}$  to within approximately  $\pm 0.15 \phi$  or 10 - 11% in poorly sorted ( $s \approx 1.5 \phi$ ) bed material. The sample size should be larger when percentiles at the distribution tails, particularly at the fine tail, are to be determined (see Section 5.2 for discussion of sample size).

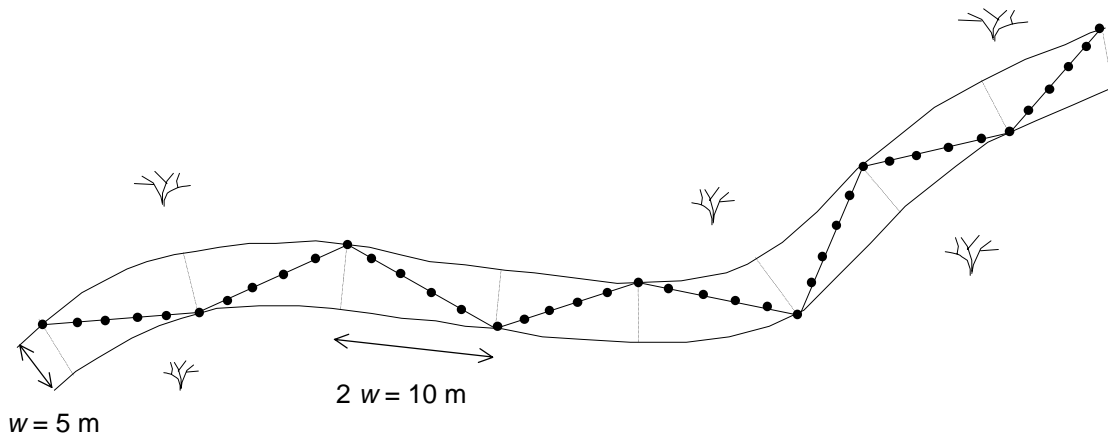


Fig. 6.2: Systematic zigzag sampling scheme with bank contact points evenly spaced at two stream widths. The ratio of thalweg length to length of the zigzag course is 0.9.

Minimum spacing for avoiding serial correlation in pebble counts is  $1 - 2 D_{max}$  diameters, i.e., 0.3 – 0.5 m in many mountain gravel-bed streams. In a stream 5 m wide, a zigzag course that collects 400 particles at 0.3 m intervals and touches the banks at intervals of two stream widths covers a total stream length of 107 m, or 21 stream widths (Table 6.2). This is equivalent to the length of a sampling reach recommended by Rosgen (1996). If the sampling objective is to detect a change in particle-size distribution over time within a stream section, the reach should extend over roughly 100 stream widths in order to average-out local effects caused by sediment deposits at the mouths of small tributaries, rockfall, or in backwater areas. Thus, the spacing between sampling points increases accordingly. Using the same scenario with bank contact points every 10 m in a 5 m wide stream and a 400-particle sample size, a zigzag pebble count with a 2.2 m spacing covers 800 m of stream length, or 160 stream widths (Table 6.2).

Table 6.2: Longitudinal extent of a 400-particle zigzag count with bank contact points every 2 stream widths in streams 5 m and 10 m wide.

	Stream width ( $w$ ):			
	5 m		10 m	
	Sample point spacing:			
	2.2 m	0.3 m	2.1 m	0.3 m
Particles per diagonal, $n_d$	5	37	11	73
Number of sections, $n_s = 400/n_d$	80	11	36	5.5
Thalweg length covered, $L_T = n_s \cdot 2w$	800 m	107 m	727 m	109 m
Number of stream widths covered, $n_w = L_T/w$	160 $w$	21 $w$	73 $w$	11 $w$
Zigzag course length, $L_Z = n_s \cdot \sqrt{w^2 + (2w)^2}$	894 m	120 m	805 m	122 m
$L_T/L_Z$	0.9	0.9	0.9	0.9

The spacing  $L_p$  between particles for zigzag pebble counts can be computed from

$$L_p = \frac{\sqrt{w^2 + 2 w^2} \cdot L_t}{n_s \cdot 2 w} \quad (6.1)$$

where  $w$  is the stream width,  $L_t$  is the thalweg stream length, and  $n_s$  is the number of particles to be sampled.

### 6.2.3 Heterogeneous reaches and complex streambeds

Sampling the surface of a heterogeneous reach with a spatially integrated sampling scheme has advantages and disadvantages that should be weighed before starting the sampling project. One aspect is time. Spatially integrated sampling is often faster than spatially segregated sampling because delineation or surveying of the various geomorphological or sedimentary units is not necessary (Sections 6.3.2.1-6.3.2.3). Another aspect is the degree of spatial heterogeneity within the reach. Information obtained from spatially integrated reach-averaged sampling may be suitable in a mountain B3-type stream with little sediment supply and a gradual transition of areas with finer and coarser sediment. However, a low gradient C-type stream with ample sediment supply is likely to have areas of distinctly different surface sediment and, in this case, reach-averaged information on surface sediment is not very informative. An increase in the amount of sand delivered to the stream, for example, could produce sand patches, but their presence might not significantly affect the reach-averaged  $D_{10}$  or  $D_{50}$  particle sizes. The presence of sand patches could be better accounted for using spatially segregated sampling (Section 6.3.1). Another aspect to consider when selecting a sampling scheme is the sample size required for a preset precision. In reaches with pronounced spatial variability of particle sizes, sample standard deviation varies between sampling locations and one-step sample-size equations (Section 5.2.1) are not applicable to the reach as a whole. Sample size either needs to be computed for individual sediment units, or a two-stage sampling approach is necessary in which samples are taken from several grid systems overlaying the reach, each slightly shifted against the other (Section 5.2.3.1) (Fig. 6.3). This may result in a large sampling effort.

#### 6.2.3.1 Grid sampling and lay-out of the grid

If spatially integrated sampling is the selected sampling scheme for a heterogeneous reach, a *tightly*-spaced systematic grid pattern that evenly covers the entire sampling reach is required for reach-averaged particle-size information (Diplas and Lohani 1997). Entire coverage implies that particles from *all* possible sampling locations are included in the sample (Fig. 6.4). If this is physically impossible because a potential sampling location is inaccessible or a particle is unretrievable, it is statistically more accurate to make an educated guess about the size class of such particles than to exclude those locations from the sample altogether.

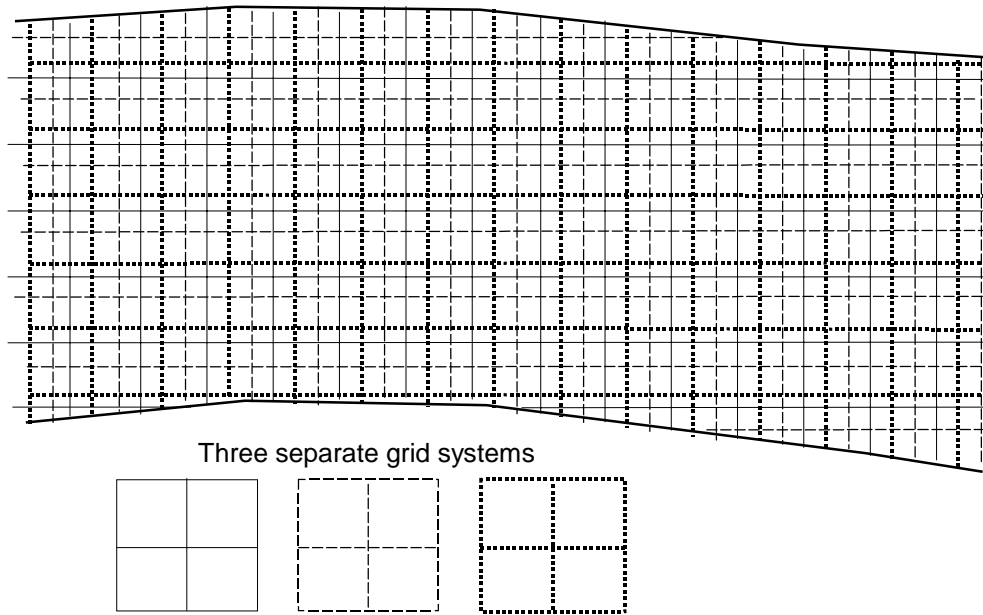


Fig. 6.3: A reach covered by three grid systems each slightly shifted relative to each other.

The grid orientation should be rectangular so that each grid point represents a streambed section of the same size. In a slightly sinuous reach, a grid of tightly-spaced transects perpendicular to the low flow streambed are widely-spaced at the outside bends, and

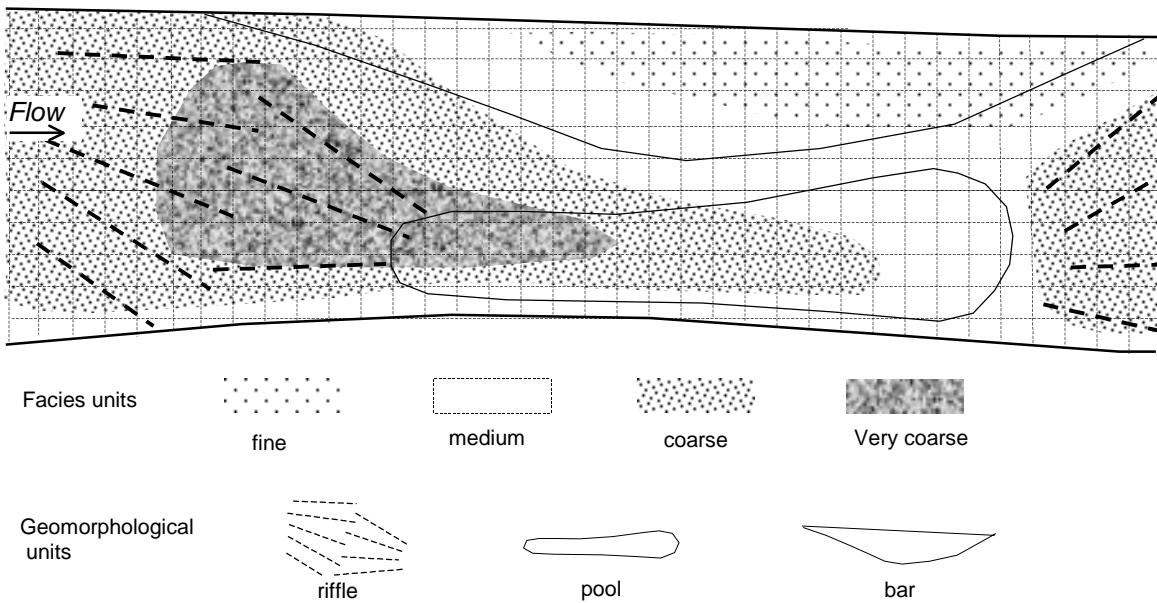


Fig. 6.4: Sketch map of a reach with its facies units, the underlying geomorphological units, and a sampling grid (sampling points at grid intersections).

tightly-spaced at the inside bend. This uneven sampling pattern underrepresents particle sizes at the outside bends, and overrepresents particle sizes at the inside bends, potentially causing samples that are biased against coarse particles. In moderately sinuous reaches, this bias can be mitigated by adjusting transects to the high flow bed which is usually less sinuous than the low flow bed. In highly meandering streams, a reach consisting of several meander bends should be sampled by a rectangular grid unconnected to stream morphology, if a reach-averaged bed-material particle size is to be obtained from a joint particle-size analysis of all sampled particles. Laterally, transects or grids should extend over the entire bankfull width when the sampling objective is to provide a reach-averaged estimate of channel bed conditions.

### 6.2.3.2 Grid spacing and areal extent of the sampling grid

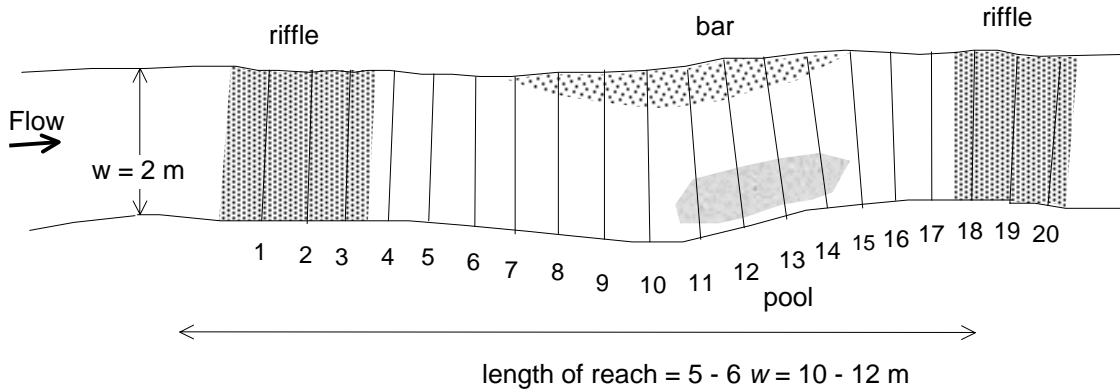
The grid spacing used for spatially integrated sampling is determined by three factors: (1) The sample size needed for a tolerable error given the sorting of the bed material, (2) the minimum grid spacing required to avoid serial correlation due to double counting of an individual clast within a particle cluster, and (3) the areal extent of the sampling reach. Recall that pebble counts of 400 particles provide an precision of about  $\pm 0.15 \phi$ , or  $\pm 10 - 11\%$  for the  $D_{50}$  particle size for gravel bed-material with a typical sorting coefficient (Inman 1952) of approximately 1.2 (Sections 5.2.3.4 and 6.1.5.2). The error is larger for more poorly sorted bed material or for the tails of the distribution (Sections 5.2.1. and 5.2.2).

For gravel- and cobble-bed streams with a  $D_{max}$  particle size of small boulders, minimum sampling-point spacing should be 0.3 - 0.5 m. This means that a stream width of 5 m can hold 10 - 17 sampling points per transect, but considerably less if the grid spacing is to accommodate large boulders. If the streambed area to be sampled is small, e.g., a stream section of 1 - 2 stream widths, it is best to select a square sampling grid which facilitates the densest sampling point spacing possible.

Representative spatially integrated sampling of a morphologically or sedimentologically diverse sampling reach must ensure that a sufficient number of sampling points falls onto each unit to ensure a fair representation of that part of the reach. A grid system with about 20 transects is required to cover the morphological and sedimentary units within a riffle-pool section (from one riffle to the next riffle) in sufficient detail (Fig. 6.5). The actual number of transects needed in a particular stream reach can be calculated based on the following considerations:

The stream reach to be sampled is a riffle-pool sequence 5 m wide and 30 m long (i.e., 6  $w$ ). The  $D_{max}$  is 0.3 m. A grid spacing of 0.3 m yields 17 sampling points per transect. 20 transects yield 340 sampling points, which is less than a sample size of 400 required in poorly sorted gravel beds. 408 sampling points are obtained by sampling 24 transects each spaced 1.25 m apart. If a grid spacing of 0.5 m was selected, with 10 sampling points per transect, the reach would be covered by 40 transects each spaced 0.75 m apart.

### Small stream



### Medium-sized stream

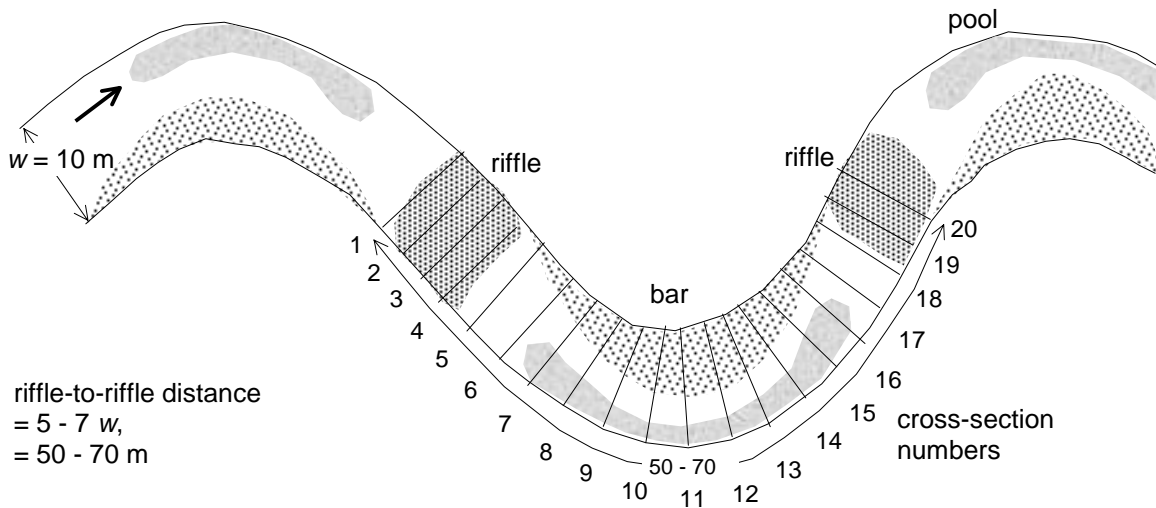


Fig. 6.5: Sampling grid with 20 cross-sections covering the entire reach in a small (top) and medium-sized (bottom) stream.

The widest spacing between individual sampling points is obtained by a distance of 0.625 m between sampling points on a transect, which allows 8 sampling points per transect. 50 transects each spaced 0.6 m apart yield a total of 400 sampling points.

Small cobble-bed streams less than 2 m wide are difficult to sample with a pebble count because a reach 12 m long may have only 200 grid points, even if the grid spacing is set to the minimal value of the  $D_{max}$  particle size. In this case, either a lower criterion for

sampling precision should be accepted, or sampling should be extended over a stream reach long enough to provide a sufficient number of grid points.

### **6.3 Spatially segregated pebble counts (sampling each unit individually)**

Whereas spatially integrative sampling ignores geomorphological or sedimentary units and the associated patterns of spatial variability in bed-material size and sorting within a reach, spatially segregated sampling distinguishes between individual streambed areas that have particle-size distributions different from neighboring areas. Depending on the study objective, a heterogeneous sampling reach can be delineated according to geomorphological, or sedimentary criteria, and sampling can either encompass all units or be restricted to one or a few.

#### **6.3.1 Geomorphologically stratified sampling**

Geomorphologically stratified sampling delineates all *geomorphological*<sup>6</sup> units within a reach, such as riffles or pools, and samples each unit individually (Kondolf 1997a). The results of geomorphologically stratified sampling provide insight into the patterns of spatial variability of bed-material size and permit comparison of particle sizes among different geomorphological units (e.g., riffles and pools, or bar head and riffle).

Alternatively, the same geomorphological units can be compared between different stream reaches or over time. The differences in particle sizes between units can provide insight into whether sediment transport is supply limited or transport limited. A reduction in sediment supply, for example, can be analyzed by comparing the dominant large particle size  $D_{dom}$  at the upstream end of bars with the riffle particle size distribution (Riffle Stability Index, RSI, Kappesser 1995).  $D_{dom}$  approaches the riffle  $D_{max}$ -particle size in aggrading streams, but is closer to the riffle  $D_{50}$  size in degrading streams. This is because when sediment supply is reduced, riffles respond by coarsening, whereas the size of dominant large particles at the upstream end of bars remains unaffected for some time.

An input of sand and fine gravel into a stream reach is not necessarily shown by fining on riffles. Introduced fine sediment is more likely to be accumulated in depositional areas, such as pools, backwaters, wakes, and along banks. Thus, a comparison of the volume of fine sediment stored in pools over time or between reaches can be used for monitoring fine sediment supply to streams (Section 6.6.2)(Lisle and Hilton 1992; 1996; 1999).

Similarly, a comparison of particle sizes from the same geomorphological units over time, space, or between streams is useful for monitoring the effects of changes in water and sediment supply. Such changes may not be detectable when monitoring reach-averaged particle-sizes.

---

<sup>6</sup> See footnote 2 in Section 6.

### 6.3.1.1 Characterization and delineation of geomorphological units

The first step in geomorphologically stratified sampling is to carefully delineate the various geomorphological units. This is performed visually based on recognition of streambed topography, flow patterns, and patterns of spatial bed-material variability. The delineation of geomorphological units may be difficult, particularly for inexperienced operators (Poole et al. 1997). Delineation requires training and the results are affected by the stage of flow. The frequent lack of well-defined boundaries between geomorphological units, and the deviation of geomorphological units from textbook descriptions, make delineation difficult and introduce subjectivity. Even trained geomorphologists may be inconsistent in their delineation of geomorphological units in different stream types. A description of the characteristics of geomorphological units is provided in Section 3.2.

### 6.3.1.2 Grid sampling on individual geomorphological units

Delineated geomorphological units and their spatial patterns of bed-material size should be shown in a sketch map of the reach to help design the optimum sampling scheme for each unit. Closely-spaced parallel transects or a square grid within a geomorphological unit ensures representative sampling in most cases. The grid spacing should not be smaller than the largest particle size to be included in the sample in order to avoid counting a large particle multiple times. Counting a large particle more than once introduces serial correlation into the sample and is not recommended. To do so overemphasizes the presence of large particles in small samples and disturbs the relation between sample size and error because sample-size statistics assume random, non-correlated sample points.

A geomorphological unit often has spatial variability in particle size distributions, and sample-size recommendations provided in Section 5.2 are not applicable because they refer only to homogeneous streambed areas. In order to establish a relation between sample size and error on heterogeneous units, a two-stage sampling approach (Section 5.2.3.1) may be used. The heterogeneous unit is sampled multiple times using a systematic grid that covers the entire unit. The grid is slightly shifted for each subsample (Fig. 6.6). The two-stage approach then determines how many subsamples are needed in order to obtain a desired precision for the sampling result.

Usually, a total sampling effort has a higher statistical validity if the total large sample is broken up into several subsamples that are each collected with a slightly shifted grid. Grid spacing may need to be tailored to each geomorphological unit within a reach since the patterns and the degree of spatial particle-size variability vary among geomorphological units.

#### ***Small geomorphological units***

Geomorphological units in small streams may be too small to provide a sufficient sample size for the smallest grid spacing usable for a given  $D_{max}$  particle size, and even when

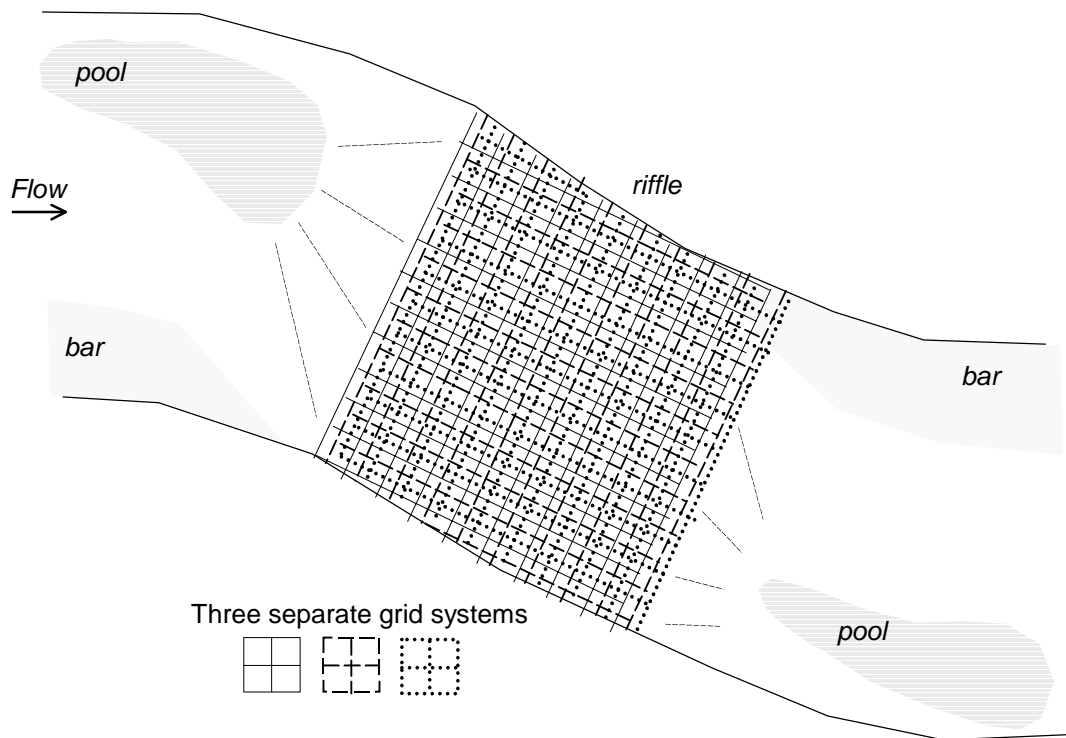


Fig. 6.6: Three replicate samples of a riffle using three grid systems, each slightly shifted relative to each other.

multiple shifted grids are used. If the precision resulting from a small sample size is not acceptable, the user may combine samples from several adjacent geomorphological units of a kind, e.g., samples from several riffles or from several bars. If the study objective focuses on one particular riffle or bar, the problem of a small sampling area may be circumvented by taking one or several areal samples (Section 4.1.3). Areal samples include *all* particles within the delineated area. Thus, the sampled area can be much smaller than required for grid samples. For small areas, areal sampling increases the potential sample size and precision. However, the conversion necessary to compare areal samples with grid samples may be difficult (Section 4.3).

### 6.3.1.3 Sampling on riffles only

Bed-material sampling is sometimes limited to riffles because the cross-sectional channel shape and flow hydraulics in a reach tend to be most uniform on riffles. In addition, riffles are commonly the shallowest areas in an inundated streambed and have comparatively low spatial variability in particle size and little sand in the surface layer. Thus, riffles are the most convenient stream location for pebble counts.

However, the analyst must keep in mind that sampling on a riffle does not provide a reach-averaged particle-size distribution. Often, but not always, riffles have coarser bed material than the reach because finer sediment is eroded off the riffle surface. Also, if boulders are supplied to the reach from rock falls or debris flows, riffles may be finer than the reach average. Riffles may be the location with the steepest local gradient, but are not necessarily coarser than the reach average (Clifford 1993). The reason for this is that riffles may be stabilized by structural elements, such as clusters, particle interlocking, and imbrication (Sear 1996) (Fig. 3.9).

While riffle particle-sizes are not necessarily indicative of the reach as a whole, the *ratio* of riffle sediment size to the sediment size of other geomorphological units is frequently used to determine whether bedload transport is supply or transport limited (Section 6.3.1). Riffle surface sediment size could also be monitored over time or compared between different sites.

Bed-material sampling for bedload-transport computations is often limited to riffles. The argument for this practice is that bedload is often computed for a riffle cross-section only, and that all stream sediment is transported through a specified cross-section. However, bed material may be entrained or deposited at many stream locations within a reach. Thus, bed material from the entire reach affects bedload transport and using the reach-averaged bed-material size distribution for bedload-transport modeling within a given cross-section seems more appropriate.

#### 6.3.1.4 Proportional sampling on long reaches

If the study aim is to estimate the average particle-size distribution over a long meandering reach and to obtain information on the different particle sizes in riffles and pools, Rosgen (1996) proposes a proportional procedure that samples riffles and pools in proportion to their occurrence along the reach. Reach length for this approach extends over two complete meander wave-lengths, which comprise four individual meander bends and thus four riffle-pool sequences. With a riffle spacing of 5 - 7 stream widths, a reach covers a stream length of 20 - 30 stream widths. While walking the reach, the stream length occupied by pools and riffles is measured. Riffle-like features such as rapids, runs, and glides (Section 3.2.2.2) are included into the riffle category. Once the percentage stream length occupied by riffles and pools is determined, transects are placed so the percentage of samples taken on riffles is equal to the percentage of channel reach length delineated as a riffle. For example, if 70% of the reach length was classified as riffle-dominated, 70% of all transects would be placed into riffle-dominated sections (Fig. 6.7). Rosgen (1996) suggested using 10 transects per reach, so the number of transects allocated to riffles and pools can be easily determined. On each transect, 10 particles are sampled with even spacing, resulting in a total sample size of 100. Since particles were sampled on a proportional basis, data from riffles and pools may be combined for a joint particle-size analysis to obtain a reach-averaged particle-size distribution.

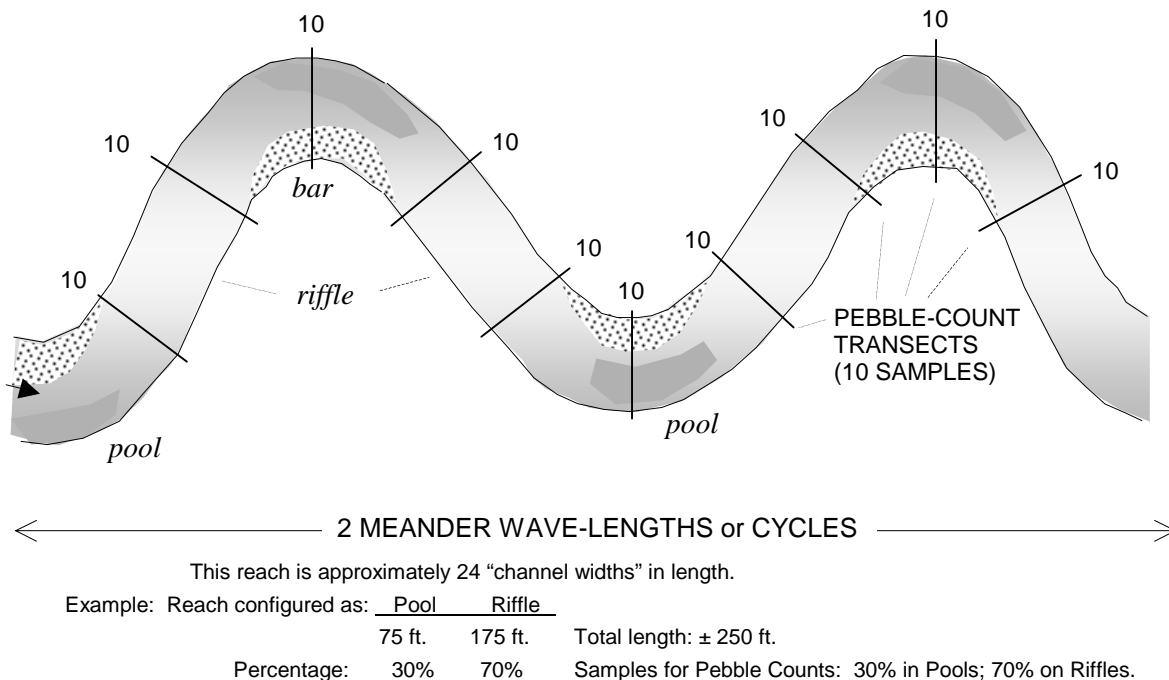


Fig. 6.7: Allocation of transects in a reach of consecutive riffle-pool sequences on a proportional basis. (Redrawn from Rosgen (1996), by permission of Wildland Hydrology).

The proportional procedure described in this section can be a quick estimate of the median particle size over a long reach if there is little spatial variability within each geomorphological unit. However, geomorphological units are often spatially non-homogeneous. When the proportional procedure with 10-transects per reach is applied to reaches where particle sizes vary between riffles and pools, and where particle sizes vary between consecutive riffles or consecutive pools, sampling is unrepresentative and unsystematic. An increase in the number of transects per reach increases sample representativeness and statistical accuracy by avoiding: (1) a misfit between the number of transects and the number of riffles and pools per reach, (2) operator arbitrariness, and (3) an unrepresentative, small sample size.

If a reach comprises four riffle-pool units, and 70% of the reach length is identified as riffle, 30% as pool, and each reach is sampled by 10 transects, then seven transects need to be allocated onto four riffles and three transects onto four pools. Consequently, one of the riffles is sampled with only one transect, and one of the pools is not sampled at all. Such a misfit could be avoided if the same number of transects is allocated to each of the riffles and the pools. The percentage stream length occupied by riffles or pools (e.g., the 70% riffles, 30% pools) may then be proportionally sampled by placing 7 transects onto each riffle and 3 transects onto each pool. This apportioning yields 40 transects per reach, 28 on riffles, and 12 on pools. Sampling 10 particles per transects yields a total of 400 particles. This sample size is more in line with recommendations suggested by other

sources and may provide an precision for the  $D_{50}$  particle size (in mm) of about  $\pm 10\%$  (Rice and Church 1996b) (Section 5.2.3.4).

Another reason why a larger number of transects for each riffle and pool is recommended is because it decreases the emphasis placed on an individual transect and its placement within the riffle or the pool. Although some systemization can be attempted by alternately placing transects at the upstream, center, and downstream sections of riffles and pools, transect placement largely depends on operator discretion.

### **6.3.2 Sedimentary stratified sampling**

If the purpose of the study is to characterize spatial heterogeneity of surface grains rather than compare geomorphological units, sampling should be stratified by sedimentary units. Sedimentary units are homogeneous streambed areas with no systematic spatial variation of bed-material size, and are sometimes termed *facies* or *patches*. The size of a patch or sedimentary unit is not fixed, but depends on the degree of spatial heterogeneity of the streambed, and the number of different facies that the study wants to distinguish. Most studies differentiate between 3 or 4 different facies, so that facies units are visually distinguishable. Fig. 3.10 provides an example of a heterogeneous stream reach with several facies units in an aggraded C-type stream. A heterogeneous streambed with four facies due to a heavy loading of large woody debris is shown in Fig. 3.12.

There are two basic methods of delineating a heterogeneous streambed into homogeneous sedimentary units: visual (Section 6.3.2.1 and 6.3.2.2) and statistical methods (6.3.2.3). Examples of both are presented below. After the various sedimentary units have been delineated, a sampling scheme needs to be established that is appropriate for the patch size and the degree of homogeneity. Various sampling schemes for spatially segregated sampling are explained in Section 6.3.2.4.

#### **6.3.2.1 Visual delineation of sedimentary units (facies or patches) based on estimates of percentile particle sizes**

Experienced operators can become proficient in visually estimating particle-sizes (Shirazi and Seim 1981; Platts et al. 1983), and thus in the distinction between areas of different particle-size composition. However, the facies delineation process remains to some degree subjective (Kondolf and Li 1992) because segregation of sedimentary units from a heterogeneous surface reduces, but not eliminates heterogeneity. In addition, there are no standards defining a meaningful degree of spatial variability within sedimentary units. For best delineation results, it is important to spend some time walking the streambed to become familiar with the particle sizes present on the bed and their spatial distribution. Based on these insights, the user can devise criteria for delineation of sedimentary units. The reach length covered by the study should be sufficiently enough (20 stream widths or more) so that each type of sedimentary unit occurs several times within the reach.

***Estimating the particle size of one or two percentiles***

Criteria for delineation of sedimentary units in gravel-bed rivers may be based on the particle size of specified percentiles. The size of one large percentile, e.g., the  $D_{75}$ , may be sufficient in some deposits (Lisle and Madej 1992), but in poorly sorted bed material, different facies can be better discriminated on the basis of the size of several percentiles, e.g., the  $D_{50}$  and the  $D_{90}$  (Hilton and Lisle, pers. comm., 1998). Each study needs to define its own delineation criteria in correspondence with the site characteristics and the study aim. Example criteria for delineation of sedimentary units (patches, facies) are provided in Table 6.3.

Table 6.3: Example criteria for delineation of sedimentary units (patches, facies).

<u>Lisle and Madej (1992)</u>		<u>Hilton and Lisle, pers. comm., 1998</u>		
$D_{75}$ (mm)	Sedimentary unit (facies)	$D_{50}$ (mm)	$D_{90}$ (mm)	Sedimentary unit (facies)
< 22	fine pebbles	<16	<45	fine pebbles
22 - 64	coarse pebbles	<16	>45	sand and pebbles
> 64	cobbles	16-45	any	coarse pebbles
sand>25%	bimodal	>45	any	cobbles

For field application, the procedure of visual delineation and the subsequent segregated sampling can be segmented into several steps:

1. Walk the reach and familiarize yourself with the different compositions of surface sediments.
2. Determine the different facies and define delineation criteria appropriate to the site and the study aim.
3. Apply the delineation criteria to distinguish between sedimentary units and mark the boundaries with surveyors' flags.
4. Conduct pebble counts covering the entire sedimentary unit or only parts of it, depending on the size of the sedimentary unit (see explanations below).
5. Survey the boundaries of all sedimentary units.
6. Prepare maps from the survey data.
7. Determine the areal extent of each sedimentary unit.
8. Determine the percent area of each facies type.

9. Compute the reach-averaged particle size distribution by adding the area-weighted particle-size distributions from each facies (Section 6.3.2.5).

The size of a sedimentary unit, or of the patches that comprise a unit, needs to be sufficiently large to accommodate a pebble count. The minimum area needed for a pebble count depends on the product of sample size and grid spacing. Grid spacing for pebble counts should be at least as large as the  $D_{max}$  particle size, about 0.3 - 0.5 m in gravel-bed rivers comprised of small boulders. Sample size depends on the desired precision and the sediment sorting. Recall that a sample of about 400 particles from a homogeneous unit determines the  $D_{50}$  to within  $\pm 0.12$  to  $\pm 0.15 \phi$  (Section 5.2.2.3), or to within approximately 10% in terms of mm-units in poorly sorted sediment. A 100-particle sample nearly doubles this error. If a facies unit is too small or too fine in bed-material size for a pebble count, areal samples should be used.

### 6.3.2.2 Visual delineation based on a two-level characterization of particle sizes

Buffington and Montgomery (1999a) devised a two-level visual particle-size classification based on the relative abundance of the major size classes (sand, gravel, and cobble) and on the subsizes of the dominant size class. The delineation procedure is described in detail in Section 4.1.3.5, but summarized below for convenience. In a Level 1 delineation, the operator visually estimates the relative abundance of the main three constituents of a particle-size distribution. For example, a deposit with 10% sand, 60% gravel, 30% cobble classifies as a **sandy, cobbly Gravel facies (scG)**. In Level 2, the operator characterizes the size of the major constituent (i.e., gravel in this example) more precisely and estimates the percentage of three out of the five classifiers: very fine, fine, medium, coarse and very coarse. The percentages of 20% fine, 50% medium, and 30% coarse gravel, for example, classify the gravel part as fine-coarse-medium. The approach provides statistically significant distinctions between particle-size distributions of facies and has the advantage of being generally applicable to all facies.

Visual delineation and sampling procedure for spatially segregated sampling on heterogeneous surfaces can be broken down into the following steps:

1. Conduct a preliminary reconnaissance of the stream reach, visually identifying the facies (sedimentary units) according to the Level 1 and 2 classifications presented by Buffington and Montgomery (1999a) (Section 4.1.3.5).
2. Do pebble counts in each facies type, using an appropriate grid spacing and sample size for the desired precision. This may be performed with one sufficiently large, facies-spanning pebble count per unit. Use areal sampling (Section 4.1.3.1 - 4.1.3.4) for facies areas too small or too fine for a pebble count of adequate extent.
3. Plot the percent frequency of the three major constituents of each facies on a triaxial diagram (Fig. 4.15 in Section 4.1.3.5). Redefine facies criteria if clusters of data points plotted in the diagrams fail to distinguish between facies.

4. Construct a textural map by surveying.
5. Compute the reach-averaged particle-size distribution by adding the area-weighted particle-size distributions from each facies (Section 6.3.2.5)

### 6.3.2.3 Statistical delineation from systematic grid data

Visual delineation of sedimentary units can be problematic, particularly when the streambed is submerged. In order to alleviate this problem, Crowder (1996) and Crowder and Diplas (1997) suggest a four-step delineation procedure, whereby visual delineation is augmented by a statistical delineation method in which hypothesis testing of sample similarity or difference is applied incrementally over the reach by a moving window technique. The steps involved in hypothesis testing and the moving window technique are:

1. Walk the reach to become familiar with the various sedimentary units and select the subsample area and the number of particles collected in each subsample. The subsample area (cell size) depends on the degree of heterogeneity of the bed and on the  $D_{max}$  particle size. For example, a  $D_{max}$  particle size of 0.3 m requires a minimum grid spacing of 0.3 m. Crowder and Diplas (1997) suggest starting with a sample size of 20 – 30 per cell, or of 25 - 36 if a square cell-size is selected. Sampling 25 particles from a 0.3 by 0.3 m grid requires a grid cell-size of 1.5 by 1.5 m. Sampling 36 particles with a grid spacing of 0.5 m requires a grid cell size of 3 by 3 m.
2. Spread a systematic grid of cells over the entire stream reach disregarding sedimentary units. For example, the reach may be covered by a 1.5 by 1.5 m grid, and subsamples of 25 particles are collected from each grid cell (Fig. 6.8). Do not use less than about 25 particles per subsample.
3. Compute the arithmetic mean particle size  $D_m$  (in mm; Eq. 2.39, Section 2.1.5.3) as well as the arithmetic standard deviation (variance  $s^2$  (Eq. 2.56, Section 2.1.5.4) for each cell. The values of  $D_m$  and  $s^2$  for each cell are plotted into a sketch map of the reach (Fig. 6.8).
4. Check whether the selected sample size and the computed sample variance  $s^2$  per grid cell allow detection of a difference in the mean particle size between all adjacent grid cells 1 and 2 using Fig. 6.9. The curve for  $s_1^2 + s_2^2 = 100$  in Fig. 6.9 indicates that 6 mm is the smallest difference detectable between two neighboring  $D_m$  with a subsample size of 30. Similarly, a 6 mm difference between two neighboring  $D_m$  requires a sample size of 800 if the summed variance is  $s_1^2 + s_2^2 = 3000$ . If the sample size per grid cell is too low, more particles need to be sampled in each grid cell.
5. Determine the boundaries between sedimentary units by performing statistical hypothesis testing and the moving windows procedure explained below.

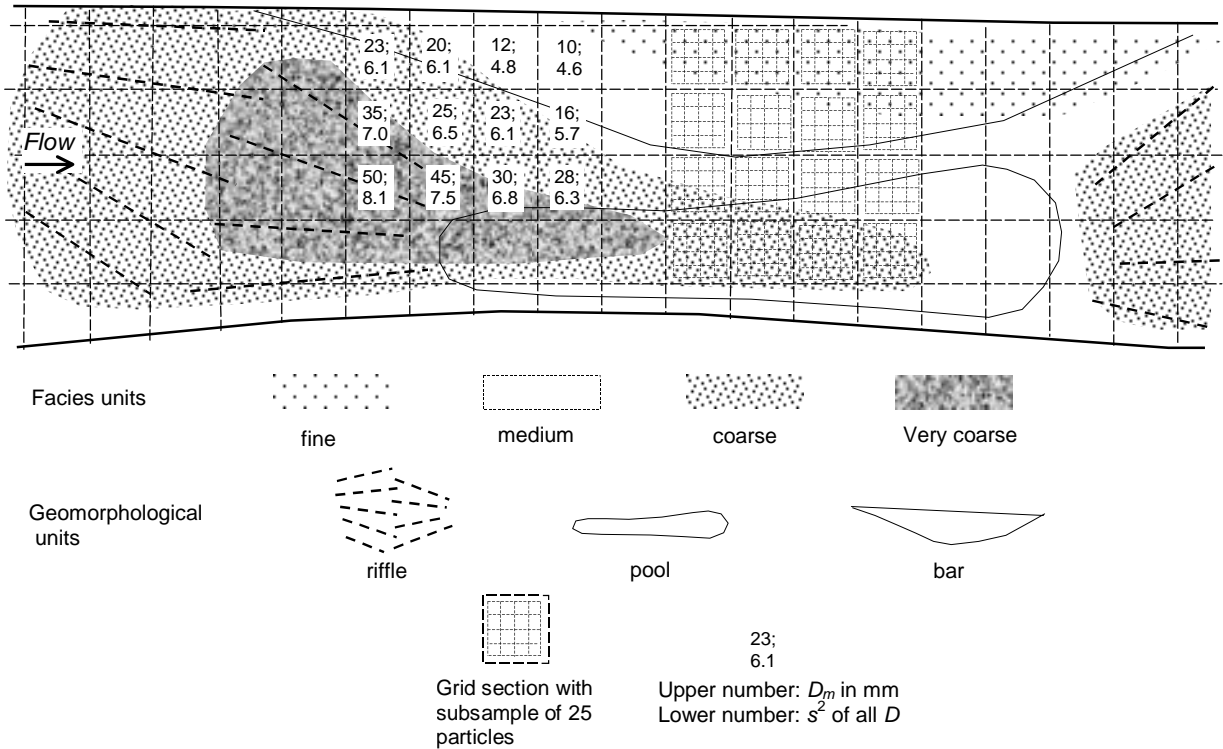


Fig. 6.8: A grid is superimposed on the sampling reach, extending over facies boundaries. The upper number in each grid section is the arithmetic mean particle size in mm, the lower number is the particle-size variance  $s^2$  obtained from a 25-particle pebble count collected in each grid section (here shown for 16 of the grid sections).

- Once the boundaries of sedimentary units are determined, combine all subsample particles within the delineated sedimentary unit and do a particle-size analysis to characterize the specified sedimentary unit.

**Example 6.1:**

Two subsamples with a sample size of  $n = 25$  were collected in neighboring grid cells. Subsample 1 had a  $D_{m1} = 6$  mm, and a  $s_1 = 4.7$ . Subsample 2 had a  $D_m = 14$  mm, and a  $s_1 = 8.8$ .  $s_1^2 + s_2^2 = 99.5$ .  $\Delta D_m = |D_{m1} - D_{m2}| = 14 - 6 = 8$  mm. The line for  $s_1^2 + s_2^2 = 100$  on Fig. 6.8 b indicates that a sample size of 25 is sufficient to detect a difference of 6 mm and thus adequate to detect an 8 mm difference between  $D_{m1}$  and  $D_{m2}$ .

**Statistical discrimination**

One method of determining a sedimentary boundary is to test whether the mean particle sizes of two neighboring subsamples are statistically different. The neighboring  $D_{m1}$  and  $D_{m2}$  are different with a 90% confidence if the value for  $Z_{12}$  determined from

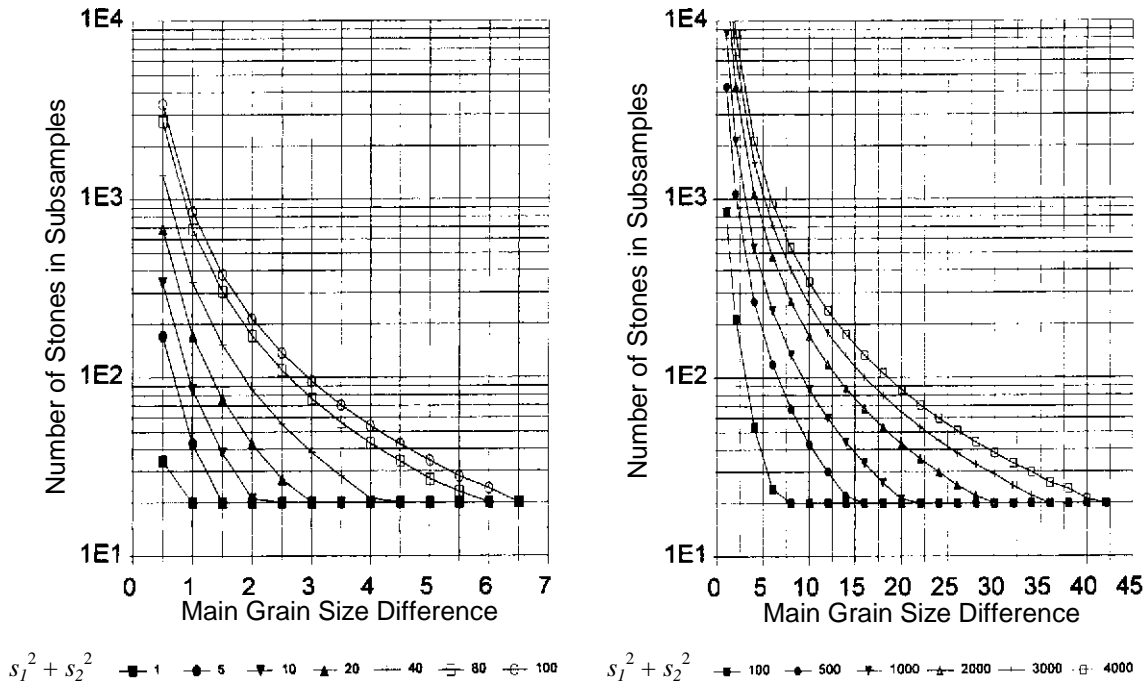


Fig. 6.9: Minimum subsample size necessary to locate a specified difference in the arithmetic mean particle size (mm); legend indicates lines of constant sums of variances  $s_1^2 + s_2^2$  ranging from 1 - 100 (left), and 100 - 4000 (right). (Reprinted from Crowder and Diplas (1997), by permission of the American Society of Civil Engineers).

$$Z_{12} = \frac{|D_{m1} - D_{m2}|}{\sqrt{\frac{s_1^2}{n_1} + \frac{s_2^2}{n_2}}} \quad (6.2)$$

exceeds the value of 1.645 or is less than - 1.645.  $s_1$  and  $s_2$  are the arithmetic standard deviations of subsample 1 and 2 and  $n$  is the subsample size which is usually the same for  $n_1$  and  $n_2$ . For a 95% probability,  $Z_{12}$  is increased to 1.96 (See Table 5.1 for values of  $Z$  for various probabilities). A statistical difference between neighboring  $D_m$  confirms the presence of a sedimentary boundary. The  $Z$ -statistic in Eq. 6.2 could be replaced by a  $t$ -statistic with  $n_1 + n_2 - 2$  degrees of freedom if the user wants to acknowledge the effect of a small samples size.  $t$ -statistics for a 95% confidence limit are listed in Table 5.2.  $t$ -statistics for other confidence levels can be found in general statistics books.

**Example 6.2:**

Two neighboring grid cells with a sample size of  $n = 25$  have a  $D_{m1} = 6$  mm,  $s_1 = 4.7$ , and  $D_{m2} = 20$  mm, and  $s_2 = 8.8$ . Solving Eq. 6.2 yields:

$$Z_{12} = \frac{|6 - 20|}{\sqrt{\frac{4.7^2}{25} + \frac{8.8^2}{25}}} = \frac{14}{\sqrt{0.88 + 3.10}} = \frac{14}{1.99} = 7.02$$

which is larger than 1.96 (and larger than 2.00 if  $t$ -statistics are used) and indicates a statistically significant difference in the  $D_m$  between the neighboring grid cells. Thus, subsamples 1 and 2 belong to different sedimentary units.

Eq. 6.2 could be applied systematically to all neighboring grid cells to locate sedimentary boundaries. However, this discrimination procedure defines a sedimentary boundary along the grid-cell margins, even if the true sedimentary boundary goes through the middle of the grid cell. In order to facilitate a more accurate detection of the true boundary location, Crowder and Diplas (1997) devised the moving windows procedure.

#### ***Moving window technique***

To apply the moving window technique (Fig. 6.10), the area of sample 1 is covered by two adjacent windows A and B which are incrementally moved towards the area of sample 2 over the area in which the boundary is expected. For each step, the difference between the mean particle sizes  $D_{mA}$  and  $D_{mB}$  is computed. The boundary between sample 1 and 2 is located where the difference between  $D_{mA}$  and  $D_{mB}$  reaches a maximum value.

The statistical delineation procedure confirms that sampled sedimentary units are sufficiently homogeneous. Since each sedimentary unit may be of different size, a reach-averaged size distribution is computed from an area-weighted average (Section 6.3.2.5).

#### **6.3.2.4 Strategies for sampling within delineated facies units**

Segregated sampling schemes may be applied to sample the surface sediment of a reach delineated into different facies units. Four basic sampling types can be distinguished:

1. Reach spanning grid that covers all facies with the same grid patterns;
2. Different grid pattern to cover each facies unit;
3. Different sampling procedures on different facies (e.g., taking areal adhesive samples in facies with particle sizes too small for pebble count or photographs in facies areas too small for a pebble count (= hybrid sampling));
4. Different sampling procedures on one facies (e.g., taking a pebble count to sample coarse gravel and areal adhesive samples for a representative sample of fine gravel);
5. Large reach with large facies units: sample extends only over a small part of large facies units and is collected at a representative location.

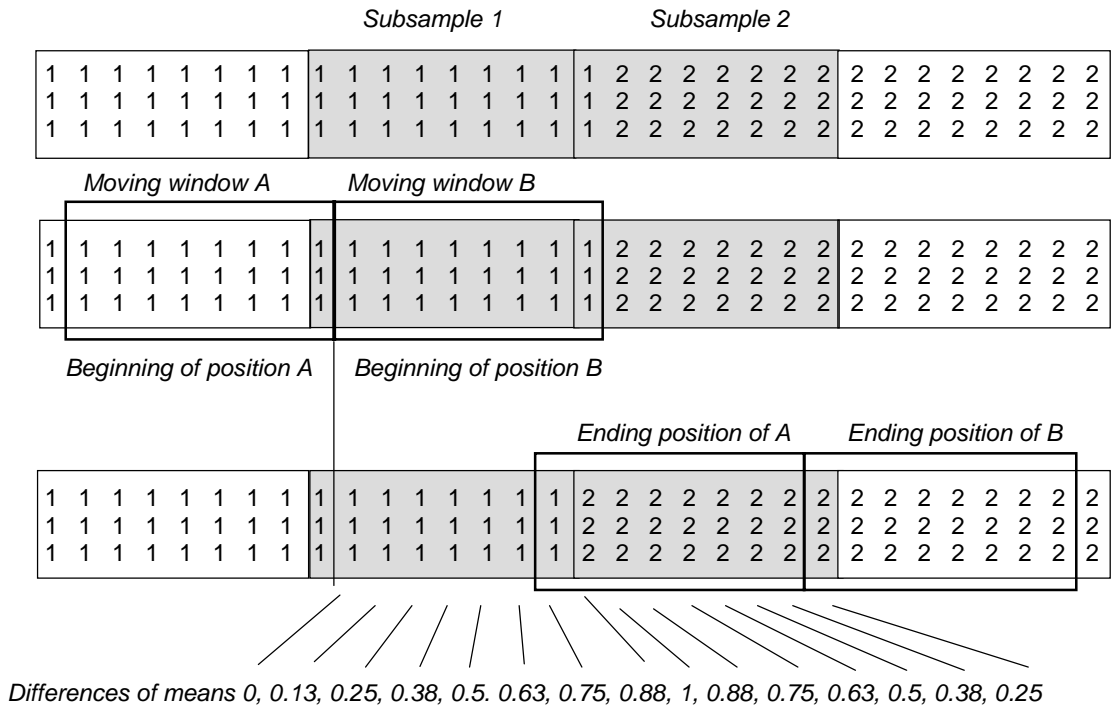


Fig. 6.10: Moving window technique: Two subsamples  that are statistically different and surrounding material  (top); Moving windows A and B in their starting position (center); Ending positions of moving windows A and B and differences in their mean particle sizes at each increment between beginning and ending position of windows. (Redrawn from Crowder and Diplas (1997), by permission of the American Society of Civil Engineers).

These five methods of spatially segregated sampling are explained below. Selection of one of the five methods depends on the characteristics of the facies units such as the  $D_{max}$  particle size, the sediment sorting, the size and orientation of facies units, and how clearly distinguishable facies units are from each other.

**1. Reach spanning systematic grid and allocation of sampled particle to respective facies**

The easiest method of spatially segregated sampling is to cover the entire reach with one grid system and segregate the particles into the various facies unit during the sampling process (Fig. 6.11) (Kondolf and Li (1992), and Kondolf (1997a)). This method requires that all facies may be covered by the same grid, which means that the grid size necessary for the coarsest facies provides a sufficient number of grid points in each facies. It also requires that the various facies units are easily distinguishable by eye.

If spatially segregated sampling with a reach-spanning grid is possible, the operator traverses the reach along transects that may span several facies units. Particles collected along each transect are categorized according to their sedimentary unit, which means

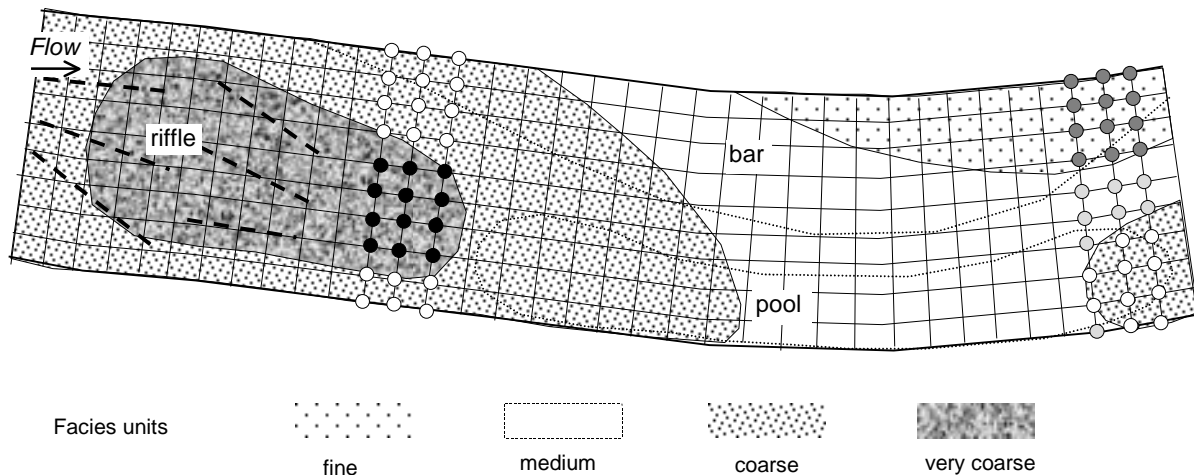


Fig. 6.11: Spatially segregated sampling using a systematic reach-spanning grid. All facies units are covered by the same grid. Examples of allocating sampling points to facies units is given for some of the transects. Equal shading of the circles indicates allocation to the same facies.

particles collected while the transect traverses the “very coarse” facies are allotted to the very coarse facies, whereas particles collected while the transect passes over the “coarse”, “medium” or “fine” facies are listed under the category “coarse facies”, “medium facies” or “fine facies”.

## 2. A separate grid system covers each facies unit

When sampling a reach delineated into sedimentary units, it may be necessary to select a separate grid pattern that varies in grid size and orientation for each unit (Fig. 6.12). The coarse facies, for example, may require a wider grid spacing than the fine facies, or the

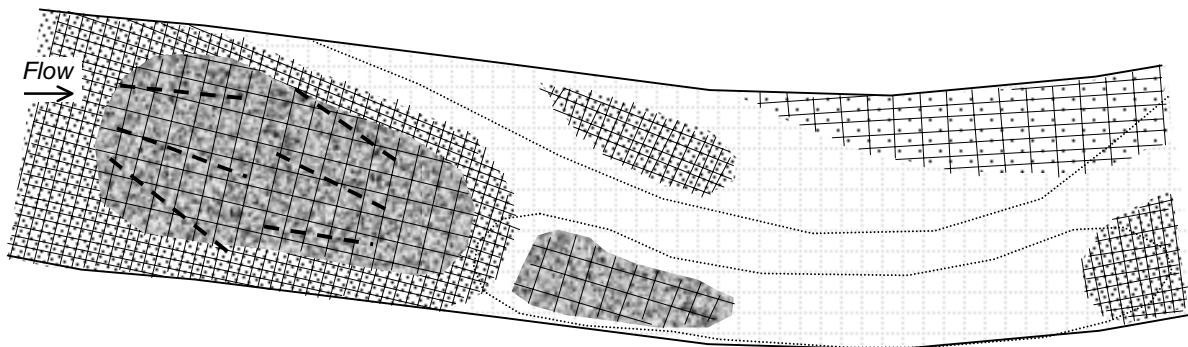


Fig. 6.12: Spatially segregated sampling using a different grid for each facies unit (same legend as Fig. 6.11).

poor sorting of particle sizes in one facies may require a larger sample size to attain a specified precision than a facies with well sorted sediment. Directional orientation of facies units may warrant still another grid orientation.

**3. Small sedimentary units: pebble counts or areal samples**

Some delineated units may be substantially smaller than the area needed for pebble counts. In this case, the user may either collect pebble counts using several grids, each slightly shifted relative to each other (Section 6.3.1.2), or use areal samples (Fig. 6.13). Areal samples, and specifically adhesive sampling (Section 4.1.3.2) may be useful if the surface sediment is mostly finer than about 15 mm, and the user wants to know an exact frequency distribution of the fine gravel and sand. A small, but coarse facies unit may be analyzed by photo sieving (Section 4.1.3.3) using photographs that cover the entire facies unit.

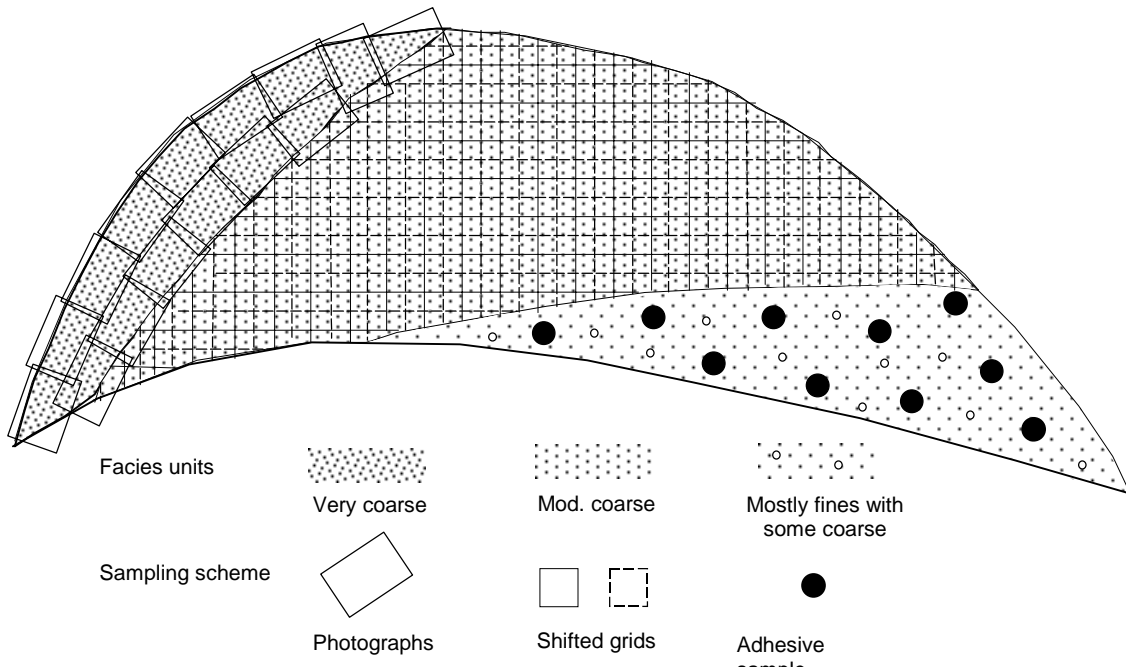


Fig. 6.13: Small sedimentary units: shifted grids, photographs, or adhesive samples are applicable.

Recall that particle-size distributions of areal samples need to be converted into equivalent grid-by-number particle-size distributions before comparison with pebble count data (Section 4.3). After the statistical conversion of areal samples into equivalent grid-by-number samples, particle-size distributions from each facies are area-weighted and summed to yield a reach-averaged particle-size distribution (Section 6.3.2.5).

#### ***4. Poorly sorted facies units containing fine and coarse gravel: hybrid sampling***

If a sedimentary unit has a wide particle-size spectrum with both a large amount of fine gravel and also coarse gravel and cobbles, both adhesive areal samples and a pebble count may need to be collected to representatively sample that facies (hybrid sampling, Diplas 1992) (Fig. 6.14). An adhesive sample (Section 4.1.3.2) can representatively sample fine gravel and sand and provide a more accurate analysis of fine gravel and sand than pebble counts, whereas the pebble count can characterize the coarse part of the distribution better than an areal sample. The particle-size distribution for the entire facies unit is obtained from a sample combination procedure (Section 4.4).

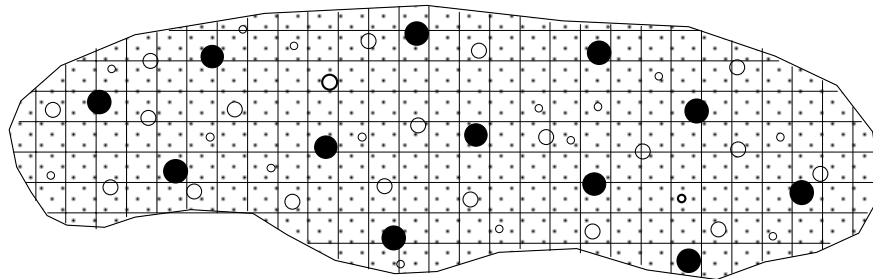


Fig. 6.14: Hybrid sampling on a poorly sorted facies unit with mostly fine but also some coarse gravel: Grid sample for a representative sample of the coarse gravel, and areal (adhesive) samples (○) for representative samples of the fine gravel and sand.

#### ***5. Long reach with large and reoccurring facies units: sample extends only over a small part of large facies units***

A sampling project may have to be conducted in a large stream about 100 m wide and over a long reach where 20 or more channel widths (4 riffle-pool sequences) result in a reach length of 2000 m. The total streambed area is 200,000 m<sup>2</sup>. If the stream has four facies with areas of 20,000, 40,000, 60,000 and 80,000 m<sup>2</sup>, and each facies occurs 4 - 6 times, then the size of individual facies may range between 4,000 (40 by 100 m) and 30,000 m<sup>2</sup> (150 by 200 m). It may still be feasible to collect a 400-particle pebble count from a 4000 m<sup>2</sup> unit, covering the entire facies unit with 20 transects and sampling in 2.5 m step spacing, but total coverage becomes inconvenient for large facies units. In this case, it seems reasonable to restrict a pebble count to a relatively small area (e.g., 20 by 20 m) and to select a representative area within each or almost each of the facies units (Fig. 6.15) for the pebble count (some judgement is required). Facies A, for example, may occur four times in the reach, and a 100-particle pebble count may be collected from each of the four areas of facies A, yielding a total sample size of 400 for facies A. Pebble count data from all four areas of that unit are eventually combined into one sample. However, each pebble count may be analyzed separately in order to evaluate the similarity between the four units. The same process is repeated for the facies units B, C, and D.

If a certain facies occurs numerous times, it may not be necessary to collect a sample from each unit belonging to that facies. A few units most representative of that facies type are

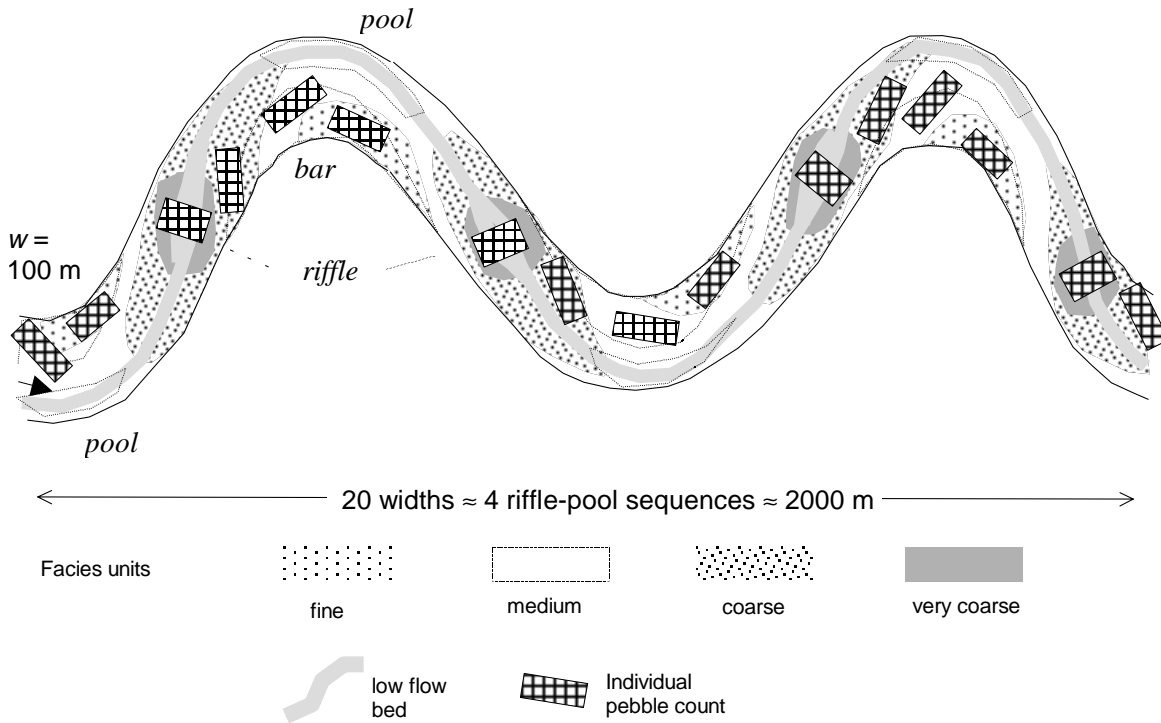


Fig. 6.15: Spatially segregated sampling in a long reach with large and reoccurring facies units: each pebble count covers only part of a facies unit.

then selected for sampling. Also, some units might be so large that they cannot be covered by one large grid count. In that case, several smaller grid counts may be used, each grid covering only a fraction of the total sedimentary unit (Lisle and Madej 1992). The total number of pebble counts to be performed on a sedimentary unit of a specific type should correspond roughly to the percentage area covered by that facies type. If, for example, the cobble, coarse gravel, and fine gravel facies comprise 30, 50, and 20% of the total reach area, then 30, 50, and 20% of all pebble counts are collected from cobble, coarse gravel, and fines gravel facies, respectively. The reach-averaged particle-size distribution is computed from area-weighted particle-size number or percentage frequencies of each unit (Section 6.3.2.5).

#### Example 6.3:

For a  $D_{max}$  or  $D_{95}$  particle size of 0.3 m, and a sample-size requirement of 400 particles, the minimum sampling area is  $400 \times 0.3 \text{ m}^2 = 36 \text{ m}^2$  (size of a small classroom). Table 6.4 provides minimum sampling areas of sedimentary units for various sample sizes and  $D_{max}$  particle sizes, anticipated absolute errors in particle size  $\phi$ -units (see Table 5.6), and relative errors as percentage based on mm-units (based on Fig. 5.8).

If the facies area is too small to accommodate grid spacing for a particular  $D_{max}$  particle size, and sample size required for a specified precision, grid spacing and sample size can be reduced, but either reduction decreases sampling precision.

Table 6.4: Minimum sampling area for various  $D_{max}$  and sample size, and sampling errors in  $\phi$  and % mm.

$D_{max}$ (m)			Sample size $n$	error in terms of	
0.1	0.3	1.0		$\phi$ -units	% mm
Minimum sampling area					
$m^2$	$m^2$	$m^2$			
1	9	100	100	$\pm 0.30$	$\pm 17$
4	36	400	400	$\pm 0.12$	$\pm 10$
10	90	1,000	1,000	$\pm 0.07$	$\pm 4$

### 6.3.2.5 Area-weighted reach-averaged particle-size distribution from stratified sampling

To compute the reach-averaged bed-material size distribution from a stratified sampling scheme, each sedimentary (or geomorphological) unit (Section 6.3.2) (e.g.,  $A$ ,  $B$ , and  $C$ ) should be surveyed and mapped. The fraction of the total area for each of the units is then computed ( $A\% + B\% + C\% = 1$ ). After the particle-size frequency distributions  $f_A$ ,  $f_B$ , and  $f_C$  are established for each unit, the reach-average size distribution  $f_{i,m}$  for the  $i$ th size class is obtained by multiplying the frequency of particles of the  $i$ th size class  $f_{i,A}$  from unit  $A$  by the percent total area  $A\%$  comprised in unit  $A$ . This multiplication is repeated for all geomorphological (or sedimentary) units and frequencies are added to obtain the area-weighted reach-average number frequency  $f_{i,m}$ .

$$f_{i,m} = f_{i,A} \cdot A\% + f_{i,B} \cdot B\% + f_{i,C} \cdot C\% \quad (6.3)$$

The process is then repeated for all size classes to obtain the area-weighted particle-number frequency distribution. The percentage frequency distribution  $f_{\%,m}$  and the cumulative frequency distribution  $\Sigma f_{\%,m}$  are then computed (Table 6.5). Alternatively, area-weighting can be deferred and applied to the percentage frequencies  $f_{\%,i}$  from all units to obtain area-weighted percentage frequencies  $f_{\%,m,i}$ .

$$f_{\%,m,i} = f_{\%,i} \cdot A\% + f_{\%,i} \cdot B\% + f_{\%,i} \cdot C\% \quad (6.4)$$

The computations are repeated for all size classes and  $f_{\%,m,i}$  is summed to obtain a cumulative frequency distribution  $\Sigma f_{\%,m,Di}$ . Both methods provide almost identical

cumulative frequency distributions (compare the two shaded columns  $\Sigma f_{\%,m,i}$  in the example computation in Table 6.5).

Table 6.5: Original frequency distributions  $f_i$  of pebble counts in geomorphological or sedimentary units  $A$  (57%),  $B$  (27%) and  $C$  (16% of total streambed area), and difference between cumulative frequency distribution derived from area-weighted number-frequencies  $\Sigma f_{\%,m,i}$  and area-weighted percentage frequencies  $\Sigma f_{\%,m,i}$ . All values larger than 10 are rounded to the nearest integer value.

$D_i$ (mm)	$f_i$			area-weighted			reach-average			area-weighted reach-average			$\Sigma f_{\%,m,i}$	
	A	B	C	A	B	C	$f_{m,i}$	$f_{\%,m,i}$	$\Sigma f_{\%,m,i}$	A	B	C		$f_{\%,m,i}$
<2	30	25	10	17	6.8	1.6	26	6.0	6.0	4.0	1.6	0.4	5.9	5.9
2	1	1	1	0.6	0.3	0.2	1.0	0.2	6.2	0.1	0.1	0.0	0.2	6.2
2.8	2	0	0	1.1	0.0	0.0	1.1	0.3	6.5	0.3	0.0	0.0	0.3	6.4
4	6	4	1	3.4	1.1	0.2	4.7	1.1	7.6	0.8	0.3	0.0	1.1	7.5
5.6	7	5	1	4.0	1.4	0.2	5.5	1.3	8.9	0.9	0.3	0.0	1.3	8.8
8	8	6	3	4.6	1.6	0.5	6.7	1.6	10	1.1	0.4	0.1	1.6	10
11.3	13	9	6	7.4	2.4	1.0	11	2.5	13	1.7	0.6	0.2	2.5	13
16	25	15	9	14	4.1	1.4	20	4.6	18	3.3	0.9	0.4	4.6	18
22.6	65	27	15	37	7.3	2.4	47	11	29	8.6	1.7	0.6	11	28
32	87	62	35	50	17	5.6	72	17	45	12	3.9	1.4	17	45
45	91	95	57	52	26	9.1	87	20	66	12	5.9	2.3	20	65
64	53	83	81	30	22	13	66	15	81	7.0	5.2	3.2	15	81
90	23	57	96	13	15	15	44	10	91	3.0	3.6	3.8	10	91
128	9	26	49	5.1	7.0	7.8	20	4.7	96	1.2	1.6	1.9	4.8	96
180	7	10	20	4.0	2.7	3.2	9.9	2.3	98	0.9	0.6	0.8	2.3	98
256	2	5	10	1.1	1.4	1.6	4.1	1.0	99	0.3	0.3	0.4	1.0	99
360	1	1	8	0.6	0.3	1.3	2.1	0.5	100	0.1	0.1	0.3	0.5	100
512	0	1	3	0.0	0.3	0.5	0.8	0.2	100	0.0	0.1	0.1	0.2	100
total:	430	432	405	245	117	65	427	100		57	27	16	100	

#### 6.4 Spatially integrated volumetric sampling (reach-averaged)

A reach-averaged mass-based particle-size distribution may be obtained by sampling an entire reach with a spatially integrated methodology or by delineating the reach into its sedimentary units which are then sampled separately (spatially segregated). Spatially integrated sampling means that sampling integrates over all sedimentary units (or any other distinguishable streambed units such as geomorphological units or habitat units) instead of sampling each unit separately (i.e., spatially segregated). Whether spatially integrated sampling is preferable to spatially segregated sampling must be determined for each stream and study situation. Criteria for making this decision will be outlined.

***Spatially integrated or segregated sampling for a reach-averaged particle-size distribution?***

Spatially integrated volumetric sampling is best used for computing the reach-averaged particle size of relatively homogeneous reaches in which the number of sampling locations is relatively low. If heterogeneous reaches are sampled spatially integrated, the number of samples needed to cover the reach is relatively high which leads to a large total sample mass. Heterogeneous reaches are therefore better sampled using a spatially segregated approach (Section 6.5.2.2). Within the delineated sedimentary unit, bed material is comparatively homogeneous. This leads to a relatively small number of samples for each unit and to a relatively small mass for each sample. Therefore, the total mass required for each sedimentary unit remains rather small.

Note, however, that the process of delineating the reach into its sedimentary units and the survey to measure the areal extent of each unit is labor intensive as well, particularly if the reach is comprised of a large number of relatively small sedimentary units (patches). The increased work effort from delineation and surveying offsets some of the work effort rendered unnecessary by the reduced sample mass of spatially segregated sampling. Thus, on moderately heterogeneous reaches or patchy reaches comprising numerous small facies units, the total work effort may actually be similar for spatially integrated and spatially segregated techniques. Finally, spatially integrated sampling is also used when the presence of facies units is irrelevant for the study.

Volumetric samples may refer to sediment from the armor layer, the subarmor, the subsurface, or the vertically unstratified bulk sediment (Fig. 4.1). Because spatially integrated sampling is used for reaches that are relatively homogeneous, or that have small patches, the user needs to evaluate the degree of spatial heterogeneity within the reach. When sampling the armor layer or the vertically unstratified bulk sediment, the surface portion of the sediment to be sampled is visible to the observer. However, when the sampling target is the subarmor or subsurface sediment, its degree of spatial variability can only be inferred from the degree of spatial variability of the surface sediment. Inference is possible based on the observations by Lisle and Hilton (pers. comm. 1998) and Buffington and Montgomery (1999 a and b) that surface and subsurface particle-size distributions are often related in a positive, linear way (Section 6.1.6.2). Fine surface sediment is likely to have fine subsurface sediment beneath, whereas coarse surface sediment is likely to have coarse subsurface sediment. The degree of subsurface homogeneity or heterogeneity, and thus the subsurface sampling scheme cannot be inferred from the surface sediment if a post-flood surface deposit (usually of fines) alters the flood-generated relation between surface and subsurface sediment size.

The following sections explain sampling schemes for spatially integrated volumetric sampling. Sampling schemes should be discussed together with sample-mass requirements because the precision obtained from a given sample mass may differ depending on the sampling scheme applied. Thus, the topic of sample size recurs throughout Sections 6.4 and 6.5.

### 6.4.1 Sampling a truly homogeneous reach

A truly homogeneous sediment deposit has very little or no variability between samples collected at various locations within the reach. Thus, all sampling schemes lead to the same sampling result. The most practical approach to sample a truly homogeneous reach is to collect one or a few unbiased samples that suffice for a predetermined precision requirement at random location(s) within the reach.

Total sample mass required for a homogeneous reach depends on a preset precision requirement, and may be determined from a relation between sample mass and error (e.g., Ferguson and Paola (1997), Fig. 5.22 or Eqs. 5.62 and 5.63 in Section 5.4.3.2). For an assumed normal distribution in terms of  $\phi$ , sample mass for a specified precision depends on the general coarseness of the sediment, the percentile of interest, and most markedly on sediment sorting (Section 5.4.3). Estimates of the  $\phi_{50}$  and the bed material sorting (i.e., the  $\phi_{16}$  and  $\phi_{84}$ ) are obtained from a pilot study. If no particular underlying distribution type can be assumed for the parent distribution, sample mass may be computed from the empirical and mathematically simple recommendations by Church et al. (1987) that are based on the  $D_{max}$  particle size (Section 5.4.1.1). The 0.1% criterion, for example, determines total sample mass  $m_{tot}$  as 1000 times the mass  $m_{D_{max}}$  of the  $D_{max}$  particle. A pilot study then only needs to determine the  $D_{max}$  particle size for the reach. When applied to a normal distribution, the 0.1% criterion provides a precision of at least  $\pm 0.4\phi$  for all percentiles up to the  $D_{95}$ , even for poorly sorted sediment with  $s \leq 2$ . Sample mass can easily amount to hundreds or thousands of kg or more in coarse gravel-bed streams, even if the less stringent 1% criterion of  $m_{tot} = 100 m_{D_{max}}$  is applied.

### 6.4.2 Sampling schemes for spatially integrated sampling of heterogeneous reaches

The statistical precision, as well as the work effort of a sampling study is affected by the spatial patterns with which samples are collected within a reach (Smartt and Grainger 1974). The sampling pattern used for spatially integrated volumetric sampling include: (1) random locations for volumetric samples, (2) volumetric samples at systematic grid points, (3) volumetric samples at random locations within systematic grid cells, and (4) volumetric samples at the grid points of several grid systems overlaying each other (two-step approach) (Fig. 6.1). Application of these sampling schemes to heterogeneous reaches in coarse gravel-bed streams are discussed below.

#### 6.4.2.1 Random sampling locations

Random sampling is appropriate for homogeneous streambed areas in which the location of sampling does not influence the outcome of the sampling result. However, spatial homogeneity is rare in mountain gravel-bed streams. Sampling at random locations is not recommended for heterogeneous reaches. One reason is that the irregular spacing of random sampling may fail to include all stream locations in a representative way. Small facies areas, in particular, are likely to remain unsampled. Thus, random sampling tends to

require more samples than systematic sampling to arrive at the point where further sampling leads only to minor improvements in precision. Analyzing volumetric samples collected on a spatially heterogeneous large gravel bar, Wolcott and Church (1991) found that random sampling resulted in a different particle-size distribution than systematic sampling and required five times more samples for the same sampling precision.

Another reason why random sampling is not recommended in coarse gravel- and cobble-bed streams is that random sampling is not as versatile as systematic sampling. Samples taken at random locations cannot be used for a retroactive delineation of the streambed area into facies units, nor can random samples collected from heterogeneous beds be combined for joint analysis in one large sample (Section 6.4.4.3 and 6.4.4.5). A joint analysis of subsamples in one aggregate sample requires that all samples represent an identical portion of the streambed area. Random samples collected from heterogeneous beds are also not usable to assess the sampling precision in a two-stage approach (see below).

#### 6.4.2.2 Sampling the reach at systematic grid points

When applying a spatially integrated sampling scheme to a heterogeneous reach, a good strategy is to cover the reach by a systematic grid and to collect volumetric samples at each grid intersection. Fig. 6.16 shows an example of a systematic grid that covers the reach with 360 grid points. Sampling a heterogeneous reach at systematic grid points ensures that all areas in the reach are representatively included in the sample.

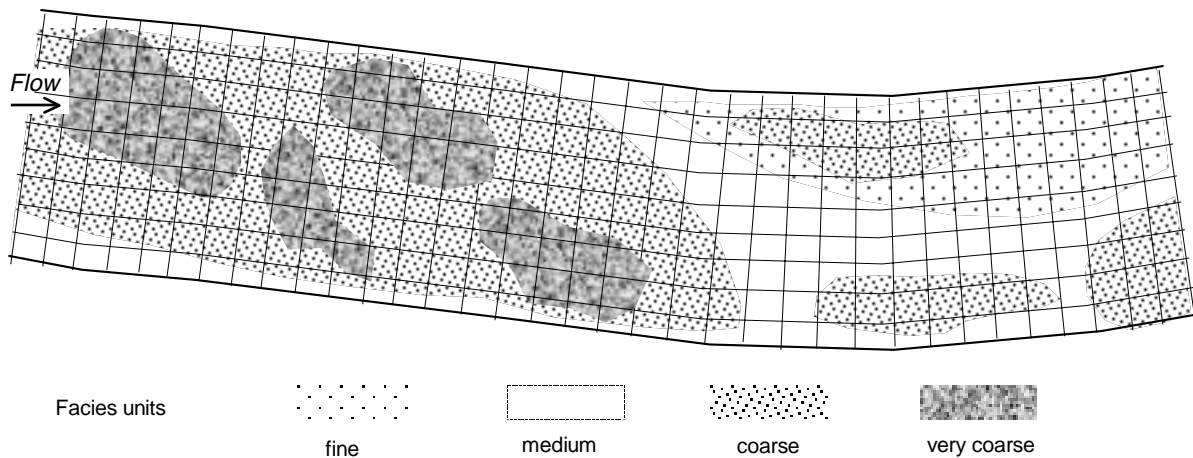


Fig. 6.16: Spatially integrated volumetric sampling (reach-averaged sampling) of a heterogeneous reach with small sedimentary units at grid points. A grid with 360 points or 324 grid cells covers the reach.

However, systematic sampling may not correctly represent sediment from units that are smaller than the grid size. Small sediment units are underrepresented if no grid points falls into that area and overrepresented if a grid point happens to fall within the area.

Misrepresentation can be avoided by choosing a grid spacing to match the smallest sampling units on the bed.

### 6.4.2.3 Random placement of sampling locations within grid cells

In a stream reach with linear structural streambed elements, such as transverse ribs, berms, or sand-filled micro-channels, some randomization in sample placement is preferable to a strict placement at grid points. Randomization avoids sample locations that align with linear bed elements. A moderate randomization of sampling locations can be achieved by sampling at a random location within the area outlined by regularly-shaped and even-sized cells (Fig. 6.17) (Wolcott and Church 1991). The outline of cells does not need to correspond to the boundaries of sedimentary or geomorphological units. Random placement of sampling locations into very large grid cells approaches the outcome of random sampling (Section 6.4.2.1). Thus, the cell size should not be too large. It is also possible to introduce more regularity into the sample point location by using algorithms. An example is to place the sample locations of the first row of cells at an equal distance  $x_1$  from the left boundary of all cells in row 1. Likewise, all sampling locations for the second row of cells are placed at an equal distance  $x_2$  from the left cell borders. The y-coordinate of the sampling locations is determined accordingly. All sampling locations in the first column of cells are placed at an equal distance  $y_1$  from the top of the cells, and at an equal distance  $y_2$  from the top for all cells in the second column (Smartt and Grainger 1974).

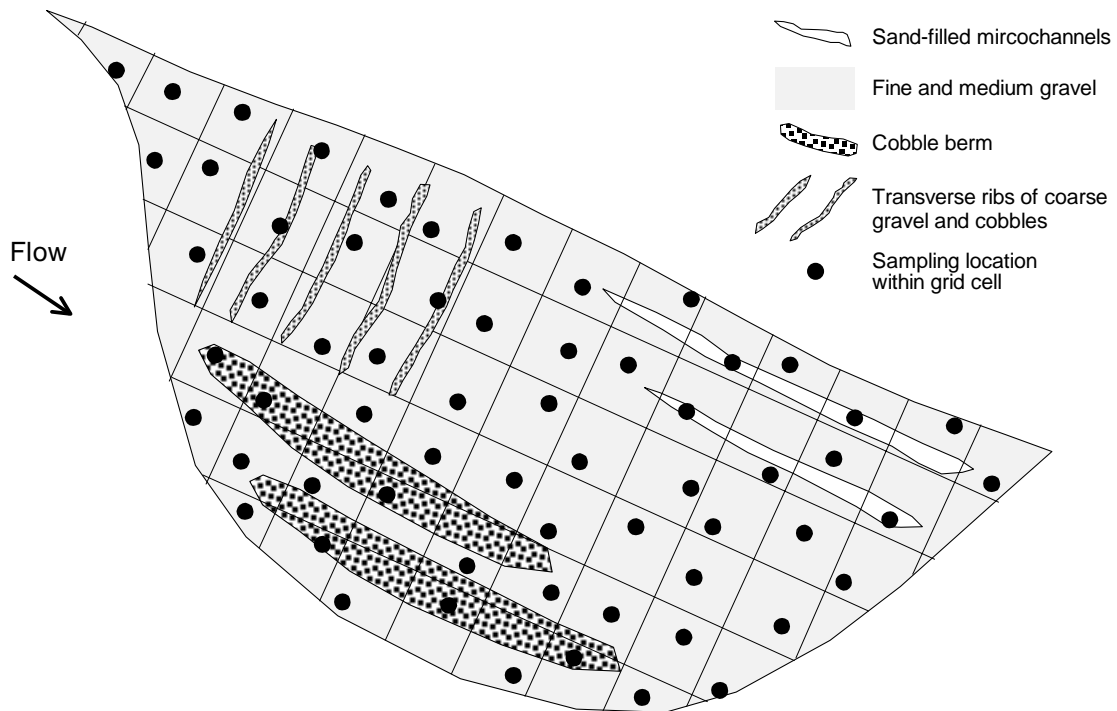


Fig. 6.17: Sampling at random locations within systematic grid cells.

If linear bed features are absent, Wolcott and Church (1991) found that sampling at systematic grid points and sampling at random locations within the same number of systematic cells produced similar reach-averaged particle-size distributions with similar sampling precision.

#### 6.4.2.4 Two-stage sampling using overlaying grid systems or a small grid pattern

Two-stage sampling is used to compute the statistical difference or precision between repetitive samples collected from the same population (Sections 5.4.2.1 and 6.4.4.4). For spatially integrated sampling on a heterogeneous bed, the requirement that all samples come from the same population means that each sample should represent the same degree of spatial variability. This demand is best achieved by sampling the reach using several grid systems, each with the same size and spacing, but each slightly shifted in position against the other grids. The sample grid systems may be laid out and sampled sequentially until a desired sampling precision has been attained. A more efficient alternative may be to use a pilot study to estimate the number of repeated samples needed to obtain a preset precision. If, for example, the pilot study suggested that each volumetric sample collected from 200 grid points should be repeated about 5 times, repetitions can be performed by laying out a small grid pattern of 1,000 points from the start. Individual samples are then allocated either randomly or systematically into one of five sets. Care must be taken to avoid any systematic difference between subsamples, which may occur when a streambed shows fining or coarsening towards one bank or in a downstream direction.

#### **6.4.3 Number of sampling points for systematic samples of heterogeneous reaches**

After the patterns for spatially integrated sampling have been determined, the user needs to determine four factors that relate to sample mass:

1. Number of sampling points in the reach (Sections 6.4.3.1 and 6.4.3.2) ,
2. Mass of sediment to be collected at each sampling location
3. Total mass of sediment to be collected in the reach, and } Sections 6.4.4.1 - 6.4.4.3)
4. Number of replications of the total sample (Section 6.4.4.4).

The number of samples required for an accurate characterization of the particle-size distribution in the reach depends on the degree of spatial variability within the reach. Purely statistical criteria may be applied to compute this number when sampling a large area in a dry streambed (e.g., 160 m by 1,000 m or 400 m by 400 m) where the resulting number of sampling locations may amount to 100 or more. Geometrical and ecological criteria need to be considered in smaller streams. When sampling in a mountain stream 10 m wide with most of the bed inundated by flow, sampling space becomes not only restricted from a geometrical standpoint, but also from an ecological one.

### 6.4.3.1 Large streams, no space limitation

Based on their study on a large and heterogeneous gravel bar of approximately 160,000 m<sup>2</sup>, Wolcott and Church (1991) suggested that 100 to 300 samples collected from even-spaced sampling points may be appropriate for an unbiased particle-size estimate of reach-averaged subsurface sediment in many gravel-bed rivers. The number of sampling locations can be determined for a specified reach by collecting a number of subsamples. The standard deviation of the subsample mean  $s_{Dm}$  is then computed for an increasing number of subsamples ( $n_2$  to  $n_{tot}$ ) and plotted. As the number of subsamples increases, the standard deviation of the subsample means decreases. Ideally, the plotted relation of standard deviation versus sample size follows the function  $s_{Dm} = f(1/\sqrt{n})$ . The graph of this curve decreases steeply for small sample sizes and flattens for larger sample sizes (Fig. 6.18 and Section 5.4.2.2; Figs. 5.10 and 5.11 in Section 5.2.3.4). At some position along the curve there is a point at which a further increase in the number of samples does not significantly improve the sampling precision. This point defines the number of samples  $n_{opt}$  needed to characterize the reach as the optimum trade off between sampling effort and sampling precision.

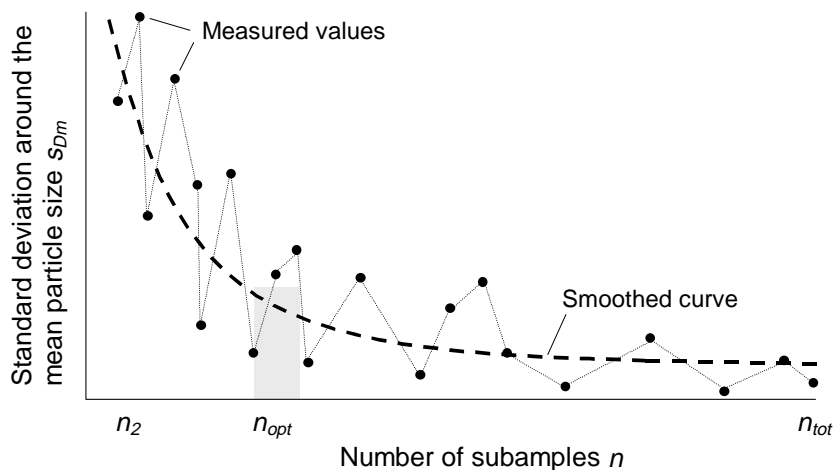


Fig. 6.18: Decrease of the standard deviation of the mean particle size  $s_{Dm}$  for subsamples increasing in number from  $n_2$  to  $n_{tot}$ .  $n_{opt}$  is the sample size at which a further increase in sample size does not lead to a further significant increase in sampling precision and the optimal sample size in the trade-off between precision and work effort.

When performing an analysis with only one data set, the resulting curve is likely to be jagged (Fig. 6.18). A smooth curve is only obtained if the standard deviation for each subsample size is computed for a large number (approximately 50 - 200) of repeated subsamples. This number of repetitions is only practical with computer sampling. When using only one data set, the user might want to fit a regression curve through the data points to better visualize the optimal number of samples for a reach (Section 5.4.2.2). However, the smoothed curve indicates an unduly high precision.

#### 6.4.3.2 Small streams, space limitation for sampling

Another aspect to consider when determining the grid size for spatially integrated sampling is the areal extent of each volumetric sample in relation to the size of the reach. Assume a mountain stream with most of the streambed inundated by flow and that volumetric samples are collected with the plywood shield (Section 4.2.4.7). Each sample then covers (and disturbs) a streambed area of approximately  $0.5 \text{ m}^2$ . If such samples were spaced 5 m apart in a stream 10 m wide, and the reach was 50 m long, 20 samples could be collected per reach. The combined area of all samples is 2% of the reach ( $10 \text{ m}^2$  of  $500 \text{ m}^2$ ). With respect to statistical precision, 20 samples may be low. From an ecological standpoint, the damage caused by 20 samples may be high. The user must decide where to place the emphasis.

#### **6.4.4 Subsample mass at each grid location and total sample mass within the reach**

The mass of individual samples taken within the reach may be computed using either an empirical or an analytical approach. The empirical approach presented by Wolcott and Church (1991) makes no assumptions regarding the bed-material distribution-type and is based on the sample mass criteria by Church et al. (1987) (Fig. 5.14 in Section 5.4.1.1). Ferguson and Paola (1997) present an analytical approach that assumes that the bed material follows a normal distribution in terms of  $\phi$ -units. The analytical approach allows computing sample mass for a specified level of precision around a given percentile (Fig. 5.22 or Eq. 5.62), but requires prior knowledge of at least one percentile of the distribution and the sorting coefficient of the bed through a pilot study.

##### 6.4.4.1 Full sample at each grid location in well sorted, fine to medium gravel beds

One means for determining the sample mass needed for an unbiased sample (Fig. 5.14) or for a preset precision requirement (Fig. 5.22) is to select a stream location that best represents the average particle-size distribution of the bed. Sample mass that satisfies a predetermined precision is then computed for that location and collected at each of the 100 or so grid locations within the reach. Collection of “full” samples at all grid points may be feasible in streams with fine gravel where a kg of sediment is adequate for a specified precision, but not for poorly sorted gravel-bed streams.

##### 6.4.4.2 Reduction of sample mass at each grid location in poorly sorted gravel- and cobble beds

When sampling in poorly sorted, coarse gravel- or cobble-bed streams, the mass required for a single sample alone can amount to hundreds or thousands of kg (Fig. 5.14 or Fig. 5.22). If such a sample is collected at each of the 100 or so grid points per reach, the total mass of sediment collected in a reach approaches several tens or hundreds of tons, a mass

that is usually impossible to collect, particularly in mountain gravel-bed streams. In order to facilitate collection of a manageable sediment sample, the sample mass needs to be reduced. To the extent possible, the reduction needs to be carried out such that the total sample mass collected remains statistically meaningful. Reducing the number of grid points is not recommended because this may lead to unrepresentative samples of the various facies in the reach. A better approach is to reduce the sample mass collected at each sampling point. Several approaches may be used.

1. Exclusion of the largest particle sizes from the analysis (truncation at the coarse end, Section 5.4.1.4, acceptable and even recommended by some if the study focuses on fines),
2. Acceptance of a larger error (see discussion of sample size, e.g., Fig. 5.22 in Section 5.4.3.2),
3. Limitation of the analysis to the  $D_{50}$  particle-size for which fewer sample are requirement than for higher or lower percentiles; see Fig. 5.22 in Section 5.4.3.2), and
4. Collection of individually small samples (grab samples) that are combined to one composite sample that is then statistically unbiased and “accurate”.

Approaches 1 - 3 have been already been discussed. The mass of the individually small samples (Approach 4) can be computed based on either empirical sample-mass recommendations (Section 6.4.4.3) or analytically (6.4.4.5). Both approaches may yield a different grab sample mass.

#### 6.4.4.3 Individually biased grab samples, empirical approach

Instead of collecting large and statistically valid samples at each grid location, Wolcott and Church (1991) proposed collection of individually small grab samples while maintaining the number of sampling locations. The reduction of sample mass at each grid location is justified on the basis of two arguments. (1) If the entire reach is sampled at regular grid points (Section 6.4.2.2) or at random locations within regular grid cells (Section 6.4.2.3), each sample represents the same fraction of the total sampling area. Since all samples represent an area of the same size, all particles collected in a reach may be combined into one large sample for joint sieving to obtain a reach-averaged particle-size. (2) If all volumetric samples are reduced by an equal amount, the sample mass per grid point may be substantially reduced to the size of a grab sample and still remain unbiased with respect to total sample mass. Based on the empirical 1%-criterion by Church et al. (1987), that makes no assumptions about the underlying distribution type, Wolcott and Church (1991) recommend the following two sample mass criteria for determining the grab sample mass:

1. Each grab sample must encompass at least 1% of the total sample mass required for an unbiased sample of the entire reach.
2. Each grab sample must be at least as large as the mass of the largest particle present in the reach ( $D_{max}$ ) to ensure a potentially equal mass of all grab samples. The sampling device used must not hinder collecting a particle of near  $D_{max}$  size.

**Example 6.4:**

A pilot study has estimated a subsurface  $D_{max}$  particle size to be 256 mm, which is approximately the  $D_{99}$  particle size of a sediment with a  $D_{50}$  of 22.6 mm and a sorting of  $s = 1.5$ . A spherical or ellipsoidal quartz ( $\rho_s = 2.65 \text{ g/cm}^3$ ) particle with a  $b$ -axis length of 256 mm has a mass  $m_p$  of approximately 23 kg ( $m_p = \pi/6 \cdot b^3 \cdot \rho_s$ ).

Each grab sample should have a mass of at least 23 kg, the mass of the  $D_{max}$  particle in order to give each grab sample the chance to contain at least one  $D_{max}$  particle. 23 kg of sediment fills a heaping household pail.

If the  $D_{max}$  particle mass is not to exceed 1% of the total sample mass (1% criterion for coarse gravel beds, Section 5.4.1.1), total sample mass allotted to a 100-point grid system is  $100 \cdot 23 \text{ kg} = 2,300 \text{ kg}$  ( $\approx 1.2 \text{ m}^3$  or 12 cubic feet). If 200 samples are needed to cover the spatial variability of the reach, total sample mass is  $200 \cdot 23 \text{ kg} = 4,600 \text{ kg}$ .

Assume, a two-stage approach (see next heading) determined that the 200 grab samples need to be repeated 5 times to arrive at an acceptable level of precision, total sample mass for the reach is  $5 \cdot 4,600 \text{ kg} = 23,000 \text{ kg}$ . Results of these computations are presented for three  $D_{99}$  particle sizes in Table 6.6.

Table 6.6: Grab sample mass  $m_{ss}$  (kg) suggested by Wolcott and Church (1991) according to the 1% criterion by Church et al. (1987):  $m_{ss} = m_{D_{max}}$ . 200 grab samples are collected in the reach, amounting to a sample size of 200  $m_{ss}$ . Five repetitions yield a total sample mass of  $m_{tot} = 1,000 m_{ss}$  for the reach.

Particles size of $D_{max}$ or $D_{99}$ (mm)	Grab sample mass $m_{ss}$ (kg)	Combined mass for 200 grid points (200 $m_{ss}$ ) (kg)	Total sample mass for 5 · 200 grid points (1,000 $m_{ss}$ ) (kg)
114	2.0	412	2,060
225	23	4,600	23,000
572	260	52,000	260,000

The sample mass required for one grab sample may exceed the capacity of the sampling device which is a few kg for a pipe sampler (Section 4.2.4.5), and nearly 50 kg for a barrel sampler (Section 4.2.4.6). In this case, a larger sampling device should be used, such as the plywood shields (Section 4.2.4.7). If several physical samples must be combined to obtain one grab sample, care must be taken that the device facilitates collecting a particle of  $D_{max}$  size. Truncation of the sample at a certain large particle size (Section 5.4.1.4) may be unavoidable.

#### 6.4.4.4 Determining sampling precision from two-stage sampling with overlaying grid systems

When taking individually small grab samples, information on sampling precision is obtained from a two-stage sampling procedure that compares several repetitions of the combined sample from the reach (Sections 5.4.2.1, 5.4.2.2 and 6.4.2.4).

##### Example 6.5:

The study objective is to determine the  $D_{50}$  particle size to a precision of  $\pm 20\%$ . The number of sampling locations was estimated at 50. Five sets of 50 grab samples of 40 kg each were collected and jointly sieved. The five values of the  $D_{50}$  particle size are 60, 70, 80, 90, and 100, mm with a mean  $D_{50m}$  of 80 mm, and a standard deviation  $s_{D84}$  of 15.8 mm. The precision of those 5 samples may be computed either with the general sample size equation (Eq. 5.13 for absolute error) or with the equation given below for relative error. The  $t$ -value for  $n = 5$  is 2.78 (Table 5.2).

$$n = \left( \frac{t_{1-\alpha/2;n-1} \cdot CV}{e\%} \right)^2 = \left( \frac{t_{1-\alpha/2;n-1} \cdot s_{50}}{e\% \cdot D_{50m}} \right)^2$$
$$= \left( \frac{2.78 \cdot 15.8}{0.2 \cdot 80} \right)^2 = 7.5 \cong 8$$

Since the computed sample size of 7.5 is smaller than 5, the computation is repeated with a  $t$ -value for  $6 = 2.57$ , yielding  $n = 6.4$ . Another iteration is not necessary, because even if a  $t$ -value for 6.2 was used and yielded a result close to  $n = 6.2$ , sample size is usually rounded up to the next integer value, which is 7. Total grab sample mass necessary to estimate the  $D_{50}$  particle size to a precision of  $\pm 20\%$  amounts to  $7 \cdot 50 \cdot 40 \text{ kg} = 14 \text{ metric tons}$ , or ca.  $7 \text{ m}^3$ .

#### 6.4.4.5 Individually unbiased subsamples for assumed normal distributions

The sample mass for individual grab samples determined in Section 6.4.4.3 and Example 6.4 ( $m_{ss} = m_{Dmax}$ , and  $m_{ss} = m_{tot} / 100$ ) was geared towards creating a total sample that is unbiased towards the  $D_{max}$  or  $D_{99}$  particle size. This sample-mass computation is free of any assumptions of an underlying distribution type. Table 6.6 illustrates that the total sample mass amounts to tons and hundreds of tons when the  $D_{max}$  particle size is in the boulder range. The sample mass for grab samples can be smaller than computed in Table 6.6 and Example 6.4, if the sampling objective requires an accurate determination of the  $D_{50}$  particle sizes only, and if a pilot study revealed that a normal distribution of particle sizes in  $\phi$  units might be assumed.

For underlying normal distributions, Ferguson and Paola (1997) provide a sample mass equation that provides bias avoidance for specified percentiles. If the study objective is to determine the  $D_{50}$  size, bias only needs to be avoided in the  $D_{50}$  particles size and the subsample mass can be accordingly small. By contrast, if the reach-averaged  $D_{95}$  is of interest, each subsample should be sufficiently large to satisfy the criterion for an unbiased  $D_{95}$  particle size. The subsample mass for bias avoidance and the total sample mass required for the reach is computed in Table 6.7 for three particle-size distributions. Each of the distributions has a  $D_{50}$  of 22.6 mm, but the sorting coefficients are 1, 1.5, and 2  $\phi$ , so that the  $D_{84}$ ,  $D_{95}$ , and  $D_{99}$  particle sizes are different for each of the three distributions. Collecting individually unbiased samples has the advantage that samples may be compared among themselves and may be used for retroactively delineating facies units (Crowder and Diplas 1997, Section 6.3.2.3).

Table 6.7: Three normal particle-size distributions (in  $\phi$ ) with equal  $D_{50}$  particle sizes of 22.6 mm, but sorting coefficients of  $s = 1, 1.5$  and 2. Total sample mass ( $m_{tot}$ , kg) required for a tolerable absolute error of  $\pm 0.3 \phi$  for the  $D_{50}$ ,  $D_{84}$ ,  $D_{95}$ , and  $D_{99}$  particle size as well as the subsample mass necessary for bias avoidance in the  $D_{50}$ ,  $D_{84}$ ,  $D_{95}$ , and  $D_{99}$ . Number of sampling points is computed from the ratio  $m_{tot}/m_{ss}$ .

Per- cent- tile	Particle size (mm)*			Total sample mass $m_{tot}$ (kg) for acceptable absolute error $\pm 0.3 \phi$ #			Subsample mass $m_{ss}$ (kg) required for bias avoidance§			Number of sampling points $m_{tot}/m_{ss}$ for		
	$s = 1$	$s = 1.5$	$s = 2$	$s = 1$	$s = 1.5$	$s = 2$	$s = 1$	$s = 1.5$	$s = 2$	$s = 1$	$s = 1.5$	$s = 2$
$D_{50}$	22.6	22.6	22.6	18	99	336	0.32	0.48	0.64	58	207	525
$D_{84}$	45	64	90	146	2.24 t	19.2 t	2.6	10.4	38	57	215	526
$D_{95}$	71	125	221	528	17.6 t	304 t	9.9	80.0	592	54	220	513
$D_{99}$	114	255	572	2.24 t	136 t	5,100 t	40	670	9.9 t	56	203	515

\* Computed from Eq. 5.58 in Sect. 5.4.3. # Values read off and determined from Fig. 5.22 b in Section 5.4.3.2. § Values read off and determined from Fig. 5.20 and Eq. 5.60 in Section 5.4.3.1.

#### 6.4.4.6 Comparison of subsample masses and total sample mass computed with two different approaches

The grab-sample mass computed by Wolcott and Church (1991) (Table 6.6) for bias avoidance of the  $D_{99}$  particle size of the total sample is sufficient to avoid bias in the  $D_{90}$  particle size when applied to subsamples from normally distributed deposits (Table 6.7). The total sample mass computed by Wolcott and Church (1991) (Table 6.6) which assumed the necessity of 200 grid points and 5 repetitions of the 200-grid (a total of 1,000 grid points) suffices for a  $\pm 0.3 \phi$  precision of approximately the  $D_{95}$  particle size. Thus, both approaches yield comparable results for high percentiles in the  $D_{90}$  to  $D_{95}$  region.

The approach by Ferguson and Paola (1997) determines a much smaller subsample mass when central percentiles are the focus of the study. If the  $D_{50}$  or the  $D_{84}$  are the only percentiles of interest, subsample mass may be reduced to 0.6 or 38 kg (Table 6.7), if a deposit sorting of  $s = 2$  and a normal distribution are assumed. This is a substantial

reduction of sample mass compared to a subsample mass of 260 kg for a deposit with a  $D_{max}$  particle size of 572 mm (Table 6.6).

#### 6.4.4.7 Retroactive computation of the number of sampling points

In the approach by Ferguson and Paola (1997) shown in Table 6.7, the number of sampling points per reach may be computed retroactively from the ratio of the total sample mass  $m_{tot}$  required for a sampling precision of  $0.3 \phi$  around a specified percentile and the subsample mass for bias avoidance  $m_{ss}$ . The ratio of the two independently determined parameters  $m_{tot}/m_{ss}$  ranges from approximately 55 for a sorting coefficient of  $s = 1$ , to 210 for  $s = 1.5$ , and to approximately 520 for  $s = 2$ . These values are similar to the sampling point numbers of 100 - 300 suggested by Wolcott and Church (1991). While the approach by Wolcott and Church (1991) points out that the number of sampling locations depends on the degree of spatial heterogeneity of the reach, results by Ferguson and Paola (1997) point out that the number of grid points strongly increases with the degree of bed-material sorting.

#### 6.4.4.8 Problems with collecting large samples in coarse gravel and cobble-bed streams

The total mass of all volumetric samples per reach can become very large. One reason for this is that heterogeneous beds require many samples to characterize a reach (Table 6.6 and 6.7). Other reasons are that individual samples become large due to a large percentile of interest, poor sorting of the bed, or a large  $D_{50}$  size. Sampling large masses not only requires heavy equipment, but is also restricted to large streams where gravel extraction of this magnitude does not result in severe environmental damage. When sampling in mountain gravel-bed streams, collecting large sample masses is often neither feasible, nor ecologically responsible. Statistical measures (e.g., truncation at the coarse end, acceptance of a larger error, limitation of analysis to the  $D_{50}$  size) help to reduce the huge sample mass. Logistical measures (e.g., sieving and analyzing the coarse portion of the sediment in the field, splitting the sample (preferably in the field) and retaining only a fraction of the medium and fine gravel and sand for laboratory analysis) improve the manageability of large sample masses (Section 2.1.3.8 - 2.1.3.10).

#### 6.4.4.9 Computation of the reach-averaged particle-size distribution

To compute the reach-averaged particle-size distribution, each subsample is sieved individually and a particle-size distribution is computed. The reach-averaged particle-size distribution is obtained from the arithmetic mean weight frequencies or percentage frequencies per particle-size class of all individual samples. This approach is mathematically identical to lumping all individual samples together for joint sieving. However, joint sieving loses all information on spatial variability. The computation of a reach-averaged percentile particle size from the mean percentile particle-size of all individual samples is not recommended and is only an option if all individual samples are

sufficiently large to be unbiased. Areal weighting is not required because each subsample represents an equal fraction of the streambed area.

## **6.5 Spatially segregated volumetric sampling (sampling each unit individually)**

For spatially segregated volumetric sampling, the reach is delineated into geomorphological units (e.g., bars, riffles, pools) (Section 6.3.1), sedimentary units (e.g., fine, medium and coarse facies) (Section 6.3.2), aquatic habitat units (e.g., areas with particular flow conditions and/or substrate), or any other stream units of interest. Depending on the study objective, sampling may be restricted to one unit that is of specific concern, to all units of a certain type, to some representative units of a type, or to all units within a reach.

Spatially segregated volumetric sampling may be applied for sampling the armor layer, the subsurface, or the vertically unstratified bulk sediment. Determining appropriate sampling schemes and sample masses has been previously discussed.

### **6.5.1 Geomorphologically stratified sampling**

Geomorphologically stratified sampling is usually used to characterize the particle-size distribution of a geomorphological unit. The geomorphological unit most commonly sampled by volumetric samples is the riffle. Samples collected from bars or pools usually focus on a particular location within the unit (e.g., the bar head), or on a particular kind of sediment (e.g., fine sediment only, or coarsest clasts only) (Sections 6.6.1 and 6.6.2).

Geomorphologically stratified sampling is not a recommended strategy for characterizing the reach-averaged bed-material size because the number and mass of subsamples required is much larger than would be the case when sampling the reach stratified into sedimentary units. This aspect is discussed in more detail in Section 6.5.2.1.

#### **6.5.1.1 Sampling on riffles only**

Information on subarmor or subsurface sediment size on riffles is important for a variety of studies. The percentage of subsurface fines, for example, is part of the evaluation of fish spawning habitat because subsurface fines can decrease the spawning success of salmonid fish (Bjornn and Reiser 1991). Watershed monitoring studies use changes in the percentage of riffle subsurface fines over time as an indication of changes in land use practices and sediment production.

Riffles that are sampled in such studies should be representative of the reach. Riffles that are considerably coarser than the reach should be avoided. Coarse riffles may result from large rockfall particles being incorporated in the riffle but not in the remainder of the

reach. Riffles that are unusually fine should also be avoided. Fine riffles can result when imbrication and particle interlocking provide the stability that would otherwise be provided by the presence of large particles (Sections 6.3.1.3, 3.2.2.2 and 3.2.2.3). Sampling should be repeated over several riffles in order to average out local effects.

Note that neither the riffle subsurface sediment, nor the armor layer, nor the vertically unstratified bulk sediment is automatically representative of the average subsurface particle-size distribution of the reach. For example, fine sediment entering the reach is not necessarily stored in the subsurface of the riffle if the stream reach contains backwater areas or pools that are more likely to be storage places for fines. If typical storage features are absent, more fines may be stored in the riffle subsurface sediment than would be if backwater areas and pools were available for storing fine sediment. Thus, the riffle subsurface sediment is not necessarily representative of the fine sediment supply to the reach. The supply of fine sediment is better determined from collecting subsurface sediment from the entire reach (Section 6.5.2.1) or from spatially focused sampling of fine sediment in pools (Section 6.6.2).

#### 6.5.1.2 Sampling patterns and sample mass for riffle samples

If the study objective focuses on an analysis of the riffle subsurface (or armor, or bulk) sediment, volumetric samples should be collected from the entire riffle either in a grid pattern (Section 6.4.2.2) or from random locations within even-spaced and even-sized cells (Section 6.4.2.3). The number of samples to be collected on the riffle depends on the spatial variability of the riffle subsurface sediment which is unknown but assumed to be similar to the spatial variability of the surface sediment (Section 6.4). The mass for each individual sample depends on the sorting of the subsurface riffle sediment, the percentile in question, and the particulars of the sampling goal (Section 6.4.4).

The user has a choice between collecting full samples, grab samples, or individually unbiased samples at each grid point. The first option may yield a large total sediment mass and is only feasible if either the number of samples is small, or when the sediment on the riffle is fine to medium gravel (Section 6.4.4.1). Grab samples are obtained in coarse gravel-beds when no particular type of particle-size distribution is assumed, and if obtaining an unbiased sample for the riffle sediment in general is the study objective (Section 6.4.4.3). The number of sampling points for grab samples should be determined from a precision analysis similar to that in Fig. 6.18 (Section 6.4.3.1). A two-stage sampling approach may be used to compute the sampling precision (Section 6.4.4.4). If, for example, a barrel sampler provides a sample mass of approximately 50 kg each, the user may begin by collecting 3 - 5 samples on the riffle. The samples are repeated 3 - 4 times at slightly shifted locations to yield a total of 9 to 20 samples weighing a total of 450 - 1000 kg. Rood and Church (1994) used a hybrid sampler (Section 4.2.4.10) that collects about 13 kg per sample. They found that about 30 - 50 samples were necessary to detect a 10% change in the percent subsurface fines on an individual riffle if particles larger than 32 mm were present. A sample mass of approximately 1 ton may be logistically or ecologically unfeasible. The user needs to either accept a higher tolerable error for

detecting a change in subsurface fines, or the samples collected must be truncated at some large particle size in order to reduce the mass of individual samples (Section 5.4.1.4).

If the particle-size distribution in the bed can be assumed to be normal, and the sediment sorting is known from a pilot study, the user may collect samples that are individually unbiased (Section 6.4.4.5). Individually unbiased samples tend to produce a higher total sample mass than the grab-sample approach if the sample is unbiased with respect of the  $D_{95}$  and higher percentiles. The total mass of individually unbiased subsamples is lower if central percentiles are of concern and sample size only needs to avoid bias in particle sizes between the  $D_{50}$  and the  $D_{84}$  (Tables 6.6 and 6.7). The total sample mass required for the reach is determined for a specified precision around a specified percentile. The number of samples per reach is the ratio between the mass of the total sample and an individual sample (Section 6.4.4.7). The number increases with the sorting of the bed material.

## 6.5.2 Sedimentary stratified sampling

Sedimentary stratified volumetric sampling is used to describe the reach-averaged particle size-distribution of the armor, the subarmor (or subsurface) and the unstratified bulk sediment (Section 6.5.2.1). Another use of sedimentary stratified volumetric sampling is to determine the reach-averaged subsurface  $D_{50}$  size (Section 6.5.2.2). The ratio of surface sediment size to the size of subsurface sediment ( $D_{50surf}/D_{50sub}$ ) is an important tool for watershed monitoring and sediment transport analysis.

The ratio of the surface sediment size to the size of the fine mode of bedload, or to the size of pool fines, is also used for analysis. These ratios may be used to determine whether bedload transport is supply- or transport limited (Dietrich et al. 1989; 1993; Lisle et al. 1993; Lisle 1995; Lisle and Hilton 1992, 1996, 1999; Buffington and Montgomery 1999 a, b, and c). A value close to 1 for the ratio  $D_{50surf}/D_{50sub}$  indicates high sediment supply, while values larger than 1 indicate low sediment supply. Subsurface sediment size is also used as an estimate of the particle-size distribution for bedload transport. Subsurface is similar in size to bedload in aggrading streams, but in degrading streams, subsurface sediment is coarser than bedload (Lisle 1995). Surface and subsurface sediment are often related in size, such that coarse surfaces have coarse subsurface sediment. In reaches where this relation is true, it is possible to segregate the reach for subsurface sampling based on the sedimentary textures visible on the surface (Section 6.4).

### 6.5.2.1 Reach-averaged information on subsurface, armor, or bulk sediment size

Sedimentary stratified sampling is recommended for computing the reach-averaged bed-material size in heterogeneous reaches because sedimentary units are more homogeneous and better sorted than either geomorphological units or the reach as a whole.

Consequently, each sedimentary unit requires a smaller total sample mass for a specified precision than does sampling from a geomorphological unit, or the reach as a whole.

**Sampling schemes for spatially segregated sampling on sedimentary units**

Several sampling schemes may be applied for spatially segregated sampling of sedimentary units. The patterns with which volumetric samples are collected depend on the size of both the reach and its sedimentary units, and on how dispersed the sedimentary units are within the reach (patchiness). The sampling patterns are summarized in Table 6.8.

Table 6.8: Approaches for spatially segregated sampling of sedimentary units for reach-averaged information on sediment size.

Sampling situation	Sampling approach
1. Small reach, few sedimentary units	An appropriate number of sampling locations is distributed evenly over each of the units.
2. Large units within large reaches	Samples are collected from representative locations within each of the sedimentary units.
3. Each sedimentary unit occurs multiple times (patchiness)	Samples are collected from a few patches that are representative for a given facies type.
4. Study objective restricted to surface and subsurface $D_{50}$ particle size	Samples are collected at locations at which the local surface $D_{50}$ is equal to the reach-averaged surface $D_{50}$ particle size (Section 6.5.2.2).

Situation 1: A reach that has only a few sedimentary units that are mostly contiguous and of approximately equal size may be sampled by collecting several subsamples from all sedimentary units either at grid points or from within grid cells (Fig. 6.19). This situation is most likely encountered in small B- and C-type (mountain) gravel-bed streams with plane-bed and riffle-pool morphology (Sections 1.3.1. and 1.3.2).

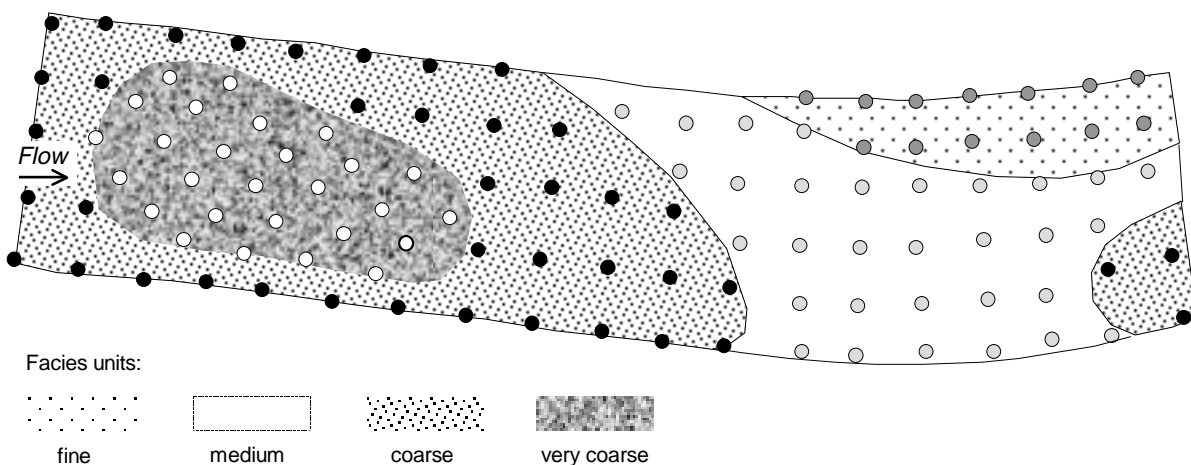


Fig. 6.19: Sampling a reach with only a few and mostly contiguous sedimentary units of approximately equal size by collecting samples from all sedimentary units using reach-spanning grid points.

Situation 2: If the sedimentary units are large and in large streams, samples may be collected from a few representative locations within each unit (Fig. 6.20). The selection of representative units for sampling allows the user to avoid an obviously unrepresentative location simply because it happens to lie under a grid point. This approach is termed *judgement sampling* (e.g., Gilbert 1987). Judgement sampling can improve the sampling results. However, note that sound judgement requires extensive experience, and that judgement may vary between operators, particularly if operators have different backgrounds or levels of training.

Situation 3: Judgement in selection of sampling locations is also required when the reach is comprised of numerous small sedimentary units so that each facies occurs multiple times (patchiness). The number of units may be too large to sample each unit individually. In this case, the user should select a few units that are representative of a specific facies and collect samples only from those units (Fig. 6.20). Situation 2 and 3 may occur together, particularly in braided streams or in gravel-bed streams that carry a large amount of sand and fine gravel.

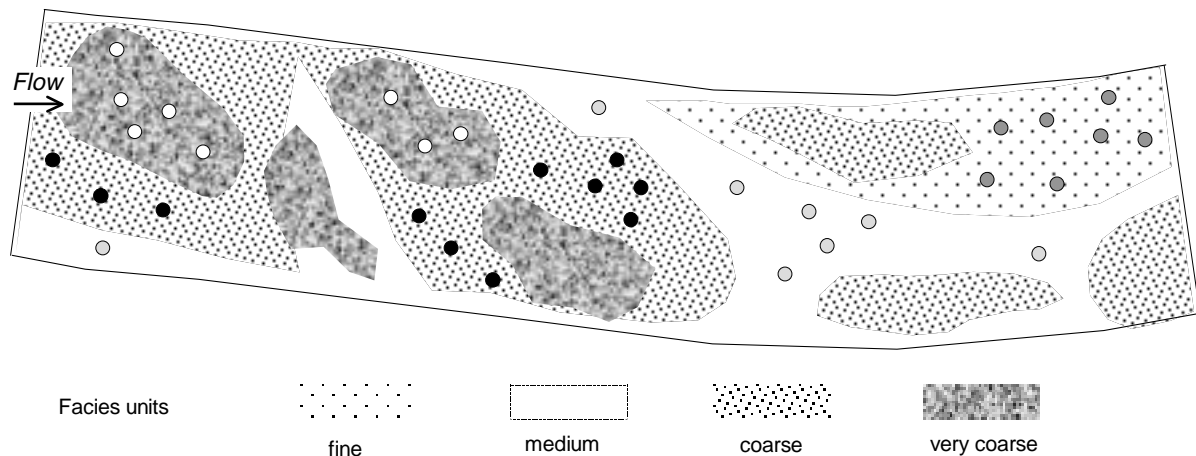


Fig. 6.20: For a reach in which a specified facies type occurs multiple times, samples are not collected from all facies of a kind, but from a few representative locations within the sedimentary units. Obviously unrepresentative locations are avoided.

Situation 4: Sampling from only one selected unit that is representative of the reach-averaged  $D_{50}$  surface or subsurface particle entire reach is discussed in Section 6.5.2.2.

### ***Sample mass for spatially segregated sampling and comparison with spatially integrated sampling***

The mass of each individual sample should be sufficiently large to qualify as a grab sample when no assumption about the underlying particle-size distribution is made (Section

6.4.4.3). If the distribution in  $\phi$ -units can be assumed to be near-normal, sample mass needs to be large enough to avoid bias with respect to a specified percentile (Section 6.4.4.5). The total sample mass is determined by the optimum number of grab samples in excess of which further sampling does not significantly improve the sampling precision (Fig. 6.18, Section 6.4.3.1). When sampling individually unbiased subsamples, total sample mass for each sedimentary unit is determined for a predetermined acceptable percentile error from Figs. 5.22 a-c. The number of individually unbiased subsamples per unit is the quotient of total sample mass to the mass of individually unbiased subsamples.

Example 6.6 demonstrates how sedimentary stratified sampling of a reach can substantially decrease the sample mass compared to the sample mass needed for spatially integrative sampling.

Example 6.6:

Assume a reach had three sedimentary units A, B, and C each with a sorting coefficient of  $s = 1$ , and a  $D_{50}$  particle size of 16, 22.6, and 32 mm, respectively. Sample mass for characterizing each unit with an acceptable error of  $\pm 0.3 \phi$  units is 6.6 kg, 18 kg, and 52 kg (Table 6.9) and sums to 77 kg for the entire reach (upper, shaded part of last column).

Table 6.9: Sample mass (kg) for bias avoidance around the  $D_{50}$ ,  $D_{84}$ , and  $D_{95}$  in individual samples and total sample mass for a tolerable absolute error of  $\pm 0.3 \phi$  for subsurface bed material from three sedimentary units with  $D_{50}$  particle sizes of 16, 22.6, and 32 mm, respectively. Computations are done for sorting coefficients of  $s = 1$  and  $s = 2$ . Sample mass for bias avoidance computed from Fig. 5.20; Total sample mass computed from Fig. 5.22 b (Section 5.4.3).

Percentile of interest	Bias avoidance in individual samples for a $D_{50}$ of (mm)			Total mass for absolute error of $\pm 0.3 \phi$ for $D_{50}$ of (mm)			
	16	22.6	32	16	22.6	32	22.6
	Unit A	Unit B	Unit C	Unit A	Unit B	Unit C	all units
<u><math>s = 1</math></u>							
$D_{50}$	0.12	0.3	0.9	6.6	18	52	77
$D_{84}$	0.9	2.6	7.3	52	146	414	612
$D_{95}$	3.5	9.8	27	188	528	1502	2,218
<u><math>s = 2</math></u>							
$D_{50}$	0.2	0.6	1.8	120	336	956	1,412
$D_{84}$	13.7	38	109	6,800	19,200	54,600	80,000
$D_{95}$	211	592	1684	96,900	304,000	773,500	1,142,000

If the reach-averaged  $D_{50}$  particle size was 22.6 mm, and the reach-averaged sorting coefficient was 2, a sample mass of 336 kg is required to estimate the  $D_{50}$  to an precision of  $\pm 0.3 \phi$  units when

using a spatially integrated sampling scheme (Table 6.10, lower, shaded part of column for total sample mass for  $D_{50} = 22.6$  mm). This is more than 4 times the sample mass accrued from spatially segregated sampling of that reach. The difference between spatially segregated and spatially integrated becomes larger if the study objective shifts from the  $D_{50}$  particle size to higher percentiles. Spatially integrated sampling would require more than 30 times the sediment mass of spatially segregated sampling to correctly sample the  $D_{84}$  particle size (Table 6.9, compare the two shaded columns). The factor by which spatially segregated sampling reduces the total sample mass over spatially integrated sampling also depends on how well the reach can be delineated into homogeneous sedimentary units.

The reach-averaged particle-size distribution is computed by areal weighting of the frequency or percent frequency of the particle-size frequency distribution from each of the sedimentary units (Section 6.3.2.5).

#### 6.5.2.2 Sampling location for reach-averaged subsurface $D_{50}$ size

Spatially segregated sampling is particularly useful for determining the reach-averaged subsurface  $D_{50}$  particle size, because sampling may be focused on a few sampling locations. The ability to focus sampling is based on two factors: (1) The ratio between the surface and subsurface particle size is such that locations with a coarse surface tend to have coarse subsurface sediment (Section 6.5.2). (2) There is a spatial relationship between the ratios of the local and reach-averaged  $D_{50}$  subsurface size and the ratios of the local and reach-averaged  $D_{50}$  surface size (Lisle and Hilton 1998 pers. communication):

$$\frac{D_{50sub;loc}}{D_{50sub;r-avg}} \approx \frac{D_{50sur;loc}}{D_{50sur;r-avg}} \quad (6.5)$$

The proportionality expressed in Eq. 6.5 is also valid for other percentiles and has been verified in several gravel-bed rivers. Thus, the sedimentary unit at which the local surface  $D_{50}$  equals the reach-averaged surface  $D_{50}$  is the ideal location for sampling to obtain the representative reach-averaged subsurface  $D_{50}$  particle size. This focus of sampling locations to representative locations provides statistically valid samples that describe the subsurface bed material relatively accurately with a relative small sample size. Stratified subsurface sampling becomes particularly important when a long (and large) spatially heterogeneous reach is to be characterized.

The procedure for identifying representative locations for subsurface bed-material sampling depends on the degree of spatial heterogeneity of the reach and on the relative size of the reach. A familiarity with the bed-surface particle sizes within the reach of

concern is therefore very important. The approach outlined below assumes that sedimentary units (e.g., fine gravel, sand and gravel, coarse gravel, cobbles), each larger than a few m<sup>2</sup>, are visually distinguishable within a spatially heterogeneous bed. The approach can be divided into the following steps<sup>7</sup>:

1. Walk the stream, look at the spatial variation in surface particle sizes and define different sedimentary units (facies or patches) based on surface particle sizes within the entire reach. Visual estimates of the  $D_{50}$  and the  $D_{90}$  particle sizes are helpful, but other criteria may be used for delineating facies units as well (Section 6.3.2.1). Determine the degree of spatial heterogeneity of the reach. Particle sizes on the streambed may have a complex appearance in which patches of similar bed-material size are intermingled with other facies types. This is common in large or aggrading streams (case A), (e.g., Fig. 6.16). In riffle-pool streams, bed-material particle size may show simple systematic lateral and longitudinal variability (case B) (e.g., Fig. 6.11).

***(Case A) Patchy, and intermingled sedimentary units: select a long sampling reach of ca. 20 stream widths***

2. Identify the length of the study reach. The reach must be sufficiently long to ensure that the proportion of the area in each mapped facies is stable. That is, if you sampled further up- or downstream, the percentage of the area allotted to each facies would be stable. A reach length on the order of 20 stream widths is usually required.
3. Flag the boundaries of the sedimentary units, survey the boundaries, and prepare a map of the various sedimentary units within the study reach. Determine the area of each patch or sedimentary unit.
4. Perform a surface pebble count on each type of sedimentary unit. If sedimentary units are patchy, i.e., small and interspersed, and there are many patches of a common facies type, select a few patches that seem most representative and cover each patch with an individual pebble count (Situation 3, Section 6.5.2.1). Sample enough patches to determine the variance within a type of sedimentary unit. If sedimentary units are few, comparatively less patchy, less intermingled and larger in size, cover the entire unit with a pebble count (Situation 1, Section 6.5.2.1). If sedimentary units extend over large areas, perform localized pebble counts at random locations within the unit (Situation 2, Section 6.5.2.1).
5. Compute the average surface sediment-size distribution for each type of sedimentary unit. The reach-averaged surface bed-material size is obtained by weighting the average surface-size distribution for each type by its percentage area of the reach (Section 6.3.2.5).

---

<sup>7</sup> Step 1 - 5 are similar to the procedure listed for spatially segregated pebble counts and visual delineation of the reach in Section 6.3.2.2. For completeness and convenience for the user, the entire procedure is repeated here.

6. Determine subsurface bed-material sampling locations. Samples that best represent the reach-averaged subsurface sediment size can either be obtained at one or several locations at which surface particle-size distributions are similar to the reach-averaged surface distribution. Alternatively, random volumetric samples can be collected from the one sedimentary unit that best represents the reach-averaged particle size. If that sedimentary unit is coarser or finer than the reach average, a few volumetric samples from a finer, or coarser type of sedimentary unit are needed to better represent the reach-averaged subsurface particle-size distribution.
7. Alternatively, establish the ratio  $D_{50surf}/D_{50sub}$  for the sampling reach. Take several randomly placed subsurface samples from each facies type. Calculate the average subsurface  $D_{50}$  for each type of sedimentary unit and the reach-averaged subsurface  $D_{50}$  as a area-weighted mean, as above. The surface  $D_{50}$  size of the various sedimentary units is known, and a relation can be established between the ratios of the surface  $D_{50}$  of the particular facies type over the reach-averaged surface  $D_{50}$  (i.e., Eq. 6.5). Plotted graphs of this relation intersect close to the point where abscissa and ordinate both have the values of 1, but the slopes of the graphs are different for various stream types (Lisle and Hilton 1998, pers. comm.). Because it is expected that sedimentary units with particle-size distributions in the medium size range best represent the reach-average particle size, sampling should be concentrated on those units.

***(Case B) Simple systematic lateral and longitudinal variability in bed-material size: a short reach may be sufficient***

If there is negligible patchiness in surface bed-material size, and only simple systematic lateral and longitudinal variability as expected in coarse-bedded riffle-pool streams with a relatively small supply of sandy and gravelly sediment, sampling may be limited to a shorter reach of a single riffle-pool sequence. However, a longer reach of about 20 stream widths provides additional representative samples, unless the study is focussed on a particular riffle-pool section.

Sampling the subsurface bed material at the location within the reach where the surface sediment is most similar to the reach-average usually provides a reasonable estimate of the reach-averaged subsurface distribution. Sampling errors can only be estimated if several samples are obtained at each sedimentary unit. The adjustment process described in Step 7 is difficult to perform in reaches with few sedimentary units, particularly if none of them has a surface  $D_{50}$  that closely matches the reach-average surface  $D_{50}$ . In this case, it is difficult to identify a facies unit with a subsurface  $D_{50}$  that is likely to represent the reach-averaged subsurface  $D_{50}$ .

## **6.6 Spatially focused sampling**

Spatially focused sampling collects a sample from a small and isolated location within the streambed area. This area may be in close vicinity of an object of concern, such as zones

of scour and deposition around bridge piers, or near fish habitat structures. Spatially focused sampling uses small-scale grids, areal samples, photo sieving and volumetric sampling. Spatially focused sampling is either used to evaluate the hydraulic and sedimentary response at a certain locally confined stream location, or to sample sediment in stream locations that are indicative of reach-averaged conditions of sediment supply.

### 6.6.1 Sampling large particles on bar heads for stream competence analysis

Stream competence analysis evaluates the largest particle size transportable by a specific stream flow, such as the annual high flow, bankfull flow or the 100-year flood. In order to measure particle sizes transportable by such flows, stream locations need to be found in which such particles are deposited.

Coarse particles that are mobile during frequent floods are commonly deposited at the upstream end of bars. Free-formed bars, such as mid-channel and diagonal bars (Fig. 3.4 in Section 3.2.1), have the most direct interaction with the free-flowing stream and are most indicative of the general flow hydraulics. This makes the upstream end of mid-channel and diagonal bars ideal sampling sites for stream competence analysis (Fig. 6.21). Next in a hierarchy of sampling sites are point bars, followed by lateral bars.

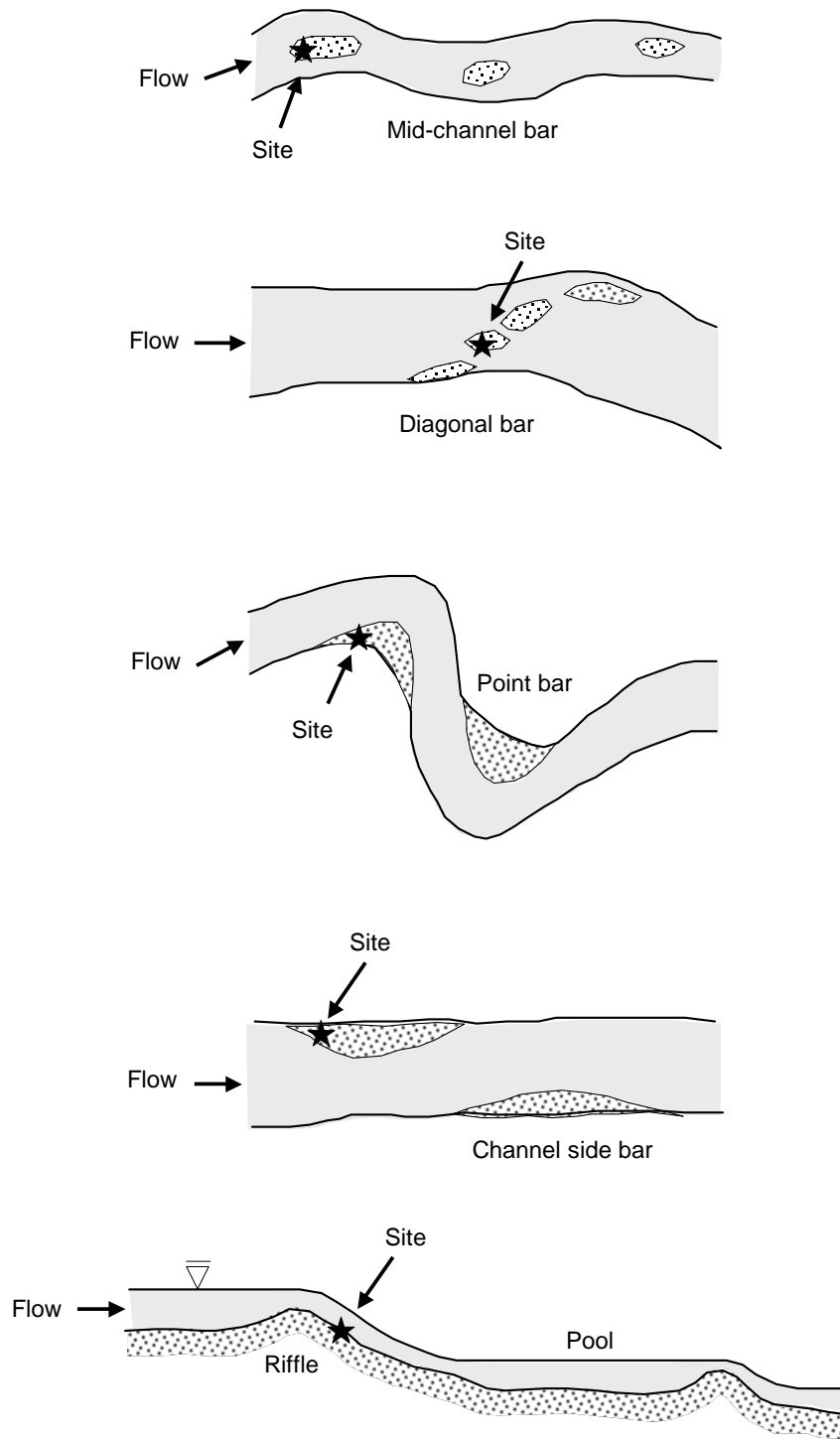
Particles deposited during infrequent large floods may be found in overbank deposits away from the main channel or in cobble and boulder berms along the channel.

### 6.6.2 Sampling fines in pools for analysis of fine sediment supply

Local deposits of fine sediment may also be indicative of reach-averaged conditions of sediment supply. A moderate supply of fine sediment may not be detectable in the main channel bed or on riffles. Fine sediment should be visible, though, in locations conducive to local deposits of fines, such as backwater areas, the wake of stream obstructions (e.g., a log), as well as in pools. Repeated monitoring of such locations may indicate whether the quantity of fines transported by the stream changes over time.

Lisle and Hilton (1992; 1999) and Hilton and Lisle (1993) developed a field analysis for monitoring the deposition of fine sediment in pools. Fine sediment (comprising mostly sand and fine gravel) is transported in gravel-bed streams long after a high flow during subsequent moderate and low flows. The fines are eventually trapped in pools and build deposits of measurable thickness along zones of low shear stress near the sides or in backwater areas of pools. The parameter  $V^*$  quantifies the ratio of the fine sediment volume in pools  $V_{fines}$  to pool volume  $V_{pool}$  and is computed from

$$V^* = \frac{V_{fines}}{V_{pool} + V_{fines}} \quad (6.6)$$

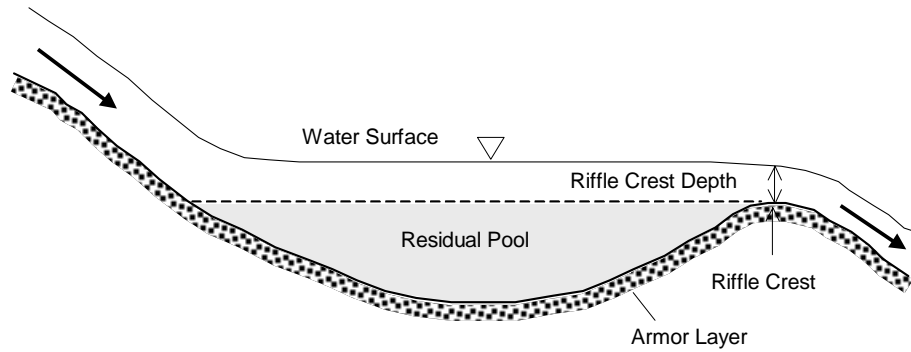


★ Preferred Sampling Locale  
(unless surface material dictates otherwise)

Fig. 6.21: Gravel-bar sampling sites for stream competence analysis (Redrawn from Yuzuk 1986).

To compute  $V^*$ , the water depth and the thickness of the fine sediment deposit is measured along a grid system spanned over the pool. The thickness of the fine sediment deposit is measured by probing with a steel rod that has a cm gradation (Fig. 6.22).

**A. Longitudinal Profile**



**B. Cross Section**

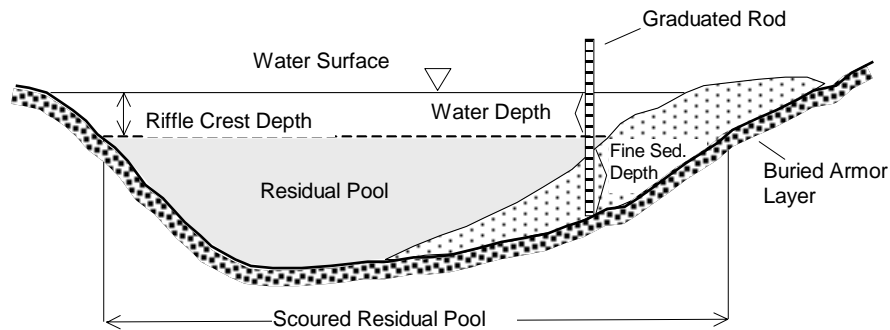


Fig. 6.22: (A) Longitudinal profile of a pool, showing the riffle crest and the area included in the residual pool volume. (B) Cross-section of a pool, showing measurement of water and fine sediment depth and volume of water and fine sediment in the scoured residual pool (Redrawn from Hilton and Lisle (1993)).

Tap the rod with a hammer to penetrate the fine sediment until a resistance is felt at the boundary with the coarse armor layer beneath. In order to measure water depth independent of a current flow depth, water depth is measured up to the residual pool volume, i.e., the minimum water depth at which water would just overflow the downstream riffle. Volumes of pool and fine sediment are computed by multiplying the cross-sectional areas of pools and fines by the distance between cross-sections.

Values of  $V^*$  can range from 0 (for no fines) to 1 if the pool is completely filled by fines.  $V^*$  is computed for about 10 - 15 pools (more if  $V^*$  varies heavily between pools) and

averaged. A change in  $V^*$  can be used as a measure to monitor spatial or temporal changes in fine sediment yield.

Volumetric samples of pool fines may be obtained using a pipe dredge (Section 4.2.4, Fig. 4.30a). Lisle and Hilton (1999) compared the particle-size distribution of pool fines to the fine mode of bedload sediment and to the subsurface sediment in order to analyze whether sediment transport is supply- or transport limited.

## 7. Steps of a sampling project

---

These guidelines have presented the various topics of bed-material sampling in a hierarchical order such that basic topics required for the understanding of higher topics were described first. However, in order to guide the user through the temporal sequence of sampling, a summary section is provided that explains the steps that may be taken before, during, and after a sampling project. The summary also highlights the principle points that should be followed or avoided when sampling in a gravel-bed stream in order to obtain successful field results.

### **Preliminary work:**

#### **State the study objective clearly.**

Specify the target population of bed material to be sampled in the study project and explain why sampling that particular population is assumed to solve the study question. Bed-material populations may be the surface or the subsurface sediment, sediment representing the entire reach or sediment from specified geomorphological locations such as riffles, pools or bar heads. Stating the study objective is critical toward making a worthwhile field effort and dictates the more pragmatic decisions of the sampling project.

#### **Get to know the stream.**

Walk as much of the stream as possible. View the stream in its environmental context (note hillslope conditions and evaluate sources of sediment supply or sediment sinks). Obtain large-scale maps and areal photographs for an overview of the stream and its watershed. This is particularly important if the stream cannot be visited prior to the sampling project. Obtain hydrologic data such as mean daily flow and annual hydrographs.

#### **Select a suitable study site.**

The proximity to sediment sources or sinks is an important factor to consider when selecting a study site. Off-stream sediment supply from banks or tributaries, or sediment retention in beaver dams or diversion structures may have to be avoided in some studies, while sampling in their vicinity may be the focus of other studies. Environmental sensitivity of the stream to the disturbance that may be caused by bed-material sampling should be considered. Vehicle access may be a crucial factor. All these factors should be part of study-site selection.

**Familiarize yourself with the stream in the sampling area.**

Walk the sampling area and determine the morphological units (e.g., riffles, pools, and bars, Section 3.2.1), their particle sizes (Section 3.2.3), and the stream type (e.g., plane-bed, riffle-pool, 1.3). Does large woody-debris affect the degree of spatial variability of bed-material size (Section 3.2.5)? Does the particle-size distribution change within the sampling area (e.g., heterogeneous or homogeneous reach?). Dig a few small pits and determine whether the streambed is armored (Section 3.3.1). Draw a sketch plan (Section 6.1.4) which may include visually estimated mean or maximum particle sizes, the amount of fines, geomorphological (Section 3.2) or sedimentary units (Section 6.3.2.1-6.3.2.3), bed-surface structures (Section 3.4), large woody debris and other parameters of concern.

**Select the sampling methods needed to accomplish the study objectives.**

If the study objective is met by analyzing the surface sediment, use a pebble count (Section 4.1.1). Combine a pebble count with areal samples (Section 4.1.3) if the bed contains areas with large amounts of fine gravel and sand interspersed with coarser particles. Restricted field time may warrant a photo sieving approach (Sections 4.1.2.2, 4.1.3.3), but requires that the bed has a negligible amount of fine sediment (or the fines are irrelevant to the study), and that surface particles are well visible and not embedded or imbricated. In addition to saving time during field work, photographic close-ups or areal overviews of the bed are useful for analyzing bed-surface structures (Section 4.1.3.4). Use volumetric samples if the armor (Section 4.2.1), or the subsurface/subarmor and the vertically unstratified bulk sediment (Section 4.2.2) are the focus of the study. Consider whether the stream site(s) are accessible by vehicle when selecting sampling equipment.

**Determine the desired/tolerable sampling precision.**

Each study requires a specific sampling precision in order to meet the study objective and make the sampling effort worthwhile. Precise sampling is particularly important when attempting to detect a change in bed-material size over time or space (Section 4.1.1.2). For example, two samples with  $D_{50}$  sizes of 40 and 59 mm are not statistically different if each result has a 20% sampling error (Section 4.1.1.5). Remember also, operator errors add to the statistical error, but are not included in the computation of statistical errors. Finally, note that sampling errors propagate through the computations for which the results are used. If the  $D_{50}$  particle size has a 20% error, this error increases to a factor of 2.25 if  $D_{50}$  is raised to a power of 2.

**Conduct a pilot study.**

A pilot study can verify the feasibility of a selected sampling method (e.g., Are the particles too wedged into the bed for retrieval? Is the stream wadable? Is the bed too fine for a pebble count? Should areal samples be collected to better account for the distribution of fine sediment? Is the bed too coarse for a volumetric armor layer or subarmor/subsurface sample?) Evaluate whether the anticipated equipment is appropriate for the bed-material particle size and a dry or inundated streambed (Sections 4.2.3, 4.2.4).

A pilot study is also needed to estimate the standard deviation or sorting coefficient (Section 2.1.5.4) of the particle-size distribution. The standard deviation largely determines the sample size needed for a preset precision (Section 5). Finally, a pilot study is needed to determine the degree of spatial variability of the reach, which determines the sampling scheme and the length of the sampling reach (Section 6.1.4).

**Estimate the necessary sample size (number of particles, sample mass, or number of subsamples) for obtaining the desired sample precision.**

Estimate the necessary sample size based on data from the pilot study. Use statistical methods that assume a normal distribution of particle sizes ( $\phi$ -units), if neither the distribution of a pilot sample, nor the study objective interfere with this assumption. If assumptions cannot be made about the underlying distribution type, determine sample size from methods that are not contingent upon this information. Table 7.1 provides sample-size procedures for pebble counts, volumetric, and areal samples for particle-size distributions for which either a normal or no underlying distribution is assumed. Compute sample size using both procedures if you cannot decide on a particular distribution type at this stage in the analysis.

The sample size required for a desired precision may be large. For pebble counts, this is usually not a problem (sampling 400 or more particles is doable), but gathering volumetric samples of several tons may be difficult. Evaluate your options before reducing the sample size. There may be ways to increase the feasibility of large samples (e.g., field sieving (Section 2.1.3.10), or collecting samples from a larger area). Optimize the information that can be obtained from a specific sample mass (by truncation and readjustment of the samples at the coarse end (Section 5.4.1.4), and by collecting grab samples (Section 6.4.4)). Increase the sampling accuracy by delineating and sampling homogeneous sedimentary units (Sections 6.3.2, 6.5.2) instead of a heterogeneous reach. Consider computer resampling of a parent sample (Section 5.4.2.2). Consider whether the study objective might even be met with a lower sample precision.

Consider using statistical analyses not described in this document. This document provides a variety of statistical analyses suitable for various study objectives, but these descriptions by no means exhaust the fund of statistical analyses. A statistical procedure might be available that satisfies your study objective with a lower sample size, or a higher precision than indicated by the analyses in this document. Consult with a statistician to find out whether a statistical procedure exists that is exactly tailored to suit the needs of your study.

**Determine the appropriate spatial sampling scheme (Section 6).**

Sample-size statistics require that all subsamples be derived from the same population. For bed-material sampling, this means that the area from which subsamples are collected must be more or less homogeneous so that all samples that are collected may be considered together. All samples must be collected from random locations. Regular

sampling patterns such as a grid with a random starting point (Sections 6.2.1, 6.2.2, 6.4.1) are preferable over completely random sampling, particularly if the bed is not exactly homogeneous (which gravel beds rarely are). Heterogeneous streambed areas may be sampled by collecting several subsamples, each along a reach-covering grid system that is slightly shifted against the other (Sections 6.2.3, 6.4.3, 6.4.4). This procedure results in a large sample size. Sample size can be reduced without compromising the sampling accuracy if a heterogeneous sampling area is (visually or statistically) delineated into several sedimentary units (e.g., a coarse, medium fine, and a bimodal facies) which are then basically homogeneous (Sections 6.3.2, 6.5.2). The reach should be sufficiently large so that each facies occurs several times. If sedimentary units are large, collect subsamples from representative locations instead of covering the entire unit.

The study objective may require that bed material be collected from a specific geomorphological unit, such as a riffle (Sections 6.3.1; 6.5.1) or a pool (Section 6.6.2), or that sampling is focused on a stream location with a particular interaction between flow hydraulics and sedimentation (e.g., bar head, backwater area, wake deposit). These samples are often used for a comparison over time or space (Section 6.6). Note that samples from individual geomorphological units or from “special” locations are usually not representative of the bed material in the reach.

### **Establishing a sampling plan and schedule.**

Allocate the number of sampling points for pebble counts or the locations of volumetric samples over the reach. Estimate the field time necessary based on the estimated sample size. Would more operators be helpful or is the operator variability for the specific sampling method so high that employing more operators is counterproductive? Can the logistics be improved? Decide whether to sieve in the field or in the lab (Sections 2.1.3.10, 2.1.3.9). Consider photo-sieving (Sections 4.1.2.2, 4.1.3.4) if the field time is very limited. Assemble all necessary equipment and estimate the lab time required for analysis.

Design field forms (Sections 4.1.1.7, 4.5). This is a worthwhile effort even if the forms are not ultimately used because the process of designing the forms helps to visualize the sampling project.

The planning process of a bed-material sampling project may require frequent revisions because a decision or a fact made or encountered at some point may not be compatible with a decision or fact encountered at some other point.

### **While collecting bed material:**

#### **Surface sampling with pebble counts (Section 4.1.1)**

##### **Tips for reducing (operator) errors.**

- Use a sampling frame when selecting particles to reduce operator preference for “handy” particles (Section 4.1.1.6), or sample along a tape measure on dry beds.

- Sample along a strictly determined grid pattern that covers the sampling area to prevent operators from omitting “unappealing” streambed locations (Section 4.1.1.4).
- Space sampling points by at least the  $D_{max}$  particle size in order to avoid counting large particles multiple times which results in a serially correlated sample (Section 4.1.1.4).
- Sample from high-flow bank to high-flow bank and record all particle sizes for each transect in sequential order (e.g., from left to right bank). Include the location of the current water line. Such a record helps to determine a systematic spatial variation of particle sizes and allows a deferred decision on whether particles from the high-flow bed are included or excluded from the study (Section 4.1.1.7).
- One operator should select and retrieve all particles. A second person may assist by taking over the template measurements.
- The use of templates (usually in 0.5  $\phi$  gradation) to measure particle sizes avoids measurement errors (Section 2.1.3.6) but requires that the size distribution approximates normality in  $\phi$ -units. Use calipers only if the measured range of particle sizes is small (less than 0.5 or 1  $\phi$  units), if particle sizes are definitely not normally distributed ( $\phi$ -units), or when measuring all particle axes for an analysis of particle shape (Section 2.1.3.7).

#### **Areal surface sampling, sample conversion and combination.**

Use areal samples if the sampling area is too small for a pebble count or when the bed contains a large amount of fines (Section 4.1.3). Select an adhesive for areal samples that will provide the optimum penetration depth for a given particle-size distribution (Section 4.1.3.2). If used to augment pebble counts, areal samples must be converted to equivalent grid-by-number distributions (Section 4.3). This conversion may not always be clear-cut. Pebble counts and converted areal samples need to be combined to obtain the complete particle-size distribution for the sampling area (Section 4.4).

#### **Volumetric samples.**

Determine the bed-material layer(s) to be sampled (armor, subarmor/subsurface or bulk) (Sections 3.3, 4.1) and the thickness of the sample (Sections 4.2.1, 4.2.2). Note that the sampling result is affected by the methods and the equipment used for sampling. Therefore, select methods and equipment that corroborate the study objective (Sections 4.2.4, 4.2.5) and avoid methodological changes. It is recommended that a three-sided plywood shield be used to define and contain the sampling area unless an undisturbed sediment core is needed. Remember to collect a sufficiently large sample mass.

#### **Post collection analysis:**

##### **Sieving**

A standard sieve set in 0.5  $\phi$  gradation is usually adequate for gravel- and cobble-beds, although well-sorted distributions may require sieving in 0.25  $\phi$  units (Section 2.1.3.1). Sieving the cobble and coarse gravel portion at the field site reduces the sediment load

hauled back to the laboratory. Split the fine part of the sample and sieve only a sufficient portion for size analysis. Large samples may require splitting the entire sample before sieving (Section 2.1.3.10).

Using square-hole sieves for the gravel portion is recommended for two reasons: Sieve results for gravel may directly be combined with sieve results for sand (typically obtained from square-hole sieves), and gravel sieve results are directly comparable with template measurements (Section 2.1.3.1). Results from square-hole sieves must be converted before they are compared with results from round-hole sieves (Section 2.1.3.5). This conversion varies with particle shape. The same conversion is necessary before comparing particle-size measurements performed with a template and a ruler or calipers.

### **Analysis of particle shape and other particle parameters.**

Particle shape affects the transportability of particles and may indicate the fluvial transport distance (Section 2.2.2). If a visual classification of particle shape is not sufficiently accurate (Sections 2.2.3, 2.2.4), all three particle axes need to be measured for a computation of particle shape (Sections 2.2.1, 2.2.3). Be sure to correctly identify the three particle axes (Section 2.1.1) and use calipers rather than a ruler to obtain accurate measurements when appropriate. Measure particle axes and any other particle properties (density, volume and mass (Section 2.3) and bulk density (Section 2.4)) directly at the field site if particle sizes and sample mass are large.

### **Statistical analysis:**

#### **The gradation curve and descriptive statistics**

Compute the frequency per size class either by weight (for volumetric samples) or by number (for pebble counts) and plot the histogram. Compute the cumulative frequency distribution and plot the gradation curve (sum curve). Determine the distribution type (Section 2.1.4) and evaluate whether the distribution is “normal enough” to warrant the use of statistics based on a normal distribution. This is a judgement call. Treat bimodal distributions (Section 2.1.5.9) as two separate distributions.

Use either a graphic approach or the moment method (Section 2.1.5) to compute the particle-distribution parameters. A graphic analysis is recommended when analyzing only a few data sets and particularly for the novice user because this method makes it easy to see the connection between computation and statistical results. Compute the seven percentiles ( $D_5$ ,  $D_{16}$ ,  $D_{25}$ ,  $D_{50}$ ,  $D_{75}$ ,  $D_{84}$ ,  $D_{95}$ ) and the descriptive statistical parameters (mean, sorting, skewness and kurtosis). The moment method computes the moments (which are largely equivalent to the graphic distribution parameters) directly from the frequency distribution. This procedure is recommended for a fully computerized analysis of a large number of data sets.

### Statistical precision of a sample (Section 5)

The first estimate of the relation between sample size and precision was based only on a pilot sample. The actual precision is determined after all samples are collected. Table 7.1 indicates the sections in this document that discuss sample-size procedures used for pebble counts, volumetric, and areal samples. Either a normal distribution is assumed, or the procedure makes no assumptions regarding the distribution type.

Table 7.1: Document sections explaining sample-size procedures for pebbles counts, volumetric, and areal samples, for an assumed underlying normal distribution, or for no assumed distribution type.

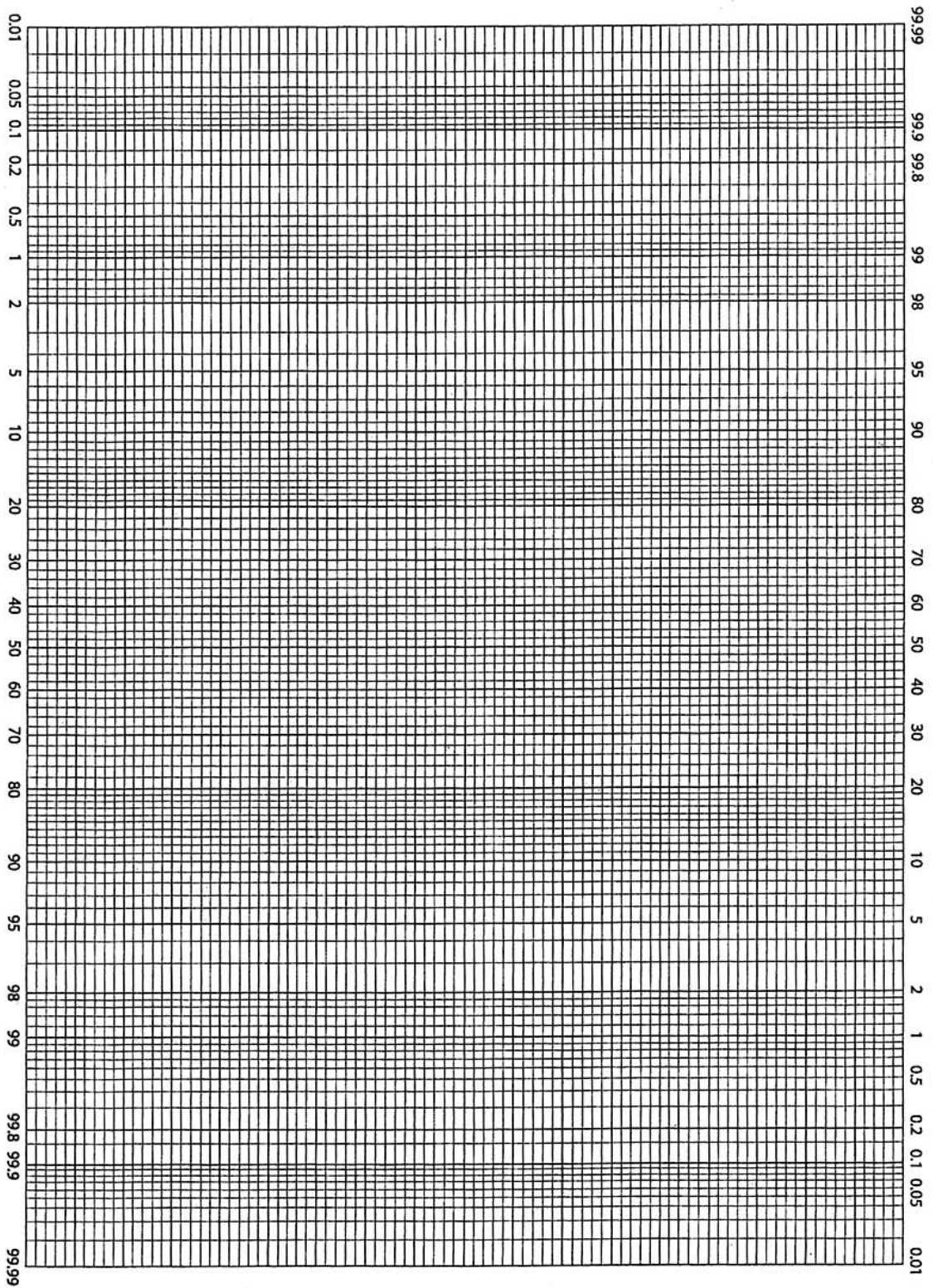
	Normal distribution assumed	No distribution type assumed
Pebble count	5.2.2	5.2.3, 5.2.4
Volumetric sample	5.4.3	5.4.1.1, 5.4.2
Areal sample	5.3.1	5.3.2, 5.3.3

If attaining a preset sampling precision is crucial to the sampling project, compute sampling precision at the field site as soon as samples are sieved and analyzed. Use a laptop computer and pre-designed spreadsheets for rapid field computations (Sections 5.2.2.9, 5.4.3.1, 5.4.3.2). Continue sampling (during the same field season) until a tolerable sampling precision has been reached.

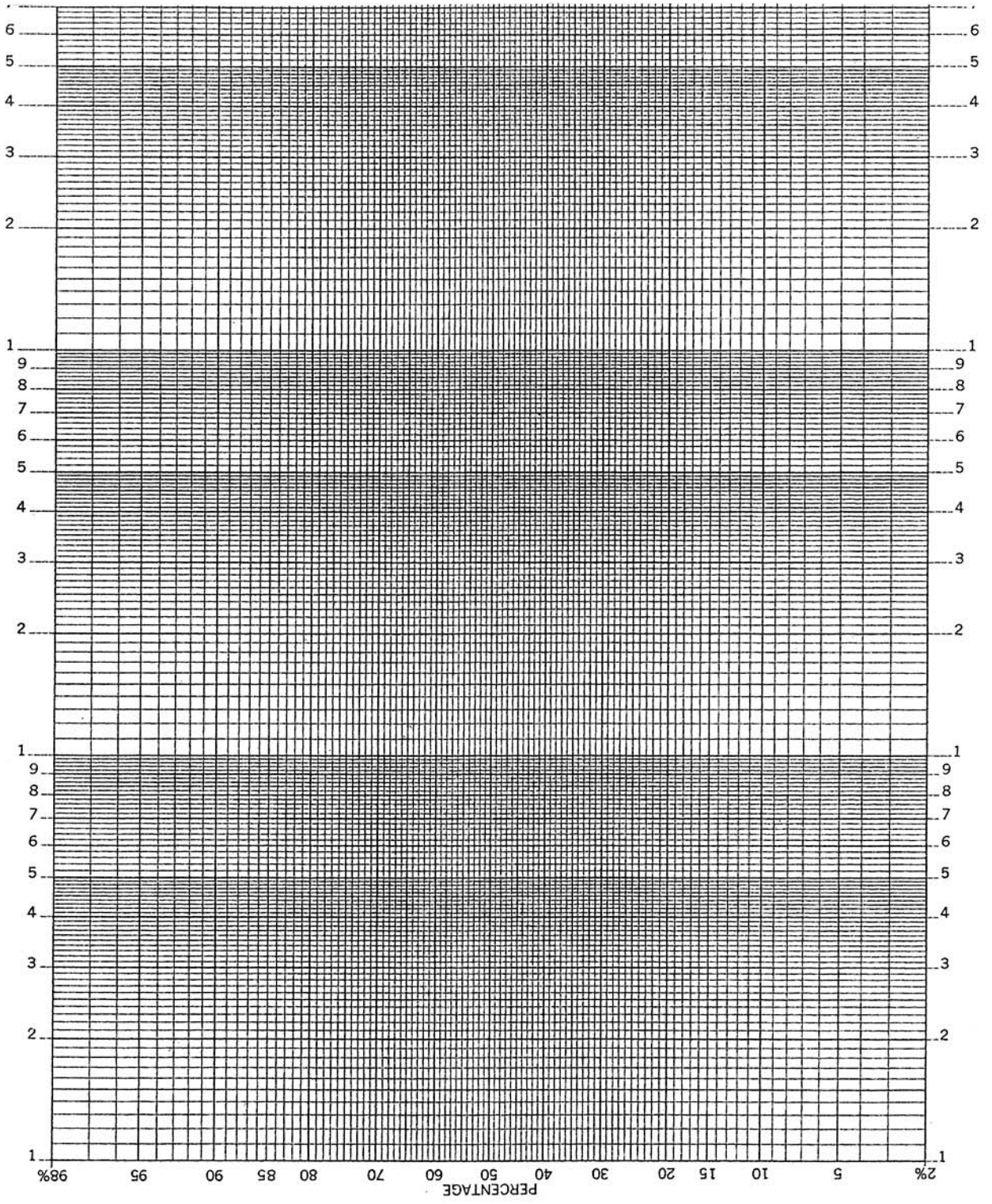
More statistical analyses than described in this document are available in the statistical literature. Consult with a statistician to identify the statistical analysis that satisfies your sampling objective as best as possible.

# 8. Appendix

Probability paper with linear divisions



Probability paper with logarithmic divisions



## 9. References

---

- Abt, S.R., R.J. Witter, A. Taylor, and D.J. Love, 1989. Human stability in a high flood hazard zone. *Water Resources Bulletin* 25 (4): 881-890.
- Adams, J., 1979. Gravel size analysis from photographs. *Journal of the Hydraulics Division, ASCE*, 105(HY10): 1247-1255.
- Adams, J.N. and R.L. Beschta, 1980. Gravel bed composition in Oregon coastal streams. *Canadian Journal of Fisheries and Aquatic Sciences* 37: 1514-1521.
- Alonso, C.V., 1993. Sediment deposition on stable gravels. In: *Advances in Hydro-Science and -Engineering*, Vol. 1, S.S.Y. Wang (ed.), p. 251-256.
- Anastasi, G., 1984. Geschiebeanalysen im Felde unter Berücksichtigung von Grobkomponenten. [Field grain-size analyses with special attention to coarse material]. *Mitteilungen der Versuchsanstalt für Wasserbau, Hydrologie und Glaziologie der ETH Zürich*, Nr. 70.
- Andrews, E.D. and G. Parker, 1987. Formation of a coarse surface layer as the response to gravel mobility. In: *Sediment Transport in Gravel-Bed Rivers*. C.R. Thorne, J.C. Bathurst and R.D. Hey (eds.). John Wiley and Sons, New York, p. 269-300.
- Anthony, D.J., and M.D. Harvey, 1991. Stage-dependent cross-section adjustments in a meandering reach of Fall River, Colorado. *Geomorphology* 4:187-203.
- Ashmore, P.E., T.R. Yuzyk and R. Herrington, 1988. Bed-material sampling in sand-bed streams. Sediment Survey Section, Water Resources Branch, Inland Waters Directorate, Report IWD-HQ-WRB-SS-88-4, 47pp.
- Ashworth, P.J. and R.I. Ferguson, 1986. Interrelationships of channel processes, changes and sediments in a proglacial braided river. *Geografiska Annaler* 68A (4): 361-371.
- Ashworth, P.J., R.I. Ferguson and M. Powell, 1992a. Bedload transport and sorting in braided channels. In: *Dynamics of Gravel Bed Rivers*. P. Billi, R.D. Hey, C.R. Thorne and P. Tacconi (eds.), John Wiley and Sons, Chichester, p. 497-515.
- Ashworth, P.J., R.I. Ferguson, P.E. Ashmore, C. Paola, D.M. Powell, and K.L. Prestegard, 1992a. Measurements in a braided river chute and lobe. 2. Sorting of bed load during entrainment, transport, and deposition. *Water Resources Research* 28(7): 1887-1896.
- Barta, A.F., P.R. Wilcock and C.C. Shea, 1993. Entrainment of gravel in steep streams (abstract). American Geophysical Union 1993 Fall Meeting, Supplement to *EOS, AGU Transactions* 74 (43): 311.
- Barta, A.F., P.R. Wilcock and C.C. Shea, 1994. The transport of gravels in boulder-bed streams. In: *Hydraulic Engineering '94*. Proceedings of the 1994 Conference, G.V. Cotroneo and R.R. Rumer (eds.), ASCE, New York, Vol. 2: p.780-784.
- Bartolomä, A., 1992. Texturelle und kompositionelle Reifung von Fluß- und Küstenschottern, Kalabrien, Süditalien. [Textural and compositional maturing of fluvial and coastal gravels and cobbles, Calabria, Southern Italy.] Ph.D. Dissertation, Fachbereich Geowissenschaften, Freie Universität Berlin, Germany.

- Bevenger, G.S. and R.M. King, 1995. A pebble count procedure for accessing watershed cumulative effects. USDA, Forest Service, Rocky Mountain Forest and Range Experiment Station, Research Paper RM-RP-319, 17 pp.
- Bhowmik, N.G. and M. Demissie, 1982. Bed material sorting in pools and riffles. *Journal of the Hydraulics Division, ASCE*, 108 (HY10): 1227-1231.
- Billi, P., 1994. Streambed dynamics and grain-size characteristics of two gravel rivers of the Northern Apennines, Italy. In: *Dynamics and Geomorphology of Mountain Rivers*. P. Ergenzinger and K.-H. Schmidt (eds.). Lecture Notes in Earth Sciences, Springer Verlag, Berlin, 197-212.
- Billi, P. and E. Paris, 1992. Bed sediment characterization in river engineering problems. In: *Erosion and Sediment Transport Monitoring in River Basins*. IAHS Publ. no. 210: 11-20.
- Bisson, P.A., R.E. Bilby, M.D. Bryant, C.A. Dolloff, G.B. Grette, R.A. House, M.L. Murphy, K.V. Koski and J.R. Sedell, 1987. Large woody debris in forested streams in the Pacific Northwest: past, present and future. In: *Streamside Management: Forestry and Fishery Interactions*. E.O. Salo and T.W. Cundy (eds.), College of Forest Resources, University of Washington, Seattle, Washington, Contribution no. 57: 143-190.
- Bjornn, T.C. and Reiser, D.W., 1991. Habitat requirements of salmonid streams. In: *Influence of Forest and Rangeland Management on Salmonid Fishes and their Habitats*, W.R. Meehan (ed.), p. 83-138, American Fisheries Society Special Publication 19, Bethesda.
- Bluck, B.J., 1982. Texture of gravel bars in braided streams. In: *Gravel-bed Rivers. Fluvial Processes, Engineering and Management*. R.D. Hey; J.C. Bathurst and C.R. Thorne (eds.), John Wiley and Sons, Chichester, p. 339-355.
- Bluck, B.J., 1987. Bed forms and clast size changes in gravel-bed rivers. In: *River Channels. Environment and Process*. K.S. Richards (ed.), The Institute of British Geographer Special Publication Series, Basil Blackwell, Oxford, p. 159-178.
- Boothroyd, J.C. and G.M. Ashley, 1975. Processes, bar morphology, and sedimentary structures on braided outwash fans, northeastern Gulf of Alaska. In: *Glaciofluvial and Glaciolacustrine Sedimentation*. A.V. Jopling and B.C. McDonald (eds.). Society of Economic Paleontologists and Mineralogists, Special Publication 23, p. 193-222, Tulsa, Ok.
- Brayshaw, A.C., 1984. Characteristics and origin of cluster bedforms in coarse-grained alluvial channels. In: *Sedimentology of Gravels and Conglomerates*. E.H. Koster and R.J. Steel (eds.), Canadian Society of Petroleum Geologists, Memoir 10: 77-85.
- Brayshaw, A.C., 1985. Bed microtopography and entrainment thresholds in gravel-bed rivers. *Geological Society of America Bulletin* 96: 218-223.
- Brayshaw, A.C.; L.E. Frostick and I. Reid, 1983. The hydrodynamics of particle clusters and sediment entrainment in coarse alluvial channels. *Sedimentology* 30: 137-143.
- Brierley, G.J. and Hickin, E.J., 1985. The downstream gradation of particle sizes in the Squamish River, British Columbia. *Earth Surface Processes and Landforms* 10: 597-606.

- Brierley, G.J., 1991. Bar sedimentology of the Squamish River, British Columbia: definition and application of morphostratigraphic units. *Journal of Sedimentary Petrology* 61(2): 211-225.
- Bridge, J.S. and J. Jarvis, 1976. Flow and sedimentary processes in the meandering river South Esk, Glen Clova, Scotland. *Earth Surface Processes and Landforms* 1: 303-336.
- Bridge, J.S. and J. Jarvis, 1982. The dynamics of a river bend: a study in flow and sedimentary processes. *Sedimentology* 29: 499-543.
- Buffington, J.M., 1996. An alternative method for determining subsurface grain size distributions of gravel-bedded rivers (abstract). American Geophysical Union 1996 Fall Meeting, Supplement to *EOS, AGU Transactions*, 77 (46): F250.
- Buffington, J.M. and D.R. Montgomery, 1999a. A procedure for classifying and mapping textural facies in gravel-bed rivers. *Water Resources Research* 35 (6): 1903-1914.
- Buffington, J.M. and D.R. Montgomery, 1999b. Effects of hydraulic roughness on surface textures of gravel-bed rivers. *Water Resources Research* 35 (11):3507-3521.
- Buffington, J.M. and D.R. Montgomery, 1999c. Effects of sediment supply on surface textures of gravel-bed rivers. *Water Resources Research* 35 (11): 3523-3530.
- Buffington, J.M., W.E. Dietrich and J.W. Kirchner, 1992. Friction angle measurements on a naturally formed gravel streambed: implications for critical boundary shear stress. *Water Resources Research* 28(2): 411-425.
- Bunte, K., 1994. Modeling bedload transport in sand-bed streams using the Ackers and White (1973) sediment transport formula. Report prepared for the Stream Systems Technology Center, Rocky Mountain Forest and Range Experiment Station, US Forest Service, Fort Collins, Colorado, 56pp.
- Bunte, K., 1995. Parameters of the Riffle Stability Index in relation to bar and riffle grain-size distributions: results of field measurements in gravel- and cobble-bed streams in northern Colorado, October 16-20, 1995. Report prepared for the Stream Technology Center, Rocky Mountain Forest and Range Experiment Station, US Forest Service, Fort Collins, CO, 40p.
- Bunte, K. and S.R. Abt, 2001. Sampling frame for improving pebble count accuracy in coarse gravel-bed streams. *Journal of the American Water Resources Association* (in press).
- Bunte, K. and J. Poesen, 1993. Effects of rock fragment covers on erosion and transport of non-cohesive sediment by shallow overland flow. *Water Resources Research*, 29 (5), 1415-1424.
- Bunte, K. and J. Poesen, 1994. Effects of rock fragment size and cover on overland flow hydraulics, local turbulence and sediment yield on an erodible soil surface. *Earth Surface Processes and Landforms* 19: 115-135.
- Burns, D.C. and R.E. Edwards, 1985. Embeddedness of salmonid habitat of selected streams on the Payette National Forest. For the Payette National Forest, McCall, ID, 30 p.
- Burrows, R.L., W.W. Emmett and B. Parks, 1981. Sediment transport in the Tanana River in the vicinity of Fairbanks, Alaska, 1977-1979. *U.S. Geological Survey Water Resources Investigation Report* 81-20, 56 pp.

- Butler, J.B., S.N. Lane and J.H. Chandler, 2000. Automated extraction of grain-size data from gravel surfaces using digital image processing. *Journal of Hydraulic Research* (in press)
- Campbell, A.J. and R.C. Sidle, 1985. Bedload transport in a pool-riffle sequence of a coastal Alaska stream. *Water Resources Bulletin*, American Water Resources Association 21(4): 579-590.
- Carling, P.A., 1989. Hydrodynamic models of boulder berm deposition. *Geomorphology* 2: 319-340.
- Carling, P.A., 1991. An appraisal of the velocity-reversal hypothesis for stable pool-riffle sequences in the River Severn, England. *Earth Surface Processes and Landforms* 16: 19-31.
- Carling, P.A. and N.A. Reader, 1981. A freeze-sampling technique suitable for coarse river bed material. *Sedimentary Geology* 29: 233-239.
- Carling, P.A. and N.A. Reader, 1982. Structure, composition and bulk properties of upland stream gravels. *Earth Surface Processes and Landforms* 7: 349-365.
- Carling, P.A. and N. Wood, 1994. Simulation of flow over pool-riffle topography: A consideration of the velocity reversal hypothesis. *Earth Surface Processes and Landforms* 19: 319-332.
- Church, M., 1987. Discussion to Andrews and Parker (1987) "Formation of a coarse surface layer as the response to gravel mobility". In: *Sediment Transport in Gravel-Bed Rivers*. C.R. Thorne, J.C. Bathurst and R.D. Hey (eds.). John Wiley and Sons, New York, p. 314-322.
- Church, M., 1992. Channel morphology and typology. In: *The Rivers Handbook*, Vol. 1. P. Calow and G.E. Petts, eds., Blackwell Science Ltd., Oxford, UK, p. 126-143.
- Church, M. and D. Jones, 1982. Channel bars in gravel-bed rivers. In: *Gravel-bed Rivers. Fluvial Processes, Engineering and Management*. R.D. Hey; J.C. Bathurst and C.R. Thorne (eds.), John Wiley and Sons, Chichester, p. 291-338.
- Church, M., D.G. McLean and J.F. Wolcott, 1987. River bed gravels: sampling and analysis. In: *Sediment Transport in Gravel-Bed Rivers*, C.R. Thorne, J.C. Bathurst and R.D. Hey (eds.), John Wiley and Sons, Chichester, p. 43 – 88.
- Church, M., M.A. Hassan and J.F. Wolcott, 1998. Stabilizing self-organized structures in gravel-bed stream channels: field and experimental observations. *Water Resources Research* 34 (11): 3169-3179.
- Clifford, N.J., 1993. Differential bed sedimentology and the maintenance of riffle-pool sequences. *Catena* 20: 447-468.
- Crofts, R.S., 1974. A visual measure of single particle form for use in the field. *Journal of Sedimentary Petrology* 44 (3): 931-934.
- Crowder, D.W., 1996. Sampling heterogeneous gravel deposits within stream beds (abstract). American Geophysical Union 1996 Spring Meeting, Supplement to *EOS*, *AGU Transactions* 77 (17): 130.
- Crowder, D. W. and P. Diplas, 1997. Sampling heterogeneous deposits in gravel-bed streams. *Journal of Hydraulic Engineering* 123 (12): 1106-1117.
- De Jong, C., 1992. Discussion of Reid, Frostick and Brayshaw (1992), in: *Dynamics of Gravel-bed Rivers*, P. Billi, R.D. Hey, C.R. Thorne and P. Tacconi (eds.), John Wiley and Sons, Chichester, United Kingdom, p. 267-272.

- De Jong, C. and P. Ergenzinger, 1995. The interrelations between mountain valley form and river-bed arrangement. *River Geomorphology*, E.J. Hickin (ed.), John Wiley & Sons, Chichester, p. 37-54.
- De Vries, M., 1970. On the accuracy of bed-material sampling. *Journal of Hydraulic Research* 8 (4): 523-533.
- Diepenbroek, M. and C. De Jong, 1994. Quantification of textural particle characteristics by image analysis of sediment surfaces - examples from active and paleo-surfaces in steep, coarse grained mountain environments. In: *Dynamics and Geomorphology of Mountain Rivers*. P. Ergenzinger and K.-H. Schmidt (eds.). Lecture Notes in Earth Sciences 52: 301-314, Springer Verlag, Berlin.
- Diepenbroek, M., A. Bartolomä, and H. Ibbeken, 1992. How round is round? A new approach to the topic 'roundness' by Fourier grain shape analysis. *Sedimentology* 39 (3): 411-422.
- Dietrich, W.B., 1987. Mechanics of flow and sediment transport in river bends. In: *River Channels. Environment and Process*. K.S. Richards (ed.), The Institute of British Geographer Special Publication Series, Basil Blackwell, Oxford, p. 199-227.
- Dietrich, W.E. and J.D. Smith, 1984. Bed load transport in a river meander. *Water Resources Research* 20(10): 1355-1380.
- Dietrich, W.E., J.W. Kirchner, H. Ikeda, and F. Iseya, 1989. Sediment supply and the development of the coarse surface layer in gravel-bedload rivers. *Nature* 340: 215-217.
- Dietrich, W.E., D. Kinerson and L. Collins, 1993. Interpretation of relative sediment supply from bed surface textures in gravel bed rivers (abstract). American Geophysical Union 1993 Spring Meeting, Supplement to *EOS, AGU Transactions* 74 (16): 151.
- Diplas, P., 1989. Areal sampling techniques. In: *Sediment Transport Modeling*. S.S.Y. Wang (ed.), American Society of Civil Engineers, New York, p. 380-385.
- Diplas, P., 1992a. Surface and subsurface granulometry. In: *Grain Sorting Seminar. Mitteilungen der Versuchsanstalt für Wasserbau, Hydrologie und Glaziologie der Eidgenössischen Technischen Hochschule Zürich*, 117: 157-162.
- Diplas, P., 1992b. Discussion to "Experimental investigation of the effect of mixture properties on transport dynamics" by P.R. Wilcock, 1992. In: *Dynamics of Gravel Bed Rivers*. P. Billi, R.D. Hey, C.R. Thorne and P. Tacconi (eds.), John Wiley and Sons, Chichester, p. 131-135.
- Diplas, P. and J. Fripp, 1991. Bed material sampling: issues and answers. In: *Proceedings of the Fifth Federal Interagency Sedimentation Conference, Las Vegas, Nev.*, Subcommittee on Sedimentation of the Interagency Advisory Committee on Water Data, p. 2.81-2.88.
- Diplas, P. and J.B. Fripp, 1992. Properties of various sediment sampling procedures. *Journal of Hydraulic Engineering* 118 (7): 955-970.
- Diplas, P. and V.K. Lohani, 1997. Discussion of: "Application of the pebble count: notes on purpose, method, and variants," by G. Mathias Kondolf. *Journal of the American Water Resources Association* 33 (6): 1397-1399.
- Diplas, P. and A.J. Sutherland, 1988. Sampling techniques for gravel sized sediments. *Journal of Hydraulic Engineering* 114 (5): 484-501.

- Dunkerley, D.L., 1994. Discussion: bulk sampling of coarse clastic sediments for particle-size analysis. *Earth Surface Processes and Landforms* 19: 255-261.
- Dunne, T. and L.B. Leopold, 1978. *Water in Environmental Planning*. Freeman and Company, New York.
- DVWK, 1988. Feststofftransport in Fließgewässern - Berechnungsverfahren für die Ingenieurspraxis. [Solid matter transport - Computation procedures for engineers.] *DVWK-Schriften* 87, Paul Parey, Hamburg.
- Edwards, T.K. and Glysson, G.D., 1988. Field methods for measurement of fluvial sediment. *U.S. Geological Survey, Open File Report* 86-531, Reston, Virginia, 118 pp.
- Ehrlich, R., 1964. The role of the homogeneous unit in sampling plans for sediments. *Journal of Sedimentary Petrology* 34 (2): 437-439.
- Ergenzinger, P., B. Kozłowski, and P. Obenauf, 1999. Eroslope II, Abschlußbericht. [EROSLOPE II, Final Report submitted to the European Programme on Climatology and Natural Hazards, Contract number EV5V-CT92-0179].
- Ettema, R., 1984. Sampling armor-layer sediments. *Journal of Hydraulic Engineering* 110 (7): 992-996.
- Everest, F.H., C.E. McLemore and J.F. Ward, 1980. An improved tri-tube cryogenic gravel sampler. *U.S.D.A. Forest Service Research Note*, PNW-350, 8 pp.
- Fraccarollo, L. and A. Marion, 1993. Non-destructive sampling procedure for flume experiments on sediment transport. In: *Advances in Hydro-Science and -Engineering*, Vol. 1, S.S.Y. Wang (ed.), p. 1183-1188.
- Fehr, R., 1987. Geschiebeanalysen in Gebirgsflüssen. Umrechnung und Vergleich von verschiedenen Analyseverfahren. [Bed material analyses in mountain streams. Transformation and comparison of various analyses procedures]. *Mitteilungen der Versuchsanstalt für Wasserbau, Hydrologie und Glaziologie an der ETH Zürich*, No. 92, 139 pp., Switzerland.
- Ferguson, R.I. and A. Werritty, 1983. Bar development and channel changes in the gravelly River Feshie, Scotland. *Modern and Ancient Fluvial Systems*, J.D. Collinson and J. Lewin (eds.). Special Publications of the International Association of Sedimentologists 6: 169-180.
- Ferguson, R.I. and C. Paola, 1997. Bias and precision of percentiles of bulk grain size distributions. *Earth Surface Processes and Landforms* 22 (11): 1061-1078.
- Ferguson, R.I., T.B. Hoey, S.J. Wathen, A. Werritty, R.I. Hardwick and G.H. Sambrook Smith, 1998. Downstream fining of river gravels: integrated field, laboratory and modeling study. *Gravel-Bed Rivers in the Environment*. P.C. Klingeman, R.L. Beschta, P.D. Komar, and J.B. Bradley, eds., 85-114, Water Resources Publications LLC, Highlands Ranch, Colorado.
- Fleiss, J.L., 1981. *Statistical Methods for Rates and Proportions*. John Wiley & Sons, New York, 321 pp.
- Folk, R.L. and W.C. Ward, 1957. Brazos River Bar: a study in the significance of grain size parameters. *Journal of Sedimentary Petrology* 27(1): 3-26.
- Folk, R.L., 1966. A review of grain-size parameters. *Sedimentology* 6: 73-93.
- Fraccarollo, L. and A. Marion, 1995. Statistical approach to bed-material surface sampling. *Journal of Hydraulic Engineering* 121 (7): 640-645.

- Fraccarollo, L. and A. Marion, 1993. Non-destructive sampling procedure for flume experiments on sediment transport. In: *Advances in Hydro-Science and -Engineering*, Vol. 1, S.S.Y. Wang (ed.), p. 1183-1188.
- Fripp, J.B. and Diplas, P., 1993. Surface sampling in gravel streams. *Journal of Hydraulic Engineering* 119(4): 473-490.
- Fujita, Y., 1989. Bar and channel formation in braided streams. In: *River Meandering*. S. Ikeda and G. Parker (eds.), Water Resources Monograph 12, American Geophysical Union, Washington, DC, p. 417-462.
- Gale, S.J. and P.G. Hoare, 1992. Bulk sampling of coarse clastic sediments for particle size analysis. *Earth Surface Processes and Landforms* 17: 729-733.
- Gale, S.J. and P.G. Hoare, 1994. Reply: Bulk sampling of coarse clastic sediments for particle size analysis. *Earth Surface Processes and Landforms* 19: 263-268.
- Gessler, D., C.C. Watson and N. Raphael, 1993. Effect of grain size on sediment transport calculations. *Hydraulic Engineering*, Vol. 1, H.W. Shen, S.T. Su and F. Wen (eds.), ASCE, New York, p. 887-892.
- Gessler, J., 1992. Armoring on the surface of gravel bed rivers revisited. In: *Grain Sorting Seminar. Mitteilungen der Versuchsanstalt für Wasserbau, Hydrologie und Glaziologie der Eidgenössischen Technischen Hochschule Zürich*, 117: 299-309, Switzerland.
- Gilbert, R.O., 1987. *Statistical Methods for Environmental Pollution Monitoring*. Van Nostrand Reinhold, New York, 320pp.
- Gomez, B., 1979. A technique for sampling the surface bed material in mixed sand and gravel streams. *British Geomorphological Research Group, Technical Bulletin* 24: 15-21, Geo Abstracts Ltd., Norwich, England.
- Gomez, B., 1983a. Representative sampling of sandy fluvial gravels. *Sedimentary Geology* 34: 301-306.
- Gomez, B., 1983b. Temporal variations in bedload transport rates: the effect of progressive bed-armouring. *Earth Surface Processes and Landforms* 8: 41-54.
- Gomez, B., 1983c. Temporal variations in the particle size distribution of surficial bed material: the effect of progressive bed armouring. *Geografiska Annaler* 65 A (3/4): 183-192.
- Gordon, N.D., T.A. McMahon and B.L. Finlayson, 1992. *Stream Hydrology. An Introduction for Ecologists*. John Wiley and Sons, Chichester, GB, 526 pp.
- Grant, G.E., F.J. Swanson and M.G. Wolman, 1990. Patterns and origin of stepped-bed morphology in high gradient streams, Western Cascades, Oregon. *Geological Society of America Bulletin* 102: 340-352.
- Haan, C.T., 1977. *Statistical Methods in Hydrology*. Iowa State University Press, Ames, 378 pp.
- Harvey, A.M., 1987. Sediment supply to upland streams: influence on channel adjustment. In: *Sediment Transport in Gravel-Bed Rivers*, C.R. Thorne, J.C. Bathurst and R.D. Hey (eds.), John Wiley and Sons, Chichester, p. 121-150.
- Hey, R.D. and C.R. Thorne, 1983. Accuracy of surface samples from gravel bed material. *Journal of Hydraulic Engineering*, 109 (6): 842-851.

- Hilton, S. and T.E. Lisle, 1993. Measuring the fraction of pool volume filled with fine sediment. *U.S.D.A. Forest Service, Pacific Southwest Research Station, Research Note PSW-RN-414*, 11 pp.
- Hirsch, P.J. and A.D. Abrahams, 1981. The properties of bed sediments in pools and riffles. *Journal of Sedimentary Petrology* 51 (3): 757-760.
- Hogan, S.A., S.R. Abt and C.C. Watson, 1993. Development and testing of a bed material sampling method for gravel and cobble bed streams. Report prepared at the Department of Civil Engineering, Colorado State University, Fort Collins, CO, 126 pp.
- Ibbeken, H., 1974. A simple sieving and splitting device for field analysis of coarse grained sediments. *Journal of Sedimentary Petrology* 44(3): 939-946.
- Ibbeken, H., 1983. Jointed source rock and fluvial gravels controlled by Rosin's law: a grain size study in Calabria, South Italy. *Journal of Sedimentary Petrology* 53(4): 1213-1231.
- Ibbeken, H., and P. Denzer, 1988. Clast measurement: a simple manual device and its semiautomatic electronic equivalent. *Journal of Sedimentary Petrology* 58 (4): 751-752.
- Ibbeken, H. and R. Schleyer, 1986. Photo sieving: a method for grainsize analysis of coarse-grained, unconsolidated bedding surfaces. *Earth Surface Processes and Landforms* 11: 59-77.
- Inman, D.L., 1952. Measures for describing the size distribution of sediments. *Journal of Sedimentary Petrology* 22: 125-145.
- Iseya, F., and H. Ikeda, 1987. Pulsations in bedload transport rates induced by longitudinal sediment sorting: a flume study using sand and gravel mixtures. *Geografiska Annaler* 69A(1): 15-27.
- ISO 1977. Liquid flow measurement in open channels - bed material sampling. *International Organization of Standardization*, publication no. ISO 4364: 1977(E): 380-392, International Organization of Standardization, Genève, Switzerland.
- ISO 1992. Liquid flow measurement in open channels - sampling and analysis of gravel-bed material. *International Organization of Standardization*, publication no. ISO 9195: 1992(E), 9pp. International Organization of Standardization, Genève, Switzerland.
- Johnston, C.E., E.D. Andrews and J. Pitlick, 1998. In situ determination of particle friction angles of fluvial gravels. *Water Resources Research* 34: 2012-2030.
- Julien, P., 1995. *Erosion and Sedimentation*. Cambridge University Press, Cambridge.
- Kappesser, G., 1995. Riffle stability index. Unpublished draft manuscript for review and comment. George Washington and Jefferson National Forests, Roanoke, VA, 21p.
- Keller, E.A., 1971. Areal sorting of bed-load material: the hypothesis of velocity reversal. *Geological Society of America Bulletin* 82: 753-756.
- Keller, E.A. and J.L. Florsheim, 1993. Velocity-reversal hypothesis: a model approach. *Earth Surface Processes and Landforms* 18: 733-740.
- Keller, E.A. and W.N. Melhorn, 1978. Rhythmic spacing and origin of pools and riffles. *Geological Society of America Bulletin* 89: 723-730.
- Keller, E.A. and W.N. Melhorn, 1981. Bedforms and fluvial processes in alluvial stream channels: selected observations. In: *Fluvial Geomorphology*. M. Morisawa (ed.),

- The "Binghamton" Symposia in Geomorphology International Series, No. 4., p. 253-283, George Allen & Unwin, London.
- Kellerhals, R. and D.I. Bray, 1971. Sampling procedures for coarse fluvial sediments. *Journal of the Hydraulics Division, ASCE*, 97 (HY8): 1165-1180.
- King, R.M. and J.P. Potyondy, 1993. Statistically testing Wolman pebble counts: changes in percent fines. In: *Stream Notes*, October 1993. USDA Forest Service, Stream Systems Technology Center, Fort Collins, CO.
- Kirchner, J.W., W.E. Dietrich, F. Iseya and H. Ikeda, 1990. The variability of critical shear stress, friction angle, and grain protrusion in water-worked sediments. *Sedimentology* 37: 647-672.
- Klingeman, P.C. and Emmett, W.W., 1982. Gravel bedload transport processes. In: *Gravel-bed Rivers. Fluvial Processes, Engineering and Management*. R.D. Hey; J.C. Bathurst and C.R. Thorne (eds.), John Wiley and Sons, Chichester, p. 141-179.
- Kondolf, G.M., 1997a. Application of the pebble count: notes on purpose, method, and variants. *Journal of the American Water Resources Association* 33 (1): 79-87.
- Kondolf, G.M., 1997b. Reply to discussion by Gregory S. Bevinger and Rudy M. King: "Application of the pebble count: notes on purpose, method, and variants." *Journal of the American Water Resources Association* 33 (6): 1395-1396.
- Kondolf, G.M., 1997c. Reply to discussion by Panayiotis Diplas and Vinod K. Lohani: "Application of the pebble count: notes on purpose, method, and variants." *Journal of the American Water Resources Association* 33 (6): 1395-1396.
- Kondolf, G.M. and S. Li, 1992. The pebble count technique for quantifying surface bed material size in instream flow studies. *Rivers* 3(2): 80-87.
- Kondolf, G.M. and M.G. Wolman, 1993. The sizes of salmonid spawning gravels. *Water Resources Research* 29 (7): 2275-2285.
- Koster, E.H., 1978. Transverse ribs: their characteristics, origin and paleohydraulic significance. In: *Fluvial Sedimentology*, A.D. Miall (ed.), Canadian Society of Petroleum Geologists, Calgary, Alberta, Canada, p. 161-186.
- Kothyari, U.C., 1995. Frequency distribution of river bed materials. *Sedimentology* 42: 283-291.
- Kozlowski, B. and P. Ergenzinger, 1999. Ring structures – a specific new cluster type in steep mountain torrents. In: *Proceedings of the 27<sup>th</sup> IAHR Congress*, held in Graz, Austria, 9 pp; for viewing see: [www.iahr.org](http://www.iahr.org)
- Krumbein, W.C., 1940. Flood gravel of San Gabriel Canyon, California. *Bulletin of the Geological Society of America*, 51: 673-706.
- Krumbein, W.C., 1941. Measurement and geological significance of shape and roundness of sedimentary particles. *Journal of Sedimentary Petrology* 11 (2): 64-72.
- Krumbein, W.C., 1942. Flood deposits of Arroyo Seco, Los Angeles County, California. *Bulletin of the Geological Society of America*, 53: 1355-1401.
- Lane, E.W., 1955. The importance of fluvial morphology in hydraulic engineering. *Proceedings of the American Society of Civil Engineers*, Vol. 81, paper no. 745.
- Lane, E.W. and E.J. Carlson, 1953. Some factors affecting the stability of canals constructed in coarse granular material. *Proceedings of the 5th IAHR Congress*, p. 37-48.

- Lauck, T., Lamberson, R. and T.E. Lisle, 1993. A simulation model for the infiltration of heterogeneous sediment into a stream bed. In: *Advances in Hydro-Science and - Engineering*, Vol. 1, S.S.Y. Wang (ed.), p. 229-236.
- Leopold, L.B., 1970. An improved method for size distribution of stream bed gravel. *Water Resources Research* 6(5): 1357-1366.
- Leopold, L.B., 1992. Sediment size that determines channel morphology. In: *Dynamics of Gravel Bed Rivers*. P. Billi, R.D. Hey, C.R. Thorne and P. Tacconi (eds.), John Wiley and Sons, Chichester, p. 297-311.
- Lewis, D.W. and D. McConchie, 1994. *Analytical Sedimentology*. Chapman & Hall, New York.
- Li, Z. and P.D. Komar, 1986. Laboratory measurements of pivoting angles for application to selective entrainment of gravel in a current. *Sedimentology* 33: 413-423.
- Lisle, T.E., 1979. A sorting mechanism for a riffle-pool sequence: summary. *Geological Society of America Bulletin*, Part. 1, 90: 616-617.
- Lisle, T.E., 1995. Particle size variations between bed load and bed material in natural gravel bed channels. *Water Resources Research* 31 (4): 1107-1118.
- Lisle, T.E. and S. Hilton, 1992. The volume of fine sediment in pools: an index of sediment supply in gravel-bed streams. *Water Resources Bulletin* 28(2): 371-383.
- Lisle, T.E. and S. Hilton, 1996. Storage of fine-grained bed material in pools of natural gravel-bed channels (abstract). American Geophysical Union 1996 Fall Meeting, Supplement to *EOS, AGU Transactions* 77 (46): F253.
- Lisle, T.E. and S. Hilton, 1999. Fine bed material in pools of natural gravel bed channels. *Water Resources Research* 35 (4): 1291-1304.
- Lisle, T.E. and M.A. Madej, 1992. Spatial variation in armouring in a channel with high sediment supply. In: *Dynamics of Gravel Bed Rivers*. P. Billi, R.D. Hey, C.R. Thorne and P. Tacconi (eds.), John Wiley and Sons, Chichester, p. 277-293.
- Lisle, T.E., F. Iseya and H. Ikeda, 1993. Response of channel with alternate bars to a decrease in supply of mixed-size bed load: a flume experiment. *Water Resources Research* 29(11): 3623-3629.
- Little, W.C. and P.G. Mayer, 1976. Stability of channel beds by armorings. *Journal of the Hydraulics Division*, 102 (HY11): 1647-1661.
- Looney, S.W. and T.R. Gullledge, Jr., 1985. Use of the correlation coefficient with normal probability plots. *The American Statistician* 39 (1): 75-79.
- Lotspeich, F.B. and F.H. Everest, 1981. A new method for reporting and interpreting textural composition of spawning gravel. Research Note, Pacific Northwest Forest and Range Experiment Station, PNW-369.
- Lotspeich, F.B. and B.H. Reid, 1980. A tri-tube freeze-core procedure for sampling stream-gravels. *The Progressive Fish Culturist* 42 (2): 96-99.
- Lotspeich, F.B. and B.H. Reid, 1980. A tri-tube freeze-core procedure for sampling stream-gravels. *The Progressive Fish Culturist* 42 (2): 96-99.
- MacDonald, L.H., E.E. Wohl and S. Madsen, 1997. Validation of Water Yield Thresholds on the Kootenai National Forest. Final Report submitted to the Kootenai National Forest, Libby, Montana, 197 pp.
- MacDonald, L.H., A.W. Smart and R.C. Wissmar, 1991. *Monitoring Guidelines to Evaluate Effects of Forestry Activities on Streams in the Pacific Northwest and*

- Alaska*. United States Environmental Protection Agency, Water Division, EPA/910/9-91-001, 166 pp.
- McDonald, B.C. and I. Banerjee, 1971. Sediments and bed forms on a braided outwash plain. *Canadian Journal of Earth Sciences* 8(10): 1282-1301.
- McNeil, W.J. and W.H. Ahnell, 1964. Success of pink salmon spawning relative to size of spawning bed materials. *US Fish and Wildlife Service Special Scientific Report, Fisheries* No. 469.
- Marcus, W.A., S. Ladd and J. Stoughton, 1995. Pebble counts and the role of user-dependent bias in documenting sediment size distributions. *Water Resources Research* 31 (10): 2625-2631.
- Marion, A. and L. Faccarollo, 1997. New conversion model for areal sampling of fluvial sediments. *Journal of Hydraulic Engineering* 123 (12): 1148-1151.
- Marshall, T.J. and J.W. Holmes, 1988. *Soil Physics*. Cambridge University Press, Cambridge, Great Britain, 336 pp.
- Milhous, R.T., 2001. Specific weight and median size of the bed material of gravel and cobble bed rivers. *Proceedings of the Seventh Federal Interagency Sedimentation Conference*, March 25-29, 2001, Reno, Nevada. (Submitted)
- Milhous, R.T., S.A. Hogan, S.R. Abt and C.C. Watson, 1995. Sampling river-bed material: the barrel sampler. *Rivers* 5 (4): 239-249.
- Miller, R.L. and Byrne, R.J., 1966. The angle of repose for a single grain on a fixed rough bed. *Sedimentology* 6: 303-314.
- Montgomery, D.R. and J.M. Buffington, 1993. Channel classification, prediction of channel response, and assessment of channel condition. Report TFW-SH10-93-002 prepared for the SHAMW committee of the Washington State Timber/Fish/Wildlife Agreement, 107 pp.
- Montgomery, D.R., J.M. Buffington, R.D. Smith, K.M. Smith and G. Pess, 1995. Pool spacing in forest channels. *Water Resources Research* 31(4): 1097-1105.
- Montgomery, D.R. and J.M. Buffington, 1997. Channel-reach morphology in mountain drainage basins. *Geological Society of America Bulletin* 109 (5): 596-611.
- Montgomery, D.R. and J.M. Buffington, 1998. Channel Processes, classification, and response. *River Ecology and Management. Lessons from the Pacific Coastal Ecoregion*. R.J. Naiman and R.E. Bilby (eds.), 13-42, Springer Verlag, New York, NY, 705 pp.
- Mosley, M.P. and D.S. Tindale, 1985. Sediment variability and bed material sampling in gravel bed rivers. *Earth Surface Processes and Landforms* 10: 465-482.
- Naden, P.S. and A.C. Brayshaw, 1987. Small- and medium-scale bedforms in gravel-bed rivers. In: *River Channels. Environment and Process*. K.S. Richards (ed.), The Institute of British Geographer Special Publication Series, Basil Blackwell, Oxford, p. 249-271.
- National Council of the Paper Industry for Air and Stream Improvement (NCASI), 1986. A comparison of four procedures for determining streambed substrate composition. *Technical Bulletin* 481.
- Neter, J., W. Wasserman and M.H. Kutner, 1990. *Applied Linear Statistical Models*. 3<sup>rd</sup> ed. Irwin, Burr Ridge, Il., 1181 pp.

- Neumann-Mahlkau, P., 1967. Korngrößenanalyse grobklastischer Sedimente mit Hilfe von Aufschluß-Photographien. [Granulometric analysis of rudites on outcrop-photographs.] *Sedimentology* 9: 245-261.
- Newbury, R.W. and M.N. Garboursy, 1993. *Stream Analysis and Fish Habitat Design. A Field Manual*. Newbury Hydraulics, Ltd., Gibsons, British Columbia, Canada.
- Parker, G., 1987. Discussion to Church, M., D.G. McLean and J.F. Walcott, 1987. "Bed load sampling and analysis". In: *Sediment Transport in Gravel-Bed Rivers*, C.R. Thorne, J.C. Bathurst and R.D. Hey (eds.), John Wiley and Sons, Chichester, p. 79-80.
- Parker, G., P.C. Klingeman and D.G. McLean, 1982. Bedload and the size distribution of paved gravel-bed streams. *Journal of the Hydraulics Division, ASCE*, 108 (HY4): 544-571.
- Petrie, J. and P. Diplas, 2000. Statistical approach to sediment sampling accuracy. *Water Resources Research* 36 (2): 597-605.
- Pettijohn, J.F., P.E. Potter, and R. Siever, 1972. *Sand and Sandstone*. Springer Verlag, New York, Heidelberg, Berlin, 619 pp.
- Platts, W.S., W.F. Megahan and G.W. Minshall, 1983. Methods for evaluating stream, riparian, and biotic conditions. In: USDA, Forest Service, Intermountain Forest and Range Experiment Station, Ogden UT, *General Technical Report INT-138*, 62pp.
- Poole, G.C., C.A. Frissell and S.C. Ralph, 1997. In-stream habitat unit classification: inadequacies for monitoring and some consequences for management. *Journal of the American Water Resources Association* 33 (4): 879-896.
- Potyondy, J.P. and T. Hardy, 1994. Use of pebble counts to evaluate fine sediment increase in stream channels. *Water Resources Bulletin* 30 (3): 509-520.
- Pye, W.D. and M.H. Pye, 1943. Sphericity determinations of pebbles and sand grains. *Journal of Sedimentary Petrology* 13 (1): 28-34.
- Ramos, C., 1996. Quantification of stream channel morphological features: recommended procedures for use in watershed analysis and TFW ambient monitoring. *Timber, Fish and Wildlife*, Report TFW-Am9-96-006.
- Reid, I, L.E. Frostick and A.C. Brayshaw, 1992. Microform roughness elements and the selective entrainment and entrapment of particles in gravel-bed rivers. In: *Dynamics of Gravel Bed Rivers*. P. Billi, R.D. Hey, C.R. Thorne and P. Tacconi (eds.), John Wiley and Sons, Chichester, p. 253-275.
- Reiser, D. and J.B. Bradley, 1993. Fine sediment intrusion and salmonid habitat. In: *Advances in Hydro-Science and -Engineering*, Vol. 1, S.S.Y. Wang (ed.), p. 257-264.
- Rice, S., 1994. Towards a model of changes in bed material texture at the drainage basin scale. In: *Process Models and Theoretical Geomorphology*. M.J. Kirkby (ed.), John Wiley and Sons, New York, p. 159-172.
- Rice, S., 1995. The spatial variation and routine sampling of spawning gravels in small coastal streams. Research Branch, British Columbia Ministry of Forests, Victoria, B.C., Working Paper 06/1995, 41 pp.
- Rice, S. and M. Church, 1996a. Bed material texture in low order streams on the Queen Charlotte Islands, British Columbia. *Earth Surface Processes and Landforms* 21: 1-18.

- Rice, S. and M. Church, 1996b. Sampling surficial fluvial gravels: the precision of size distribution percentile estimates. *Journal of Sedimentary Research* 66 (3): 654-665.
- Rice, S. and M. Church, 1998. Grain size along two gravel-bed rivers: statistical variation, spatial pattern, and sedimentary links. *Earth Surface Processes and Landforms* 23: 345-363.
- Richards, K.S., 1976. The morphology of riffle-pool sequences. *Earth Surface Processes and Landforms* 1: 71-88.
- Ritter, J.R. and E.J. Helley, 1969. Optical methods for determining particle sizes of coarse sediment. In: *Techniques of Water-Resources Investigations of the United States Geological Survey*, Book 5: Laboratory Analysis, Chapter 3. Preliminary Report Open File, 33 pp.
- Rood, K. and M. Church, 1994. Modified freeze-core technique for sampling the permanently wetted streambed. *North American Journal of Fisheries Management* 14: 852-861.
- Rosgen, D.L., 1994. A classification of natural rivers. *Catena* 21: 169-199.
- Rosgen, D.L., 1996. *Applied River Morphology*. Wildland Hydrology, Pagosa Springs, Colorado.
- Sahu, B.K., 1964. Transformation of weight frequency and number frequency data in size distribution studies of clastic sediments. *Journal of Sedimentary Petrology* 34(4): 768-773.
- Sambrook Smith, G.H. and R.I. Ferguson 1995. The gravel-sand transition along river channels. *Journal of Sedimentary Research A*, 65: 423-430.
- Sambrook Smith, G.H., A.P. Nicholas and R.I. Ferguson, 1997. Measuring and defining bimodal sediments: Problems and implications. *Water Resources Research* 33 (5): 1179-1185.
- Schleyer, R., 1987. The goodness-of-fit to ideal Gauss and Rosin Distributions: a new grain-size parameter. *Journal of Sedimentary Petrology* 57(5): 871-880.
- Schnackenberg, E.S. and L.H. MacDonald, 1998. Detecting cumulative effects on headwater streams in the Routt National Forest, Colorado. *Journal of the American Water Resources Association* 34 (5): 1163-1177.
- Schuett-Hames, D., B. Conrad, A. Pleus, and D.Smith, 1996. Field comparison of the McNeil sampler with three shovel-based methods used to sample spawning substrate composition in small streams. Timber, Fish and Wildlife, TFW-AM-9-96-005, 33 pp.
- Seal, R. and C. Paola, 1995. Observations of downstream fining on the North Fork Toutle River near Mount St. Helens, Washington. *Water Resources Research* 31(5): 1409-1419.
- Seal, R., C. Toro-Escobar, Y. Cui, C. Paola, G. Parker, J.B. Southard and P.R. Wilcock, 1998. Downstream fining by selective deposition: theory, laboratory, and field observations. *Gravel-Bed Rivers in the Environment*. P.C. Klingeman, R.L. Beschta, P.D. Komar, and J.B. Bradley, eds., 61-84, Water Resources Publications LLC, Highlands Ranch, Colorado.
- Sear, D.A., 1996. Sediment transport processes in pool-riffle sequences. *Earth Surface Processes and Landforms* 21: 241-262.
- Shirazi, M.A. and Seim, W.K., 1981. Stream system evaluation with emphasis on spawning habitat for salmonids. *Water Resources Research* 17(3): 592-594.

- Simons, D.B. and F. Sentürk, 1992. *Sediment Transport Technology. Water and Sediment Dynamics*. Water Resources Publications, Littleton, Colorado, 897pp.
- Smartt, P.F.M and J.E.A. Grainger, 1974. Sampling for vegetation survey: some aspects of the behavior of unrestricted, restricted, and stratified techniques. *Journal of Biogeography* 1: 193-206.
- Smith, L. and S.W. Wheatcraft, 1993. Groundwater flow. In: *Handbook of Hydrology*, D.R. Maidment (ed.), McGraw-Hill, New York.
- Sneed, E.D. and R.L. Folk, 1958. Pebbles in the lower Colorado River, Texas: a study in particle morphogenesis. *Journal of Geology* 66: 114-150.
- Stedinger, J.R., R.M. Vogel, and E. Foufoula-Georgiou, 1993. Frequency analysis of extreme events. In: *Handbook of Hydrology*, D.R. Maidment (ed.), McGraw-Hill, New York.
- Stream Notes*, April 1996. Newsletter published by the Stream Technology Center, USDA Forest Service, Rocky Mountain Range and Experiment Station, Fort Collins.
- Sullivan, K., T.E. Lisle, C.A. Dolloff, G.E. Grant, and L.E. Reid, 1987. Stream channels: The link between forests and fishes. In: *Streamside Management: Forestry and Fishery Interactions*, E.O. Salo and T.W. Cundy (eds.), College of Forests Resources, University of Washington, Seattle, WA, Contribution No. 57: 39-97.
- Surian, N., 2000. Downstream variation in bed material size along a braided river, Piave River, Italy. in: Nolan, T. and C. Thorne (eds.), *Gravel-Bed Rivers 2000 CD Rom*. A Special Publication of the New Zealand Hydrological Society.
- Sutherland, A.J., 1987. Static armor layers by selective erosion. In: *Sediment Transport in Gravel-Bed Rivers*. C.R. Thorne, J.C. Bathurst, and R.D. Hey (eds.), John Wiley, Chichester, p. 243-267.
- Swan, B., 1974. Measures of particle roundness: a note. *Journal of Sedimentary Petrology* 44 (2): 572-577.
- Teleki, P.G., 1972. Areal sorting of bed-load material: the hypothesis of velocity reversal: discussion. *Geological Society of America Bulletin* 83: 911-913.
- Thomas, E.L. and E.E. Rand, 1991. Methods to measure sedimentation of spawning gravels. USDA Forest Service, Los Angeles, California, *Research Note PNW-411*.
- Thompson, A., 1986. Secondary flows and the pool-riffle unit: a case study of the processes of meander development. *Earth Surface Processes and Landforms* 11: 631-641.
- Thompson, D.M., 1995. The effects of large organic debris on sediment processes and stream morphology in Vermont. *Geomorphology* 11: 235-244.
- Thompson, D.M., E.E. Wohl and R.D. Jarrett, 1996. A revised velocity-reversal and sediment sorting model for a high-gradient, pool-riffle stream. *Physical Geography* 17 (2): 142-156.
- Thoms, M.C., 1992. A comparison of grab- and freeze-sampling techniques in the collection of gravel-bed river sediment. *Sedimentary Geology* 78: 191-200.
- Todd, S.P., 1996. Process deduction from fluvial sedimentary structures. In: *Advances in Fluvial Dynamics and Stratigraphy*. P.A. Carling and M.R. Dawson (eds.), John Wiley and Sons, Chichester.
- Trask, P.D., 1932. *Origin and Environment of Source Sediments in Petroleum*. Gulf Publishing Company, Houston, Texas, 324 pp.

- Triola, M.F., 1995. *Elementary Statistics*. 6<sup>th</sup> ed. Addison-Wesley Publishing Company, Reading, Massachusetts, 726 pp.
- Wadell, H., 1932. Volume, shape, and roundness of rock particles. *Journal of Geology* 40: 443-451.
- Walkotten, W.J., 1973. A freezing technique for sampling streambed gravel. USDA Forest Service, Portland, Oregon, Research Note PNW-205.
- Walkotten, W.J., 1976. An improved technique for freeze sampling streambed sediments. U.S.D.A. Forest Service Research Note PNW-281, 11 pp.
- Warren, G., 1974. Simplified form of the Folk-Ward skewness parameter. *Journal of Sedimentary Petrology* 44: (1): 259.
- Whiting, P., 1996. Sediment sorting over bed topography. In: *Advances in Fluvial Dynamics and Stratigraphy*, P.A. Carling and M.R. Dawson (eds.), John Wiley and Sons, Chichester, p. 203-228.
- Whiting, P.J. and J.B. Bradley, 1993. A process-based classification system for headwater streams. *Earth Surface Processes and Landforms* 18: 603-612.
- Whiting, P.J. and W.E. Dietrich, 1993. Experimental studies of bed topography and flow patterns in large-amplitude meanders. 1. Observations. *Water Resources Research* 29 (11): 3605-3614.
- Whiting, P.J., W.E. Dietrich, L.B. Leopold, T.G. Drake, and R.L. Shreve, 1988. Bedload sheets in heterogeneous sediment. *Geology* 16: 105-108.
- Wilcock, P.R., 1993. Critical shear stress of natural sediments. *Journal of Hydraulic Engineering* 119 (4): 491-505.
- Wilcock, P.R. and R.S. Stull, 1989. Magnetic paint sampling of the surface and subsurface of clastic sediment beds. *Journal of Sedimentary Petrology* 59: 626-627.
- Williams, O.R., R.B. Thomas and R.L. Daddow, 1988. Methods for collection and analysis of fluvial-sediment data. USDA Forest Service, Watershed and Air Management Staff, Report WSDG-TP-00012, 85 pp.
- Wohl, E.E., D.J. Anthony, S.W. Madsen, D.M. Thompson, 1996. A comparison of surface sampling methods for coarse fluvial sediments. *Water Resources Research*, 32 (10): 3219-3226.
- Wolcott, J. and M. Church, 1991. Strategies for sampling spatially heterogeneous phenomena: the example of river gravels. *Journal of Sedimentary Petrology* 61(4): 534-543.
- Wolman, M.G., 1954. A method of sampling coarse bed material. *American Geophysical Union, Transactions*, 35: 951-956.
- Wood-Smith, R.D and J.M. Buffington, 1996. Multivariate geomorphic analysis of forest streams: implications for assessment of landuse impacts on channel conditions. *Earth Surface Processes and Landforms* 21: 377-393.
- Yang, C.T., 1971. Formation of riffles and pools. *Water Resources Research* 7(6): 1567-1574.
- Yang, C.T., 1996. *Sediment Transport. Theory and Practice*. McGraw-Hill, New York.
- Young, M.K., W.A. Hubert, and T.A. Wesche, 1991. Biases associated with four stream substrate samplers. *Canadian Journal of Fisheries and Aquatic Science* 48 (10): 1882-1886.

- Yuzyk, T.R., 1986. Bed material sampling in gravel-bed streams. Sediment Survey Section, Water Survey of Canada, Water Resources Branch, Inland Waters Directorate, Conservation and Protection, Environment Canada, Report IWD-HQ-WRB-SS-86-8, 62 pp.
- Yuzyk, T.R. and T. Winkler, 1991. Procedures for bed-material sampling. Lesson Package No. 28. Environment Canada, Water Resources Branch, Sediment Survey Section, Ottawa, Canada, 100 pp.

## 10. Index

---

### A

- a*-axis, 14-17, 86, 136-137, 140
- Abrasion, 85, 88, 107
- Absolute error, 242. *See* Error around mean, median, *and* percentiles
- Accuracy, 243-245, 259, 277  
and precision, 244, 225  
definition of, 244
- Adhesive areal samples, 224-226, 284, 351, 355  
methods, 172-177  
for fine gravel surfaces, 172  
clay and flour dough, 176-177, 230  
effect of sedimentary properties, 173  
freeze technique, 173  
various substances, 172  
wax, 225, 229  
modeling, 224
- Adhesive penetration depth, 173-175, 217  
computed, 226-229
- Adhesive properties, 173-176
- Adjustment of frequency distributions, 237-238
- Aggrading stream reach, 120, 122, 191, 228, 340, 345, 373, 378
- Air-drying, of particles, 32, 33
- Alluvial, free-formed streams, 117
- Alluvial wedge, 124
- Alternate bars, 109, 113
- American Society for Testing and Materials. *See* ASTM
- Anastomosing stream, 9
- Angle of repose. *See* Pivot angles
- Angularity. *See* Particle shape
- Antidunes, 134
- Aquatic habitat, 105, 128, 132, 146, 178, 277, 279, 371  
for spawning 131, 203, 371
- Area-by-number, 171, 178, 219, 221, 228
- Area-by-weight, 171, 217-220, 222-227, 229
- Areal overview, 166, 183-184
- Areal samples, 132, 144-146, 154, 168, 170-173, 176-178, 184, 188, 230, 234, 325, 342, 347, 351, 354-355, 380  
adhesive methods. *See* Adhesive methods  
area covered per sample, 171, 197, 283-286  
bias towards fines, 224  
converted to grid-by-number by:  
computed penetration depth, 226-229  
modified cube model, 224-226  
split plane surface model, 227-229  
voidless cube model, 218-224, 227  
combined with pebble counts by:  
adjustment of frequency distributions, 237-238  
flexible combination, 233-236  
rigid combination, 230-233  
definition of, 145, 170  
from photographs. *See* Photographic areal samples *and* Photo sieving  
hand-picking, particle retrieval, 145, 170-172  
magnetic paint, 172  
operator variability, 176  
sample size and number of samples, 171  
suitability of, 146  
thin-section technique, 173, 176  
time requirement of, 146  
to expose subsurface, 192
- Areal weighting, of particle-size distributions, 347, 351, 354, 356-358, 371, 377-379
- Arithmetic progression, 59
- Armor layer, 129-132, 143, 188, 191, 199, 201, 207, 213, 333, 359, 371, 373  
definition of, 188  
development of, 182, 188  
diagram, 143  
difference between armor and subarmor, 190  
poorly developed, 188  
removal of to expose subarmor, 191-192  
representativeness for the reach, 372  
sample, 191, 330  
sampling, 210  
sampling depth, 188, 190  
thickness, 188-190, 192, 330
- Armored beds, 228
- Armoring, 128, 130-131, 199  
degree of, 188, 191
- ASTM C136-71, 296
- ASTM D75-71, 296
- ASTM E-11, 21
- A-type streams, 4, 9, 122-123, 325, 326

### B

- Backfill, of transverse clast dams, 133-134
- Backhoe, 203
- Backwater, 123-124, 126, 277, 340, 372

Bankfull, 118, 289, 338, 380  
 Bank line, 120  
 Banks, 283, 326, 346  
     self formed, 120  
 Bankward fining, 120  
 Bar graph, 38  
 Bar head, 113, 117, 119-120, 371, 380  
 Barrel samplers, 206-208, 331, 367, 372  
 Bars, 107-111, 113, 119-121, 326, 333, 340  
     alternate bars, 109, 112  
     bed-material size, 113-114  
     downbar fining, 108, 114, 323, 326  
     forced by obstacle, 114  
     free-formed, 114, 380  
     in braided streams, 112, 114  
     in B-type streams, 122  
     in mountain streams, 111  
     in streams with large sediment supply, 112  
     lobe front, 109, 133  
     medial bars, 113  
     point bars, 109  
     representativeness for sampling location, 114  
     riffle bars, 109  
     sampling on, 380-381  
 Bar toe, 114  
 Bar types, 111  
 Bar unit, 109-111, 113, 115-117, 122  
*b*-axis 14-17, 21-25, 27-28, 86, 136-137, 168-169, 179  
     and square-hole sieve size, 21  
     lengths, 16, 21, 23-24  
     measurements of, 28, 30, 164. *See also*  
         Measurements of particle size  
     of the  $D_{max}$ , 189  
     on photographs, 166, 168-169, 178-179, 184  
     plane, position of, 168-170, 178, 184  
 Beaver dams, 123  
 Bedform morphology, 120  
 Bedload, 107-108, 119, 123-124, 127, 130-132, 343  
     particle-size distribution of, 373  
     blockage of conveyance by LWD, 123-124, 126  
 Bedload sheets, 135-136  
 Bedload transport  
     prediction of, 141, 188, 343  
     rates, 127, 136, 148, 289  
     supply-limited and transport limited, 340, 343, 373, 383  
     three-dimensional patterns of, 108  
 Bed-material sampling. *See* Sampling,  
 Bed-material size, 107-108, 113, 126  
     and sediment supply, 114  
     around boulders, 124, 127  
     around LWD, 116, 125-126  
     chaotic patterns, 126  
     coarse, 115  
     coarsest parts of the reach, 117  
     heterogeneity (heterogeneous). *See*  
         Heterogeneity  
     homogeneity (homogeneous). *See*  
         Homogeneity  
     in pools, 113, 118, 119  
     in riffle-pool reach, 120, 122  
     on bar heads, 120  
     on bars, 113, 114  
     on riffle crests, 113  
     on riffle-related features, 117  
     on riffles, 108, 116, 118, 120  
     patchy, 126, 323. *See also* Patch, patchiness  
     reach-averaged. *See* Reached-averaged bed-material size  
     spatial variability. *See* Spatial variability of bed-material size  
     vertical stratification, 128-132, 143  
     wide size range of, 199  
 Bed stability, 136, 362, 372  
 Bed-surface plane, 173, 175, 177  
 Bed-surface structures, 114, 133-141, 154, 156, 183, 327  
     analysis by photo sieving, 181  
     and photographic methods, 133  
     effects on bed-material sampling, 119  
     effects on hydraulic roughness, 142  
     effects on particle mobility, 141  
 Bias, 243-245  
     against fines  
         in pebble counts, 224, 229  
         in photographic grid counts, 170  
         in photo sieving  
         in shoveled samples, 199  
     against large particles, 338  
         in heel-to-toe samples, 154, 156-157  
         in small samples, 304  
         in volumetric samples, 192, 194  
     and percentiles, 311-314  
     and sample mass, 313  
     and sorting, 311-314  
     in areal samples, towards fine sediment 224  
     in pebble counts, against fines, 224, 229  
     in photo sieving against fine and large particles, 178, 181  
     in poorly accessible stream locations, 333  
     towards large particles, 300-301, 341  
         in areal samples, 285  
         in small samples, 304  
 Biased sample, 298  
 Bimodal, 51, 62, 82-84, 108, 275  
 Bimodality, 62, 83-85  
 Binned data, 71  
 Binning, of particle sizes, 42, 328  
 Binomial approach (sample size), 261, 264-265

Boom trucks, 203  
 Bootstrap approach (sample size and sample mass), 152-153, 162, 243, 261, 268-277, 288, 309, 315-320  
     and multinomial approach, 277  
     and total error, 276-277  
     computer program for, 309  
     versus one-step approach, 276  
 Bootstrap error, 268-275, 315-320  
 Bootstrapping. *See* Bootstrap approach  
 Boulder and cobble berms, 135, 362, 380  
 Boulder-bed streams, 1  
 Boulders, 17-18, 20, 326, 327, 338  
     avoided in heel-to-toe samples, 154  
     effect on flow and sediment transport, 116, 124, 127  
     effect on local bed-material size, 124, 127  
     excluded from sampling, 127, 289, 327  
     in cascades, 117  
     included in the sample, 127, 289  
     in step-pool streams, 123  
     in transverse clast dams, 133  
     measurements of, 33-34  
     selection in pebble counts, 161  
     untransportable (immobile), 127, 131, 141, 326, 327, 342  
 Braided stream, 9, 109-110, 122-115, 131, 375  
 B-type streams, 4, 9, 122, 325, 326, 333, 334, 374  
 Bulk density, 100-101, 106, 294, 297, 313, 317  
     computation of, 104  
     effect of particle packing, 100, 104  
     for shoveled sediment, 196  
     for various sediments, 104  
     in dry channels, 101  
     in inundated channels, 100  
     in situ, 196  
     in situ measurements, 100-104  
     relation to sediment porosity, 105  
     required sample mass, 103

## C

Calipers, 16, 20, 27-28, 30, 33, 86, 164-165, 329  
 Cascades, 6, 8-9, 116-117  
*c*-axis, 14-17, 24, 33, 86  
     estimation in photo sieving, 179  
     of the  $D_{max}$ , 189  
 Censored layer, censored gravel, 130-132  
 Center of class, 23-24, 47-48, 61, 65, 72  
 Central tendency, 62  
 Channel. *See* Stream  
 Chi-square, 265  
 Clay and flour dough for areal samples, 176-177  
 Clusters, clustered 107, 114, 118, 121, 136-138, 142, 144, 169, 327, 338, 342

Coarse gravel-bed streams, 114  
 Coarse mode, 84  
 Coarse particles, 108, 117, 131, 137  
 Coarsest locations in the streambed, 118  
 Cobble beds, 208  
 Cobbles, 17, 24, 28, 117, 123, 128, 133  
     and sample mass, 299  
     measurements of, 32-34  
     mobile and immobile, 326  
     selection in pebble counts, 161  
 Coefficient of variation, 252  
 Combination of particle-size distributions from different methods of sampling and analysis, 216, 355  
     adjustment of frequency distributions, 237-238  
     flexible combination, 233-236  
     rigid combination, 230-233  
 Computed adhesive penetration depth, 226-229  
 Computer sampling, 364. *See also* Bootstrap approach  
 Confidence interval, 264-265  
     around all particle-size classes, 265-268  
 Confidence level, 243, 247-250, 266-267, 271, 280, 287, 316, 349, 350  
     definition of, 247  
 Contents of the pan, 60  
 Contingency table, 278  
 Conversion of particle-size distributions 216-217, 278, 342, 354  
     computed penetration depth, 226-229  
     modified cube model, 224-226  
     split plane surface model, 227-229  
     voidless cube model, 218-224, 227  
 Cookie-cutter sampler, 206-207  
     using divers, 207  
 Core samples, 132  
 Coupled streams, 12  
 C-type streams, 111, 120-122, 325, 326, 333, 345, 374  
 Cumulative particle-size frequency distribution, 23, 27, 31, 38, 40-41, 43-44, 47, 57, 62, 66, 357-358  
     in mm, 38  
     in  $\phi$ -units, 38  
     of equivalent Gaussian distribution, 52  
     of small samples, 63  
     percent finer, 38, 47, 74  
     percent coarser, 38, 74  
     plotting; curve, 38-39, 41

## D

D'Agostino test, 54  
 Dams, 130-131  
 Data sheet, for sieving, 31

Debris flows, likelihood of reaching stream, 12  
 Degrading stream, 120, 122, 124, 340, 373  
 Delineation of geomorphological units, 340-341, 343, 371  
 Delineation of sedimentary units, 326, 336, 340-341, 345-351, 359, 371, 377, 378  
   criteria for, 346  
   for subsurface sampling, 373  
   moving window technique, 329, 348, 351  
   retroactively, 329, 361, 369  
   statistical, 329, 348-352, 357  
   visual, 345-348  
 Deposition, 326  
   of coarse sediment, 113, 118, 123-128, 130, 188. *See also* Lag deposits  
   of fines, 120, 125-126, 133, 138, 140, 191, 340, 380. *See also* Fine sediment  
   on riffles, 118  
 Deposits,  
   of debris flows and landslides, 123, 136-137  
   non-stratified, 132  
 $D_{50surface}/D_{50subsurface}$  ratio, 131, 191, 373, 379  
 $D_{50armor}/D_{50subarmor}$  ratio, 188  
 $D_{50surface}/D_{bedload\ fines}$  ratio, 373  
 $D_{50local}/D_{50\ reach-avg.}$  ratio, 379  
 Dissipation of flow energy, 118  
 Distribution, 57  
   central parts, 46  
   fine and coarse tails, 40, 44-46, 56, 60-61, 74, 76, 78  
 Distribution parameters, 38, 41, 45, 55-60, 108  
   accuracy of, 60  
   and near-normality, 57  
   arithmetic approaches, 56-59  
   central tendency, 62  
   comparison between methods, 80-81  
   compilation of (Table 2.8), 58  
   computerized computation, 61  
   frequency distribution method. *See* Moment method  
   geometric approaches, 56-60  
   graphic approaches, 56-59, 61  
   moment method, 56-58, 60-61, 63. *See also* Moment method  
   number of percentiles needed, 60  
   overview, 57  
   various approaches, 56  
 Distribution types,  
   assumed. *See* Underlying distribution type testing for, 42  
 Divers, 131, 181, 204, 207  
 Double (or multiple) counting, 147-148, 156, 166, 168, 327, 338, 341. *See also* Serial correlation  
   effect on particle-size distribution, 156  
 Downbar fining, 108, 114, 323, 326

Downstream conveyance of sediment,  
   blockage by LWD, 123-124, 126  
 Downstream fining, 107-108  
 Downwelling flows, 132  
 Dredge, 215, 216, 383  
 Dune-ripple stream, 6, 8

## E

Eddy, eddies (wake), 137-138  
   recirculating eddy, 118  
 Ellipsoid, ellipsoidal. *See* Particle shape.  
 Embedded, embeddedness, 139-142, 169, 189-190  
   effect on photographic analysis, 182  
 Entrenchment ratio, 7  
 Equal mobility transport, 128, 130-131, 188  
 Erosion pavement, 124, 128, 130-131. *See also* Lag deposit  
 Erosion threshold, 136, 141  
 Error (mass-based computation and general). *See also* Precision  
   around mean, 309  
   around median, 309, 368. *See also* Two-stage approach  
   around percentiles, 315-320  
     absolute, 305-309, 318-320, 320-322  
     central percentiles, 301-304  
     computed analytically, 315-320  
     estimated from regression function, 304-306  
     percent, 305, 307, 320-322  
     standard error, 315-320  
   conversion between absolute, standard, and percent, 272  
   effect of large particles, 291, 298  
   from bootstrap approach, 315-320  
   in distribution tails, 60  
   preset acceptable, 242, 315, 323, 326, 331, 338, 366, 372, 376  
 Error (number-based computations and general). *See also* Precision  
   around mean, 245-246, 249-258, 276  
     absolute, 249-252, 254-255, 257, 272, 276  
     comparison of absolute and percent, 251-252, 258  
     comparison of sample-size eqs., 256-258  
     limited population size, 254-256  
     percent, 250-257  
   around median, 261-263, 276, 285. *See also* Two-stage approach  
     absolute, 262-263, 272, 276, 285  
   around percentiles, 247, 261, 264-277, 284,  
     absolute, 152, 271  
     central percentiles, 261-263  
     computed analytically, 274

- in symmetrical and skewed distributions, 272-273
    - percent, 152, 157, 264-268
    - standard error, 242, 247, 268-275
  - conversion between absolute, standard, and percent, 272
  - from bootstrap approach, 268-275
  - in 100- and 400-particle pebble counts, 149, 152, 157, 250, 266, 271, 276-277, 327-328, 334, 338, 347, 352
  - in distribution tails, 60
  - in percent fines, 283
  - in skewed distributions, 272, 276-277
  - in symmetrical distributions, 271
  - preset acceptable, 242, 246, 248, 250, 258-259, 285, 323, 326, 338
  - Type I and Type II, 278-280, 282
  - Error band around entire particle-size distribution, 265-268, 277
  - Error curves around percentiles, 273-274, 305-307
    - and replicate sampling, 307, 364
    - comparisons, 320-322
    - trumpet curve, 305-306
    - from best-fit regression function, 305-306
    - scatter in, 305, 308, 364
- F**
- Facies units. *See* Sedimentary units
  - Familiarization with reach or facies units, 326, 345, 346, 348, 377
  - Field, 25, 27-28, 30, 32
  - Field book, 166, 240
    - rain-proof, 240
  - Field computations, 260
    - of sample size, 263
  - Field forms 240. *See also* Data records and data sheets
    - developing, 240
    - for pebble counts, 165
  - Field notes, 300
  - Field sieving and weighing, 33-34, 36, 181
  - Field site, 32-34, 177
    - number of, 181, 182
    - remoteness of, 199, 208
  - Field time, 144-146, 170, 181
    - for photographic analysis and photo sieving, 181, 184
  - Field work, 240, 241
    - experience necessary, 5
  - Filled gravel, 129
  - Fine particles
    - accumulation in poorly accessible areas, 151
    - between low and high flow water line, 151
    - inclusion or exclusion from sample, 166
    - in interstitial voids, 229
    - partially hidden, 171, 283
    - underrepresented in pebble counts, 151, 153
    - variability between samples or operators, 151-152
  - Fine sediment in gravel beds, 105, 108, 131, 371
    - 151, 191, 386
    - abundance of, 128, 139
    - accumulation of, 277
    - around embedded particles, 140
    - at the downstream end of the bar, 114
    - deposits of, 133, 138, 380
    - exclusion from sample, 153
    - in backwater, 124, 372, 380
    - in bedload, 373
    - in bed-surface structures, 133-141
    - infiltration of, 130-132, 182, 188
    - in pools, 118-119, 323, 340, 372, 373, 380, 382-383
    - in spawning gravel, 203
    - in subsurface sediment, 372
    - intrusion, 131
    - in wake of boulder, 127
    - scour of, 124, 128, 130
    - storage of, 372
    - stream locations indicative of, 380
    - supply of, 119, 130, 132, 372,
    - tallying in one size class, 154
    - veneer of, 330
    - washed away during sampling, 13, 199, 203
    - wide size range < 0.1 to > 8 mm, 203
  - Fisheries biologists, 139
  - Fish habitat (studies), 185, 203, 371. *See also* Aquatic habitat
  - Flexible combination, 233-236
  - Floods, very large, 133, 326, 380
  - Flow
    - around boulders, 127
    - energy, dissipation of, 118
    - helical, 113
    - high energy, 131, 134
    - subcritical, critical, supercritical, 117
    - three dimensional pattern, 108, 126
  - Flow depth, 110, 113, 117, 184
  - Flow hydraulics, 128, 139-140, 326
  - Flowlines, 138
  - Flow separation zone, 137
  - Flow velocity, 113, 117
    - fast, 199
    - in pools, 118
    - on riffle-related features, 117
    - on riffles, 117-118
    - reversal of, 118
    - surface and bottom, 114
  - Fluvial transport distance, 16, 24, 51, 83, 88-89
  - Form-sphericity diagram, 179

Framework subsurface sediment, 188  
 Framework-supported gravels, 128, 131, 225  
 Fredle index, 76-77  
 Free matrix particles, 104-141  
 Free particle space, 140-141  
 Freeze-core samplers, 198, 204-205, 208, 210-213  
     problems with large particles, 213  
 Freeze-core samples, 100, 104  
     comparison with other samples, 213  
     sample mass, 211  
     stratification, 210  
 Freeze technique, for areal samples, 173  
 Frequency-by-number, 40, 216-217, 219-222, 237  
 Frequency-by-weight, 216-217, 219-222  
 Frequency distribution. *See* Particle-size frequency distribution  
 Froude number, 117, 135

## G

Gaussian distribution. *See* Normal distribution  
 Geometric progression, 59  
 Geomorphological units, 323, 325, 326, 337, 340, 341, 344, 371  
     comparison of particle sizes between, 340, 343  
     delineation of, 326, 336, 340-341  
     retroactive delineation of, 329  
     sampling on, 341-342  
     size of, 331  
     small, 341  
     sorting on, 373  
     spatial variability on, 341  
 Geomorphologically stratified sampling,  
     surface sampling, 340-345  
     volumetric sampling, 371-373  
 Glide. *See* Riffle  
 Goodness-of-fit, 45, 47-48  
     and computational consistency, 47  
     and sieve size, 47  
     effect of skewness, 51  
     effect of truncation, 51  
     for fine or coarse part of distribution, 51  
     to lognormal distribution, 47  
     to normal (Gaussian) distribution, 45, 47, 51, 243  
     to Rosin distribution, 51  
 Grab samples, 372, 373  
     comparison between computations, 369  
     mass of, 366-369  
     number of, 367, 376  
     repetitions of, 368  
     small and biased, 366  
 Gradation coefficient. *See* Sorting

Gradation curve. *See* Cumulative particle-size frequency distribution curve  
 Grain-to-grain contact, 136-137  
 Gravel, 17, 20, 30-31  
 Gravel- and cobble bed streams, 2  
 Gravel lobes, 114. *See also* Lobe fronts  
 Gravel mobility, 141  
 Gravelometer. *See* Template  
 Gravel pits, 132. *See also* Sampling pits  
 Gravel sheets, 135  
 Gravel sheltered in pockets, 141  
 Grid-by-number, 154, 168, 171, 178, 197, 217, 219, 221-225, 227-228, 230, 233, 237, 354  
     correspondence with volume-by-weight, 227  
 Grid-by-weight, 219  
 Grid counts, 145-146, 166, 169-170, 184  
     definition of, 145, 166  
     photographic. *See* Photographic grid counts  
 Grid sampling, 324, 334, 361, 363, 382  
     for each facies unit, 351, 353  
     for volumetric riffle samples, 372  
     in heterogeneous riffle-pool reach, 338  
     reach spanning, 351-353, 362-363, 374  
     several, overlaying, 324, 336, 341, 354, 363  
 Grid spacing, 327, 338-339, 341, 347-348, 353, 361, 365. *See also* Pebble count, sampling point spacing  
     cell size, 362  
     in different geomorphological unit, 341  
     in meander bends, 337-338  
     in streams of different widths and  $D_{max}$ , 339  
     minimum, 348  
     selection of, 362  
     small-scale, 380  
     tightly spaced, 332, 336-337, 341  
     widely-spaced, 333, 334, 337  
 Guidelines for bed-material sampling, 2, 5  
     in mountain streams, 5  
     in sand-bedded streams, 2  
     no substitute for experience, 5  
     problems of, 4  
     wide variety of, 5  
 Gullies, 9

## H

Hand-picking subsurface particles, 197  
 Hand-picking surface particles in areal samples, 172  
 Hanging scale, 33-34  
 Heel-to-toe sampling, 146-149, 152-159, 161-164  
     comparison with sampling frame, 161  
     mean percent error, 153  
     overrepresentation of mid-sized particles, 156  
     total error, 152

underrepresentation of fines and cobbles/  
boulders, 156-157  
Helley-Smith sampling bag, 200-201  
Heterogeneity of bed material, 333, 336, 345,  
360, 363  
degree of, 323, 332, 333, 345, 348, 359, 363,  
377, 378  
definition of, 326, 370  
effect on selected sampling scheme, 336  
example of,  
evaluation of, 359  
reduced by delineation into facies units, 345  
sampling of. *See* Sampling patterns in  
heterogeneous reach  
High flow, 113, 117-118, 121, 131  
Histogram, 38, 40, 239  
Homogeneity of bed material, 117, 120, 122,  
323, 360  
degree of, 323, 332, 333, 345, 359  
definition of, 326  
near-homogeneity, 326, 333  
truly homogeneous, 326, 360  
relatively homogeneous, 332, 334, 359, 373  
reach-averaged particle-size, 334  
homogeneous units, 345  
sampling of. *See* Sampling patterns in  
homogeneous reach  
Horseshoe vortex scour, 127, 138-139, 142  
Hybrid pipe-freeze-core sampler, 199, 213-215,  
372  
Hybrid sampling, 217, 351, 354, 355

## I

Imbricated, imbrication 118, 121, 134, 136-137,  
141-142, 144, 169, 343, 372  
Imhoff cone, 204  
Immobile particles and object, 127, 131, 138  
Infiltration of fines, 130-132, 182, 188  
Initial motion, 141, 146  
Intergranular friction angle. *See* Pivot angles  
Interstitial fines, 333  
Interstitial flow, 131  
Interstitial space index, 141  
Interstitial spaces, 277  
Iterations in sample-size computation, 250-251,  
262, 285-286, 303. *See also* Two stage  
approach  
ISO (1977, 1992), 290, 293, 299, 301

## J

Joined sieving, 343, 361, 366, 367, 370  
Judgement in selection of sampling locations,  
375  
Judgement sampling, 355, 375

## K

Kurtosis, 42, 56-58, 79, 149  
classification of, 78  
comparison between methods, 82  
definition of, 78  
fourth moment, 79, 80  
graphic arithmetic, 78  
graphic geometric, 79

## L

Laboratory time, 144-146, 181  
Lag deposit of coarse sediment, 117-118, 120,  
123-127, 130-131  
Landscaping cloth, for particle drying, 32  
Landslide deposits, 123  
Landward fining, 108, 114, 122, 323, 326  
Large woody debris. *See* LWD  
Lateral fining, 108, 122, 334, 378, 379  
Liquid nitrogen, 210, 215  
Lobe front of coarse sediment, 114, 133, 330  
Local hydraulics, 191  
Logarithmic transformation, 41-42, 46, 54, 60,  
65, 72  
Log jams, 107, 124, 130  
duration of, 124  
sequences of, 127  
Lognormal distribution, 17, 42-43, 45-47, 69, 73,  
82, 242, 253, 256, 263  
standard equation for, 46  
Lognormality, 41, 43, 54  
Longitudinal clast ribs, 134, 136  
Longitudinal stream profile, 108, 117  
Low flows, 113, 115, 117-119, 121, 124, 135  
LWD (large woody debris), 108, 116, 123-127,  
326, 327, 334,  
effect on bed-material size, 123, 125  
effect on flow and sediment transport, 116,  
124, 127  
heavy loading of, 126, 345

## M

Magnetic paint, 172  
Map, mapping,  
of facies units, 337, 346, 348, 378  
sketch map of reach, 326, 341, 348, 357  
textural, 346-347, 378  
using photographs, 142  
Matrix of finer sediment, 136, 139  
Matrix-supported gravel, 128, 225  
Meander bend, 114, 325, 337, 338, 343  
Meandering streams, 109-111, 113, 115, 325,  
343  
meadow meanders, 9  
valley meanders, 9

- Mean particle size, 41-42, 46, 56-57, 59, 62-65  
 arithmetic, 46, 59, 62, 348-350  
 comparison of computations, 80-81  
 definition of, 62  
 first moment, 65  
 geometric, 59, 64, 223  
 graphic arithmetic, 62, 64  
 graphic geometric, 63-64  
 in skewed distribution, 63  
 visual assessment of, 327
- Measurement of particle size, 20, 27-30, 323  
 in pebble counts, 164  
 operator error in, 148, 164, 329  
 record of, 164
- Measurement of particle volume, 98, 310
- Median particle size, 40, 46, 59-60, 62, 74  
 basis for stream classification, 1, 7  
 definition of, 40, 62  
 in skewed distribution, 62  
 visual assessment of, 345
- Mesh-bag scoop, 200-201, 210
- McNeil samplers, 198-200, 203-206, 213  
 and percent fines, 204  
 comparison with other samplers, 204  
 comparison with shoveled samples, 200-201  
 diagrams, 205  
 dimensions, 204  
 representative collection of fines, 200  
 sample mass, 204  
 sampling suspended bed sediment, 203-204  
 truncation of coarse particles, 203
- Micro-channels, sand-filled, 363
- Modality, 62
- Mode, 46, 62, 66, 83  
 definition of, 62  
 in Rosin distribution, 48  
 in skewed distribution, 62
- Modified cube model, 217, 224-226
- Moment method, 56-58, 60-61, 63, 82  
 advantage/disadvantage of, 61  
 effect of truncation, 61  
 exclusion of "pan", 80  
 first moment (mean), 65  
 fourth moment (kurtosis), 79  
 second moment (sorting), 71, 246  
 suitability, 61  
 third moment (skewness), 77
- Monitoring bed-material size, 148, 188, 335  
 for detecting change in  
 amount of fines, 128, 132, 203, 277, 340, 371, 380, 382-383  
 channel bed, using photographs, 184  
 riffle sediment size, 343  
 for watershed effects analysis, 146, 343, 371, 373  
 using visual estimates, 185
- Mountain streams, 12, 111, 114, 131, 143, 150, 158, 164, 199, 243, 258, 271, 275, 277, 326, 327, 335, 336, 360, 370,  
 volumetric sampling in, 319, 331, 332, 360, 363, 365
- Moving window technique, 329, 348, 352
- Multinomial approach (sample size), 261, 265-268, 275, 277, 284, 287
- Multiprobe freeze-core sampler, 199
- ## N
- Nominal diameter, 16-17, 221, 291
- Non-normal distribution, 44-45
- Non-parametric statistics, 43
- Non-random sample, 148, 156
- Normal distribution, 17-18, 24, 28, 40, 42-48, 51-52, 57, 59-60, 62, 67, 69, 73, 78, 242, 243, 248, 253, 264, 272, 273  
 as prerequisite for statistical applications, 42  
 assumption of. *See* Underlying distribution type  
 binned data, 45  
 change of curvature, 40  
 comparison with best-fit normal distribution, 45
- Normality, 41-43, 46, 54, 57. *See also* Normal distribution  
 approximate, 327  
 assessing the degree of, 51-52, 57  
 assessment by regression analysis, 45  
 D'Agostino test for, 54  
 departure from, 42-43, 54  
 effect on sample size, 42  
 Kolmogorov-Smirnov test for, 54, 270  
 near-normality, 51, 54, 376  
 not in a strict statistical sense, 42  
 null-hypothesis of, 54-55  
 resemblance with, 45  
 summary statistics of, 51  
 testing by regression coefficients, 45  
 testing for, 43, 45  
 visual assessment of, 43, 52  
 wrongly assumed, 42
- Number-based frequency. *See* Frequency-by-number
- Number of volumetric samples, 331-332  
 effect of heterogeneity and sorting, 370, 373  
 for spatially integrative sampling, 359, 363, 364, 366, 368, 370, 371,  
 geometrical and ecological criteria, 363, 365, 370, 372  
 grab sample repetitions, 368  
 grab samples, 372, 376  
 in large streams, 364  
 in small streams, 363

individually unbiased subsamples, 376  
on riffles, 372  
per area, 331  
per reach, 363, 364, 373  
retroactive computation of, 370  
subsample repetitions, 364  
subsamples, 364  
Null hypothesis, 51, 54, 281, 348

## O

Obstacle clast, 137-138  
One-step vs. Multinomial approach, 277  
Operator arbitrariness, 344  
Operator bias, 147, 243, 245, 259, 279, 334  
    and sample size, 245  
    against cobbles and boulders in pebble counts, 154-155, 244, 333  
    effect of boot size, 154  
    in heel-to-toe samples, 157, 161  
    reduction by sampling frame, 161  
    against small particles in pebble counts, 60, 149-153, 157, 244, 277, 283, 333  
    due to poor streambed accessibility, 151  
    in visual particle-size estimates, 185  
    towards cobbles and boulders, 147-148, 156  
        in areal samples, 172  
    towards fines in areal samples, 172  
    towards mid-size particles, 244  
Operator error, 20, 28, 148-149, 162, 259, 277, 283, 304  
    and sample size, 259  
    effect of multiple operators, 259-260  
    in heel-to-toe samples, 152  
    in particle-size measurements, 148, 164, 329  
    in pebble counts, 148-149, 152  
    when using sampling frame, 162-164  
Operator training, 5  
Operator variability, 25, 27  
    in areal sampling, 176  
    in pebble counts, 151, 154  
    in visual particles-size estimates, 185  
Optical particle-size analyzer, 169, 178  
Oven-drying, of particles, 32  
Overbank deposits, 380  
Overbank flow, 135

## P

Parent population, 245, 248, 250, 252, 259, 261-262, 264-265, 268, 275, 285-286, 321  
    computer generated, 288, 308  
    generated from sample, 288  
    surrogate for, 304  
Particle area, 284  
Particle availability for sampling, 243, 254-256

Particle axes, 14-16, 20, 28-29, 86, 164. *See also*  
    *a*-axes, *b*-axes, and *c*-axes  
    ellipse-approximation, 86, 178-179  
    position of, 136  
    ratios, 86, 87  
Particle breakdown, 107  
Particle counting  
    number of per photograph, 178, 181  
    number of per size class, 36, 38  
Particle density, 14, 34, 36-37, 98, 290, 301, 310, 313, 317  
    for different materials, 98  
Particle interlocking, 118, 343, 372  
Particle mass, 367  
    measurement of, 98  
Particle mean weight and sieve size, 36-37  
Particle mobility, 138, 141  
Particle number  
    per photograph 178, 181  
    per size class, 36, 38  
Particle packing, 94-97, 100, 103-104, 133, 136, 142, 165, 170, 182, 184, 287. *See also*  
    Framework gravels, Matrix gravels, and  
    Bed-surface structures  
    and compaction, 104  
    and effect of particle-size distribution, 104  
    void containing, 224  
    voidless, 193, 218, 221  
Particle paths for coarse and fine bedload, 114  
Particle position  
    effect on embeddedness, 190  
    effect on photo sieving, 179  
Particle protrusion, 141  
Particles  
    irretrievable, 150, 151, 336  
    large and wedged, 13, 122-123, 141, 155, 165, 333  
    partially hidden, 144, 169, 171-172,  
        effect on photo sieving, 184  
        on photograph, 179, 184  
    to be included in a sample, 148, 166  
    unsized, 95, 104  
    untransportable, 108, 117, 124, 127, 131, 138  
Particle shape, 14-17, 21-25, 28, 36-37, 60, 85-91, 94, 98  
    analysis by photo sieving, 181  
    and abrasion, 83, 88, 90  
    and particle mobility, 90  
    angular, angularity, 16, 27, 85-86, 90-92, 94-97  
        and transport distance, 90  
    bladed, bladedness, 86-90, 179  
    categories, 91  
    classification, 87  
    compact, compactness, 36, 87-90, 179  
    Corey shape factor, 89, 90

- diamond-shaped, 30
- disc, 86-87, 89
- dominant shape, 97
- effect of fluvial transport distance, 88-89
- effect on embeddedness, 190
- effect on photographic analysis, 182, 184
- effect on photo sieving, 179
- effect on pivot angle, 93
- effect on suspensibility, 88
- ellipsoidal, 14-17, 23-25, 89-90, 95-97, 189, 284, 290-291, 310
- elongated, elongatedness, 36, 86-91, 95
- flat, flatness, 20-25, 90-92, 94, 136
- form factor  $F$ , 87, 89
- form-factor  $S$ , 88
- per sieve class, 24
- platy, platyness, 86-90, 95, 179
- rhombic, rhomboidal, 14-16, 30
- rod, 86
- rounded, roundness, 88-91, 94, 97
  - visual chart for, 90-91
- roundness and abrasion, 90
- roundness index, 90
- sample size for identification of, 98
- shape/roundness matrix, 91
- spherical, sphere 16-17, 21, 23-25, 86, 88-91, 94, 96-97, 104, 221, 284, 290, 291, 310
- sphericity, 86-90. *See* Sphericity
- sphericity-form diagram, 87, 97
- variability at a site, 97
- visual field identification, 97
- Particle sieve-diameter, 17
- Particle size, 14, 16-20, 24, 28, 32-33
  - analysis, 3, 21, 31-32
  - categories, 17
  - classes, 14, 16-28, 30, 32-34, 36-37
  - conversion between measurements, 28, 30
  - $D_{max}$ , 289, 290, 327
  - dominant large,  $D_{dom}$ , 29, 289, 340, 371
  - fraction. *See* Size class
  - gradation, 18, 20
  - gradation curves. *See* Cumulative particle-size frequency distribution
  - mean, 14, 17. *See* Mean particle size
  - measurements of, 20, 27-30, 323
    - in pebble counts, 164
    - operator error, 148, 164, 329
  - median, 17. *See* Median particle size
  - metric, in mm, 17
  - per sieve class, 24
  - ratios, 343
    - $D_{50surface}/D_{50subsurface}$ , 131, 191, 373, 379
    - $D_{50armor}/D_{50subarmor}$ , 188
    - $D_{50surface}/D_{bedload\ fines}$ , 373
    - $D_{50local}/D_{50reach-avg.}$ , 379
- Particle-size distribution, conversion between
  - sampling methods, 216-217
  - computed penetration depth, 226-229
  - modified cube model, 224-226
  - split plane surface model, 227-229
  - voidless cube model, 218-224, 227
- Particle-size frequency distribution, 17-18, 38, 40-41, 43-48, 51, 56, 61-62, 64, 67, 80, 84
  - advantage of plotting, 158
  - analysis of, 39
  - bimodal, 82-83
  - computation of, 38, 370
  - example of, 39
  - in various stream types, 1
  - irregular, 46
  - obtained by different methods of sampling and analysis, 216-217
  - symmetrical, 62
  - tail of fines, 42, 48
  - wide, 230
  - with different sorting coefficients, 69
- Particle-size measurements. *See* Measurements of particle size
- Particle-size parameter. *See* Distribution parameters
- Particle sliding, 136
- Particle specific gravity, 99
- Particle specific weight, 99
- Particle submerged specific weight, 100
- Particle volume, 16, 34, 293
  - ellipsoid approximation, 178-179
  - estimation from particle shape, 98
  - measurement of, 98, 310
- Particle weight, 31, 34
  - per size class, 36-37
  - weighing in the field, 34, 36, 370
- Patch, patchiness, 108, 120, 126, 323, 330, 336, 345, 374, 375, 378-379
- Pavement, 124, 130, 131
- Peakedness. *See* Kurtosis
- Pebble box, 16, 20, 28-30, 86
- Pebble counts, 25, 38, 54, 123, 132, 145-165, 182, 184, 191, 230, 248, 250, 271, 276-278, 283, 323, 325, 328, 332-340, 340-345, 345-358, 378
  - and fines, 149-153, 157
  - and volumetric sample, 191
  - adjustment with areal sample, 237-239
  - along transects, 108, 333, 334, 344
    - at measuring tape, 147, 151, 155, 158-159, 333, 334
    - in meandering reach, 337-338
    - number of to cover the reach, 338-339, 343-345, 352, 355
    - paced, 332-334
    - parallel, 333, 334, 341

spanning facies units, 352  
 tightly / widely spaced, 332, 333, 336-337, 341  
 area needed for, 354  
 bias against fines, 224, 229  
 data record for, 164-166, 329  
 definition of, 144, 146  
 combination with areal sample. *See also*  
   Hybrid sampling, 354-355  
   flexible, 233-236  
   rigid, 230-233  
 geomorphologically stratified sampling, 340-345  
 grid spacing. *See* Grid spacing  
 heel-to-toe sampling. *See* Heel-to-toe sampling  
 inherent bias towards coarse particles, 156  
 in poorly accessible stream locations, 150, 151, 283, 332, 333, 336  
 in presence of bed surface-structures, 156  
 in small cobble-bed streams, 339  
 in submerged beds, 150  
 methodological differences, 148  
 of particles large and wedged, 13, 122, 123, 141, 155, 165, 333  
 on dry beds, 150  
 on exposed subsurface, 197-198  
 on facies units, 346-347  
 operator bias. *See* Operator bias  
 operator error. *See* Operator error  
 particle identification, 146-150, 332, 333  
   based on foot placement, 154  
   using sampling frame, 161  
 particle retrieval, extraction from bed, 122-123, 133, 149-150, 161, 164, 333, 334, 336  
 error in 100- and 400-particle pebble counts, 149, 152, 157, 250, 266, 271, 276-277, 327-328, 334, 338, 347, 352. *See also* Error (number-based computations)  
 sample size, 250. *See also* Sample size (number-based) *and* Sample size - error relation  
 sampling path, 151, 332  
   avoiding cobbles and boulders, 155  
   obstructed, 333  
   systematic, 333-336  
   unplanned, 333-334  
 sampling point spacing, 142, 145-148, 156, 159, 165, 168, 198, 327, 335, 338-339, 355. *See also* Grid spacing  
 sedimentary stratified sampling (within facies units), 345-358  
 sources of errors, 148  
 spatial aspects of, 327  
 spatially integrated sampling, 332-340  
 spatially segregated sampling, 340-358  
 statistical error 148-149, 152, 157, 162-164, 259, 271, 283  
   around small percentiles, 278  
   in heel-to-toe samples, 152  
   when using the sampling frame 162-164  
 subsamples, 341  
 time requirement, 145  
 unbiased, 157  
 within representative area of facies unit, 355  
 zigzag sampling, 278, 325, 332, 329, 333-336  
 Pebbles, 28, 32-33, 36  
 Penetration depth of adhesive. *See* Adhesive penetration depth  
 Percent error, 242. *See* Error around mean, median *and* percentiles.  
 Percentile error. *See* Error around percentiles  
 Percent finer, 38, 47, 74  
 Percent fines, 82-83, 108, 146, 148-149, 153, 278-279, 327  
   and error, 283  
   comparability of, 204  
   in McNeil samplers, 204  
   sample size for determining, 277-283  
   variability in pebble counts, 151, 153  
 Percentage frequency distribution, 38  
 Percentiles, 39-41, 48, 57-58, 62-63, 66-67  
   analytical computation of, 310-311  
   at points of curvature, 59  
   at tails of the distribution, 59  
   central, 61, 261  
   computation of, 40  
   example computation, 41  
   graphically determined, 39, 41  
   linear interpolation, 41  
   of normal distribution, 247  
   quartiles, 40, 60, 63, 76, 78  
   usage for, 146  
 Photographic analysis  
   areal overviews > 100 m<sup>2</sup>, 166, 182-184  
   close-ups < 0.1 m<sup>2</sup>, 182, 184  
   for small sampling areas, 146, 351  
   intermediate scale > 1 m<sup>2</sup>. *See* Photographic grid counts *and* Photo sieving  
   under water, 181, 184  
   variety of spatial scales, 167, 184  
 Photographic areal sampling, definition of, 178. *See* Photo sieving  
 Photographic grid counts, 166-170, 178  
   bias against fines, 170  
   deviation from sieve results, 169  
   problems of, 169-170  
   projection onto a screen with grid lines, 168  
   suitability of, 170  
 Photographs, 144-146, 167-168, 170, 178, 181-182, 184

for mapping bed surfaces, 142  
 of imbricated surfaces, 142  
 Photo sieving, 86, 171, 178-181, 184, 351, 354, 380  
   calibration, 181  
   comparison with mechanical sieving, 179, 181  
   field time vs. lab time, 181  
   flow chart for analysis, 179-180  
   for particle-shape analysis, 181  
   using divers, 181  
 Pilot study, 241, 246, 251, 252, 274, 288, 308, 325, 326, 360, 363, 365, 367, 373  
 Pipe dredge, 383. *See also* Dredge  
 Pipe samplers, 195, 203, 331, 367. *See also* McNeil samplers, 203  
 Pivot angle, 93-97, 119  
 Plane-bed stream, 6, 8, 117, 122, 275, 325, 326, 334, 374  
 Planimetric particle-size measurements and analysis, 166, 169. *See also* Photo sieving  
 Plotting particle-size distribution  
   advantage of, 158  
 Plywood shield, 210, 365, 367  
   to enclose the sampling area, 200, 209,  
 Pocket gravel, 141  
 Point bar, 111. *See also* Bar  
 Pool, pools, 107-109, 111, 113, 116-123, 325, 326, 334, 372  
   backwater pool, 126  
   bed-material size in, 113, 326  
   caused by LWD, 116  
   dammed pool, 124  
   deposition of fines in, 119, 373, 380, 382-383  
   forced pool, 326, 334  
   location of, 111  
   plunge pools, 124, 127, 130  
   residual pool volume, 382  
   scour in, 117  
   scour pool, 124, 126-127, 130  
   various kinds of, 116  
 Pool-exit-slope, 117  
 Pool-riffle-bar triplet, 109, 116  
 Pool-riffle stream, 6, 8, 111, 120-122. *See also* Riffle-pool  
 Population size  
   and sample size, 254-255, 270  
   limited, 242-243, 254-257, 269-270  
   unlimited, 255  
 Pores, 100, 131  
 Porosity, 104, 105, 106, 224  
 Polymodal, 62, 83  
 Precision, 241-245, 247-248, 250, 261, 268, 275-276, 284, 288, 323, 327, 328, 336, 338, 359, 360, 364, 368, 372, 376. *See also* Error and accuracy, 245  
   definition of, 244-245

for all percentiles, 284, 287  
 for set of subsamples, 286, 288, 304  
 mean, for given sample size, 286-287  
 stringent criteria, 328  
 unduly high, 364  
 Probability, 43-44  
 Probability graph paper, 41, 43, 50, 57. *See* Appendix  
 Probability plotting, 41  
   and regression analysis, 51  
   approximation of probability scale, 43  
   of residuals, 51  
   visual assessment, 43-44  
 Proportional sampling, 343-344

## Q

Quantiles, 55  
 Quartiles, 40, 63, 76, 78

## R

Random, randomness of  
   particle selection, 146  
   sample, 146, 151, 155-156  
   sampling locations, 324, 333, 360  
   within grid cells, 324, 360-363, 366, 372, 374  
 Randomization of locations for volumetric samples, 324, 361, 362, 363  
 Randomized grid patterns, 331  
 Rapids. *See* Riffles  
 Reach, 107-108, 113-114, 116-117, 120-121, 127, 141-142. *See also* Sampling area  
   definition of, 325  
   delineation of. *See* Delineation  
   familiarization with, 326, 345, 346, 348  
   large, 351, 355, 374  
   length of, 325-326, 335, 343-345  
   long, 323, 343-344, 355  
   size of, 338, 365  
   small, 332, 338-339, 340-341, 347, 374  
 Reach-averaged bed-material size, 114, 323, 325, 332, 334, 336, 338, 340, 342, 343, 348, 354, 356, 357-358, 359, 364, 366, 370, 371, 373, 376, 378  
   area-weighted, 347, 348, 351, 354, 356-358, 377-379  
   of subsurface sediment size, 364, 373, 377-379  
 Reach-spanning grid system, 351-353, 362-363, 374  
 Recording field results, 240. *See also* Field book, -computations, -forms, and -notes  
 Regression analysis, 55, 305-306, 364  
 Replicate sampling, 307-310, 363, 368  
 Resampling procedure. *See* Replicate sampling  
 Residuals, 43, 51-54

Resin cores, 213  
 Rigid combination, 230-233  
 Riffle crest, 108-109, 113, 117, 325, 326, 382  
 Riffle-pool sequence, 9, 108-109, 111, 113, 118-120, 122, 128, 323, 325, 338, 343, 344, 379  
 Riffle-pool morphology, 120-122, 325, 374  
 Riffle-pool stream, 275, 378  
 Riffles, 9, 107-109, 113, 116-121, 371  
   as sampling locations, 120, 342, 343, 371-372  
   bed-material size on, 114, 121, 326  
   coarser or finer than reach, 342, 371-372  
   flow hydraulics and cross-section, 342  
   glide, 117, 326, 343  
   location of, 111  
   pebble counts on, 342-343  
   rapids, 9, 116-117, 326, 334, 343  
   related features, 116  
   response to sediment supply, 340  
   runs, 116-117, 120, 122, 326, 334, 343  
   structural stability on, 118, 121, 343, 373  
   unrepresentativeness for the reach, 343, 372  
   volumetric sampling on, 371-372  
 Riffle spacing, 118  
 Riffle splitter, 32, 35. *See also* Sample splitting  
 Riffle Stability Index, 340  
 Riparian areas  
   damage to, 203  
 Riprap, 94  
 Rockfall, 97, 127, 131, 371  
 Rosin distribution, 48-51  
 Rotary scoop sampler US RBMH-80, 202-203  
 Round-hole sieves, 168  
 Roughness  
   form, 127  
   hydraulic, 133, 142  
   of bed, 135, 146, 289  
 Ruler, 16, 20, 25, 27-28, 30, 33, 36, 86, 164-166, 168-169, 178, 184, 329  
 Runs. *See* Riffles

## S

Sample, 25, 27, 30-31  
   coarse portion, 32  
   computer generated, 288  
   large, 32  
   largest particle to be included, 123, 127  
   partitioning into gravel and sand fraction, 51  
   representative, 74  
   unsieved portion, 33  
   with coarse particles, 34  
 Sample combination  
   adjustment of frequency distributions, 230, 237-238  
   flexible, 230, 233-236  
   rigid, 230-233

Sample conversion  
   computed penetration depth, 226-229  
   split plane surface model, 227-229  
   modified cube model, 224-226  
   voidless cube model, 217-224, 227  
 Sample mass (volumetric samples), 32-33, 191, 195-197, 200, 213, 363, 368, 371  
   effect of large particles, 291, 298  
   effect of sampling scheme on, 359, 360  
   for grab samples, 366-368, 373  
   for identifying particle shapes, 97  
   for measuring embeddedness, 141  
   for riffle samples, 372  
   for subsamples, 363, 365, 373  
     for bias avoidance in, 304, 365, 368-370, 372, 373, 376  
     grab samples, 366-368  
     reduction of, 366, 376  
   for total sample, 199, 331, 332, 359, 363, 365, 366, 368, 369-370, 373, 376  
     comparison between computations, 369  
     ecological criteria, 363, 365, 370, 372  
     for homogeneous reach, 360  
     in poorly sorted, coarse stream, 360, 365  
     large, unfeasible, 359, 370, 372  
     manageability of, 370, 376,  
     reduction of, 299-301, 365, 366, 370, 373  
     sedimentary stratified vs. integrated  
       sampling, 375-377  
   from barrel samples, 206, 208  
   from freeze core, 211  
   from hybrid sampler, 215  
   from McNeil samplers, 204  
   from plywood shield, 210  
   from tri-tube samples, 212  
   in coarse, poorly sorted mountain stream, 319, 331, 360, 365  
 Sample mass equations  
   analytical, 365  
     based on normal distribution, 308-320  
     for specified percentile error, 315-320  
   empirical, 288, 289-298, 299, 365  
     0.1, 1, 5, and 10% criteria (constant CV), 293-294, 315, 320, 360, 365, 366  
     American, 296  
     as function of  $D_{max}$ , 196, 289-299  
     based on error due to largest particle, 291  
     based on sample volume, 294-295  
     Canadian, 297  
     field criterion (5  $D_{max}$  particles), 295  
     for low, normal, and high precision, 293  
     German (DVWK), 297  
     Swiss, 297  
 Sample mass - error relation, 288, 301, 311, 316, 331, 360. *See also* Error curves, 376

- and assumed distribution type, 288-289, 293, 304, 309
- and standard deviation, 316-320, 372
- and study objective, 372
- bootstrap approach, 315-320
- for bias avoidance, 311-314, 331, 369, 370, 372-373, 376
- for error around mean, 309
- for error around median, 309, 376
- for percentile error, 372
  - absolute, 305-309, 318-320, 320-322, 365
  - central percentiles, 301-304
  - estimation from regression function, 304-306
  - percent, 305, 307, 320-322
  - standard error, 315-320, 365
- Sample depth in volumetric samples, 192-194, 197
  - thickness of strata, 132
- Sample size (for areal samples), 242, 283
  - geometrical consideration, 284
  - multinomial approach, 287
  - two stage sampling, 285-287,
- Sample size (number based), 241-243, 245, 247-249, 253, 255-256, 271, 275-276, 278, 282, 347
  - and confidence levels, 248
  - and cost and benefits of field work, 241
  - and error. *See* Error (number-based computation)
  - computation in the field, 260, 263
  - computation of, 249, 283
  - effect of limited population size, 243, 254-256
  - effect of multiple operators, 259
  - effect of preset acceptable error, 259
  - effect of sorting, 258
  - effects of bed-material characteristics, 241, 258-259
  - effects of spatial variability, 328
  - estimating from pilot study, 326
  - factors affecting, 242
  - for characterizing a population, 275
  - for detecting change in percent fines, 278-283
  - for low percentiles, 277, 328
  - geometric approximation, 287
  - in skewed distributions, 276
  - of subsamples, 262
- Sample-size computation, iteratively, 250-251, 262, 285-286, 303
- Sample-size equations (number-based), 245, 261, 272, 276
  - comparison of, 256-257
  - for areal samples, 283-284
  - for error around mean, 249-258
    - absolute 249-252
    - limited population size, 254-256
    - percent, 252-254
  - for error around median, 261-263, 272, 285. *See also* Two-stage approach
  - for error around percentiles, 261, 264-275, 284. *See also* Binomial, Multinomial, and Bootstrap approach
    - absolute, 271
    - central percentiles, 261-263, percent, 264-268
    - not applicable for heterogeneous reach, 341
- Sample size – error relation, 242-243, 247, 250, 256, 258, 269, 275, 327, 341
  - and assumed underlying distribution type, 242-243, 249, 264-265, 268, 271-274
  - and sorting (standard deviation), 276
  - around any percentile, 285
  - around mean and median, 276
  - binomial approach, 265-266
  - computation in the field, 260
  - for heterogenous reaches, 341
  - from bootstrap approach, 270, 274
- Sample-size statistics, 243, 277. *See also* Error and Precision
- Sample splitting, 31-35
  - in the field, 33, 370
- Sample storage 31
- Sample volume, 32-33, 195-197
  - fixed and small, 199
  - manageable, 323
  - relative, 310-320
- Sampling area, 347, 348. *See also* Reach
  - disturbance by sampling, 158, 299, 323, 331, 365
  - for areal samples, 197, 283-286
  - for pebble counts, 145, 328
  - for volumetric samples, 195, 198
  - large, 355, 363, 364. *See also* Streams, large
  - small, 242, 249, 323, 332, 338, 342, 354
- Sampling bed material, 141
  - challenge of, 3
  - coarsest clasts only, 371
  - finest only, in pools, 372, 380, 382-383
  - in entire reach, 150
  - in fast and deep flow, 13
  - in gravel- and cobble-bed streams, 2, 4
  - in heterogeneous reach. *See* Sampling patterns
  - in homogeneous reach. *See* Sampling patterns
  - in mountain streams, 4, 370. *See* Mountain streams
  - in plane-bed streams, 122
  - in presence of bed-surface structures, 133, 142
  - in presence of structural features, 119
  - in reaches with much LWD, 126, 127, 345
  - in step-pool streams, 123
  - in turbid water, 13
  - in various stream types, 2

- in vertically stratified sediment, 132
- in vicinity of boulders, 127
- locations of. *See* Sampling locations
- methodological differences, 4
- non-destructive, 143, 170, 171, 184
- on bar heads, 371, 380-381
- on bars, 114
- on riffles only, 120, 342, 372
- purpose of, 2
- to demonstrate downstream fining, 108
- with no replications, 304
- with replications, 307-310, 363, 368
- Sampling bias, 243, 245
- Sampling effort, 336, 341, 359, 360, 364, 370
- Sampling equipment and procedures
  - and coarseness of the bed, 331
  - combination of, 351, 354. *See also* Hybrid sampling
  - effect of natural and man-made factors, 143
  - for volumetric samples, 195, 198-216, 367
- Sampling errors. *See* Error(s) and Precision
- Sampling frame, 153, 158-166, 198, 259, 276, 283
  - comparison with heel-to-toe samples, 161
  - construction of, 158
  - operator error, 162
  - reduction of operator error, 161, 163-164
  - usage of, 159
- Sampling grid. *See* Grid sampling
- Sampling locations, 108, 114, 331, 366, 368. *See also* Sedimentary and Geomorphological units, and Pebble counts
  - accessibility, 332
  - at locations representative of reach-avg.  $D_{50}$  or  $D_{50\ sub}$
  - at representative locations within each or almost every facies unit, 351, 355, 374, 375
  - effect of heterogeneity and sorting, 370
  - extending over bankfull width, 338
  - for stream competence analysis, 380
  - for reach-avg. subsurface sediment and  $D_{50\ sub}$ , 374, 377, 379
  - inaccessible, 13, 151, 336, 283
  - indicative of fine sediment, 380
  - in high- or low-flow bed, 120, 151, 166, 338. *See also* Stream width
  - number of, 331-332. *See* Number of volumetric samples
  - patterns of. *See* Sampling patterns
  - representative selection of, 2, 355, 359, 374, 375, 377-379
  - retroactive computation of, 370
  - where local  $D_{50} \cong$  reach-averaged  $D_{50}$ , 374
  - within grid cells, 324, 362, 363, 372, 374
- Sampling method
  - selection of, 3, 4, 145
  - "standard", 4
  - suitability, 145
- Sampling patterns. *See also* Sampling locations
  - in heterogeneous reach, 242-243, 245, 304, 323, 325-326, 328, 332-333, 336, 340-341, 347, 373, 377. *See also* Sedimentary segregated and Geomorphologically segregated sampling
  - in homogeneous reach, 241, 254, 261, 275, 284, 304, 323, 325-326, 328, 330, 332-334, 341, 344-345, 359, 360, 373. *See also* Sedimentary integrated and Geomorphologically integrated sampling
  - overlapping, shifted grids, 324, 336, 341-342, 360, 363
  - random, 324, 333, 360-361
  - randomization of, 331, 362
  - random locations within cells, 324, 360-363, 366, 372, 374
  - spatially focused sampling. *See* Spatially focused sampling
  - systematic grid, 324, 333, 334, 336, 338, 341, 348-349, 351, 366, 372, 374
    - facies-spanning, 351, 353
    - pebble count combined with areal sampling (hybrid sampling), 351, 354, 355
    - reach-spanning, 351, 352, 360, 362-363, 374
- Sampling patterns for pebble counts. *See* pebble counts
- Sampling pit, 189, 191, 195, 197-198, 208
- Sampling point spacing. *See* Pebble counts and Grid spacing
- Sampling protocol, 151
- Sampling reach. *See* Reach
- Sampling results,
  - comparability of, 145
  - effects of sampling schemes, 323
- Sampling schemes, 323, 324, 335, 345, 374. *See also* Sampling patterns
  - and degree of spatial variability, 333, 360
  - and sample mass, effort and precision, 359, 360
  - based on surface facies, 331
  - errors in, 148
  - for subsurface sediment, 331
  - for volumetric samples, 331
  - geomorphologically stratified (segregated)
    - pebble counts, 340-345
    - volumetric samples, 371-373
  - overview, 324
  - sedimentary integrated, 333, 336, 345
  - sedimentary stratified (segregated), 373-379
    - pebble counts, 336, 345-358

- sampling patterns for, 351-355, 374-377.
  - See* Sampling patterns
  - volumetric samples, 373-379
- selection of, 3, 332, 333, 336, 358-359
- spatially focused, 323, 379
- spatially integrated, 323, 324, 331, 336, 358-371
  - pebble counts, 332-340
  - volumetric samples, 358-371
- spatially segregated, 245, 323-325, 331, 336-338, 371-379
  - pebble counts, 340-358
  - volumetric samples, 358-359, 371-379
- unsuitable, 333
- Sampling suspendable bed material, 203-204, 208
- Sand, 17-21, 24, 30-33, 36, 132, 134, 336, 362, 375
- Sand-bed streams, 1, 2
- Scour, 107, 116-118, 121, 123-124, 126-128, 130, 141, 326
  - around boulders or LWD, 127
  - around bridge piers, 138
  - in horse-shoe vortex, 127, 138-139, 124
  - in pools, 117, 124
  - of fines, 124, 128, 130
  - on riffle, 118-119
- Sedimentary stratified (segregated) sampling. *See* Sampling schemes
- Sedimentary (facies) units, 126, 145, 185-186, 303, 323, 324, 326, 328-330, 332, 345, 348, 352, 359, 371, 372, 374
  - definition of, 330, 345
  - delineation of. *See* Delineation
  - familiarization with, 348
  - few per reach, 374, 378
  - identification of, 127
  - large, 355-356, 373, 375, 378
  - many small ones, 359
  - map of, 346, 347, 378
  - multiple occurrences of, 374-375
  - particle-size distribution on, 378
  - representative sampling of, 332
  - size of, 331, 345, 347, 559
  - small, and fine sediment, 347, 360-361
  - sorting on, 355, 373
  - visually distinguishable, 378
- Sediment entrainment
  - delay of, 118
- Sediment strata (layers), 132, 189, 329
- Sediment stratigraphy, 211
- Sediment supply, 107, 112, 116, 122, 128, 131
  - and transport capacity, 119
  - cut off from, 124, 130
  - effect on bed-material size, 114
  - from debris flow, 12, 97
  - from fluvial sources only, 12
  - from non-fluvial sources, 12, 108
  - from rockfall, 97, 127
  - from rock source, 51
  - from tributary, 107
  - high, 133, 135, 188, 336, 373
    - of coarse sediment, 135
    - of sand and silt, 119
  - low, 111, 114, 124, 136, 336, 355, 379
  - of fine sediment, 151, 191, 372, 386
  - of non-transportable large clasts, 108, 289
- Sediment transport analysis, 188, 373
- Sediment volume, 106
- Serial correlation, 123, 142, 147-148, 156, 166, 168, 327, 335, 338, 341
- Settling velocity
  - effect of particle shape, 89
- Shear stress, 117
  - excess, 124
  - reversal of, 118
  - zones of highest, 113
- Shovels, 195, 198-199, 204
- Shovel samples
  - comparison with McNeil sampler, 200-201
  - on dry beds, 195
  - under water, 199
- Sieve, 14, 16-17, 20-25, 27, 30-31, 33
  - analysis. *See* Sieving.
  - box, 33-34
  - class, 16-17, 21, 24-25, 28, 33-34, 36
  - curve. *See* Cumulative particle-size frequency distribution curve
  - diameter, 17, 25, 33
  - round-hole sieve, 20, 23-25, 28
  - set, 16, 25, 32-33
  - size, passing, 17, 23-25, 27, 31, 49
  - size, retaining, 17, 23-24, 36, 37, 49
  - square-hole sieve, 20-25, 28, 30, 37
- Sieving, 20-27, 30-35
  - contents of the pan, 43
  - in the field, 32-34
  - in the lab, 30
  - manually, 30
  - ROTAP, 30
  - subsamples, 30-33
    - jointly, 343, 361, 366, 367, 370
- Significance level, 54-55
- Silt, 18, 132
- Single-thread streams, 122
- Single-tube freeze-cores, 199, 213
- Single-tube freeze-core sampler, 210-211
- Sinuosity, 7
- Sketch map of reach, 326, 341, 348
- Skewness, 38, 41-42, 56-58, 61, 75, 149
  - and departure from normality, 73
  - and sample size, 263, 272-275

- classification of, 75
- comparison between methods, 82
- computation of, 74
- definition of, 73
- graphic arithmetic, 74, 78
- graphic geometric (Fredle index), 76
- in mountain gravel-bed rivers, 73
- in Rosin distribution, 48
- moment method (third moment), 77-78
- negative, 73-74
- numerical values of, 75
- positive, 73-74
- quartile, 76
- range of percentiles used, 74-75
- sensitivity of data range, 74
- towards tail of fines, 128, 270-272, 276-277, 307, 320-322, 327, 328
- Sorting, 38, 41-42, 46-47, 56-58, 61, 73-74, 96, 149, 157, 162, 185, 242-243, 246, 257-260, 271, 310, 333, 364, 373
  - and standard deviation, 67
  - chart for visual estimation, 67-68
  - classification of, 68
  - coefficient. *See* Sorting
  - comparison between methods, 80, 82
  - for Rosin distribution, 49
  - gradation coefficient, 70-71
  - graphic arithmetic, 67, 73
  - graphic geometric, 69-72
  - in skewed distributions, 67
  - longitudinal, 123, 136
  - moderately-well sorted gravel bed, 149
  - moment method (second moment), 71-73
  - number of percentiles used, 67
  - of different facies, 126
  - poorly sorted gravel, 147, 149, 214, 244-245, 250, 253, 258, 276, 291, 311, 314, 315, 327, 333, 334, 346, 365, 370
  - values in gravel-bed rivers, 68
  - well sorted sediment, 134, 188, 241, 252, 332, 365
- Spacing between sampling points or grid points. *See* Pebble counts *and* Grid spacing
- Spatially focused sampling, 323, 377, 379
  - in pools, 372, 380, 382-383
  - on a few (representative) locations only, 375, 377
  - on bar heads, 371, 380-381
- Spatial sampling schemes. *See* Sampling schemes
- Spatial scale of sampling project, 323, 325
- Spatial variability of bed-material size, 114, 171, 326, 329, 332-334, 340, 341
  - and LWD, 126
  - and sampling patterns, 332
  - complex, 332
  - covered by sampling, 332, 367
  - degree of, 326, 330, 333, 345, 359, 363
  - downbar fining, 108, 114, 323, 326
  - downstream fining, 107
  - ignored, 340
  - inferences of, 330, 359
  - insight in, 340
  - landward fining, 108, 114, 122, 323, 326
  - lateral, 108, 122, 334, 378, 379
  - longitudinal, 334, 378, 379
  - moderate, 332, 344
  - no information on, 334, 370
  - none, 326, 345
  - of fines, 60
  - of subsurface sediment, 330-331, 372
  - on bars. *See* Downbar *and* Landward fining, *and* Bar heads
  - on geomorphological unit, 107, 114-115, 120
  - on riffles, 108, 120, 342, 372
  - patchy, patchiness, 108, 120, 126, 323, 330, 336, 345, 374, 375, 378-379
  - patterns of, 107
  - pronounced, 336
  - within reach, 108, 120, 363
  - within sedimentary (facies) units, 331
- Spawning
  - gravel, 178, 198, 203. *See also* Aquatic habitat success and fines, 82
- Sphericity, 86-90
  - and fluvial transport distance, 88-90
  - effective settling, 89-90
  - effect of geological parent material, 88-89
  - effect of sediment source, 97
  - effect on suspensibility, 90
  - effect on transportability, 88-90, 92
  - sphericity-form diagram, 87, 97
- Split plane surface model, 227-229
- Splitting apparatus, 34. *See also* Sample splitting
- Spreadsheet, 19, 31, 38, 41, 43-44, 57, 61, 260, 261, 263
- Square-hole sieves, 164, 168, 179
- Standard descriptive statistical parameters, 42
- Standard deviation, 38, 40-41, 46, 55-56, 59, 66-67, 69, 72-73, 80, 82, 242-243, 245-246, 248, 252, 257, 259-261, 268, 270-271, 285-286, 327
  - between or of subsamples, 262, 263, 302, 364
  - comparison between original and log-transformed data, 72
  - computation of, 66
  - definition of, 66
  - graphic geometric, 253
  - logarithmic geometric, 250, 251
  - of population, 245
- Standard error, 242, 247, 268-275, 316. *See also* Error around percentiles

Standing waves, 134  
 Statistical bias, 243, 245  
 Statistical error. *See* Pebble counts  
 Step-pool stream, 6, 8, 9, 123-124, 325, 326  
 Stilling well. *See also* Plywood shield  
     to enclose sampling area, 200  
     to prevent loss of fines in shoveled samples, 199  
 Stone cells, 136  
 Stoss deposit, 137-138  
 Straight streams, 108-110, 113, 115  
 Streambed  
     disturbance by sampling, 158, 299, 323, 331, 365, 376  
     heterogeneity. *See* Heterogeneity of bed material  
     homogeneity. *See* Homogeneity of bed material  
     monitoring. *See* Monitoring  
 Stream blockage, 124, 126. *See also* log jams  
     effect on stream morphology, 124  
 Stream classifications, 6  
     applicability of, 9  
     based on median particle size, 1, 7  
     difference between Rosgen and Montgomery-Buffington, 9  
     educational aspect of, 6  
     Montgomery and Buffington (1993, 1977, 1998), 6-8, 11  
     Rosgen (1994, 1996), 1, 6-7, 9-11  
 Stream competence, 107, 118, 130, 141, 380-381  
 Stream gradient, 1, 7, 107, 112, 116-118, 122  
     local, 117, 343  
     steep, 1, 133-134, 343  
     in Montgomery-Buffington and Rosgen classification, 11  
 Stream morphology, 1, 6, 9, 108, 116, 122-124, 323, 325, 338  
     and spatial variability of bed-material size, 114  
     around boulders and LWD, 116, 124  
     of riffles, pools, and bars  
     studies, 146  
     units, 108, 116  
 Stream morphometry, 7, 9  
 Streams  
     aggrading, 120, 122, 191, 229, 340, 345, 373, 378  
     degrading, 120, 122, 124, 340, 373  
     large, 326, 355, 364, 370, 375  
 Stream type, 325, 341  
     anastomosing, 9  
     A-type streams, 4, 9, 122, 123, 325, 326  
     boulder-bed, 1  
     B-type streams, 4, 9, 122, 325, 326, 333, 334, 374  
     braided (D-type), 9, 109-110, 112-115, 131, 375  
     cascades, 9, 116-117  
     classification by Montgomery and Buffington, (1993, 1997, 1998), 6-8, 11, 325  
     classification by Rosgen (1994, 1996), 1, 6-7, 9-11, 325  
     C-type streams, 4, 9, 111, 120-122, 325, 326, 333, 345, 374  
     common in Pacific Northwest, 9  
     coupled stream, 12  
     distinction by sediment source, 12  
     gravel- and cobble-bed, 1, 2  
     gullies, 9  
     meandering, 109-111, 113, 115  
     mountain streams, 12. *See* Mountain streams  
     plane-bed, 6, 8, 117, 122, 275, 325, 326, 334  
     pool-riffle, 6, 8, 111, 120-122. *See also* Riffle-pool  
     relict/non-fluvial, 12  
     sand-bed, 1, 2  
     self-formed, 12  
     single-thread streams, 112  
     step-pool, 6, 8, 9, 123-124  
     straight, 108-110, 113, 115  
     uncoupled stream, 12  
     wadable and unwadable, 13  
 Stream width, 117-118, 151, 161, 185, 325, 336, 338  
 Student's *t*, 247-248, 251, 257-258, 286, 302, 350  
 Study methods, 2, 4  
     selection of, 3-4  
 Study objective, 2-4, 120, 150, 371, 372, 374  
 Subarmor sediment, 188, 199, 201, 330, 359, 373. *See also* Subsurface sediment  
     definition of, 191  
     diagram, 143  
     sample depth, 192  
     sampling of, 191, 210  
 Subsamples, 261, 286  
     area for, 348  
     area represented by, 361  
     combination of several, 199  
     difference between, 363  
     grab samples. *See* Grab samples  
     joint analysis of, 361, 366  
     for armor layer sampling, 330  
     for sieving, 30-33  
     mass for bias avoidance, 304, 365, 368, 369, 370, 372, 373, 376  
     reduction of mass, 366, 376  
     number of, 248, 261-263, 284-285, 288, 301-305, 364, 370, 372, 373, 376  
 Subsurface particles, hand-picking, 197

Subsurface sediment, 128, 130-131, 188, 199, 359, 364, 371-373, 383  
 and bedload particle size, 373  
 definition of, 191  
 diagram, 143  
 example particle-size distribution, 39  
 in facies units, 331, 379  
 fining of, 128, 130  
 reach-averaged  $D_{50}$  size, 364, 373, 377-379  
 relation to surface sediment size, 330, 359  
 sample depth, 192  
 sampling of, 191, 377-379  
 size, controlled by, 191  
 Summary statistics, in normal distribution, 51  
 Surface coarsening, 128, 130-131, 191  
 Surface fines, 277  
 sampling of, 278  
 veneer of, 191  
 Surface fining, 132  
 Surface particles, 128-129  
 distinction from subsurface particles, 172  
 marking with spray paint, 172  
 problem of identification, 144  
 removal of, 197  
 Surface sampling. *See also* Pebble counts and  
 Areal sampling  
 definition of, 144  
 differences between methods, 145  
 in small sampling areas, 146  
 Surface sediment, 188, 199, 330  
 definition of, 144  
 diagram, 143  
 relation to subsurface sediment size, 330, 359  
 removal of, 191  
 Surveying sedimentary units, 346, 359, 378  
 Suspended sediment concentration, 132  
 Systematic sampling along measuring tape, 147, 151, 155, 158-159

## T

Tape recorder, voice activated, 164  
 Tarps, 32-34  
 Template, for gravel measurements, 16, 20, 25-28, 30, 32-33, 148, 161, 164-165, 328  
 Ternary (triaxial diagram), 186-187, 347  
 Textural map, 346-348, 378  
 Thalweg, 108, 113-114, 120-121  
 stream length, 335-336  
 Thin-section analysis  
 for areal resin samples, 173, 176  
 for resin cores, 213  
 Total error (statistical and operator), 152, 162, 271, 277  
 Traction carpets, 136-137  
 Transportability, 90

Transport capacity, 107, 113, 119, 122, 131  
 Transport competence, 107, 118, 130, 141, 380-381  
 Transport controlled (limited), 51, 340, 343, 373, 383  
 Transport distance, 16, 24, 51, 88-89  
 Transverse clast dams, 133-134  
 Transverse ribs, 117, 134-135, 327, 362  
 Triaxial (triangular) diagram (ternary), 186-187, 347  
 Tri-tube freeze-core sampler, 212-213  
 Truncation of sample, 61  
 and comparison of samples, 61  
 and surface fines, 82  
 at coarse end, 60, 82, 204, 366-367, 373  
 and readjustment, 299-300  
 at fine end, 60, 80, 153  
 effect on distribution curve, 60  
 effect on Fredle index, 77  
 effect on moment method, 61  
 effect on second moment, 80  
 effects on sorting, 46  
 effects on summary statistics, 61  
 of distribution tails, 45  
 Turbulence, 118  
 Two-stage sampling approach, 149, 171, 261, 263, 275, 284-286, 288, 301-307, 309, 328, 331, 341, 360, 361, 363, 367-368, 372  
 and  $\phi$ -units, 263, 287, 301  
 computerized, 304-307  
 for heterogeneous reaches, 336  
 with resampling, 307, 309

## U

Underlying distribution type, 242-243, 271-274  
 assumption of (normal distribution), 45, 249, 264-265, 288-289, 309, 311, 318, 328, 360, 365, 368, 369, 373, 376  
 no assumption, 264-265, 268, 288, 293, 304, 360, 365, 368  
 Underwater storage box for shoveled samples, 199  
 Unimodal, 62, 83-84, 243  
 Unstratified bulk sediment, 188, 336, 359, 371-373  
 Untransportable objects or clasts, 117, 127, 131, 289

## V

$V^*$ , 380, 382-383  
 Vehicle access, 32-33  
 Velocity reversal, 118  
 Visual chart for  
 degree of sorting, 67-68  
 particle roundness, 90

- particle size-categories (ternary), 93
- shape/roundness matrix, 91
- Visual delineation of sedimentary (facies) units, 185, 329, 345-348
- Visual estimates
  - of bed-surface parameters, 327
  - of particle sizes, 142, 184-185, 345-348
- Visual field identification of particle shape, 97
- Visual image of bed stratigraphy, 213
- Visualization of sampling process, 240
- Voidless cube model, 218-224, 227
- Void ratio, 100, 105-106
- Voids, 128, 132, 227, 287
  - filled with fines, 130
  - neglecting presence of, 227
- Void volume, 106
- Volume-by-number, 219
- Volume-by-weight, 171, 197, 217, 219, 221, 223-230
- Volumetric samples, 132, 323, 325, 329, 359
  - areal extent of, 365
  - at random locations within systematic grid cells, 360
  - at several overlaying grid systems, 360
  - at systematic grid points, 360
  - definition of, 188
  - depth of, 192-194, 197
  - grab samples, 366
  - in dry beds, 195
  - of subsurface, 277
- Volumetric sampling, 288-320, 325, 329, 380
  - armor layer, 330. *See* Armor layer
  - equipment and procedures, 195, 198-216, 367
  - geometrical and ecological criteria, 363
  - geomorphologically stratified, 371-373
  - in homogeneous reaches, 359-360
  - in large streams, 364
  - in mountain streams, 370
  - number of samples or sampling points, 359, 363, 364, 366, 368, 370-373, 376
  - reduction of, 366
  - retroactive computation of, 370
  - number of subsample replications, 363, 372
  - on riffles, 372
  - problems of, 199
  - sample mass. *See* sample mass
  - sedimentary stratified, 373-379
  - spatial aspects of, 329
  - spatially integrated, 358-371
  - spatially segregated, 371-379
  - under water, 198-199, 202, 207

## W

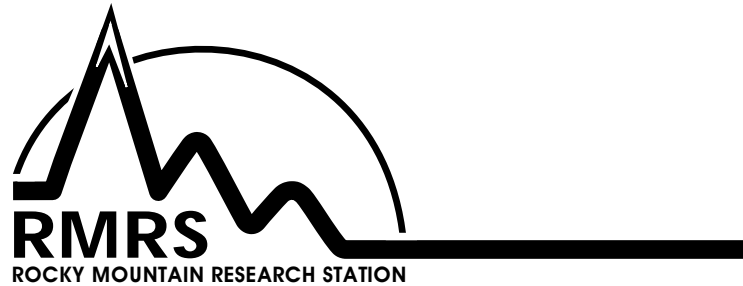
- Wading, wadable, wadability, 13, 25, 146, 147, 151, 181, 202, 203, 207, 215, 332, 333, 334

- Wake deposit, 137-139, 142, 156, 340, 380
- Weight-based frequency. *See* Frequency-by-weight
- Weight per size class, 38
- Wentworth scale, 17-18
- Wet-sieving, 173, 177
- Width-depth ratio, 7

## Z

- Zigzag paths for pebble counts. *See* Pebble counts





The Rocky Mountain Research Station develops scientific information and technology to improve management, protection, and use of the forests and rangelands. Research is designed to meet the needs of National Forest managers, Federal and State agencies, public and private organizations, academic institutions, industry, and individuals.

Studies accelerate solutions to problems involving ecosystems, range, forests, water, recreation, fire, resource inventory, land reclamation, community sustainability, forest engineering technology, multiple use economics, wildlife and fish habitat, and forest insects and diseases. Studies are conducted cooperatively, and applications may be found worldwide.

### **Research Locations**

Flagstaff, Arizona  
Fort Collins, Colorado\*  
Boise, Idaho  
Moscow, Idaho  
Bozeman, Montana  
Missoula, Montana  
Lincoln, Nebraska

Reno, Nevada  
Albuquerque, New Mexico  
Rapid City, South Dakota  
Logan, Utah  
Ogden, Utah  
Provo, Utah  
Laramie, Wyoming

\*Station Headquarters, Natural Resources Research Center,  
2150 Centre Avenue, Building A, Fort Collins, CO 80526

The U.S. Department of Agriculture (USDA) prohibits discrimination in all its programs and activities on the basis of race, color, national origin, sex, religion, age, disability, political beliefs, sexual orientation, or marital or family status. (Not all prohibited bases apply to all programs.) Persons with disabilities who require alternative means for communication of program information (Braille, large print, audiotape, etc.) should contact USDA's TARGET Center at (202) 720-2600 (voice and TDD).

To file a complaint of discrimination, write USDA, Director, Office of Civil Rights, Room 326-W, Whitten Building, 1400 Independence Avenue, SW, Washington, DC 20250-9410 or call (202) 720-5964 (voice or TDD). USDA is an equal opportunity provider and employer.